THE BEHAVIOUR OF SKEWED MASONRY ARCH BRIDGES

John A. Hodgson

Department of Civil Engineering
University of Salford, Salford, UK

Submitted in Partial Fulfilment for the Degree of
Doctor of Philosophy, April 1996

Contents

List of illustrations

List of tables

List of plates

1.0 Introduction

1.1 Background

Masonry arch bridges have been used throughout the world. Many thousands exist in Europe. The number of arch bridges in the United Kingdom has been estimated at 75,000 with approximately equal numbers occurring within the road and railway networks.

The arch is very pleasing to the eye. Many arch bridges are listed structures so that replacement schemes are not options. In 1880 Baker was commissioned to report on the deterioration of Telford's Bridge at Over. Baker wrote, "The abutments had gradually gone over, and had been continuing to go over for sixty years. The result was that certain barbarians were actually urging the magistrates to take down the bridge...". He continued, "... cracks in the spandrels were big enough to walk through quite comfortably. It would be a disgrace to the country if they pulled down Telford's historical work and substituted a hideous iron lattice-bridge", (Heyman & Threlfall, 1973).

Masonry arch bridges were built to carry a road, a railway or sometimes a waterway over an obstacle. A right arch bridge was used where the crossing could be perpendicular to the obstacle. In contrast, a skewed arch was built wherever the obstacle and over-road intersected at any angle other than 90°. Thus, a right arch is a special case of the more general class of skewed arch. The extent of existing knowledge of the behaviour of arch bridges is limited to the right arch in which many effects have either been omitted or have been simplified. These effects include the spandrel walls, the backfill, irregular geometry, and eccentric loading. Clearly, there is scope for an advancement of knowledge so that these effects may be considered and ultimately the behaviour of the skewed arch bridge can be described.

The construction of arch bridges in Great Britain reached its zenith at around the beginning of the Nineteenth century. At this time, if conditions prevailed, there was a general desire for each new bridge to exceed the span of any that had gone before (Ruddock, 1979). However, Séjourné (1913) could only find eight structures in the United Kingdom that had at least one span with a clear opening of more than 40.0 m.

In the United Kingdom, the first revival of interest in the behaviour of masonry arch bridges was at the time of the Second World War. This led to the development of the MEXE (Military Engineering Experimental Establishment) method which provided a quick method of load assessment before military vehicles were allowed to cross a particular bridge. Since its inception, it has been used almost universally as the Engineer's primary assessment tool. However, it is generally felt to be inadequate since it was based on a number of dubious

assumptions and empirical modification factors. The fact that no catastrophic failures have been recorded must not be used to conclude that the method is conservative and is therefore safe.

The second revival of interest in the masonry arch began approximately fifteen years ago and was due to the ever increasing volumes of both commercial and private traffic on the road network. Freight is opting for the road network rather than the railway network. The Government is bringing the country into line with the rest of Europe by permitting heavier vehicles with weights of up to 40 Tonnes onto the road network. The deadline for this upgrading of permissible loads is 1999. However, there are many advocates for vehicles of up to 44 Tonnes to be allowed on the road network. These are, at present, allowed on the roads but only when travelling to and from rail freight terminals and only when six axles are adopted. Thus, the establishment of heavy load routes following the assessment of all bridges is of prime importance. The financial implications of imposing unnecessary weight restrictions would be enormous. Longer journeys would be required which would impair the economic growth of those regions effectively isolated by the weight restrictions.

The situation of the railway network is in stark contrast to that of the road network. Railway traffic has decreased over the past few decades. Lighter rolling stock are now in service but higher speed trains may offset this. In addition, the trend towards welded tracks is a further benefit. However, the fact remains that most of the arch bridges in the United Kingdom are in excess of 150 years old and, like the Victorian brickwork sewers, may be approaching the end of their life.

Bridge owners require an assessment technique to satisfy several objectives. These include the necessity for it to possess a sound theoretical background. This would increase the confidence of the Assessment Engineer. This confidence would be enhanced if the assessment technique could produce the necessary information to enable the Engineer to obtain a "feel" for the validity of the analysis. Additionally, the quality of an assessment technique will be judged on its ability to permit further investigation into the effects of proposed strengthening measures. The M.E.X.E. method can only produce a permissible axle weight. However, it does permit an investigation into the effects of repairs although, without a sound theoretical basis, there can be little confidence in its conclusions.

Research intended to provide the Assessment Engineer with the means for determining the effects of several parameters remains outstanding. These parameters include structural defects and proposed strengthening measures, the influence of the spandrel walls upon the behaviour of the entire structure, the behaviour of the backfill and its interaction with the arch, and other three-dimensional effects such as eccentric loading, impact loading on the parapets and irregular geometries. Fundamental to the above is a knowledge of how load is transferred through the

three-dimensional structure into the abutments.

The revival of interest in masonry arch bridges has also led to the construction of a small number of new arch bridges, viz., Ellerbeck Bridge which was built in 1989, Kimbolton Bridge in Cambridgeshire which was built in 1992, and Monk Bridge which was also built in 1992. It has been realised that when calculating the relative costs of various proposals for a bridge scheme, the inclusion of maintenance costs leads to masonry structures being, by far, the most cost effective. Modern bridges of steel or concrete construction are designed for a life of 120 years. In many cases, material weathering has led to expensive remedial measures and to a greatly reduced life span. In contrast, the cost of maintenance associated with masonry arch bridges is negligible.

Research into construction methods is ongoing. Modern headroom requirements would result in the need for very flat arches. These present very great forces to their abutments. The alternative solution, which would be to construct regular shaped arch bridges with increased spans, is not feasible because of the constructional difficulties involved. Additionally, increased spans do not satisfy the headroom requirements because of the interpretation of the relevant clauses imposed by the client.

1.2 Scope of the research

This thesis will be primarily concerned with a study of the load carrying behaviour of skewed masonry arch bridges.

The first relevant aspect to be dealt with will be some of the most commonly occurring construction details found in single span skewed masonry arch bridges. The development of arch theory will then be discussed with particular emphasis on the current analysis methods and their limitations.

At the inception of this project there existed no satisfactory theoretical or empirical model pertaining to the load carrying behaviour of skewed arch bridges. Moreover, the performance of this type of structure was even less well understood when constructed from multiple rings of brickwork. In cases such as these, ring separation may be an inevitable consequence of the dynamic loads that the bridge has been subjected to throughout its life as well as being a distinct possibility if it were to be subjected to a monotonically increasing static load. This thesis will be concerned with the behaviour of these bridges under static loading because without a knowledge of how these loads are transferred through the structure the effects of dynamic loading cannot be considered. The absence of data pertaining to the behaviour of skewed

masonry arch bridges resulted in the requirement for the model arch bridge tests documented herein. The interpretation of the results of these tests and the formulation of a theoretical analysis technique will provide the means of describing the behaviour of these structures.

The experimental work was carried out at the large-scale model testing laboratory at the Bolton Institute of Higher Education. Here, four 3.0 m single span skewed arch bridges were constructed in a way that was similar to a previous set of four square span, multi-ring, segmental, brickwork arch bridges. Additionally, a further series of seven single ring, barrel only, arches were tested. The design and construction of the reinforced concrete test bed, upon which all testing was carried out, and all aspects of the construction, instrumentation, and testing of each arch bridge came under the direct supervision of the author. The results of the load tests on the 3.0 m span large-scale skewed arch bridges have been documented elsewhere. However, the pertinent points from these bridge test reports will also be included within this thesis together with the pertinent points from the bridge test reports on the corresponding square span arch bridges. It is only through a comparison of these two series of tests that a knowledge can be acquired of the effect that skew has upon the behaviour of masonry arch bridges.

Each large-scale model arch bridge was extensively instrumented although the skewed arch series was more so. Parameters that were measured included the magnitude and position of the applied load, deflections, surface strains, backfill pressures and temperatures. Each bridge was subjected to a series of non-destructive patch load tests in which the load was repeatedly increased and decreased until the reaction of the bridge became repeatable. The data from these tests are documented with a view to extending the proposed analytical model to incorporate serviceability effects at some future date.

Each arch bridge was ultimately subjected to a monotonically increasing line load that was parallel to the abutments and positioned at the quarter span of the bridge. When the bridge failed the loading was instantaneously reduced and thereafter incremental displacements were applied until collapse occurred.

The results of the load tests on the 1.2 m span barrel-only arches will be contained within this thesis. They will serve to highlight the generic movements involved in the deformation of the voussoir arch as it accommodates the displacement of the ultimate load. In other words, the movements of each block of masonry that are required within a three-dimensional collapse mechanism, as predicted by the proposed mechanism method, can be verified against visual observations of each of these failure mechanisms. These tests will therefore enable the behaviour of the 3.0 m span skewed arch bridges to be described as well as providing information necessary for the development of a three-dimensional mechanism method.

The development of a three-dimensional mechanism analysis method will be described. The method will make use of the upper-bound theorem of collapse and will utilise the assumption that the formation of fractures divides the arch into several rigid blocks. The magnitude of the collapse load can be determined directly from the change in potential energy of this system of rigid blocks since their movements, in accommodating the displacement of the collapse load, must be such that they remain in contact with each other. This analytical technique will be used to describe the behaviour of each skewed arch bridge documented within this thesis. Finally, its limitations will be discussed and proposals for its development will be made since it is possible for it to be extended to include other forms of collapse mechanisms and the spandrel walls.

A new application of the finite element method will be presented which can incorporate the phenomenon of ring separation. This aspect of the work was carried out by the author at the head office of his sponsors, viz. L.G. Mouchel and partners, using a commercial finite element analysis package (ANSYS v5.1 58). Prior to the development of this model there existed two other models that had attempted to incorporate ring separation. The first model was the two-dimensional finite element analysis carried out by Choo et al. (1991b) and the second was a two-dimensional mechanism analysis method developed by Gilbert (1993).

The former model was calibrated against experimental data obtained from tests carried out at the Bolton Institute of Higher Education. This model was reported to produce a close correlation between its predicted collapse load and the actual measured value of two 5.0 m span arch bridges. However, it could not accurately reproduce the measured load-deflection response of either structure. There was a reasonable correlation between the predicted load-deflection response and the measured response of the first 5.0 m span model arch bridge with the exception that they became divergent as the maximum load was approached. In contrast a close correlation between the finite element predictions and the measured load-deflection response of a similar structure that had been constructed with the defect of total ring separation existed only at the ultimate load and at the initial unloaded state. Furthermore, it appeared that the material properties (Choo et al. 1991b) used in this model were lower than those that were obtained experimentally.

The latter method could reproduce the experimentally observed collapse mechanisms but overestimated the associated load if the analysis was performed using the measured shear bond strength. Furthermore, the method of modelling of the bond between the adjacent rings led to incorrect predictions that a multi-ring arch could be stronger than the equivalent voussoir arch. This is because, although a rigid-plastic model of the bond could prevent ring separation if a sufficiently strong mortar was assumed and in this case the two forms of structure would become identical, localised ring separation associated with the formation of a hinge leads to an

increase in the predicted collapse load.

It was therefore decided that an independent theoretical model should be developed which must use actual measured material properties. To be credible, a single theoretical model must be capable of predicting the behaviour of an arch bridge that may either suffer ring separation as a result of incremental loading or which already contains ring separation. A finite element model of a square span multi-ring brickwork arch will be presented within this thesis which can incorporate ring separation. This model will be discussed and a method will be outlined to show how it can be extended to deal with skew.

It can therefore be seen that the scope of the work is wide. Masonry arch behaviour is complex and it would be unrealistic to suggest that this work will resolve all, or even more than a few, of the problems which exist. In particular, the strength of a masonry arch bridge may be influenced by the ability of it to mobilise backfill pressures which will restrain the deformation of the arch barrel. Furthermore, the type of fixity that may exist between the spandrel walls and the arch barrel and the resistance to their movement that the wing walls may offer will also greatly influence the behaviour of the structure. These effects will be included as realistically as possible. However, the formulation of more sophisticated models will be beyond the scope of this thesis except for providing suggested ways in which these effects might be incorporated.

1.3 Constructional Aspects

In England, early attempts to construct skewed arch bridges were largely unsuccessful. Benjamin Outram (Schofield; 1979) built several arch bridges of up to 20° skew with unskewed masonry, i.e. as if they were square span structures.

In a skewed arch that was constructed with unskewed masonry, shown in figure 1.1, each acute angled haunch is effectively unsupported. These regions do not form part of a contiguous set of masonry which, in a direction normal to the bedding joints, span between two facing abutments. The integrity of these regions is dependent upon the ability of the arch to disperse its load in the transverse direction.

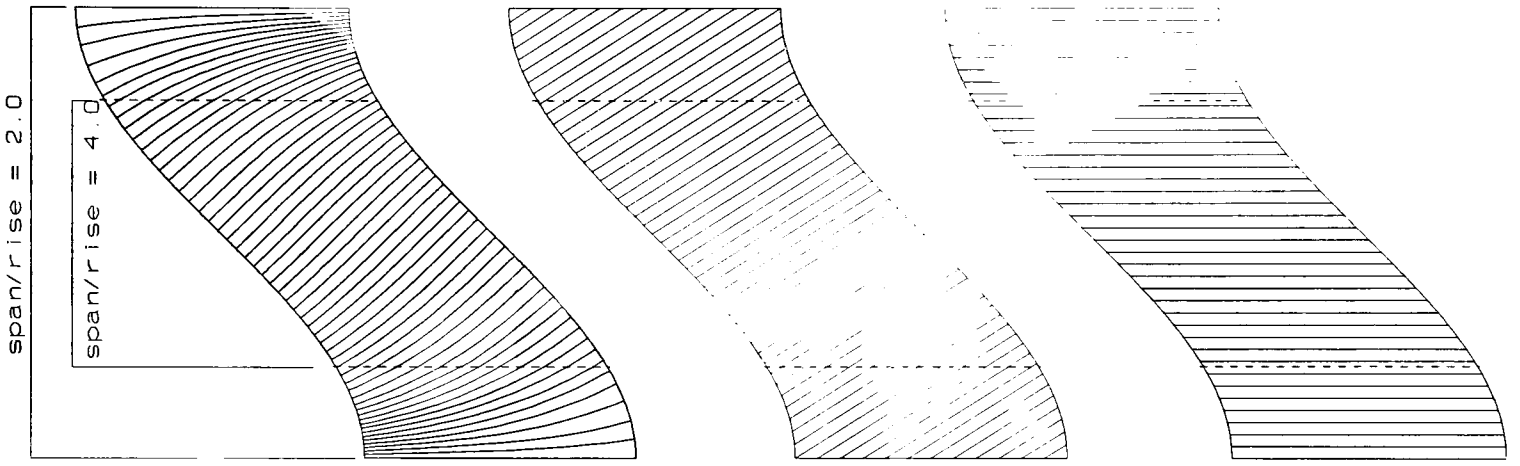

Figure 1.1 Setting out of skewed arch

Figure 1.1 shows the development of a 45° skewed segmental arch with three possible methods of construction consecutively illustrated. The edge of the developed shape forms part of an inverse sine curve, when rolled up to form the desired arch the edge is a straight line when viewed from above. The three methods illustrated above are the Orthogonal, Helicoidal and unskewed respectively. Several authors have outlined the steps required in order to generate the above construction details (Rankine, 1898; Encyclopaedia Britannica, 1876; Gay, 1924) and readers are referred to these texts for a detailed mathematical description of the curves.

Chapman (1787) devised a method for setting out the masonry in a skewed arch. His method became known as the Helicoidal, or English, method but is actually only partially correct. The more exact method known as the Orthogonal, or French, method ensures that bedding joints are perpendicular to the direction of the skew span throughout the arch. In 1797 Jessop superseded Outram's construction method by using the Helicoidal method to build the first "correct" skewed arch bridges in England, across the Rochdale canal (Ordnance survey sheet SJ8811SE grid reference 88625 11065). Plates 1.1 and 1.2 show Jessop's bridge.

Plate 1.1 Jessop's Bridge: the first skewed arch

Plate 1.2 Jessop's Bridge: the first skewed arch

The Orthogonal method is not applicable to skewed brickwork arch bridges since it requires the use of varying sized masonry blocks. Furthermore, this method requires that the shape of the arch is a "basket handle" (Gay, 1924), i.e., the arch and each abutment form a continuous curve and that each abutment is vertical. Figure 1.1 illustrates this requirement. For a semi-circular arch, the first course of masonry, adjacent to the skewback, is placed parallel to the abutment and does not require much effort to ensure that it curves around so that it is perpendicular to each fascia. Likewise, each subsequent course can also be gently eased into the structure. If the span/rise ratio is increased to form a segmental arch, the detailing of the blockwork adjacent to each abutment resembles that which is required in the Helicoidal method. Gay (1924) pointed out that a further drawback of this method is that each voussoir is unique and therefore the cost of such a solution is great.

The Helicoidal method provides a saving in the cost of construction since each voussoir is similar to all other voussoirs. However, this method produces an untidy edge detail in multi-ring skewed brickwork arch bridges. In this method, the bedding joints are only perpendicular to the direction of skew at the crown of the arch. Thus, each brick course is generally not perpendicular to the intended line of the fascia. Therefore, if special bricks are not used, or if normal bricks are not cut to shape in situ, a saw-toothed effect is produced. Furthermore, the brickwork is inclined in each acute angled haunch, whilst the brickwork is declined in each obtuse angled haunch. Hence, a vertical face can not be achieved unless the bricks are cut to shape in situ.

The problems associated with the aesthetics of skewed arches can be overcome through the use of large stone blocks positioned at each edge of the arch. These can be cut to the desired shape and therefore provide an attractive solution. The interior of the arch can then be infilled with brickwork built following the Helicoidal method. The infill brickwork is sometimes placed on its ends so that the number of discrete rings is halved. This is a common feature of square span arch construction but is not feasible in highly skewed arches if the large edge blocks ,as described above, are omitted.

Plates 1.3 and 1.4 show details of a skewed arch bridge in which large masonry edge blocks were used to both stiffen the arch and to provide an aesthetically pleasing fascia. The brickwork infill follows the Helicoidal method with each brick being placed as a header.

It was often the practice to construct skewed arch bridges from multiple brickwork rings and simply cut the fascia bricks in situ so that a uniform edge was produced. Gay (1924) presents several illustrations of how the masonry in skewed arch bridges was set out. He suggested that the Léveillé method was often used in stead of the Orthogonal method when the skew was very pronounced and the arch had a "basket handle" profile.

Plate 1.3 Edge detail adopted on skewed arch bridges

Plate 1.4 Edge detail adopted on skewed arch bridges

This method uses unskewed masonry up to 30° from the springing and Helicoidal masonry beyond this point. The Léveillé method was intended to produce an effect similar to the Orthogonal method without the construction difficulties and associated costs.

The acute angle formed at the corner of the abutments of a highly skewed arch bridge presents a potentially weak section. This weakness continues within the arch barrel and is often removed by chamfering the masonry at these locations. The chamfer is gradually reduced so that it is no longer required at the crown.

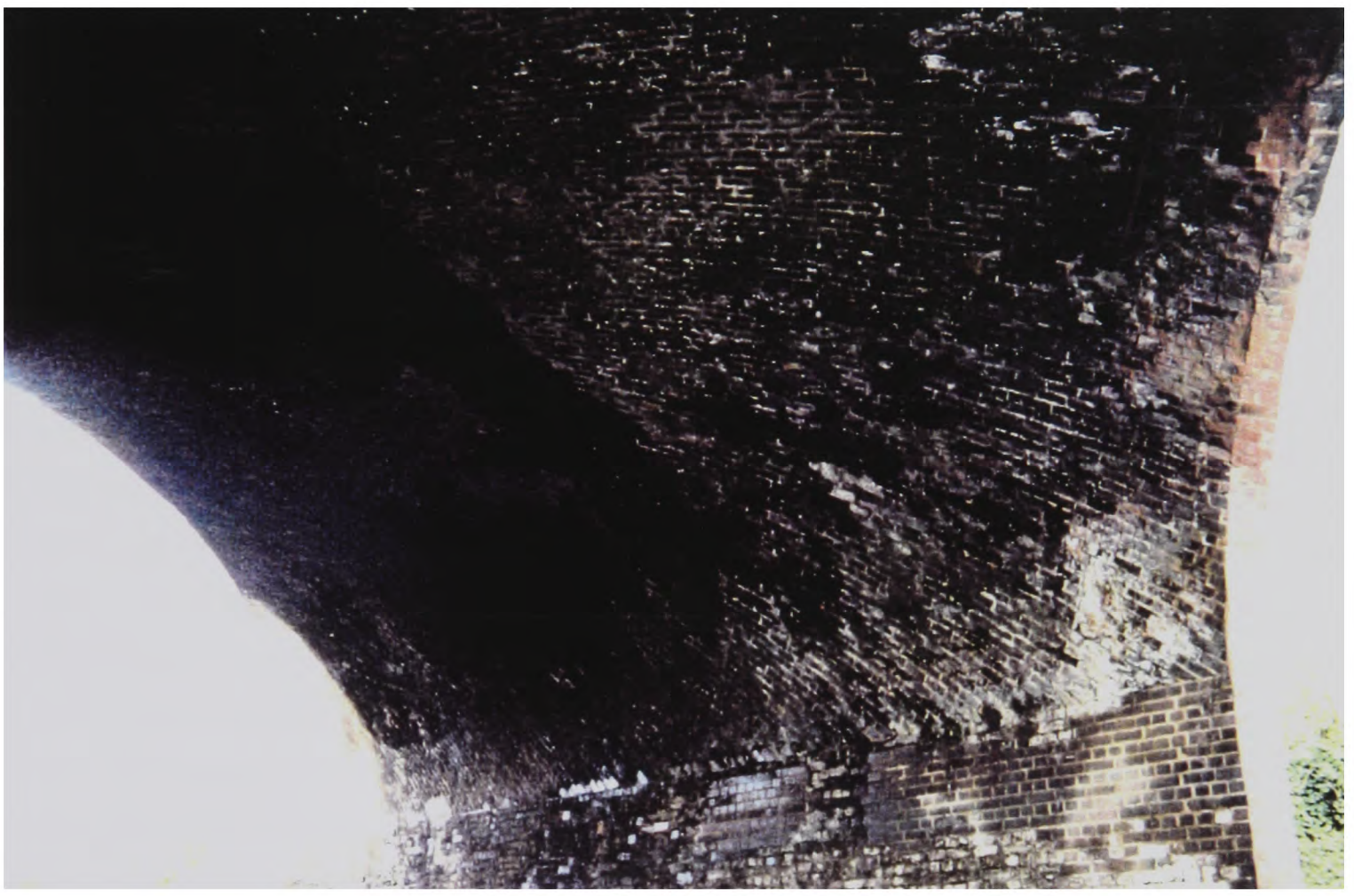

Plate 1.5 Edge detail adopted on highly skewed arch bridges

Without the incorporation of large edge blocks the amount of workmanship required to construct a skewed arch bridge was much greater than that required to construct a similar square span arch bridge.

2.0 Review of Literature on masonry arches

2.1 Early History

The masonry arch has been used for approximately 5000 years. Van Beek (1987) claims that its origins can be traced back to before the golden age of Egypt or Mesopotamia. At the dawn of these civilisations, buildings were constructed by using reeds as permanent formwork. The reeds were bent at the top and tied together to form the roof. The whole structure was then daubed with mud (Encyclopedia Britannica, 1978a). As the population expanded and larger buildings were required, more sophisticated construction techniques were developed including the use of adobe. These had the advantage that they could be produced where mud was plentiful and transported to the required construction site. It is therefore reasonable to assume that the first voussoir arch was an adobe structure. Later, quarried stone could also be transported to wherever required since labour costs were low in those days. The natural development of Engineering led to voussoir arch bridges being constructed from quarried stone blocks.

It is not known when the arch was first used in the Far East. Howe (1897) stated that Public Works were executed in China from 2900 B.C. and may have involved the construction of arch bridges. However, he provided no evidence to substantiate this. There are some ancient Chinese arch bridges such as the Seventh century Chauchow Bridge (Ling-Xi, 1987). Knapp (1992) pointed out that the earliest Chinese artifact found which provided evidence of the use of arch bridges was in a Han tomb (25-220 A.D.). There were many well documented, equally ancient, European arch bridges, for example the old London Bridge and the medieval Exe Bridge (Brierley, 1979), which were constructed in the Twelfth Century. The economic development of this part of the world dictated that many of these bridges have since been demolished to make way for structures which are wider, stronger and provide less of an obstruction to the waterway below. A different economic situation in China may have led to their bridge stock being subjected to fewer heavy vehicles and resulted in their survival. Therefore, it may be a mistake to observe ancient Chinese arch bridges and conclude that this was where this structure originated.

In the west, the ancient Greeks knew of the arch but their architecture precluded their use. An exception to this were the beehive tombs at Mycenae. Instead, massive stone and timber lintels were preferred. Once again, the longevity of stone has meant that only structures with stone lintels have survived whereas no structure has retained its original timber roof. However, the greatest bridge builders of antiquity were the Romans. Three of their most important contributions to Civil Engineering were the discovery of a natural cement, the cofferdam, and the semi-circular masonry arch (Encyclopedia Britannica, 1978b).

Many Roman bridges had timber superstructures; none have survived. Masonry arch bridges were only used where economics, ground conditions, and resources were favourable. Smith N.A.F. (1993) pointed out that, "those Roman structures on which we are encouraged to base our historical and structural interpretations are not necessarily typical".

Many Roman masonry arch bridges were built with adequate piers which sometimes incorporated flood relief tunnels within them. In spite of these precautions only the well maintained or unused bridges have survived. Many Roman bridges were made good by the addition of medieval downstream weirs, starlings and break waters. However, the magnificence of the Pont du Gard aqueduct, shown diagrammatically in figure 2.1, and the Pons Milvius, amongst others, cannot go unnoticed.

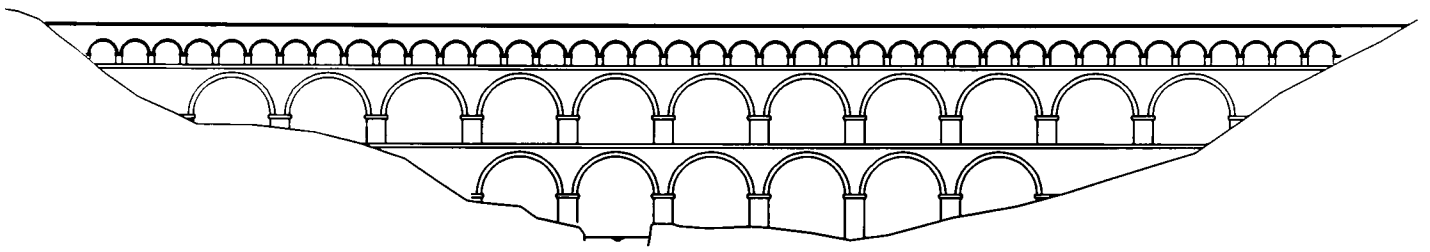

Figure 2.1 Impression of the Pont Du Gard Aqueduct

The Roman Engineer must have possessed some knowledge of arch stability. Variations in the dates and styles of successive piers in the Narni Bridge indicate a construction sequence which was from end-to-end rather than bottom-to-top. In the Pont du Gard, it appears that the same set of three falsework frames were used, one at each level, as the aqueduct was constructed from end-to-end.

After the waning of the Roman empire there was a prolonged period in the west in which the arch, amongst other things, was forgotten. In medieval times, the pointed gothic arch became fashionable and actually represented a significant step forward in arch construction. As shown in figure 2.2, the pointed gothic arch solved the problem of intersecting unequal spans. Within this period, aesthetics appeared to take priority over stability. Builders tried to minimise the thickness of the arch and consequently there were many disasters.

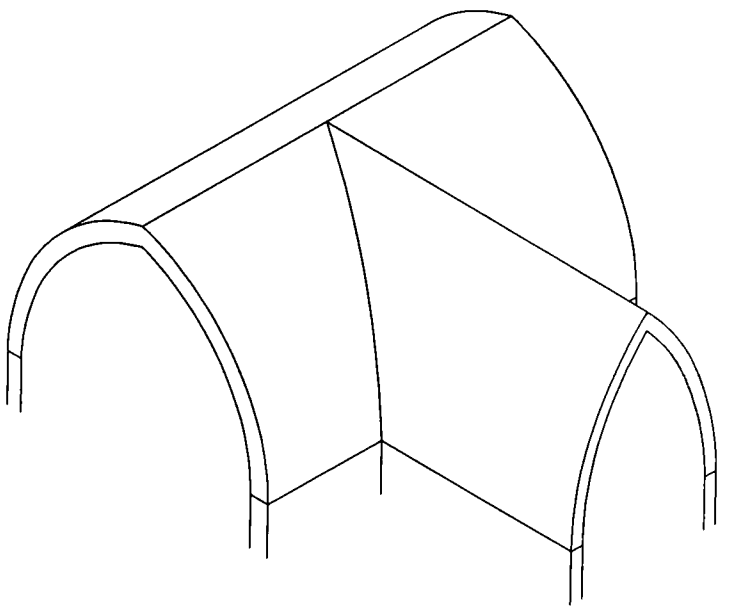

Figure 2.2 Pointed Gothic Arch

2.2 Seventeenth and Eighteenth Centuries

2.2.1 Theoretical Development

Hooke (1675) was the first modern Engineer to consider the behaviour of the masonry arch. He wrote, "Ut pendet continuum flexile, sic stabit contiguum rigidum inversum", which translates thus, "as hangs the flexible line so but inverted stands the rigid arch". It was a criticism of Hooke that he *anticipated* the results of others. Whilst this was certainly possible given his position as Curator of experiments at the Royal Society, in this case it seems unlikely since the above statement was issued twenty two years before Gregory (1697) continued with this approach. Hooke had been unable to present a mathematical solution to the problem although he had experimentally demonstrated his idea to the Royal Society.

Gregory used Newton's recently invented method of fluxions, i.e., differential calculus, to determine the shape of an infinitely thin suspended chain. Gregory explained that the catenary is the shape that is required to maintain equilibrium and is therefore, when inverted, the true shape of an arch.

La Hire (1695) set out to determine the thrust that an arch exerts on its abutments. He assumed that the voussoirs were frictionless and attempted to calculate the vertical force required on each to maintain equilibrium. He solved the problem graphically by constructing the polygon of forces and the corresponding funicular polygon. However, as shown in figure 2.3, when he

examined a semi circular arch with horizontal springings he realised that voussoirs having infinite weight would be required at the springing and thus such an arch could not stand.

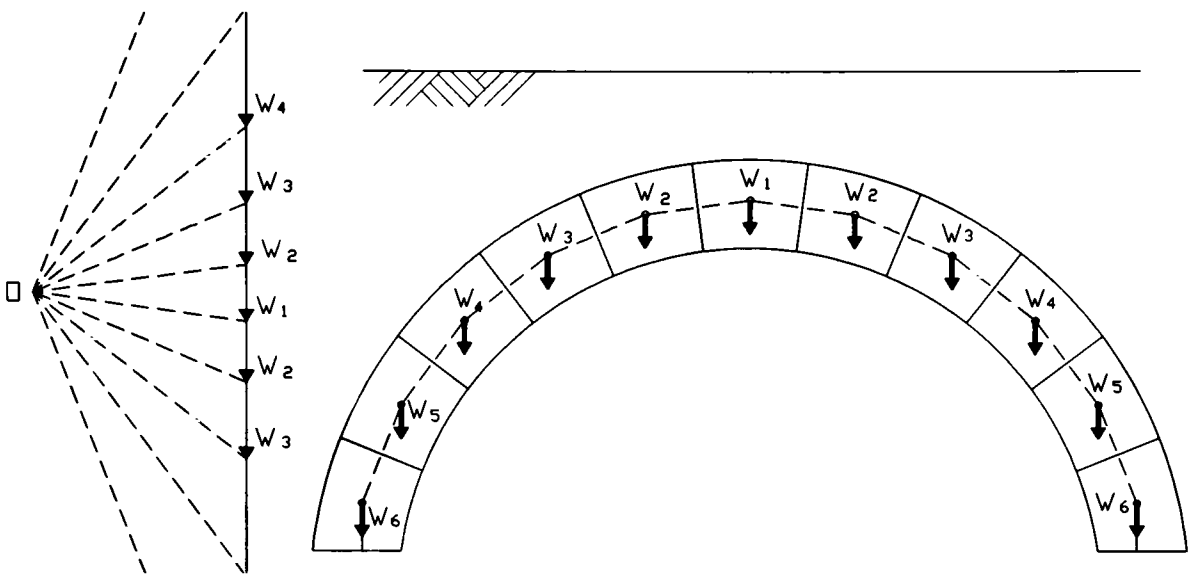

Figure 2.3 Arch Analysis after La Hire

The minimum vertical load was required at the keystone. Each successive voussoir required a larger vertical force in order to equilibrate it and thereby complete its triangle of forces. At the voussoir adjacent to the springing, the triangle of forces cannot be formed. Thus, La Hire realised that friction must be incorporated into the analysis.

La Hire (1712) returned to the problem of the masonry arch but considered the way in which it failed. As shown in figure 2.4, it had been observed that when the piers were not strong enough the arch failed at some point along its haunch. He described the mode of failure as a rupture although modern Engineers now describe it as a hinge. He developed a relationship which expressed the arch thrust and self weight as an overturning moment so that the stability of the pier could be checked. However, no rule for determining the exact location of the rupture was given. His positioning of the arch thrust at the crown also demonstrated a less than complete understanding of the problem.

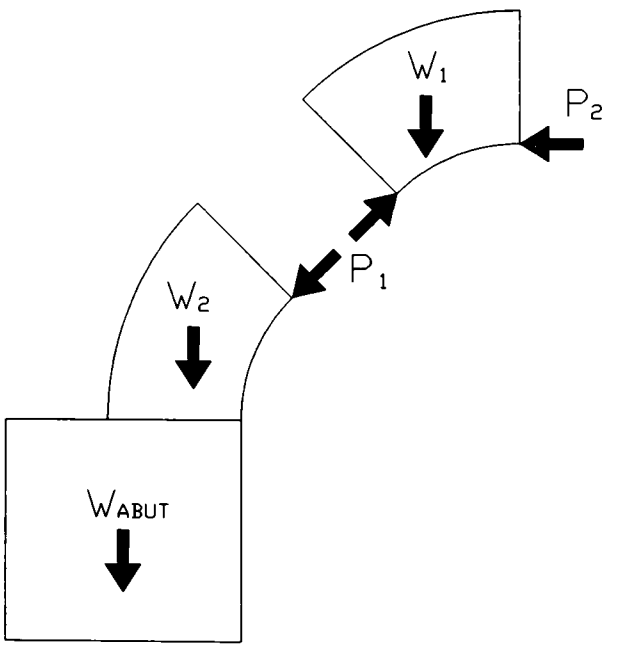

Figure 2.4 Arch Failure after La Hire

Couplet (1729) attempted to determine the correct dimensions of piers. In order to do this he needed to analyse the arch and assumed that the voussoirs were frictionless. In his later work Couplet (1730) corrected this mistake and stated that it was more realistic to assume that friction

was sufficiently great to prevent sliding. He also stated that voussoirs would offer no resistance to the opening of their joints at collapse and that, due to infinite compressive strength, failure could only take place by hinging at the extremities of the arch section. Couplet considered only symmetrical loading and concluded that an arch could not collapse if the chord of half its extrados could be contained within the thickness of its barrel. He pursued this point in search of the minimum arch thickness. Herein lies his only mistake. He assumed that intrados hinges would form at 45° to the horizontal and hence arrived at the conclusion that $(t/R)_{min}=0.101$.

Couplet's understanding of the mechanics of collapse and the notion of a line of thrust clearly distinguish him as being considerably ahead of his time. He had actually stated the assumptions required for the basic mechanism method as used today.

In 1748 Poleni (Heyman, 1972; 1988) was the first to apply the existing theory to a three-dimensional problem. In 1743 he was commissioned to report on the cracking which had been observed in the dome of St. Peter's Cathedral in Rome. He divided the dome into a number of radial slices (lunes) and postulated that if a line of thrust could be contained within each lune it is safe and if each lune is safe the dome must also be safe.

Coulomb (1773) made no reference to the work of Couplet and it cannot be disproved that he arrived at similar conclusions independently. Coulomb was generally much more rigorous in his approach and did not make the same mistake regarding the position of the intrados hinges. Hence, he arrived at the correct solution that $(t/R)_{min}=0.106$.

2.2.2 Constructional Developments

Gautier (1717) published what was considered to be the most significant contribution to arch construction of its time although it did not advance arch theory. His book was a practical guide on all aspects of arch construction and included empirical rules for proportioning piers and the thickness of the arch. It also discussed hollow spandrels as a means of both reducing the weight of the structure and flood protection but did not consider the effect that this might have on the overall stability of the structure; a point recently taken up by Melbourne and Tao (1995).

In 1736 construction began on Westminster Bridge. Batty Langley's design (Ruddock, 1979) was to use, for the first time in Great Britain, voided spandrels to balance the thrust from adjacent unequal spans. However, during construction one of the piers began to sink. The contractor, Labelye (1751), received proposals for remedial measures and eventually constructed a counter arch springing off the haunches of the two adjacent arches so that the pier was effectively isolated. Consequently large internal voids were created. The development of

construction techniques and Engineering judgement had reached a level that enabled Engineers to carry out these measures with confidence.

Edwards' four attempts to bridge the River Taff at Pontypridd (Morgan, 1764) provided an invaluable opportunity to extend the current understanding of arch behaviour and construction requirements. His first three attempts failed. It was noted that the third failure occurred because there was insufficient material above the crown to resist the effects of relatively large amounts of material above the haunches. His fourth attempt, as shown in figure 2.5, included circular openings through the spandrels and remains to date.

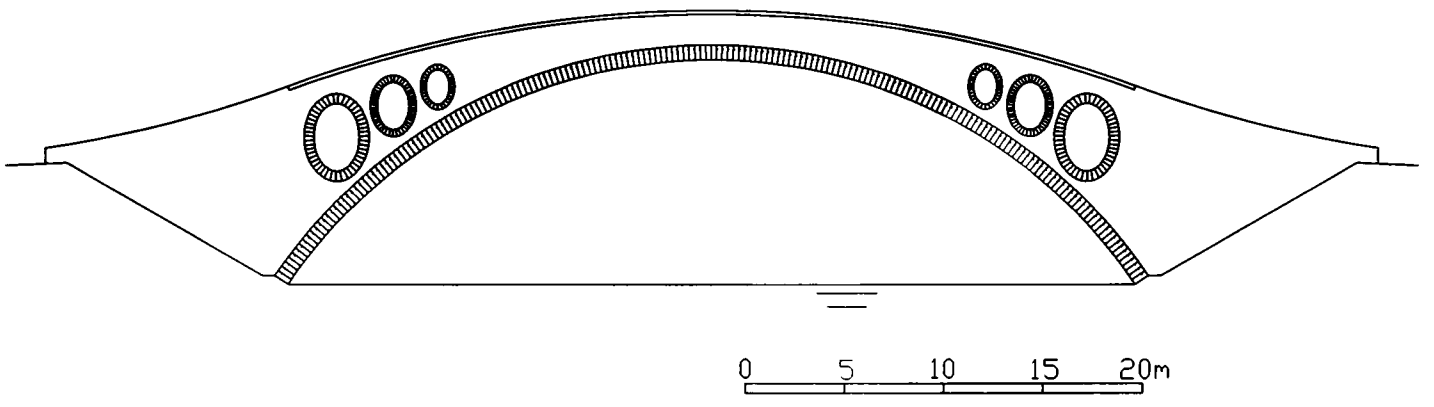

Figure 2.5 Edwards' fourth bridge at Pontypridd

The construction of Blackfriars Bridge by Smeaton (1754) illustrates the lack of theoretical knowledge coupled with a rapidly developing sense of what was, at least, safe. Smeaton prepared a list of dimensions of existing arch bridges. His list revealed that, when the ratio of span to crown thickness was greater than 36, counter arches had been used as in Westminster Bridge. Some of the bridges had shown signs of what had been concluded to have been the cause of collapse of the third bridge over the River Taff. Thus, Smeaton had acquired some knowledge of what was required without depending on the earlier work of Gautier.

Smeaton (Ruddock E., 1974) felt that hollow spandrels were a compromise between strength and foundation loads. After the failure of a bridge at Edinburgh he recommended, "any method of arching in the spandrils between great arches that will effectually save weight [sic.] ". At Perth he decided to use internal spandrel walls and thereby effectively setting a precedent. Smeaton was sufficiently knowledgeable to realise that, depending on ground conditions, such measures were not always necessary.

Perronet (1780) was the first director of the newly formed École des Ponts et Chaussées. He realised that the thrust from adjacent spans could be used to balance each other. Thus, he understood that only the abutments needed to be designed to resist horizontal forces. This gave

other Engineers the confidence to be able to reduce the width of piers, which had previously been taken as one-fifth of the span, to one-tenth of the span. The fact that adjacent spans could be used to balance each other led him to conclude that flatter arches could also be constructed with confidence. However, he may not have appreciated the extent to which the abutments would need to be enlarged in order to resist the increased horizontal forces.

2.2.3 Experimental Research

Gautier (1717) was the first to record the results of a series of model tests. He was attempting to determine the magnitude of the abutment thrust. He built half-arches from wooden blocks and piled up other blocks at the springing in order to maintain equilibrium. He removed the backing blocks incrementally until failure occurred, at which point the weight of the remaining backing blocks was recorded.

It was Frézier (1737) who discussed the determination of arch thrusts and the required dimensions of piers. He published the work of Danyzy (1732), as shown in figure 2.6, who had experimentally verified Couplet's predictions using model arches which were formed from plaster voussoirs.

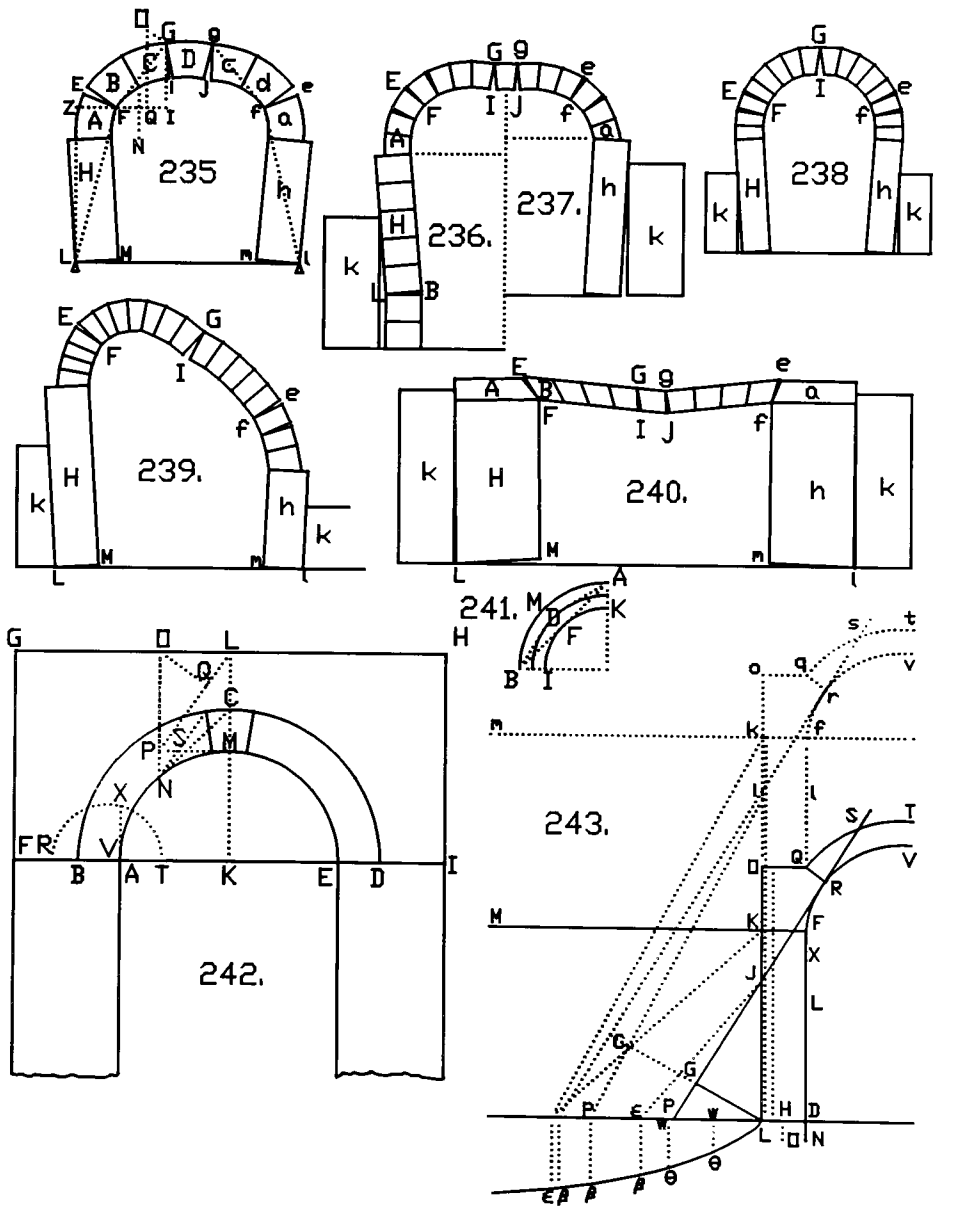

Figure 2.6 Results from Danyzy's Tests (1732)

2.3 Nineteenth Century

2.3.1 Experimental Research

Boistard (1800) carried out a series of tests on model voussoir arches with the intention of determining the exact mode of collapse, the minimum size of piers, and the force exerted on the centring during construction. He noted that during construction and before the keystone was fitted, several voussoirs in the haunch were no longer in contact with the centring. He concluded that this fact had probably been exploited by the Romans and explained the construction sequence employed on the Pont du Gard aqueduct.

Robison (1822) carried out model tests on arches whose voussoirs were formed from chalk. He was able to reproduce the failure of a real bridge that he had recently observed. The voussoirs of this bridge were of soft stone and collapse had been due to a compressive failure of the masonry. The practice of constructing and testing model arches was therefore verified.

Barlow (1846) concluded that if the thickness of an arch was more than sufficient to contain the single line of thrust that a thinner arch would contain at failure, then more than one such curve could be drawn, each of which was as possible as any other. He proved this by experiment, as shown in figure 2.7, in which voussoirs were separated by joints formed from several wooden blocks. He demonstrated that many different combinations of blocks could be removed whilst preserving equilibrium.

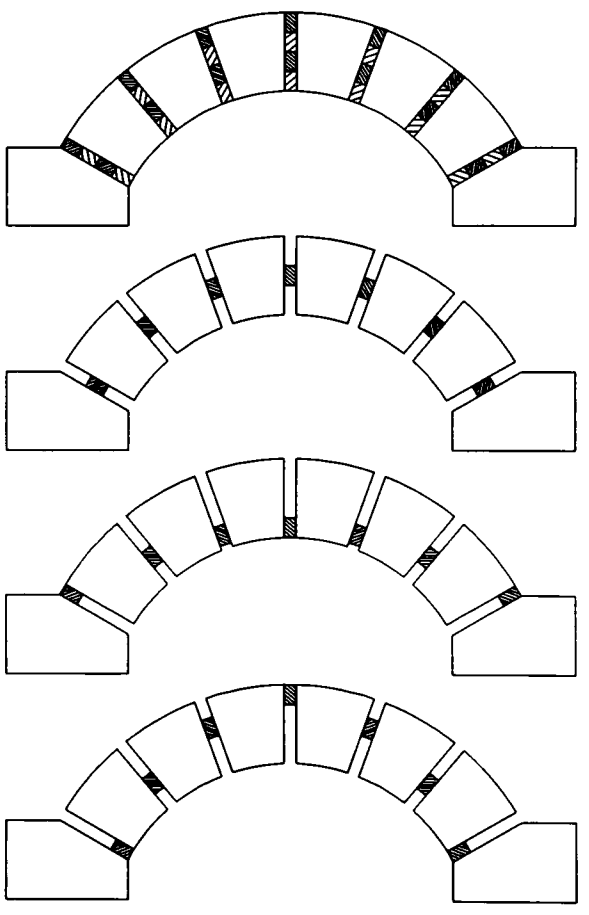

Figure 2.7 Barlow's Experimental arch

Jenkins (1876) was well aware of the notion that more than one line of thrust exists within an arch when the applied load was small. He devised an ingenious model to demonstrate that the line of thrust adjusted itself in order to maintain equilibrium. His model arch was constructed with curved voussoirs so that they could rock when loaded and the change in the position of the line of thrust could be observed.

The Austrian Society of Engineers (1890) carried out a series of tests to determine the load-deflection response of arches and to establish whether it was linear or non-linear. They concluded that, since it was approximately linear, Castigliano's assumptions were valid.

2.3.2 Theoretical Development

Ware (1809) added to Gregory's work, the statement, "and when an arch of any other figure is supported it is because in its thickness some catenary is included". Thus, it is possible to interpret this as the origin of the lower bound theorem of collapse.

Rondelet (1812) presented a resumé of early work but unlike Gauthey concentrated on theoretical developments. His experimental results led to the development of new theories by researchers such as Lamé and Navier in the following few years.

Hutton (1812) gave an account of what is now referred to as the lower bound theorem of collapse. His work is a useful record of the state of knowledge up to that point.

Lamé and Clapeyron (1823) claimed to have developed the concept of a hinged failure mechanism in ignorance of the work of Couplet and Boistard. Likewise, they also determined the position of the intrados hinges by a method similar to that used by Coulomb.

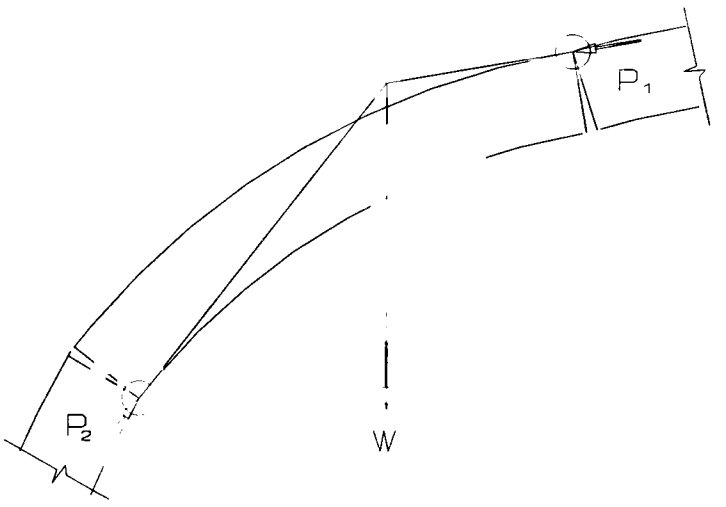

Figure 2.8 Force Equilibrium after Lamé and Clapeyron

They stated that the three forces viz., the thrust at two adjacent hinges (which must also be tangential to the arch) and the weight of the material between the hinges (see figure 2.8), must act through the same point in order that the structure be in equilibrium. This, they stated, once again in ignorance of its earlier use by Coulomb 50 years earlier.

Navier (1826) established a straight line law for the pressure distribution across the bearing surface of a voussoir. Thus, he also showed that tensile strains occur if the line of thrust falls outside the middle third. Coulomb had stated that if an arch was stable then the thrust must lie between certain limits. Navier now defined these limits as the middle-third and said that the arch would be safe if the thrust line is contained within these limits.

Moseley (1835) developed arch theory independently of Coulomb but made similar conclusions. His contribution is noteworthy since he was the first British scientist to develop the line of thrust principle. He concluded that the line of thrust must be contained within the arch and its inclination to each joint must not exceed the angle of friction of the arch material.

Villarceau (1845) knew that an infinite number of possible thrust lines exist in a statically indeterminate structure such as the arch. He assumed that one possible line of thrust was coincident with the centre line of the arch and developed a safe design method. His numerical solutions of the equations were presented in the form of tables to be used by bridge designers.

Snell (1846) considered the stability of arches. He determined the amount of thickening towards the abutments that was required to ensure that the line of thrust remained within the barrel. He introduced material failure so that the position of the line of thrust could be modified. He used Lamé's method and extended it into a trial and error method for analysing unsymmetrical load cases.

Rankine (1862) adopted the middle-third rule and produced a design method based on it. This method required that the line of thrust produced by a symmetrical system of distributed loads is initially assumed to be parallel to the intended shape of the intrados. He used Navier's formula for the thrust at the crown and found that, in order to preserve equilibrium, a system of horizontal pressures were required. The pressures were required to change direction at a certain height. Below this point. the arch is included in the abutments and is backed accordingly. Above this point, the arch is designed for the maximum horizontal pressure. Rankine stated that, "the stability of an arch is secure if a linear arch (line of thrust) balanced under the forces which act on a real arch can be drawn within the middle third of the arch ring".

Fuller (1875) developed a graphical method for determining the location of the line of thrust due to any symmetrical set of loads. However, Jennings (1985) showed that, in order to analyse unsymmetrical load cases, the method must be extended to include shear effects. This would require an iterative process in which the line of thrust was adjusted until equilibrium was established. He remarked that the arrival of the computer has rendered this method redundant particularly when the method is used correctly, i.e. iteratively.

The search for the true line of thrust continued with several authors proposing rules for how it might be calculated. Winkler (1879) was the one who came closest to what Castigliano eventually produced. He defined the line of thrust to be the locus of points for which the sum of the squares of its distance from the centre line of the arch was a minimum. This was almost stating that the strain energy due to bending must be minimised.

Castigliano (1879) developed the theorem of minimum strain energy. This theorem expressed the elastic extension of a body due to the imposition of a load in terms of the bending moment, shear force and axial force developed within it. He deduced that the elastic extension would be such that the strain energy would be minimised. He assumed that the arch was an encastré rib and minimised the strain energy to calculate the resultant reactions. He repeatedly analysed an arch until all tensile sections within it had been removed and an effective arch depth whose section was entirely in compression was produced.

2.3.3 Constructional Developments

Gauthey's (1809) "Traité de la construction des ponts" appeared two years after his death. It assembled all theoretical and experimental work known to the École des Ponts et Chaussées at that time. However his references to the masonry arch tended to concentrate on practical guidelines.

Perronet's Pont du Neuilly was completed in 1774. It was constructed with a tapering section in order to ease the effects of the River Seine when in flood and incorporated flood relief tunnels and hollow spandrels. In 1826 Telford replicated the architectural details of this bridge when he constructed the 45.7 m span bridge at Over, shown diagrammatically in figure 2.9.

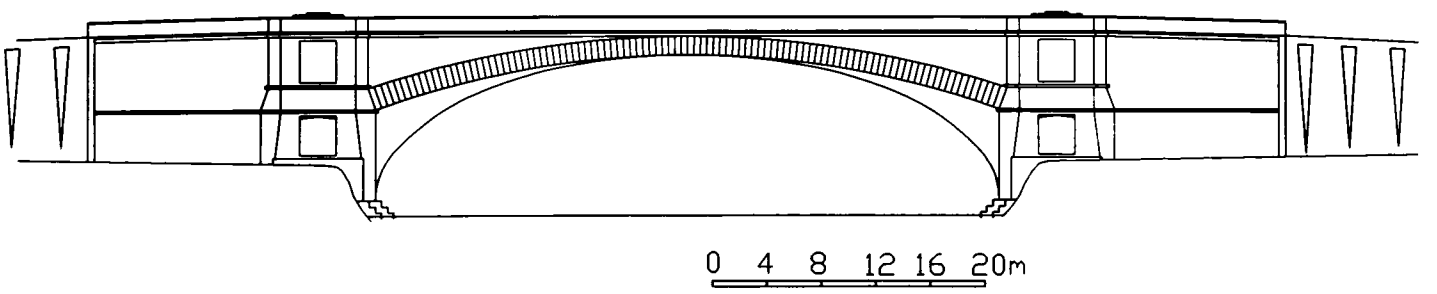

Figure 2.9 Telford's Bridge at Over

Given the limited theoretical and experimental developments that had taken place by 1826 it is reasonable to assume that the proportions of new bridges were determined by examining what had been successful or unsuccessful elsewhere. An empirical method such as this may produce a conservative design. However, in this case, it led to the survival of this bridge.

Telford had been misled by the ground investigation crew who reported that, "strong coarse indurated gravel existed at foundation level". The eastern abutment was actually founded on

very poor ground, this caused it to suffer continual settlement. The bridge survived because its proportions were such that it could accommodate this movement.

Upon removal of the centring, Telford observed a 50 mm deflection of the crown which was subsequently followed by a further 200 mm as the piers settled when loaded. Similarly, at the Pont du Neuilly, Perronet had recorded a total deflection of 600 mm. However, Perronet had pre-set his bridge by 380 mm to allow for this; Telford did not. Telford's bridge had been reduced to a three-pinned arch and had continued to deteriorate until in 1880 it was underpinned and the deterioration arrested.

2.4 Twentieth Century

2.4.1 Constructional Development

The construction of masonry arch bridges continued well into the twentieth century. The Pont Adolphe in Luxembourg by Séjourné, as shown diagrammatically in figure 2.10, was completed in 1903. It has a massive 84.66 m span and was thought to be the largest masonry arch in the world until the arch at Plauen (89.0 m span) was completed in 1923 by Liebold.

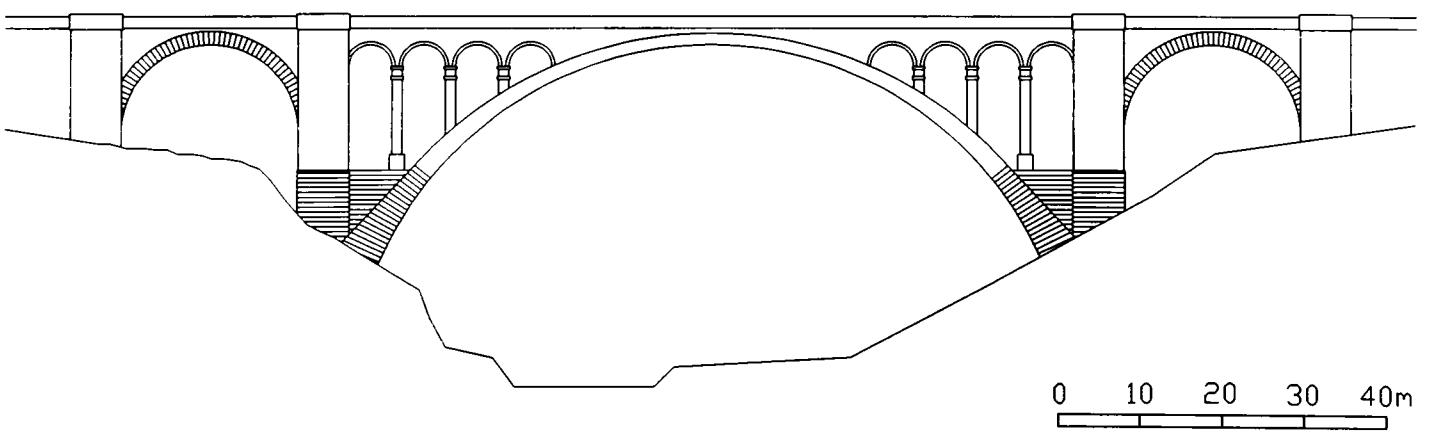

Figure 2.10 Pont Adolphe at Luxembourg

The details adopted by Séjourné highlight the advances made in arch construction. The massive span, hollow spandrels and light weight structure indicate a practical understanding of the masonry arch which extended far beyond theoretical developments.

In China, the cost of materials and available labour still make masonry arch construction economically viable. Yi-Sheng (1978) described several masonry arch bridges built throughout China during the latter part of this century. Many of these bridges were architecturally similar to the Chauchow Bridge, as was the Pont Adolphe, such as the 112.5 m. span Changhung Bridge over the Nanpun River, Yunnan which was completed in 1961. In 1972, the span of this bridge was exceeded by the 116.0 m span Chiuhsikou Bridge in Szechuan Province. However, the largest masonry arch bridge today is the 120.0 m span bridge over the Wachao River in Hunan Province which was built in 1990.

2.4.2 Experimental Research

Pippard et al. (1936) carried out a series of tests on arches which comprised accurately machined steel voussoirs. They did this so that the elastic properties of the arch components could be reliably established. Each voussoir was formed so that they could be fitted together in any order and the arch constructed with either pin, roller or encastré supports. When the experimental results were compared with predictions made by Castigliano's strain energy theory good correlations was noticed.

Pippard and Ashby (1939) carried out a series of 23 tests on concrete voussoir arches with two different types of mortar viz., with lime or with cement. All arches were supported encastré. The experimental results obtained by loading each successive arch on consecutive voussoirs revealed that with lime mortar the line of thrust was often well outside the middle third before tensile cracking was observed. When cement mortar was used, the line of thrust could fall outside the bounds of the arch without causing failure since significant tensile stresses could be resisted. Crushing of the voussoirs was observed to cause premature instability in a few tests and was accompanied by sliding failures at these locations.

This work enabled Pippard to determine the criteria upon which his elastic method of analysis was based. He allowed tensile stresses to be developed provided that the line of thrust did not leave the middle half of the section and he prescribed a permissible compressive stress. Pippard's work was later incorporated into the MEXE method.

Davey (1953) reported the results of load tests on twenty one existing bridges. Several of these bridges were skewed but unfortunately none of these were included in the three which were tested to destruction. His objectives were to determine the amount of load dispersion through the backfill, investigate the transverse distribution of load within the arch barrel, assess the contribution of the backfill and spandrel walls and examine the effect of spreading abutments.

Davey concluded that movement of the abutments is both significant and highly variable. When the load is above the abutment, they move inwards which may be accompanied by an upward movement of the crown. When the load is above the span they move outwards. The non-uniform movement of the abutments is a function of the variability of the masonry within the barrel, the quality of the backfill and the quality of the foundations. Transverse cracking between voussoirs occurred under a relatively low load. These cracks closed when the load was removed. Thus, Davey rightly concluded that the presence of cracks does not entail collapse. He noted that during the destructive tests, diagonal cracking within the arch barrel occurred and he likened these to the yield lines observed within a flat slab when subjected to similar loading. He also concluded that the backfill material could make a significant contribution to the strength of the arch and that creep under a heavy and sustained load could be significant.

Chettoe and Henderson (1957) extended the work of Davey except that they did not carry out any destructive tests nor did they use such an extensive array of deflection gauges. Four of the eight single span arches that were tested were skewed and it appears that the structures were selected for testing on the basis of maximising the possibility of comparing similar bridges. They remarked on the difficulties such a comparative study posed. This was especially true when one tries to compare Davey's tests to their own. In this case, not only was the geometry of each bridge different in some way but the loading arrangement also differed.

They concluded that the load-crown deflection was approximately linear. Pippard pointed out that the response was actually bi-linear and suggested that this was due to the reduction of the structure's indeterminacy caused by the formation of the first hinge.

Just as Davey had done, Chettoe and Henderson observed non-uniform abutment movements. Some hysteresis was observed after each load-unload cycle and cracks which had opened during loading closed when it was removed. They concluded that it was reasonable to assume a 45° spread of load through the backfill since this assumption led to a close correlation between measured values and their effective width calculations.

At one of the bridges viz., Crawley Down, vertical cracks in the parapet above the springings were noticed before the tests. These cracks were observed to open at a quite early stage of loading and to close after the removal of the load. They wrongly deduced that since the spandrel walls moved freely that their influence upon the carrying capacity of the arch was negligible. By comparing two similar arches in which the 34° skewed arch produced a crown deflection of 60% of the square span arch, they concluded that the difference was attributable to the randomly produced composite action of backfill and arch. These errors will be discussed later.

Significantly, they incorrectly concluded that they could see no reason to deduce that skew weakens the structure. This conclusion is fallacious; their measurements concurred with those of this project, i.e., that skew increases the stiffness of the structure. Furthermore, the results of this project also indicate that skew weakens an arch bridge. Thus, a correct conclusion would have been that it is incorrect to base the safety of an arch on its stiffness.

Beginning in the mid-1980's, the Transport and Road Research Laboratory, T.R.R.L. (now called T.R.L.) carried out a series of destructive tests on arch bridges. Some of these tests were carried out by themselves and others were contracted out. With the exception of two bridges, all were tested to collapse.

Hendry et al. (1985) carried out the T.R.R.L. field test on Bridgemill Bridge. This was a fairly flat voussoir arch constructed from dressed sandstone. This bridge was not tested to failure due to the limited travel in the loading system.

Hendry et al. (1986) carried out the T.R.R.L. field test on Bargower Bridge. This was a 16° skewed semi circular voussoir arch with a large depth of cover. Failure was due to a compressive failure of the arch beneath the loading position. However, the results must be assumed to be unreliable since the rock backfill above its haunches meant that the load was actually being applied near the springings.

Page (1987) carried out the T.R.R.L. field tests on the Preston and Prestwood bridges. The former bridge was a 17° skewed elliptical voussoir arch with brick spandrels. Failure was by a compressive failure under the load. The latter bridge was a deformed brick arch which had its parapets removed before testing. It failed due to the formation of a four-hinge mechanism.

Page (1988) carried out the T.R.R.L. field tests on the Torksey and Shinafoot bridges. The former bridge was a segmental brickwork arch with a small amount of backing. Its failure was reported as a three-hinge snap through. The latter bridge was a random rubble segmental arch which failed due to the formation of a four-hinge mechanism.

Page (1989a) carried out the T.R.R.L. field tests on the Barlae and Strathmashie bridges. The former bridge was a 29° skewed segmental voussoir arch. It failed due to the formation of hinged mechanism. The hinges were generally parallel to the abutments, this was facilitated by the stiffening effect of internal spandrel walls and a masonry backing. The latter bridge was a disused random rubble arch. It had stepped spandrel walls which probably supported the loading beam. Thus, it failed when the spandrel walls collapsed.

Harvey et al. (1989) carried out the T.R.R.L laboratory test on a full scale model bridge.

Unfortunately, due to the poor design of the test rig, in which structural deformations were inhibited, failure of the arch was not possible and, had it been possible, would not have been through a realistic mechanism.

Melbourne and Walker (1990a) carried out the T.R.R.L laboratory test on a full scale model bridge. Failure was due to a diffused four-hinge mechanism which was facilitated by ring separation. An interpretative analysis of the results including the effect of the spandrel walls and the backfill was attempted. This work substantiated the significant effects that each of these parameters had upon the behaviour of the arch bridge.

Royles and Hendry (1991) carried out a series of tests on 24 model arches with the aim of investigating the influence that backfill material, spandrel walls and wing walls had upon the behaviour of the masonry arch. It had been noted that in earlier work (Hendry, 1985; 1986) the results of full scale tests indicated that the strength of an arch may considerably exceed that which is predicted by the analysis of a two-dimensional section of it. Two of the arches tested were actually scale models of bridges which had been tested either to failure or as close to failure as possible (Bridgemill and Bargower) so that validation and comparisons could be carried out.

It was concluded that a substantial strengthening effect is produced when spandrel and wing walls interact with the arch barrel. This effect increases as the span/rise ratio decreases. They illustrated this conclusion with the two-dimensional models shown in figure 2.11. Without spandrel walls, the maximum load that the arch sustained was 100 N. When spandrel walls were included, the capacity of the same arch increased to 150 N. When the movement of the walls was restrained the capacity increased to 320 N.

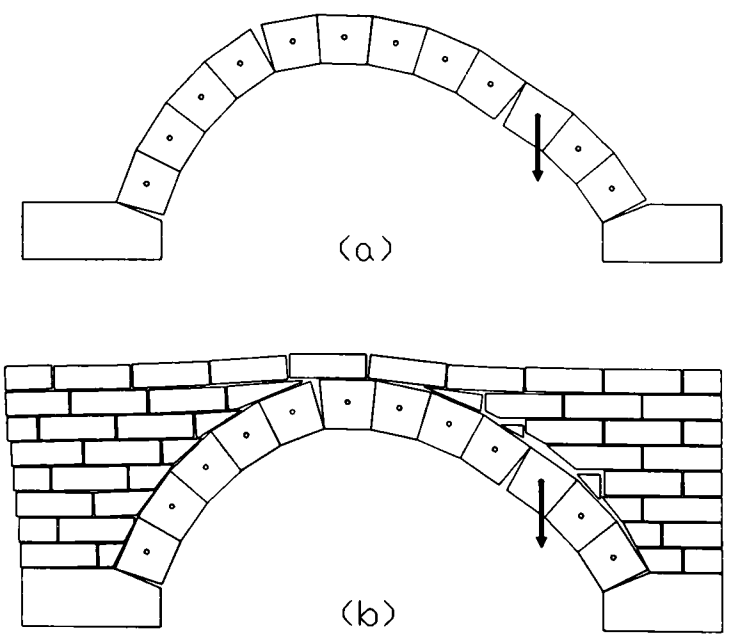

Figure 2.11 Hendry's Models

The presence of spandrel walls produced a shift in the location of the second, in-span, hinge. The minimisation of the effort required by the structure to balance the applied load produced the above shift. In its earlier location, additional effort would have been required since a larger number of spandrel blocks would have been involved in the collapse mechanism. A kinematically admissible collapse state demanding less load could be found as shown in figure 2.11b.

2.4.3 Theoretical Developments

Selberg (1953) produced the first analytical method which could incorporate the spandrel walls. He realised that the arch could not be converted into a four-hinged mechanism if the "superstructure" could provide an effective restraint to it.

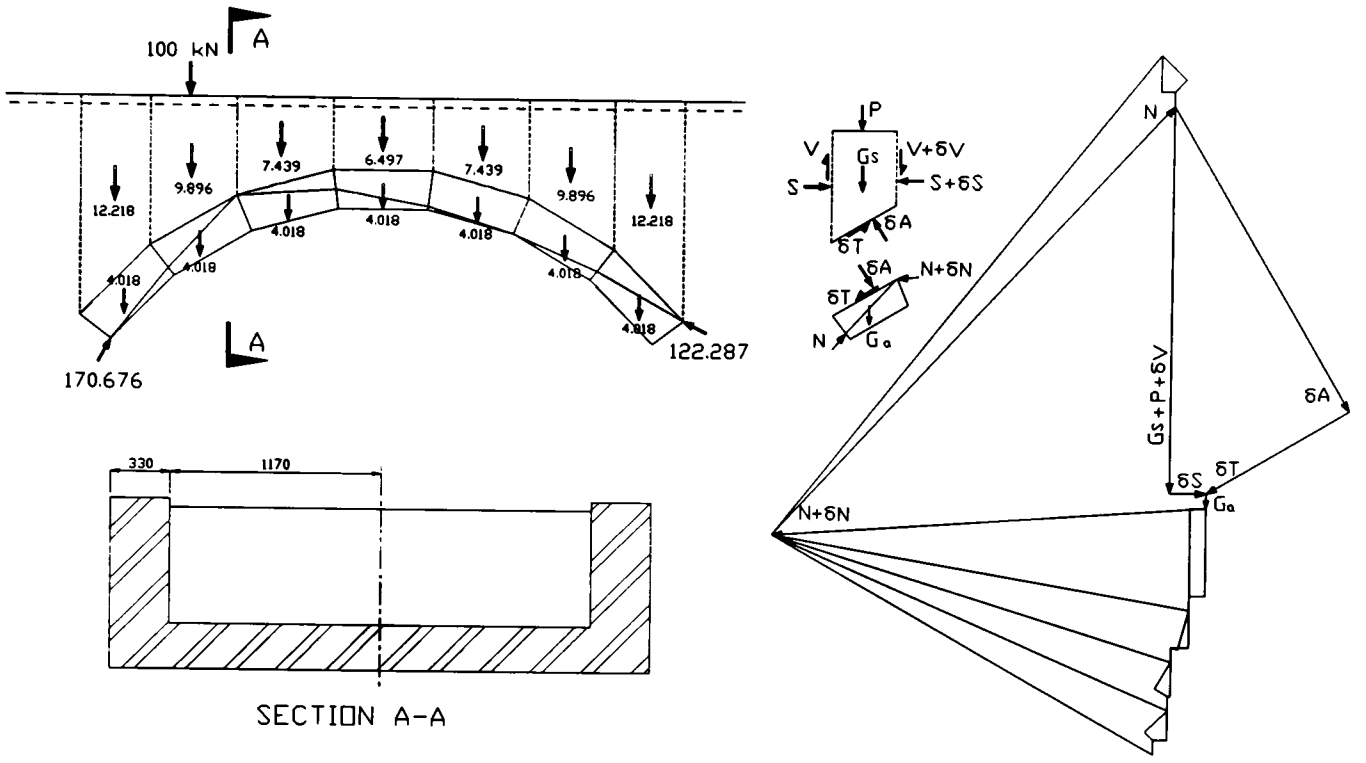

Figure 2.12 Arch Analysis after Selberg

In his method, the superstructure was divided into a finite number of vertical slices each of which had an accompanying section of arch. The superstructure element was subjected to self weight, any live load, and frictional forces between it and the three adjacent blocks. The arch element was subjected to its weight and the thrust within the arch. The graphical method involves drawing the force polygon and by adjusting the forces on each block eventually achieving equilibrium. However, it is possible to equilibrate the system under any live loading. This problem is overcome by the inclusion of a yield criterion which forces the Engineer to adjust the gradient, and hence the eccentricity, of the thrust line. It is worth noting that the spandrel walls play an important part in this method. In the case of hollow spandrels, the maximum load that is predicted is greatly reduced but is not zero.

Pippard et al. carried out many tests on model voussoir arches. It was concluded that at low loads the response of such structures was linear. It was also observed that failure was due to a hinged mechanism.

When Pippard (1948) worked at the Military Engineering Experimental Establishment he continued with Castigliano's minimum strain energy theorem. His earlier experimental work

had shown that restricting the line of thrust to the middle third was too conservative so the limiting tensile stress of 1.4 N/mm^2 was adopted. The basis of the M.E.X.E. method has been dealt with by several workers including Heyman (1966) and can also be found in the Department of Transport standard (1984). Thus, it is not proposed that a further summary of this method be given in this text. However, it must be noted that for many years the M.E.X.E. method has been the Assessment Engineer's primary tool and that it continues to attract its advocates owing to its simplicity and speed of use.

Pippard and Baker (1957) presented details of the calculations necessary to determine the load required to produce a mechanism. This was a repeat of earlier work carried out by Pippard (1951) in which a review of the theory of the voussoir arch was presented in conjunction with a summary of his work to date.

Greenberg and Prager (1951) proved that limit analysis of perfectly plastic beams depended upon two fundamental theorems. Drucker, Greenberg and Prager (1952) later proved that the theorems remained valid when applied to more general problems and yield conditions. Kooharian (1952) was the first to demonstrate that masonry could be treated in a similar manner to the way in which steel beams were treated in limit analysis.

The two theorems were stated:

1. Collapse will not occur if at each stage of loading a safe, statically admissible state can be found,
2. Collapse will occur if a kinematically admissible collapse state can be found.

Heyman (1966) produced the yield surface for masonry in terms of a bending moment-axial force interaction diagram. He thereby demonstrated that masonry could be analysed using either of the two limit state theorems. He expressed these two theorems in language that was specific to the masonry arch and which was more useable for the Engineer.

Heyman's "safe" theorem states:

> The structure is safe if a line of thrust can be found which is in equilibrium with the external loads and which lies wholly within the masonry.

Embedded within his uniqueness theorem was the upper bound theorem:

> If a line of thrust can be found which represents an equilibrium state for the structure under the action of the given external loads, which lies wholly within

the masonry, and which allows the formation of sufficient hinges to transform the structure into a mechanism, then the structure is on the point of collapse. Further, it the loads are each proportional to one of their member and are increased from their working values to their collapse values by a load factor, the value of the load factor at collapse is unique.

Heyman stated the assumptions required in order that his two theorems remained valid. Firstly, friction between adjacent blocks was assumed to be so great that sliding failures were not possible. Secondly, the arch comprised infinitely strong blocks. Thirdly, these blocks were incompressible ,i.e., that each block possesses an infinite modulus of elasticity. This meant that collapse was only possible through a hinged mechanism; the strength of the blocks ensured that the hinges occurred at the extremes of the arch. Fourthly, the arch had no tensile strength. Thus, cracking occurred when the line of thrust moved outside the middle third and collapse when it moved outside the arch.

Heyman (1969) developed his earlier ideas into his "plastic" analysis method which was based on the above assumptions. He also defined a geometric factor of safety which was simply the ratio of the actual arch thickness to its theoretical minimum thickness.

Figure 2.13, below, shows the ultimate load and associated line of thrust for a 3.0 m span segmental arch with span/rise=4.0 and span/depth=13.95 when horizontal backfill pressures are ignored. The applied load is dispersed through the backfill but otherwise it resembles Heyman's method.

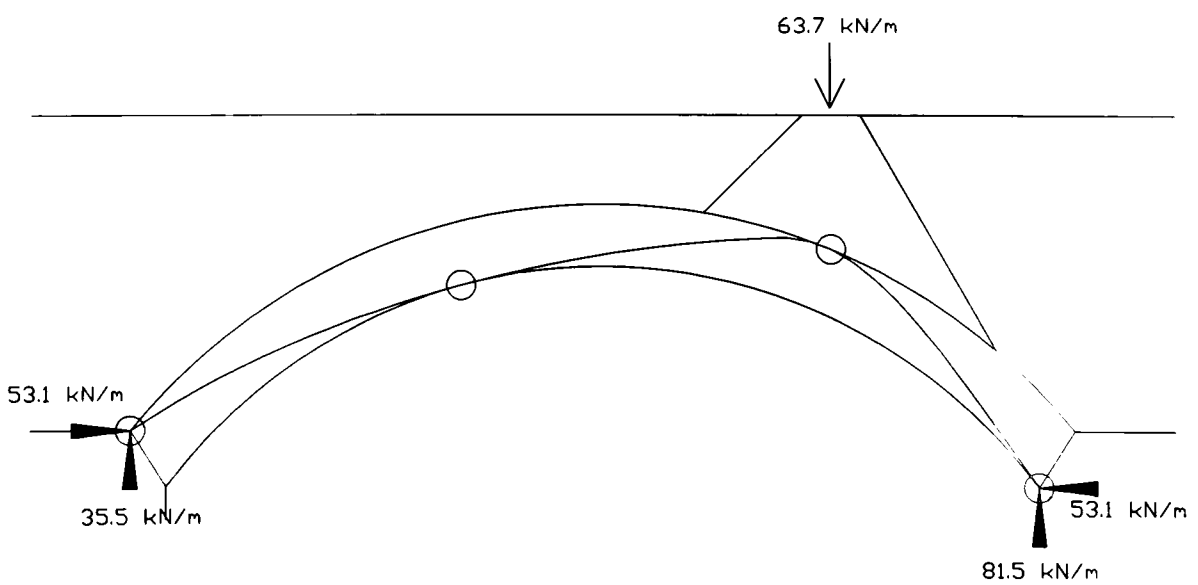

Figure 2.13 Mechanism without horizontal soil pressures

Heyman et al. (1972; 1980) used the limit state theorems to assess the stability of a number of bridges and thus demonstrated the applicability of these theorems. In his later work (Heyman,

1972), the development of arch theory described in Coulomb's Memoirs was interpreted in terms of present day limit state theory. This book provides an excellent review of the theoretical developments up to the beginning of the Nineteenth century.

The uniqueness theorem was of some relevance to Livesley whose early work (Livesley, 1973a; 1973b; 1974) concentrated on the development of an efficient computer algorithm for obtaining an optimal solution to a bounded variables problem. He used this for obtaining the best design of steel framed structures.

The first systematic method of finding an optimal solution to a bounded variables problem was due to Dantzig et al. (1951). Charnes and Greenberg (1951) proved that the lower-bound and the upper-bound theorems, when applied to the analysis of a truss, were actually dual linear programming problems. Charnes, Lemke and Zienkiewicz (1959) provided a more general proof of duality.

Livesley (1978) considered the limit state analysis of the masonry arch. He adapted his earlier algorithm for this task. He considered the arch, in section, as a collection of contiguous rigid blocks. In this method of determining a lower-bound on the collapse load it was necessary to find the maximum value of the applied live load whilst ensuring that equilibrium was maintained for each voussoir. Equilibrium equations expressing the applied live load and dead load in terms of the three inter-block forces were developed. These three forces consisted of normal forces at the extremes of the section, and a frictional force acting along the block interface. The maximisation of the applied load was carried out subject to constraints that limited each frictional force to a fraction of the total normal force at the particular interface. In other words, the maximum possible live load was determined subject to equilibrium being maintained. The use of Coulomb friction to model the shear force that resists sliding movements contravenes limit state theory. However, as discussed in more detail in chapter 6, Livesley was able to correct his predicted mechanism so that the lower-bound theorem of collapse was satisfied.

Walklate and Mann (1983; 1984) used Eddy's theorem to develop an analysis technique in which the position of the line of thrust was calculated. The applied load could then be adjusted until the line of thrust is contained within bounds depending on whatever criteria the Engineer wished to adopt. Eddy's theorem is as follows:

> The line of thrust in an arch has the same shape as the bending moment diagram for those loads which placed on a simply supported beam of the same span. The free bending moment at any section is equal to the product of the horizontal thrust in the arch and the height of the line of thrust above the base line at that point.

This theorem is precisely that used by Pippard, Heyman and others when the line of thrust is drawn.

Harvey (1986; 1987; 1988) adopted the method which had been described by Heyman in 1969. Heyman had intended to demonstrate the usefulness and ease of application of plastic analysis. Thus he had omitted horizontal backfill pressures. Harvey included them and justified it on the grounds that the collapse load that the method now produced was closer to the load produced by load tests. The method is based on small deflection theory in which changes to the geometry of the structure are ignored. Passive backfill pressures are known to be related to the movement of the arch and not proportional to the depth of backfill. Nevertheless, Harvey included pressures which might be expected to occur behind a vertical wall but recommended that a reduction factor be applied to these pressures.

Figure 2.14 shows the ultimate load and associated line of thrust for the same 3.0 m span arch shown in figure 2.13. Horizontal backfill pressures are included in a more realistic way than simply being proportional to depth.

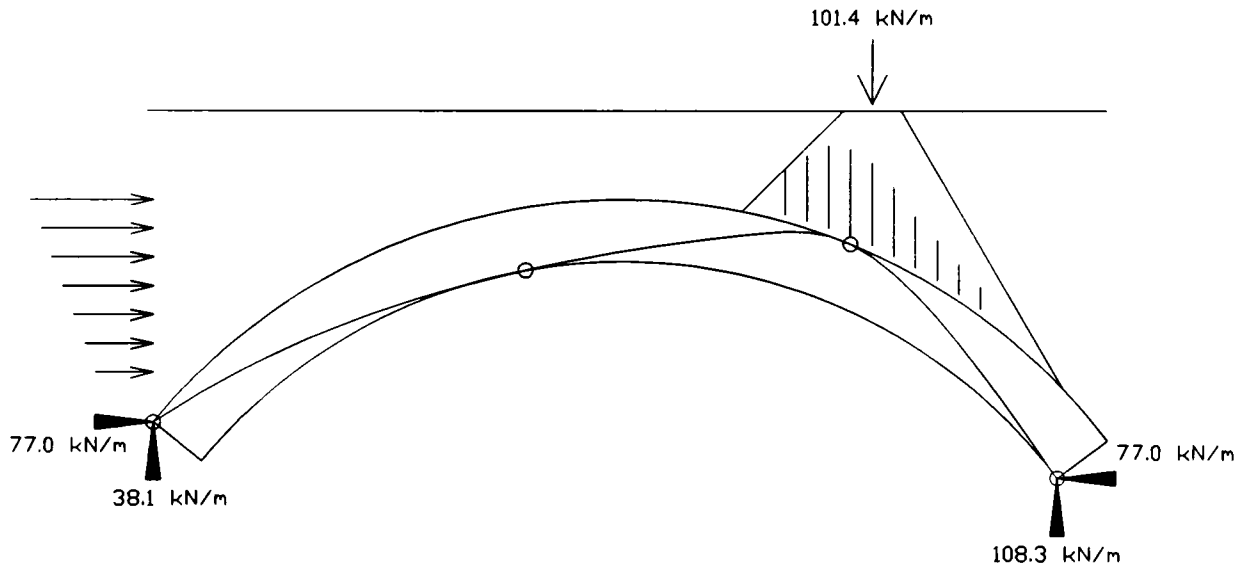

Figure 2.14 Mechanism with Horizontal soil pressures

Crisfield and Packham (1987) produced a mechanism method in which material failure was introduced as a further constraint to the problem. Their method also permitted the inclusion of horizontal backfill pressures. However, like Harvey had done, and without any better theoretical guidance, they continued to apply these pressures as if they were those which would be expected behind a vertical wall. They pointed out that whatever method was used, viz., moment equilibrium or virtual work, the collapse load would be the same. They also stated that virtual work would be the better method since this does go some way to allowing passive movement related pressures to be calculated.

Smith, Harvey and Vardy (1990) continued with the concept of a zone of thrust as opposed to

a line of thrust (Harvey,1991). They described it as a band of material beyond the normal line of thrust which is at the estimated compressive strength of the arch ring material. This description relies on the assumption that the material is elastic-perfectly plastic. Material tests would be required to justify the use of such an assumption since it has often been observed that brittle failures occur when compression is high.

Taylor and Mallinder (1987; 1993) and Taylor (1991) have demonstrated that beyond the peak stress there is a descending branch of the stress-strain curve for concrete voussoirs. Load tests on other material reveal that sometimes the rate of descent is rapid, i.e. an elastic-brittle material.

Smith (1991) produced his "load path analysis of masonry arches" in which the zone of thrust, horizontal backfill pressures, the dispersal of the applied load through the spandrel fill and several other features were included. It would appear that many of these features were included to appease the practising Engineer. However, further research is required into the effects of these features before the level of confidence implied by the method is realised.

Vilnay and Cheung (1986) made no reference to limit state analysis nor to non-linear programming. They presented an example of a three voussoir arch. However, if they had presented an example of an arch comprising more voussoirs they would have required the above mathematical technique in order to solve it. They investigated the stability of an arch by deriving an expression which related the applied load to the change in potential energy of the arch. They stated that, "failure of the arch is conditioned by the existence of tensile forces". They went onto explain this statement and actually meant that the line of thrust must be contained within each joint. By checking that this was satisfied, the range of allowable horizontal abutment thrusts could be determined. In their model, failure could only take place by the formation of a hinged mechanism. They developed expressions for the horizontal and vertical displacement of each block relative to its neighbour due to a rotation. They retained second order terms in the expansion of these expressions. By summing these terms for all blocks and equating them to the relative movement of the abutments further constraints to the problem were generated. The potential energy of the system when displaced by a load was minimised subject to the above constraints in order that the collapse load could be determined.

Cooke (1987) proposed a technique for the analysis of the masonry arch in which the change in its potential energy was maximised in order to determine the collapse load. He based his calculations on large deflection theory in which changes to the geometry of the arch were incorporated as it reacted to the load. He incorrectly assumed that stability was maintained beyond the stage at which a mechanism forms. He calculated the collapse load as the sum of the load required to create a mechanism and the additional load required to cause instability.

Crisfield, Jennings, Hughes and Vilnay (Cooke, 1988) corrected his formulation of the potential energy and thus proved that the maximum load occurs when the mechanism is formed. In other words, as Jennings pointed out, stability is lost when a mechanism forms. This fact has been demonstrated many times during load tests.

Hughes and Vilnay (1988) produced details of an elastic method which extended the work of Castigliano into an iterative procedure which was capable of predicting the collapse load of a masonry arch. Their model was also able to include soil-structure interaction (Blackler, Hughes and Bridle, 1990) in the form of linear springs attached to the arch whose stiffness was equal to the modulus of subgrade reaction (Fomba, 1990).

In the elastic method, the arch is divided into a number of beams. The support reactions were calculated using the principle of minimum strain energy. From equilibrium, the internal forces within each beam could be calculated. These forces can then be used to calculate the deflections and the stress distribution within each beam. Tension zones are removed and the stresses redistributed until equilibrium is achieved. The applied load can then be increased and the above process repeated until equilibrium can no longer be achieved, at which point the collapse load is produced.

Jennings (1988) produced a mechanism method which required a repeated use of linear programming to determine the correct mechanism and collapse load. He assumed that, "the fill above each hogging/sagging hinge was in a state of active/passive failure when the arch collapses". Thus, for an assumed value of the horizontal abutment reactions, it is possible to calculate the upper and lower bounds of a zone representing the permissible region within which the line of thrust must be contained. This region defines the constraints of the problem. The magnitude of the applied load is maximised subject to these constraints. Thus, in effect the geometry of the arch is changed during this method so that the haunches of the arch are thickened as if backing was included. Consequently, a significant increase in the load bearing capacity of an arch can be achieved.

However, the basic assumption is questionable. Jennings adopted a pressure distribution within the backfill which was proportional to depth. Experimental evidence reveals that this is incorrect; backfill pressures are related to the movement of the arch barrel. Furthermore, the arch must deform quite considerably before anything like maximum passive pressures can be generated. At this point the collapse mechanism has already formed and the instability of the structure is mirrored by the fact that the applied load would have to reduce in order to achieve equilibrium and avoid a sudden collapse. When the arch is just on the point of being converted into a mechanism, backfill pressures are much smaller than those produced during the post-failure stage.

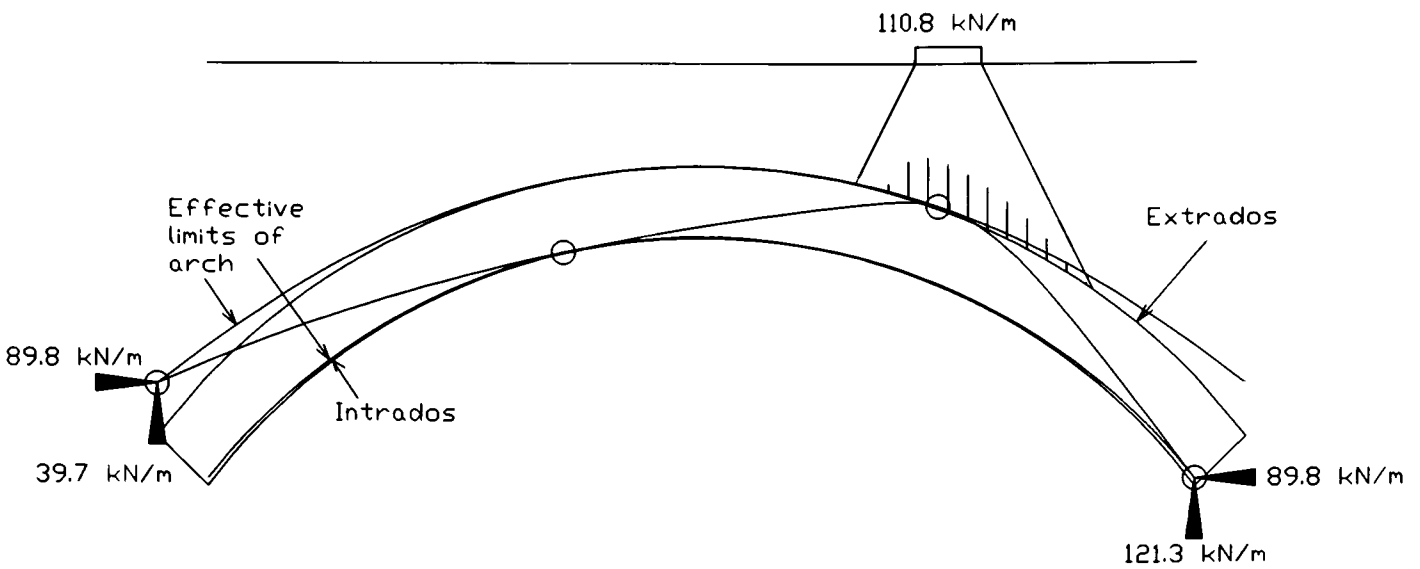

Figure 2.15 Mechanism method after Jennings

Figure 2.15 shows the ultimate load and associated line of thrust for the same 3.0 m span arch as shown in figure 2.13. Horizontal backfill pressures are included, but are limited to 50% of the full passive capability, for the calculation of the revised geometry of the structure as suggested by Jennings.

Livesley (1992a) extended his work to deal with multi-span structures and material yielding. He attempted (Livesley, 1992b) to extend his method for the analysis of three-dimensional structures. He remarked on the difficulty encountered when selecting a set of forces which realistically modelled the behaviour of the joints. He also discussed the problems involved with sliding and with transforming the constraints to a linear form. However, he obtained some results for a three-dimensional analysis of a square span arch subjected to an eccentric point load. His model consisted of only four blocks, a single block wide, and highlights the computing effort required to solve realistic problems of a three-dimensional nature. However, this work represents the first attempt to analyse a three-dimensional model through the use of a mechanism method.

Boothby (1992b; 1992c) used the upper bound theorem of collapse to analyse an arch consisting of a set of contiguous rigid blocks. He omitted sliding mechanisms and retained second order terms in his formulation of the constraints. He therefore required non-linear programming to obtain the minimum collapse load which satisfied the kinematic constraints.

Gilbert (1993) used the upper bound theorem of collapse to analyse the square arch bridge. This, upper bound, technique will be discussed in more detail in chapter 6. However, Gilbert proposed two extensions of this model for the analysis of multi-ring arches. The first model, viz. the "plastic shearing" model, allowed blocks within adjacent rings to slide relative to each other but these shear failures were associated with dilatant movements in accordance with the

normality rule. The change in potential energy associated with these movements was adjusted accordingly. The second model, viz. the "plastic cohesion" model, attempted to incorporate the shear bond strength of the mortar by assuming that a force exists along each block at the interface so that the potential energy associated with relative shear movements was enhanced by the movement of these forces. However, in conflict with the findings of Stöckl and Hofmann (1988) the mortar bond was modelled as rigid-plastic so that, if a shear bond strength was sufficiently high so that ring separation was prevented, the predicted failure load was identical to that of a voussoir arch. This is not correct, it will be shown in chapter 7 that the actual elastic-plastic behaviour of the mortar bond will result in the behaviour of a multi-ring brickwork arch being fundamentally different to that of a voussoir arch. Furthermore, it was shown (Gilbert, 1993) that the predicted capacity of the multi-ring arch continues to increase in proportion to the mortar bond strength beyond that of the voussoir arch.

Gilbert proposed several other extensions of this upper bound technique in order to incorporate material yielding, multi-span arches and spandrel walls. Thus, neglecting Selberg's method, this was the first model to include spandrel walls. However, like all other theoretical models to date, Gilbert's was also two-dimensional. The inclusion of the spandrel walls was done by analysing a section at mid-width and one at the edge and producing an estimate of the combined collapse load on a pro rata basis.

Boothby (1994) again expressed the potential energy function in terms of the possible movements of the structure but this time included an energy dissipation term to represent the loss of energy due to sliding. In order to achieve this, he needed to calculate the set of normal and tangential forces between each set of contiguous blocks. His method was a hybrid approach, in which sliding was included in a similar manner to that adopted by Livesley, and the movement of blocks was incorporated in a similar manner to that adopted by Gilbert. However, he required non-linear programming techniques to determine the optimal solution to his problem.

Chandler H.W. and Chandler C.M. (1995) attempted to use shell theory to produce a safe lower-bound estimate of the load carrying behaviour of the skewed arch bridge. Their initial statement that, "any stress field, regardless of its reasonableness, that satisfies equilibrium and the boundary conditions and which does not exceed the yield criterion can be used to construct a lower bound on the collapse load" is certainly safe and would naturally lead to a conclusion that, "given suitable edge support, a skewed arch can withstand a normal pressure purely by compressing the bedding joints of the brickwork". This may be true, and is certainly a lower-bound on the actual method of load transfer and suggests that a two-dimensional analysis based on the skew span is acceptable. However, although this is safe, a higher lower-bound, making use of the lower-bound theorem of collapse which refers to a yield criterion, is required in order

to increase the usefulness of this technique. Furthermore, the detachment of spandrel walls will result in the loss of the required suitable edge support.

In the mid 1950's efforts to solve continuum problems in elasticity by notionally dividing the structure into small general element were very much overcome. Previously, such problems had been attempted through the use of finite difference methods which became progressively more tedious and frustrating as the problems were enlarged. Argyris was the first, in 1954, to publish on a new numerical technique which, in 1960, Clough named the "finite element method" (Argyris & Kelsey, 1960)

The basis of the finite element method is simple. A model of a structure is discretised into a finite number of elements. Rules are developed which govern how a general element deforms when loaded. When all elements are assembled and certain parts of it are restrained and other parts of it are subjected to load, the structure can be solved in terms of the deformation of each of its members.

A considerable amount of research into the finite element method has been carried out on the use of arch and shell elements. Crisfield (1989) reviews this work. It was not specifically aimed at masonry or brickwork and most of it tended to be within the elastic range.

The first application of the non-linear finite element method applied to the study of the brickwork arch was due to Towler (1981). He adopted a one-dimensional model in which the arch was idealised as a set of straight beam elements. Material non-linearity was incorporated through the use of a no-tension material together with a parabolic compressive stress-strain relationship. This enabled them to model the actual behaviour of their model arches which they had load tested to destruction. The development of this approach was continued by Towler and Sawko et al. (1982a; 1982b; 1984; 1985).

Crisfield (1984) also developed a non-linear finite element method using one-dimensional elements. He idealised the arch as a set of locally shallow arches consisting of curved beam elements. Geometric non-linearities were incorporated by large deflection theory. Material non-linearities were incorporated by a bi-linear compressive stress-strain relationship and a no-tension material.

Later, (Crisfield, 1985a; 1985b) a two-dimensional finite element model was developed. The arch was modelled by eight-node plane stress quadrilaterals using the same elastic-perfectly plastic material that had been used in the one-dimensional model. He found that the adoption of an isotropic no-tension criterion allowed circumferential cracks to develop under dead load. These cracks adversely affected the behaviour of the model when subsequently subjected to

incremental live loading. He corrected this by resolving the material properties into the circumferential and radial directions and specified the no-tension criterion in the circumferential direction only. He also found that the usual way of calculating elemental strains was not accurate enough and therefore developed a more accurate element with 2×8 Gaussian integration points so that crack development could be monitored more closely. His model also included the backfill which he modelled using eight-node plane strain quadrilateral elements with which the Mohr-Coulomb yield criterion was adopted (Crisfield,1987).

Choo et al. (1990a; 1991b) developed a non-linear finite element analysis technique for the masonry arch. Material non-linearities were modelled by assuming that the arch possessed no-tensile strength and exhibited an elastic-perfect plastic behaviour in compression. The model comprised one-dimensional beam elements. The load was applied in increments and the structure solved at each stage. The nodal forces were used to calculate the depth of tensile regions, which were subsequently removed. The stress distribution at each joint was also found so that it balanced the nodal forces. The depth of any plastic zones, thus calculated, was retained but was not included in the calculation of the elemental stiffness for the subsequent load increment. The effective depth of the arch was reduced until it was no longer able to balance the nodal forces.

Choo et al. (1990b; 1991b; 1992) extended their finite element work into two dimensions. The arch was idealised as a set of eight-node quadrilateral elements. To simulate radial cracking, elements were disconnected when tensile stresses greater than tensile strengths occurred in the circumferential direction. To simulate ring separation, the quadrilateral elements within adjacent rings were connected by joint elements. These elements had no lateral strength so that adjacent rings were free to slide. However their normal stiffness ensured that no element would impinge upon another. Frictional forces were calculated and applied at each end of the joint element when sliding occurred. This model was also based on a more realistic parabolic stress-strain relationship and instead of reducing the section when tensile stresses occurred, elements were simply disconnected until no further load could be sustained.

Choo et al. (1993) developed a three-dimensional finite element method using curved shell elements. The backfill was modelled by one-dimensional spring elements attached to the extrados as had been done in each of the two previous models. They returned to the simplified linear elastic-perfect plastic material with no tensile strength. The solution was sought in much the same way as it had been done in the one-dimensional model, i.e., that the shell elements were reduced in thickness until they could no longer sustain load. The model was used to analyse a skewed arch, viz., Barlae Bridge and thus represents the first attempt to realistically analyse skew.

It was claimed that each of their finite element models could be adjusted so that the results of load tests could be reproduced reasonably accurately. In particular, their three-dimensional analysis of Barlae bridge (Choo et al., 1993) appeared to depend of this adjustment process; it produced a value for the collapse load that was within 2% of the actual measured value. However, their model should have predicted the twisting that the skewed arch undergoes when it supports a load; it did not. Instead, it predicted a uniform deformed shape as if the arch was not skewed. Despite being stiffened by internal spandrel walls and backing, Barlae bridge also exhibited this twisting phenomenon. Furthermore, their analysis could not reproduce the measured load-deflection response (Page; 1989). This suggests that there is a flaw in their modelling procedure. The above phenomenon can be reproduced accurately by a finite element analysis provided that the model is able to behave in a realistic way. If this is achieved, it is unnecessary to adjust material properties; this will be demonstrated in the finite element modelling presented in chapter 7.

Loo and Yang (1991a; 1991b) produced a non-linear finite element method which incorporated more realistic failure criteria than simply imposing upper limits on the compressive stresses. They adopted the results of the research of Dhanesehar et al. (1985) to model the arch behaviour as a linear elastic-brittle material. However, convergence problems were encountered so they introduced strain softening as a falling branch of the stress-strain relationship after the peak value had been attained. They developed a biaxial failure surface with von Mises being adopted when uniaxial compression occurred. Four-node isoparametric elements were used to model the masonry and the backfill. When partial failure occurred, i.e., only one of the principal stresses reached its limiting values the material was changed from having isotropic properties to orthotropic properties. Thus the method used a smeared crack approach in which discrete cracks were not introduced but were modelled by a change in the material properties.

Loo and Yang produced reasonable results when their model was subjected to concentrated loads only. Their conclusion, when abutment settlement or spread was analysed, suggest that very small movements would cause collapse. This does not seem reasonable and further work should be carried out to investigate this phenomenon.

3.0 Experimental Test Programme

3.1 Objectives

The principal objective of the experimental test programme was to develop the database of quantitative information pertaining to the load bearing behaviour of skewed masonry arch bridges. Thus, the behaviour of the above type of bridge would be unequivocally described and the database used to facilitate the development of arch theory.

At the outset of this project very little information was available regarding the load carrying behaviour of skewed arch bridges. Much of the documented knowledge was based on the non-destructive field tests on skewed arch bridges that were carried out by Davey (1953) and those that were later carried out by Chettoe and Henderson (1957). These testing programmes produced data pertaining to the three-dimensional behaviour of skewed and square span arch bridges. Unfortunately, the extent of this data was limited by the amount of instrumentation and visual observations which were made. The data were rendered qualitative because of the unknown material properties and construction details. These problems are significant arguments against carrying out field tests. Certainly, the T.R.R.L. series of tests appeared to be beset by such problems. The destructive field test carried out on Barlae Bridge (Page, 1989a) was the first test on such a highly skewed arch bridge. Its internal construction details, as discovered only after its collapse, dramatically influenced its behaviour. Internal spandrel walls and thickened haunches caused it to behave almost like a square span structure. Without considering its internal construction it could be possible to wrongly conclude that skew does not affect the behaviour of arch bridges.

Laboratory tests have the advantage that the construction details can be unambiguously defined and that material properties can be ascertained more reliably. The argument that laboratory tests may not be realistic representations of actual structures can easily be refuted. Careful planning of a test structure can remove the possibility that it will be forced to behave in an expected manner and thereby verify some arbitrary theory. This is a comment frequently used to describe the manner in which many arch bridges have been tested, viz., that applying a line-type load parallel to the abutments will produce a certain type of behaviour. Multiple or single point loads, or, in skewed arches, a line-type load perpendicular to the spandrel walls may produce other types of behaviour which may be more onerous.

Whilst actual structures, when field tested, may behave in a "true" manner, their behaviour can not be predicted by current arch theory. Factors which cannot be readily quantified include variations in material properties, localised geometrical anomalies, non-uniform spreading and rotation of the abutments, differential settlement, the type and degree of consolidation of the

spandrel fill, the quality of the wing walls and their foundation, and the type and nature of the soil outside the structure. It is with great difficulty that the above are incorporated into laboratory test structures. However, they should not be incorporated unless the research is aimed specifically at the effects produced by them. A further advantage of laboratory tests is that it is more possible to isolate a particular parameter and thence determine its importance. Other parameters can either be removed or more reliably predicted. Arch theory is not advanced by carrying out tests on structures which contain so many parameters that it becomes impossible to determine their respective contributions to the observed behaviour.

3.2 Development

Many factors exist which can influence the behaviour of masonry (Melbourne and Walker, 1990a; Hendry, 1990). These "randomising" factors are difficult, if not impossible, to quantify. The experimental methodology adopted throughout this programme of testing was selected in order to maximise the likelihood that the magnitude of the above "randomising" factors can be made constant throughout the programme. Thus, the construction of each arch bridge would follow a consistent style. Subsequently, each structure would be treated and finally tested in a similarly consistent manner. Each structure would be notionally identical, in every detail except one, to one other structure within the programme. Thus, by a process of superimposition it was intended that the single altered feature between any two structures would enable the influence of that feature to be ascertained.

Table 3.1 summarises the 3.0 m span two-ring arch bridges which form part of the test programme. The relevant square span arch bridges which were part of previous research projects are also shown.

Arch Ref:	Nominal Skew	Square Span	Description
3-0a	zero	3.0 m	Attached spandrel walls, backfilled
3-0b	zero	3.0 m	Attached spandrel walls, backfilled, total ring separation
3-0c	zero	3.0 m	Detached spandrel walls, backfilled, total ring separation
3-0d	zero	3.0 m	Detached spandrel walls, backfilled
3-1	**22.5°**	**3.0 m**	**Detached spandrel walls, backfilled**
3-2	**45.0°**	**3.0 m**	**Barrel only**
3-3	**45.0°**	**3.0 m**	**Attached spandrel walls, backfilled**
3-4	**45.0°**	**3.0 m**	**Detached spandrel walls, backfilled**

Table 3.1 Full Scale 3.0 m span arch bridge tests

Superficially, it would appear that varying the angle of skew but otherwise constructing a set of similar arch bridges would lead to a successful outcome. However, if such a programme was devised, it would be possible that the "randomising" factors would make it difficult to clearly define how skew affected the behaviour of an arch bridge. Such behavioral traits could be overshadowed by the behaviour produced by the "randomising" factors.

It was reasoned that a potentially more successful programme would be to carry out tests on structures in which the single altered feature could produce a significant change in behaviour. Thus, tests on highly skewed arch bridges were carried out in which the effects produced by detached spandrel walls and well compacted backfill could be examined. To adopt this approach, similar square span structures would be required as control structures so that the effects of skew could be ascertained.

The required square span control structures were part of previous research programmes carried out at the Bolton Institute of Higher Education (Melbourne & Qazzaz, 1989; Melbourne & Walker, 1990a, 1990b; Melbourne & Gilbert, 1991, 1992; Gilbert, 1993). These previously tested square span arch bridges had been constructed and tested in similarly controlled circumstances therefore using them as the control structures was both feasible and scientifically justifiable.

Each square span control structure was constructed so that ring separation might occur as a consequence of the monotonically increasing load. However, in two of them (refs: 3-0b and 3-0c), the occurrence of ring separation was prearranged so that its effects could be studied. It was anticipated that the relative geometric simplicity of these structures would provide the necessary information to enable a theoretical model to be developed. This would be a logical starting point in the development of a modelling technique which could then be extended to include similar ring separation phenomena in skewed arch bridges. Therefore, it was concluded that the skewed arch bridges should also be constructed in a way that would not preclude ring separation.

Ring separation may be the single most significant behavioural trait of multi-ring brickwork arch bridges and could potentially overshadow any other "randomising" factor and the effect produced by a change in the geometry or construction detail of an arch bridge. Thus, the single in-built change in the common construction details was designed to have an effect large enough to be observable whatever the magnitude of the "randomising" factors. This was the most important reason for the selection of the test programme as summarised in table 3.1. The alternative would have been to physically prevent ring separation by either constructing voussoir arch bridges or to use headers in order to ensure that multiple rings acted compositely. However, it is impractical to construct multi-ring skewed arch bridges with headers and this

would have meant that the previous square span arch test results would not have been applicable.

In spite of these positive arguments in favour of the selected test programme, the data was supplemented by a second series of destructive tests carried out on single ring 1.2 m span arch barrels as highlighted in table 3.2.

Bridge ref:	Width	Span	Skew	Loading
1-1	1.0 m	1.2 m	zero	eccentric at ¼-point
1-2	1.0 m	1.2 m	zero	eccentric at crown
1-3	2.5 m	1.2 m	zero	eccentric at ¼-point
1-4	1.2 m	1.2 m	45.0°	obtuse haunch ¼-point
1-5	1.2 m	1.2 m	45.0°	obtuse haunch ¼-point*
1-6	1.2 m	1.2 m	45.0°	acute haunch ¼-point*
1-7	1.2 m	1.2 m	45.0°	acute haunch ¼-point+

* paraffin applied to bricks before laying with the intention of reducing the bond strength
+ ratio of cement:plasticiser decreased to 10:1 with the intention of reducing the bond strength

Table 3.2 1.2 m span model arch barrel tests

3.3 Material Properties and Construction Details

The centring on which each 3.0 m span arch barrel was constructed comprised curved steel beams supporting timber formwork. Each steel beam was supported on two individual brickwork prisms. Thus, after construction was complete, the centring was struck by simply removing the brickwork prisms.

The centring on which each 1.2 m span arch barrel was constructed was formed in timber which was cut to the required profile. This was supported on several brickwork columns which were removed when the formwork was struck.

A release agent was applied to the timber formwork of the centring prior to bricklaying in order to minimise bonding of the masonry to the timbering and facilitate easy removal of the centring.

The test bed on which each model arch bridge was constructed was a massive reinforced concrete structure with abutments fixed 3000 mm apart, parallel to each other and possessing 60° springings. Portable abutments for the 1.2 m span arch bridges were bolted to the test bed 1200 mm apart and parallel to each other. These abutments possessed 36.87° springings.

Full size, solid class A Engineering bricks described as "Nori" bricks and supplied by "Marshalls Products plc." of Accrington were used in the construction of the arch barrel of each model arch bridge. The properties of the bricks are contained within table 3.3.

Brick type	Compressive Strength	24 hour Absorption	Nominal Dimensions	Density
Class A	154 N/mm^2	3.9% *	215×102×65	2370 kg/m^3

* In accordance with BS 3921

Table 3.3 Brick properties

Spandrel walls and wing walls, when present, were constructed from Engineering bricks reclaimed from previous tests. End retaining walls were required for each backfilled bridge in order to retain the backfill. A "real" bridge would not require these walls since the continuation of the road would perform a similar function. In accordance with BS 5628, the mortar used throughout this project was of designation (iv) having a mix proportioned in the ratio 1:2:9 (cement: lime: sand). After consulting with the bricklayer, plasticiser was also prescribed in the ratio 22:1 (cement: plasticiser) so that the quality of the mortar could be maintained throughout the test programme.

Structure Ref:	Compressive Strength*	Initial Tangent modulus	Density
3-0a	3.2 N/mm^2	–	1609 kg/m^3
3-0b	2.4 N/mm^2	–	1525 kg/m^3
3-0c	2.5 N/mm^2	–	1550 kg/m^3
3-0d	2.4 N/mm^2	–	1674 kg/m^3
3-1	2.5 N/mm^2	2.5 kN/mm^2	1550 kg/m^3
3-2	2.4 N/mm^2	3.0 kN/mm^2	1530 kg/m^3
3-3	2.6 N/mm^2	2.0 kN/mm^2	1625 kg/m^3
3-4	2.2 N/mm^2	3.2 kN/mm^2	1580 kg/m^3

* mean values from mortar cured with bridge

Table 3.4 Mortar Properties

The properties of the mortar used throughout the test programme are listed in table 3.4. The value of its initial tangent modulus is a rather qualitative assessment of this parameter since insufficient data could be obtained from these material tests before the vibrating wire strain gauge became detached from each mortar cube.

Each arch barrel was constructed with stretcher bonded brickwork set out in the Helicoidal method and comprised two individual rings which acted compositely by virtue of the strength of the mortar-brick bond. The spandrel walls, wing walls and end retaining walls were constructed with English bond brickwork. The material properties of the brickwork used in each arch bridge are summarised in table 3.5.

Structure Ref:	Compressive Strength* (N/mm^2)		Initial Tangent modulus+ (kN/mm^2)		Poisson's Ratio	Mean Shear Strength (N/mm^2)
	Mean	Std. Dev.	Mean	Std. Dev.		
3-0a	26.5	5.4	15.90	1.69	0.15	0.29
3-0b	27.6	2.7	22.40	1.85	0.20	0.29
3-0c	24.8	4.7	15.25	1.35	0.17	0.25
3-0d	25.3	3.2	17.10	2.05	0.16	0.24
3-1	25.5	5.2	15.50	0.75	0.15	0.29
3-2	24.4	4.3	15.30	1.13	0.20	0.19
3-3	26.6	3.7	16.25	1.55	0.17	0.25
3-4	27.9	4.2	15.80	0.75	0.16	0.24

* mean values from 5-course brickwork prisms cured with bridge
+ obtained from results within linear range (typically 0-3.0 N/mm^2)

Table 3.5 Brickwork Properties

Attached spandrel walls were constructed on top of the arch barrel with no physical connection between them other than that created by the strength of the mortar bond. Detached spandrel walls were constructed so that there was a gap between them and the barrel so that the arch could not come into contact with the spandrel walls when large deformations occurred. A nominal 25 mm gap was incorporated between each end retaining wall and the appropriate wing wall. These gaps were plugged with Polythene sheets to prevent spillage of the backfill. This gap ensured that the spandrel walls were not stiffened by the end retaining wall and equally, that movement of the wing walls would not cause collapse of the end retaining wall.

The sample stress-strain relationships, obtained from five course high brickwork prisms, as shown in figure 3.1 illustrate the variability of the material.

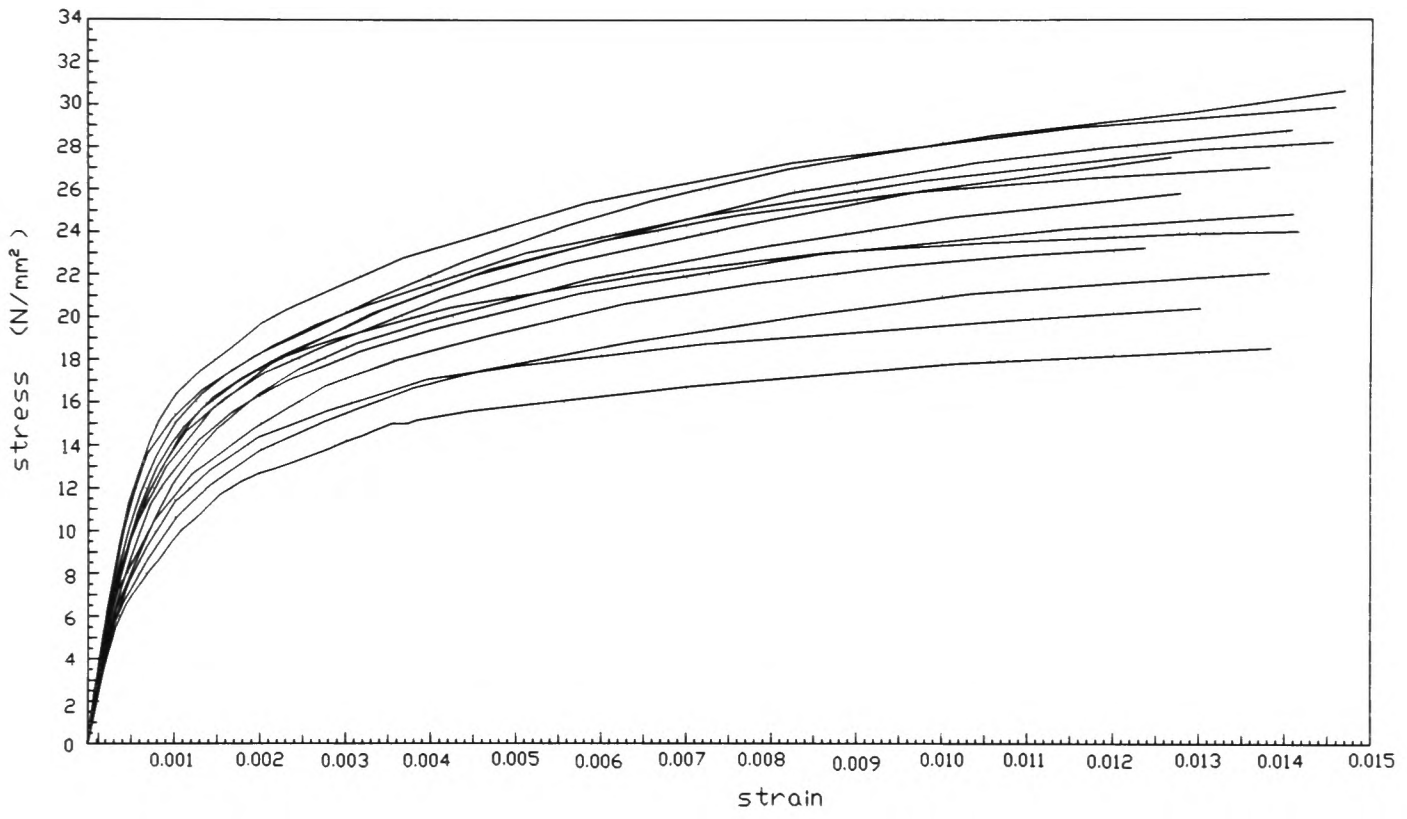

Figure 3.1 Stress-Strain relationships for brickwork prisms

The tensile strength of the mortar is not a parameter that was measured. However, the tensile bond strength of the mortar is a more important parameter and, although an insufficient number of specimens were tested, a value of 0.15 N/mm^2 was obtained. Given the variability of this parameter, it is proposed that any value of the same order of magnitude as this is acceptable for use in a theoretical model.

It was common practice to use Engineering bricks in the construction of masonry arch bridges. These bricks were often used in conjunction with mortars which tolerated relatively large movements (Temple & Kennedy, 1989; Hendry, 1990). Hence, the construction of the models was reasoned to be closely representative of actual bridges.

Backfilling of each model bridge was carried out using a 50 mm graded crushed limestone fill material. This material was selected because it had been used in the previous square span model arch bridges and had to be continued in order to produce comparable test results. The backfill was compacted in 150 mm thick layers with six passes of a vibrating "wacker" plate. Table 3.6 shows the results of a sieve analysis carried out on the backfill material.

Sieve Size	Test % Passing (cumulative mean)	DoT Type 1 standard
75.0 mm	100	
37.5 mm	97	83-100
10.0 mm	45	40- 70
5.0 mm	28	25- 45
600 μm	13	8- 22
75 μm	1	0- 10

Table 3.6 Sieve Analysis of Backfill

A large shear box test was carried out on the backfill material which established that its properties were such that it was cohesionless (c = 0 kN/mm^2) and possessed an angle of internal friction of 60°. The results of this test are shown in figure 3.2 and a brief outline of the data pertaining to the test is outlined within table 3.7.

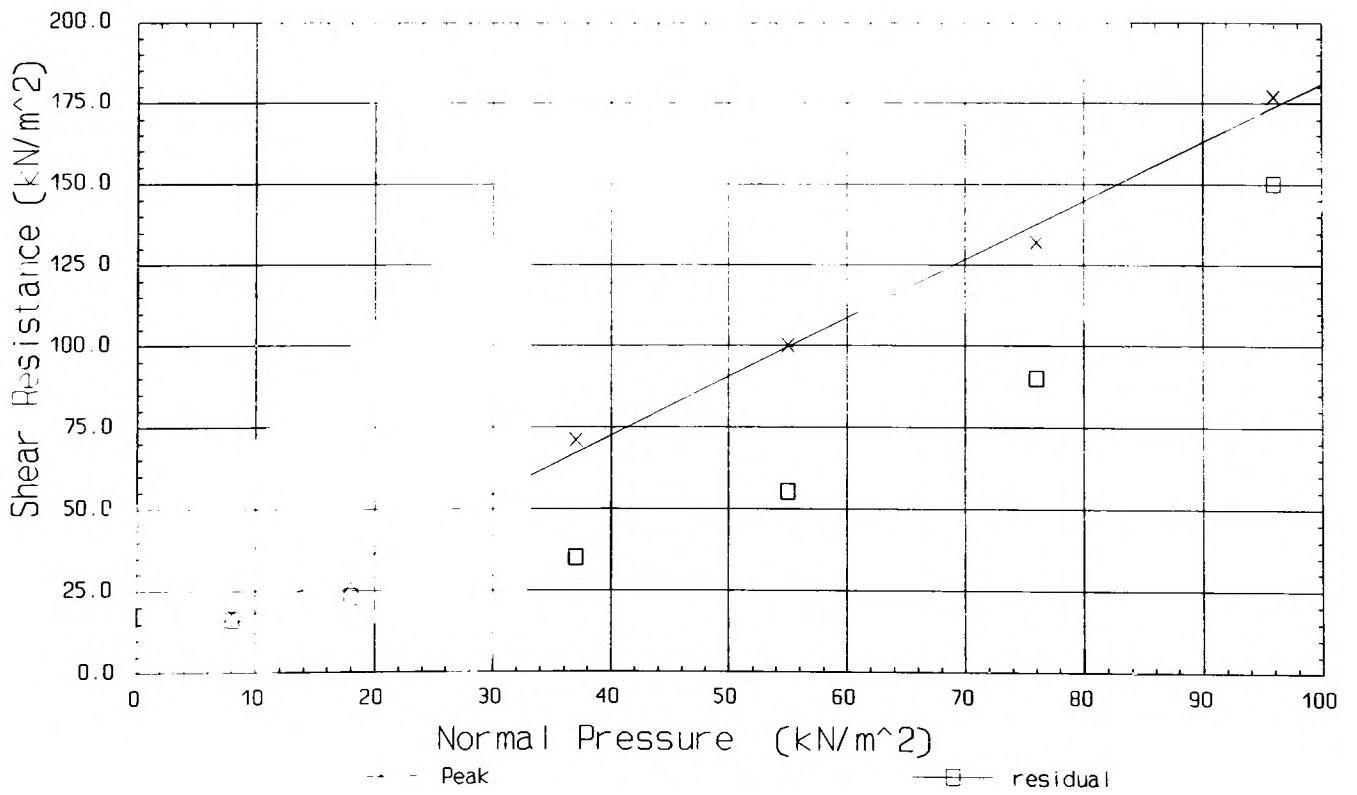

Figure 3.2 Results of the Large shear box test

Data:	Large shear box (300 ×300 ×200 mm deep).
	Dried Limestone fill, sieved to less than 25 mm, compacted in 3 no. layers using a Kango hammer to a density of 2250 kg/m^3.
	Sheared at "quick" rate, readings taken every 30 seconds (initially) for 30 minutes.
	Residual values on graph correspond to a horizontal movement of 30 mm.

Table 3.7 Large shear box results

After each arch was backfilled in situ density measurements obtained by a sand replacement technique in accordance with BS 1377 indicated that the mean bulk density of the backfill was 2250 kg/m^3. The properties of the backfill are summarised in table 3.8.

Test Property	Result
A.I.V.	8.5%
Bulk Density	2265 kg/m^3 *
Max. dry density	2420 kg/m^3 +
Optimum water content	5.0%
Natural water content	1.3%
Internal friction angle	59.5° **
Cohesion	0 kN/m^2 **

* insitu by sand replacement (BS 1377)
\+ 4.5 kg rammer method using C.B.R. mould (BS 1377)
** see figure 3.2

Table 3.8 Properties of the Backfill material

3.4 Description of Load Tests on model bridges

The dimensions of the apparatus through which loads were applied to each structure precluded the application of point loads and knife edge loads. Furthermore, had the application of such loads been possible, localised failures of the materials would have occurred. However, these terms will be retained when referring to the applied loading which actually comprised patch loads. For the 3.0 m span arch bridges these patches measured 330 × 330 mm and 2200 × 200 mm respectively. For the 1.2 m span arch bridges point loads only were applied over a patch measuring 150 × 150 mm.

3.4.1 3.0 m span arch bridges

Each bridge was eventually loaded to failure through the application of a monotonic increasing line load positioned at the South quarter-point parallel to the abutments. Prior to the failure test, a number of vertical point loads and line loads were applied at various positions. The intention was to simulate the passage of a vehicle albeit without any dynamic effects.

The instrumentation was monitored throughout all tests. The tests carried out prior to the failure test were carried out for several reasons, including:

(i) to obtain data pertaining to the three-dimensional behaviour of the bridge to loads within the serviceability range,

(ii) to provide data to enable the performance of the instrumentation to be ascertained prior to the failure load test.

Figures 3.3 to 3.6 show the general arrangement of the bridge reference 3-1 to 3-4 respectively:

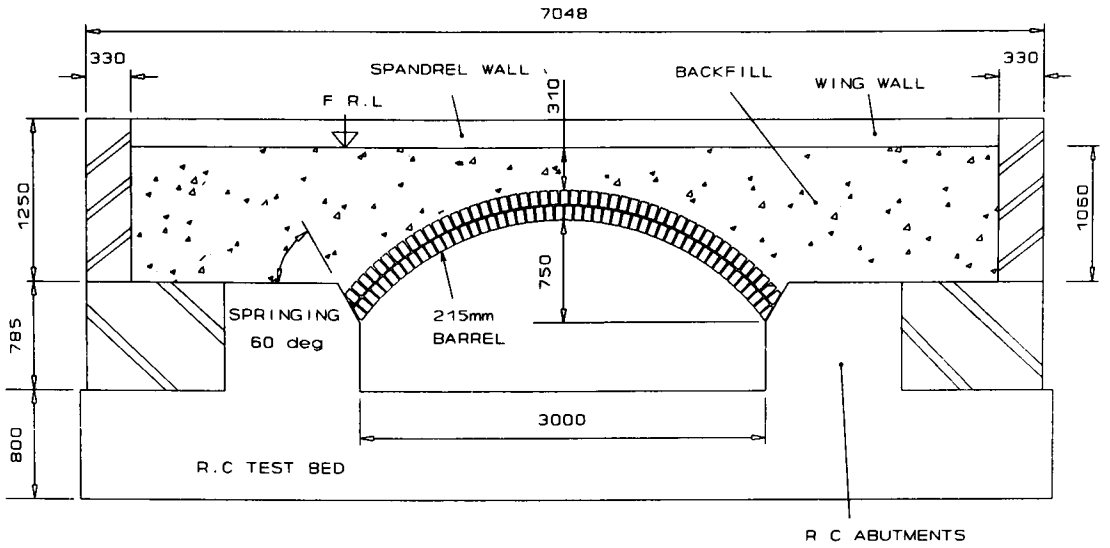

SECTION A-A

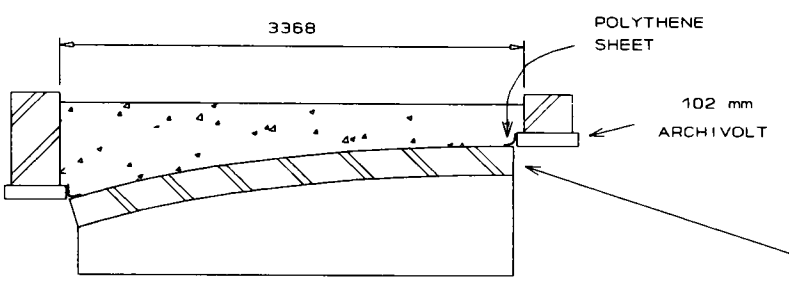

SECTION B-B

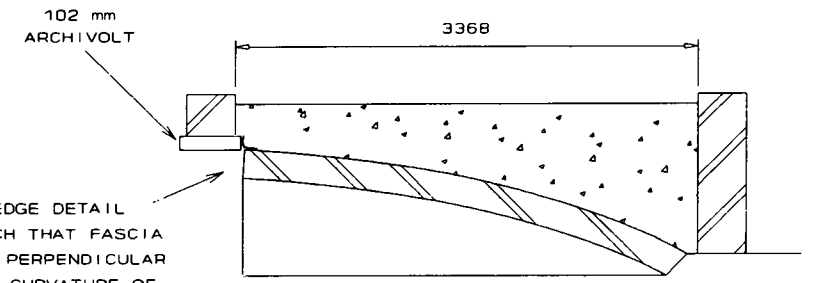

SECTION C-C

EDGE DETAIL
SUCH THAT FASCIA
IS PERPENDICULAR
TO CURVATURE OF
ARCH

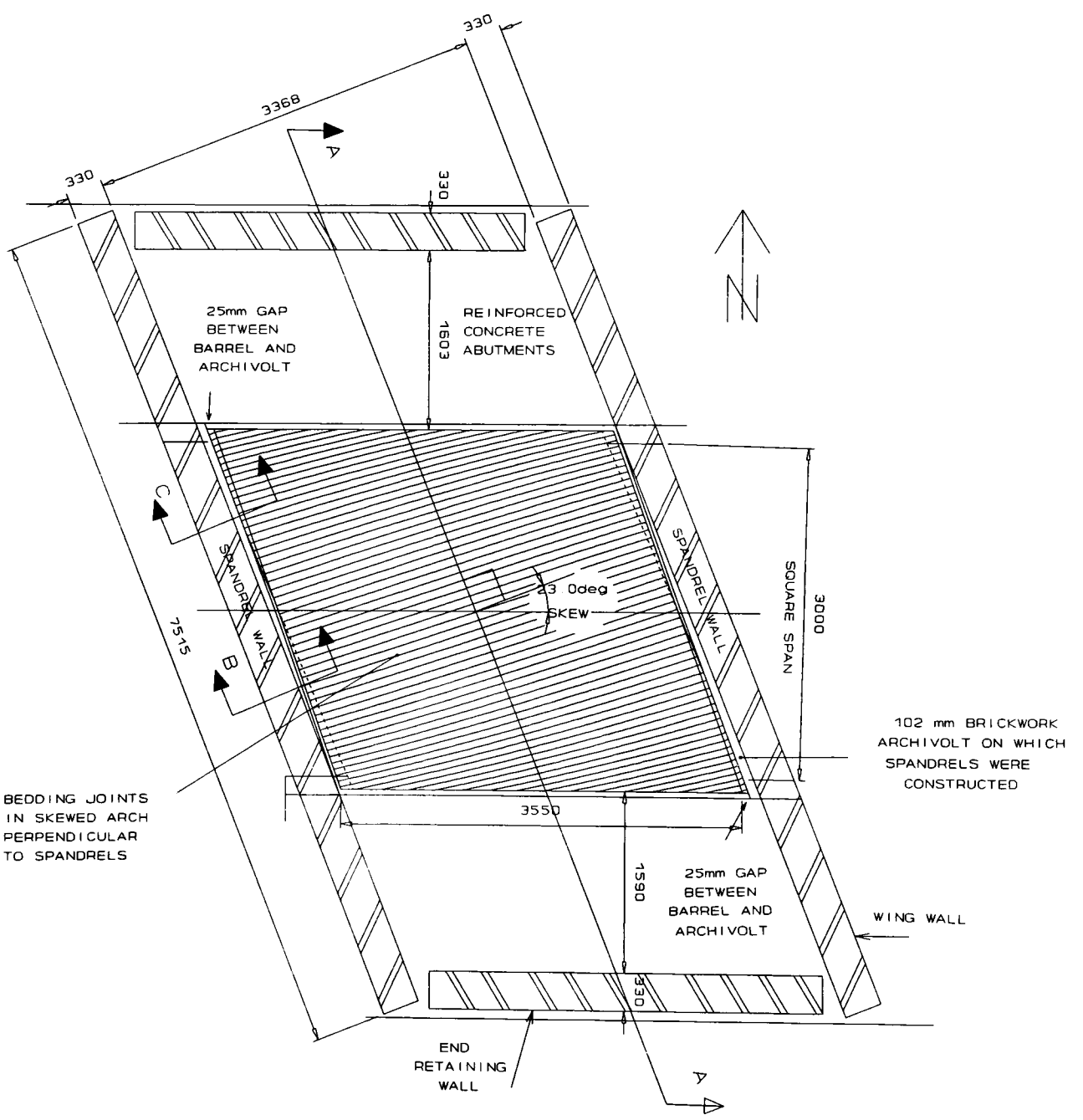

PLAN

Figure 3.3 General Arrangement of bridge 3-1

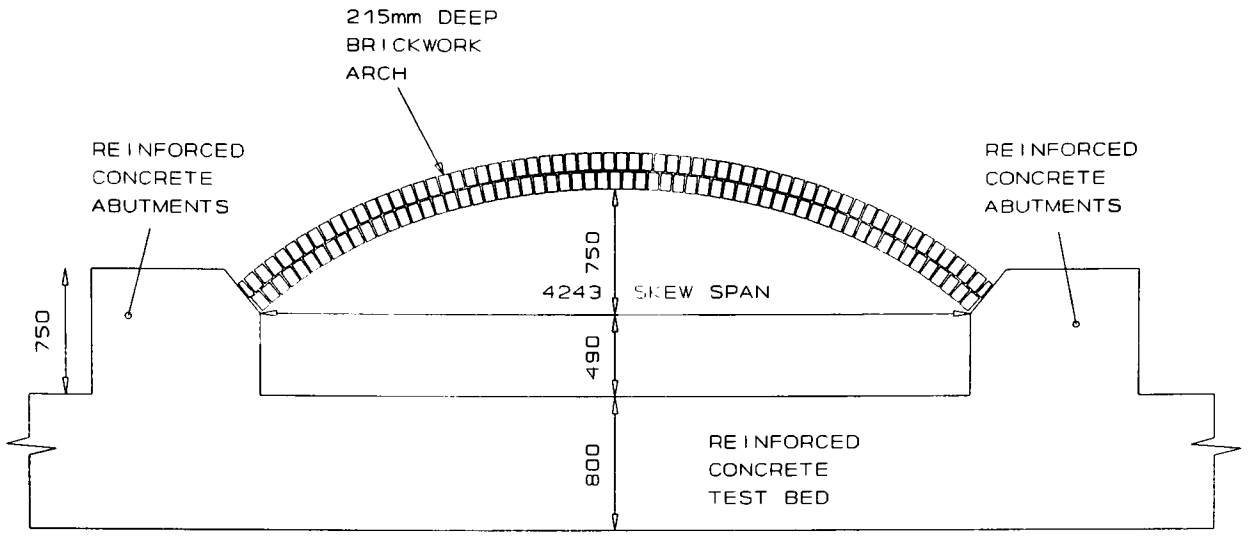

SECTION A-A

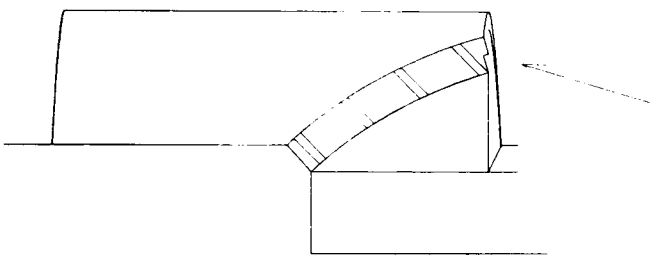

SECTION B-B

EDGE DETAIL SUCH THAT FASCIA IS PERPENDICULAR TO CURVATURE OF THE ARCH AND STEPPED SO THAT BOTTOM EDGE OF EACH RING ARE DIRECTLY ABOVE EACH OTHER

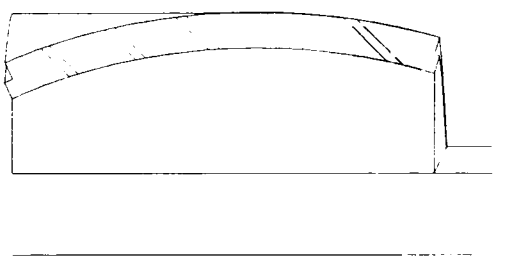

SECTION C-C

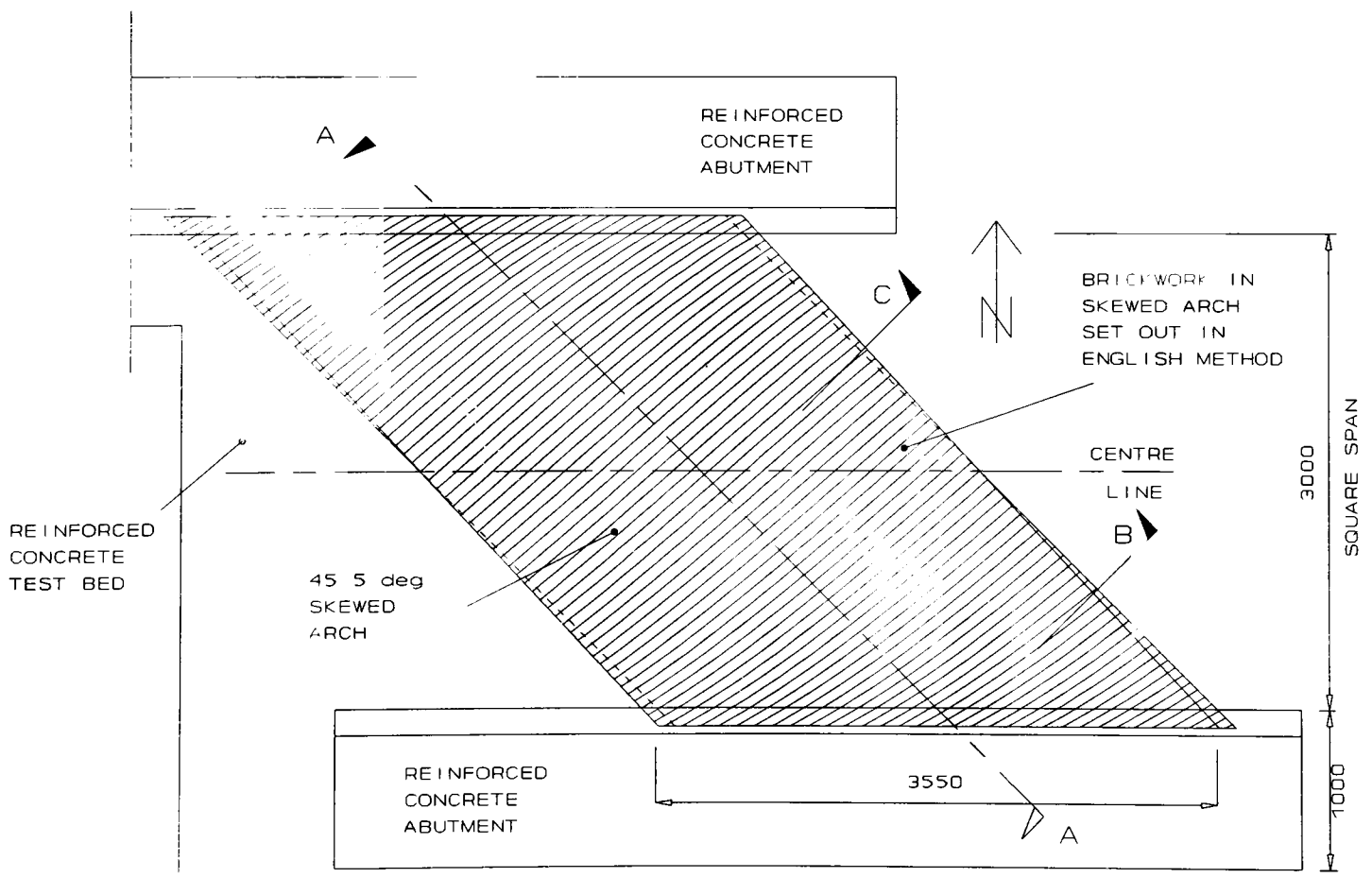

PLAN

Figure 3.4 General Arrangement of bridge 3-2

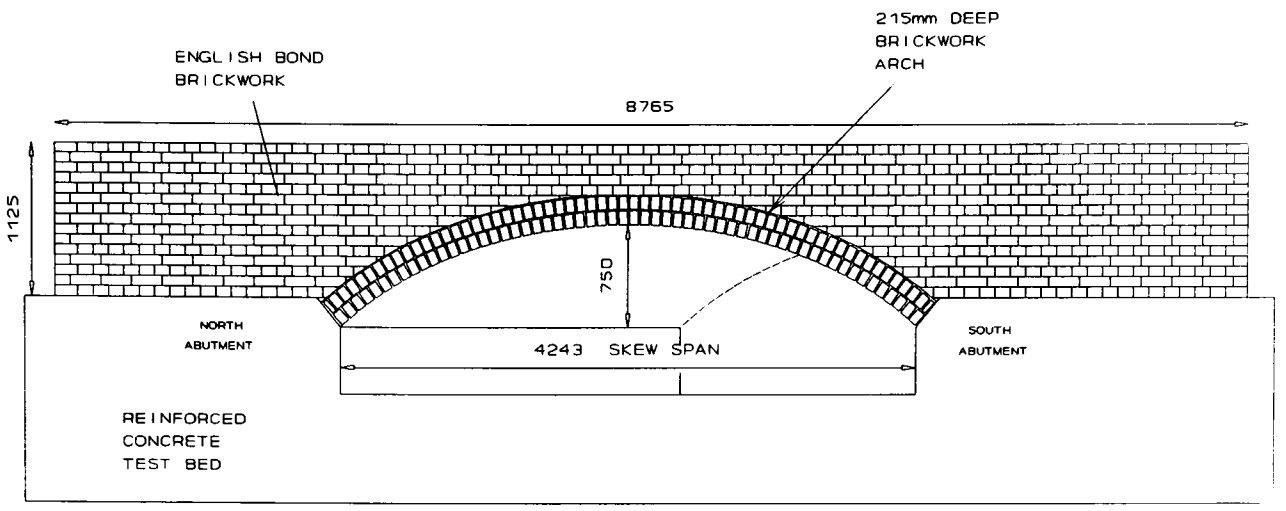

ELEVATION A-A

WEST ELEVATION

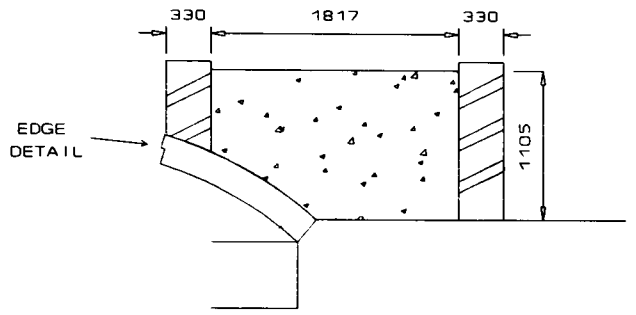

SECTION C-C

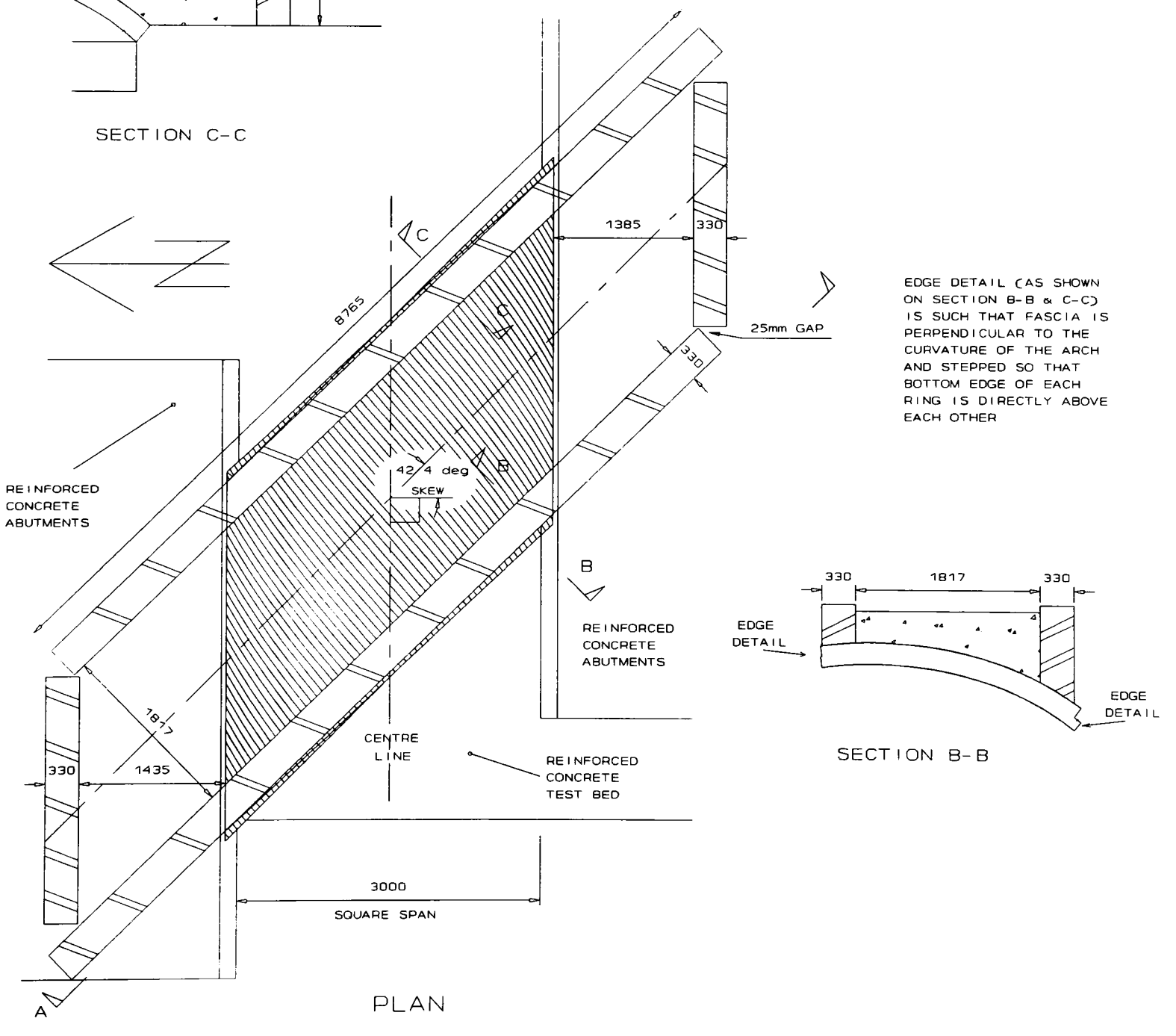

Figure 3.5 General Arrangement of Bridge 3-3

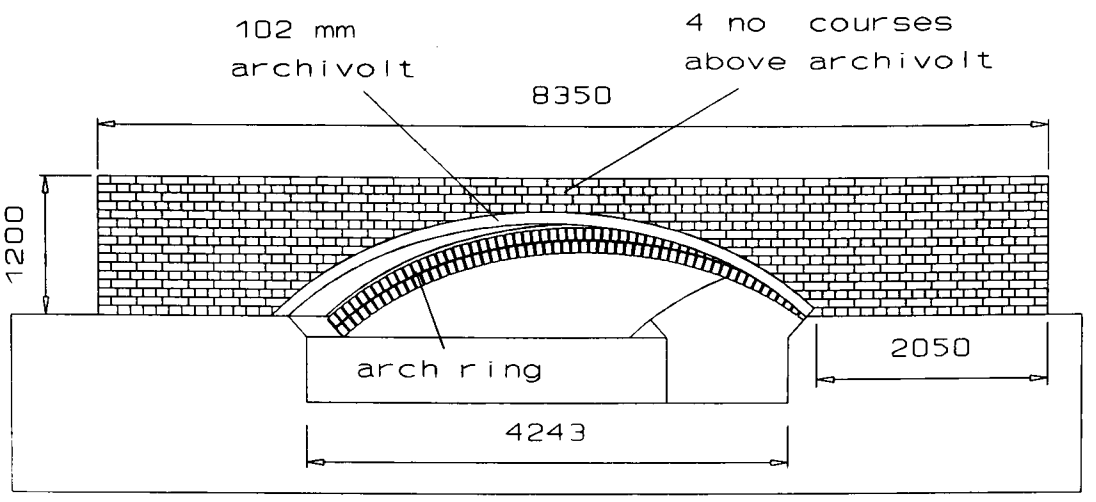

West Elevation

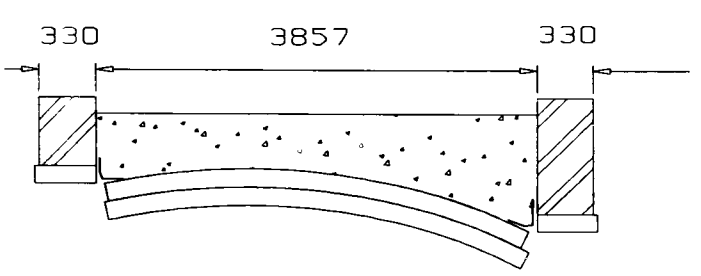

section
A-A

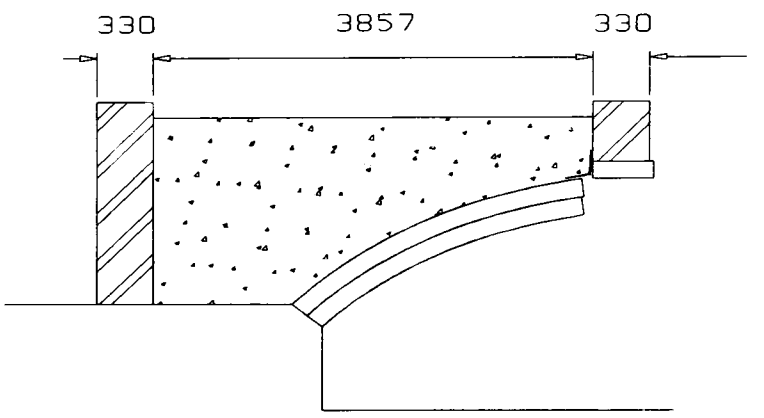

section
C-C

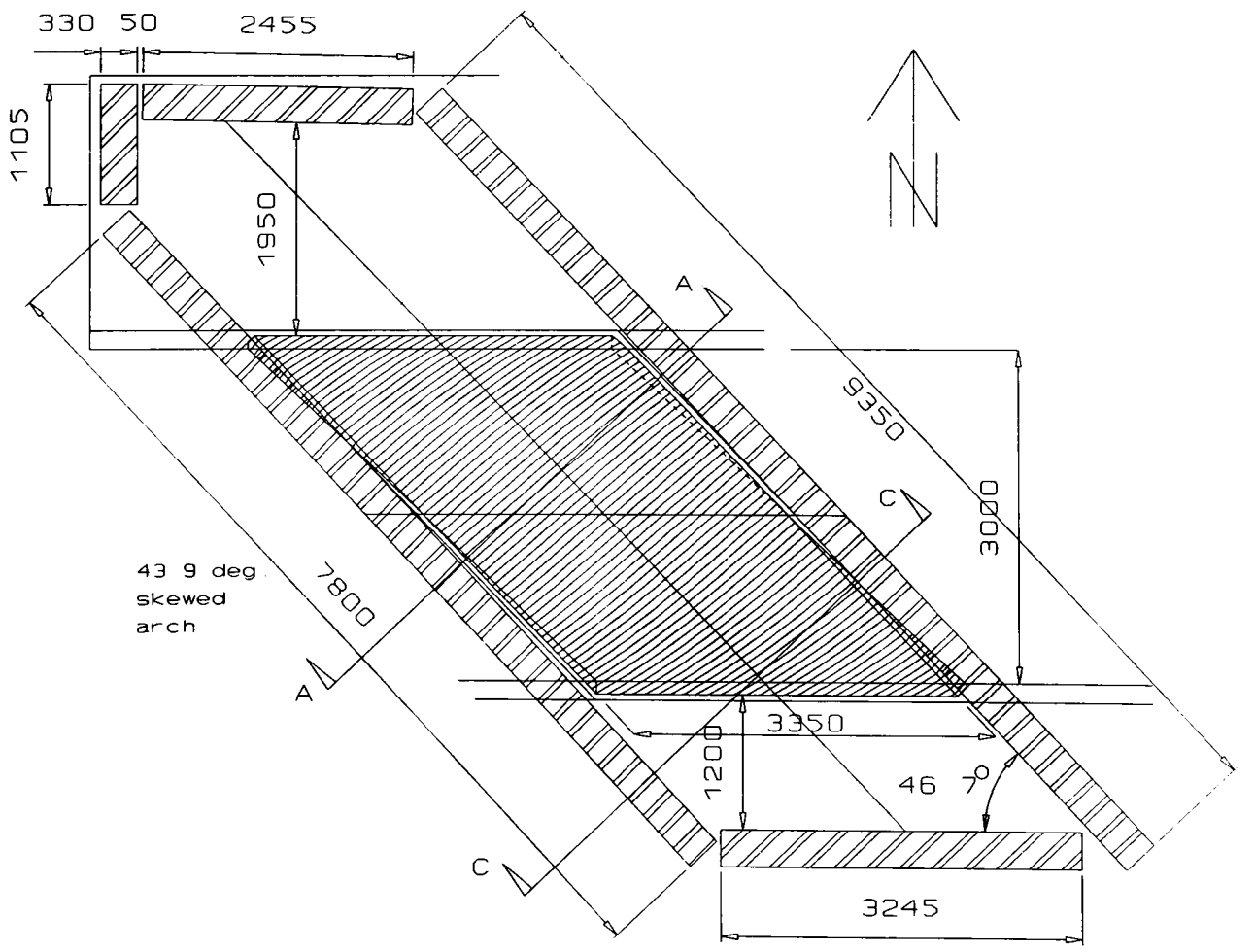

Plan

Figure 3.6 General Arrangement of bridge 3-4

Figure 3.7 shows diagrammatically the loading arrangement whilst plate 3.1 repeats this as employed on full scale model skewed arch 3-1.

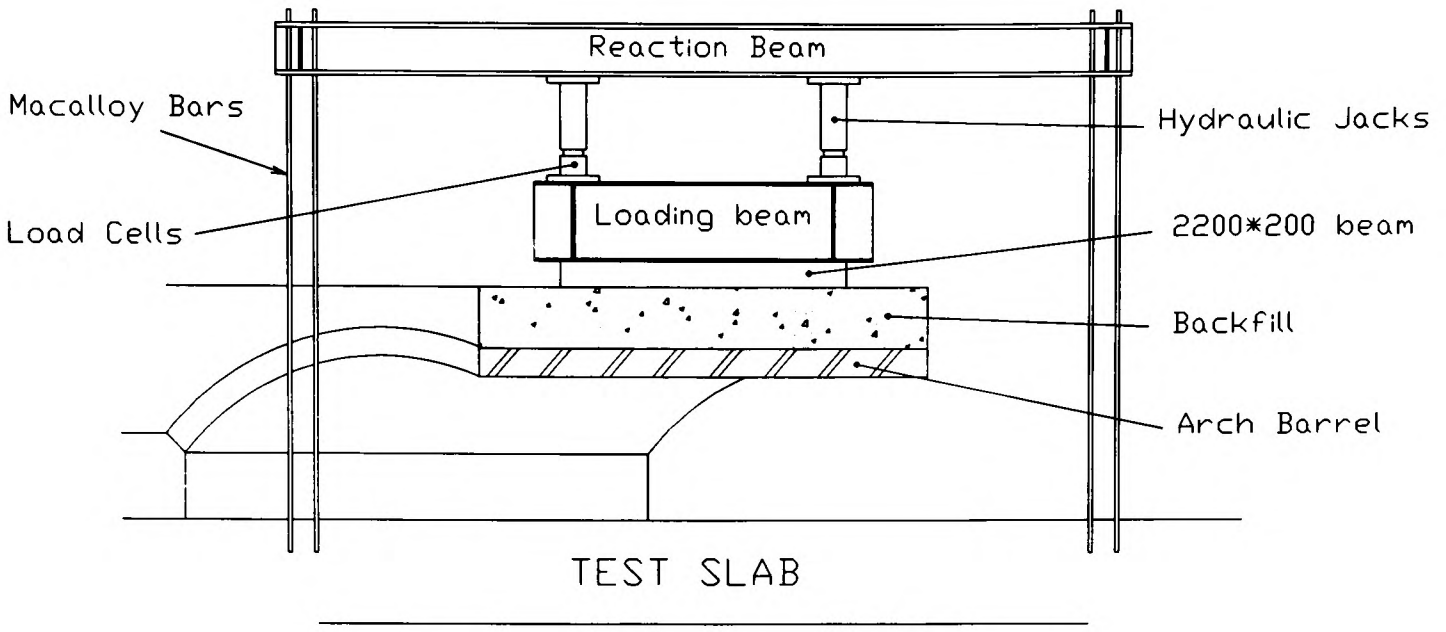

Figure 3.7 Loading arrangement for the 3.0 m span model arch bridges

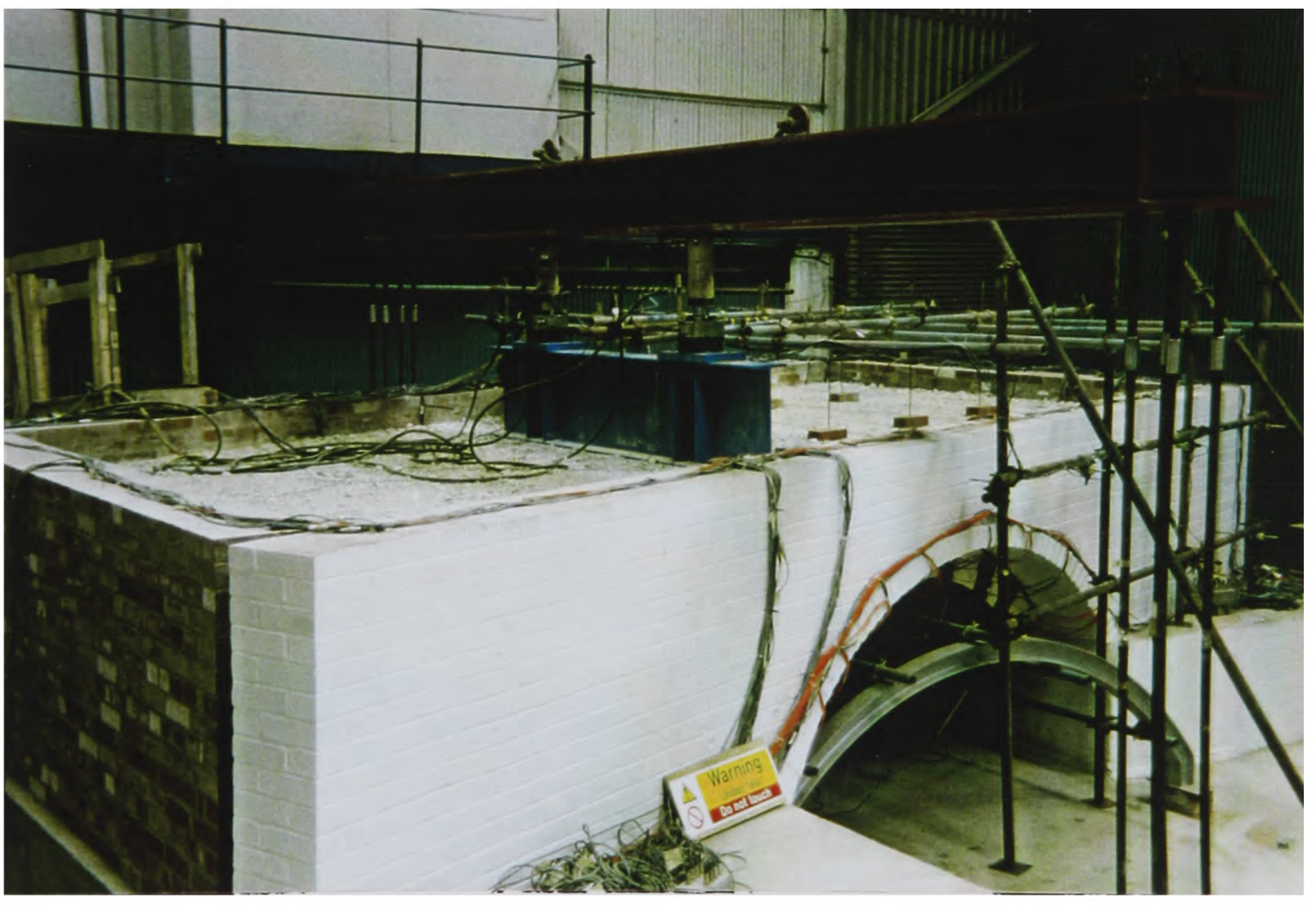

Plate 3.1 Bridge 3-1 awaiting testing at quarter-span

In the case of the line load tests, a 2200 × 200 mm steel loading beam was placed on the surface of the backfill and jacked downwards against a steel reaction beam. The latter beam was supported by two sets of four Macalloy bars which were fixed into the reinforced concrete test bed. Line loads were not applied to bridge reference 3-2. On all other structures, they

were applied at the crown and then at 200 mm. increments towards the South abutment and parallel to it. The load was applied in increments until the maximum was reached at which point the structure was unloaded. This procedure was carried out three times so that "plastic" deformations, if present, could be distinguished from "elastic" deformations.

In the case of the point load tests a 330 × 330 mm steel loading block was substituted for the loading beam and a similar triple load-unload cycle was performed. Figure 3.7 shows the position of point loads applied to the arch bridges.

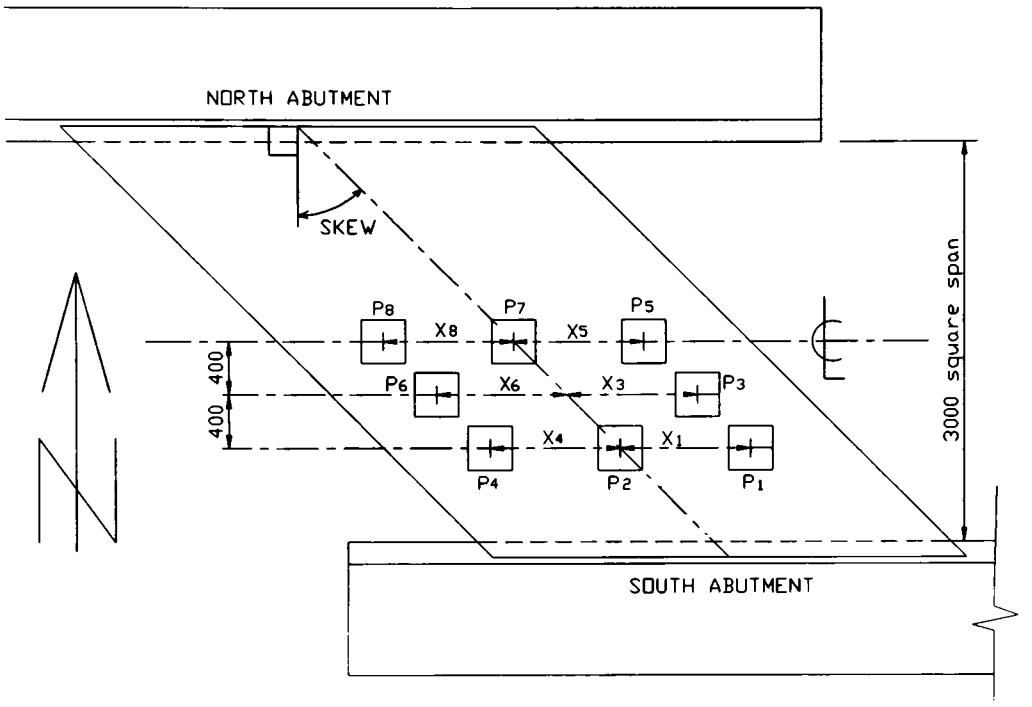

Bridge Reference	skew	Maximum Point Load	Offset+ (m)							
			x_1	x_2	x_3	x_4	x_5	x_6	x_7	x_8
3-1	23.0°	100kN	1.22	0.00	1.32	1.16	-	1.16	-	1.20
3-2	45.5°	50kN	1.18	0.00	-	1.18	1.18	-	-	1.18
3-3	42.2°	125kN	0.77	0.00	0.77	0.77	0.77	0.77	0.00	0.77
3-4	43.9°	100kN	1.20	0.00	1.20	1.20	1.20	1.20	0.00	1.20

+ "-" indicates that a patch load was not applied at this location

Figure 3.8 Point Loads applied to skewed arch bridges

Finally, with the loading beam offset by 700 mm from the South abutment, the load was increased in increments until failure occurred. After the maximum load had been achieved the hydraulic jacks were used to apply incremental deformations, with the load undergoing corresponding reductions, until the structure collapsed. This provided an excellent opportunity to study the post-failure behaviour in "slow-motion".

3.4.2 1.2 m span model arches

Each arch was subjected to a single point load which was applied over a patch measuring 150 × 150 mm. The load was increased monotonically until failure occurred.

3.5 Instrumentation

It is important to briefly explain the instrumentation strategy followed during the experimental test programme. The main considerations affecting the development of the strategy were as follows:

(i) to avoid positioning the instrumentation where their presence would affect the behaviour of the structure,

(ii) to site the instrumentation in positions which will enable a comparative study of the behaviour of each model arch bridge,

(iii) to permit the relocation of gauges in order to investigate phenomena observed in previous model bridges whilst attempting to preserve continuity,

(iv) to position the instrumentation so that data recorded by several of them can be combined so that a more thorough knowledge of the entire area can be obtained,

(v) to consider the usefulness of the information that each gauge is expected to produce.

(vi) to minimise the risk of damage.

3.5.1 Deflections

Deflection gauges were used to measure the radial movement of the arch barrel, the outward movement of the spandrel, wing and end retaining walls, and the vertical movement of the surface of the backfill. Typical arrangements of these gauges are shown in figures 3.9 and 3.10.

Two types of gauges were used. The majority of the gauges were potentiometer type linear displacement transducers. The manufacturers reported their precision as ± 0.1 mm although they tended to exhibit responses of the order of ± 0.05 mm which were proportional to the applied load during the non-destructive tests. A relatively small number of linear varying differential transformer (LVDT) displacement transducers were also used. These possessed a precision of ± 0.01 mm although when operated over large movements calibration tests revealed that they were slightly non-linear.

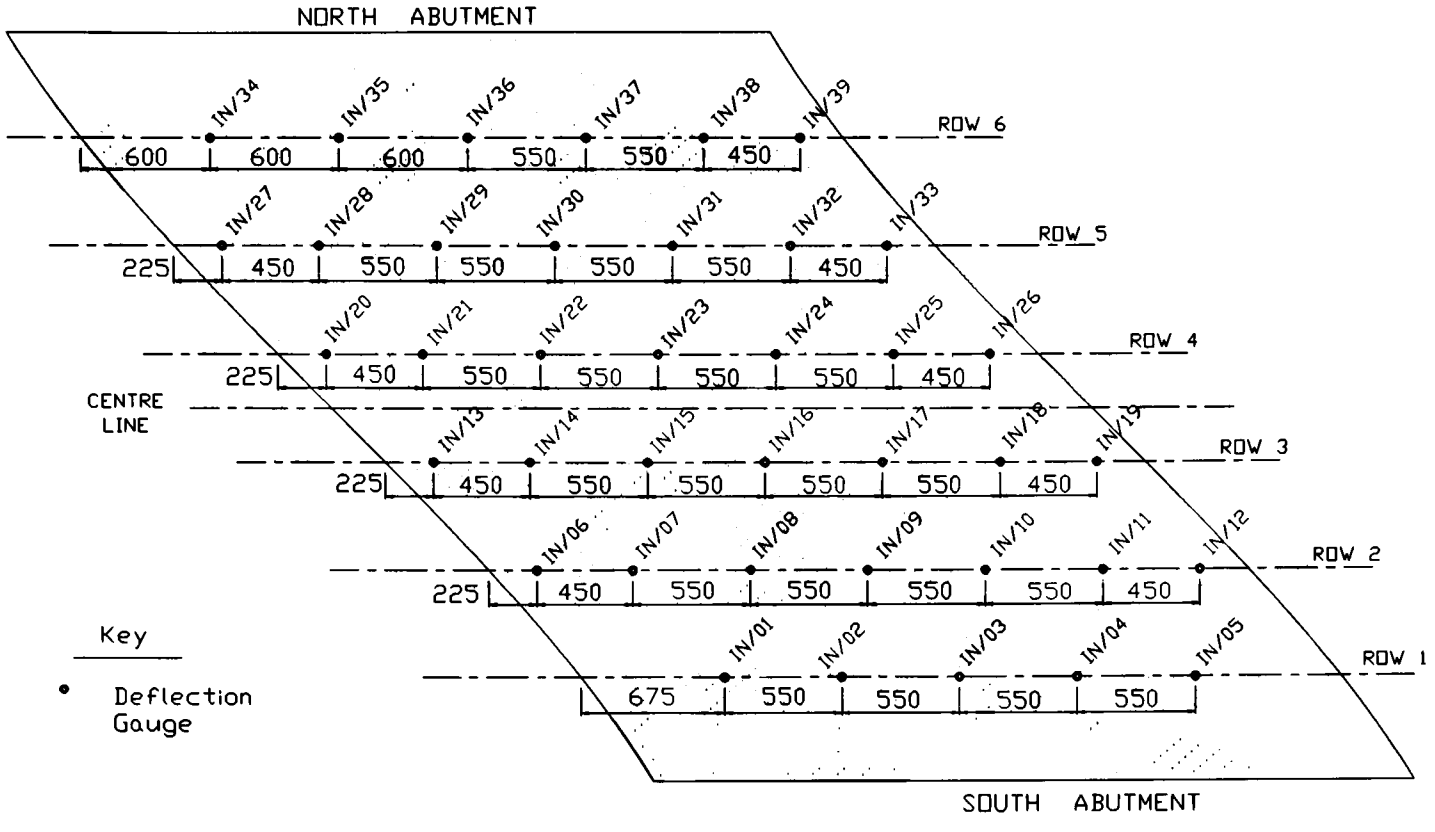

Figure 3.9 Development of the intrados showing the deflection gauges

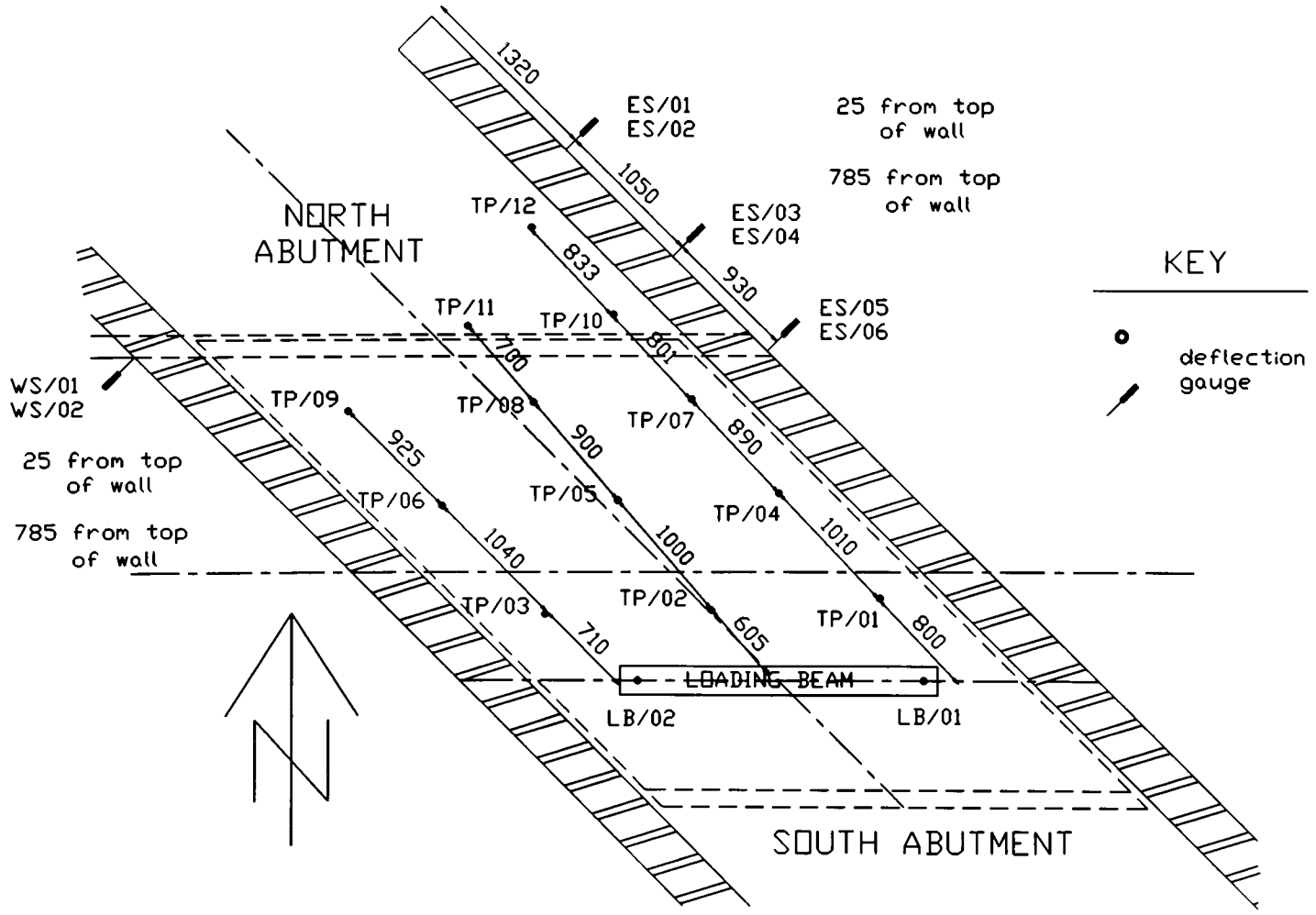

Figure 3.10 Plan on typical bridge showing surfacing deflection gauges

The deflection gauges were clamped to steel scaffolding positioned beneath the arch and around the structure. The gauges positioned on the surface of the backfill and on the intrados were arranged in regular patterns to enable contours of the deformed shape of the respective surface to be plotted. Figure 3.9 shows a typical lay out of gauges on the intrados (actually that used for monitoring bridge reference 3-3) and figure 3.10 shows a typical lay out of gauges on the surface of the backfill.

3.5.2 Surface Strains

Surface strains were measured using recoverable surface mounted vibrating wire strain gauges manufactured by "Gage Technique". These were attached to the masonry with an epoxy resin adhesive. These gauges were capable of measuring strains of the order of 2.0×10^{-6}. Their gauge length was 140 mm, which means that a tensile strain of 1789.5×10^{-6} would be required to produce a 0.25 mm crack width. This gauge length is considered to be short for application to masonry. However, the curvature of the arch and the rapid rate of change of strain with distance precluded the use of longer gauge lengths.

The measurement of surface strains was intended to provide a means of identifying the position of the line of thrust and to determine its magnitude. However, for this latter task a detailed knowledge of the constitutive stress-strain relationship for masonry having bedding joint inclined to the direction of the principal stress would be required.

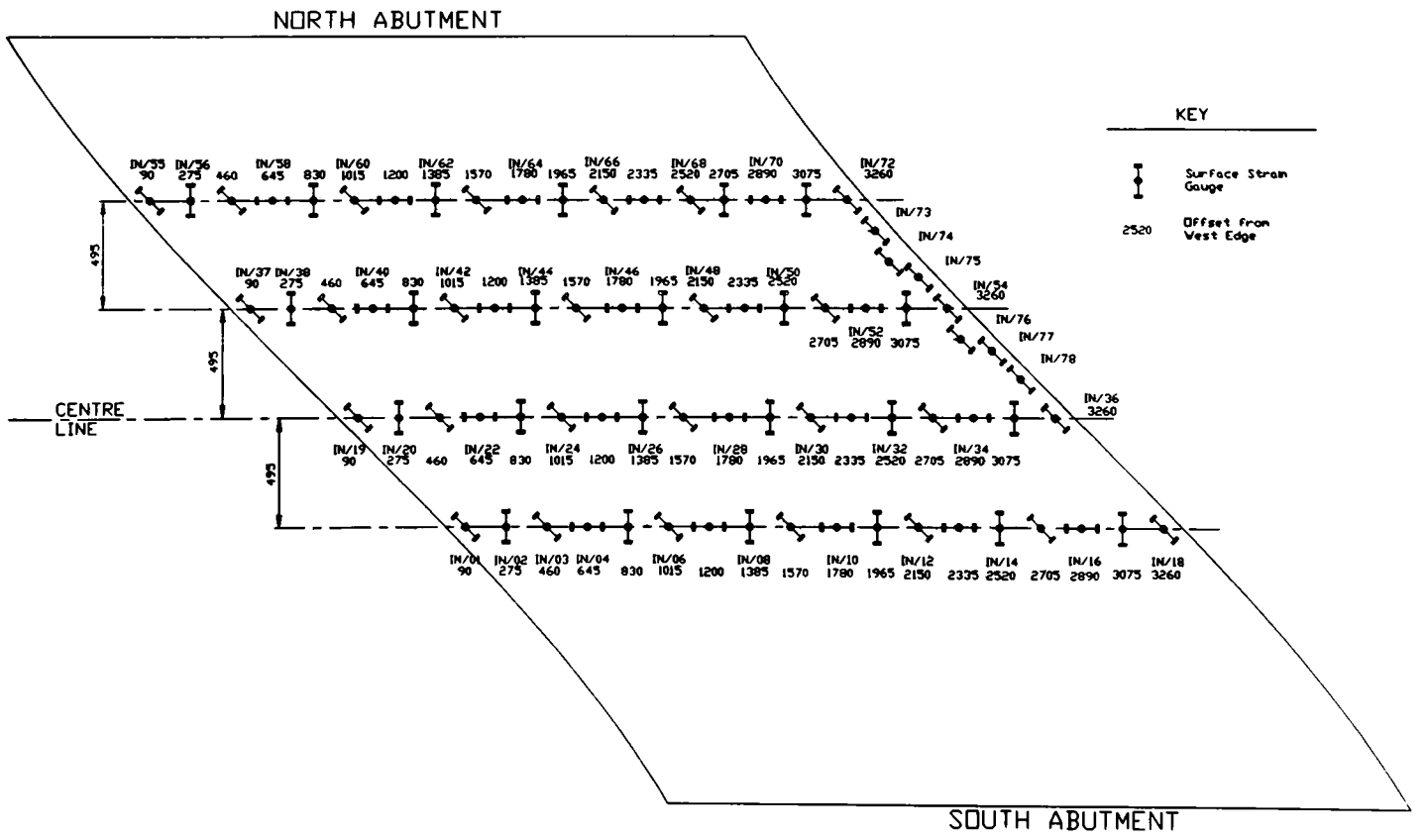

Figure 3.11 Intrados surface strain Gauges

Surface strain gauges were attached to the intrados, extrados and to each fascia. Figure 3.11 shows a typical arrangement of gauges attached to the intrados and figure 3.12 shows a typical arrangement of fascia surface strain gauges. Surface strain gauges attached to the extrados were protected from the backfill by aluminium boxes which were bolted to the masonry.

The coverage of surface strain gauges which were attached to the intrados and extrados was as dense as possible. Four rows of gauges were used on each surface to form a series of continuous virtual rectangular strain gauge rosettes. Every third gauge was oriented in the same direction. Thus, three plots were produced, one for each orientation, of the strain versus distance across the bridge. After employing curve fitting techniques the three strains at any point across the width of the bridge could be determined and used to calculate the principal strains and their orientations.

Consistency of measurements was attempted by ensuring that within the gauge length of each strain gauge a constant width of mortar joint was included. In order to achieve this, the measurements were adjusted on a pro-rata basis so that the apparent width of mortar in each direction was constant. This procedure relied upon the assumption that the strain of the mortar was much greater than the strain of the brickwork. It was hoped that this procedure would reveal information pertaining to the direction of load transference.

Two mortar joints were contained within the gauge length of those gauges which were perpendicular to the bedding joints. The number of joints contained within the gauge length of other gauges was dependent upon the skew of the bridge. However, in the direction of each gauge, the ratio of brick to mortar was comparable and thus it was reasoned that adjusting them on a pro rata basis would be sufficiently accurate to enable subsequent data manipulation.

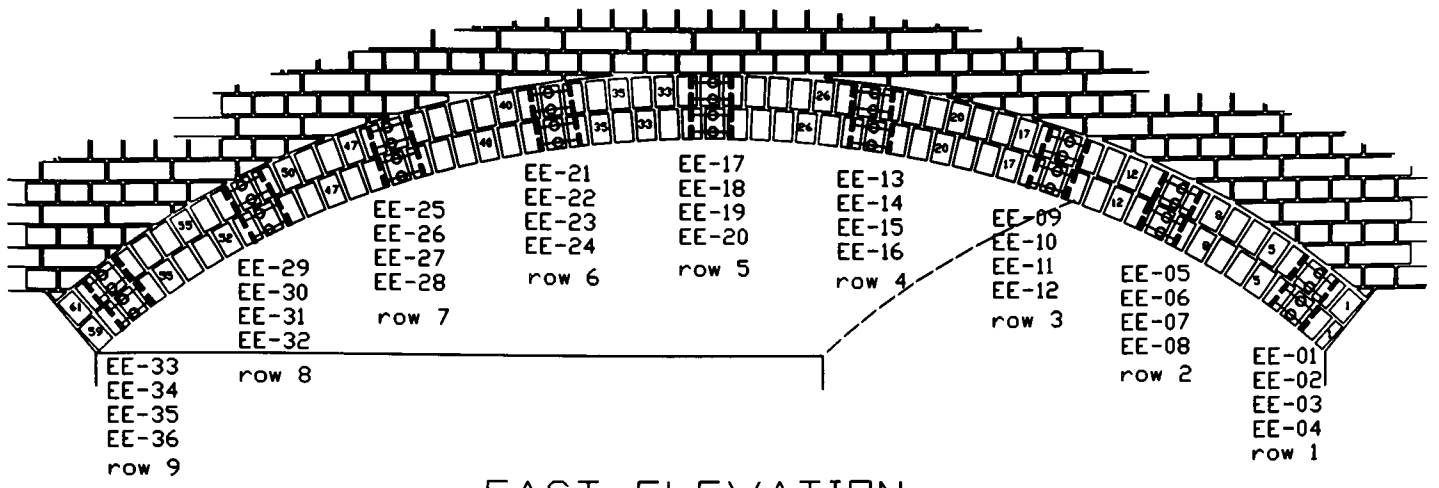

EAST ELEVATION

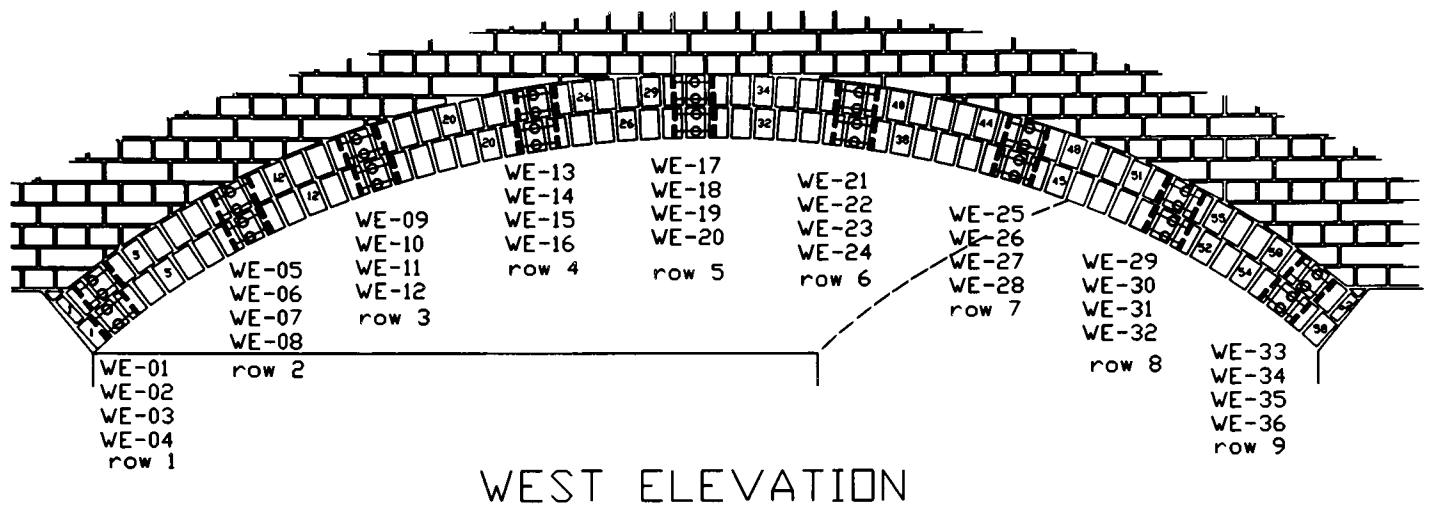

WEST ELEVATION

Figure 3.12 Fascia surface strain gauges

3.5.3 Backfill Pressures

All of the pressure cells that were used throughout this research were based on the vibrating wire principle. When each gauge had been installed into the structure a layer of fine backfill was placed over its diaphragm. This ensured that the sharp edges of larger particles could not make direct contact with the diaphragm and produce stress concentrations.

The majority of the pressure cells were Boundary Soil Pressure (B.S.P.) cells which had a 150mm diameter diaphragm. Thus, these cells were particularly susceptible to sharp edged particles. These cells were cast into a 150 × 150 mm no-fines lean-mix reinforced concrete cube. This was carried out in order to ensure that lateral pressures did not produce a Poisson's effect, i.e. an apparent reduction of the normal pressure due to a large lateral pressure. The previous practice of constructing recesses in the masonry within which cells were installed was terminated after discovering that the above Poisson's effect could be significant. Furthermore, the presence of soft-spots within the arch barrel could effect its behaviour and make measured surface strains difficult to interpret.

Figure 3.13 shows a typical response of a B.S.P. that was cast into a concrete cube and was subjected to lateral pressure only. The induced normal pressure created a very substantial apparent suction when the lateral pressure was increased to approximately 6 N/mm^2. Within the arch barrel, the compression is considerable and could cause pressure cells to register lower pressures than those which actually occurred.

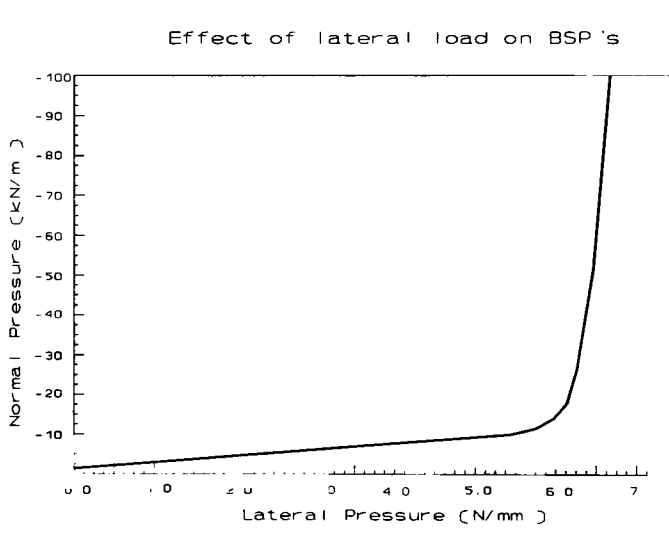

Figure 3.13 lateral loading on pressure cells

Other pressure cells which were used consisted of an oil filled double 300 mm diameter diaphragm. These tended to be more reliable since stress concentrations were alleviated by their increased size.

The principal objective behind the measurement of backfill pressures was to determine how the outward deformation of the arch affected the build up of passive pressure. The secondary objective was to determine the radial pressures which were thereby applied onto the arch. The distribution of load through the backfill was assigned a lower priority since it had been investigated under similar conditions by Gilbert (1993). Consequently, attention was given to the objectives in proportion to their relative priorities.

Figure 3.14 shows a typical arrangement of pressure cells installed within the backfill of a 3.0 m span model arch bridge (actually within bridge reference 3-4).

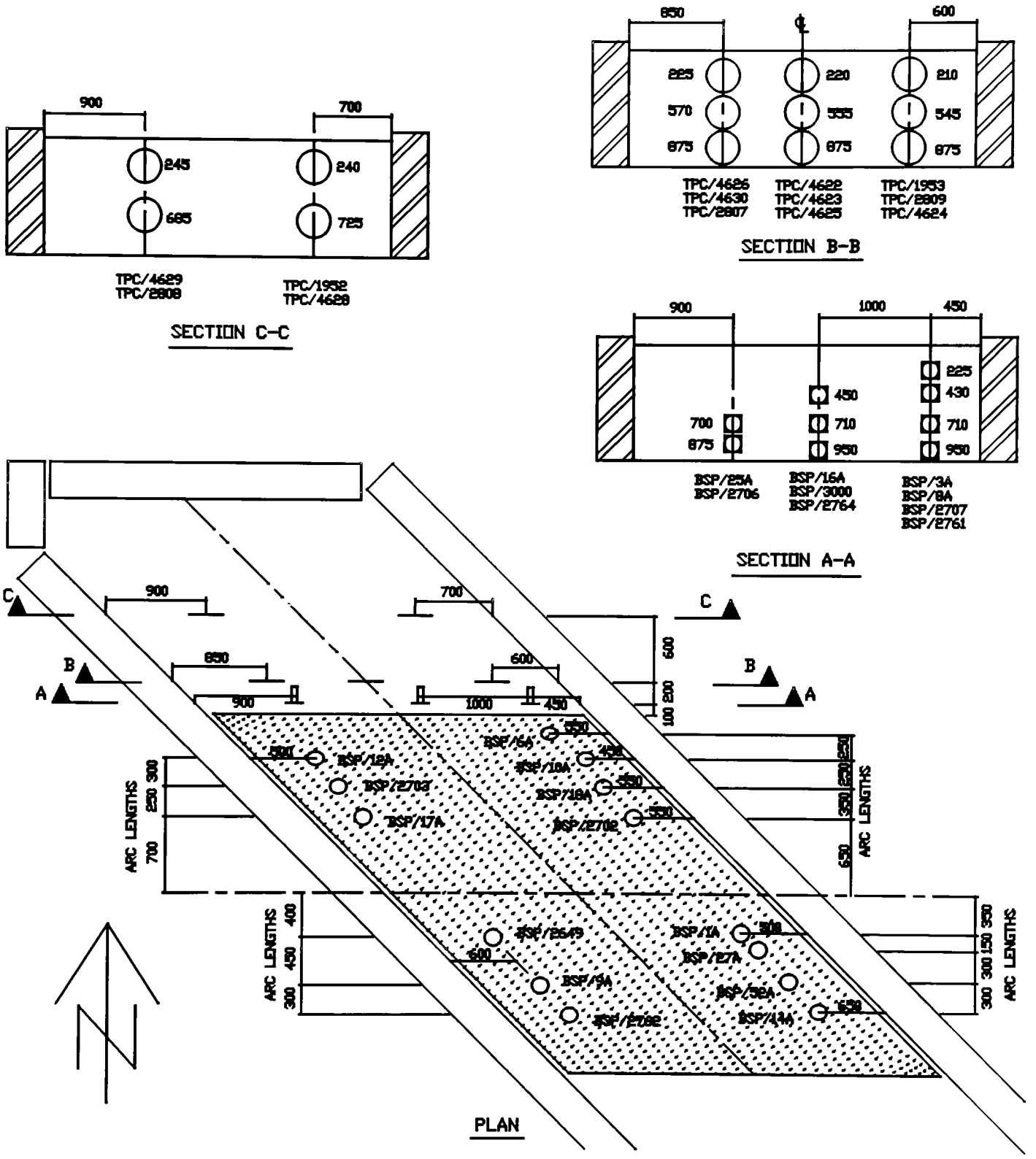

Figure 3.14 Typical arrangement of backfill pressure cells

3.5.4 Applied Load

All hydraulically applied load was measured using 1000 kN electrical resistance load cells.

3.5.5 Temperature

The ambient temperature was measured in order to adjust the data recorded on the various instruments so that results from differing load tests were more comparable. Temperatures were also recorded in order to measure how it affected each bridge.

3.6 Monitoring during Construction and prior to Load Testing

3.6.1 During Backfilling

In general, no significant changes in surface strain occurred during construction and, consistent with this, there were no observable signs of distress within any of the 3.0 m span arch bridges tested at the B.I.H.E. The exception to this was bridge reference 3-4, viz., the 45° skewed arch bridge without attached spandrel walls.

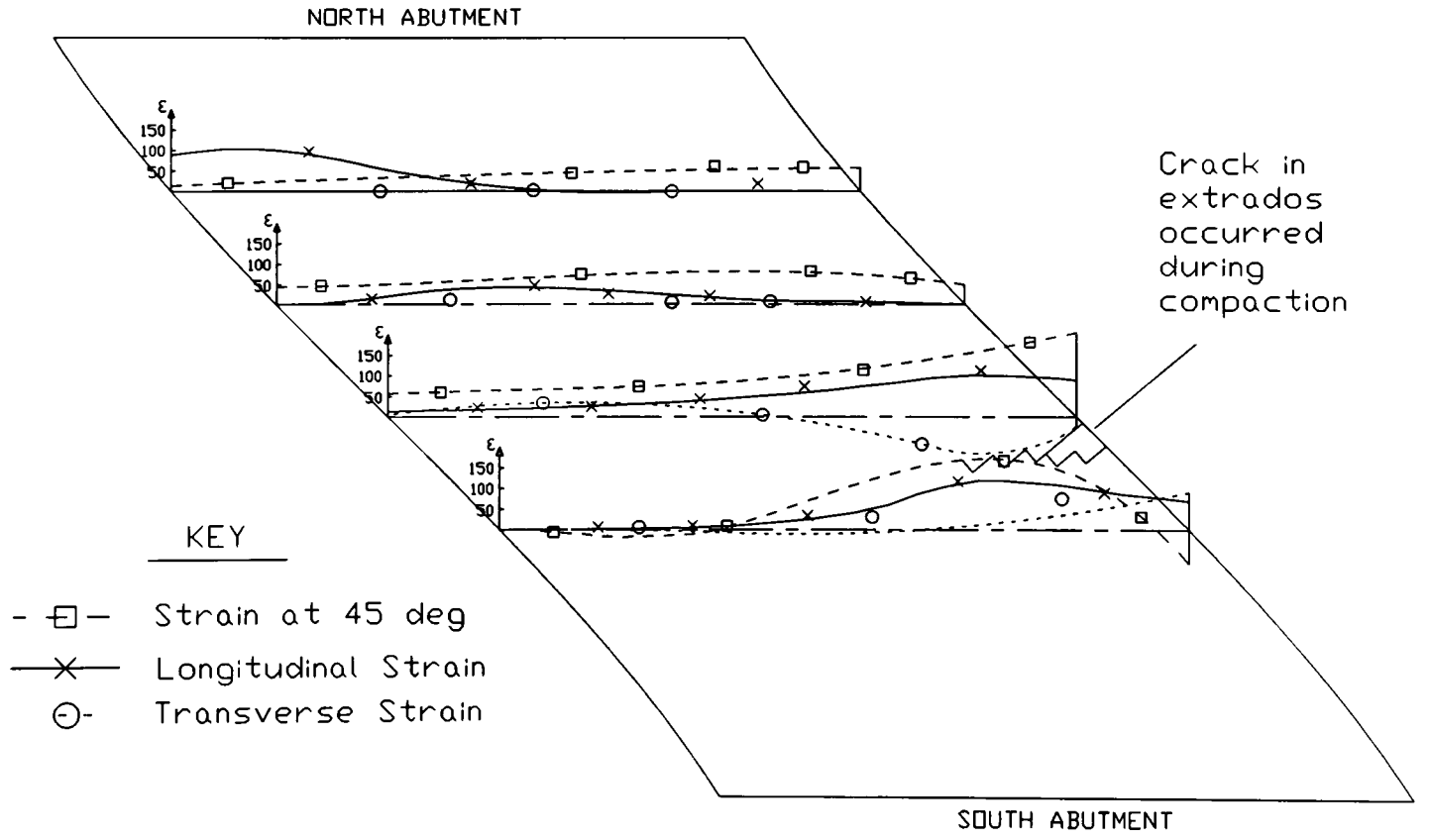

Figure 3.15 Extrados surface strains created during backfilling

The change in surface strains recorded on the extrados of Bridge 3-4 due to the backfilling operation are shown in figure 3.15. Temperature effects have been removed by subtracting strains which occurred at similar temperatures before and after construction.

Within bridge 3-4, a crack appeared in the extrados at the South side of the crown at its east edge (see figure 3.14) after the fourth 150 mm layer of backfill had been placed but not yet compacted. This crack occurred during the night and must have involved some creep effects since no immediate damage was observed when the fourth layer was placed and work suspended at the end of the working day. A feasible explanation for this crack is that this bridge suffered a downward deformation of its acute angled south haunch in conjunction with an upward movement of its crown. This was caused by the horizontal backfill compaction pressures. The absence of fill above the crown meant that the arch, and in particular each relatively weak acute angled haunch, was not capable of resisting these pressures.

The method of construction of bridge 3-3 was similar to that of bridge 3-4. Therefore the presence of attached spandrel walls must have prevented a similar crack appearing in bridge 3-3. Assuming rotational symmetry, bridge 3-4 may have cracked at the North side of the crown at its west edge. However, the dense array of pressure cells installed within this region inhibited the same degree of compaction and so no crack appeared.

The flexibility of the acute angled haunch of a highly skewed arch increases the likelihood of the above damage. The obtuse angled haunches are much stiffer as are the acute angled haunches of lesser skewed arch bridges (Bridge 3-1 did not suffer any distress during backfilling).

Clayton and Symons (1992) showed that a vertical retaining wall which is not rigid would be subjected to relatively high horizontal pressures when the retained fill is compacted. They showed that the pressure distribution shifts from being a linear function of depth to being hyperbolic i.e., asymptotic to both the pressure axis and the original active pressure line. However, due to yielding of the fill, the pressure near the surface reduces to a value which is proportional to depth as defined by the K_r ($= 1/K_a$) line.

When the soil is placed and compacted in layers, yielding of successive layers results in an approximately constant pressure distribution down to a depth at which active pressures become more significant. They concluded that this depth would not exceed 3.0-4.0 m and that compaction pressures would not exceed 20-30 kN/m^2.

Figure 3.16 shows the increase in pressure recorded above the North abutment of bridge 3-1, 3-3 and 3-4. High compaction pressures were recorded which were far in excess of "at-rest" pressures. Although compaction pressures did not exceed 30 kN/m^2, as Clayton and Symons concluded, they remained proportional to depth and extrapolation of figure 3.16 would reveal that they would remain significant well below their proposed 4.0 m limit. This may indicate that complete yielding of the surface of each layer did not occur, so the horizontal pressure did

not reduce to zero and a build up of pressure occurred.

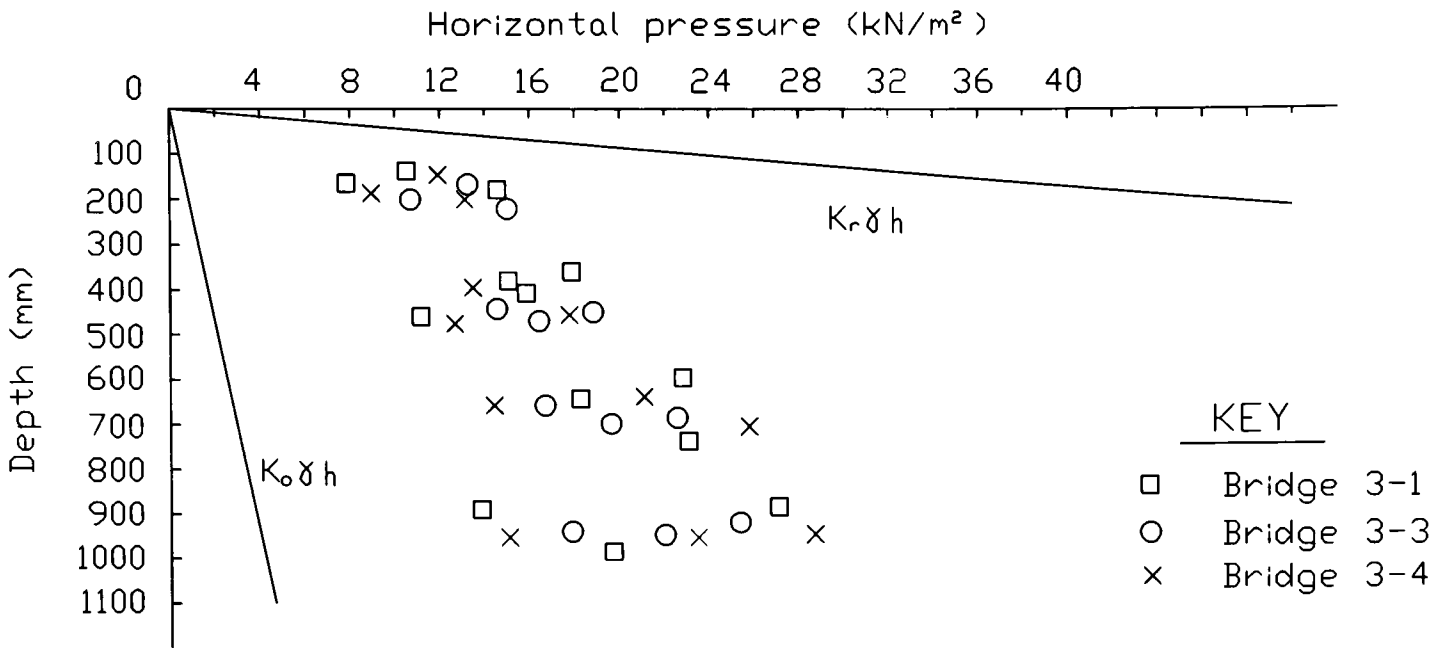

Figure 3.16 Horizontal Compaction Pressures

In actual bridges, the compaction pressure is not known. However, it is logical to conclude that the first few metres of backfill may be highly compacted due to modern trafficking. Below this layer, poor waterproofing may permit erosion of fine material and prohibit the build up of stabilising passive pressures that are required to assist the arch in supporting applied loads.

Mechanical compaction of the spandrel fill has the effect of enabling relatively large passive pressures to be generated through small outward deformations of the arch barrel. The maximum outward deflection of an arch bridge at failure is small enough for analysts to rightly assume that geometrical changes need not be taken into account. Large deformations only take place after failure. However, in a well compacted material the small pre-failure movements can still produce significant backfill pressures.

It is not possible to accurately measure the deflection of the arch during backfilling. A similar square span segmental arch would experience a ubiquitous strain of 157×10^{-6} if its shape remained segmental whilst its crown deflected downwards by 0.5 mm. Therefore, in the case of Bridge 3-4, oblique compressive strains of approximately 100×10^{-6} were consistent with a deflection of 0.5 mm at the crown.

3.4.2 During Decentring

There were no significant changes in either surface strains or backfill pressures which occurred during decentring any of the four skewed arch bridges within this research.

3.4.3 Effects of Temperature Change

Figure 3.17 shows typical ambient temperatures of the laboratory within which each model arch bridge was constructed. In addition, the temperature 100 mm above the crown of the arch within the spandrel fill is also shown.

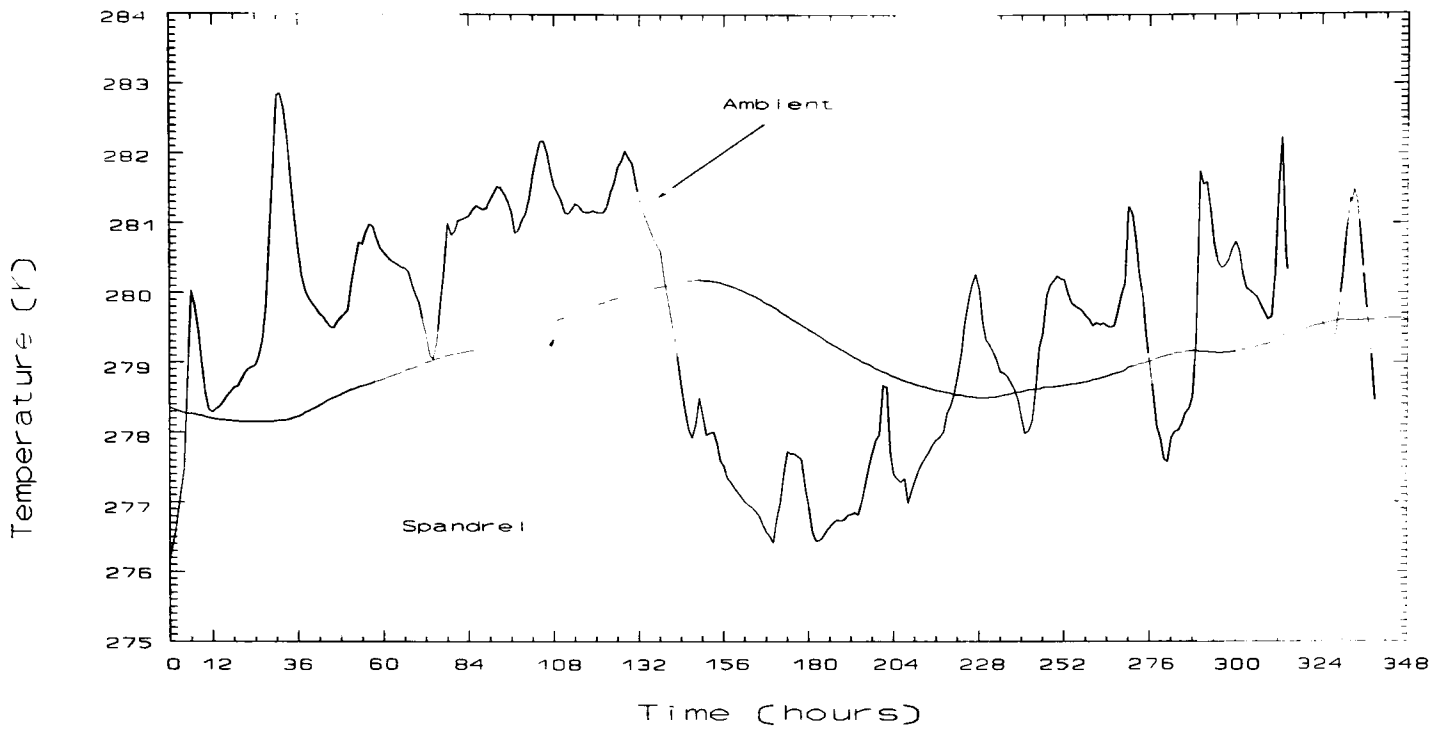

Figure 3.17 Changes in temperature

Figure 3.18 shows the recorded surface strains measured at two corresponding points at the crown of arch bridge reference 3-4 (one on the intrados and the other on the extrados) when subjected to the above temperature changes.

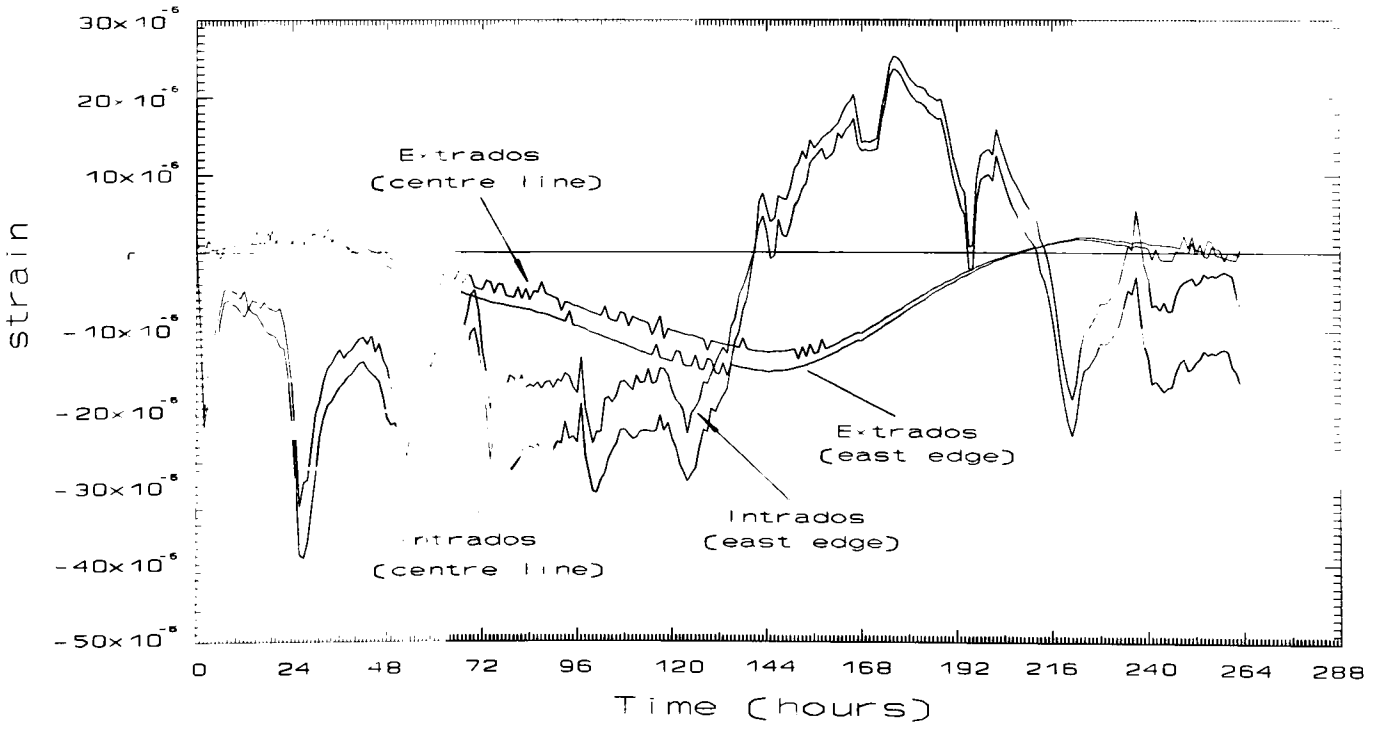

Figure 3.18 Temperature strains at the crown of skewed arch 3-4

It is noticeable that the backfill acts as an insulation material which does not create a lagging effect upon the temperature-time relationship but dampens it so that the temperature change within the backfill is always towards the ambient temperature.

The response of the arch barrel to temperature changes, as shown in figure 3.17, was calculated by taking the sum of the recorded strains and the theoretical thermal expansion of the vibrating wire. The latter term was calculated as the product of the measured temperature difference near the appropriate surface and the coefficient of thermal expansion of steel (12×10^{-6}).

Figure 3.19 is a repeat of the temperature response presented in figure 3.18 with the exception that surface strain gauge reference IN/29 is included. The data extracted from this gauge appeared to poses a time dependent component which gradually increased compressive strains.

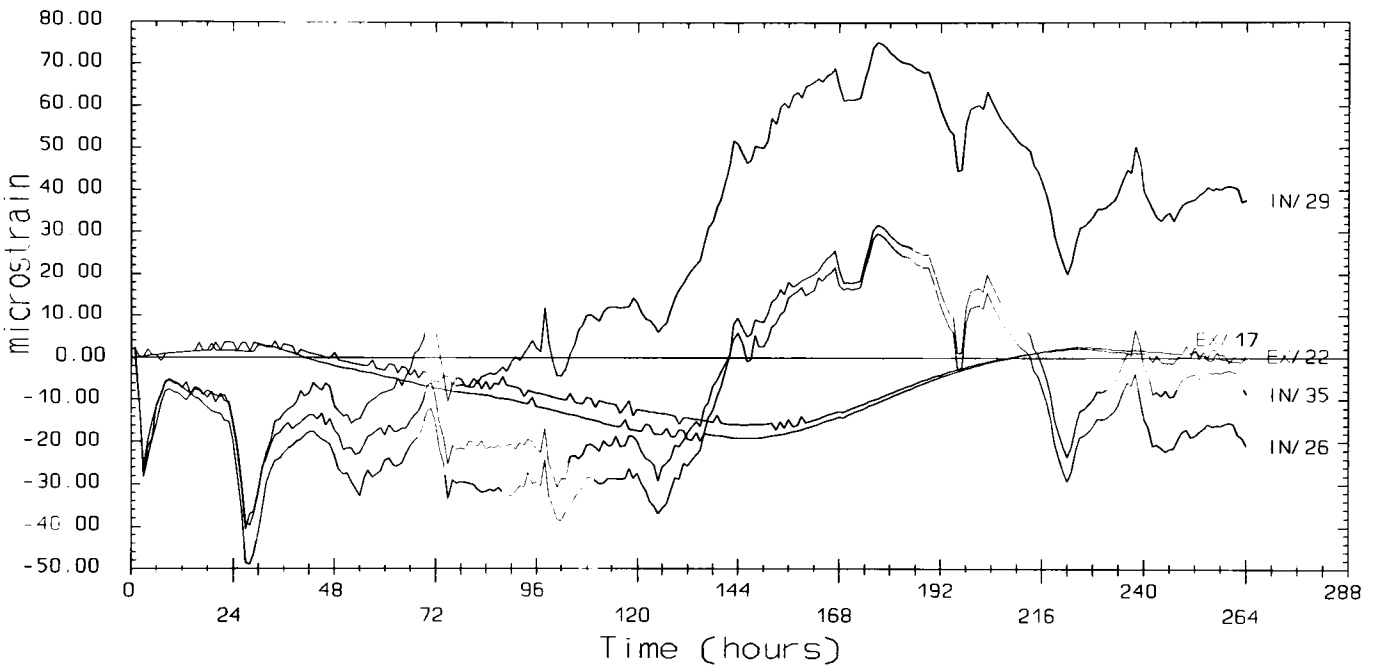

Figure 3.19 Temperature strains

This phenomenon is due to poor quality adhesive which had remained malleable after the strain gauge had been attached to the masonry. The tension within the vibrating wire was thus able to pull together the end blocks so that an apparent compression was produced.

Many gauges exhibit this effect to a lesser or greater degree; when it becomes too great the gauge must be reattached. Obviously, an increase in strain of approximately 80×10^{-6} over a period of 264 hours is small since over the duration of the failure load test (say 12 hours) this would amount to an increase in strain of 4×10^{-6}. However, in this case, this was deemed to be unacceptable since there would be a lengthy time between monitoring temperature effects and carrying out the destructive test. Therefore gauges producing effects as pronounced as this were removed and reattached prior to the start of the non-destructive tests.

4.0 Results of the Non-destructive Tests

4.1 Visual Observations

The application of the 10.0 T, or 12.5 T, point loads onto the 3.0 m span model arch bridges did not produce any observable cracks within the arch barrel of any of the bridges tested in this manner. Similar observations were made when the barrel-only structure, bridge reference 3-2, was subjected to a 50 kN point load. The exception to this was the ring separation that propagated within the 45° skewed arch bridge without attached spandrel walls, i.e. bridge reference 3-4. This structure suffered distress during backfilling since the relatively weak acute angled haunches were unable to resist the compaction pressures. Thus, a crack was observed in the extrados at its crown which was accompanied by the initiation of ring separation. This ring separation was propagated by the application of successive point loads.

Cracks between the attached spandrel wall and the arch barrel of bridge reference 3-3 were observed in the vicinity of the point of application of the eccentric point loads. These cracks were propagated when the load was repositioned and a further load test performed.

4.2 Deflections

It is necessary to introduce some terms that will be used throughout the remaining text to describe the behaviour of the model arch bridges. Longitudinal arching occurs along a line that passes through the point of application of the load when drawn from one abutment to the other. This type of behaviour has been understood for many years since the two-dimensional experiments of Danyzy (1732). Beneath the load, the downward (i.e. inward) deflection of the arch will be ascribed a negative value. Remote from the point of application of the load, the upward (or outward) deflection of the arch will be ascribed a positive value. This type of upward and downward deflection may also occur in the case of transverse arching action along a path that is parallel to the abutments.

A significant proportion of the deflection of each arch barrel was found to be non-recoverable. The redistribution of the spandrel fill and its increased compaction would contribute towards the arch being unable to return to its original form when the load was removed. Another contributory factor is that the superimposed patch loads cause the arch to undergo localised shortening due to the increased compression within it.

Figure 4.1 shows the deflection of an arch as measured by deflection gauges positioned along the row nearest to the point of application of the load. Figure 4.1 shows a typical response of an arch bridge but is actually that of bridge 3-3 along row 2 (see figure 3.8) when subjected to

a point load at position P_1 (see figure 3.7).

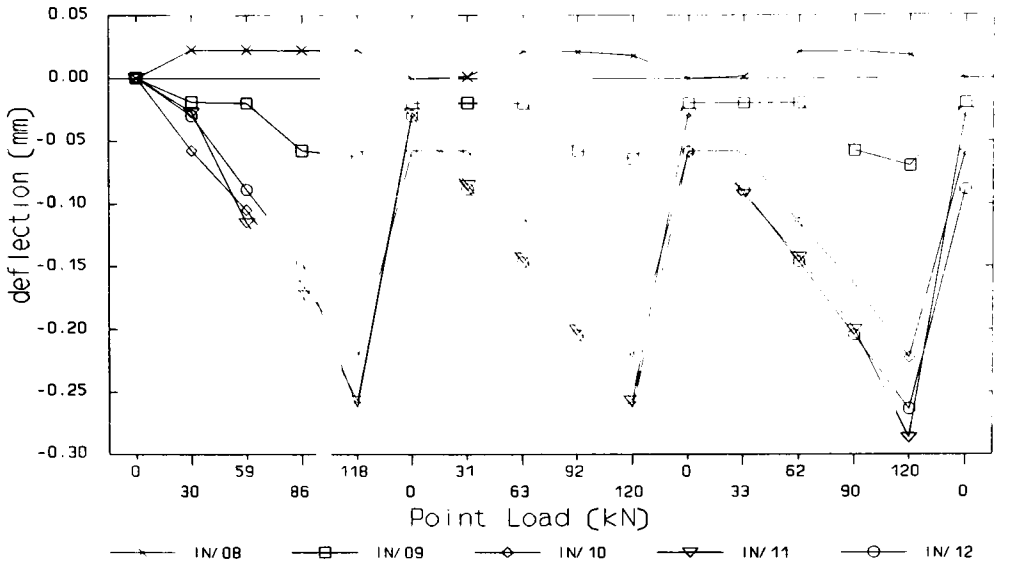

Figure 4.1 Typical Load-Deflection Response

It can be seen that the majority of the non-recoverable deflection generally occurred during the first load-unload cycle. The amount of additional non-recoverable deflection that occurred in subsequent load-unload cycles was a small proportion of that which occurred in the initial cycle.

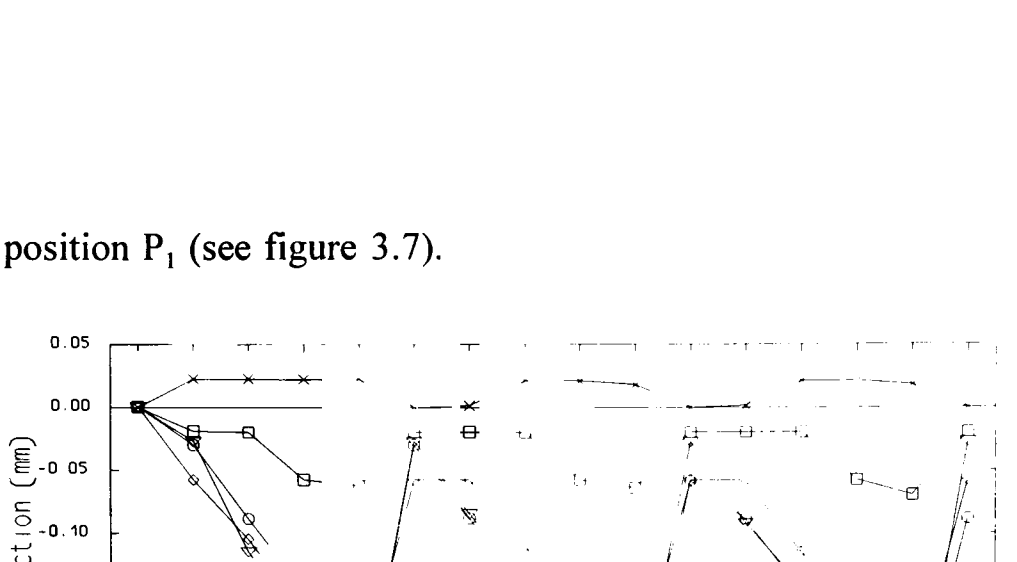

Figure 4.2 Intrados deflections along row 4 of bridge 3-3 during test P_1

The exception to this, as shown in figure 4.2, was that very early in its working life the arch bridge with attached spandrel walls, viz. reference 3-3, lost the mortar bond between the arch and its spandrel walls and thus the barrel became more flexible. A non-linear response to the applied load was produced, especially during the first load cycle, and non-recoverable deflections continued to occur during each subsequent load cycle.

In figure 4.2, during the first load cycle, and in figure 4.1, throughout each load cycle, it can be

seen that deflection gauges located remote from the load position recorded a small reaction to the load which was less than the reported accuracy of the instrumentation. However, it cannot be coincidental that, even at this magnitude, their response was dependent on the magnitude of the load and not random. Hence, data recorded by all gauges which exhibited a definite response to the load were used in the curve fitting exercise through which the contour plots of the deformed shape of each arch (see figure 4.3 to 4.12 inclusive) were generated.

Figure 4.3 and 4.4 show the development of the intrados of arch bridge 3-1 on which its deflected shape, when subjected to an eccentric point load applied above the acute and obtuse angled haunch respectively, is shown as a series of contours. Transverse arching action can also be observed.

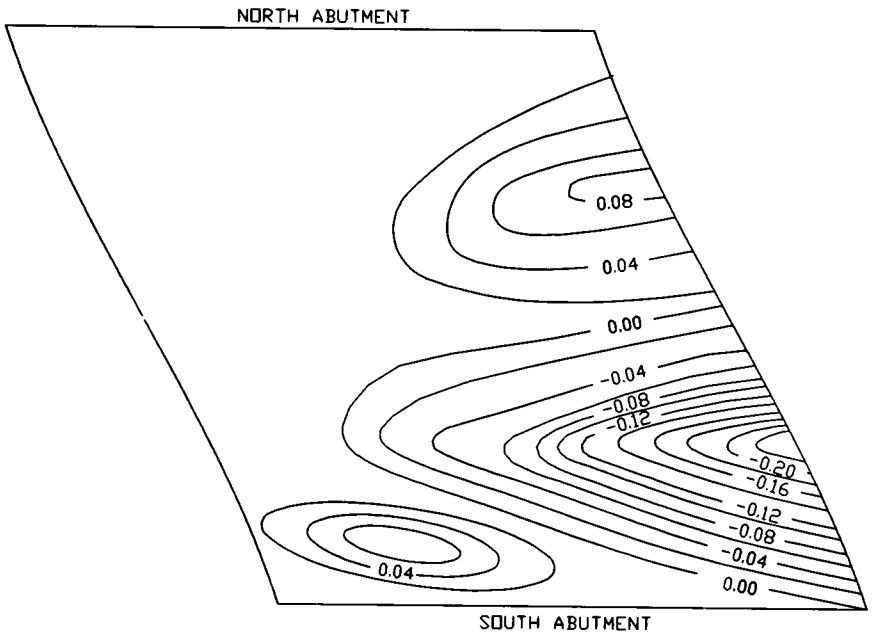

Figure 4.3 Deflected shape of bridge ref. 3-1 with 100 kN point load at P_1

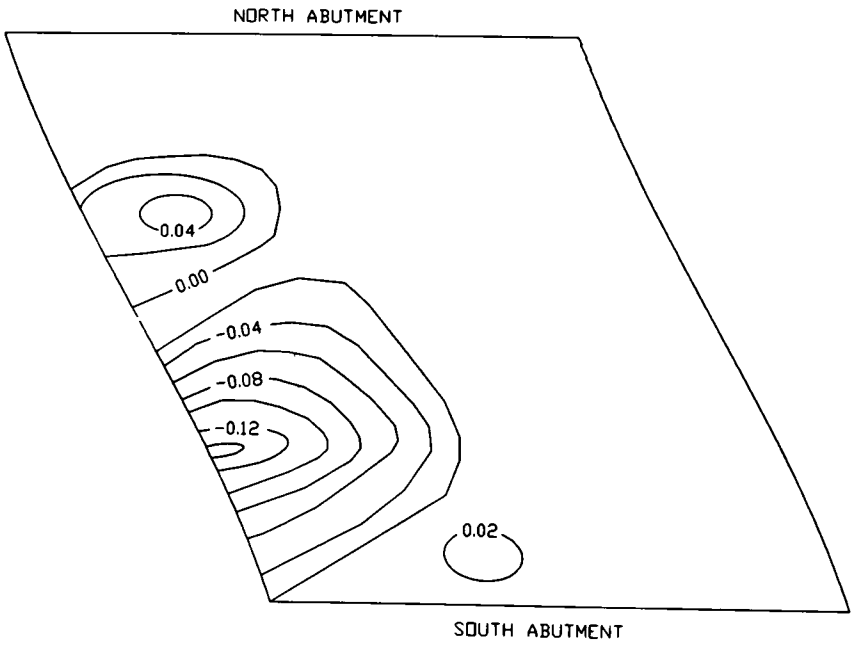

Figure 4.4 Deflected shape of bridge ref. 3-1 with 100 kN point load at P_4

Figures 4.5 and 4.6 show the development of the intrados of arch bridge 3-2 on which its deflected shape, when subjected to eccentric point loads applied on the acute and obtuse angled haunches respectively, is plotted as a series of contours.

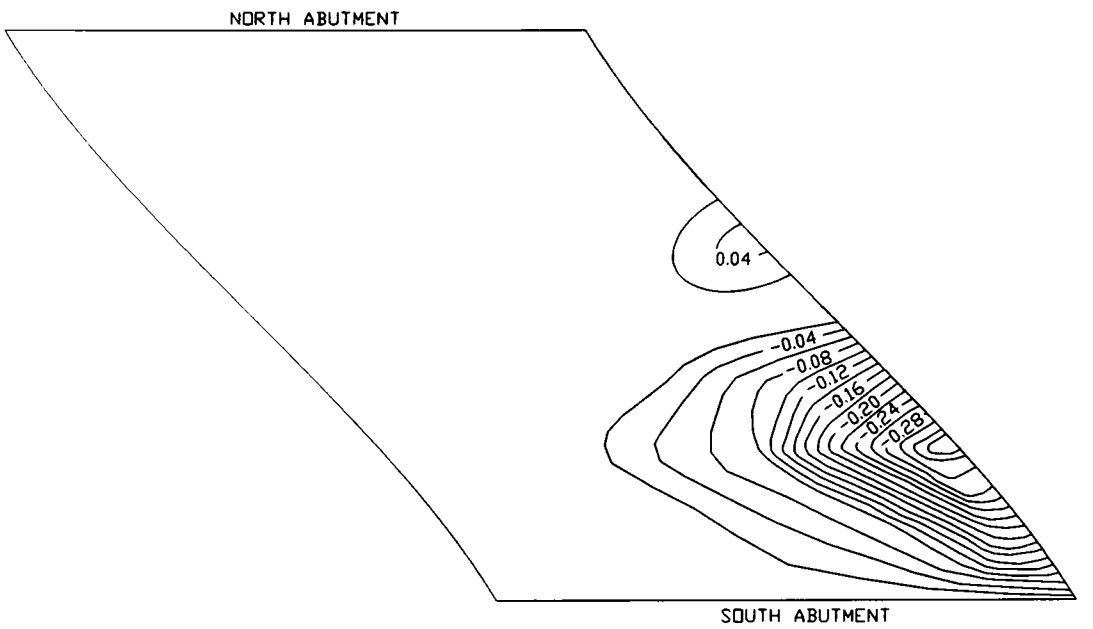

Figure 4.5 Deflected shape of bridge ref. 3-2 with 50 kN point load at P_1

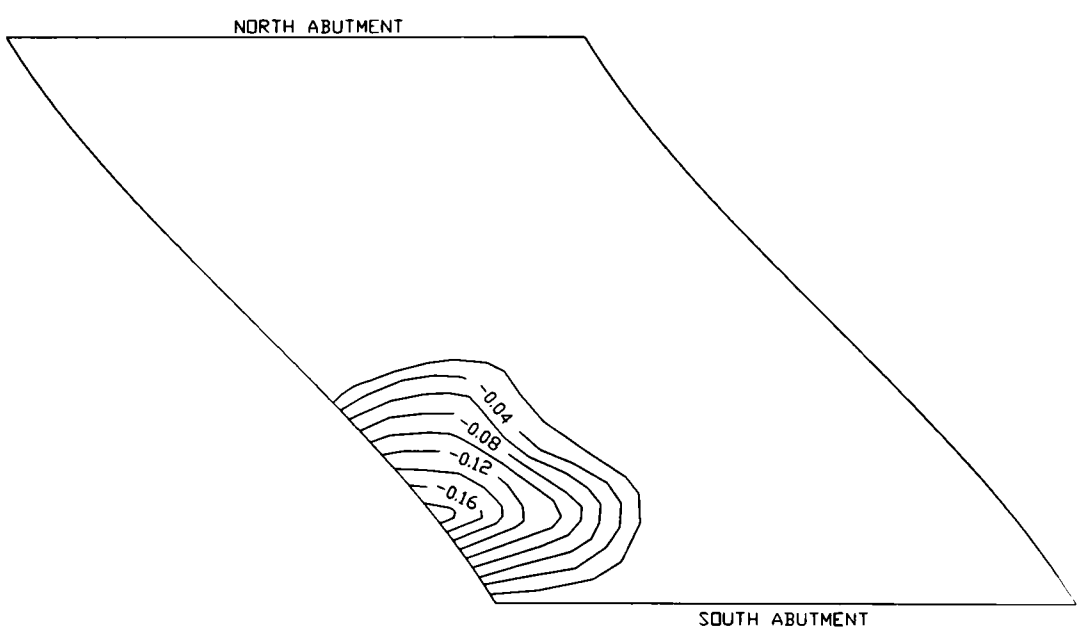

Figure 4.6 Deflected shape of bridge ref. 3-2 with 50 kN point load at P_4

Mortar pads were cast onto the extrados of this arch so that localised stress concentrations could not be created. However, despite this precaution, the magnitude of the load was not increased beyond 50 kN because it was felt that, without backfill to disperse the applied load, localised failures could occur which would influence the future behaviour of the arch. Consequently, the deflections were small and it was unlikely that outward deflections would be recorded in this case.

Figures 4.7 and 4.8 show the development of the intrados of arch bridge 3-3 on which its deflected shape, when subjected to an eccentric point load applied above the acute and obtuse angled haunch respectively, is plotted as a series of contours.

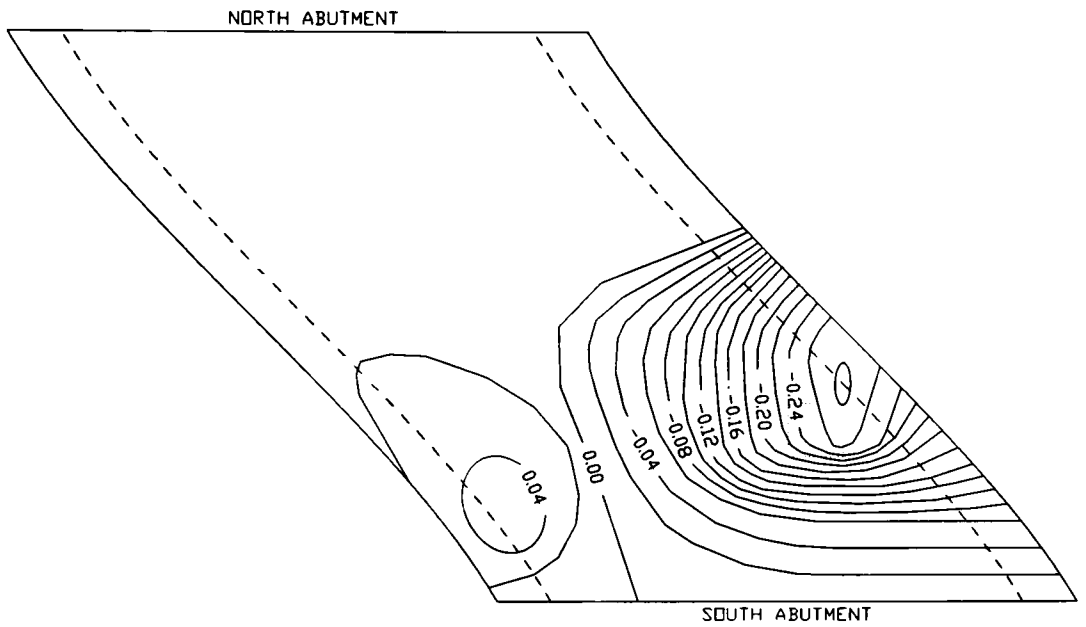

Figure 4.7 Deflected shape of bridge ref. 3-3 with 125 kN point load at P_1

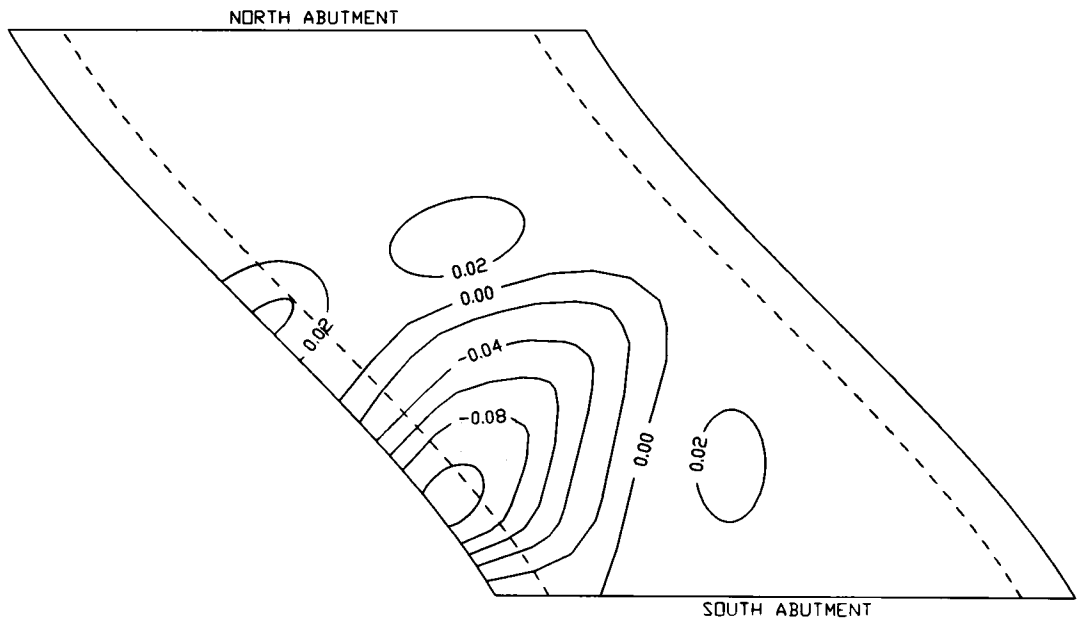

Figure 4.8 Deflected shape of bridge ref. 3-3 with 125 kN point load at P_4

When loaded at position P_1, it can be seen that small outward deflections occurred at a transverse distance from the load. When loaded at position P_4, it can be seen that small outward deflections occurred at locations situated around the periphery of the region of inward deformation. In this case, both transverse and longitudinal arching action occurred.

The difference between the two haunches is evident; the acute angled haunch had the apparent stiffness of 445 kN/mm whilst the obtuse angled haunch was much stiffer with an apparent stiffness of 1250 kN/mm.

Figures 4.9 and 4.10 show the development of the intrados of arch bridge 3-4 on which the deflected shape, when subjected to an eccentric point load applied above the acute and obtuse angled haunch respectively is plotted as a series of contours.

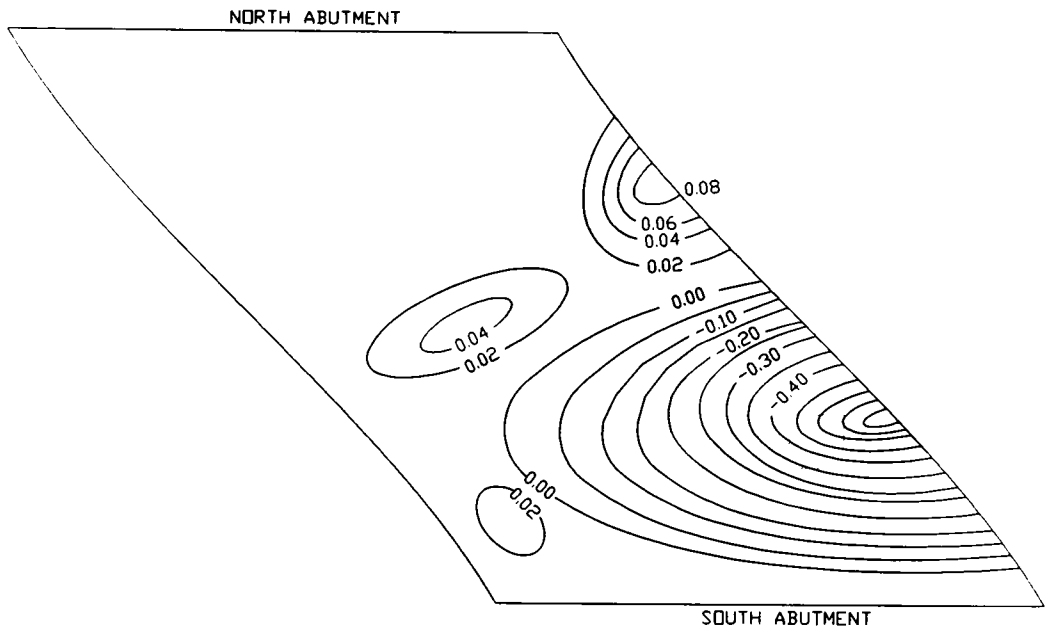

Figure 4.9 Deflected Shape of Bridge ref. 3-4 due to a 100 kN Point Load at P_1

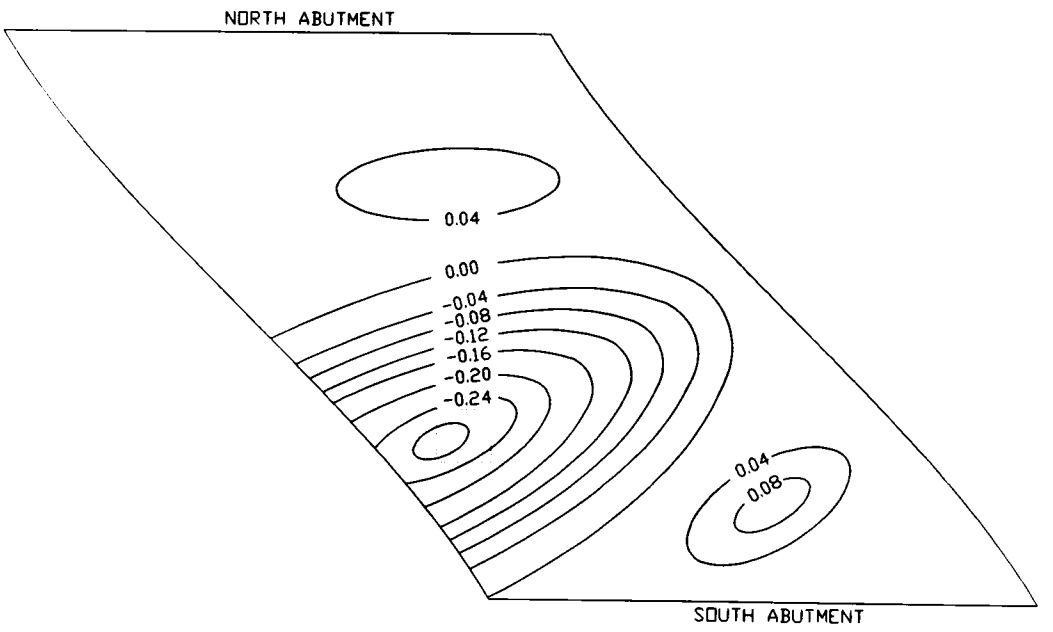

Figure 4.10 Deflected Shape of Bridge ref 3-4 due to a 100 kN Point Load at P_4

As with the arch bridge with attached spandrel walls, this bridge also reacted to eccentric point loads by twisting which produced both transverse and longitudinal arching action. This bridge was much more flexible than the arch bridge with attached spandrel walls (the acute angled haunch had an apparent stiffness of 165 kN/mm whilst that of the obtuse angled haunch was 355 kN/mm) although, as will be seen later, this was not solely attributable to the detachment of the spandrel walls.

Figure 4.11 and 4.12 show the development of the intrados of arch bridge 3-0a and 3-0d on which the deflected shape, when subjected to an eccentric point loads applied at the south quarter-point and offset by 750 mm from the centre line, is plotted.

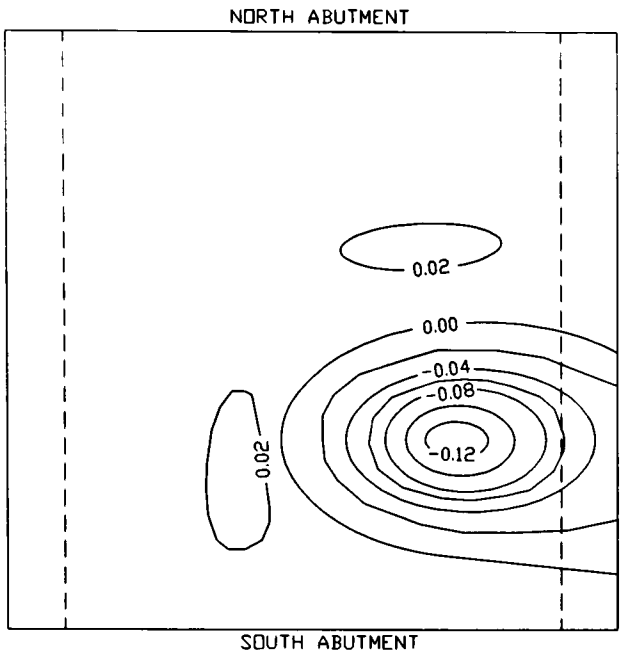

Figure 4.11 Deflected shape of arch 3-0a with 125 kN point load at P_1

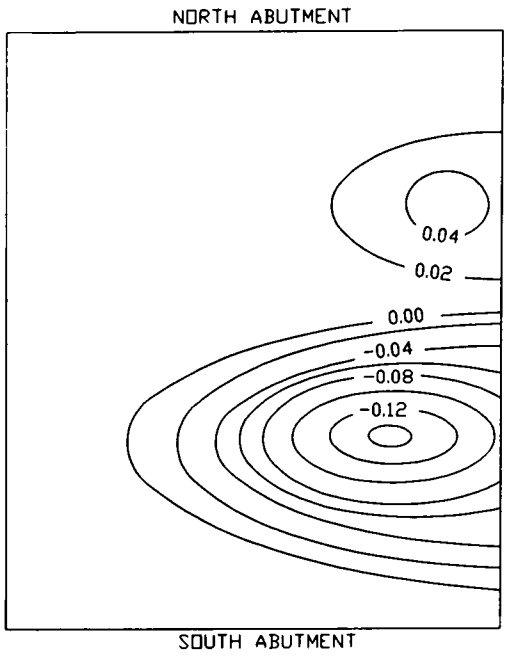

Figure 4.12 Deflected shape of arch 3-0d with 100 kN point load at P_1

Several observations can be made following a comparative study of the deflected shapes of each of the arch bridges when subjected to eccentric concentrated loads (Melbourne & Hodgson, 1995b). Both longitudinal and transverse arching action occurred in each arch bridge except bridge 3-2 in which only a localised reaction to the load was recorded.

The acute angled haunch of a skewed arch is much more flexible than the obtuse angled haunch. The deformation produced by a load positioned above the acute angled haunch is much more widespread than a similar load above the obtuse angled haunch. In this case, significant transverse arching was produced. Longitudinal arching is inhibited by attached spandrel walls. The difference between the response of bridge 3-0a and 3-0d and the response of bridge 3-3 and 3-4 illustrates the effects of spandrel walls. When spandrel walls are detached the arch becomes more flexible and permits more pronounced longitudinal arching action.

The deflected shapes reveal that the response of a skewed arch bridge to an applied load has an affinity for the obtuse angled corners. When loaded above the obtuse angled haunch, bridge 3-3 with its attached spandrel walls caused the deformed region to extend towards the north abutment obtuse corner.

4.3 Surface Strains

Surface strain measurements were generally in agreement with the data extracted from the deflection gauges. However, a more global response to the applied load was observable since the sensitivity of the strain gauges was much greater than that of the deflection gauges. Transverse arching was detected as a reversal in the sign of the measured strains at locations that were remote from the applied loads.

Figure 4.13 shows the surface strains as recorded by gauges positioned along row 1 (see figure 3.10) on the intrados of bridge reference 3-1 when it was subjected to a load at position P_1 (see figure 3.12).

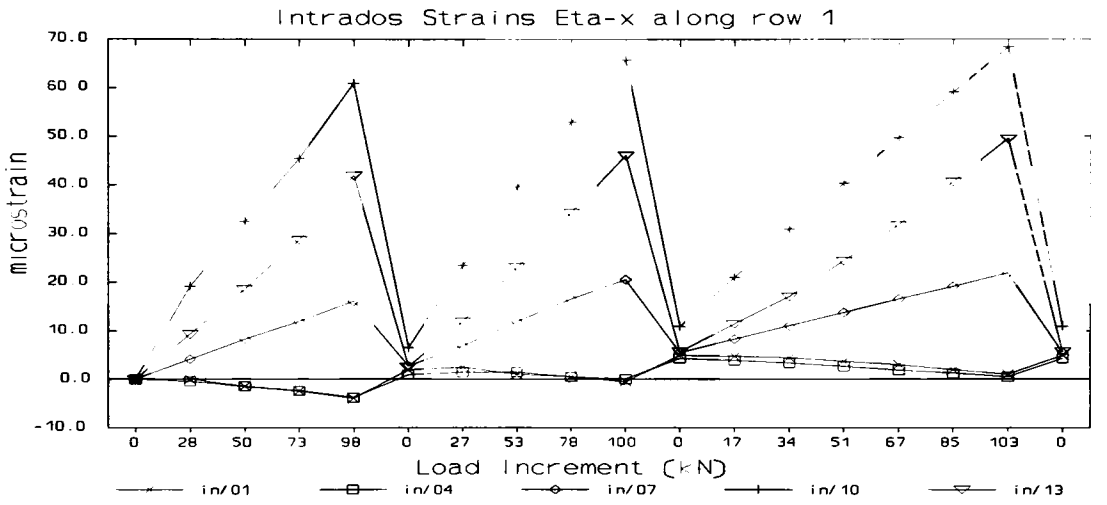

Figure 4.13 Intrados Surface strains along Row 1 of Bridge ref. 3-1 during the test at P_1

As can be seen, the response of the arch as measured by each surface mounted strain gauge was linear and proportional to the magnitude of the load. These responses were typical of each gauge situated throughout the arch provided that it was sufficiently sensitive to detect structural movements. Furthermore, the distribution of the strain in the transverse direction is immediately noticeable. A relatively large compressive strain occurred along the perpendicular between the point of application of the load and the south abutment. The strains adjacent to this path were compressive but not as great. Towards the obtuse angled haunch there was a reversal of the sign of the strains as tensile strains were recorded albeit relatively small strains.

Figure 4.14 and 4.15 illustrate the distribution of surface strain far more effectively than figure 4.13. It is evident that, even at a moderate skew of 23°, when a point load is situated above the acute angled haunch the response of the arch is very much different from its response when the load is situated above the obtuse angled haunch. Thus, the creation of simple rules by which the behaviour of a skewed arch can by modelled in two-dimensions will be difficult.

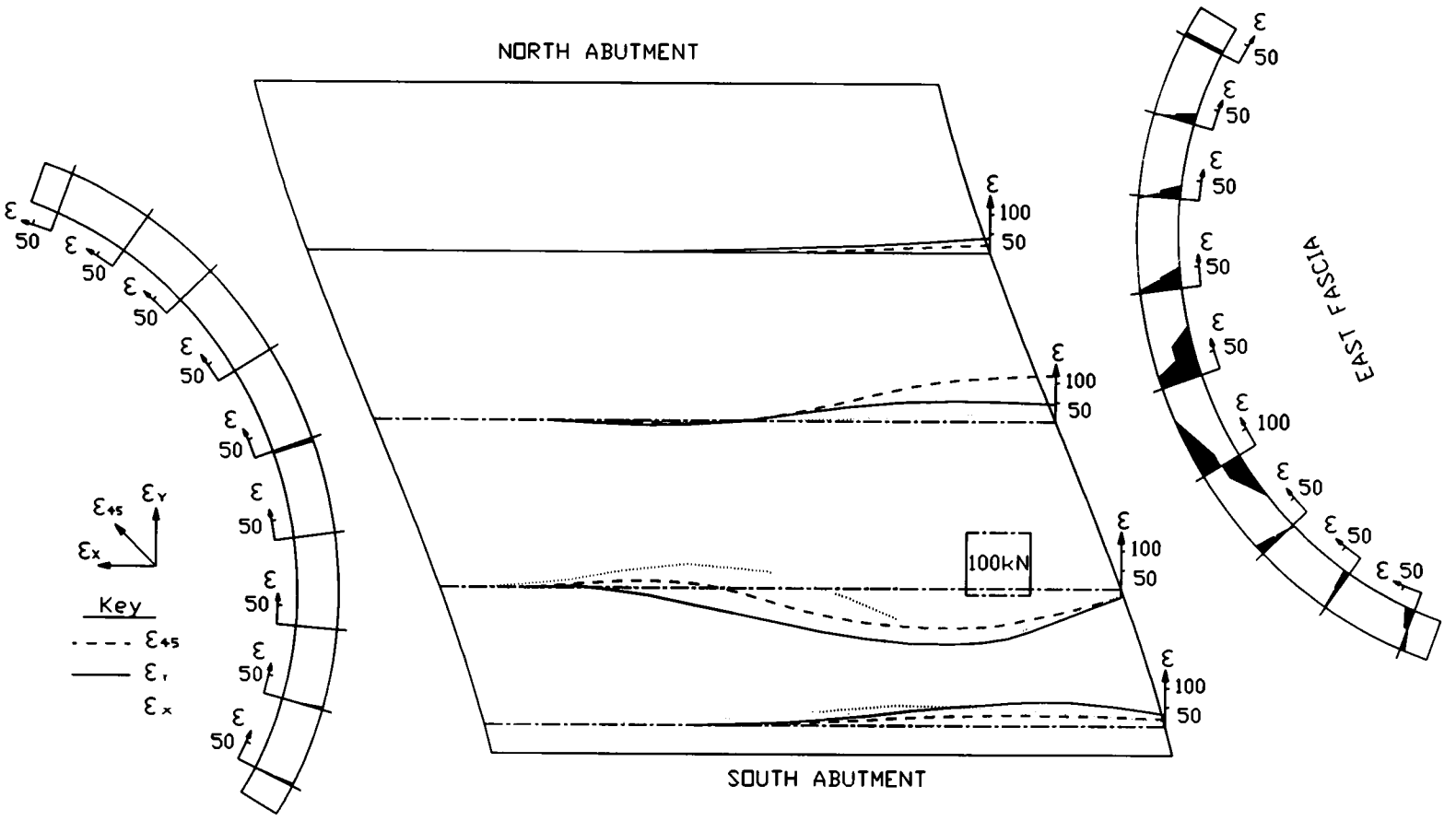

Figure 4.14 Surface Strains on bridge 3-1 due to a 100 kN Point Load at P_1

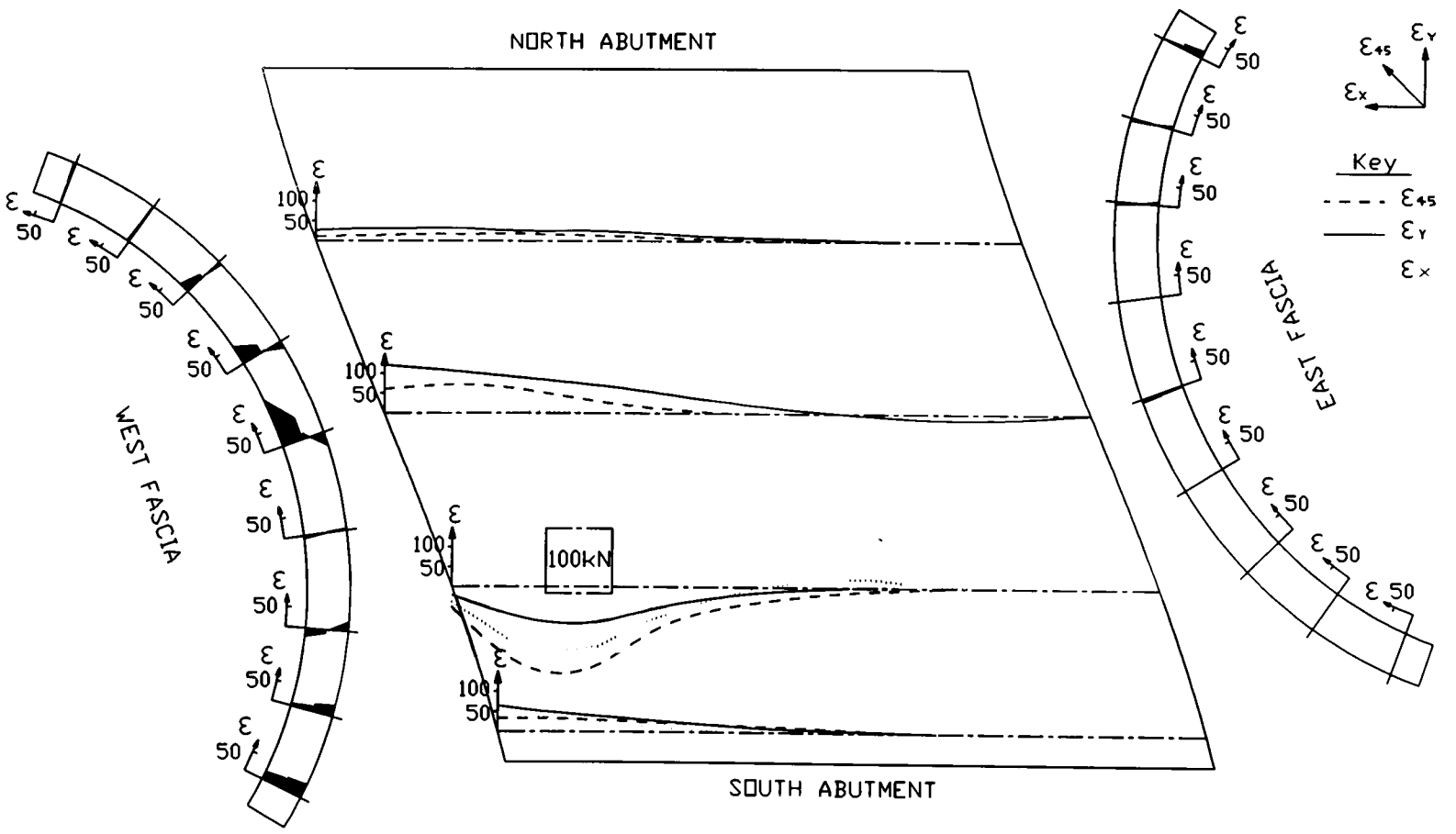

Figure 4.15 Surface Strains on bridge 3-1 due to a 100 kN Point Load at P_4

As described in chapter 3.3, the curves superimposed on the development of the intrados of bridge 3-1 in figures 4.14 and 4.15 represent the distribution of strain measured perpendicular, parallel, and inclined at 45° to the abutments. They were generated by fitting the best smooth curve though each set of data. Fascia surface strains, where sufficiently large to enable detection are also shown. These were generated by fitting a straight line through the data obtained from each pair of strain gauges attached to each brickwork ring and extrapolating it to the edges of that ring.

The highly strained region extended across almost the entire width of the arch at row 1 when the load was applied at position P_1. The extent and magnitude of this region diminished as it passed through successive rows of surface strain gauges. In contrast, when the load was applied at position P_4, a relatively localised distribution of strain along row 1 of the intrados was produced. The width of this zone became progressively wider and less severe as it passed through successive rows of surface strain gauges.

During the load test at position P_1 surface strains recorded on the east fascia were relatively large and were recorded throughout the length of the span. As can be seen, although these fascia strains were large they were not necessarily the maximum strains. No strains were recorded on the West fascia during this test.

During the load test at position P_4 fascia strains were only recorded on the South side of the West fascia. The direction of the load path appears to be perpendicular to the abutments and thus as the distance between it and the west fascia increased the strains measurable on the West fascia diminished and were eventually too small to measure.

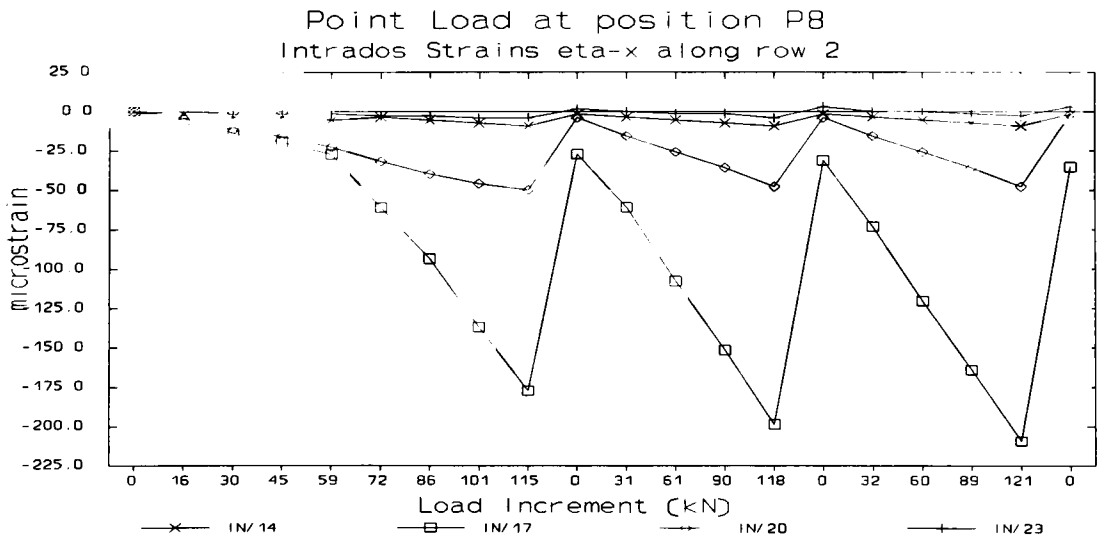

Figure 4.16 Bridge 3-3 Intrados Strains along Row 2

Figure 4.16 shows the surface strains as measured by gauges positioned along row 2 (for their

location see figure 3.10) on the intrados of bridge reference 3-3 when it was subjected to a load at position P_8 (see figure 3.12).

Load tests on this bridge were carried out in reverse order with P_8 being the first. Hence, the first non-destructive test was carried out at the west side of the structure at the crown. When the applied load had been increased to approximately 6.0 T the bond between the arch and the spandrel walls was overcome and the arch became more flexible. The surface strain gauge reference IN/17 (see figure 4.16), which was positioned directly beneath the load, recorded a bi-linear response to the load. The response of the structure after the bond had been broken was much more pronounced and was repeatable during subsequent load cycles. The strain which had occurred before the bond had been broken became an unrecoverable permanent set. This was a typical reaction of bridge 3-3 measured by gauges within the vicinity of the applied load. During subsequent load tests the extent of the spandrel wall separation increased which produced similar non-linear reactions during the first load cycle.

Figures 4.17 and 4.18 show the distribution of surface strain on the intrados of arch bridge 3-3 when it was subjected to a 12.5 T point load applied above the acute and obtuse angled haunch respectively.

When subjected to a load situated above the acute angled haunch, surface strains were measured throughout the extent of the east fascia but were relatively small further down the haunch towards the south abutment. In contrast, only relatively small strains were recorded on the west fascia. However, the significant aspect of these was that tensile strains at the crown extended throughout the depth of the barrel. It is suggested that this region of full-depth tension indicates that elements of the arch would be required to undergo complex three-dimensional rotations in order to accommodate the displacement of the load if it had been increased to the point at which it would have created a mechanism. Consistent with these observations, the maximum compressive strain on the intrados occurred at the eastern extremity of row 3. Thus, it is likely that a fracture line would occur between these two points and would involve a rotation, on plan, of one block of brickwork relative to another about a point in the vicinity of the eastern extremity of row 3.

Relatively large surface strains were recorded throughout row 1 on the intrados. Along this row, large tensile strains occurred in each direction in the vicinity of the load and smaller compressive strains were recorded towards the west edge of the barrel. This reversal of the sign of the strains was coincident with the transverse arching that was detected by the deflection gauges. Further around the intrados, towards the north abutment, the extent of the highly strained region diminished at each successive row of surface strain gauges.

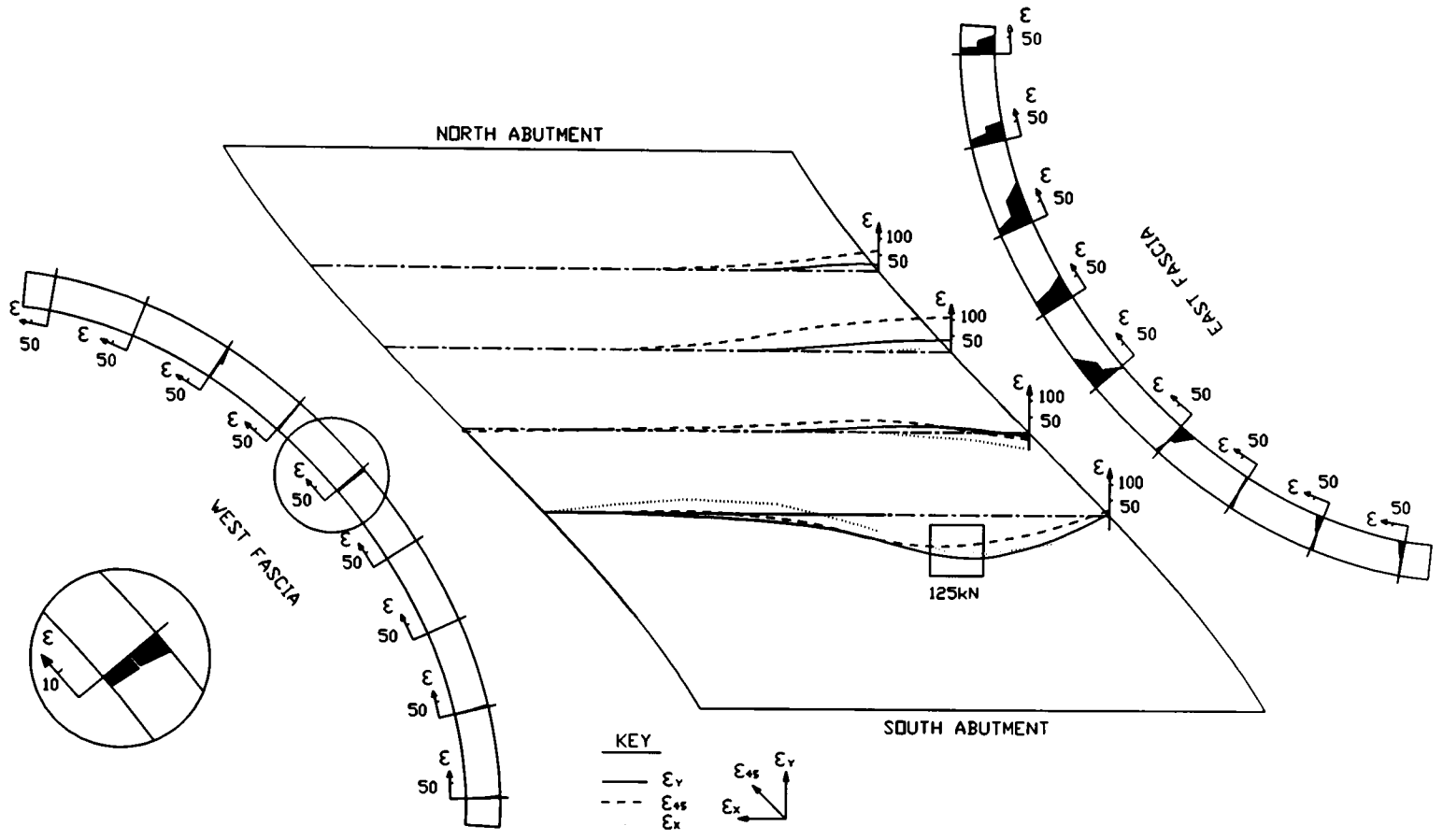

Figure 4.17 Surface Strains on bridge 3-3 due to a 125 kN Point Load at P_1

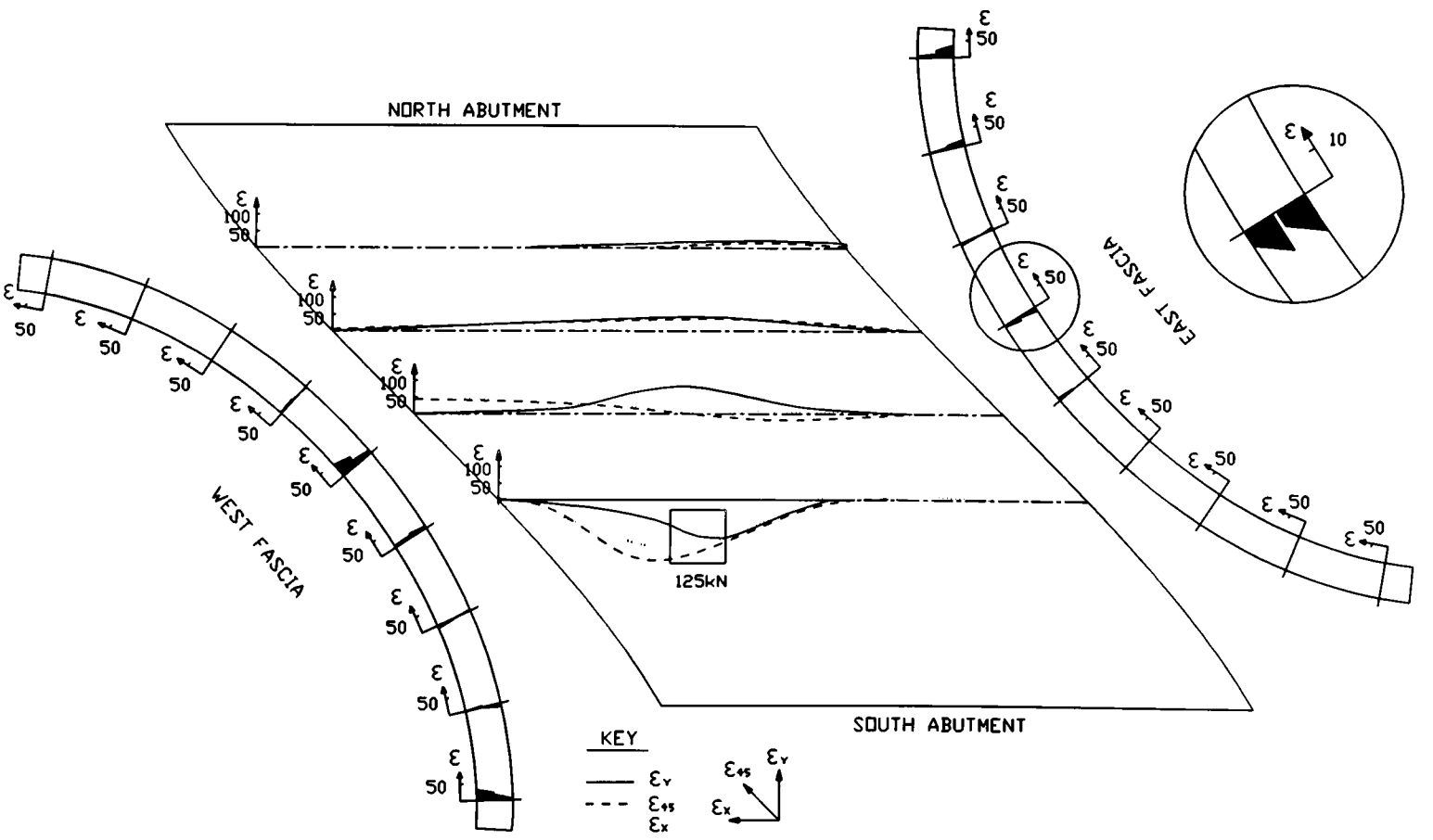

Figure 4.18 Surface Strains on bridge 3-3 due to a 125 kN Point Load at P_4

When subjected to a load situated above the obtuse angled haunch a region of full-depth tension was recorded on the east fascia. Thus, if a similar reasoning is used to explain this observation as was used when the load was situated above the acute angled haunch, the distribution of surface strain would indicate that a complex three-dimensional mechanism would occur if this load had been monotonically increased until failure. However, surface strains on each fascia were generally small except for those in the vicinity of each obtuse angled haunch. This would indicate that the direction of the load path was perpendicular to the abutments and, despite the presence of attached spandrel walls, was not in the skew direction.

Relatively large compressive strains were also recorded at the crown of the arch at its west side. At this location, the arch would tend to lift the west spandrel wall when its deformation was sufficiently great. This would indicate that this wall provided some restraint to the deformation of the arch barrel. However, it can only perform this function for as long as it remains contiguous with the arch. The relative magnitude of the longitudinal and oblique strains would indicate that the west spandrel wall did not resist anything more than a small proportion of the load even when the load was positioned close to it and the mortar bond between it and the arch was sound. The extent of the highly strained region along each row indicates that the load was transferred through the arch barrel along a path that was perpendicular to the abutments as opposed to parallel to the spandrel walls. Thus, the arch cannot rely on the support of the spandrel walls even when subjected to loads within the serviceability range.

As can be seen in figure 4.17, the surface strains recorded on the west fascia were small. Surface strains recorded on the east fascia were much larger, between the crown and the north quarter-point they revealed a discontinuity across the mortar ring which may be attributable to ring separation although this was not observed. However, it is possible that the ductility of the mortar bond will permit such discontinuities without the occurrence of ring separation.

Figures 4.19 and 4.20 show the distribution of surface strain on the intrados of arch bridge 3-4 when it was subjected to a 10.0 T point load applied above the acute and obtuse angled haunch respectively.

There was very little difference between the response of bridge 3-3 and the response of bridge 3-4 to a load applied above either haunch. The only significant difference was that bridge 3-3 was very much stiffer because of its attached spandrel walls. In each case, a region of full-depth tension was observed which occurred opposite a region of high compressive strains. The formation of a complex hinged mechanism is inferred from these observations. Furthermore, the presence of the spandrel walls did not have a significant effect upon the behaviour of the structure; the distribution of surface strain was unaffected whilst its magnitude was diminished.

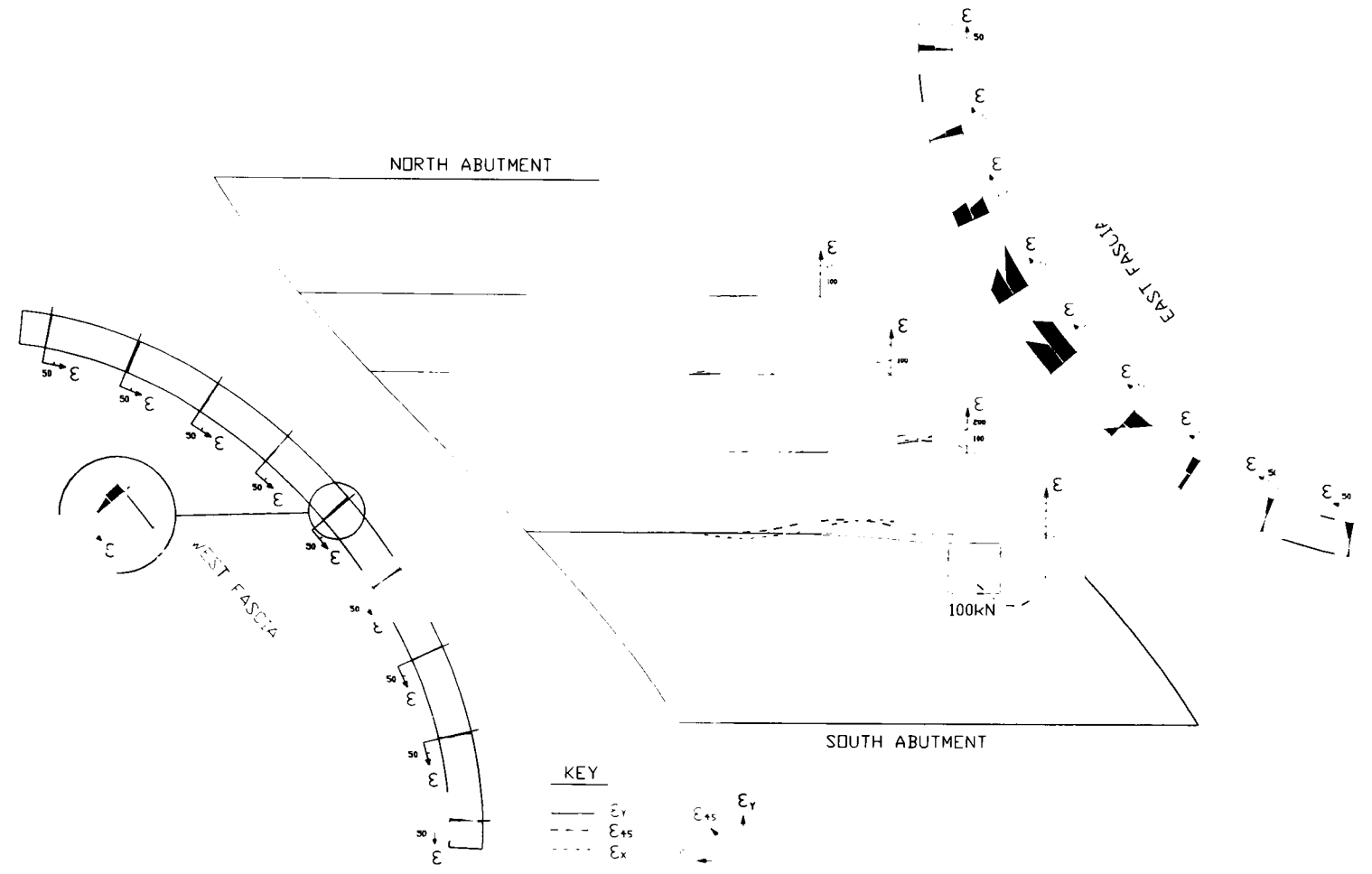

Figure 4.19 Surface strains on bridge 3-4 due to 100 kN point load at P_1

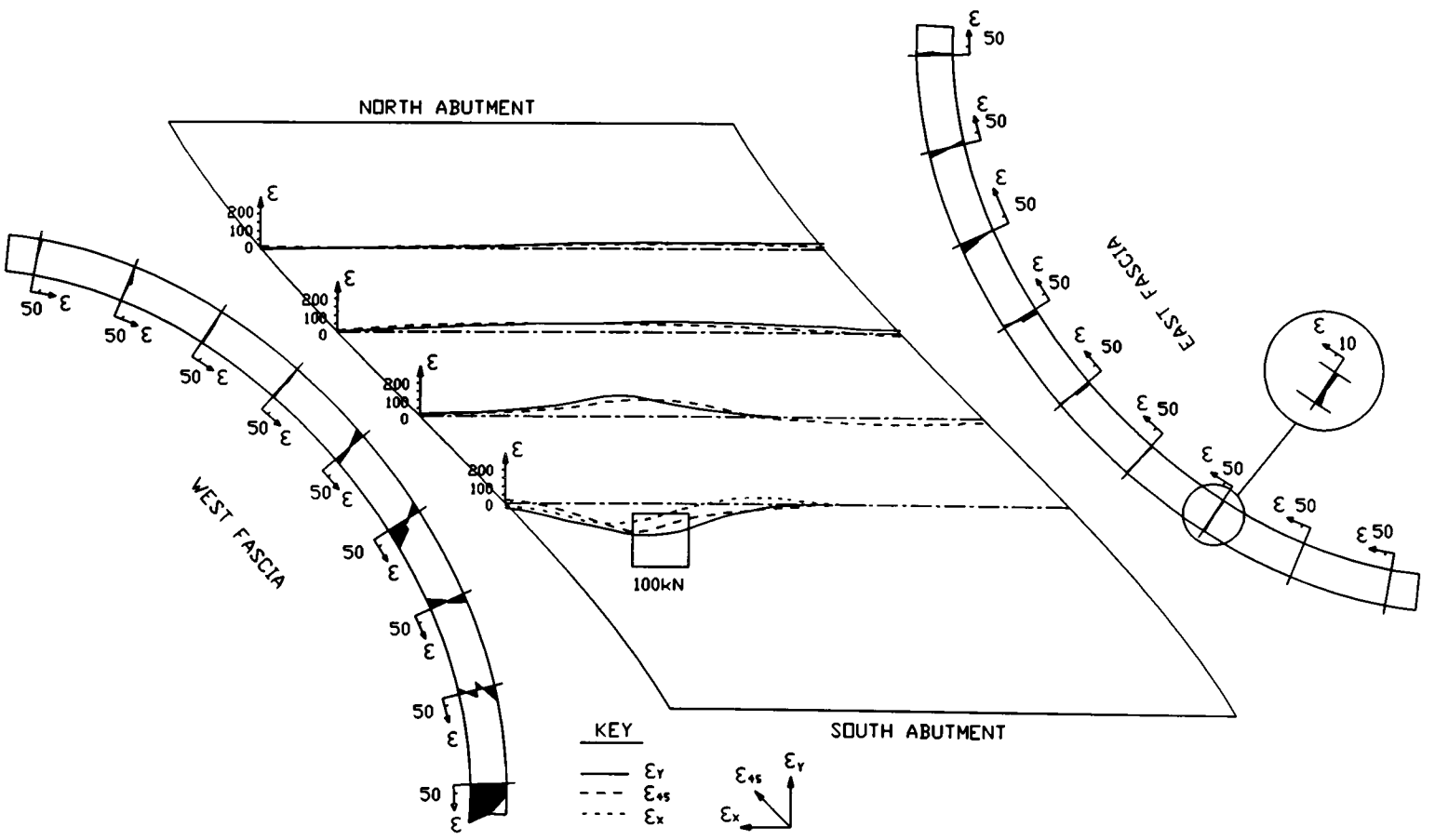

Figure 4.20 Surface strains on bridge 3-4 due to a 100 kN point load at P_4

Surface strain profiles measured on each fascia were seldom linear. Possible contributory factors include the variability of the brickwork, i.e. partially filled joints, and local variations in material properties. Another factor would be the presence of tapering joints which create an elastic modulus that varies with depth. However, the most important contributory factor is the presence of the continuous band of mortar in between the two brickwork rings. Stöckl & Hofmann (1988) carried out shear tests on brickwork specimens built with weak mortars similar to those used for the construction of the model arch bridges tested as part of this research. Their tests revealed that brickwork built with weak mortars exhibit a high degree of ductility when loaded in shear. They found that the non-linear relationship between shear stress and deformation could be accurately represented by an elastic-plastic relationship. This was a very important finding and is exactly that which will be used in the finite element analyses presented in chapter 7. Furthermore its use is justified because it explains the observed discontinuity in the surface strain profiles.

The relatively high flexibility of the mortar ring is not fully responsible for the observed discontinuity although its shear deformation will account for part of it. The strength of the mortar bond will be such that in some regions there may be no bond whilst the yield stress at which plastic flow is initiated will vary considerably throughout the remainder of the structure. As the load is progressively increased, the brickwork rings will act non-compositely without separating. The extent of the regions of mortar that are in a state of plastic flow will be enlarged whilst the extent of the region of mortar remaining within the elastic range will diminish. The diminution of the regions in which the mortar bond remains elastic enables the brickwork rings to undergo increasingly large shear deformations. In itself, this may initiate ring separation. However, the failure of the remaining regions is likely to be more brittle and is likely to initiate ring separation if it has not already occurred.

During the load test at position P_1 on bridge reference 3-4, the response measured by the east fascia row 3 strain gauges shifted significantly during the first load cycle when the load was increased beyond 60 kN. This can be seen in figure 4.21.

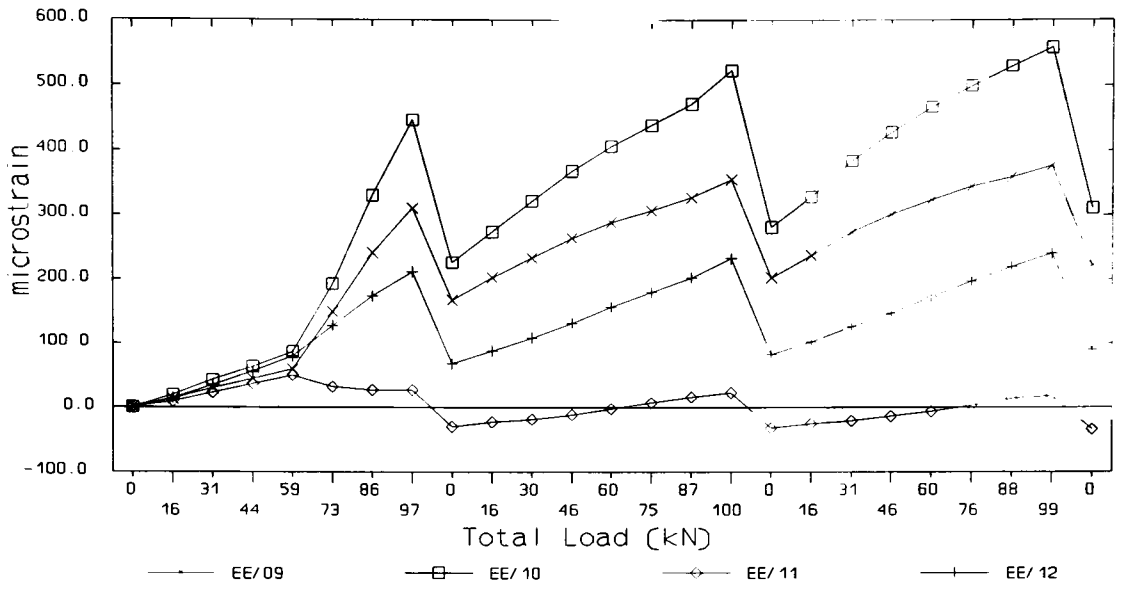

Figure 4.21 East fascia strains along row 3 of bridge 3-4 during test P_1

Prior to this load increment, the strain profile at this location was proportional to depth but was stepped by approximately 35×10^{-6} across the mortar bed. The sudden propagation of ring separation to just beyond this location produced a marked non-linearity in the response of this part of the structure to the applied load. This caused it to become much more flexible and created permanent deformations when the load was removed. After ring separation had propagated through this section, the response of the gauges attached to the upper ring was greater than the response of the gauges attached to the lower ring. This indicates that ring separation destroys the composite action of the arch barrel although friction and the plasticity of the mortar bond will creates some load sharing.

4.4 Backfill Pressures

Figures 4.22a and 4.22b show the changes in radial backfill pressure on the extrados of arch bridge 3-3 and 3-4 when subjected to a 125 kN, or 100 kN, point load at position P_1 respectively.

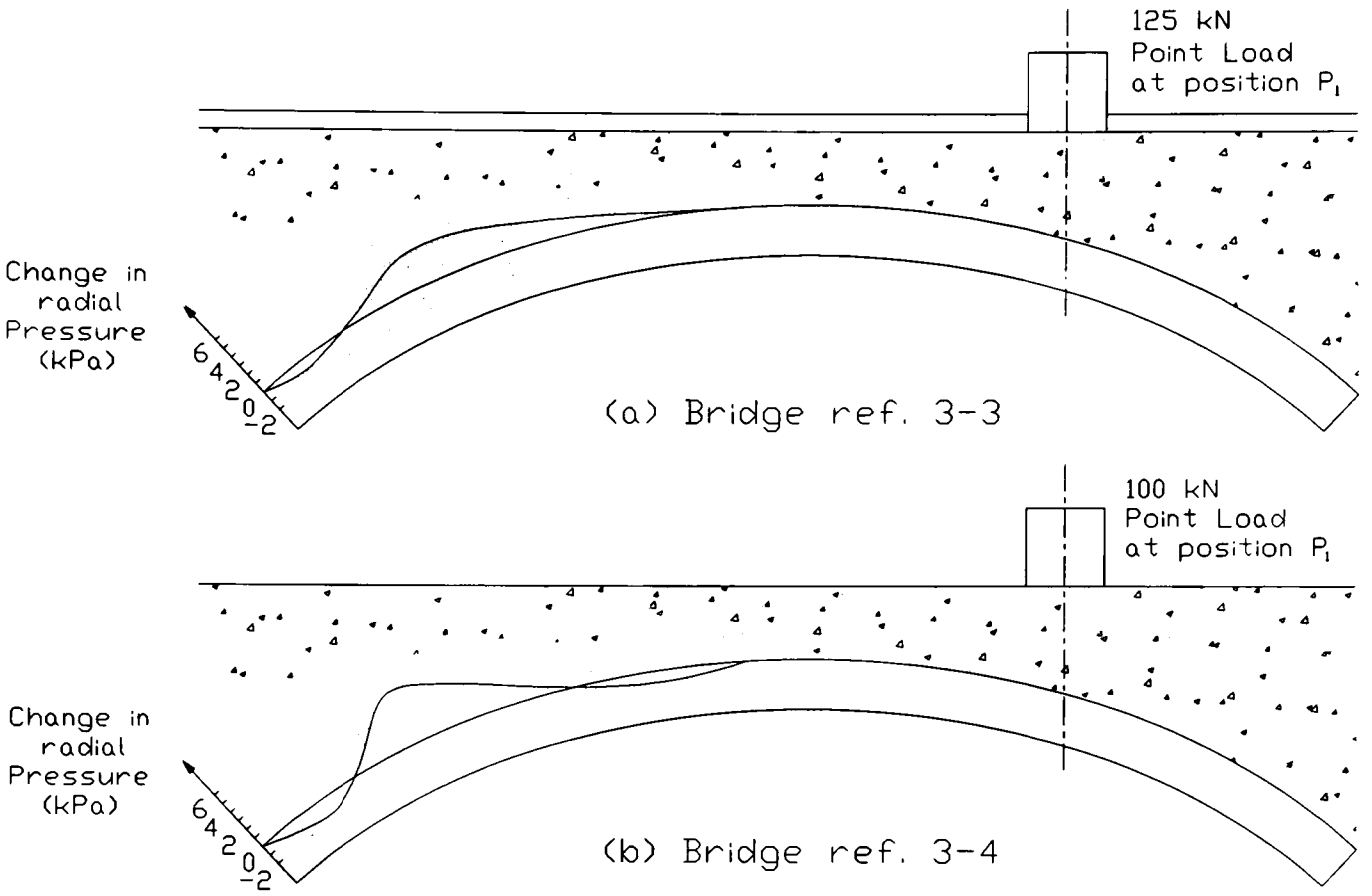

Figure 4.22 Radial Backfill pressures on passive side of each arch bridge during test P_1

The pressure distribution shown was that which was recorded by cells seated on the extrados adjacent to the north east spandrel wall (see figure 3.13 for their location). This was where the greatest outward deflections occurred and consequently the changes in pressure within this region were larger than those which were recorded on the north west haunch.

The absence of attached spandrel walls resulted in arch bridge 3-4 having a greater flexibility than arch bridge 3-3. Thus, the larger outward deformation of arch bridge 3-4 enabled it to create larger changes in backfill pressures as compared with those created by 25% higher loads applied to bridge 3-3. However, in each case, the changes in pressure were relatively small. Furthermore, there were regions along each arch that appeared to be subjected to decreasing pressures. This can be accounted for by the shearing of the backfill along the extrados as the arch deforms into it. This shearing movement will cause the pressure cells to produce erroneous results.

4.4.1 Results of the 25.8 kN Point Load Tests

A single point load was applied to arch bridge 3-4 at the position and orientation marked as R_1, in figure 4.23. The load was applied by supporting a 24.4 kN concrete block on top of a 1.4 kN, 335 mm × 335 mm steel block. After monitoring the changes in backfill pressures produced by the load at each position, both blocks were removed from the structure to enable it to recover. The blocks were then re-positioned on the surface of the backfill in a new position 50 mm towards R_{41}.

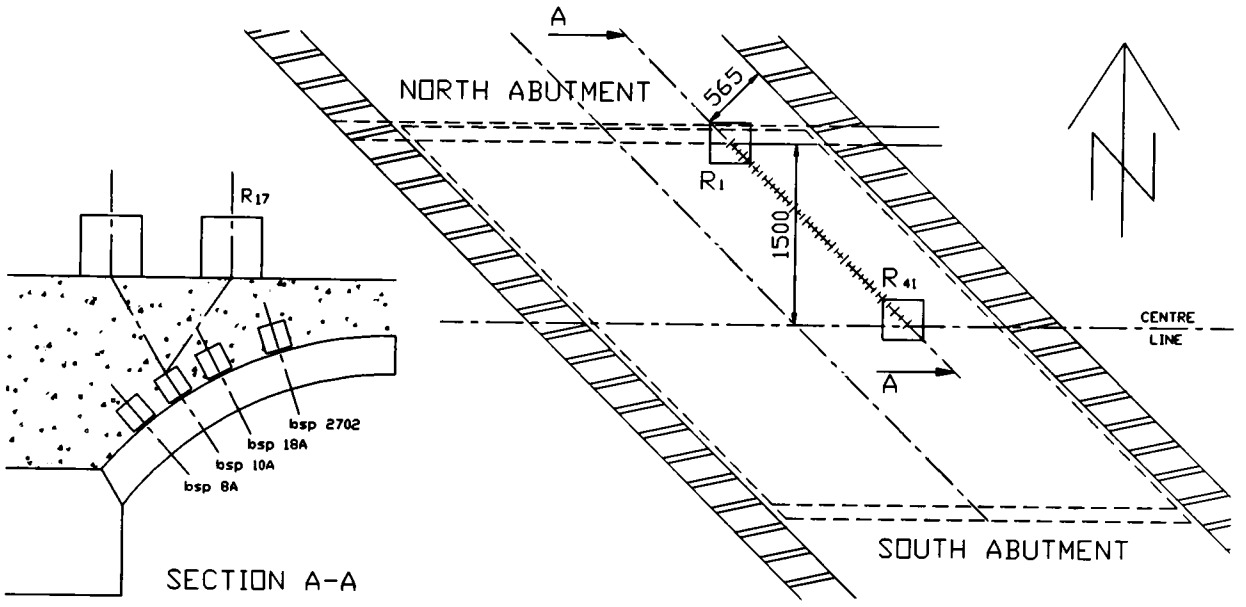

Figure 4.23 Position of 25.8 kN Point Loads on arch bridge 3-4

It is impossible to measure the change in pressure, due to a single point load, at more than two or three locations on the extrados of an arch bridge. The size of the pressure cells and the limited zone over which the load disperses creates this problem. A more effective method is to generate the influence line for each pressure cell by applying the single point load at many positions.

Figure 4.24 shows the influence line of the change in radial pressure at the site of each pressure cell that was seated on the extrados of arch bridge 3-4. Each curve was used to determine a mean value for the angle of load dispersal which was found to be 30°. However, it was found that the dimensions of the patch loads were such that it became progressively more difficult to obtain a true angle of load dispersal as the load was moved towards the crown of the arch. Each value of the load dispersal angle was determined by drawing a vertical section through the structure along the route of these patch loads as shown in figure 4.23. The position of each patch load which, according to figure 4.24, produced a detectable increase in pressure, i.e greater than 5 kN/m^2, could be plotted on the section so that the load dispersal angle could be measured. Figure 4.25 shows the influence lines of the change in horizontal pressure for each cell that was situated above the east edge of the north abutment of arch bridge 3-4 during this test.

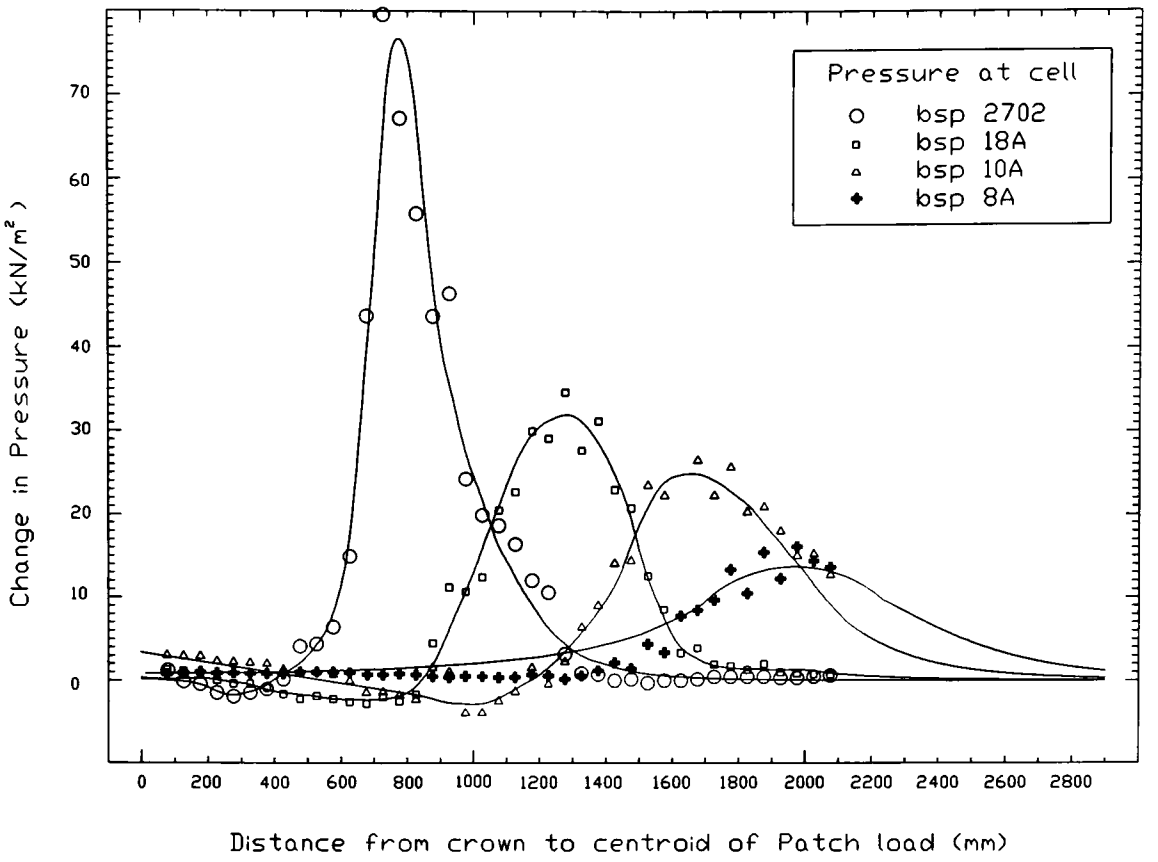

Figure 4.24 Influence lines of Radial pressure

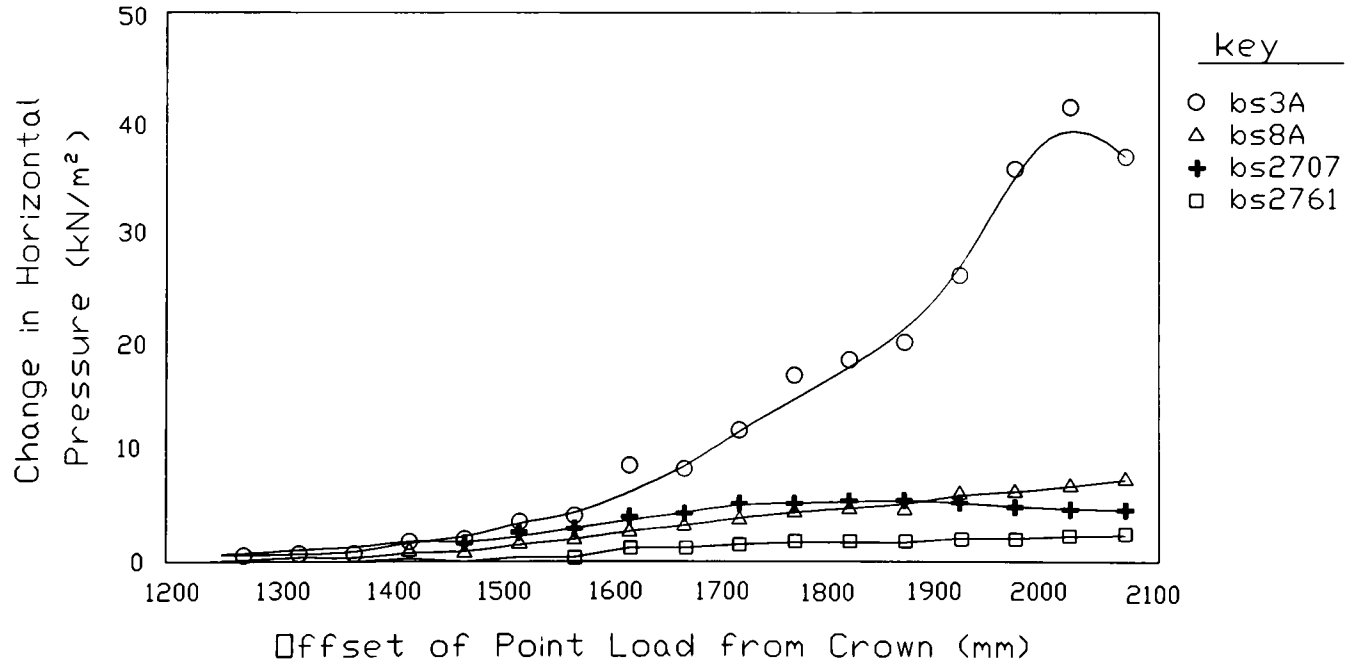

Figure 4.25 Influence lines of Horizontal Pressure

It can be seen that there are significant increases in both horizontal and radial pressure caused by the application of a vertical patch load at the surface. The largest increase in horizontal pressure occurred near the surface, at greater depths, the change in horizontal pressure was less pronounced.

5.0 Results from the Destructive Tests

5.1 3.0 m span model arch bridges

5.1.1 General Observations

5.1.1.1 Application of Load

Two hydraulic jacks, as shown in figure 3.6, were used to apply load through a 2200 × 200mm patch placed parallel to the south abutment and 700 mm offset from it. The intensity of the load was adjusted by operating the jacks individually until both load cells registered an approximately equal load. It was always the case that creep occurred during each load increment. As the structure deflected, the pressure within each jack reduced and a corresponding reduction in the load occurred. This phenomenon became more pronounced as the load test progressed.

The rate at which load was applied to each bridge was dependent upon the size of load increment, the number of gauges monitored, the time taken to visually detect and record cracks, and the "time outs" in which the data were saved, examined and backed-up. The loading rate was inversely proportional to the magnitude of the applied load since, after the occurrence of the first crack, crack monitoring became more lengthy. The mean loading rate up to failure for bridges 3-1, 3-2, 3-3, 3-4 was 100, 50, 70, 70 kN/hour respectively.

5.1.1.2 Mode of failure

Each bridge was ultimately broken into a number of blocks of brickwork by the formation of several fractures. The occurrence of fractures was hastened by ring separation. Nevertheless, the formation of a complex hinged mechanism brought about the collapse of each structure.

Beyond the maximum load regions of spalling brickwork were observed as each bridge approached collapse. Compressive failures occurred only after the brickwork blocks had undergone large rotations. The exception to this was bridge 3-2 which showed no signs of compressive failures at any time during its loading.

5.1.1.3 Post Collapse Inspection

The backfill material was able to stand almost vertically above each abutment after each bridge had collapsed. An inspection of the brickwork generally revealed that many joints were only partially filled with mortar and that the quality and distribution of these regions was random.

5.1.2 Crack Monitoring

The formation and propagation of cracks within each bridge was monitored throughout the entire duration of each load test. Each bridge was whitewashed to facilitate this. Cracks can be categorised as follows:

1. Tensile cracks within the arch barrel due to the formation of a fracture line,
2. Shear cracks at fracture lines where a block of brickwork moved radially along an adjacent block instead, or as well as, rotating about one of its edges,
3. Ring separation as adjacent brick rings sheared relative to each other,
4. Tensile cracks within the spandrel and wing walls caused by their involvement in the failure mechanism,
5. Other cracks such as thermal cracks and shrinkage cracks which occurred at the crown in detached spandrel walls.

5.1.2.1 Cracking of the arch barrels

Several tensile regions occurred within each arch barrel. These regions were generally situated alternately on the intrados and extrados in the vicinity of the eventual locations of the fracture lines. The exception to this was the occurrence of a fifth fracture line which extended from a point on the north west haunch to a point near the eastern edge of the north abutment. A crack in this location was observed in the intrados of each skewed arch and effectively isolated the north east acute angled corner. However, the absence of backfill on bridge 3-2 made it possible to examine its extrados. It was found that the fifth fracture line created a crack in the intrados and extrados. Hence, this fracture line was not associated with a simple hinge but some other form of relative block movement.

A further set of cracks occurred within the extrados of arch bridge 3-2. These were perpendicular to the loading beam and were probably a function of the application of the load, i.e without backfill it is possible for the loading beam to be supported on several discrete areas rather than on a single discrete 2200 × 200 mm patch.

The helicoidal method of bricklaying meant that any fracture that was required to form in an orientation other that parallel to the bedding joints would be saw-toothed in appearance. This would naturally facilitate the diffusion of in-span fractures although Gilbert also pointed out that diffused hinges are a fundamental requirement of a multi-ring brickwork arch as a means of ensuring that the deformation of its component parts are compatible with each other.

Extensive ring separation was also observed within each arch bridge. In the case of bridge 3-3, very little cracking was observed within the arch barrel up to the point at which failure occurred. Failure appeared to be due to a system of hinge like cracks within the spandrel walls together with extensive ring separation within the arch barrel. The stiffness of bridge 3-3 was greatly increased by the attached spandrel walls to such an extent that its response to the load was diminished so that the mortar bond strength was sufficient to prevent visual detection of hinge formation within the barrel.

Ring separation was coexistent with a transverse movement of the top ring relative to the bottom ring in the easterly direction. Attached spandrel walls, in the case of bridge 3-3, resisted this movement. This movement did not occur when square span arch bridges were tested.

The loads at which cracks, corresponding to primary hinges, were first observed in each region of tensile strain for each bridge are shown in table 5.1.

Bridge Ref	1st in-span Hinge	2nd in-span Hinge	3rd South Hinge	4th North Hinge	Failure Load
3-0a	460	600	600	600	600
3-0b	220	310	310	310	320
3-0c	220	240	360	320	360
3-0d	240	300	480	400	540
3-1	290	350	310	490	540
3-2	187	182	202	202	202
3-3	280	372	372	372	372
3-4	240	300	320	320	337

Table 5.1 Occurrence of cracks within each arch bridge

The appearance of tensile cracks is governed by the strength of the mortar. However, with similar prescribed mortars being used throughout the test programme, the degree of variability was minimised. Thus it can be concluded, from table 5.1, that attached spandrel walls stiffen the arch and delay the appearance of tensile cracks. Figures 5.1 to 5.4 inclusive show the development of cracks within arch bridge reference 3-1, 3-2, 3-3 and 3-4 respectively up until failure[1].

[1]In this thesis, failure is defined as the maximum load. Collapse is defined as the event at which the arch falls to the ground. The difference between the two terms is attributable to the hydraulic loading system which allows instantaneous removal of load when failure occurs. Thus, incremental displacements can be applied after failure and a slow motion collapse achieved.

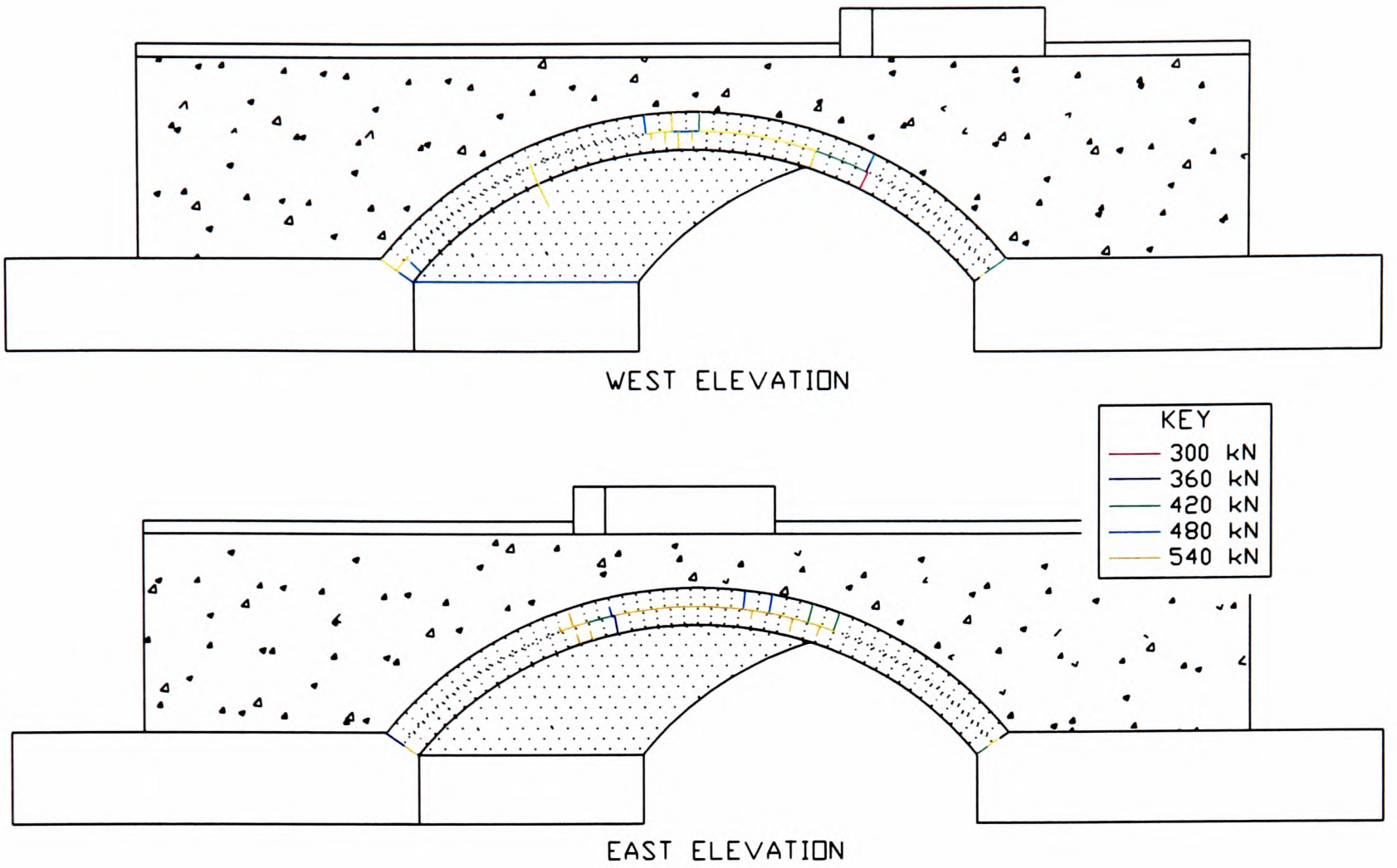

Figure 5.1 Development of cracks up to failure within skewed arch 3-1

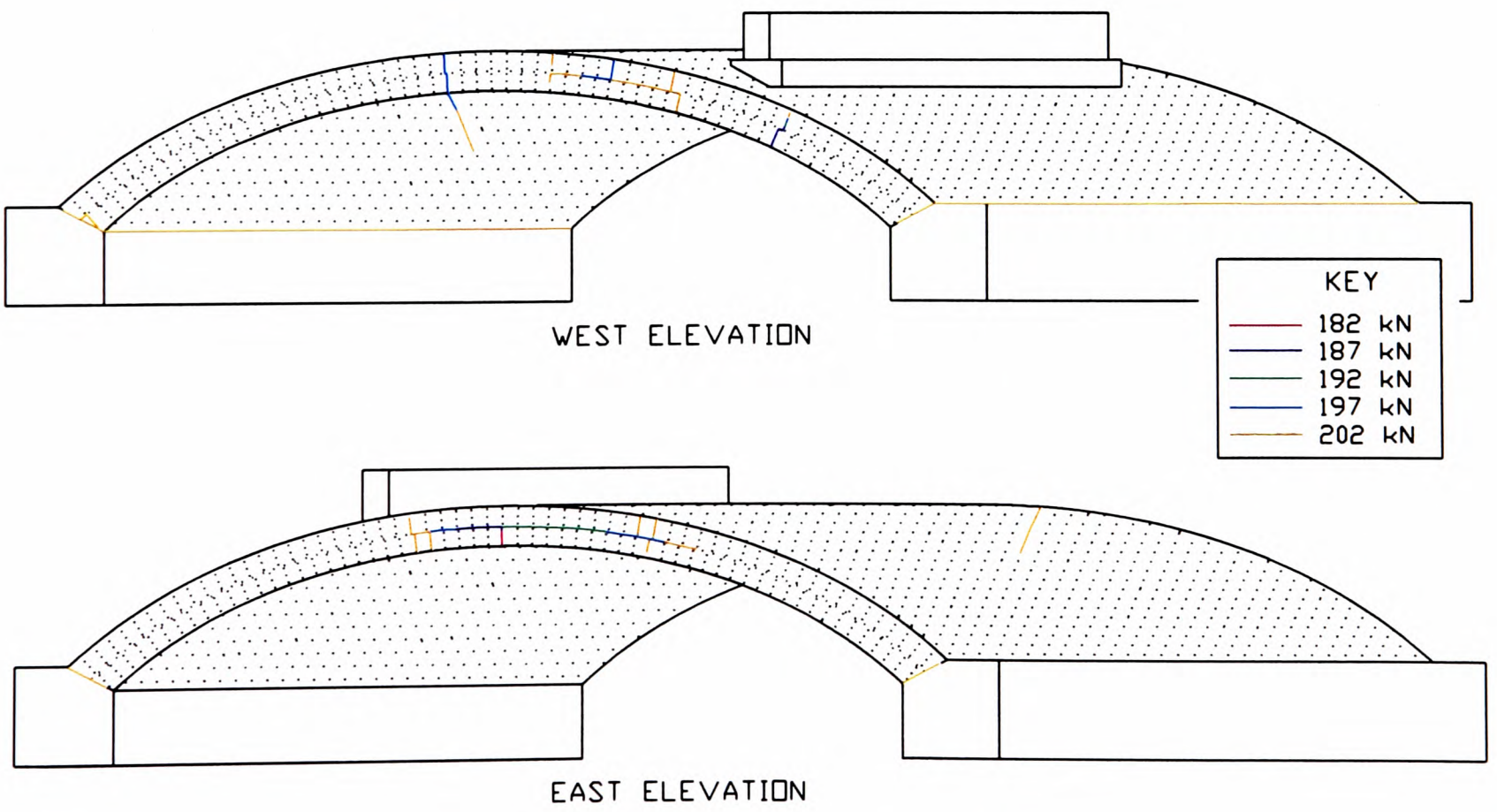

Figure 5.2 Development of cracks up to failure within skewed arch 3-2

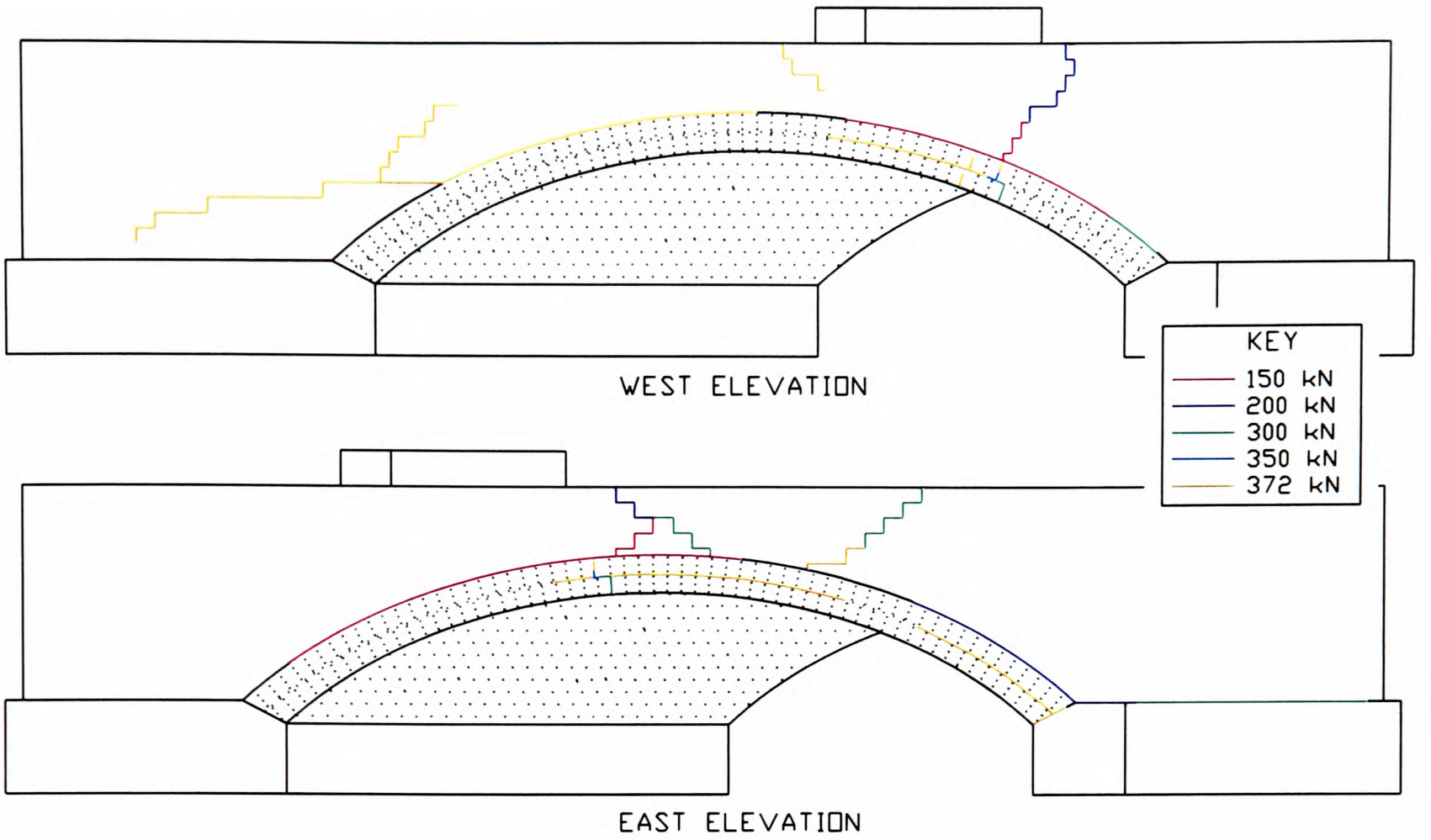

Figure 5.3 Development of cracks up to failure within skewed arch 3-3

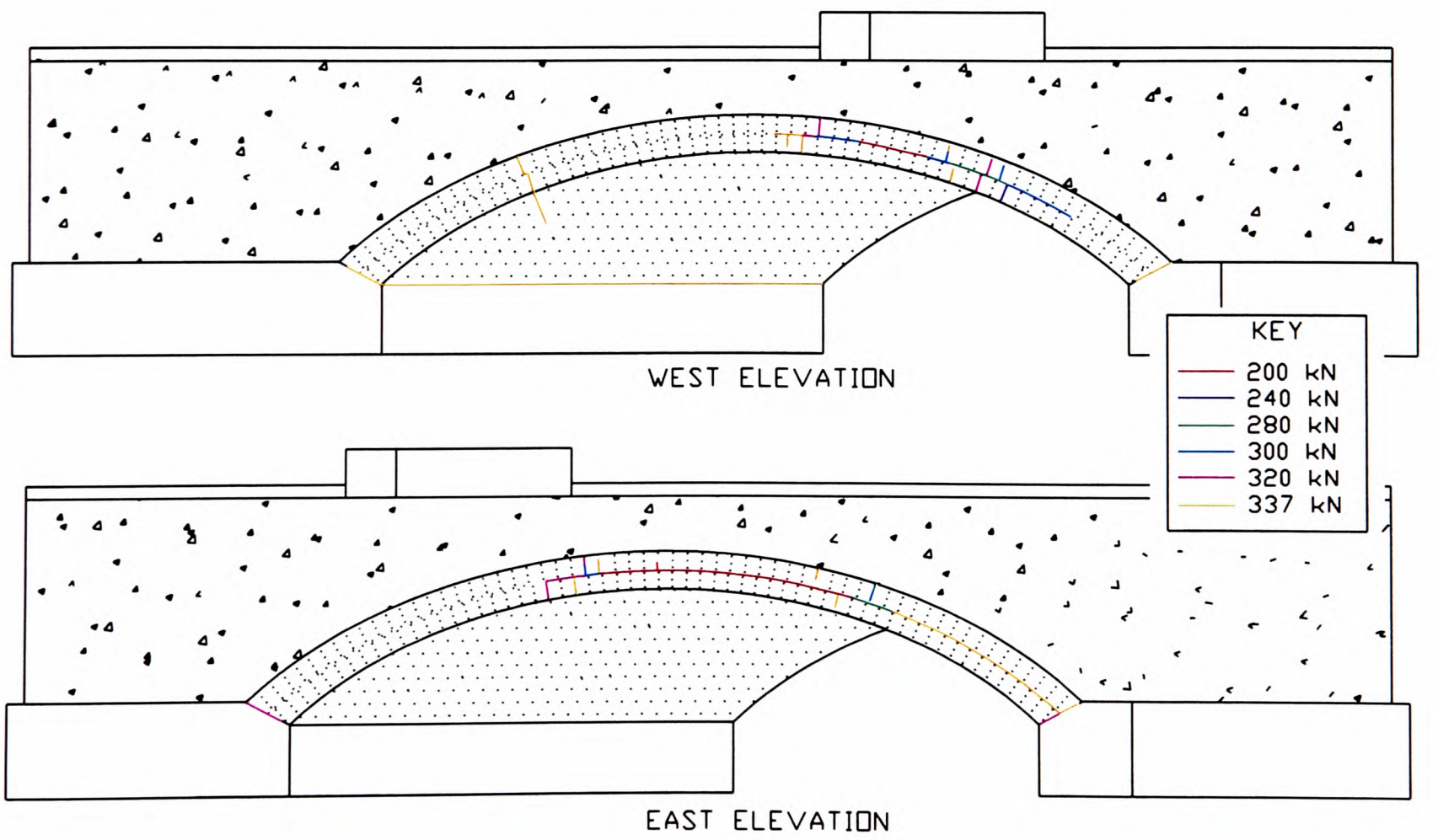

Figure 5.4 Development of cracks up to failure within skewed arch 3-4

5.1.2.2 Cracking of the spandrel walls

In the case of bridge 3-3, cracks between the arch barrel and the spandrel walls were observed during the non-destructive tests at the relatively low load of 60 kN. As this bridge approached failure cracks were observed within the spandrel walls in the vicinity of the loading beam. These cracks propagated upwards as the load was increased. Concurrently, cracks in the north east spandrel wall propagated downwards and a further crack occurred at the base of the north east wing wall. Similar cracks occurred within the west spandrel and wing walls but were displaced around the arch.

In the case of bridge 3-1 and 3-4, hairline cracks within the detached spandrel walls were observed in the vicinity of the crown at the east side of the structure. Here, thermal cracks had occurred soon after construction had been completed and these were extended by the build up of backfill pressure pushing the walls outwards.

5.1.3 Collapse Mechanisms

Figures 5.5 to 5.8 show full-scale model skewed arch bridge 3-1 to 3-4 respectively approaching collapse. Each elevation has been shown so that the effects of the angle of skew is noticeable since there are marked differences between the pattern of cracks observed in each elevation.

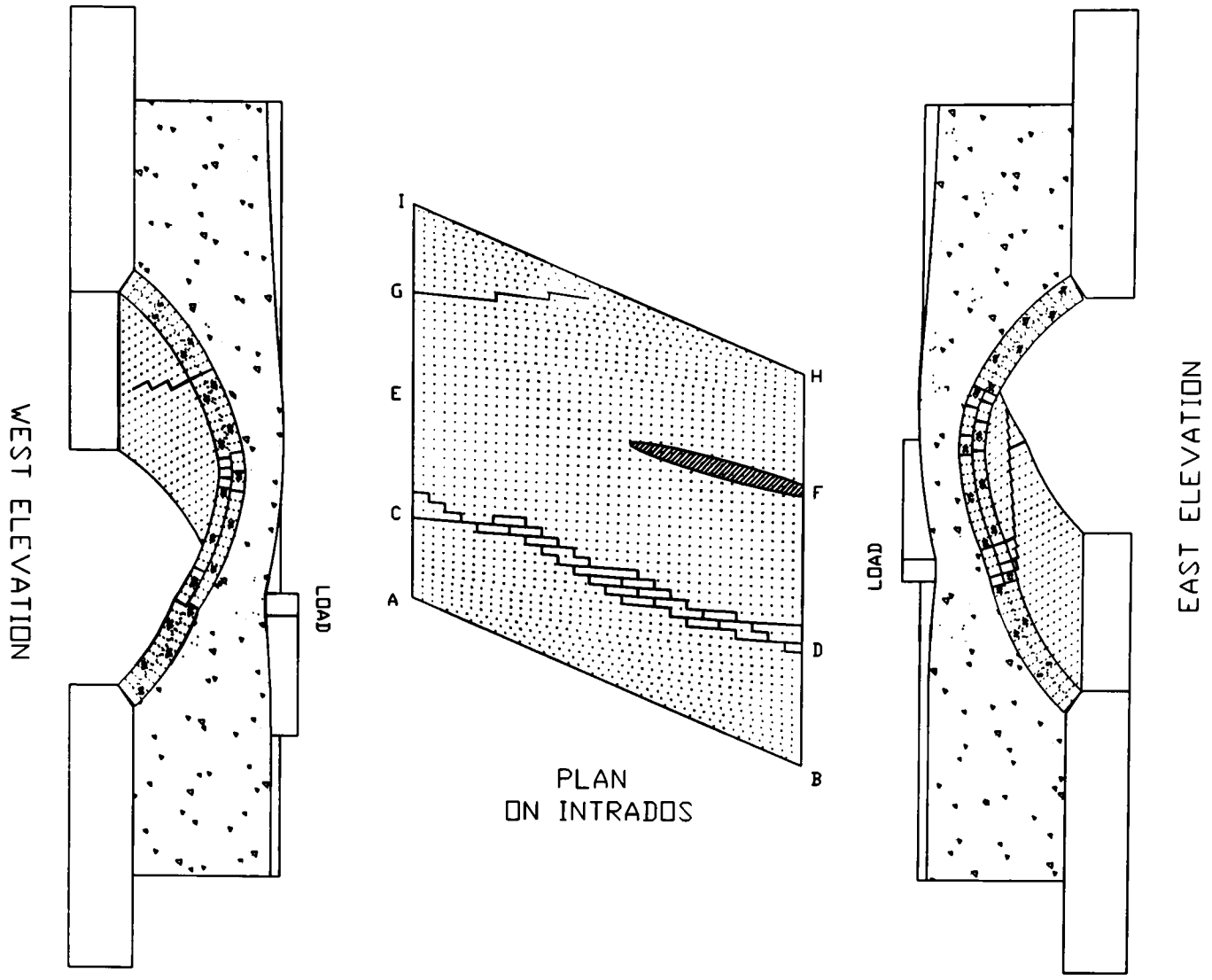

Figure 5.5 Collapse mechanism of skewed arch bridge 3-1

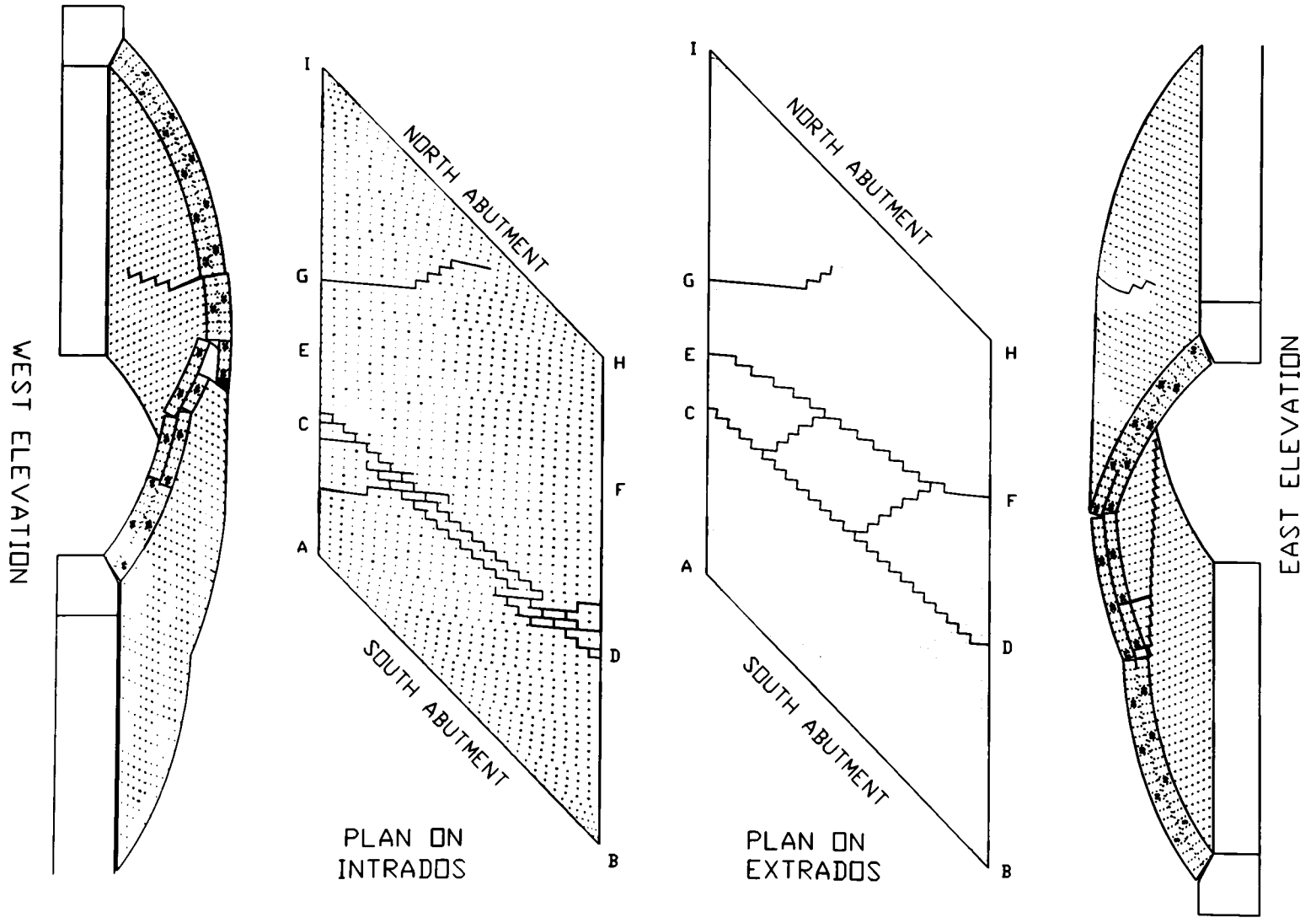

Figure 5.6 Collapse mechanism of skewed arch 3-2

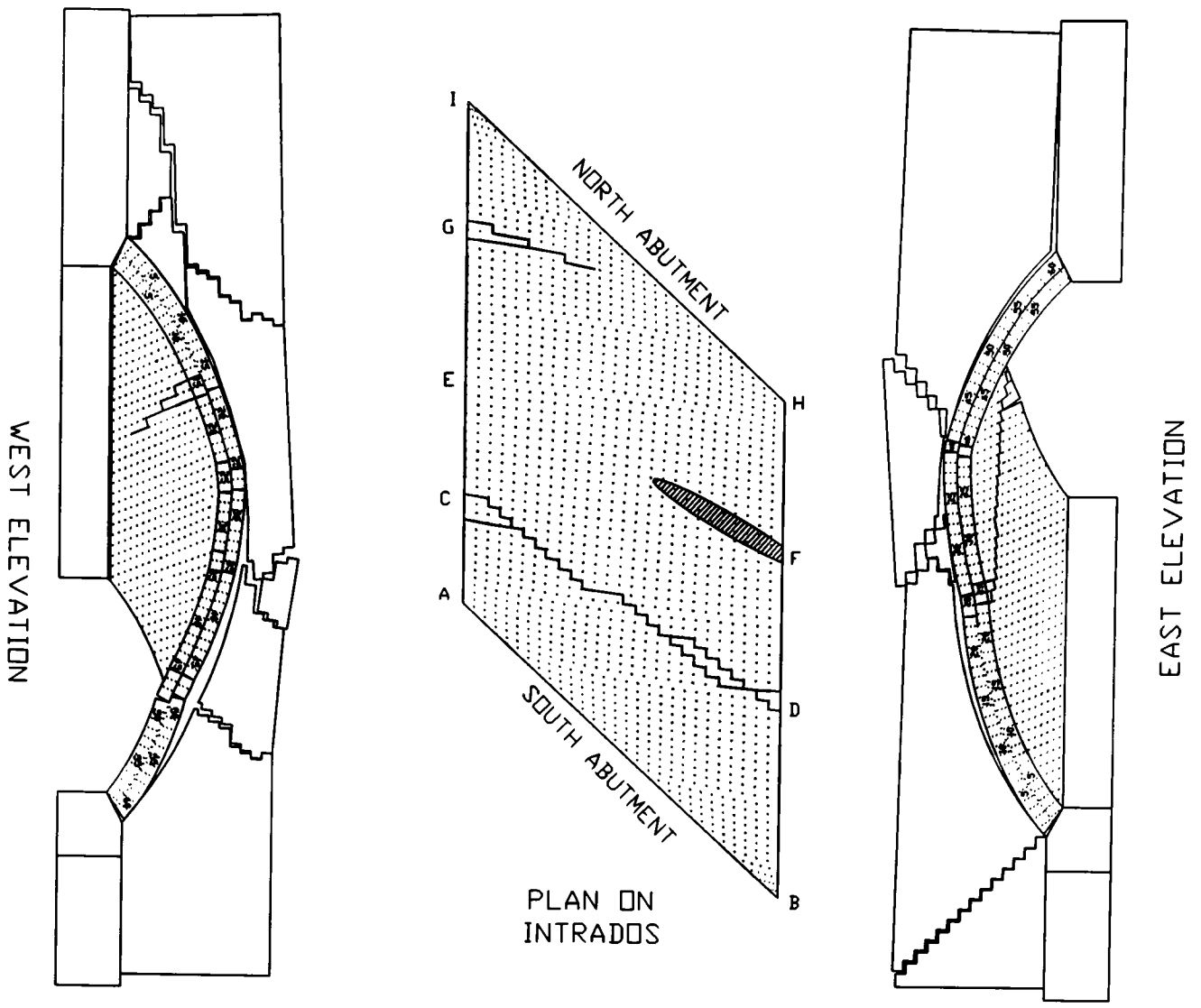

Figure 5.7 Collapse Mechanism of skewed arch bridge 3-3

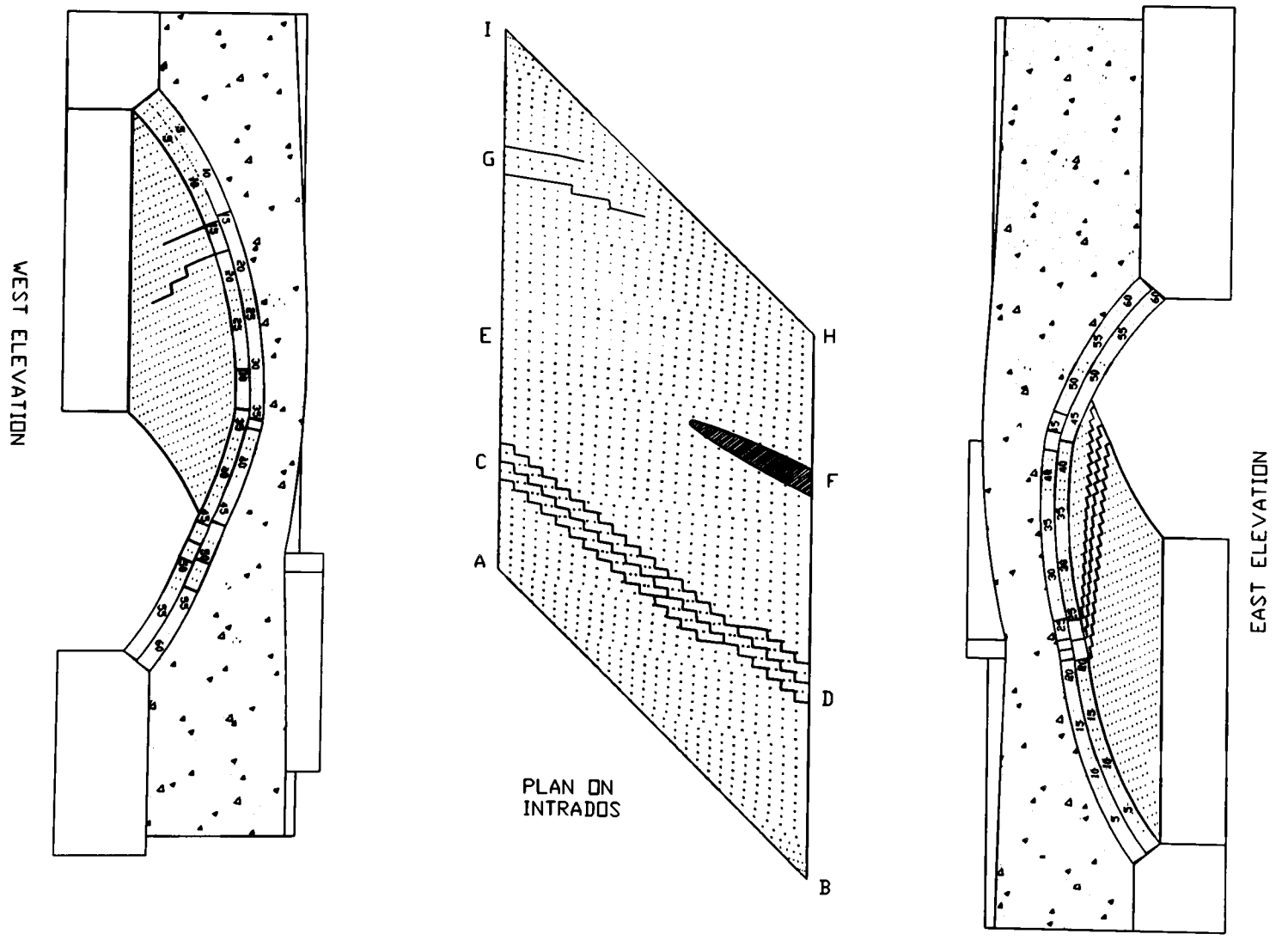

Figure 5.8 Collapse Mechanism of skewed arch bridge 3-4

5.1.4 Deflections

5.1.4.1 Deflection of the Arch Barrels

The load-deflection response of each skewed arch bridge varied depending on where the response was measured. As discussed in chapter 4.2, the stiffness of the structure varied across its width. The obtuse angled haunch was much stiffer than the acute angled haunch. Figure 5.9 which shows two load-radial deflection relationships for each full-scale model arch bridge. The load-outward deflection relationship of each skewed arch bridge was measured at the eastern extremity of the second in-span hinge where the deflection was greatest. All other relationships were measured at the centre line of the structure, i.e beneath the centroid of the loading beam or at a similar location in the vicinity of the second in-span hinge.

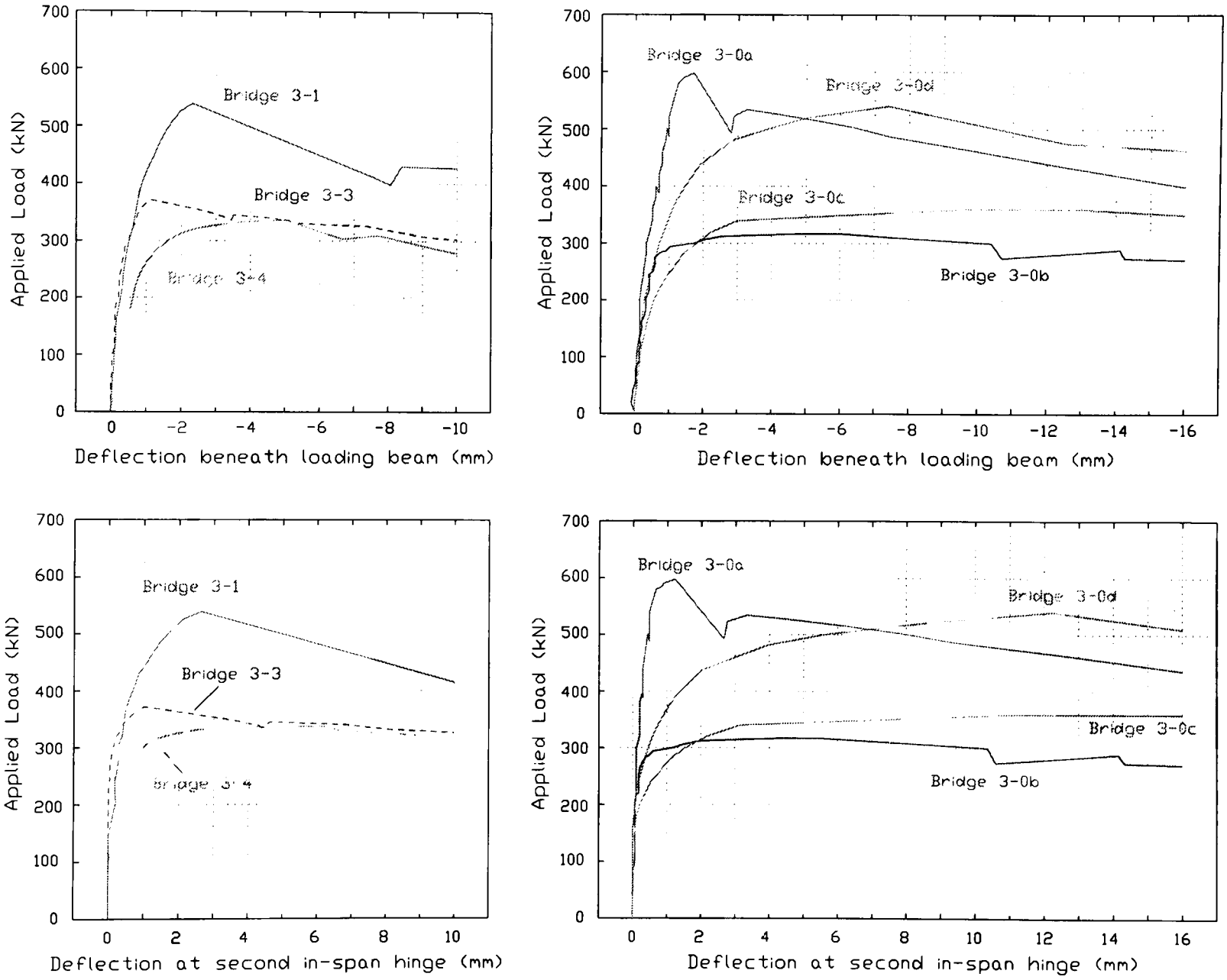

Figure 5.9 Load-deflection response of each full-scale model arch bridge

Figures 5.10 to 5.13 each show the development of a 3.0 m span arch bridge tested at the B.I.H.E. on which the deflected shape just before failure is superimposed as a set of contour

lines. These contour plots were created by combining the data recorded by each intrados deflection gauge. Curve fitting was invoked along each row of gauges and linear interpolation was used between each row. The development of each 3.0 m span right arch bridge previously tested at the B.I.H.E. (Melbourne: & Qazzaz, 1989; & Gilbert, 1991; & Walker, 1990b; & Gilbert, 1992) are shown in figures 5.10a to 5.10d respectively. The deformed shape at failure of each bridge is shown as a series of contours in which positive values represent outward radial deformations and negative values represent inward radial deformations.

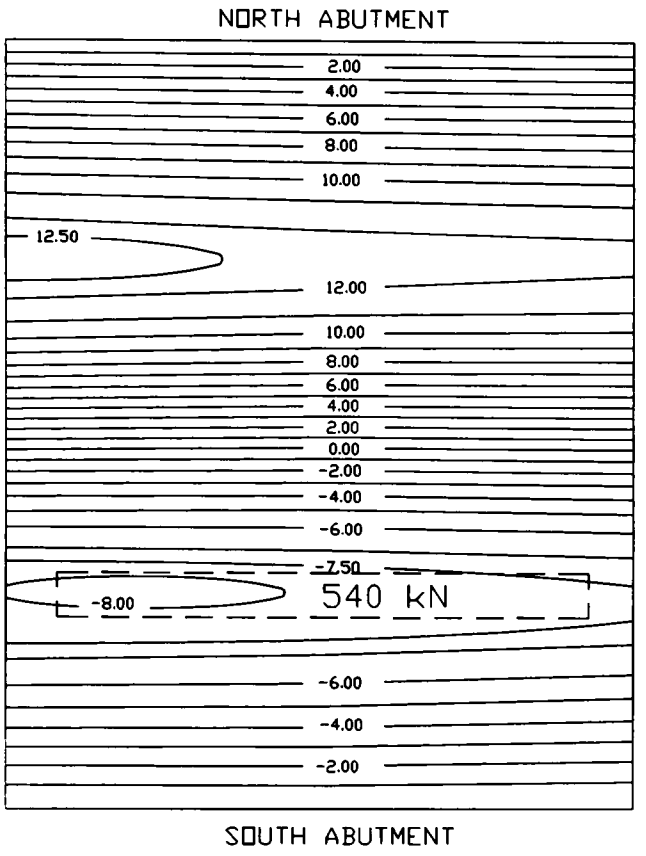

Figure 5.10a
Deflected shape at failure of bridge 3-0d

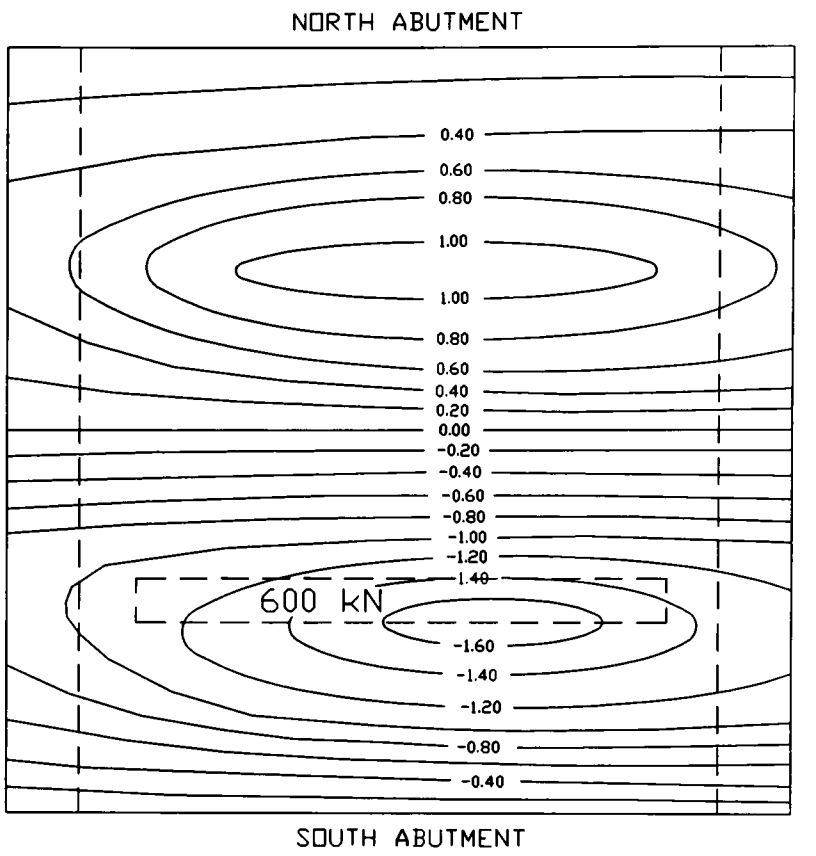

Figure 5.10b
Deflected shape at failure of a bridge 3-0a

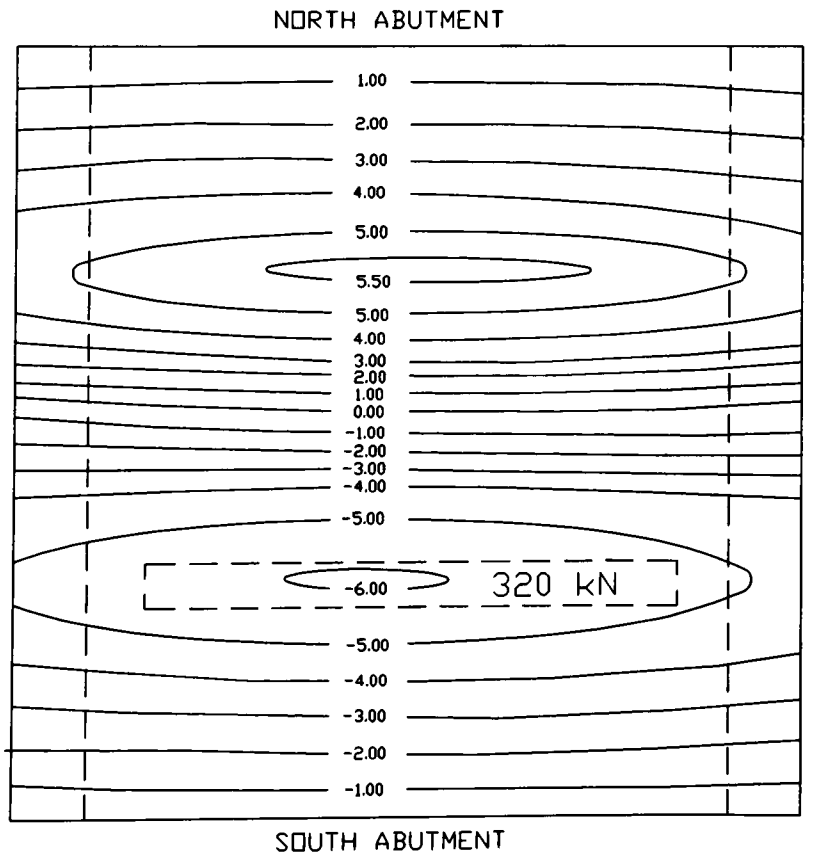

Figure 5.10c
Deflected shape at failure of bridge 3-0b

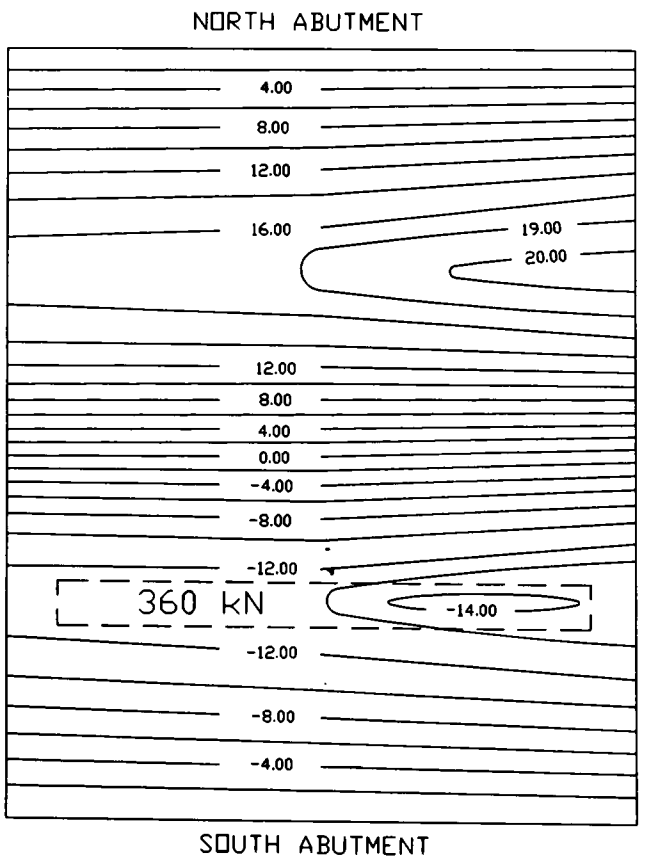

Figure 5.10d
Deflected shape at failure of bridge 3-0c

It can be seen that, without attached spandrel walls, the maximum inward and outward radial deflections at failure of the 2.88 m wide bridge shown in development in figure 5.10a were 8.0 mm and 12.5 mm respectively. In this case the failure load was 54 Tonnes. A similar bridge with attached spandrel walls but 3.54 m wide, as shown in figure 5.10b, failed at a load of 60 Tonnes and was approximately five times as stiff. It is noteworthy that, on a pro rata basis, if the bridge in figure 5.10a had been 3.54 m wide its failure load would have been in excess of 67 Tonnes despite its reduced stiffness caused by the absence of spandrel walls.

The bridge shown in figure 5.10c was similar to that shown in figure 5.10b except that instead of the two brickwork rings being mortar bonded together, they were separated by a 10 mm thick layer of sand. As a consequence of the total ring separation, the failure load reduced to 32 Tonnes. In this case the flexibility of the arch was in excess of six times greater than the flexibility of the corresponding bridge with mortar bonded brickwork rings.

The arch bridge shown in figure 5.10d (ref: 3-0c) was representative of a most poorly maintained structure, in which ring separation was prevalent and spandrel walls had become detached. Its flexibility was almost three times as great as the flexibility of the corresponding structure with mortar bonded rings (ref: 3-0d). However, the failure load of this bridge was 36 Tonnes, and would have been 45 Tonnes on a pro rata basis, which was greater than the failure load of the corresponding bridge with attached spandrel walls (ref: 3-0b).

Thus, some of the conclusions that can be made from the results of the right arch bridges tested at the B.I.H.E. are as follows (Melbourne & Hodgson, 1995b).

1. The attachment of spandrel walls (at least those whose proportions are similar to those used in this test programme) does not significantly alter the strength of an arch bridge although it causes the stiffness of the arch barrel to be increased.

2. The presence of ring separation produces a large decrease in the load carrying capacity of an arch bridge in conjunction with a similarly large reduction in the stiffness of the arch.

3. The four fractures that formed within each right arch at failure were consistent with the formation of a mechanism comprising simple hinges (in which each hinge was parallel to the abutments).

4. Partial ring separation occurred within each arch bridge that had mortar bonded brickwork rings. The stiffness of these structures was therefore reduced following the propagation of this ring separation.

The above conclusions are important when examining the corresponding results of the skewed arch bridges tested as part of this research programme.

The deflected shape at failure of the skewed arch bridges tested at the B.I.H.E. are shown in development in figures 5.11, 5.12, 5.13 and 5.14. The bridges depicted in the first three figures are comparable with the previously tested right arch bridges because of the inclusion of the spandrel fill. The fourth figure pertaining to bridge 3-2 is included for completeness.

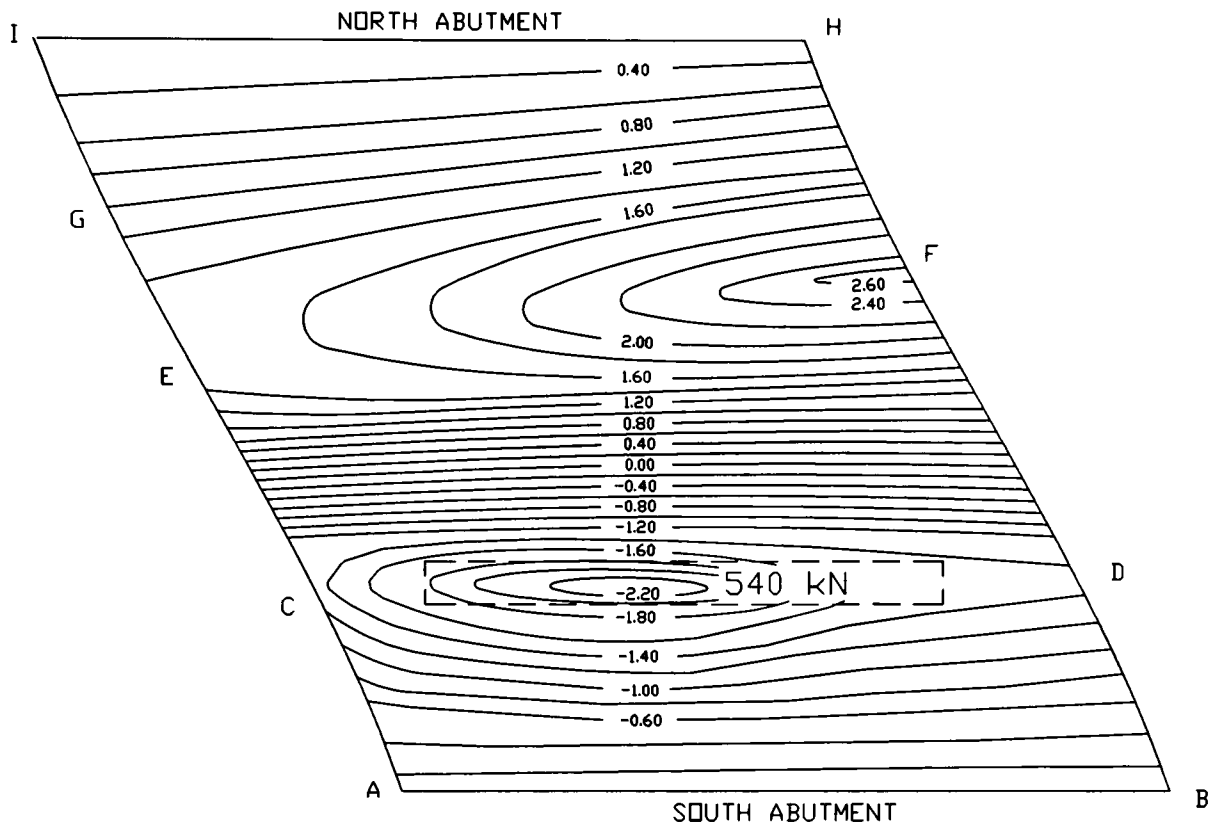

Figure 5.11 Deflected shape at failure of arch bridge 3-1

A comparison of the deflected shape at failure of the 22.5° skewed arch bridge shown in figure 5.11 with the deflected shape at failure of the right arch bridge shown in figure 5.10a reveals that the stiffness of the arch is increased by skew. A reduction in strength can also be observed if the strength of the right arch is increased pro rata based on the width of the barrel measured parallel to the abutments.

A comparison of the deflected shape at failure of the 45° skewed arch bridge shown in figure 5.12 with the deflected shape at failure of the right arch bridge shown in figure 5.11b also indicated that the stiffness of the arch is increased by skew. The inward radial deflections beneath the load were similar but the outward deflections were much smaller and limited to a comparatively small region, marked F, in the obtuse angled haunch. This decreased flexibility created by the skew and the change in geometry enabled the arch to form a mechanism at the much smaller failure load of 37 Tonnes.

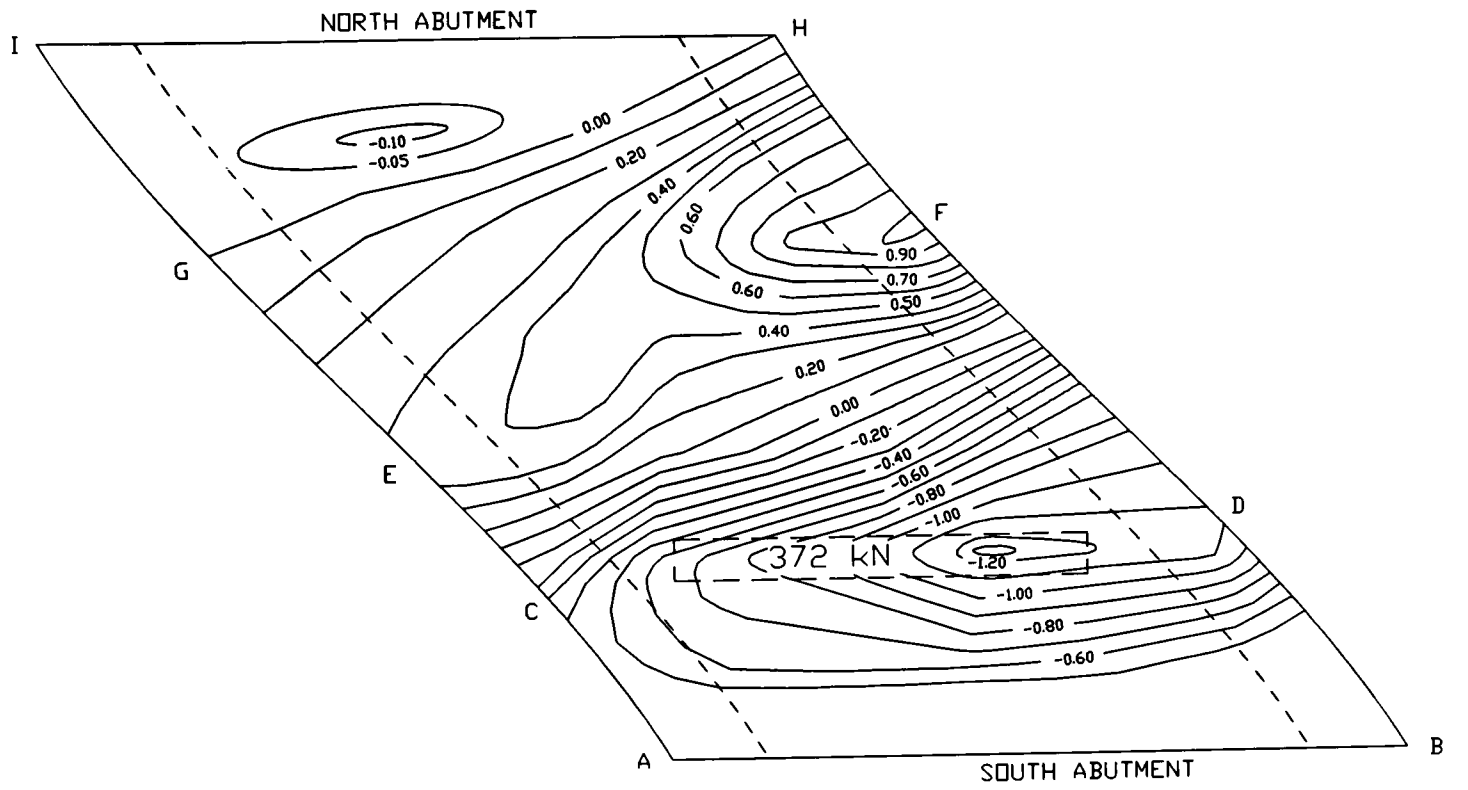

Figure 5.12 Deflected shape at failure of arch bridge 3-3

Based on previous observations it could be expected that the final single span 45° skewed arch bridge without spandrel walls, viz. bridge 3-4, shown in figure 5.13, would fail at a load that was similar to that which was required to fail the corresponding bridge with spandrel walls. Equally, it could be expected that an increase in the flexibility of the structure would occur but not so that it became as flexible as an arch bridge with a lesser skew (compare with figure 5.12 and figure 5.11a).

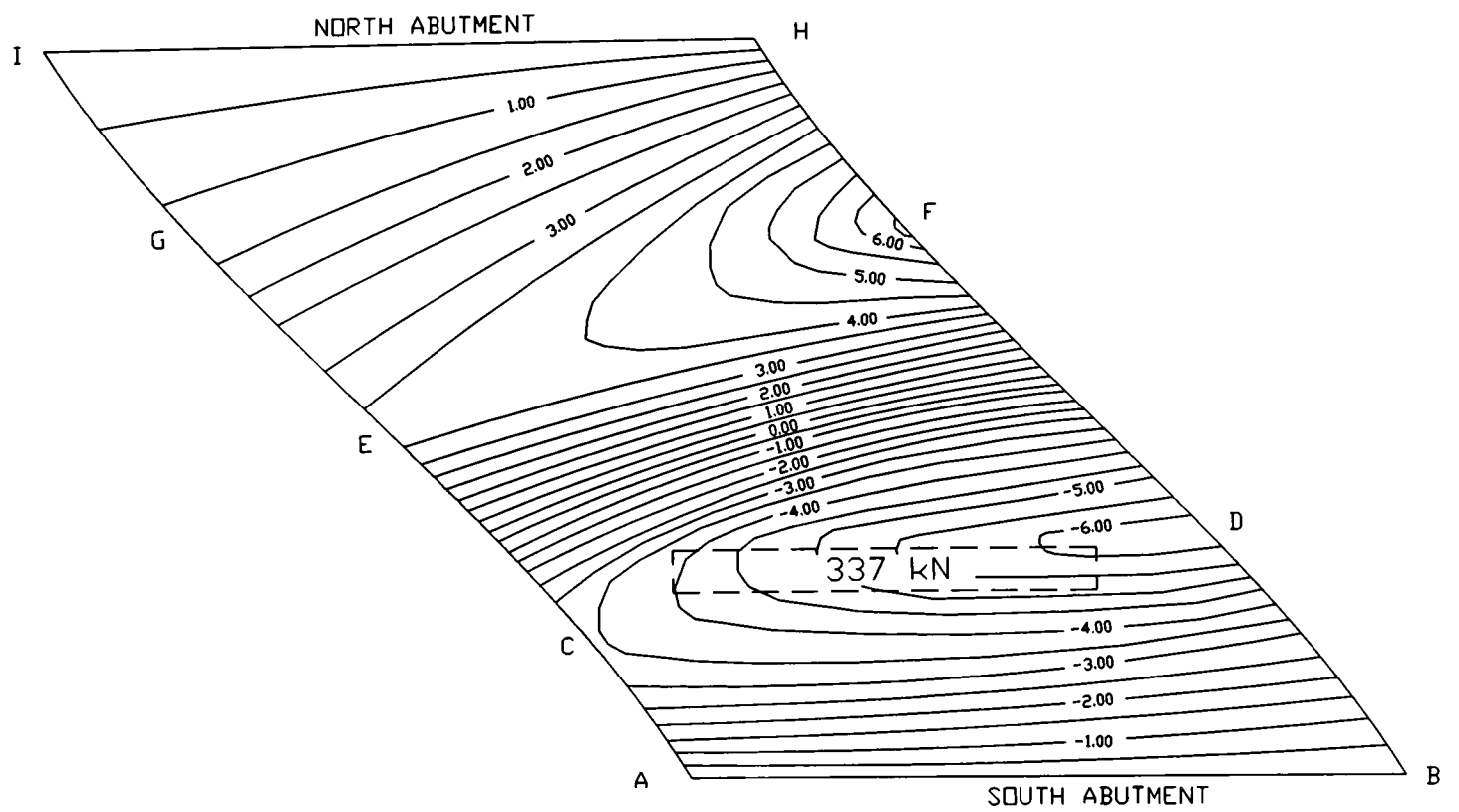

Figure 5.13 Deflected shape at failure of arch bridge 3-4

It can be seen that arch bridge 3-4 was relatively very flexible. However, this bridge was damaged during construction. Ring separation was initiated during the backfilling operation and was propagated during the non destructive tests. This was unavoidable since without spandrel walls the acute angled haunches are weak and are unable to resist the backfill compaction pressures. Thus, at the outset of the failure load test, the bridge was more comparable with the ring separated, detached spandrel walled right arch bridge shown in figure 5.11d. Thus, in this case, it can be seen that the notion that skew stiffens the arch remains valid.

Figure 5.14 shows the development of the intrados of bridge 3-2 on which the deflected shape just before failure is represented by a series of contours. The deformed shape of this bridge was similar to the shape of each other skewed arch bridge tested at the B.I.H.E. However, based on maximum inward deflections, the presence of backfill (in the case of bridge 3-4) which was in a relatively poor condition, enabled this arch to undergo much larger movements before it was reduced to a mechanism.

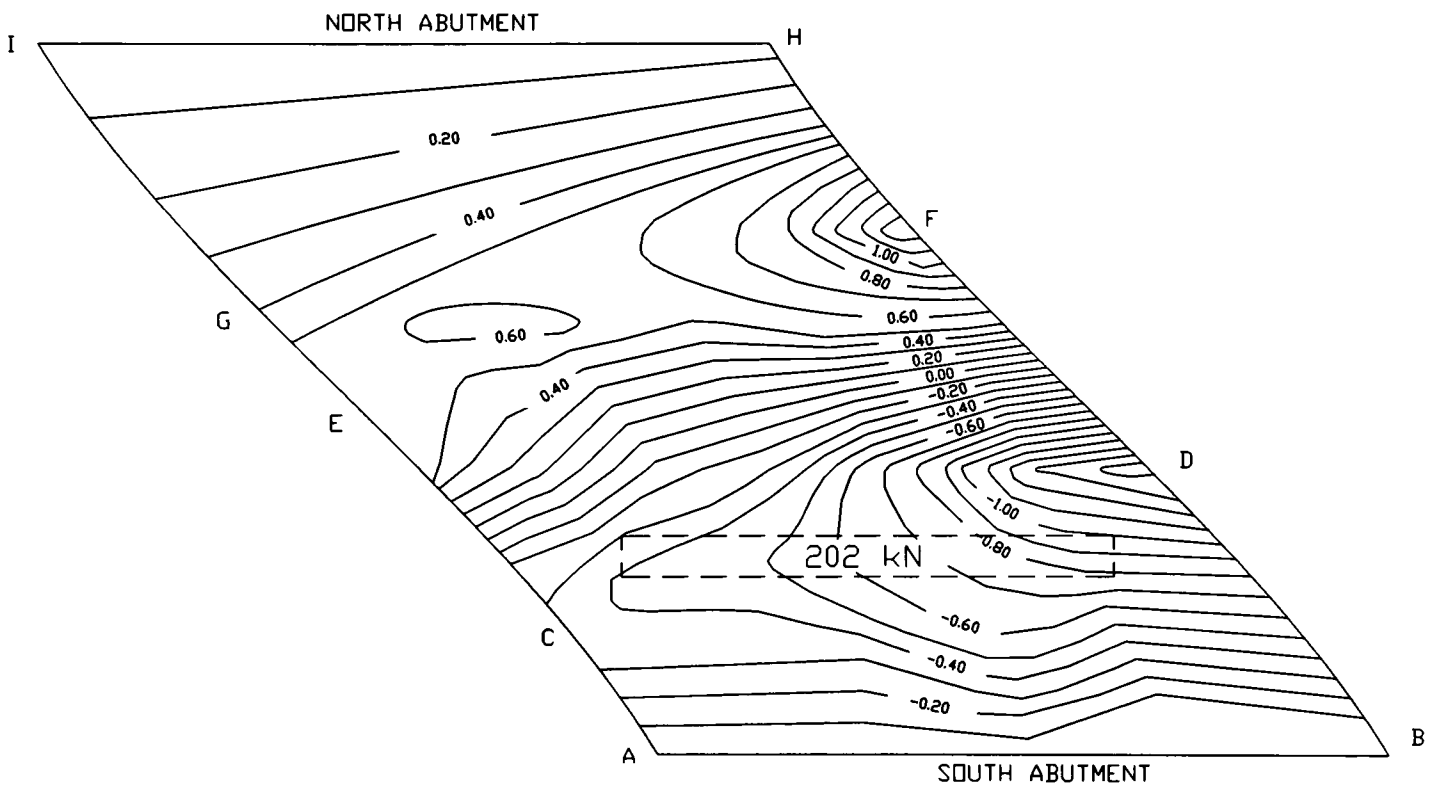

Figure 5.14 Deflected shape at failure of arch bridge 3-2

As can be seen in figures 5.11 to 5.14 the maximum outward deflection of the arch always occurred at the eastern edge of the north obtuse angled haunch. The difference between the outward deflection of the obtuse angled haunch and that of the acute angled haunch was significant and was associated with a fifth fracture. In the case of bridge 3-3, a region of downward deflections were recorded within the acute angled haunch which would serve to exaggerate the transverse bending and affirm the formation of the additional fracture.

5.1.4.2 Deflection of the spandrel and wing walls

Deflection measurements taken of the spandrel walls, wing walls and the end retaining walls revealed that these walls underwent outward movements which would tend to prevent the build up of passive pressures. The movement of these walls was small before failure since the backfill pressures generated by the deflection of the arch were not large.

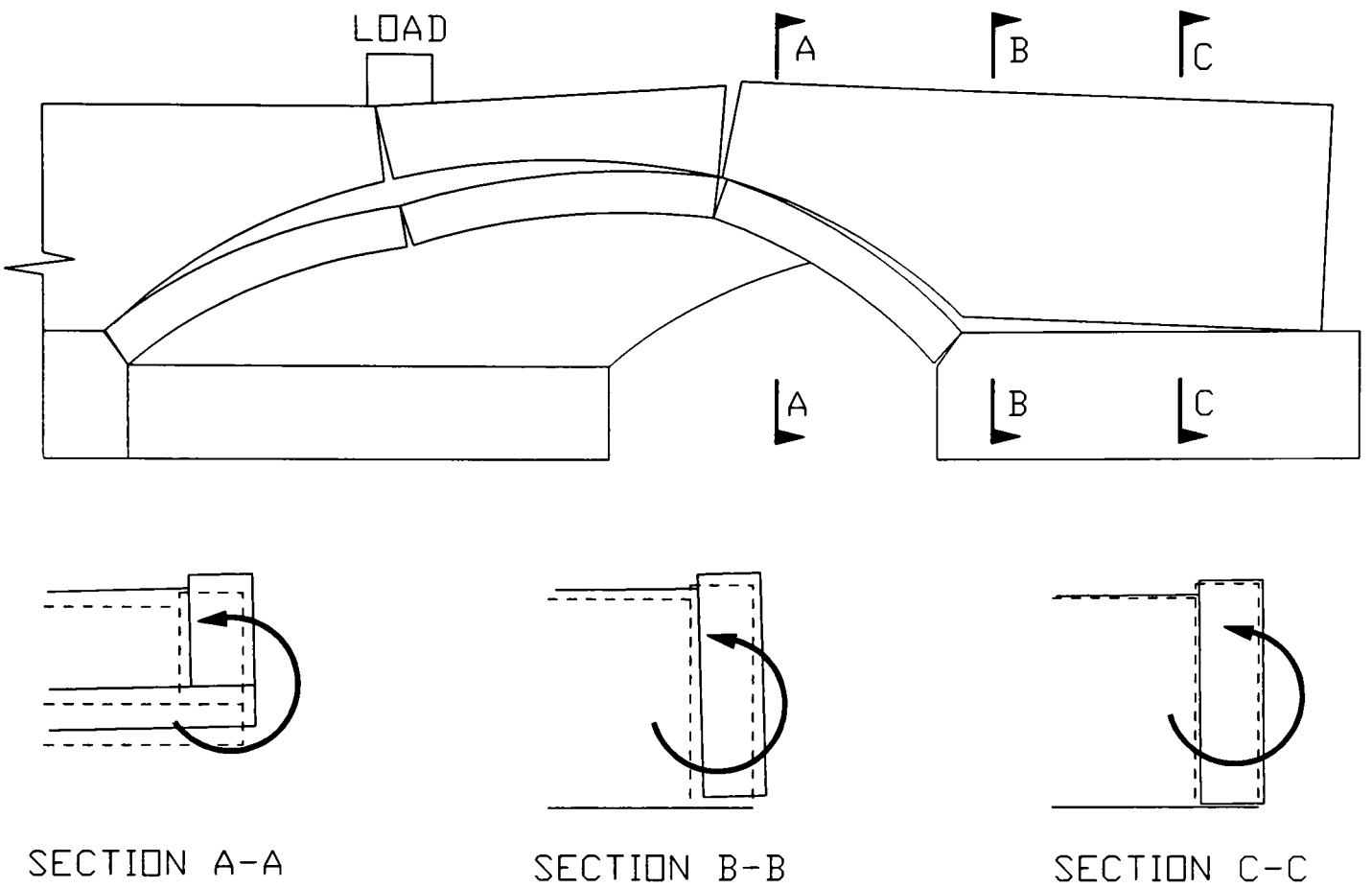

Figure 5.15 Deflection of Bridge 3-3 North East walls just before failure

In the case of bridge 3-3, upward and outward movements of the north east spandrel and wing wall occurred. The outward movement of these walls was greater at their base than at their top. The deflection of the arch lifted the above walls so that they became simply supported by the arch and the northern extremity of the wing wall. The confinement that could then be offered to the backfill was restricted and pressures were then capable of causing an outward rotation of the wall about its base since this was where pressures were greatest. Figure 5.15 shows the outward deflection of the north east walls just before failure.

5.1.4.3 Deflection of the surface of the spandrel fill

The heave of the surface of the backfill closely mirrors the deflected shape of the arch. A typical contour plot of the surfacing heave is shown in figure 5.16, which is actually the heave of the surfacing of bridge 3-3 at failure. It can be seen that the heave is greatest above the obtuse angled haunch. It can also be seen that the outward deflection of this arch was approximately equal to the heave of the fill, this point will be discussed further in section 5.1.6.1.

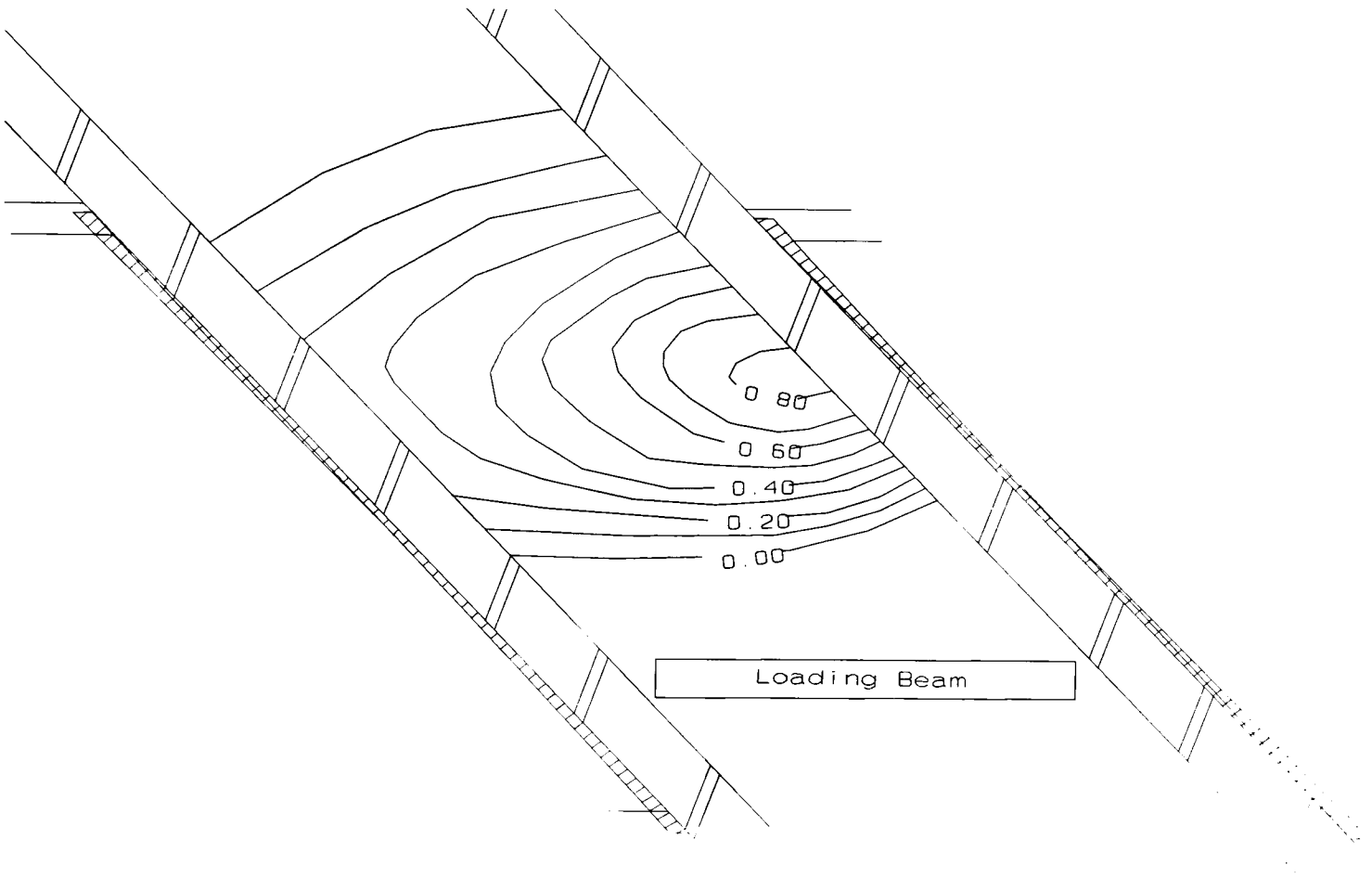

Figure 5.16 Heave of Surfacing of Bridge 3-3 at failure

5.1.5 Surface Strains

Surface mounted strain gauges generally recorded data which were difficult to interpret after cracking had occurred. A strain gauge that was situated within a tensile region but not so that its vibrating wire bridged the primary crack would record strains which would diminish when the crack opened.

Figure 5.17 contains typical load-strain responses, actually those of bridge 3-1, as recorded by a selection of intrados strain gauges that were situated in the vicinity of the first hinge.

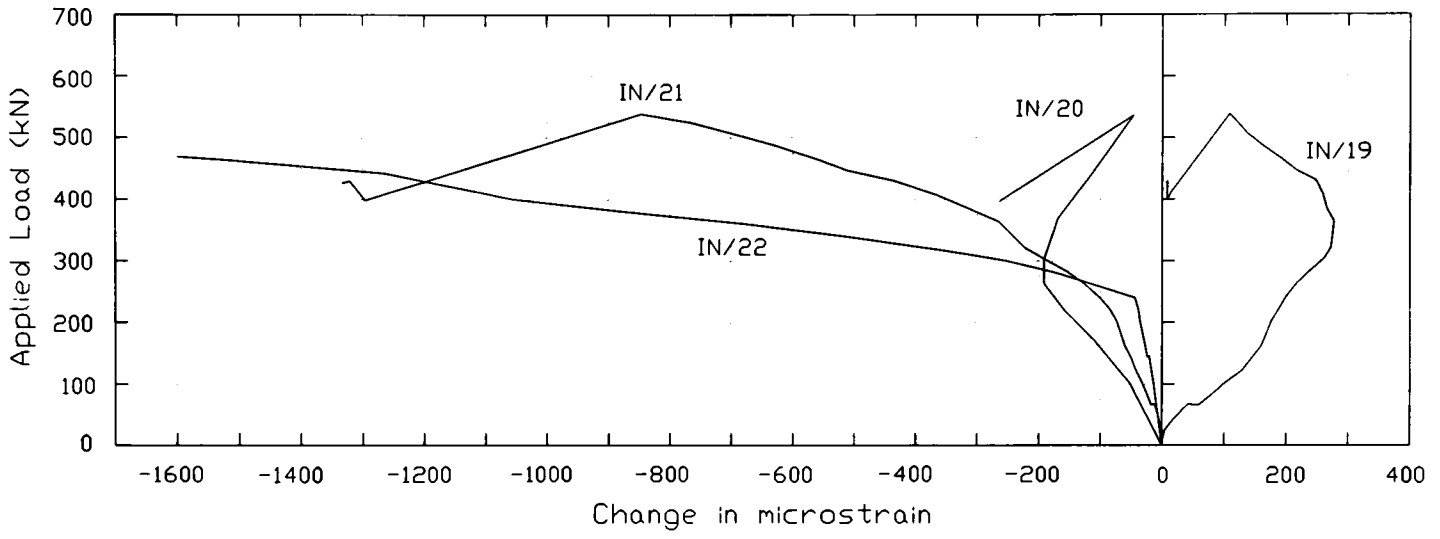

Figure 5.17 Typical surface strains within a tensile region

Gauges IN/21 and IN/22 were fortuitously situated across the tensile crack and recorded non-linear responses which revealed a marked increase in the flexibility of the arch when the tensile bond strength of the mortar was overcome and the first in-span hinge was created. Nearby gauges, viz. IN/19 and IN/20, were unfortunate enough to have been situated adjacent to the eventual position of the hinge and recorded only strain relief effects. The turning point in their strain-load response corresponded to the formation of the crack as did the change in gradient of the previously mentioned gauges. In fact, the marked change in gradient in any load-strain response is indicative of some significant change to the structure such as hinge formation, ring separation, or the detachment of spandrel walls.

Strain relief effects were generally prevalent within the load-strain relationships obtained from gauges situated within each tensile zone within each arch bridge tested at the B.I.H.E. As shown in figures 5.18 to 5.21, strain relief produced an apparently random distribution of surface strain where only large tensile strains would be expected. Figures 5.18 to 5.21 show the distribution of surface strain at failure on the intrados of each skewed arch bridge tested as part of this research. The strain distributions in compressive zones are more easily accounted for.

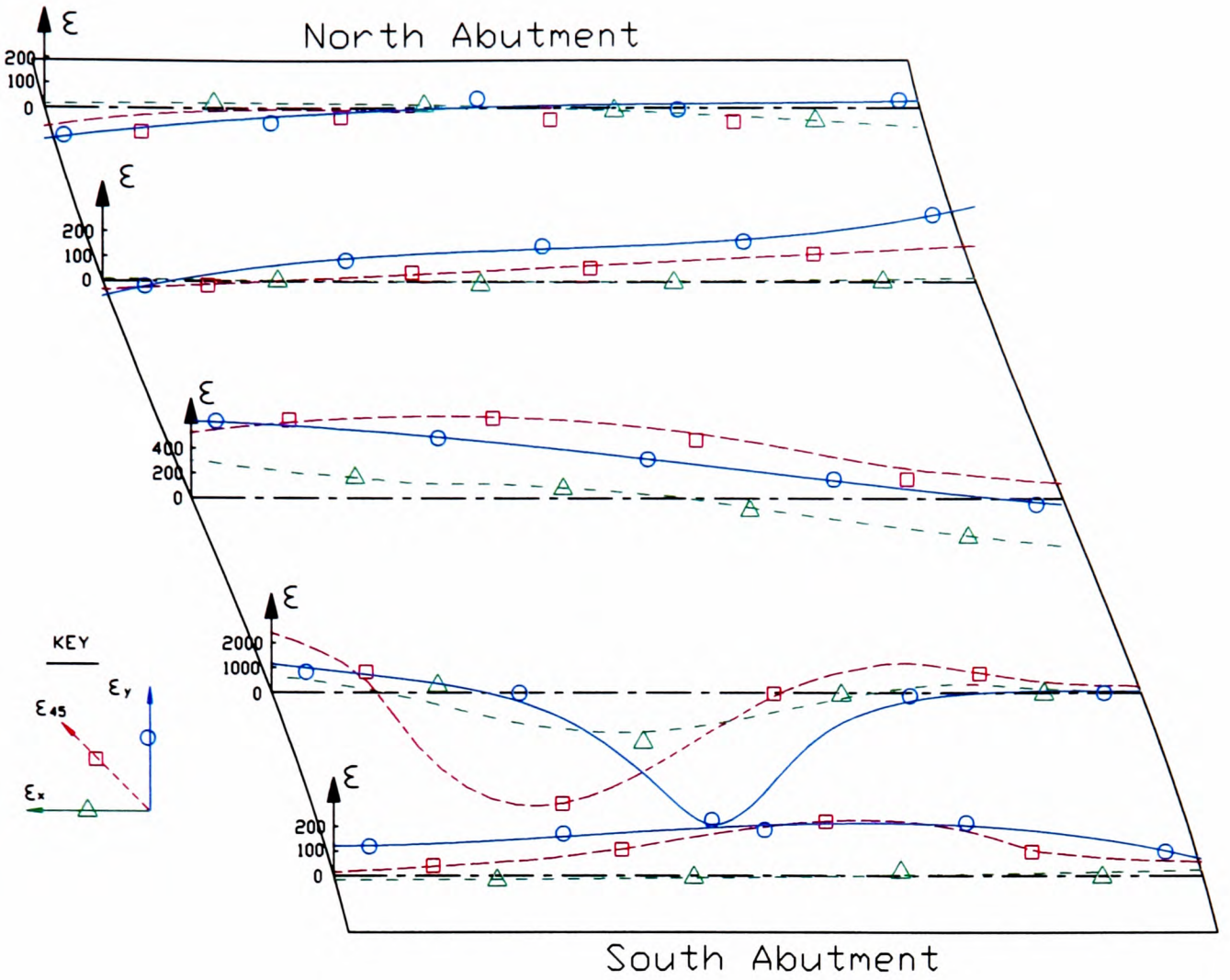

Figure 5.18 Distribution of surface strains on the intrados of skewed arch 3-1

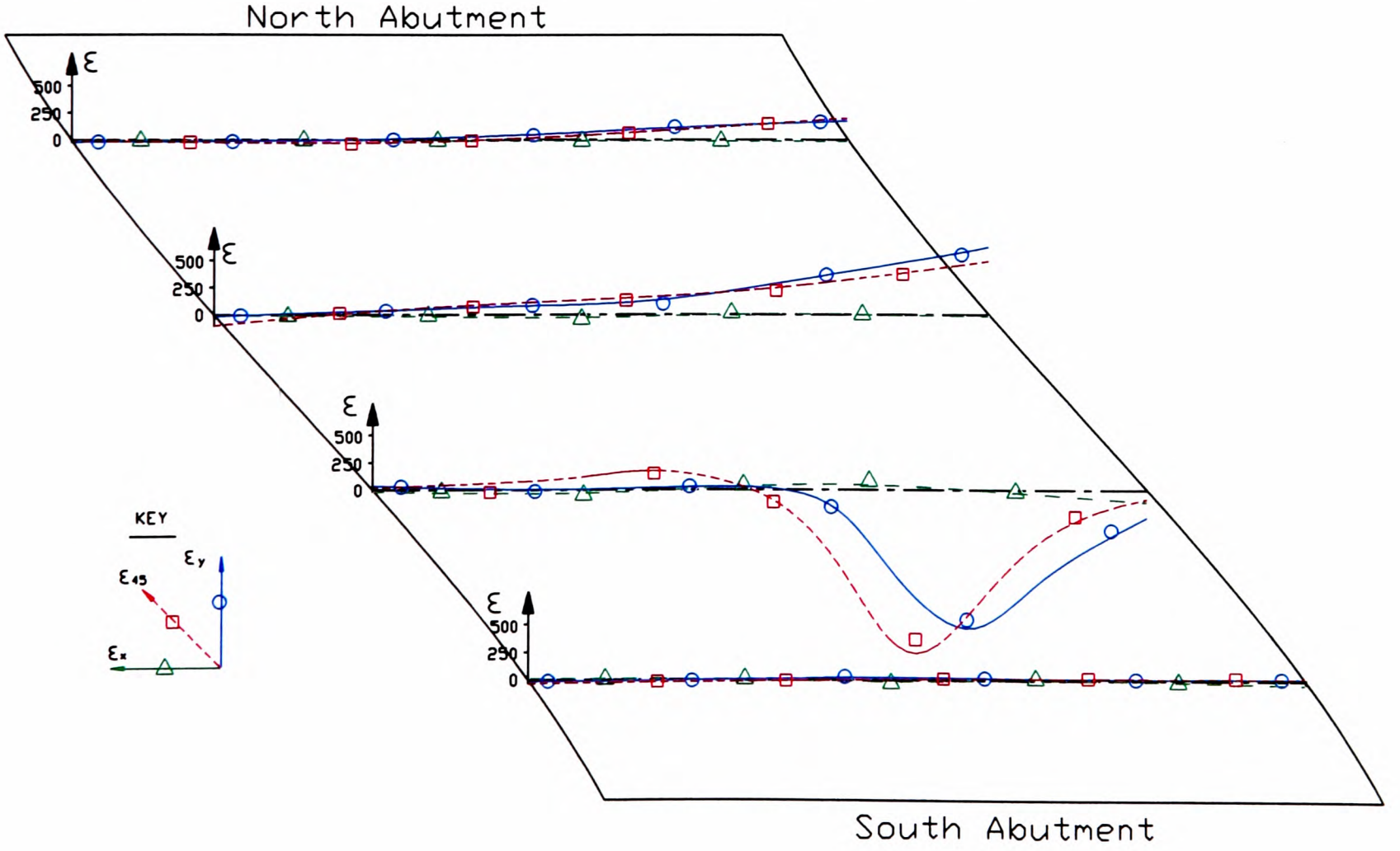

Figure 5.19 Distribution of surface strains on the intrados of skewed arch 3-2

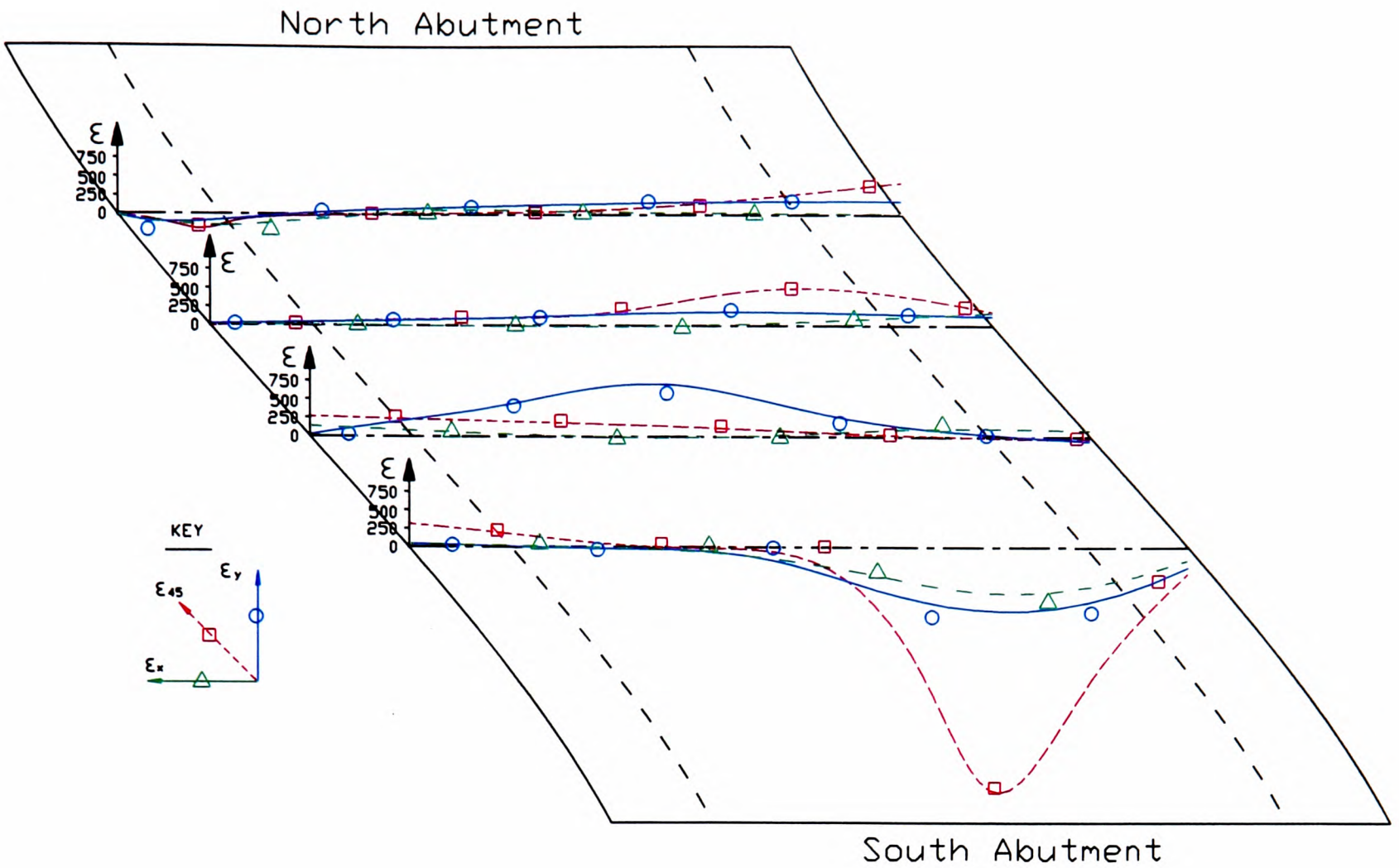

Figure 5.20 Distribution of surface strains on the intrados of skewed arch 3-3

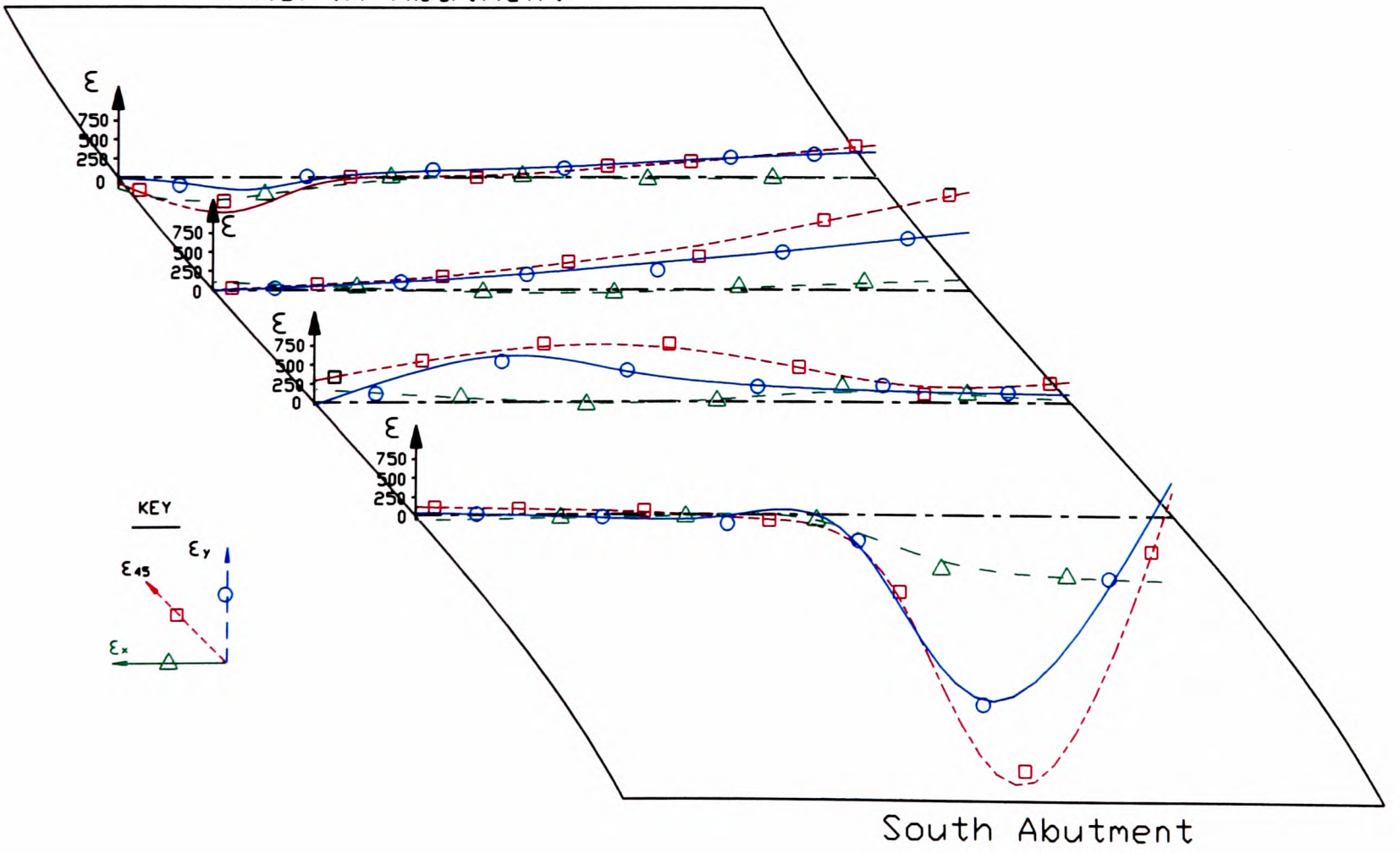

Figure 5.21 Distribution of surface strains on the intrados of skewed arch 3-4

The strain distributions on the intrados of the previously tested square span arch bridges were not linear (Gilbert, 1993) although this was partially due to the variability of the masonry. In the structures in which spandrel walls were attached some transverse bending occurred which would account for other non-linearities in the strain distributions. However, these effects were not significant enough to change the mode of behaviour which remained essentially two dimensional.

In this research, the arrangement of surface strain gauges shown in figure 3.11 evolved through an iterative process from one bridge test to the next. It was found that the distribution of surface strain along a row of gauges that were close to the abutments was small and uniform, see figures 5.18 and 5.19. Furthermore, as previously described, the strain distribution within the tensile zone surrounding the first in-span hinge was not representative of the large tensile strains that occurred in this region. Thus, the close proximity of each row of gauges shown in figure 3.11 enabled the strains created by the non-destructive point loads to be investigated and facilitated an overall understanding of the behaviour of the arch since in models of this size the rate of change of strain from one row to the next was large.

The orientation of each in-span hinge can be confirmed as being inclined to all three global cartesian axes. The fact that row 2 in each figure 5.18 to 5.21 did not record consistently high tensile strains nor did subsequent rows record consistently high compressive strains verified this statement.

In the case of bridge 3-1, shown in figure 5.18, the second in-span hinge occurred between the second and third rows of strain gauges and was inclined to these rows so that its western extremity was closer to row 2 than to row 3 whilst the reverse was true at its eastern extremity. This created the false impression that the largest compressive strains occurred at the west side of the arch.

In the case of bridge 3-2 shown in figure 5.19, the second in-span hinge also occurred between rows 2 and 3 and, whilst the largest compressive strains occurred at the eastern edge of the arch, surface strains were small at the west edge within each row. The attraction of surface strain towards the obtuse angled haunch was evident despite the fact that the spacing between each row of gauges may have allowed peak values to go unrecorded. To investigate this further, the spacing between rows of gauges was subsequently diminished.

In the case of bridge 3-3, shown in figure 5.20, the spacing between each row of gauges enabled the peak strains to be determined because the hinge intersected both row 2 and row 3. The largest strain was not measured at the eastern edge but occurred within the interior of the structure. However, the largest compressive stress would have occurred at the eastern edge since

this is a consequence of the behaviour of skewed arches. The spandrel and wing walls were also involved in the failure mechanism and were supported by the arch at this region. Their presence stiffened the arch and inhibited the development of surface strain in particular within the vicinity of the point of contact.

In the case of bridge 3-4, shown in figure 5.21, the absence of attached spandrel walls meant that the largest compressive surface strain occurred at the eastern extremity of the second in-span hinge. This hinge intersected row 2 but here the strains were not as great as those at the eastern edge of the obtuse angled haunch.

Along the fourth row of strain gauges, in a region which was remote from the second in-span hinge, compressive strains were larger at the obtuse angled haunch than they were elsewhere along this row. This was a phenomenon which occurred in each skewed arch bridge tested at the B.I.H.E. In the case of bridges 3-1, 3-3 and 3-4, tensile strains were recorded at the western extremity of this row which indicated the presence of the additional fifth hinge.

As described in section 3.5.2, the objective behind the arrangement of gauges shown in figure 3.11 was to determine the direction of the principal strains by measuring strains in the three directions required in a rectangular strain gauge rosette. However, this was unsuccessful. These arch bridges were not formed from an elastic continuum material but actually comprised a set of very stiff blocks separated by relatively flexible mortar. This meant that the movement of the bricks often resulted in compressive strains, or tensile strains, occurring in each direction. Thus, there were generally no Poisson's effects and the measured strains were more readily combined through taking components rather than via Mohr's circle of strain. Furthermore, the presence of bedding and perpendicular joints within the brickwork would cause the elastic modulus to be related to direction and make it difficult to convert strains into stresses. The exercise proved useful only in a qualitative manner in which strain concentrations could be highlighted.

Figures 5.22 to 5.25 show the development of surface strain on each fascia of each full-scale model skewed arch bridge at failure and at two intermediate loads.

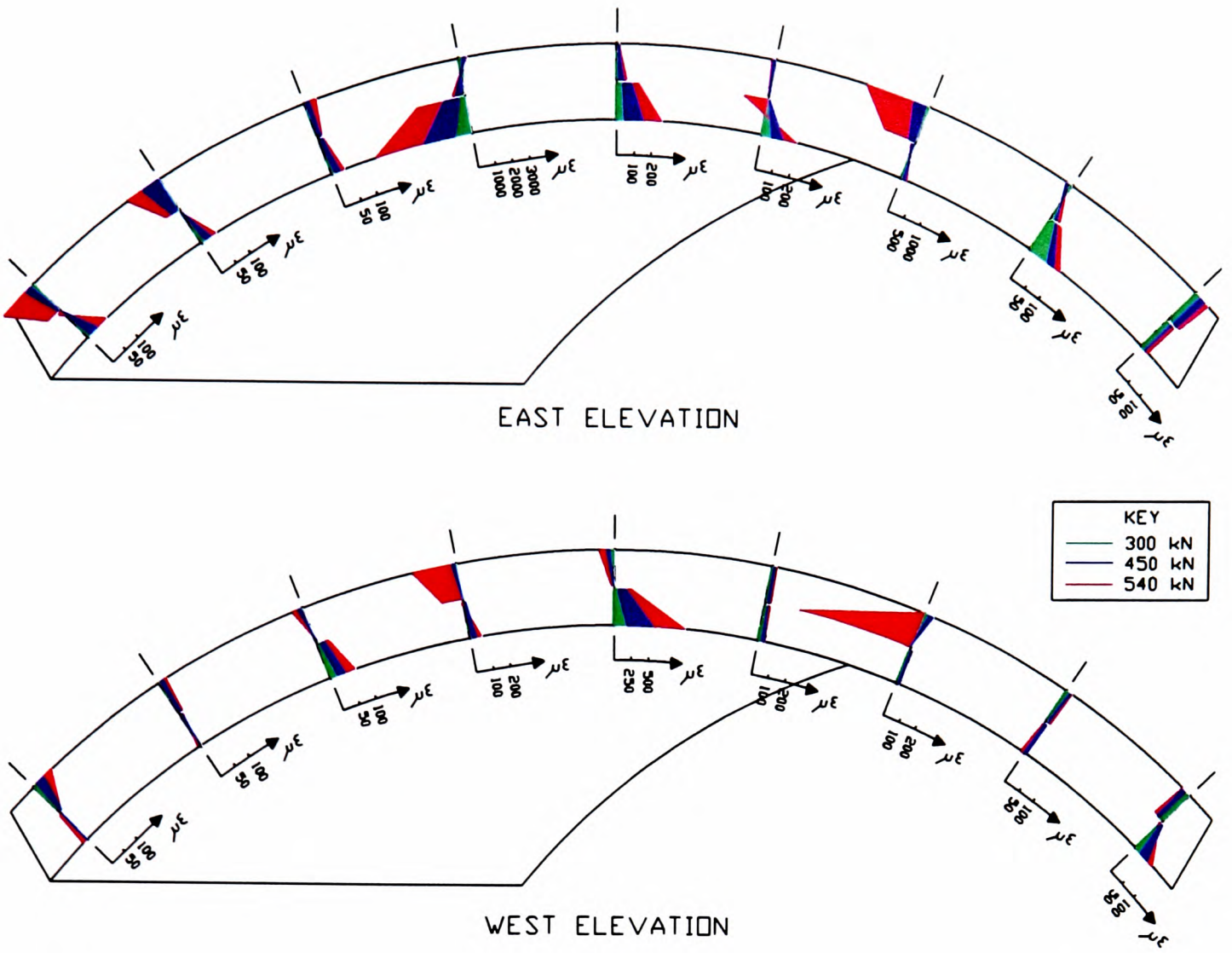

Figure 5.22 Change in surface strains on each fascia of skewed arch 3-1

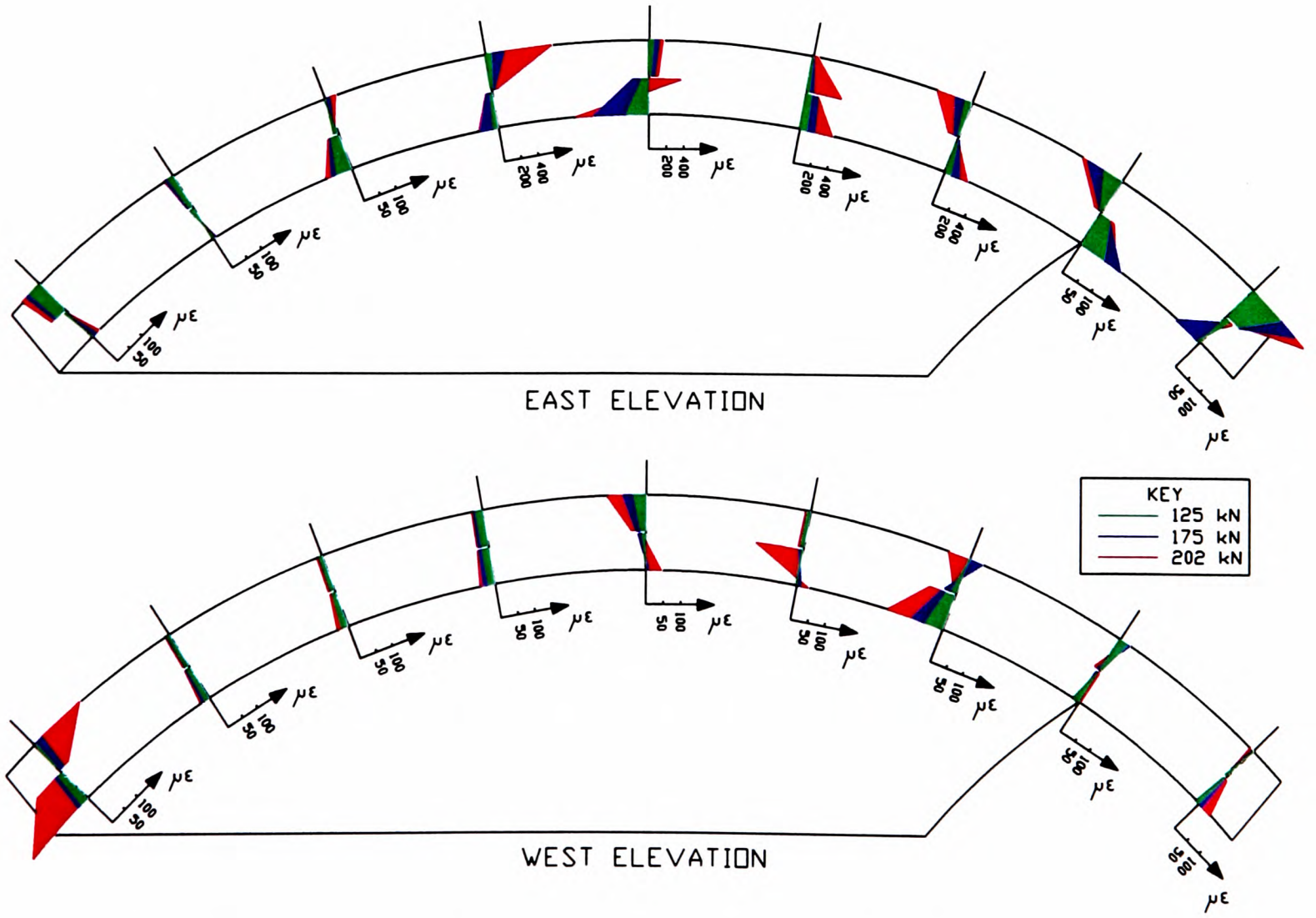

Figure 5.23 Change in surface strains on each fascia of skewed arch 3-2

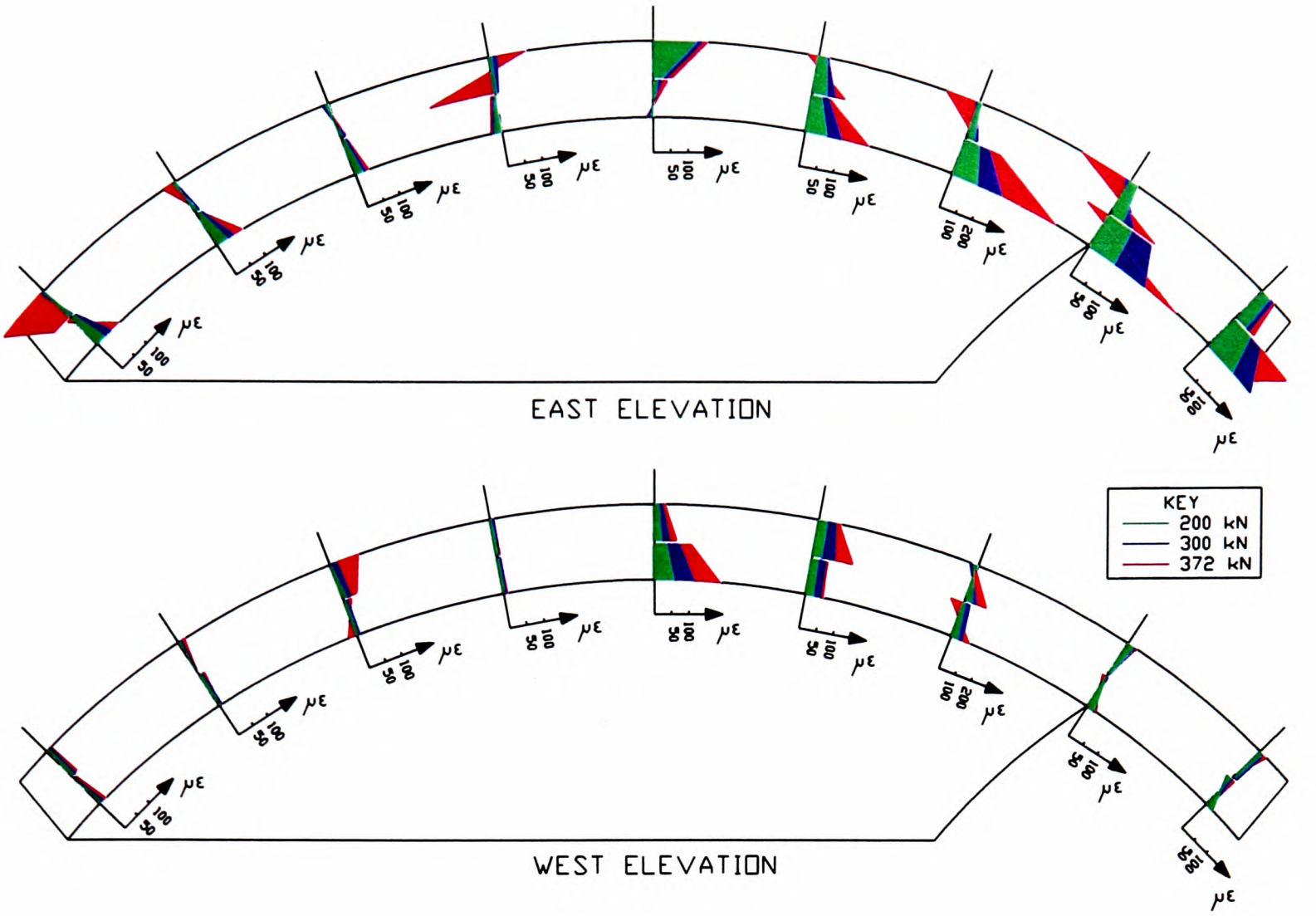

Figure 5.24 Change in surface strains on each fascia of skewed arch 3-3

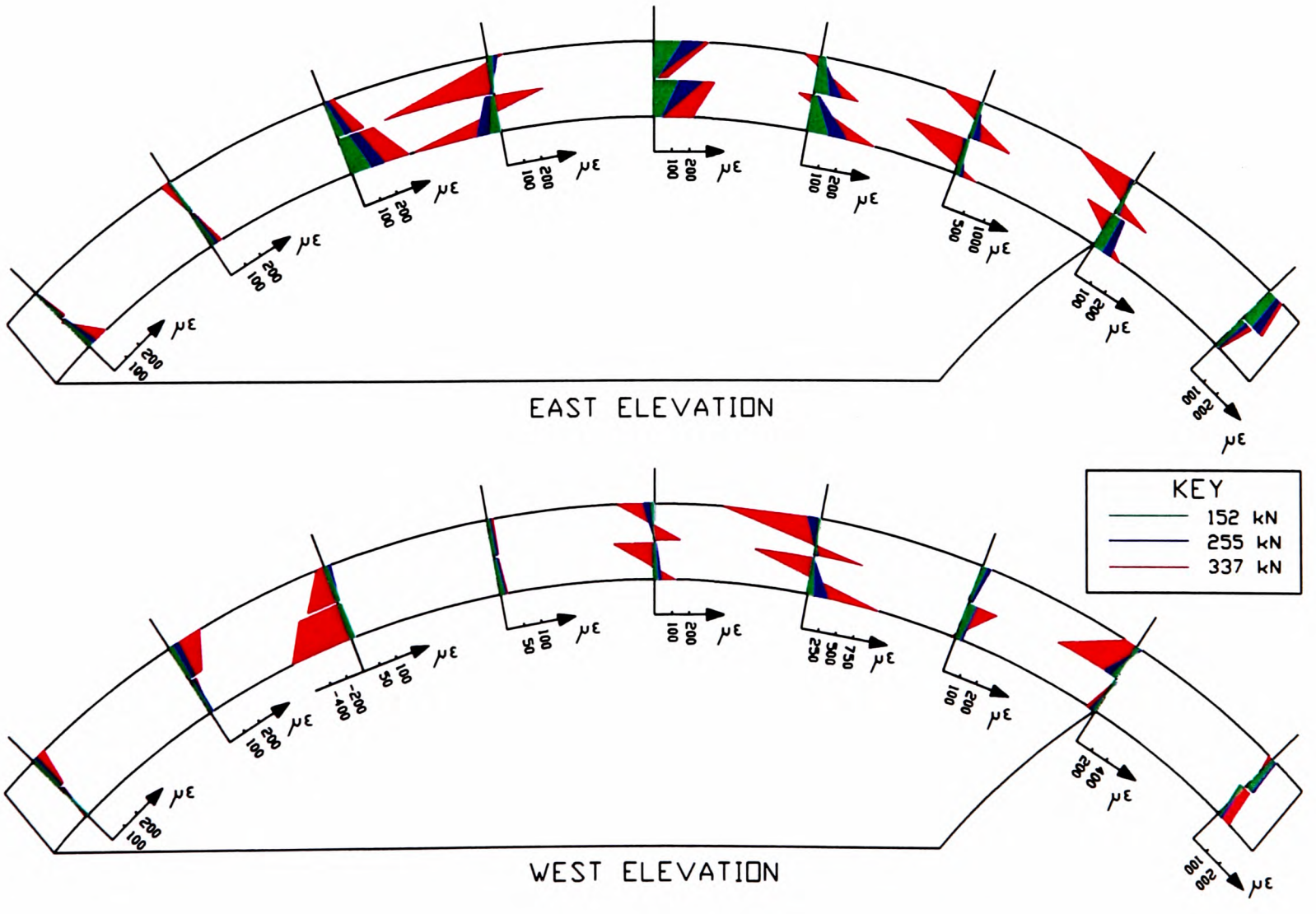

Figure 5.25 Change in surface strains on each fascia of skewed arch 3-4

A common feature observed within the fascia strain profiles shown in figures 5.22 to 5.25 was the non-linearity which occurred at the mortar joint between individual brickwork rings. This was generally observed at the ultimate load and indicated the presence of ring separation at failure. However similar observations can be made at pre-failure loads, this is particularly valid in the case of bridge 3-4 which was visually observed to have widespread ring separation at the outset of the failure load test. The discontinuity within the strain profiles of the remaining arch bridges at pre failure loads was generally not coexistent with ring separation. This must have been a consequence of the fact that the band of mortar between each brickwork ring had relatively low material properties and therefore, as discussed in chapter 4.3, could undergo shear deformation as the two brickwork rings moved relative to each other. Ring separation would not occur until the bond strength or the shear strength was exceeded.

The surface strains on each fascia were also susceptible to strain relief effects if a strain gauge had the misfortune to have been attached adjacent to where a crack occurred. However, figures 5.22 to 5.25 inclusively show that regions of tension and compression alternated on the extrados and intrados which was as expected in a square span arch bridge given the formation of a hinged mechanism. In the case of these skewed arch bridges, the general exception to this was on the north west haunch where this simple rule was violated.

In the case of skewed arch 3-2, shown in figure 5.23, tension was recorded on the intrados throughout the acute angled north west haunch which, despite its small magnitude, extended over the full depth of the section at three locations. A hinge was observed at the extrados at the north abutment which obviously could not be recorded by strain gauges. An fifth fracture was also observed at the extrados within this haunch and was associated with these regions of full depth tension.

In the case of bridges 3-3 and 3-4 shown in figures 5.24 and 5.25 respectively, the strain profile at each north west quarter point was indicative of the formation of an extrados hinge in the vicinity of this location. A further extrados hinge was observed at the north abutment. Strain profiles between these regions revealed that compressive strains on the intrados separated these two discrete regions of tension. In the case of bridge 3-3, the strain profile at the north west quarter point revealed that full depth tension occurred at this location.

It is obvious, both visually and through the instrumentation, that there is a requirement for an additional hinge which must be of a more complex nature than the simple hinges that occur in a square span arch bridge since full depth tension is a phenomenon associated with it.

Figure 5.26 shows the response of bridge 3-4 to the applied load as measured by a surface strain gauge that was situated at the eastern extremity of the second in-span hinge. The length of this

gauge was 140 mm which meant that, although this was the location of the greatest compressive strain, it was averaged over a length of 140 mm.

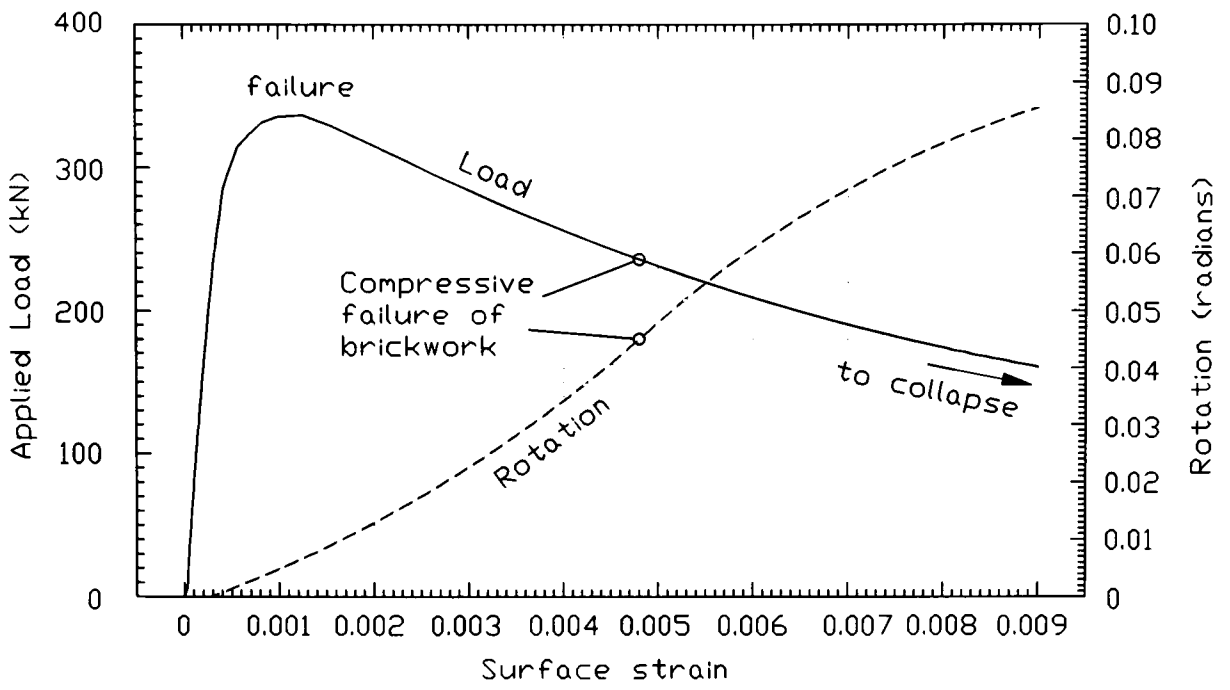

Figure 5.26 Load versus surface strain relationship for skewed arcg bridge 3-4

The above load versus surface strain relationship was approximately linear up to 80% of the maximum load. Beyond this turning point, the relationship was hyperbolic down to the point at which collapse occurred. Despite the high strength of the bricks used in the construction of this bridge, see table 3.3, it is noteworthy that compressive failures of the brickwork occurred beyond the point at which the maximum load occurred. The strain at which the brickwork crushed was 0.0048 which when compared with the stress-strain relationships shown in figure 3.1 can be seen to be far lower than the compressive strains within a typical brickwork prism when it failed in uniaxial compression. Extrapolation of figure 3.1 based on mean values given in table 3.5 would indicate that at failure the compressive strain within a typical brickwork prism was 0.02.

It can be concluded that within the skewed arch the stress state is not uniaxial and the principal stress is not perpendicular to the bedding joints as is the case during the uniaxial compressive tests on brickwork prisms. However, for analytical purposes, it may not be necessary to adopt a three-dimensional yield surface (and thereby undergo the necessary complex experimental investigation in order to describe it) because material failure may occur beyond the point at which structural failure occurs.

The surface strain versus rotation relationship was based on the rotation about the north springing of the point at which the strain gauge was situated. A point of inflexion in this relationship can be seen to concur with the compressive failure of the masonry.

5.1.6 Backfill Pressures

5.1.6.1 Pressures on the soil-structure interface

The measurement of backfill pressures on the surface of the perimeter walls and on the extrados of the arch produced unrealistic results. Pressure cells were cast into recesses within the extrados and perimeter walls of the 22.5° skewed arch, i.e. bridge 3-1, and each square span arch bridge. Pressure cells were installed only within the spandrel fill of the remaining bridges. The cells which were designated for the measurement of soil-surface pressures within bridge 3-3 faced towards the relevant masonry surfaces whilst those within bridge 3-4 faced away from the relevant masonry surfaces. Each method was unsuccessful which is why no attempt was made to record the change in pressure on the detached spandrel walls of bridge 3-4.

Figure 5.27 shows the change in pressure on the extrados of bridge 3-4 as it was monotonically loaded to failure. The load versus pressure relationships are typical, similar curves having been obtained from the load test on each model arch bridge tested at the B.I.H.E. (Melbourne & Gilbert, 1991; 1992, Melbourne & Hodgson, 1993a; 1993b; 1994a; 1995a)

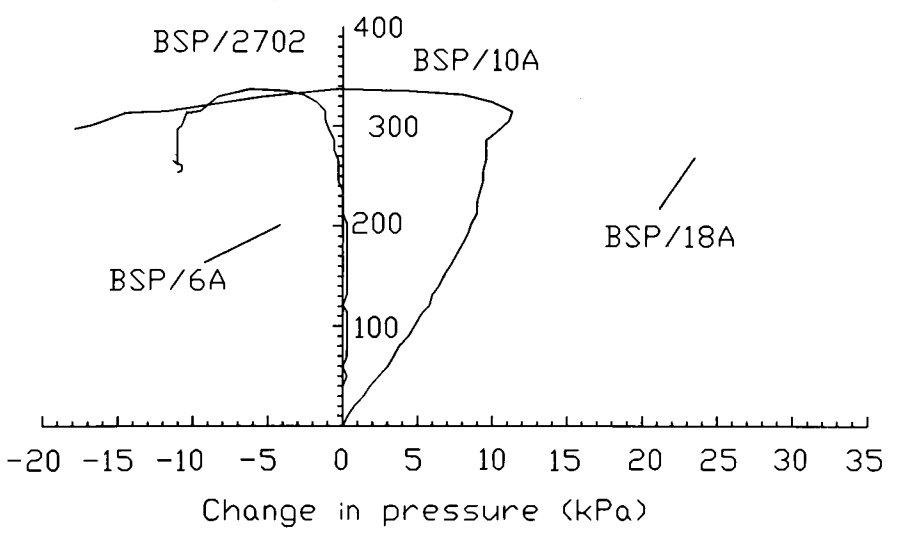

Figure 5.27 Change in pressure on the north east haunch of bridge 3-4

On the north east haunch of bridge 3-4 (see figure 3.14 for the location of pressure cells), cell BSP/6A and BSP/2702 each recorded decreasing pressure as the load was increased and the arch deflected into the fill. Cell BSP/10A recorded increasing pressure which dissipated as the bridge approached failure. The only cell to record increasing pressure throughout the test was the cell that was positioned above the hinge, viz. BSP/18A.

Similar readings were obtained from cells positioned to measure changes in pressure on the spandrel walls. These cells also recorded either small increases in pressure which later dissipated or non-linear decreases in pressure. A simplistic explanation for this non-linear

behaviour is that whilst the walls remained intact they could confine the backfill and permit the development of pressure. However, when the perimeter walls began to overturn or to crack an upper limit was imposed on the ability of the structure to mobilise further backfill pressures. However, this explanation does not account for the behaviour of cells positioned on the extrados of the arch.

Figure 5.28 shows how the fill above the arch is required to move in order to satisfy compatibility with the surrounding elements of the structure.

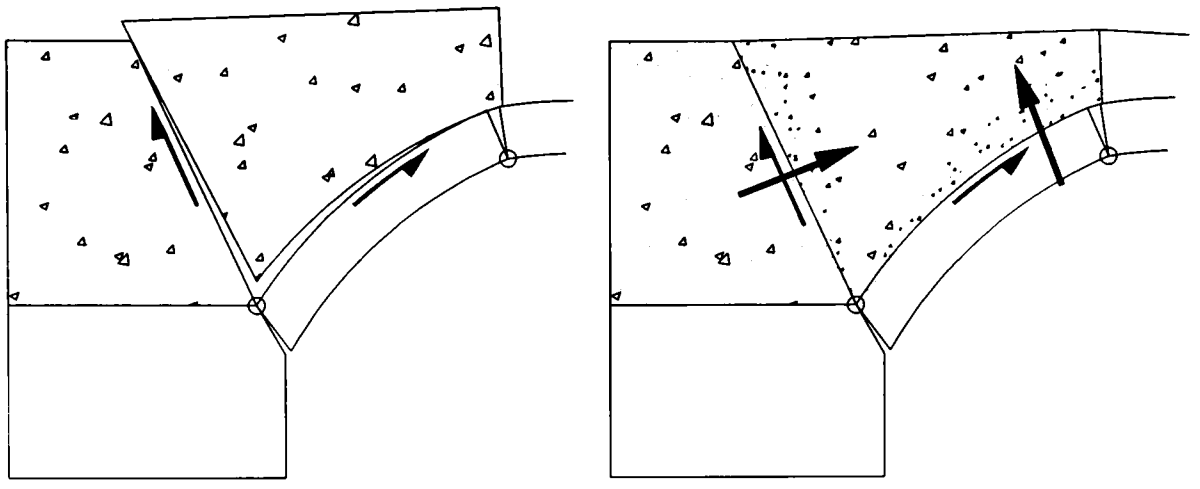

Figure 5.28 Kinematics of the soil mass above the arch

A comparison of figure 5.12 with figure 5.16 will reveal that, at failure of bridge 3-3, the magnitude of the heave of the spandrel fill was approximately equal to the outward deflection of the arch barrel. Initially, the outward deformation of the arch causes the backfill to compress which produces an increase in the generated passive pressures. However, when it can no longer be compressed and if it is not adequately confined, the backfill will displace en masse as shown in figure 5.28 so that the mobilisation of passive pressure is curtailed. If the spandrel fill is confined there will effectively be no upper limit on the passive pressure mobilisation and failure of the arch will become impossible since the backfill will prevent its deformation (Harvey; 1989). However, in practice the backfill can not be confined. Its upward displacement is resisted only by its internal friction. Its longitudinal movement is resisted by the presence of additional fill, which in the case of these model arch bridges is represented by the end retaining wall. Its lateral displacement is resisted by the presence of the spandrel walls. Paradoxically, detached spandrel walls appear to provide more confinement that attached spandrel walls because, when attached, the walls are displaced by the arch and are involved in the failure mechanism and so are relatively easy to displace outwards.

The frictional forces to which the arch and surrounding walls will be subjected as the block of backfill is displaced upwards would account for the measured load-pressure relationships typified in figure 5.27. The expected relationship between applied load and surface pressure on this part

of the structure would be such that its gradient was positive throughout and gradually reduced as the upper limit on the ability of the structure to permit further increases in pressure was approached. It must be the presence of these frictional forces which create the anomalies in the response of the pressure cells. The shear failure between the block of fill and the extrados of the arch would cause the interface to dilate and permit redistribution of the backfill. The movement of the backfill may cause slight rotations of those cells which were not cast into recesses. Each of these effects would cause a reduction in measured pressure.

The above highlights the difficulty in reliably measuring backfill pressures on a moveable soil-structure interface especially when the soil is a course compacted stone backfill and the pressure cells are relatively small. However, the presence of stabilising frictional forces in conjunction with the weight of the backfill and the passive pressure that it generates was proven despite it being unquantifiable.

Figure 5.29 shows the change in pressure on the south east haunch of bridge 3-4, i.e in the vicinity of the loading beam. It can be seen that the two cells which were positioned furthest away from the applied load recorded similar effects as those observed in figure 5.27.

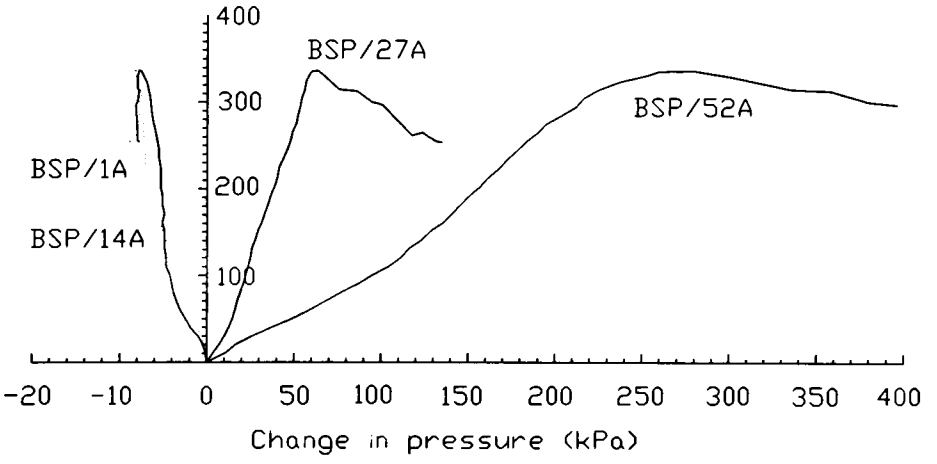

Figure 5.29 Change in pressure on the south east haunch of bridge 3-4

The movement of the backfill along the extrados of the arch was responsible for the difficulty in interpreting the measured changes in pressure. Consequently it is impossible to determine the magnitude of this effect within the response of cell BSP/52A which recorded the maximum pressure beneath the loading beam. Its response and that of cell BSP/27A showed that beyond failure, as the applied load began to diminish, pressures continued to increase. This may indicate that the dispersal of the load through the backfill diminished as the load was increased (or rather, as the arch deformed). However, it is not possible to make any firm conclusions from these observations except that the measurements of pressures within the soil mass were more reliable.

5.1.6.2 Pressures within the spandrel fill

Pressure cells were not installed within the spandrel fill of bridges 3-0c and 3-0d so no comparisons can be made between these and the remaining arch bridges. The mobilisation of passive horizontal backfill pressure above the north abutment of the remaining bridges was monitored through an array of cells situated in this region (see figure 3.14 for a typical arrangement of cells).

Figure 5.30 shows the relationship between applied load and change in horizontal pressure above the north abutment for each model arch bridge. The relationships appertain to a point at a depth of approximately 500 mm beneath the surface of the backfill at the centre line of the square span arch bridges and at a similar level but offset 600 mm from the east edge of the north abutment in the skewed arch bridges.

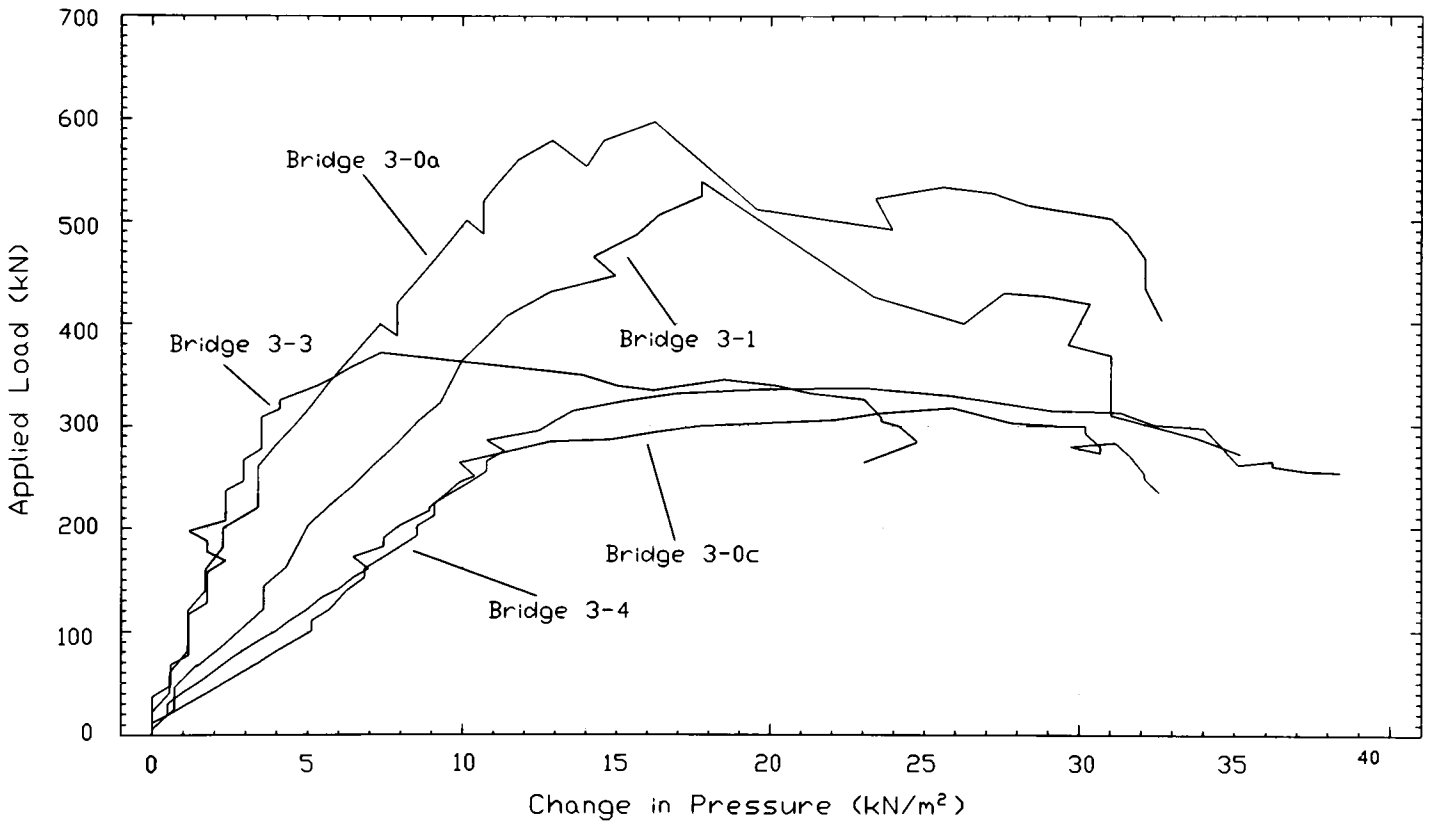

Figure 5.30 Change in horizontal pressure above the north abutment

It is difficult to make any positive conclusions from figure 5.30 because each relationship was unique to each structure. The flexibility of each structure was dependent upon the presence of ring separation, the attachment of spandrel walls, and the skew of the arch barrel. In fact, the load-pressure relationship at any point within this section through each model skewed arch bridge varied considerably depending on where it was measured. It was not possible to ensure that the backfill had a uniform density although the effort used to compact the spandrel fill within each bridge was standardised. Localised variations in the density of backfill would result in the arch deflection versus pressure change relationship varying throughout the sample section even if the deflection of the arch was uniform throughout its width and the perimeter walls were

immovable. However, if the data presented in figure 5.30 are reduced to a form in which they are based on a common value comparisons are more readily made.

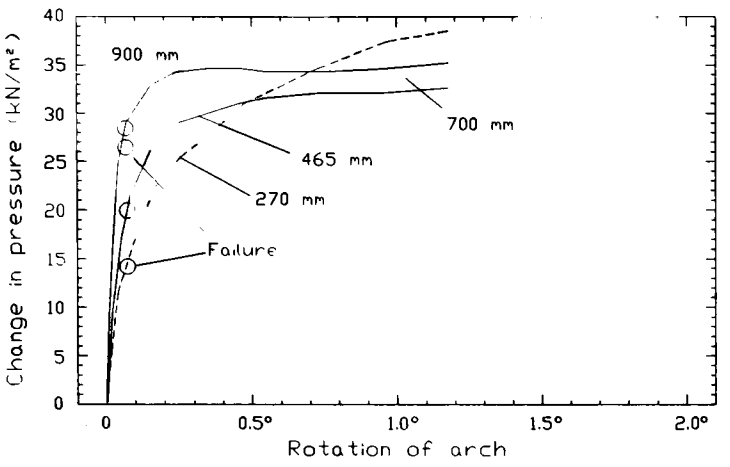

Figure 5.31a Pressure increase versus arch rotation for bridge 3-0a

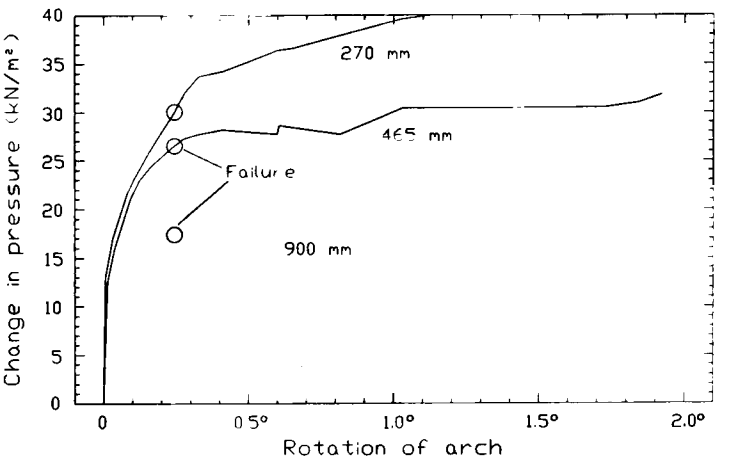

Figure 5.31b Pressure increase versus arch rotation for bridge 3-0b

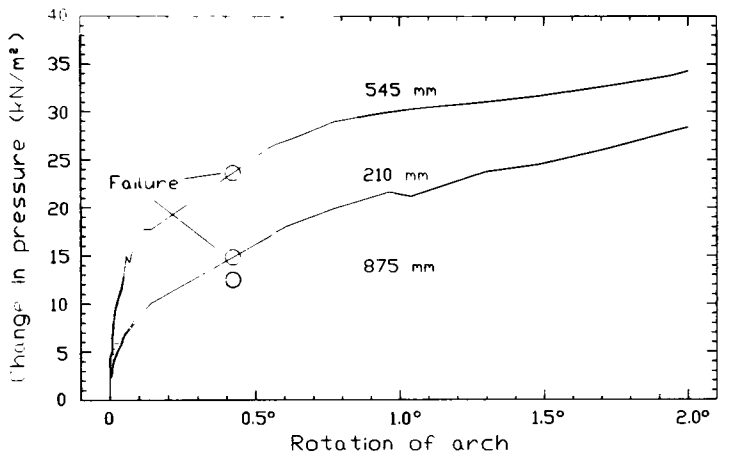

Figure 5.31c Pressure increase versus arch rotation for bridge 3-1

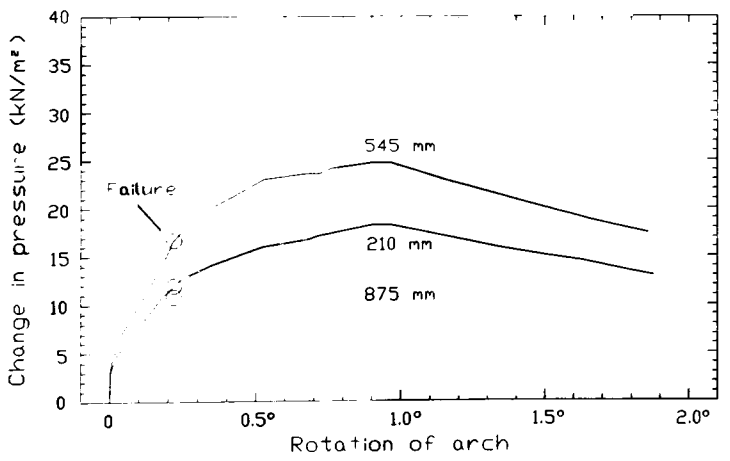

Figure 5.31d Pressure increase versus arch rotation for bridge 3-3

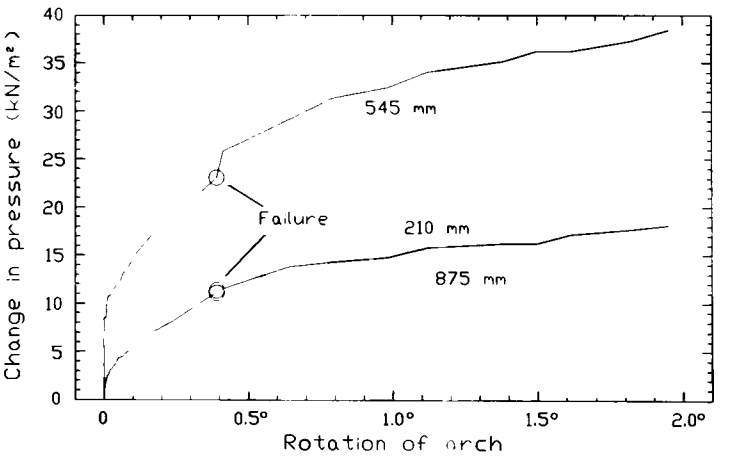

Figure 5.31e Pressure increase versus arch rotation for bridge 3-4

Figure 5.31 shows the change in horizontal passive pressure as a function of the rotation of each arch about its north springing. The multiple relationships presented for each arch bridge express the change in pressure at the same location as that which was adopted in figure 5.30 but at three different levels beneath the surface of the spandrel fill.

It can be seen that the mobilisation of passive backfill pressure was a non-linear function of the outward rotation of the arch barrel. As a consequence of this, the greatest increases in pressure were found to occur at mid-depth although, as rotations became large (after failure), the rate of change of pressure near the surface of the backfill would indicate that the location of maximum pressures migrated upwards as the arch approached collapse.

In the structures with attached spandrel walls, there was an upper limit on the available passive resistance that the backfill could generate as a reaction to the outward movement of the arch. This was due to the movement of the perimeter walls. With the exception of the surface layer of the backfill, pressures within bridges 3-0a and 3-0b increased only marginally after the rotation of the arch barrel exceeded 0.5°. In the case of bridge 3-3 the aforementioned upper limit on the passive backfill pressures was more noticeable because its east spandrel wall was displaced upwards and rotated outwards by the arch and the backfill pressure. Consequently, backfill pressures dissipated when the east spandrel wall began to move. It should be noted that backfill pressure remote from the spandrel walls did not dissipate to a similar extent, this can be seen in figure 5.35.

The most feasible explanation for the difference between the behaviour of the backfill at depths of 700 mm and 900 mm in the two square span arch bridges, viz. Bridge 3-0a and 3-0b, was the degree of compaction. Initially, in bridge 3-0a, large backfill pressures were generated at these depths by relatively small rotations of the arch barrel. In contrast, larger rotations of the arch barrel of bridge 3-0b were required in order to increase the backfill pressures. This is indicative of inconsistent compaction. However, given that bridge 3-0b contained total ring separation, it would have been expedient not to risk damaging the structure by compacting its fill by applying a similar effort to that which had been used in compacting the spandrel fill of bridge 3-0a until, at least, the barrel was covered.

In the structures built with spandrel walls detached from their arch barrel, viz. bridges 3-1 and 3-4, the corresponding relationships between pressure and rotation at each depth (at the locations shown in figure 5.31) were similar to each other. Backfill pressures continued to increase with increasing rotations of the arch since the spandrel walls were more capable of confining the backfill because they were not subjected to movement as a direct result of the deformation of the arch. However, they did suffer displacement which was produced by the pressure within the backfill. Outward movement of the detached spandrel walls of the square span arch bridges was recorded despite the fact that the deformation of the arch occurred predominantly in a direction which was parallel to the walls.

Figures 5.32 to 5.36 show the increase in horizontal pressure within the backfill above the north abutment of each arch bridge at the load increment at which failure occurred. The distribution

of pressure is shown as a series of contours which were generated by fitting the best smooth surface through the data obtained from the array of cells positioned at this location.

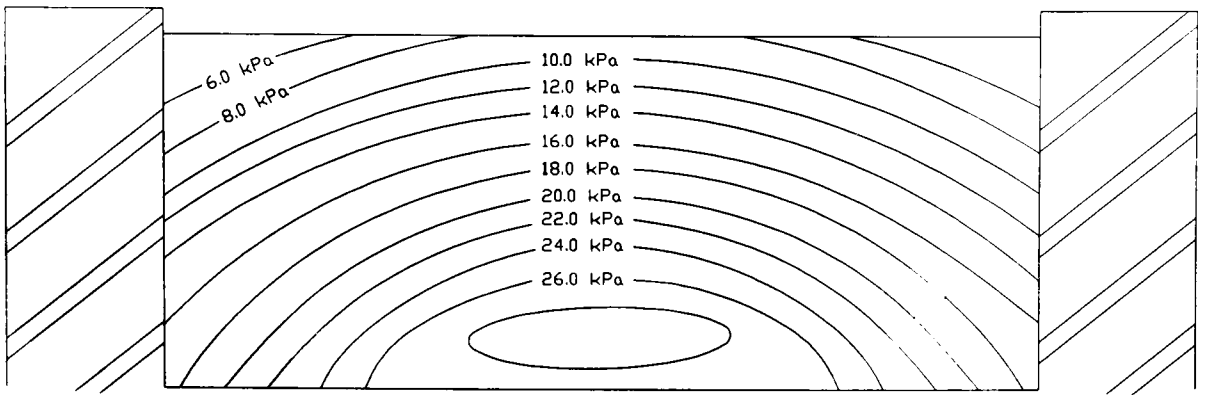

Figure 5.32 Change in passive backfill pressure within bridge 3-0a

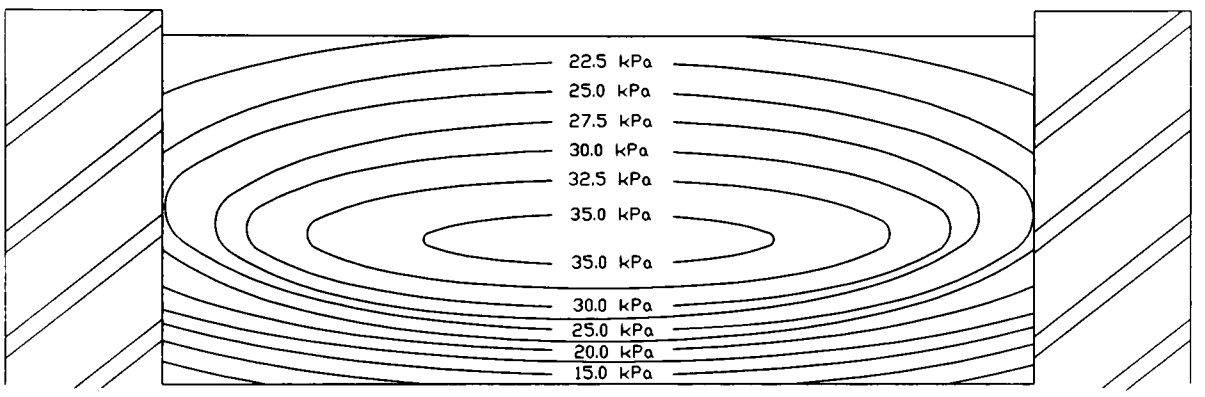

Figure 5.33 Change in passive backfill pressure within bridge 3-0b

It can be seen, in figures 5.32 and 5.33, that the increase in passive pressures behind each square span arch bridge were greater and more widespread than those behind the skewed arch bridges. The maximum passive pressures behind each skewed arch bridge were limited to a comparatively small region in the vicinity of the obtuse angled corner. However, the east spandrel wall of bridges 3-3 and 3-4 displaced outwards during the failure load test which produced a curtailment of passive pressures in its immediate vicinity. Thus, peak pressures behind each 45° skewed arch bridge were shifted slightly away from the east edge of the north abutment. The movement of the east spandrel wall of bridge 3-1 was much less than that of the more severely skewed arch bridges. This prevented similar dissipation of the maximum passive pressures which consequently remained at the east edge of the north abutment.

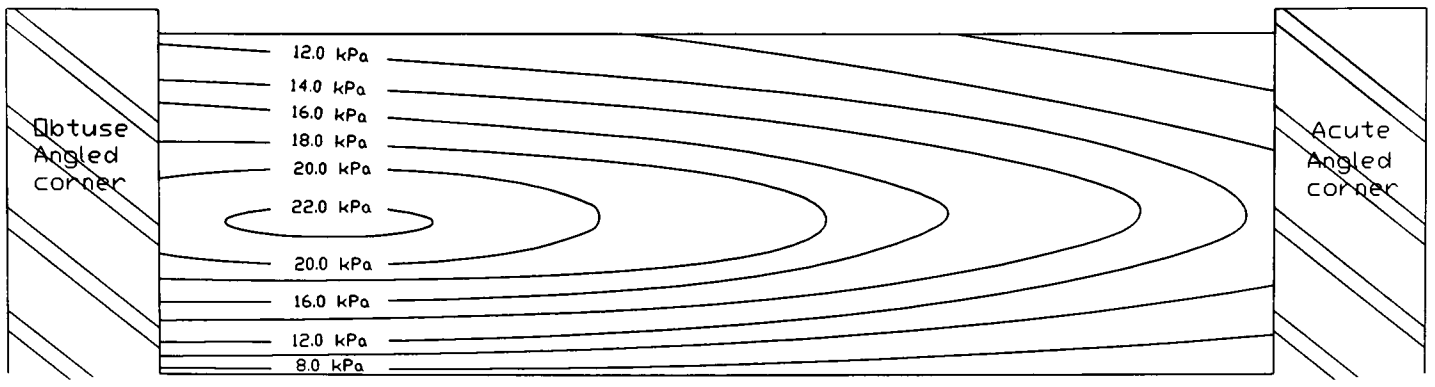

Figure 5.34 Change in passive backfill pressure within bridge 3-1

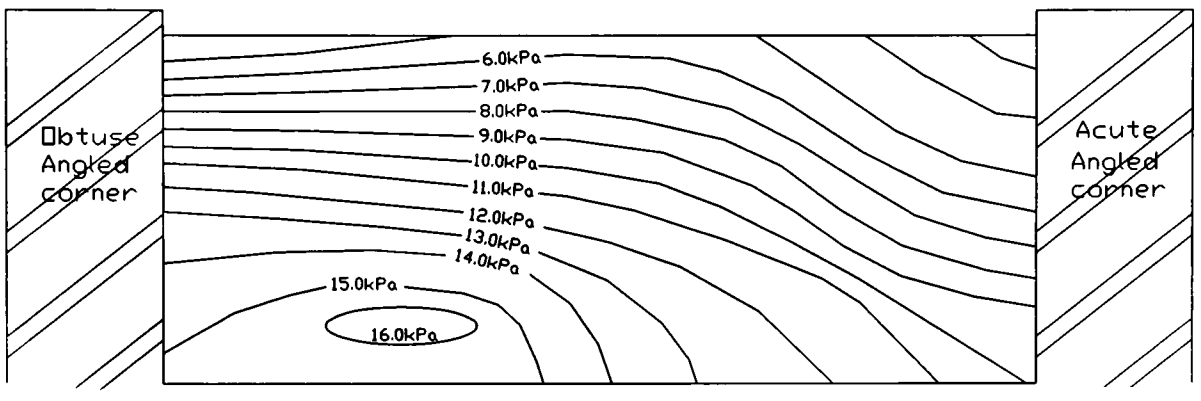

Figure 5.35 Change in passive backfill pressure within bridge 3-3

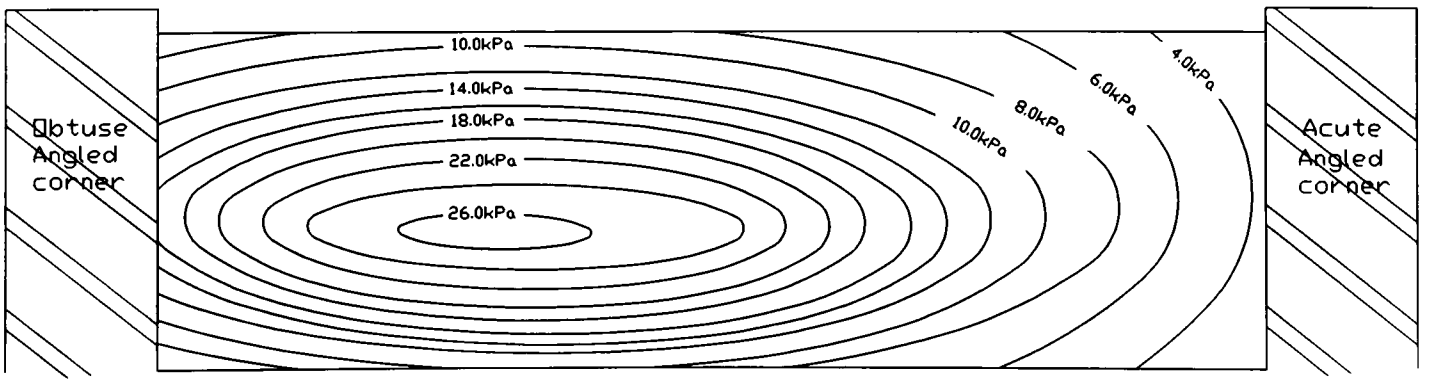

Figure 5.36 Change in passive backfill pressure within bridge 3-4

5.2 1.2 m span model arch bridges

5.2.1 Overview

Each 1.2 m span model arch was subjected to a single point load which was monotonically increased until failure occurred. The principal objective of this series of tests was to determine the generalised configuration of each failure mechanism. This would facilitate the development of the three-dimensional mechanism analysis method described in chapter 6.

It was important to use a mortar that was strong enough to resist the rigours of construction, particularly during the removal of the centring, but not so strong that it would produce catastrophic failures. A high bond strength of the mortar enables the line of thrust to lie outside the bounds of the arch without a failure mechanism being created. The arch can then undergo larger pre-failure deformations than those which would otherwise be possible. The deformed shape of the arch is equivalent to a post-failure state in which the load carrying capacity is greatly reduced. Thus, when the mortar bond strength has been exceeded the load is much higher than the deformed state can resist which, unless the loading system can rapidly reduce the applied load, may produce a simultaneous collapse.

The inherent assumption of the mechanism method that the tensile strength is zero means that it would be unable to reproduce the exact collapse load obtained from tests such as these. Furthermore, its predictions would become increasingly inaccurate as the strength of the mortar was increased. The mortar was prescribed so that its tensile strength was as low as possible, its mix was similar to that used in the construction of the 3.0 m span arch bridges. In this way, catastrophic failures were avoided since the residual load carrying capacity of the arch after failure occurred was sufficient to resist the residual applied load so that collapse and failure were two distinct events. The advantage of the mechanism method lies in the fact that the bond strength of mortar in actual arch bridges will undoubtedly be random and will be sufficiently low in some regions to enable it to make reasonable predictions of the location of each fracture line and the associated collapse load.

If the strength of the mortar is randomly distributed throughout the arch, the cracks that form during the formation of the failure mechanism may not occur within the joints where they would if the mortar was of a uniform strength. In other words, the failure mechanism would not correspond to the mechanism which required the least load to create. However, this is not important because the objective of these tests was to verify and determine generalised forms of rigid block movements that can occur in the formation of a mechanism so that a mathematical description of these movements could be obtained.

5.2.2 General Arrangements

As outlined in table 3.2, the square span of each small scale arch was 1.2 m and its span/rise ratio was equal to 4.0. Each arch was not backfilled and comprised the single ring brickwork barrel only. Load was applied through a mortar pad which provided a level surface and ensured that localised stress concentrations did not occur. Figure 5.37 shows a typical general arrangement of a square span and a 45° skewed arch. The figure also shows typical arrangements of deflection and surface strain gauges.

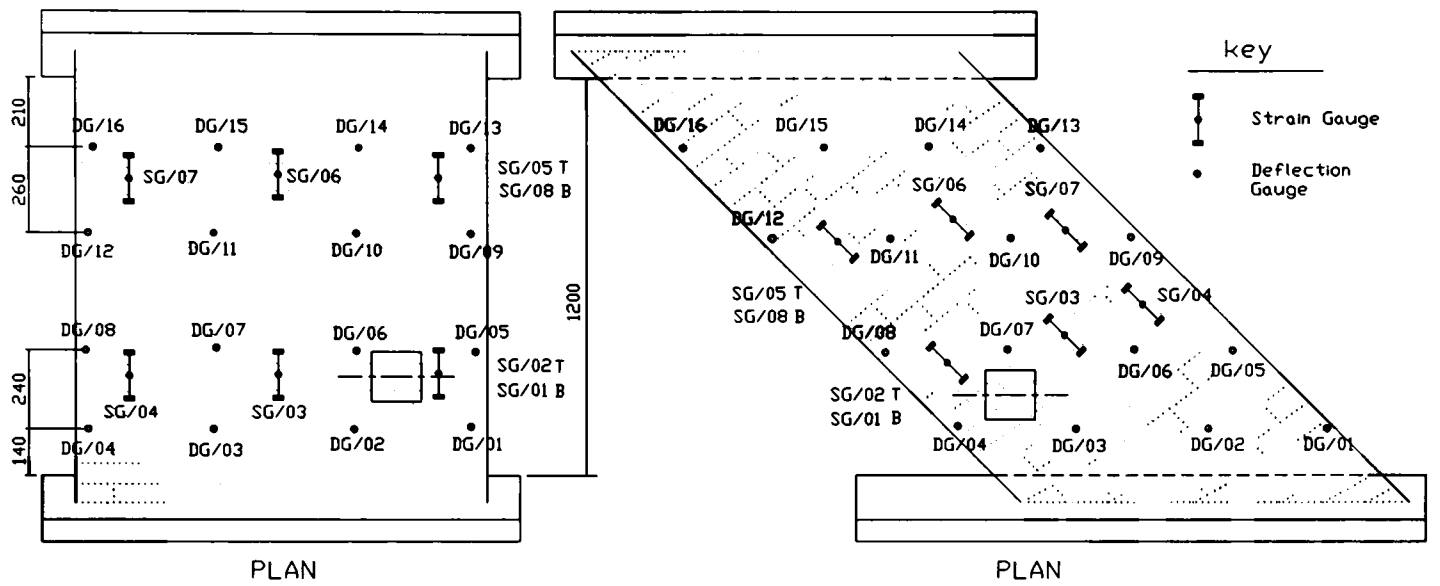

Figure 5.37 Typical general arrangements and location of instrumentation

Deflection gauges were positioned in a uniformly spaced 4×4 array in which the first and last gauge along each row was situated 25 mm from the edge of the arch. Surface strain gauges were uniformly spaced across each structure at locations where it was anticipated that hinges would occur. Two strain gauges were attached to the intrados at locations opposite to those on the extrados at the same side of the structure as the load.

5.2.3 General Observations

5.2.3.1 Application of Load

A single hydraulic jack was used to apply a monotonically increasing load through a 150 × 150 mm patch positioned eccentrically at either the quarter-point or crown. The load was increased in 0.5 kN increments until failure occurred; the mean loading rate being 25 kN/h.

5.2.3.2 Mode of failure

Each square span arch ultimately formed a hinged mechanism that was essentially two-dimensional and which brought about its collapse. The collapse mechanism of each skewed arch contained fracture lines that were consistent with both sliding and rotational movements. These mechanisms were clearly three-dimensional in which each block of masonry rotated about the line of each fracture as well as about radial or circumferential axes at the end of each fracture line. The complexity of the fractures increased as the number of fracture lines decreased.

5.2.4 Crack Monitoring and failure mechanisms

The formation and propagation of cracks within each bridge was monitored throughout each destructive test. Each bridge was whitewashed to facilitate this. There was generally little warning that failure was imminent. The load at which the first crack occurred was either one or two load increments before failure, i.e. at approximately 90% of the failure load.

Figure 5.38 shows the pattern of cracks as observed in the extrados of bridge 1-1. This arch was not loaded to failure so the collapse mechanism has not been shown in elevation.

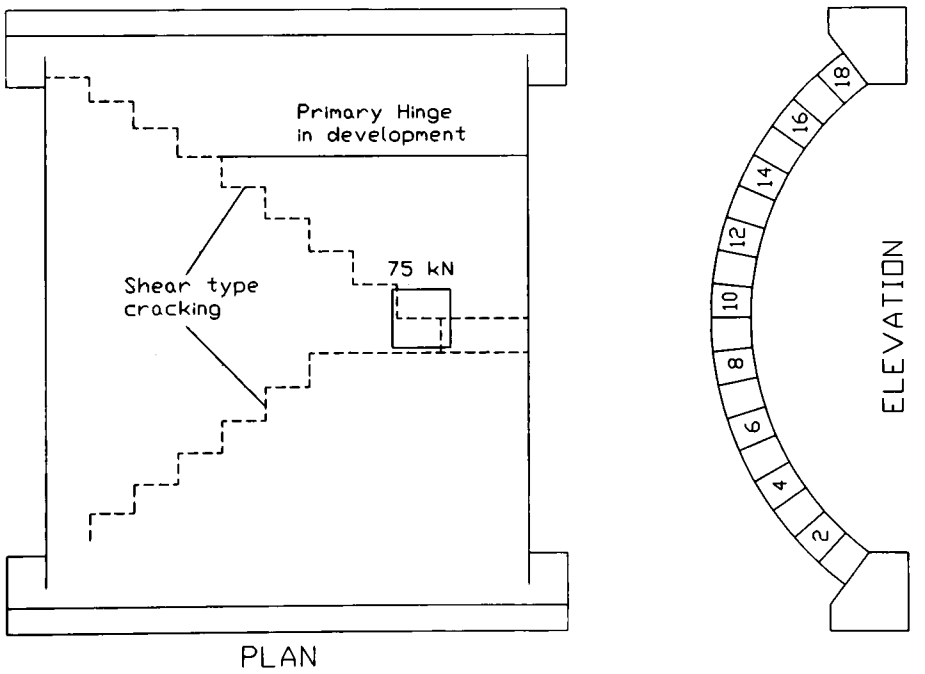

Figure 5.38 Crack pattern and failure mechanism of arch 1-1

In the case of the square span arches, arch 1-1 was an almost perfect structure in which, barring material failure, structural failure could not occur. This arch was not loaded to failure although the crack pattern may indicate that a complicated three-dimensional mechanism would have formed. It is equally possible that the cracks observed as propagating from the load towards the remote corners of the arch were due to elastic shortening of the part of the structure which was supporting the load whilst the remaining triangular region was redundant. Alternatively, catastrophic failure of the loading rig may have brought the test to a premature conclusion; this

was why the application of further load increments was curtailed when the load reached 75 kN.

The square span arch that was subjected to an eccentric point load at its south quarter point failed by the formation of a four hinged mechanism in which each hinge was parallel to the abutments. The crack pattern and collapse mechanism of this bridge are shown in figure 5.39.

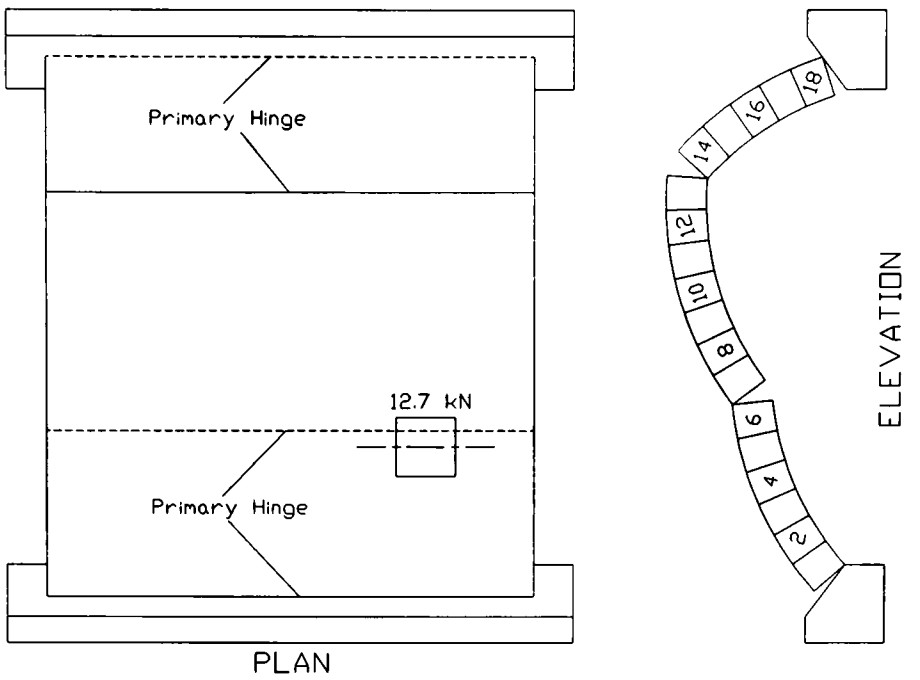

Figure 5.39 Crack pattern and failure mechanism of arch 1-2

The above arch, viz. arch reference 1-2, was of regular dimensions in which the ratios span/thickness, span/rise, and span/width were 11.7, 4.0, and 1.2 respectively. It can be concluded that for similarly proportioned arches, and provided that they are well maintained and comprise adequate materials, local failures do not occur.

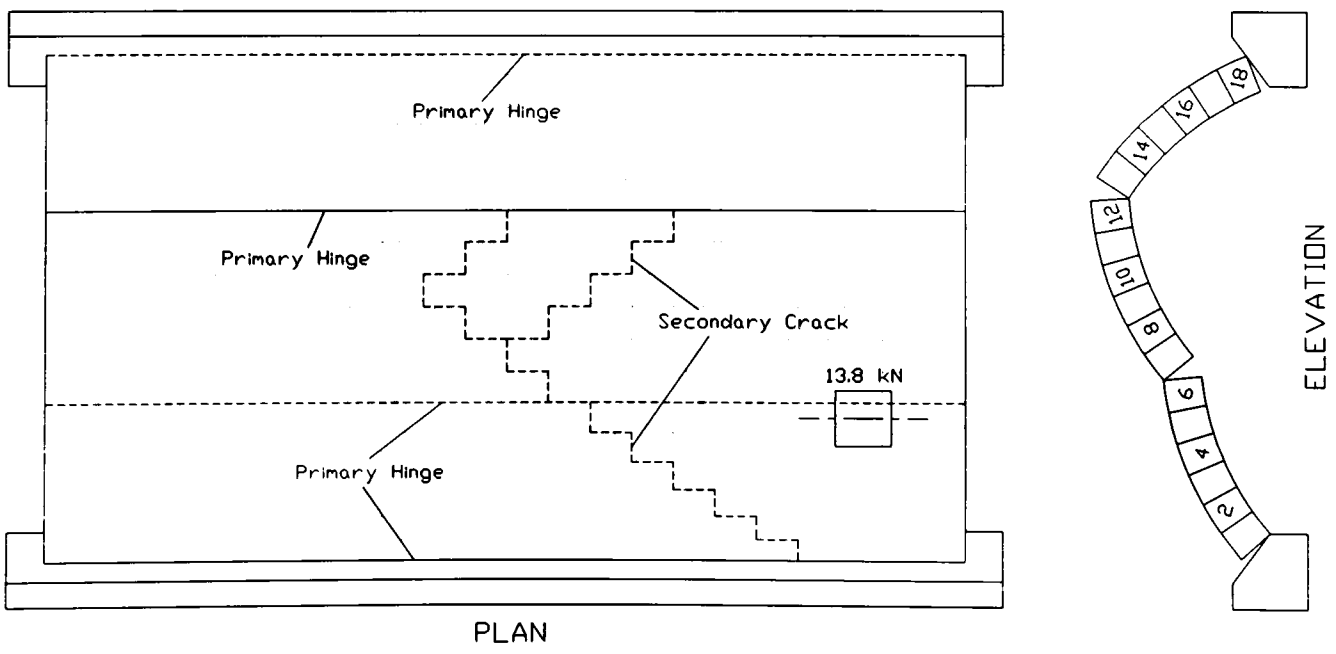

Figure 5.38 Crack pattern and failure mechanism of arch 1-3

A similar square span arch, as shown in figure 5.40, in which the ratio of span/width was decreased to 0.5, viz. arch reference 1-3, also failed due to the formation of a two-dimensional

hinged mechanism. Secondary cracks were prevalent within this arch. This would indicate that there exists a threshold value of the ratio span/width below which local effects may become more onerous than global effects. In other words, the load required to form a three-dimensional localised mechanism would be relatively low as compared with the load required to form a two-dimensional global mechanism if the structure could artificially be held together in order to permit this. Figure 5.40 shows the crack pattern and collapse mechanism of arch reference 1-3. It is immediately apparent that, although the width of the structure was approximately twice as great as the width of arch 1-2, the loads required to cause failure were similar to each other.

Despite efforts having been made to ensure that the bond strength of the mortar was minimised, failures were typically almost catastrophic. This indicates that the strength of the mortar was sufficient to maintain structural integrity by resisting tensile strains created by the line of thrust whose eccentricity was such that it lay outside the bounds of the arch. Thus, the load required to cause failure of each arch was the load required to overcome the bond strength rather than the load required to form the mechanism.

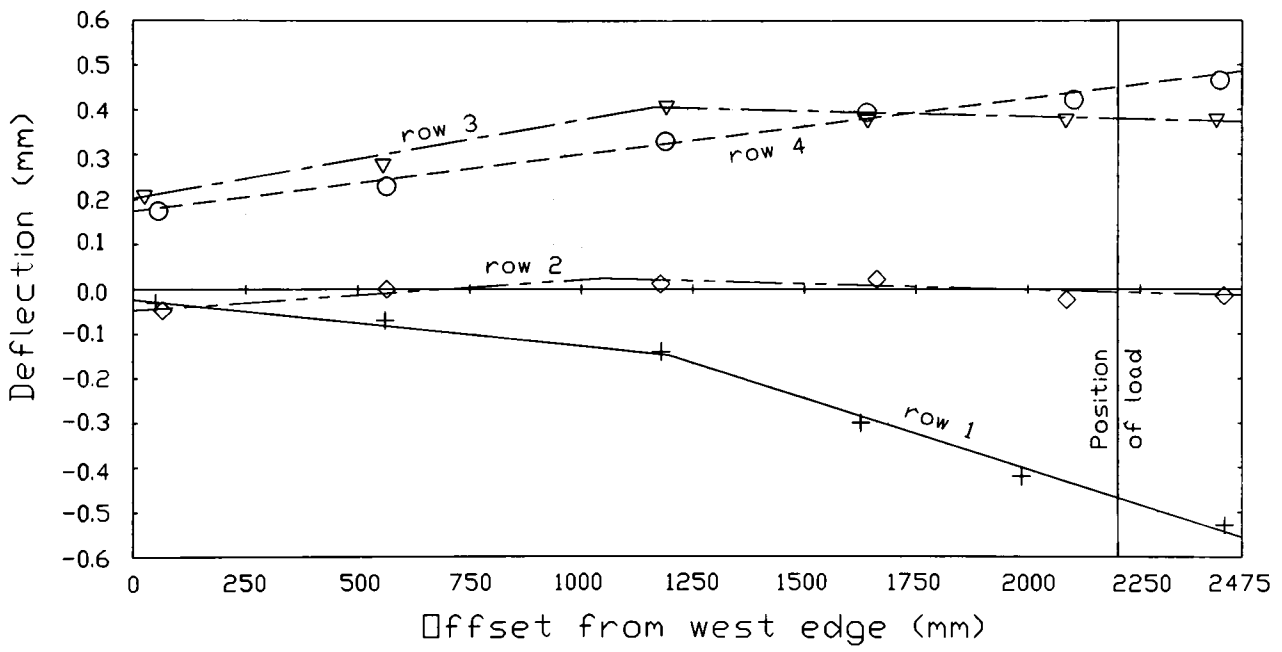

Figure 5.41 Deflected shape of arch 1-3 at failure

Figure 5.41 shows the deflected shape of arch reference 1-3 just before failure. It can be seen that, corresponding to the secondary cracks shown in figure 5.40, the deflected shape along each transverse row of gauges was a bi-linear function of distance from the edge of the structure. This would indicate that the secondary cracks were actually fracture lines at which rotations took place. However, the magnitude of these rotations was small compared with the magnitude of the rotations that occurred at the primary fracture lines. Hence the failure mechanism was essentially two-dimensional although if the structure had been wider the secondary cracks may have become more significant so that a three-dimensional failure mechanism may have formed.

The 45° skewed arches, viz. 1-4 and 1-5 (shown in figures 5.42 and 5.43 respectively), were each subjected to a monotonically increasing point load that was positioned on the obtuse angled haunch. Simple[1] hinges marked 1 and 6 occurred at each abutment. The hinge at each south springing occurred at the intrados. This hinge was accompanied by a further fracture line, marked 2, which extended from the west edge of the south springing to the east fascia in the vicinity of the crown. Sliding movements consistent with a torsional rotation were observed at this fracture line. Additionally, a simple hinge rotation about the intrados at this fracture line was also observed. Thus, in the skewed arch tensile zones do not alternate between the intrados and extrados as they do in the square span arch. The combination of relative block movements that occurred at fracture lines 1 and 2 was equivalent to a rotation about each global cartesian axis. Each of these rotations must be eliminated by the movement of the remaining blocks, marked B to E inclusive, so that the nett effect is that a simple hinge can occur at the north springing. Otherwise, the north abutment must rotate and translate in order to accommodate the discrepancy.

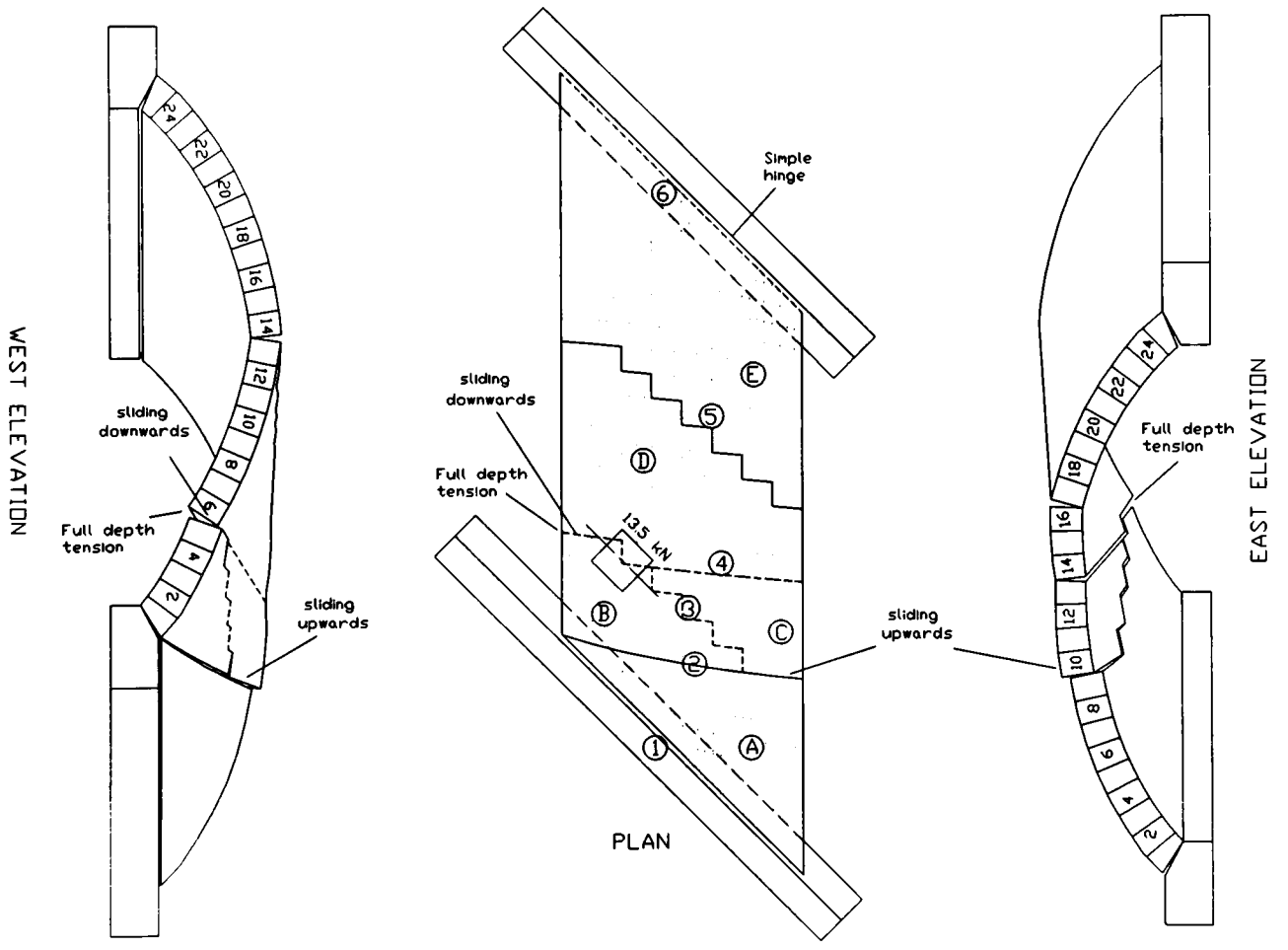

Figure 5.42 Crack pattern and failure mechanism of arch 1-4

The only region of arch 1-4 which did not behave in a way which was similar to the

[1]A simple hinge is defined as a rotation which takes place about the axis of the fracture line as in the case of the two-dimensional failure mechanism of a square span arch. A complex hinge is defined as a rotation which takes place about an axis that is perpendicular to the fracture line and can be likened to a ball and socket joint which therefore allows three-dimensional rotations to take place.

corresponding region of arch 1-5 was the region containing blocks B and C. However, these two regions were equivalent to each other. In arch 1-4, a saw-toothed fracture line, marked 3, occurred at which the principal relative block movement was a simple hinge rotation about the extrados. This fracture merged with fracture line 2 at its eastern extremity. At this location, the principal movement of block C relative to block A was an upward sliding which was accompanied by a less pronounced simple hinge rotation. At the western extremity of fracture line 3 several movements of block D relative to block B occurred. The most notable observation was that these two blocks were no longer contiguous. This separation was accompanied by a relative rotation and downward movement of block D. It was clear that at fracture line 3 a complex set of relative block movements occurred about the axis of the hinge and also about a tangential axis passing through the position of the load. At this location a tributary fracture, marked 4, occurred which was inclined to hinge 3 by 45° on plan and elevation. This was a simple hinge but when combined with fracture 3 produced a rotation about the remaining axis, viz. a radial axis through the load position. This is precisely what happened in arch 1-5 in which there was one fewer fracture line but the one marked 3/4 performed an equivalent function as the combination of fracture lines 3 and 4 in arch 1-4.

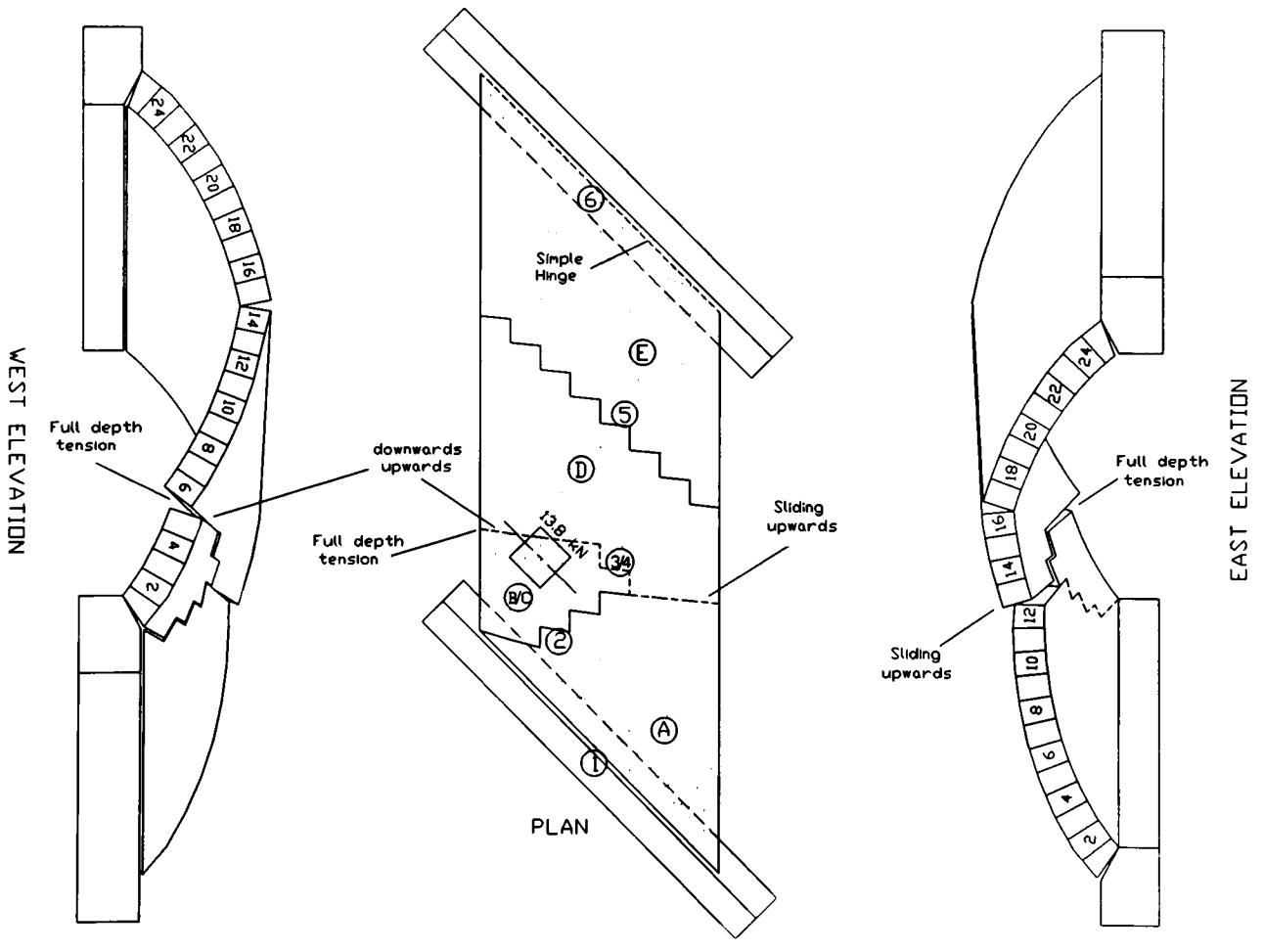

Figure 5.43 Crack pattern and failure mechanism of arch 1-5

In each arch, fracture lines 5 and 6 were simple hinges and were approximately parallel to the abutment. It is noteworthy that if fracture line 3 is omitted the crack pattern of bridge 1-4 resembles the crack pattern of the 3.0 m span skewed arches previously presented. Hence, the requirement for a complex fifth fracture line in the failure mechanism of these structures and the

necessity for the other fracture lines to allow more complex movement than simple hinge rotations.

Each 45° skewed arch shown in figures 5.43 and 5.44 (arches 1-6 and 1-7 respectively) was loaded monotonically to failure through a point load positioned on the acute angled haunch. A simple hinge marked 1 occurred at the intrados of each arch 1-6 and 1-7 at the south abutment. Each of these two arches was divided into three similar blocks A, B and C by a set of four fracture lines which were generally complex.

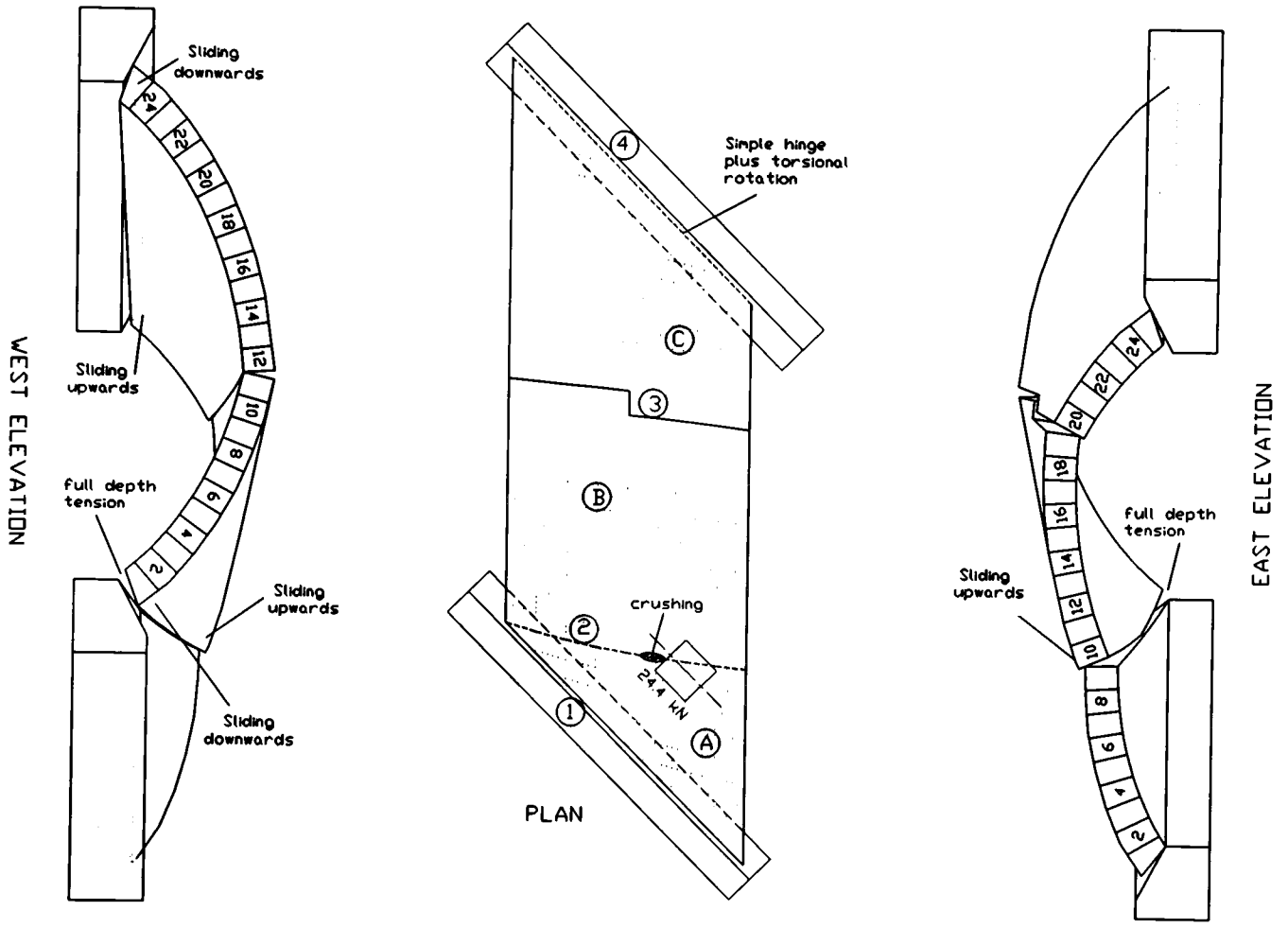

Figure 5.44 Crack pattern and failure mechanism of arch 1-6

Fracture line marked 2 extended from the obtuse angled corner of the arch to the east edge of the structure and passed through the position of the load. Relative block movements which occurred at this fracture line included a simple hinge rotation about the extrados. However, this was not the only form of movement that occurred at this fracture line. This was confirmed by the region of crushed brick that occurred in the vicinity of the load at failure. At the western extremity of this fracture line, block B also underwent a relative downward movement. Furthermore, at this location blocks A and B were no longer contiguous. At the eastern extremity of this fracture line, block B underwent a relative upward movement. The rotation of block B about a tangential axis at the position of the load produced these upward and downward movements of its extremities. This, in conjunction with the formation of the opening along the intrados enabled block B to rotate about a radial axis which passed through the load position. This latter rotation produced the separation of the blocks at the western extremity of the hinge

and the overlap at the eastern extremity. Blocks A and B were effectively in contact with each other only in the vicinity of the load, this produced a stress concentration which created the region of spalling brickwork.

The principal movements that occurred at fracture line 3 was simple hinging. However, at its eastern extremity block C also underwent a relative downward movement associated with a torsional rotation.

The interesting phenomenon that occurred within these two arch tests was that in each case, four fracture lines were formed at failure. However, the necessity for complex three-dimensional rotations to take place was demonstrated by the torsional and simple hinge rotations that were required at fracture line 4 in order for the deformation of each block to be kinematically admissible.

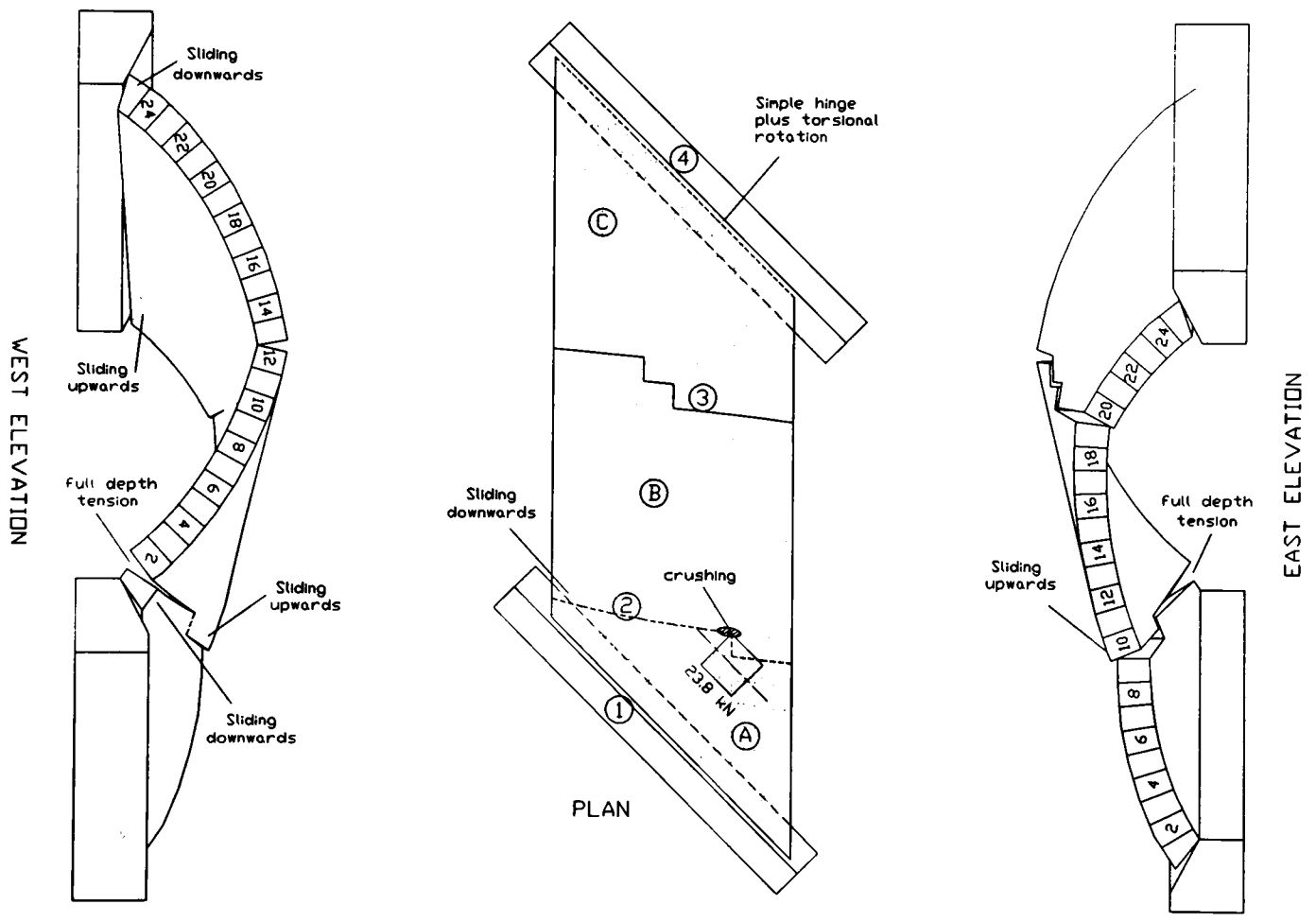

Figure 5.45 Crack pattern and failure mechanism of arch 1-7

In other words, a simple hinge could not form at the north abutment unless the abutments were permitted to displace. In the case of immovable abutments, the complex relative block movements that occurred at each other fracture line could not be accommodated by a simple hinge at the north springing. In order to accommodate the movement of blocks A, B and C the arch was required to undergo additional three-dimensional rotations either by the creation of a further fracture line or by more complex behaviour at fracture lines 3 or 4.

6.0 The mechanism method of analysis

6.1 Introduction

The use of the basic mechanism method was first demonstrated by Pippard (1951). However, it was Heyman (1966) who began its advocation. He demonstrated its simplicity and consequently the method has become popular among practising engineers as an alternative to the MEXE method. In recent years a third option has become available viz. the finite element method but this generally requires much greater computer effort and considerable care in the modelling technique since a theoretical model which resembles a particular structure in appearance may not necessarily resemble it in behaviour. A brief résumé of the use of the finite element method for the analysis of the masonry arch has been given in chapter 2 and will be elaborated upon in chapter 7 where the use of this method in the present work will also be discussed.

At present, the mechanism method is limited to two-dimensional problems and as such is confined to the analysis of structures whose geometry or loading would result in the formation of essentially two-dimensional mechanisms. The developments of this method have been reviewed in chapter 2 and, where appropriate in the context of the present work, will now be discussed in more detail. This will be done as a means of identifying the reasons for the adoption of the technique presented in this thesis for the extension of this method into the study of three-dimensional collapse mechanisms.

Discrete rigid block models, based on either the upper-bound or lower-bound theorem of collapse, increase the generality of the method since the possibility of sliding failures can be included in the analysis. However, optimisation techniques are required in order to produce the minimum collapse load or the maximum equilibrated load respectively. These modelling techniques are particularly important because their constraints can be written in linear form so that relatively simple linear programming (LP) techniques can be used to obtain the optimum solution.

The mechanism method described in this thesis abandons the discrete rigid block modelling technique in favour of an indiscrete rigid block model, i.e. one that must also isolate the position of each fracture and, therefore, must determine the shape of each block created by the formation of the surrounding fractures. The previous approaches idealised the arch as comprising many elements so that the formation of a hinge between two contiguous blocks implicitly defined the position of the hinge. The simplification adopted in the present work greatly reduces the computer effort although the constraints can no longer be linearised. However, a technique is described which enables this potential drawback to be overcome.

In the present work, the arch is idealised as a set of contiguous incompressible blocks bounded by fracture lines whose position is controlled by a set of linear vectors. This modelling technique was used in preference to one that contains many discrete rigid blocks because its relative simplicity enables the mechanism method to be extended into three-dimensions. The method will be used to analyse a two-dimensional idealisation of a square span arch and will be compared with analyses of the equivalent discrete rigid block system. The relationship between the results of the analyses of the discrete rigid block systems using the upper-bound and lower-bound theorems of collapse will also be explored.

The behaviour of the skewed arch bridge will be described by first illustrating a type of mechanism which is infeasible. A feasible mechanism will then obtained by advancing the method further so that phenomena observed during the destructive load tests, as described in chapter 5, may be explained. Finally, the limitations of the method and possible ways in which the method may be extended will be discussed.

6.2 The basic mechanism method

The basic mechanism method applies only to a two-dimensional section of the arch in which its spandrel walls are neglected and, implicitly, the live loading must be essentially two-dimensional. Thus, multiple full-width patch loads may be analysed by considering a unit width of the structure. The underlying assumptions of the basic mechanism method include the prohibition of sliding failures and that masonry is incompressible and has both infinite compressive strength and zero tensile strength. Friction must be considered to be sufficiently great so that sliding failures can not occur. This ensures that failure must occur due to the formation of a hinged mechanism so that equations 6.1 to 6.3 remain valid. This method also relies on the fact that strains are negligible at failure which means that geometrical rules can be based on the undeformed shape of the arch.

The method seeks a solution that simultaneously satisfies both upper-bound and lower-bound collapse theorems. If the loading is unsymmetrical as shown in figure 6.1, the upper-bound theorem is satisfied provided that a four hinged mechanism is formed. The lower-bound theorem is satisfied if the line of thrust can be contained within the bounds of the arch. In the limit at which each theorem is simultaneously satisfied, the magnitude of the applied load and the position of the hinges must be adjusted so that the line of thrust is tangential to the intrados or extrados at the appropriate hinge position and only exits the barrel through each springing.

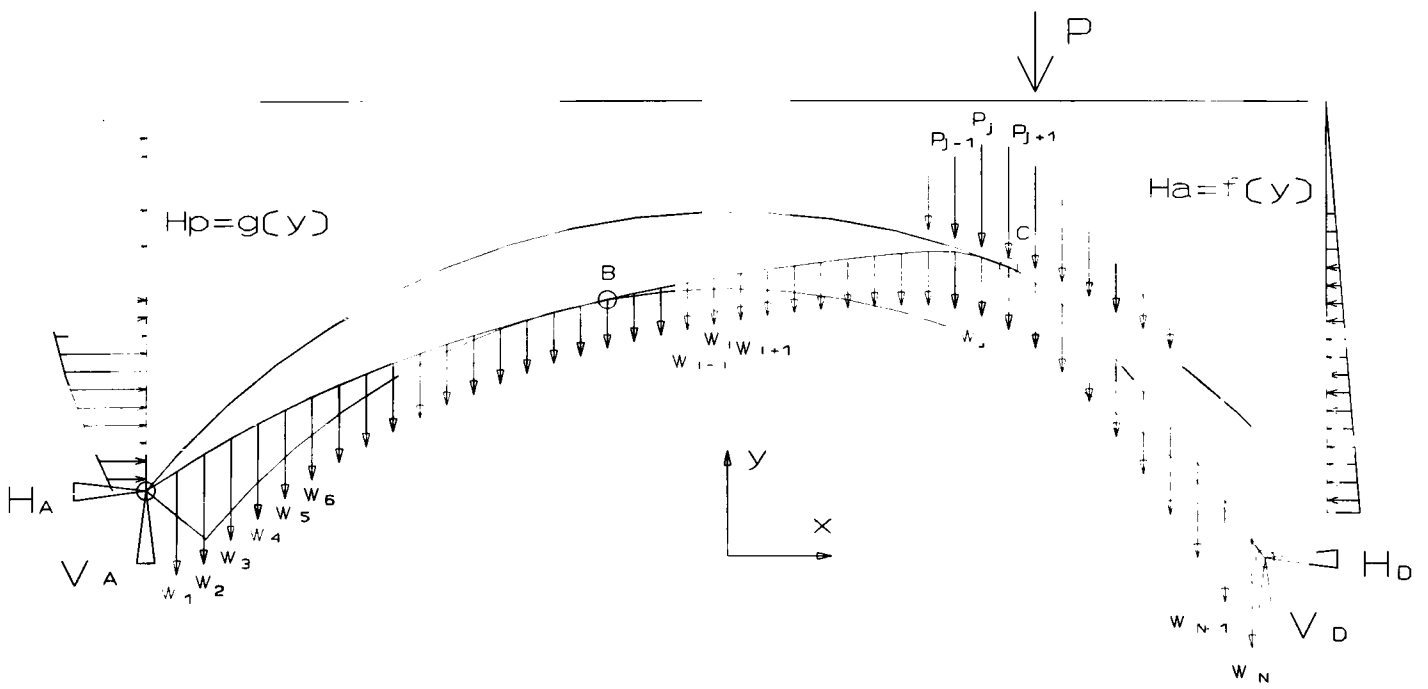

Figure 6.1 Basic Mechanism Method

Figure 6.1 shows the idealisation of an arch bridge in readiness for the application of the basic mechanism method. In this example, horizontal backfill pressures have been included so that the method represents a more advanced technique than the one proposed by Heyman (1969).

The arch is notionally divided into a finite number of vertical sections (1 to N inclusive) each with self weight, W_i, acting at the point (x_i, y_i). The dimensionless live load can be distributed through the backfill to the arch and the equivalent proportions of it which act at each section thereby calculated and denoted P_i.

Sufficient hinges are assumed to occur at (x_A, y_A), (x_B, y_B),(x_C, y_C) and (x_D, y_D) to satisfy the upper-bound theorem of collapse. The support reaction and the applied load can then be found by solving three simultaneous equations representing moment equilibrium at hinges C, B and A as detailed in equations 6.1, 6.2 and 6.3 respectively.

$$V_D(x_D-x_C) = H_D(y_C-y_D)+\sum_{i=C}^{i=D}(W_i+P_i).(x_i-x_C)+\sum_{j=C}^{j=D}Ha_j(y_C-y_j) \qquad \textbf{(6.1)}$$

$$V_D(x_D-x_B) = H_D(y_B-y_D)+\sum_{i=B}^{i=D}(W_i+P_i).(x_i-x_B)+\sum_{j=C}^{j=D}Ha_j(y_B-y_j)+\sum_{j=B}^{j=C}Hp_j(y_j-y_B) \qquad \textbf{(6.2)}$$

$$V_D(x_D-x_A) = H_D(y_A-y_D)+\sum_{i=A}^{i=D}(W_i+P_i).(x_i-x_A)+\sum_{j=C}^{j=D}Ha_j(y_A-y_j)+\sum_{j=A}^{j=C}Hp_j(y_j-y_A) \qquad \textbf{(6.3)}$$

Eddy's theorem (Walklate & Mann, 1983) is used to determine the trajectory of the line of thrust, (x_i, y_i). The position of each hinge must be adjusted if necessary until it lies wholly within the bounds of the arch and thereby satisfy the lower bound theorem of collapse.

The list of assumption of this method is also a list of its limitations. The most significant one is that the method is limited to the determination of two-dimensional mechanisms in which the only type of admissible fracture is a simple hinge. This method has been extended to incorporate the possibility of the compressive failure of the arch material (Crisfield, 1985a; Smith et al. 1990). However, it does not appear to be a method that can be extended so that it can analyse three-dimensional mechanisms in which fractures may be of a more general form. In particular, it cannot be used to analyse a skewed arch unless it was incorrectly assumed that the skewed arch behaves in a two-dimensional manner in a direction either parallel to the spandrel walls or perpendicular to the abutments. Furthermore, there is no justification that its incorrect use as just described will enable bounds on the correct failure load of a skewed arch to be ascertained.

6.3 The application of optimisation techniques

The collapse load produced by the basic mechanism method can be obtained by a trial and error technique. One possible technique would be to adjust hinge positions until the lower bound theorem of collapse is satisfied. The line of thrust will pass through each of the assumed hinge positions but may not be contained within the bounds of the arch. The position of each hinge can be adjusted to the site at which the eccentricity of the line of thrust is greatest until it can be contained within the arch. This technique requires only two or three iterations and is therefore preferable to the use of optimisation techniques. However, Ling-Xi (1987) and Jennings (1988) each used linear programming techniques to obtain the optimum collapse load from this method.

Optimisation techniques are essential in theoretical models of a more general nature in which there are many possible configurations of collapse mechanisms. Sliding failures and the possibility of the compressive failure of the constitutive material may be included as well as different forms of rigid body rotations as in the case of three-dimensional systems. In models of this complexity there is no obvious way of determining the one that would optimise the required load. Mathematically, the problem can be expressed as examining each permutation of variables until the set is found that would either minimise, or maximise (depending on the nature of the problem), the value of a given function.

The choice of optimisation technique is not difficult. Where possible, one should attempt to represent the problem by a series of linear mathematical functions known as constraints. Thus, linear programming techniques can be used provided that the function to be optimised, viz. the objective function, can also be expressed as a series of linear terms similar to the constraints. This technique is relatively simple and efficient whereas non-linear programming techniques require much more effort and tend to be problem oriented.

The optimisation technique that is used in this thesis is simplex linear programming. More specifically, the two-phase method (Foulds, 1981), otherwise known as the artificial basis method (Gass, 1969) was adopted. It is important to discuss this method here because the conclusions from the work presented in chapters 6.5 and 6.6 depend on an understanding of the output from this technique. The outcome of the final first phase tableau and each subsequent second phase tableau are of particular interest.

The simplex method assumes that the constraints form a closed boundary around the region that contains feasible solutions. This feasible region is convex which so that the optimum solution will be found at a vertex of the region. It is possible that a hyperplane of the boundary is parallel to the objective function so that at all points on it the value of the objective function is

a constant. In this case, the statement that the optimum solution will be found at a vertex of the region remains valid except that there will be more than one set of variable that will produce it. The simplex method examines the solution at each vertex to see if the objective function has been optimised. If not, it provides a means of determining the best direction of movement from the present vertex so that the next vertex to be examined will produce the largest improvement in the value of the objective function. The simplex method also contains a means of signalling unboundedness. This occurs when the value of the objective function can be increased ad infinitum without activating a constraint that would restrict its movement. In such cases the objective function can not be optimised. A solution could only be found by the imposition of additional or revised constraints or the introduction of an objective function of a different form.

The two-phase method is used in problems where it is not possible to select an initial set of variables which would coincide with a vertex of the boundary. In these situations, an "artificial" variable is added to each constraint. This creates an identity matrix within the initial first phase tableau. Basic variables, i.e. those whose coefficients form a column of the embedded identity matrix are ascribed values contained in the corresponding row of the final column of the tableau. This column initially contains the constant terms of the constraints and is therefore called the right hand side (rhs) column. The remaining variables are non-basic and therefore have zero value. The process of moving from one vertex to another is equivalent to adjusting the coefficients of the linear programming tableau until the identity matrix occurs in a position whose variables would describe a simultaneous solution of the constraints corresponding to the new vertex. Thus, an initial solution to the problem is described by the artificial variables.

The objective function used in the first-phase is the sum of the artificial variables. The entry of a unit term in the objective function row of each artificial variable destroys the identity matrix. A series of Gauss-Jordan iterations are required in order to recover the identity matrix i.e. to transform the tableau into canonical form. The value of the objective function is now contained within the rhs column. It is the objective of the first phase to drive this value to zero. If this can be achieved, the set of non-zero basic variables and the zero non-basic variables represent a basic feasible solution. A non-zero value of the first phase objective function which can not be improved upon signals an infeasible problem. Thus the successful completion of the first-phase is a significant step because it indicates the validity of the constraining equations.

The process of determining which vertex is examined next is based on finding the variable which would produce the greatest improvement in the objective function if it was to enter the basis. This choice is made by selecting the variable with the greatest negative coefficient in the objective function. The variable which is removed from the basis is the one that has the smallest positive ratio of rhs term to entering variable coefficient. Thus one variable in the

basis is replaced by another until the process can proceed no further. If the above ratios are all negative the procedure terminates due to unboundedness. If there are no negative objective function coefficients the procedure has completed successfully depending on the value of the objective function if during the first-phase.

The presence of an artificial variable within the basic feasible solution is significant; it indicates that one of the constraints was redundant. Hence the number of active constraints dictates the complexity of the solution; in this case the complexity of the collapse mechanism.

The second-phase of the simplex method begins with the removal of the artificial variables since they have served their purpose in enabling a basic feasible solution to be obtained. The actual objective functions can now be introduced so that when the tableau is transformed into canonical form the value of the objective function corresponds to a valid solution of the problem. In the case of minimisation problems the basic feasible solution and each second phase solution correspond to an upper bound. Therefore any solution obtained during the second phase is a valid answer to the original problem. However, the final second phase solution is the one that optimises the original problem.

6.4 The two-dimensional discrete rigid block mechanism method

6.4.1 Application of the principle of virtual work

The application of a general load system **[P]**, which includes the support reactions, produces internal actions **[F]** from which the stresses **[σ]** may be calculated. The structure will undergo deformations **[e]**, associated with the internal actions and the loads will undergo corresponding displacements **[Δ]**.

Consider a structure that is assumed to comprise a finite number of discrete rigid blocks such as an arch. The work done by a set of applied loads as they undergo virtual displacement is balanced by the work done by the structure as it deforms. In this case, the load system, **[P]**, consists of a single unknown load which displaces vertically through a unit distance, **[$\delta\Delta$]**. The internal actions, **[F]**, consist of a set of inter-block forces which are derived by considering equilibrium of each block. The incompressibility of the constituent blocks means that the deformation of the structure, **[δe]**, consists only of a set of relative movements between each pair of adjacent blocks. Thus, there is no strain energy and the virtual work equation, as shown in equation 6.4, is equivalent to the change in potential energy of the loaded system.

$$[P]^T .[\delta\Delta] - [F]^T .[\delta e] = 0 \qquad \textbf{(6.4)}$$

A formal proof of the principle of virtual work can be found within most structural analysis text books for example Charlton (1973). It can be seen that the work done by the structure is equal to the work done by the loads. Furthermore, there exists an equilibrium, or force, set consisting of the applied loads and internal actions and a compatibility, or displacement, set consisting of external deflections and internal deformations.

The upper bound theorem of collapse states that the load obtained from the work equation written for any arbitrarily assumed mechanism is greater than, or at least equal to, the true collapse load. In other words, collapse will occur if a kinematically admissible displacement configuration can be found. This provides the basis of one possible method of analysis in which the minimum collapse load is determined by searching through all possible admissible mechanisms. This task is made easier through the use of linear programming techniques as adopted by Gilbert (1993) and this author.

The lower bound theorem of collapse states that if at any load, an equilibrium state can be found which also satisfies the yield condition, then the load is less than, or at most equal to the true collapse load. This provides the basis of other methods such as all elasticity methods including non-linear finite element analyses and, as in this case, an alternative discrete rigid block

approach. Thus, approaches using this theorem do not assume a mechanism but seek to maximise the applied load subject to maintaining equilibrium. The process of maximising the applied load under these conditions can be automated by evoking linear programming techniques as demonstrated by Livesley (1978) and adopted by this author. Hence, despite being impossible, an increase in the load beyond the maximum value would violate equilibrium and infer the formation of a mechanism.

The third theorem of collapse, viz. the uniqueness theorem, states that the collapse load which simultaneously satisfies the upper bound and lower bound theorems must be the value of the true collapse load. Thus, when the two approaches are converted into linear programming form, the optimum values of each approach are equal and hence satisfy the uniqueness theorem. Furthermore, it is a consequence of the duality of the two approaches, a fact reported by Charnes and Greenberg (1951), that in their linear programming form, the optimal structural variables pertaining to either method can be extracted as a by-product of the other method.

The minimum upper bound technique produces the smallest possible load, **[P]**, that would still cause the arch to collapse, and the set of relative block movements, **[δe]**, in which there will be as many non-zero terms as is required to produce a kinematically admissible displaced configuration. The coefficients of the objective function correspond to the set of inter-block forces that would be produced by the maximum lower bound technique. The maximum lower bound technique produces the largest possible sustainable load, **[P]**, and the set of associated inter-block forces, **[F]**, in which each term that has reached its limiting value corresponds to a relative block movement that would be required to ensure that the mechanism is compatible with the displacement of the applied load.

In seeking the values of the parameters of the other approach, the value of each objective function term must be factored by an unknown constant. It is a phenomenon of the principle of virtual work that in order to facilitate the solution of a given problem either set, i.e compatibility or equilibrium, can be chosen arbitrarily and usually so that it consists of as many zero and unit terms as possible. Thus, it is not necessary to initially produce actual values of the internal actions if the minimum upper bound technique is used, a feasible set is displayed on the optimal linear programming tableau so that the virtual work equation 6.4 is satisfied.

When using the maximum lower bound technique, a frictional force that is required to reach its limiting value will correspond to a relative block movement along the interface. However, the occurrence of this shear failure in the minimum upper bound technique will produce a dilation of the two surfaces because of the normality rule. Thus, in cases where sliding occurs, duality of the two techniques does not exist. However, Livesley (1978) showed how this dilation could be removed so that the lower-bound theorem was satisfied and duality reestablished.

6.4.2 The minimum upper bound technique

This is a mechanism method, adopted by Boothby (1992b) and developed independently by Gilbert (1993), which, unlike the basic mechanism method, is not restricted to searching for hinged failure mechanisms. As previously described, the objective of this method is to determine the minimum collapse load from an associated set of admissible failure mechanisms.

The example shown here is a simplification of the more general model developed by Gilbert (1993) but is adequate in illustrating the method in readiness for a comparison with the lower bound approach and a study of the duality of the two methods.

The arch is idealised as comprising a system of identically shaped contiguous incompressible blocks that are hypothetically "linked" to each of their neighbours, as shown in figure 6.2.

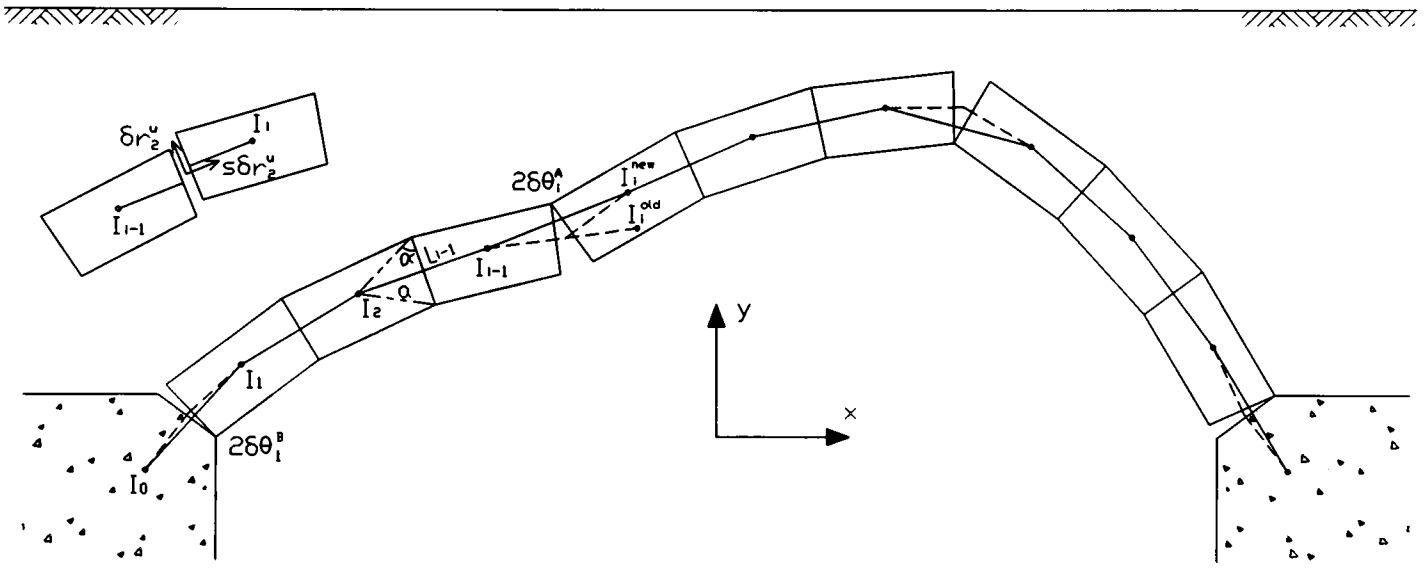

Figure 6.2 The idealised arch for the minimum upper bound technique

Admissible mechanisms are assured because the mathematics permit only certain types of relative movements. These include rotations about the top edge, $\delta\theta^A$, or bottom edge, $\delta\theta^B$, of the preceding block, and upward, δr^u, or downward, δr^d, sliding movements across the surface of the preceding voussoir.

The arch is caused to collapse by an unknown load which is applied to it and which undergoes a downward unit virtual displacement. A kinematically admissible displacement configuration is one in which adjacent blocks remain contiguous whilst undergoing translations or rotations in order to accommodate the displacement of the applied load. Furthermore, the nett effect of each relative block movement must be that the deformation of the system of blocks is compatible with the displacement of the applied load and the zero movement of the abutments.

The change in orientation and extension of each link can be expressed in terms of the permissible block movements. Each type of movement is associated with a change in the potential energy of the system. The collapse mechanism may consist of any combination of sliding movements and rotations; the set which minimises the change in potential energy is obtained through the use of LP techniques. Each block is permitted to take up any kinematically admissible position. The non-negativity constraint assumed by the simplex method of linear programming ensures that this is partially satisfied since it prevents adjacent blocks from moving through each other.

Drucker (1953) showed that, in limit state theory, sliding movements create a dilation of the two contact surfaces. This is incorporated in this theoretical model through the use of a coefficient of separation, s, which, Gilbert (1993), showed need only be as great as 0.5 to prevent sliding failures. For values greater than 0.5, only hinged failures would occur because this would correspond to minimum effort being expended in creating the mechanism. The dilation associated with sliding failures would require additional effort i.e increased load.

Each block is assumed to be similar to all other blocks. Link i, which is initially inclined to the x-axis by θ^{old}_i in the undeformed configuration, connects points denoted by I_i and I_{i-1}. Each of these points is defined to be equidistant, a, from the vertices of their respective block. As illustrated in figure 6.2, I_i lies at the apex of an imaginary isosceles triangle of base angle α within the block. The initial length of each link is given by equation 6.5.

$$L_i^{old} = 2a.\sin\alpha \tag{6.5}$$

The new length and inclination of link i after block i undergoes a rotation of either $2\delta\theta^A_i$ or $2\delta\theta^B_i$ are given by equations 6.6 and 6.7.

$$L_i^{new} = 2a.\sin(\alpha+\delta\theta_i^A+\delta\theta_i^B) \tag{6.6}$$

$$\theta_i^{new} = \theta_i^{old}+\delta\theta_i^A-\delta\theta_i^B+\sum_{j=1}^{j=i-1}(\delta\theta_j^A-\delta\theta_j^B) \tag{6.7}$$

The change in the vertical and horizontal position of block i due to its rotational movement can be found by taking the difference of the corresponding components of equation 6.6 and 6.5. At this stage, Boothby (1992b) retained second order terms in his expansion of the sine and cosine series and therefore required non-linear programming techniques to solve the problem whereas Gilbert (1993) retained only the linear part of the expansions of these series.

Taking each block in turn, its orientation and location in the deformed arch is a function of all possible rotations and translations of the preceding blocks. This results in the extension of link, i, in the vertical and horizontal directions being as shown in equations 6.8 and 6.9 respectively.

$$\delta y_i = 2a.(\delta\theta_i^A+\delta\theta_i^B).\sin\theta_i^{old}.\cos\alpha + 2a[\delta\theta_i^A-\delta\theta_i^B+2\sum_{j=1}^{j=i-1}(\delta\theta_j^A-\delta\theta_j^B)]\cos\theta_i^{old}.\sin\alpha + (\delta r_i^u-\delta r_i^d).\cos\theta_i^{old} + s.(\delta r_i^u+\delta r_i^{old}).\sin\theta_i^{old} \quad \textbf{(6.8)}$$

$$\delta x_i = 2a.(\delta\theta_i^A+\delta\theta_i^B).\cos\theta_i^{old}.\cos\alpha - 2a[\delta\theta_i^A-\delta\theta_i^B+2\sum_{j=1}^{j=i-1}(\delta\theta_j^A-\delta\theta_j^B)]\sin\theta_i^{old}.\sin\alpha - (\delta r_i^u-\delta r_i^d).\sin\theta_i^{old} + s.(\delta r_i^u+\delta r_i^d).\cos\theta_i^{old} \quad \textbf{(6.9)}$$

By taking the summation of the above expressions and equating each to the relative displacement of the abutments , viz. zero, two of the constraints ($\nabla y_{n+1}=0$, $\nabla x_{n+1}=0$) of the problem can be established as shown in equations 6.10 and 6.11.

$$2a.\cos\alpha\sum_{i=1}^{i=n+1}(\delta\theta_i^A+\delta\theta_i^B).\sin\theta_i^{old} + 2a.\sin\alpha\sum_{i=1}^{i=n+1}[\delta\theta_i^A-\delta\theta_i^B+2\sum_{j=1}^{j=i-1}(\delta\theta_j^A-\delta\theta_j^B)]\cos\theta_i^{old} + \sum_{i=1}^{i=n+1}(\delta r_i^u-\delta r_i^d).\cos\theta_i^{old} + s.\sum_{i=1}^{i=n+1}(\delta r_i^u+\delta r_i^d).\sin\theta_i^{old} = 0 \quad \textbf{(6.10)}$$

$$2a.\cos\alpha\sum_{i=1}^{i=n+1}(\delta\theta_i^A+\delta\theta_i^B).\cos\theta_i^{old} - 2a.\sin\alpha\sum_{i=1}^{i=n+1}[\delta\theta_i^A-\delta\theta_i^B+2\sum_{j=1}^{j=i-1}(\delta\theta_j^A-\delta\theta_j^B)]\sin\theta_i^{old} - \sum_{i=1}^{i=n+1}(\delta r_i^u-\delta r_i^d).\sin\theta_i^{old} + s.\sum_{i=1}^{i=n+1}(\delta r_i^u+\delta r_i^d).\cos\theta_i^{old} = 0 \quad \textbf{(6.11)}$$

The third constraint (equation 6.12), $\nabla\theta_{n+1}=0$, is formed by summing the rotations of the blocks and equating this to the relative rotation of the abutments.

$$\sum_{i=1}^{i=n+1}(\delta\theta_i^A-\delta\theta_i^B) = 0 \quad \textbf{(6.12)}$$

The fourth constraint (equation 6.13), $\nabla y_w=-1$, is formed by imposing a unit vertical displacement of the loaded block, w. Thus by taking the summation of equation 6.8 over the first w blocks the loading is specified.

$$2a.\cos\alpha\sum_{i=1}^{i=w}(\delta\theta_i^{A}+\delta\theta_i^{B}).\sin\theta_i^{old}+\ 2a.\sin\alpha\sum_{i=1}^{i=w}[\delta\theta_i^{A}-\delta\theta_i^{B}+2\sum_{j=1}^{j=i-1}(\delta\theta_j^{A}-\delta\theta_j^{B})].\cos\theta_i^{old}$$
$$+\sum_{i=1}^{i=w}(\delta r_i^{u}-\delta r_i^{d}).\cos\theta_i^{old}\ +s.\sum_{i=1}^{i=w}(\delta r_i^{u}+\delta r_i^{d}).\sin\theta_i^{old}\ =\ -1 \qquad \textbf{(6.13)}$$

Finally, the objective function used in the linear programming solution can be generated. This equation expresses the total change of potential energy of the structure in terms of the unknown block movements. The objective function is actually an alternative form of the virtual work equation in which it is not necessary to calculate the set of inter-block forces but use is made of the fact that these may be derived from the weight of each block.

$$2a\sum_{k=1}^{k=n}w_k.\ [\ \cos\alpha\sum_{i=1}^{i=w}(\delta\theta_i^{A}+\delta\theta_i^{B}).\sin\theta_i^{old}+\ \sin\alpha\sum_{i=1}^{i=w}[\delta\theta_i^{A}-\delta\theta_i^{B}+2\sum_{j=1}^{j=i-1}(\delta\theta_j^{A}-\delta\theta_j^{B})]\cos\theta_i^{old}\ ]$$
$$+\sum_{k=1}^{k=n}w_k\sum_{i=1}^{i=w}(\delta r_i^{u}-\delta r_i^{d}).\cos\theta_i^{old}\ +\sum_{k=1}^{k=n}w_k s\sum_{i=1}^{i=w}(\delta r_i^{u}+\delta r_i^{d}).\sin\theta_i^{old}\ =\ P \qquad \textbf{(6.14)}$$

6.4.2.1 Discussion

Figure 6.3 shows a two-dimensional example of a 3.0 m span arch without backfill. Its rise at its crown is 750 mm and it comprises seven voussoirs which are 220 mm deep.

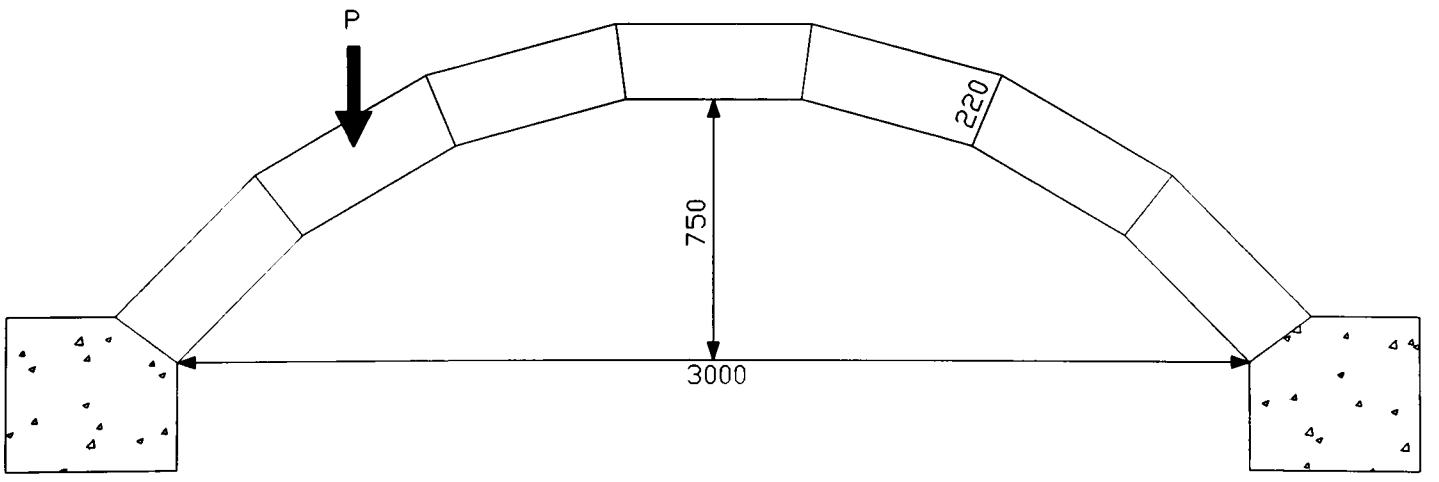

Figure 6.3 A seven block, 3.0 m span, voussoir arch

Figure 6.4 shows the initial linear programming tableau which was set up by applying the constraining equations 6.10 to 6.13 inclusive and assuming that the coefficient of separation is 0.5. The final linear programming tableau is shown in figure 6.5.

$\delta\theta_1^A$	$\delta\theta_1^B$	δr_1^u	δr_1^d	$\delta\theta_2^A$	$\delta\theta_2^B$	δr_2^u	δr_2^d	$\delta\theta_3^A$	$\delta\theta_3^B$	δr_3^u	δr_3^d	$\delta\theta_4^A$	$\delta\theta_4^B$	δr_4^u	δr_4^d	$\delta\theta_5^A$	$\delta\theta_5^B$	δr_5^u
6.84	-6.49	1.00	-0.20	6.07	-5.80	1.09	-0.48	5.11	-4.94	1.11	-0.72	4.04	-3.98	1.05	-0.92	2.94	-2.99	0.92
0.55	-0.29	-0.50	1.10	1.34	-0.99	-0.22	1.01	1.90	-1.49	0.07	0.84	2.19	-1.75	0.36	0.62	2.19	-1.75	0.62
1.00	-1.00			1.00	-1.00			1.00	-1.00			1.00	-1.00			1.00	-1.00	
-1.32	0.97	-1.00	0.20	-0.55	0.28	-1.09	0.48											
-7.07	6.80	0.50	-1.10	-7.86	7.51	0.22	-1.01	-8.02	7.44	-1.19	-0.12	-7.24	6.74	-1.42	0.29	-6.13	5.75	-1.55

δr_5^d	$\delta\theta_6^A$	$\delta\theta_6^B$	δr_6^u	δr_6^d	$\delta\theta_7^A$	$\delta\theta_7^B$	δr_7^u	δr_7^d	$\delta\theta_8^A$	$\delta\theta_8^B$	δr_8^u	δr_8^d	Q_1	Q_2	Q_3	Q_4	rhs
-1.05	1.87	-2.04	0.72	-1.11	0.91	-1.18	0.48	-1.09	0.14	-0.49	0.20	-1.00	1.00				0.00
0.36	1.90	-1.49	0.84	0.07	1.34	-0.99	1.01	-0.22	0.55	-0.29	1.10	-0.50		1.00			0.00
	1.00	-1.00			1.00	-1.00			1.00	-1.00					1.00		0.00
																1.00	1.00
0.69	-4.77	4.54	-1.57	1.04	-3.26	3.18	-1.49	1.31	-1.69	1.78	-1.30	1.50	0.00	0.00	0.00	0.00	-1.00

Figure 6.4 Imtial L.P. tableau for the primal upper bound problem

$\delta\theta_1^A$	$\delta\theta_1^B$	δr_1^u	δr_1^d	$\delta\theta_2^A$	$\delta\theta_2^B$	δr_2^u	δr_2^d	$\delta\theta_3^A$	$\delta\theta_3^B$	δr_3^u	δr_3^d	$\delta\theta_4^A$	$\delta\theta_4^B$	δr_4^u	δr_4^d	$\delta\theta_5^A$	$\delta\theta_5^B$	δr_5^u
-1.24		-1.74	-1.09	-0.47	-0.69	-2.38	-0.27		-0.55	0.10	-1.36	-0.62		-0.32	-1.08	-0.83	0.19	-0.73
-2.06		-2.95	-1.74	-0.71	-1.21	-4.00	-0.37		-0.84	0.53	-2.44	-1.35	0.37	-0.18	-2.05	-2.05	1.00	-0.88
-1.18		-2.23	-0.44	0.19	-1.23	-2.74	0.39	1.00	-1.28	0.42	-1.08	0.26	-0.63	0.14	-0.97	-0.22	-0.19	-0.15
-1.36	1.00	-1.02	0.20	-0.56	0.28	-1.12	0.49											
15.7	0.00	22.3	13.4	6.36	7.62	27.5	4.26	0.00	7.48	2.75	14.2	5.10	2.63	5.14	12.4	7.95	0.08	7.67

δr_5^d	$\delta\theta_6^A$	$\delta\theta_6^B$	δr_6^u	δr_6^d	$\delta\theta_7^A$	$\delta\theta_7^B$	δr_7^u	δr_7^d	$\delta\theta_8^A$	$\delta\theta_8^B$	δr_8^u	δr_8^d	Q_1	Q_2	Q_3	Q_4	rhs	
-0.72	-0.61		-1.08	-0.32	0.00	-0.56	-1.36	0.11	1.00	-1.44	-1.55	0.53	0.19	-1.44	1.77	2.65	2.65	$\delta\theta_1$
-1.52	-2.05	1.00	-1.52	-0.88	-1.35	0.37	-2.05	-0.18		-0.84	-2.44	0.53	0.63	-2.33	1.20	4.75	4.75	$\delta\theta_2$
-0.79	-0.43		-0.43	-0.56	-0.36	-0.06	-0.68	-0.28		-0.39	-0.89		0.44	-0.89	0.43	3.12	3.12	$\delta\theta_3$
																1.02	1.02	$\delta\theta_4$
10.5	8.36	0.00	10.5	8.50	5.90	2.74	13.7	5.91	0.00	8.80	17.3	2.61	-11.5	17.9	-8.31	-24.8	-24.8	

Figure 6.5 Final L.P. tableau for the primal upper bound problem

This technique is clearly very efficient, the computer storage requirements are relatively low and an estimate of the collapse load was obtained after only seven Gauss-Jordan iterations. However, despite Gilbert (1993) using this technique to analyse his model arch bridges with attached spandrel walls it remains a two-dimensional analytical technique. Gilbert had analysed a section at the edge of the structure which included the spandrel walls and a section at the centre line of the arch and had produced an assessment of the capacity of each structure on a pro rata basis.

An attempt was made to extend this technique for the analysis of three-dimensional systems of rigid blocks. However, as discussed below, this was abandoned because it was found to be impractical.

A two-dimensional array of blocks is required in order to represent the skewed voussoir arch so that the correct location for each fracture can be determined. The formulation of the mathematical description of each rigid block movement is extremely complex and non-linear and would require non-linear programming techniques to enable the optimum solution to be obtained.

For the construction of the constraints for the two-dimensional problem, described above, each rigid block can be thought of as a link in a chain which must remain contiguous during its deformation. Commencing at the first joint, i.e. the first possible location of a fracture,

and proceeding along the chain a joint at a time, the location and orientation of each block to the right of the particular joint is obtained due to each form of movement that can occur as a result of the fracture. Thus, the location and orientation of each block in the deformed system can be expressed in terms of the summation of each possible simple hinge and shear failure at each joint that is intersected by the portion of the chain to the left of the block. Similarly, the change in the position of the abutment at the right hand side of the structure is described by mathematical expressions involving each possible rigid block movement. These expressions are equated to zero in order to obtain a solution to the problem. The existence of a single chain is a fundamental part of this two-dimensional approach. The significance of which will become more apparent in the three-dimensional problem.

When this methodology was used in the equivalent three-dimensional problem several difficulties were encountered. The end of the chain is fixed within one of the abutments. The route that it takes through the structure from one block to the next dictates how the change in position of each block along it is described. The constraints are developed, as in the two-dimensional model, by summing the effects of each type of rotation and translation that can occur at each joint through which the chain passes. Hence, more than one chain can be used to specify the change in position of a given block. Constraints are required to ensure that whatever route is taken through the structure the change in position of a given block is unique. Therefore, as well as prescribing zero movement of the blocks within each abutment, admissible movements of every other block must also be ensured. The number of constraints required to model a particular structure therefore would make the method impractical even if the mathematics to describe each relative block movement could be developed.

Secondly, the observed phenomenon of full-depth tension would require special treatment because this would violate one of the fundamental assumptions of the method, viz. that a mechanism is admissible only if its blocks remain contiguous.

Thirdly, compatibility violations may result in the method being unusable. Consider, a regular array of blocks. Each possible movement of blocks $(i,j+1)$ and $(i+1,j)$ relative to block (i,j) can be described, albeit with some difficulty. However, any movement of block $(i+1,j+1)$ relative to one of its neighbours may be incompatible with its other neighbour. The solution algorithm would avoid this scenario by preventing any form of movement. This would result in a system of blocks that were effectively locked in position. In reality the highly compressible mortar may permit movements that could not occur if the system was idealised as a set of rigid blocks. Hence, other analytical techniques were pursued.

6.4.3 The maximum lower bound technique

The arch is idealised as comprising a set of contiguous rigid blocks. Load is transferred through the system by a set of three forces present at each joint. These forces consist of a frictional force and two normal forces, R and Q, at the intrados and extrados respectively. The simplex method requires that all variables are non-negative. Therefore, to determine the direction of the frictional force it must be replaced by two forces, S and T, which occur in opposing directions.

A set of equations for the entire structure can be formed which express the self weight of the structure and the applied load, after it has been dispersed through the backfill, in terms of the four inter-block forces. These equations represent horizontal, vertical and moment equilibrium of each block. The objective is to maximise the value of the applied load whilst satisfying the lower-bound theorem of collapse, i.e., whilst ensuring that equilibrium is maintained.

Figure 6.6 illustrates a typical set of rigid blocks subjected to the above inter-block forces.

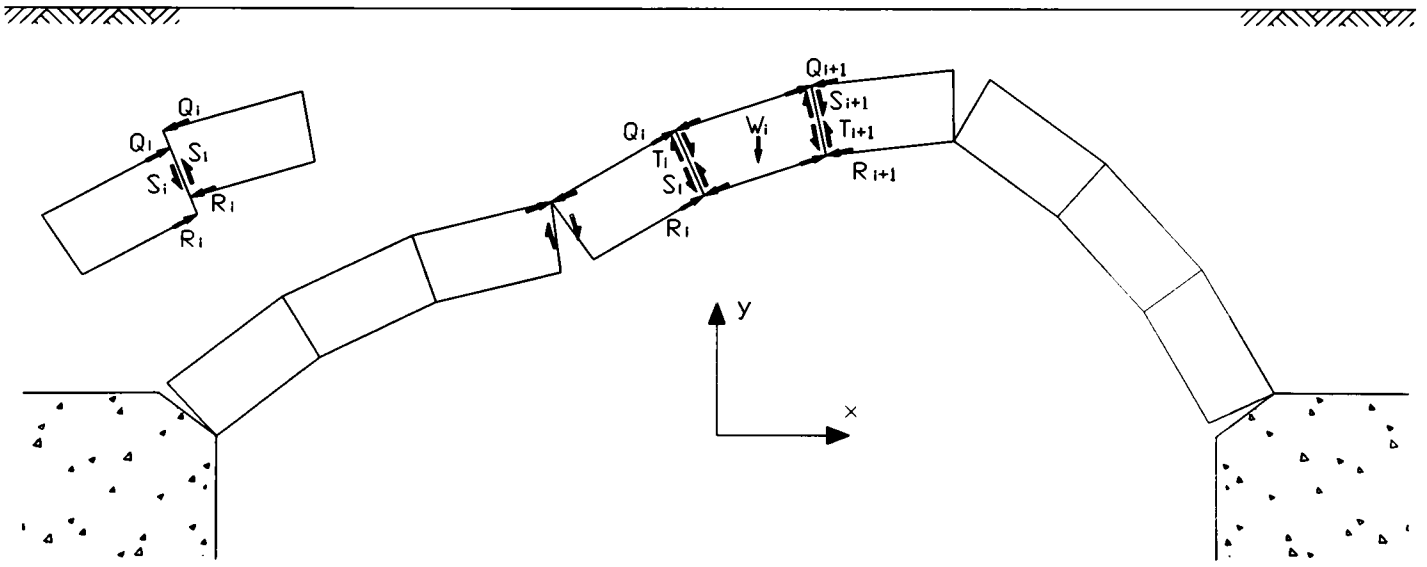

Figure 6.6 The idealised arch for the maximum lower bound technique

The method is concerned with maximising the applied load. The limiting case at which equilibrium is about to be violated occurs when a sufficient number of forces reach their limiting values. The deformed configuration, as shown in figure 6.6, is never reached. However, the eventual mechanism can be determined from the set of inter-block forces which have reached their limiting values. Furthermore, the required relative block movements describing the mechanism can be extracted from the optimal tableau.

The assumption that the joints have zero tensile strength is readily incorporated. The normal inter-block forces are constrained to be non-negative; a fact that is implicit in the use of linear

programming techniques. Therefore, in the limit at which either force is zero, a hinge is about to form at the other extreme. Similarly, the assumption that the blocks have infinite compressive strength requires no further constraints to be specified in order to produce the analysis although the imposition of a finite strength would.

The frictional forces are each constrained to be non-negative so that when one is positive the other must be zero. A further constraint is applied to each frictional force, viz., that it is limited to a fixed proportion of the total normal force acting at the corresponding joint. Thus the relationship between each frictional force and the normal forces resembles that proposed by Coulomb.

Coulomb friction and plastic shearing posses similar properties (Drucker, 1953). In a surface to surface contact situation the resistance to sliding is proportional to the normal force. However, if the force that is attempting to create sliding is increased so that it can no longer be resisted by the friction created by the normal force, a shear failure will ensue. Under these conditions the direction of movement predicted by Coulomb friction will be along the contact surface. However, plastic shearing is linked to the yield function so that the movements predicted by it also include a separation of the two contact surfaces. Drucker (1953) explained the way that plastic shearing resists sliding movements within the collapse mechanism in terms of the negative work done against the normal forces. This normality rule[1] was also defined by Gavarini (1966) thus, "if the plastic strain components are depicted in the stress space, the plastic strain vector has the direction of the outward normal to the yield surface".

Livesley (1978) showed that the predicted maximum sustainable load produced by his lower bound technique agreed with the predicted minimum collapse load of the upper bound technique. However, he found that the predicted mechanism violated the Coulomb friction law that he had used to model the resistance to sliding movements. This was not surprising since these movements belong to the upper bound technique in which the normality rule determines that shear failures must be accompanied by both sliding and dilatant movements. He demonstrated a technique which could be used to correct his predicted mechanism so that it satisfied the lower bound collapse theorem. In the event of a frictional force reaching its limiting value, the active constraining inequality which limited friction to a proportion of the normal force was replaced with one which merely specified a fixed upper limit.

---

[1] Fully plastic states are defined by an interaction curve known as a yield surface which is the boundary of the elastic domain. Whether the material is rigid-plastic or rigid-brittle makes no difference. The normality rule, otherwise known as the plastic potential flow rule, relates the strain components to the yield function. In other words it specifies the direction of movements at failure.

Livesley (1978) also demonstrated that his efficient computerised linear programming algorithm did not require two frictional forces per joint, nor did it require as many artificial and slack variables as the simplex method requires.

The three equilibrium equations, 6.15 to 6.17, for each block express the joint forces in terms of the self weight, live load (and backfill pressure if included) as follows:

$$P+w_i+(Q_{i+1}+R_{i+1}).\sin\theta_{i+1}+(T_{i+1}-S_{i+1}).\cos\theta_{i+1}-(Q_i+R_i).\sin\theta_i-(S_i-T_i).\cos\theta_i = 0 \qquad \textbf{(6.15)}$$

$$(Q_{i+1}+R_{i+1}).\cos\theta_{i+1}-(T_{i+1}-S_{i+1}).\sin\theta_{i+1}-(Q_i+R_i).\cos\theta_i-(T_i-S_i).\sin\theta_i = 0 \qquad \textbf{(6.16)}$$

$$(Q_i-Q_{i+1}).A.\cos\frac{\gamma}{2} -(R_i-R_{i+1}).B.\cos\frac{\gamma}{2} +(S_i-T_i+T_{i+1}-S_{i+1}).C = P.A.\cos\frac{1}{2}(\theta_i+\theta_{i+1}) \qquad \textbf{(6.17)}$$

Where the coefficients A,B,C depend on the geometry of each voussoir and are simply the length of the lever arm from the centroid of the block to the point of application of each load. The angle, γ, is the angle that each voussoir subtends at the centre of the vertical circle defining the intrados.

Equation 6.18 shows the aforementioned constraint on the magnitude of the frictional forces.

$$(Q_i+R_i).\mu \geq (S_i-T_i) \geq -(Q_i+R_i).\mu \qquad \textbf{(6.18)}$$

In the case of the arch shown in figure 6.3, the above equilibrium equations and constraints have been used to set up the linear programming tableau shown in figure 6.7 which, after 38 Gauss-Jordan iterations, is reduced to the final tableau shown in figure 6.8.

A comparison of figure 6.8 with figure 6.5 will reveal that the value of the maximum sustainable load obtained using the lower bound technique is equal to the minimum collapse load obtained using the upper bound technique. The slight discrepancy is due to numerical errors produced during the iterative reduction of each tableau. The fact that the optimal values obtained from each technique are equal indicates that the uniqueness theorem is satisfied. However, it should be pointed out that the negative value of the collapse load obtained from the upper bound technique is a consequence of the optimisation procedure in which the collapse load was obtained using a minimisation procedure. In contrast, a maximisation problem can be carried out simply by multiplying each objective function term by -1. This leads to the positive sign of the maximum equilibrated load obtained from the lower bound technique.

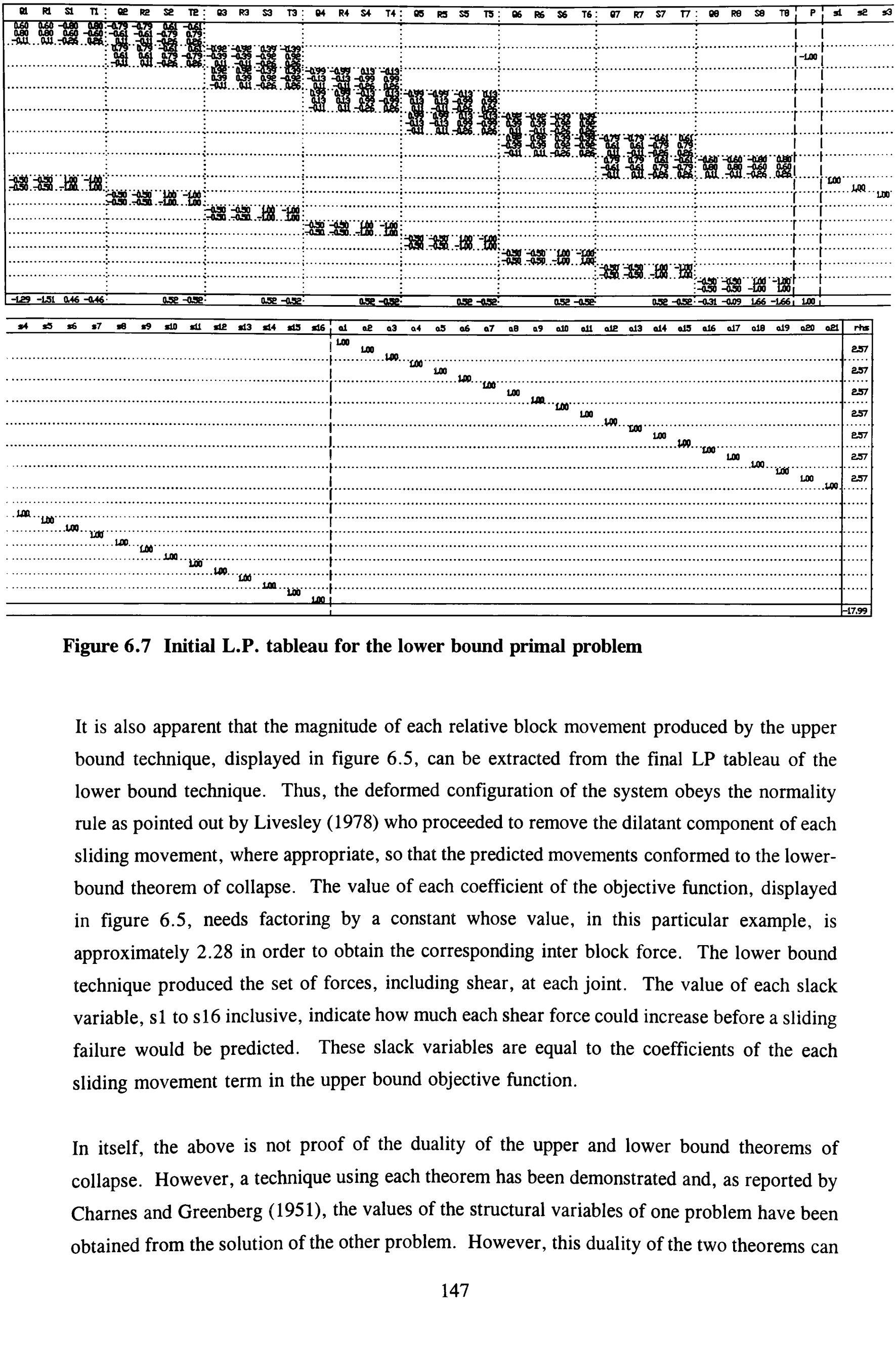

Figure 6.7 Initial L.P. tableau for the lower bound primal problem

It is also apparent that the magnitude of each relative block movement produced by the upper bound technique, displayed in figure 6.5, can be extracted from the final LP tableau of the lower bound technique. Thus, the deformed configuration of the system obeys the normality rule as pointed out by Livesley (1978) who proceeded to remove the dilatant component of each sliding movement, where appropriate, so that the predicted movements conformed to the lower-bound theorem of collapse. The value of each coefficient of the objective function, displayed in figure 6.5, needs factoring by a constant whose value, in this particular example, is approximately 2.28 in order to obtain the corresponding inter block force. The lower bound technique produced the set of forces, including shear, at each joint. The value of each slack variable, s1 to s16 inclusive, indicate how much each shear force could increase before a sliding failure would be predicted. These slack variables are equal to the coefficients of the each sliding movement term in the upper bound objective function.

In itself, the above is not proof of the duality of the upper and lower bound theorems of collapse. However, a technique using each theorem has been demonstrated and, as reported by Charnes and Greenberg (1951), the values of the structural variables of one problem have been obtained from the solution of the other problem. However, this duality of the two theorems can

be exploited, as shown in appendix B, in so far as it is not necessary to independently develop a technique based on each theorem. The initial LP tableau of either technique, known as the primal problem, can be manipulated so that it becomes the equivalent LP tableau of the dual problem.

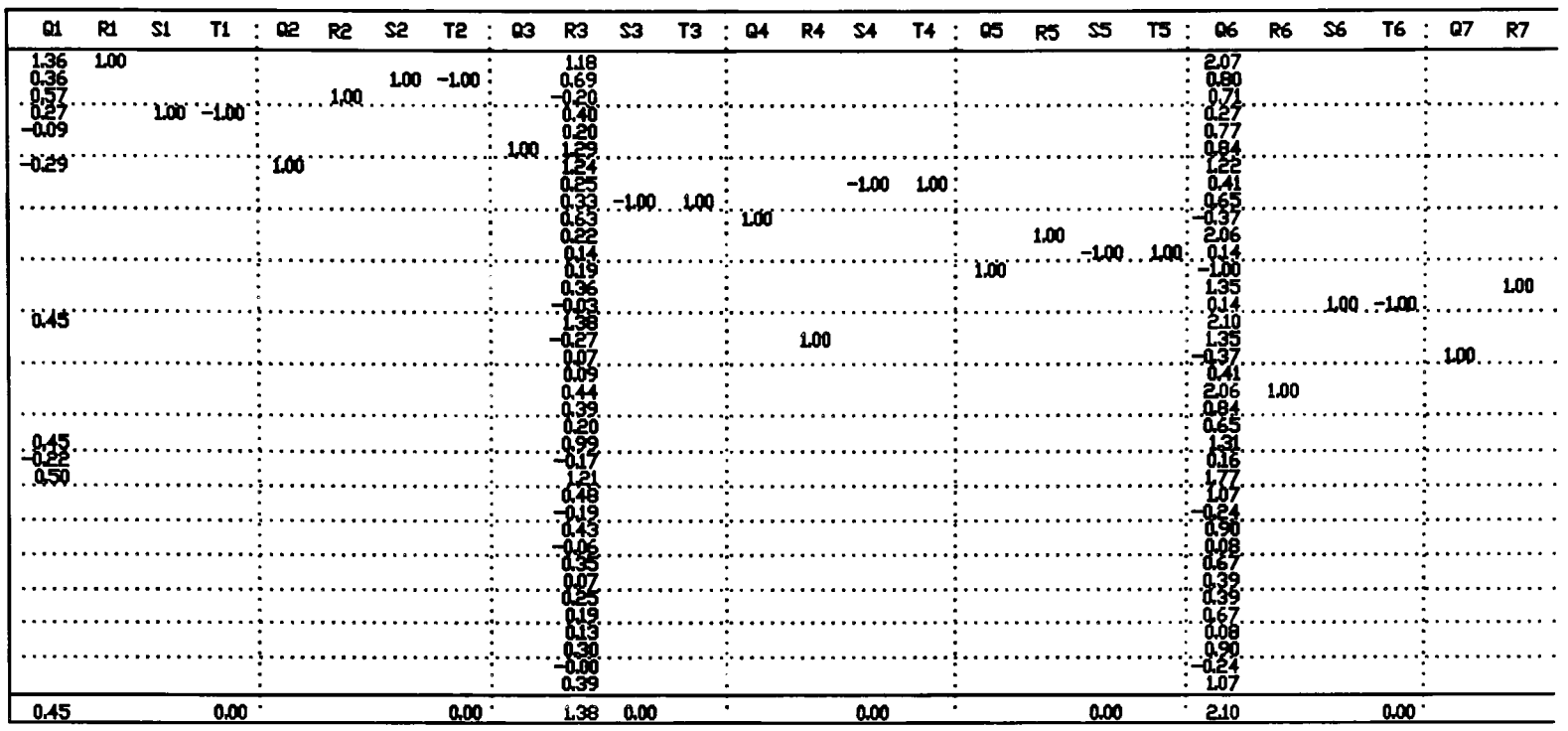

Figure 6.8 Final L.P. tableau for the lower bound primal problem

In terms of computer efficiency, the upper bound technique is preferable. However, the lower bound technique is very simple to initiate; a mathematical description of each admissible movement is not required. However, the yield function must be put into a convenient linear form. A further disadvantage of the lower bound technique is that the LP tableau is very much larger than the equivalent upper bound tableau so that without the use of sophisticated optimisation software which require only a small part of the matrix to be stored, the technique can only be applied to small problems and is therefore of no use for the analysis of three-dimensional problems.

Livesley (1992b) attempted to extend this technique for the analysis of three-dimensional rigid block systems. He commented on the difficulty involved in producing a satisfactory model of the interface and noted that if modelled incorrectly, the arch could fail without any live load being applied to it. However, he had success in modelling an arch that comprised four voussoirs which were capable of hinging, sliding and twisting relative to each other but had to make several assumptions regarding possible mechanisms and invoked symmetry to be able to analyse a segment of a dome in which there were 48 blocks. This was because the lower-bound technique becomes impractical when the number of blocks in increased. However, the validity of his analysis of the four block arch cannot be confirmed although it predicted that the span/width ratio of arch reference 1-3, documented in section 5.2, would have to be 0.16 before a three-dimensional mechanism would form. Arch 1-3 was not formed from four rigid blocks but from a two-dimensional array of rigid blocks which would behave in a more complicated manner than that which was permitted in Livesley's model.

The lower bound technique was not investigated further for its application to three-dimensional systems of rigid blocks. Livesley's success in creating a three-dimensional rigid block model prompted this author to seek an alternative model based on the upper-bound theorem of collapse which could potentially be used to validate each other. Furthermore, Livesley's difficulties in producing "a tractable computational model" (Livesley, 1992b) meant that an upper-bound approach was preferable since the only problem that was anticipated with this approach would be the production of the appropriate mathematical description of each permissible movement. Furthermore, the inability to extend the size of either model without using a commercial linear programming package to solve it resulted in this author's modelling technique as described in the proceeding chapters.

6.5 Two-dimensional indiscrete rigid block mechanism method

6.5.1 Introduction

This approach is based on the same principles as the minimum upper bound approach described in section 6.3.2. The purpose of its presentation here is to demonstrate its simplicity as compared with the previous technique and thereby show its appropriateness for the analysis of three dimensional mechanisms.

This model is applicable only to the analysis of the square voussoir arch with detached spandrel walls. It is assumed that the coefficient of separation is sufficiently great so that sliding failures cannot occur and can therefore be neglected. Hence, the arch fails due to the formation of a hinged mechanism. This is done to simplify the presentation although it should be noted that no great difficulties are encountered in including shear failures. However, the inclusion of these would result in the necessity for optimisation techniques if the minimum collapse load is required. Its exclusion enables a simple graph to be drawn of collapse load versus hinge position from which the optimum load can be obtained. Otherwise, complex non-linear programming techniques would be required.

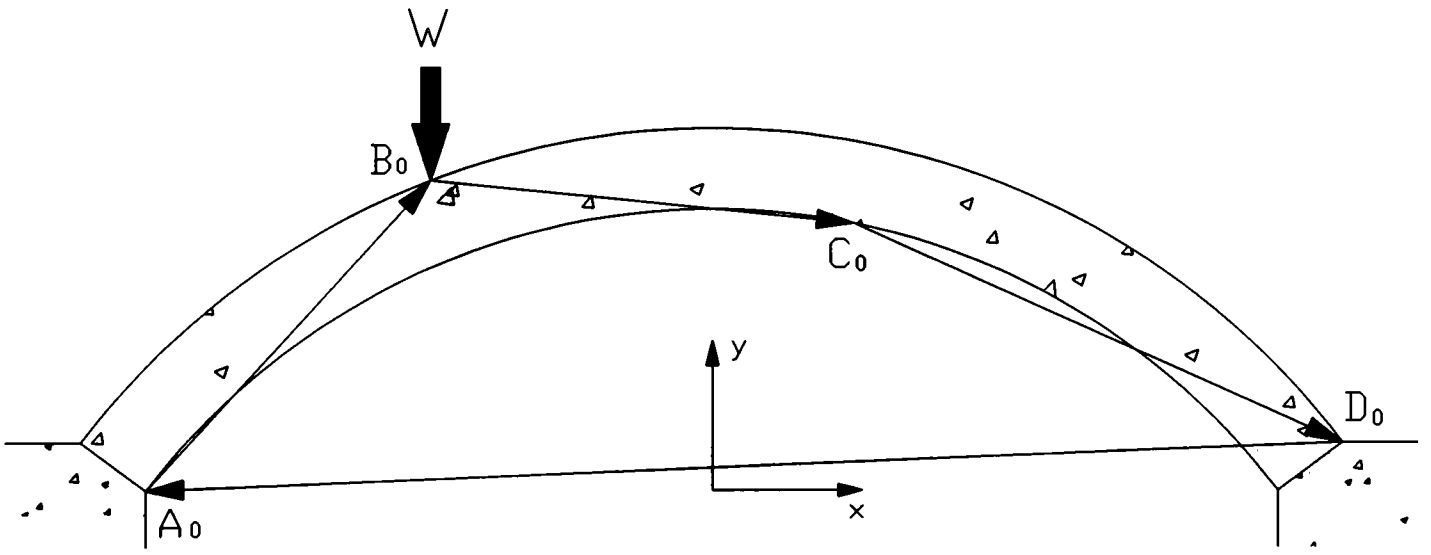

Figure 6.9 Initial geometry of the two dimensional arch

The hinges within the voussoir arch are assumed to be discrete, although their location is unknown, so that only four will form and the assumption that "masonry has zero tensile strength" can be relaxed to "the mortar between each indiscrete block of masonry has zero tensile strength". The tensile strength of the masonry at locations within each block is unimportant since a tensile failure will only occur at the hinge location. Thus, the arch can be idealised as a set of three contiguous effectively rigid blocks. The position of each fracture is described by a set of vectors which pass through consecutive hinge positions. The optimum position of each hinge can be found by allowing these reference vectors to vary, this changes

the length of each rigid block, hence the "indiscrete" nature of the model. Figure 6.9 shows the initial geometry of the two dimensional arch including the four vectors which pass through the assumed position of each hinge.

An assumption is made that the two abutment hinges are fixed in position although the required rotation taking place at them remains unknown. A further, equally reasonable, assumption is that the first in-span hinge, B, is coincident with the point of application of the load. This means that, despite the in-span hinge locations being described by non-linear functions, only one of them, C, is unknown. Varying the position of the first in-span hinge and plotting the collapse load versus position of second in-span hinge produces a series of curves from which the most onerous position of the applied load can be found in conjunction with the associated mechanism.

6.5.2 Development of the model

The imposition of the applied load causes the arch to deform by forming hinges. As each of these open, vectors $\mathbf{A_0B_0}$, $\mathbf{B_0C_0}$, $\mathbf{C_0D_0}$, and $\mathbf{D_0A_0}$ will rotate about successive hinge positions but these rotations are constrained by the fact that points A and D must remain fixed at the respective springing. Figure 6.10 shows a deformed configuration of the arch.

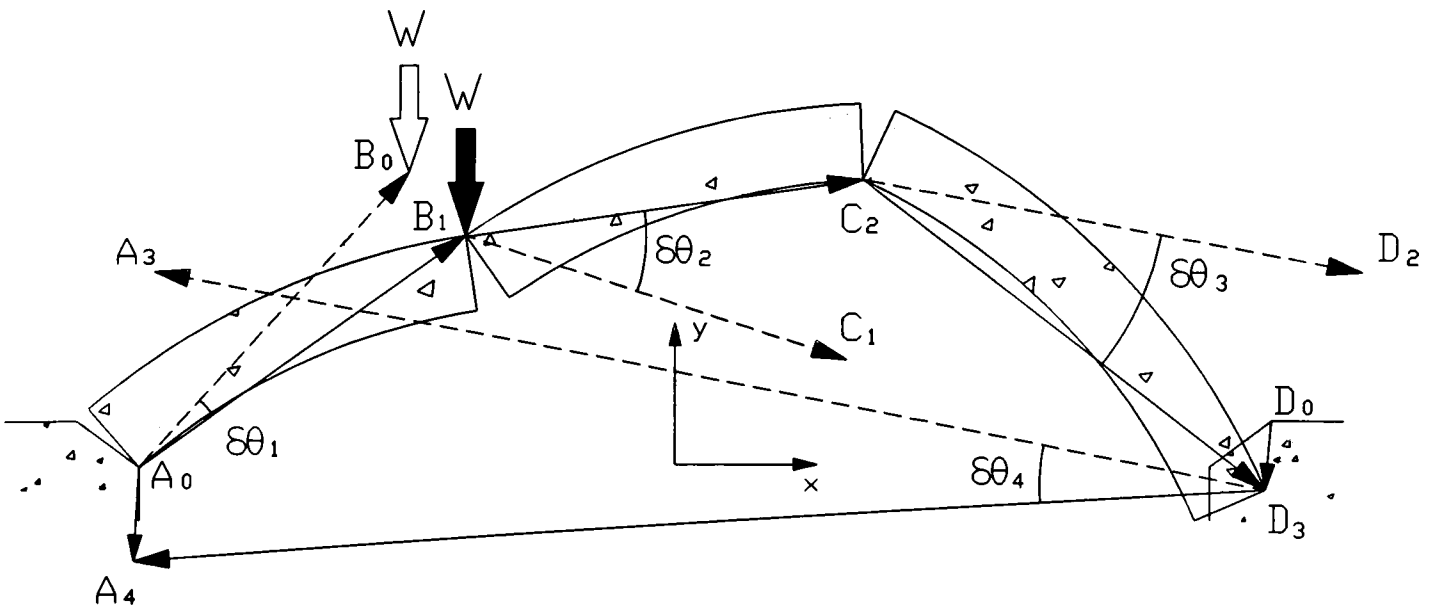

Figure 6.10 Deformed geometry of the two dimensional arch

The assumption that the mechanism is described by a set of alternating clockwise and anticlockwise hinge rotations ensures that it is kinematically admissible. Furthermore, the immovable abutment constraint can be expressed by the additional vectors $\mathbf{A_0A_4}$ and $\mathbf{D_0D_3}$ which must have zero value, see equation 6.19, for the upper bound theorem of collapse to be completely satisfied.

$$D_0D_3 = 0 \quad , \quad A_0A_4 = 0 \tag{6.19}$$

In the two dimensional arch it is sufficient to ignore the vector $\mathbf{A_0A_4}$ since the existence of a null vector $\mathbf{D_0D_3}$ ensures that the mechanism is admissible. The constraint that the sum of all rotations equals zero, i.e. constraint 6.12 of the minimum upper bound method, can be simplified to equation 6.20. In this case, where the position of the hinges are known, equation 6.20 enables the magnitude of the final rotation, $\delta\theta_4$, to be determined.

$$\delta\theta_4 = \delta\theta_1 - \delta\theta_2 + \delta\theta_3 \tag{6.20}$$

The magnitude of the hinge rotation at the remote abutment, i.e. $\delta\theta_4$, can therefore be found in a post-analysis calculation after the mechanism has been determined. The imposition of a unit displacement of the applied load leads to the pre-analysis calculation of the required hinge rotation at the near abutment. This is given by equation 6.21. The exclusion from the mechanism analysis of these two hinges greatly simplifies the procedure.

$$\delta\theta_1.(x_B - x_A) = 1 \tag{6.21}$$

Let us consider a general vector **EF** which initially is as defined in equation 6.21. The length of this vector is denoted L_{EF} and its inclination to the x-axis is denoted θ_{EF}.

$$\boldsymbol{EF} = (x_F - x_E)\boldsymbol{i} + (y_F - y_E)\boldsymbol{j} \tag{6.22}$$

A clockwise rotation, $\delta\theta$, of an intrados hinge is defined as being positive whereas an anticlockwise rotation, of an extrados hinge, is defined as being negative. Therefore, if this vector undergoes a clockwise rotation of $\delta\theta$ about its end E then the change in position of its end F, $(\delta x, \delta y)$, is as defined in equation 6.23.

$$\begin{aligned} \delta y &= L_{EF}\sin(\theta_{EF} - \delta\theta) - L_{EF}\sin\theta_{EF} \\ &= -L_{EF}\,\delta\theta.\cos\theta_{EF} \\ &= -(x_F - x_E).\delta\theta \end{aligned} \qquad \begin{aligned} \delta x &= L_{EF}\cos(\theta_{EF} - \delta\theta) - L_{EF}\cos\theta_{EF} \\ &= L_{EF}\,\delta\theta.\sin\theta_{EF} \\ &= (y_F - y_E).\delta\theta \end{aligned} \tag{6.23}$$

Therefore, after a clockwise rotation, $\delta\theta$, vector **EF** becomes $\mathbf{EF_1}$ as defined in equation 6.23 where the sign of the rotation must be selected as shown in figure 6.12.

$$\boldsymbol{EF_1} = [\,(x_F - x_E) + (y_F - y_E).\delta\theta\,]\,\boldsymbol{i} + [\,(y_F - y_E) - (x_F - x_E).\delta\theta\,]\,\boldsymbol{j} \tag{6.24}$$

Equation 6.24 can now be used to describe the deformation of the structure during the formation of a mechanism. If each rotation is allowed to occur consecutively, Points B_0, C_0 and D_0 move to points B_1, C_1 and D_1 after rotation $\delta\theta_1$. Similarly, after further clockwise rotations of $-\delta\theta_2$ and $\delta\theta_3$ about hinges B and C respectively, D_0 will have taken up the position marked D_3 and its movement from its original position, $\mathbf{D_0D_3}$, is given by equation 6.25.

$$\boldsymbol{D_0D_3 = A_0B_1 + B_1C_2 + C_2D_3 - A_0D_0} \qquad \textbf{(6.25)}$$

The constraint that point D must remain at rest can be formed by carrying out multiple substitutions of equation 6.24 into equation 6.25 and equating it to zero. This results in the formation of the following constraint equations.

$$(y_D - y_A).\delta\theta_1 - (y_D - y_B).\delta\theta_2 + (y_D - y_C).\delta\theta_3 = 0 \qquad \textbf{(6.26)}$$

$$(x_D - x_A).\delta\theta_1 - (x_D - x_B).\delta\theta_2 + (x_D - x_C).\delta\theta_3 = 0 \qquad \textbf{(6.27)}$$

It should be noted that equations 6.26 and 6.27 represent the constraints of the analysis in which the rotation $\delta\theta_1$ is known as is the position of hinges A and D. Furthermore, the relationship between x_i and y_i is non-linear so the solution would require non-linear programming techniques if it was to remain in this form. However, since the position of the first in-span hinge, B, is assumed and trial positions of the second in-span hinge are selected in a sequential order the problem becomes one of the simultaneous solution of two linear equations in $\delta\theta_2$ and $\delta\theta_3$.

The objective function expresses the change in potential energy of the applied load (P x 1.0) in terms of the vertical movement of the blocks of the arch represented by the three vectors $\mathbf{B_0B_1}$, $\mathbf{C_0C_2}$ and $\mathbf{D_0D_3}$. If the arch is assumed to comprise three straight sections so that the centroid of each is situated at the mid-point of the respective vector, and utilising the relationship in equation 6.21, the following potential energy equation 6.28 can be produced.

$$P = \tfrac{1}{2}t.w[L_{AB} + L_{BC}(1 + X_{AC}\delta\theta_1 - X_{BC}\delta\theta_2) + L_{CD}(X_{AC}\delta\theta_1 - X_{BC}\delta\theta_2 + X_{AD}\delta\theta_1 - X_{BD}\delta\theta_2 + X_{CD}\delta\theta_3)] \qquad \textbf{(6.28)}$$

where, $w = 22.5$ kN/m^3 ,

$t = 0.215$ m ,

$L^2_{EF} = (X^2_{EF} + Y^2_{EF})$ for $L_{EF} = L_{AB}, L_{BC}, L_{CD}$

6.5.3 Discussion

The linear vectors are intended to act as a means of referencing the hinge points, as such it is only their end points that are important. In fact, it is only for convenience that the hinge points are connected by linear vectors; any higher order vector would suffice. However, the assumption that the arch comprises three straight sections that are coincident with the linear vectors will lead to an underestimation of the collapse load because there is more weight associated with a curved member. Furthermore, the centroid of each curved section will not coincide with the mid-point of the corresponding vector. However, as previously mentioned, this simplified approach is meant to serve as an illustration of the feasibility of this approach. Additionally, the graphical solution provides the engineer with a greater understanding of the analysis than would a set of linear programming tableaux, if such an approach was possible.

Figure 6.11 shows the predicted capacity of the 3.0 m span right arch that was depicted in figure 6.3. The load was applied at various positions from -1.0 m to -0.5 m offset from the crown and the capacity of the arch is shown as a function of the position of the second in-span hinge as its offset from the crown is varied from 0.0 m to 1.2 m.

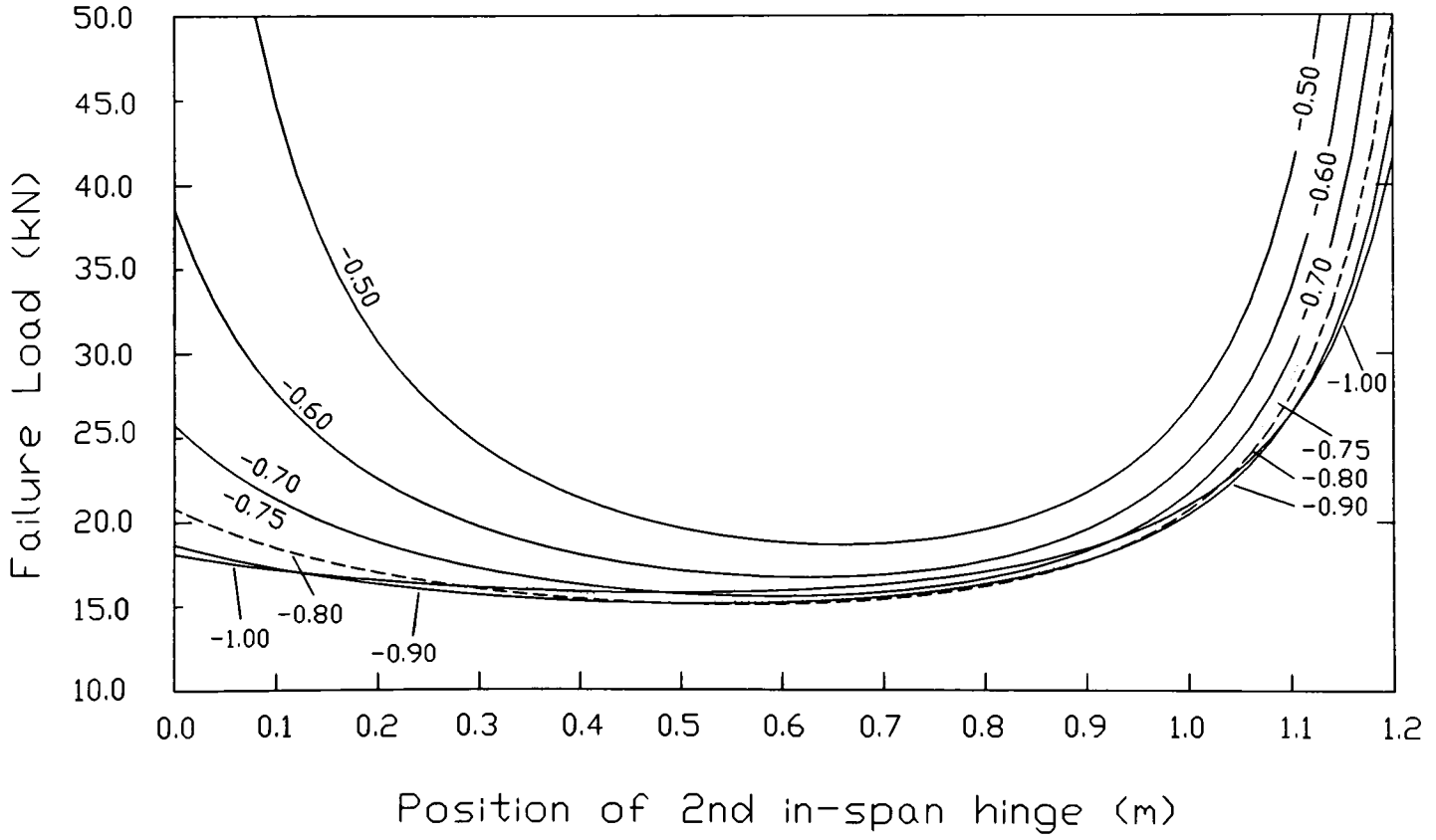

Figure 6.11 Capacity of the 3.0 m square span voussoir arch

It can be seen that the relationship between the arch capacity and the second in-span hinge position resembles a wide bottomed steep sided valley. This is significant because it indicates that the position of the second in-span hinge does not have a significant effect upon the capacity

of the arch (provided that it is situated in the valley). Therefore, by selecting a reasonable position of this hinge the error in the predicted capacity will be small.

The minimum collapse load was found to be 14.98 kN/m. However, with the load applied at the quarter-span, i.e. at -0.75 m, the minimum collapse load was 15.21 kN/m (or 54.0 kN for a 3.55 m wide arch) in which the mechanism was described by the relative block rotations: $\delta\theta_1=1.333$, $\delta\theta_2=4.682$, $\delta\theta_3=6.453$, $\delta\theta_4=3.104$. When the offset of the load was -0.66 m from the crown the minimum collapse load was 15.91 kN/m (or 3.58 kN total load for a 225 mm wide arch).

Gilbert (1993) tested a series of barrel only structures of this width and recorded a residual load capacity of 3.6 kN. This close correlation verifies the proposed method although it would be incorrect to base its accuracy on this prediction alone since Gilbert's models ring separated, this is a phenomenon that, at present, the proposed technique cannot incorporate.

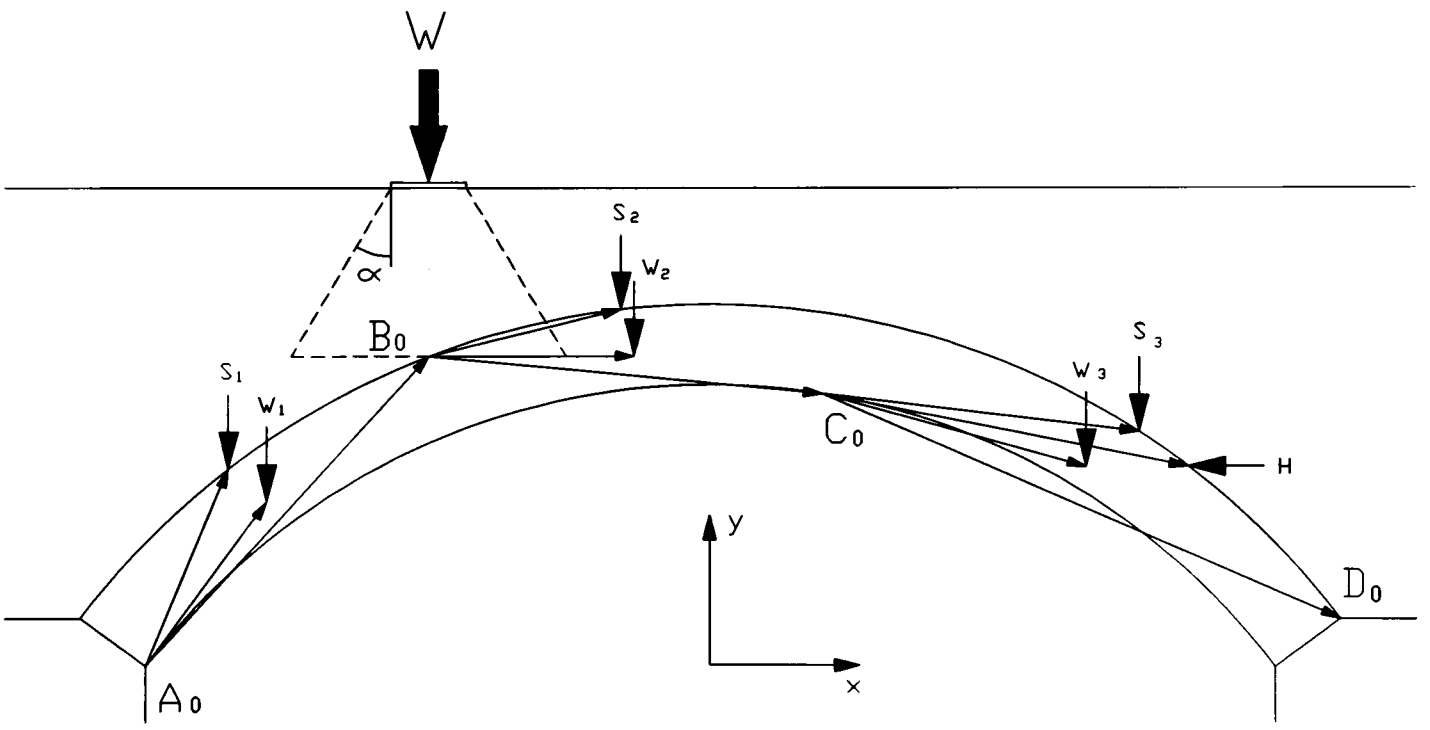

Figure 6.12 Idealisation of arch including backfill effects

It was convenient to derive the expression for the collapse load, equation 6.28, based on the three vectors that represent the arch. In so doing, the inherent assumption was that the arch comprises three straight sections. This approach will greatly reduce the complexity of the equivalent function in the three-dimensional model in which fractures may be inclined to the global cartesian axes. However, in the two-dimensional model, additional vectors can be introduced which link each hinge to the centroid of the proceeding block and to the point of application of the applied loads. Thus, it is possible to correct the work equation so that it takes account of the curvature of the arch and to enhance it so that it includes the vertical weight of

the backfill and the horizontal passive pressure as shown in figure 6.12. The collapse load can also be dispersed through the spandrel fill down to the extrados, the simplest method being that which is advocated in the DoT design note, BD 21/93.

Figure 6.13 shows the results of several analyses of a 3.0 m span arch with a rise of 0.75 m and a ring thickness of 0.215 mm. The arch is assumed to be 3.55 m wide and the depth of cover at its crown is 0.31 m. A rectangular passive pressure block was assumed and its magnitude was varied from 0 to 150 kN/m^2. The applied load was assumed to be 0.2 m wide and was dispersed through the spandrel fill at various angles. In accordance with the DoT design note, BD 21/93, the load was dispersed through the fill by applying it as a uniformly distributed load on the extrados of the arch over a loaded length equal to the base length of a trapezium formed from the dispersal lines as shown in figure 6.12.

It can be seen that there is a close correlation between the predictions of the discrete rigid block model proposed by Gilbert (1993), although his model contained separable rings, and those of the proposed indiscrete model. It can also be seen that the analysis of the indiscrete model is quicker and very much simpler than that of its discrete counterpart. However, figure 6.13 also reveals how the results of an analysis of any model that does not calculate movement related passive pressures are dependent upon the assumed magnitude of the passive pressure and load dispersal method. For example, there is an infinite number of combination of load dispersal angle and passive pressure magnitude that will produce a predicted load capacity of 600 kN. Thus, it is very important that both of these parameters are correctly selected.

Figure 6.14 shows the load carrying capacity of the voussoir arch as predicted using the indiscrete rigid block mechanism method. The applied load was assumed to disperse through the spandrel fill at 30° to the vertical and was applied uniformly in accordance with the DoT design note BD 21/93. In each case the deformation of the arch, whatever it may be, was assumed to be such that it mobilised a rectangular passive pressure block of magnitude 50H kN/m^2 (Gilbert, 1993). In each case the width of the arch was 3.55 m, and its spandrel walls were assumed to be detached. A constant span/rise ratio of 4.0 was assumed and various span/depth of ring ratios were examined. Thus, as the span was increased so was the ring thickness.

Following a comparison with the discrete rigid block mechanism methods, viz. the upper bound and lower bound methods, it can be seen that the vector approach requires much less computer effort than the latter method and much less human effort in formulating the kinematics of the problem than the former method. Thus, its extension into three-dimensions in order to analyse the skewed arch was undertaken.

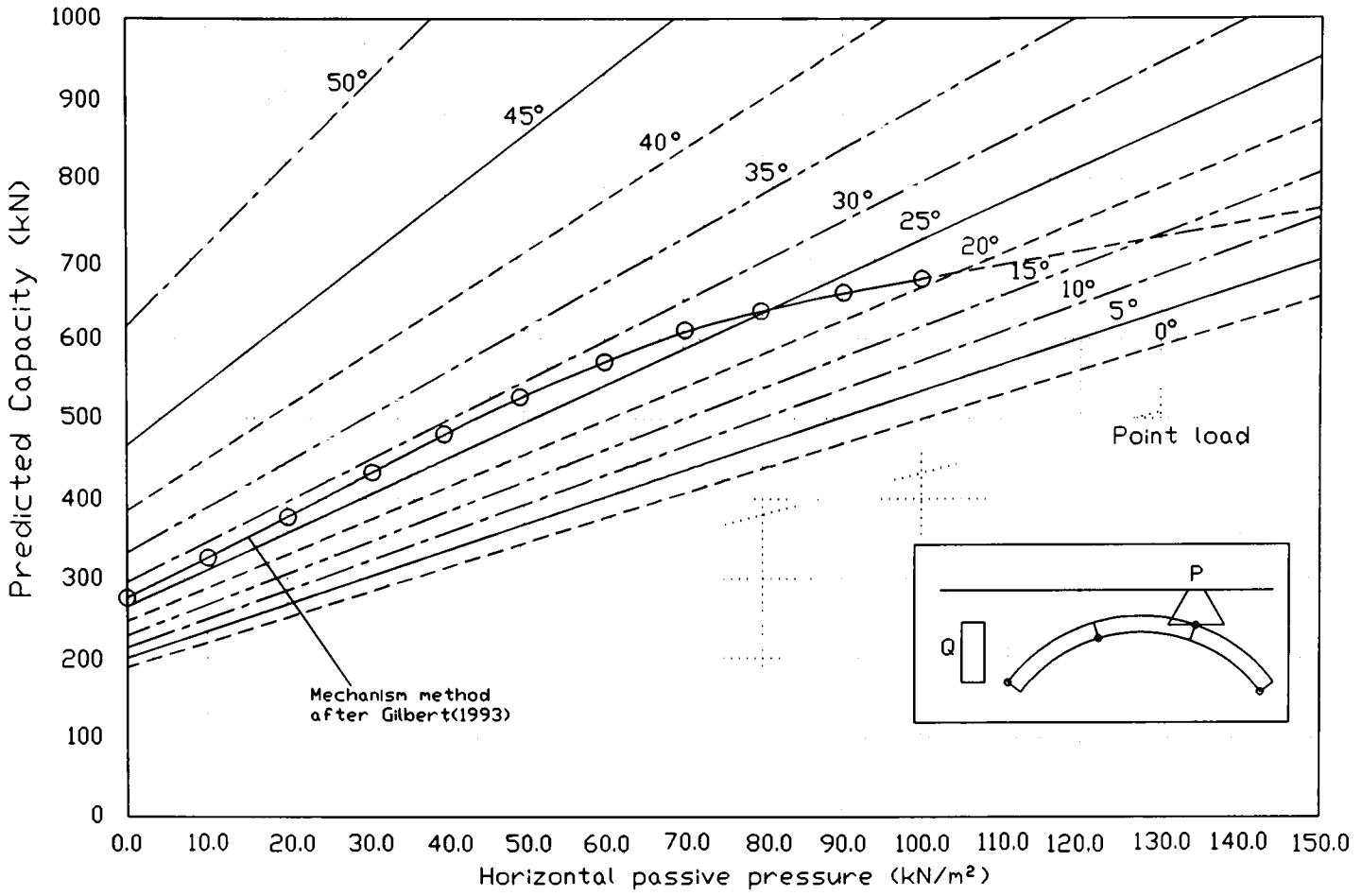

Figure 6.13 Predicted capacity versus passive pressure and load dispersal angle

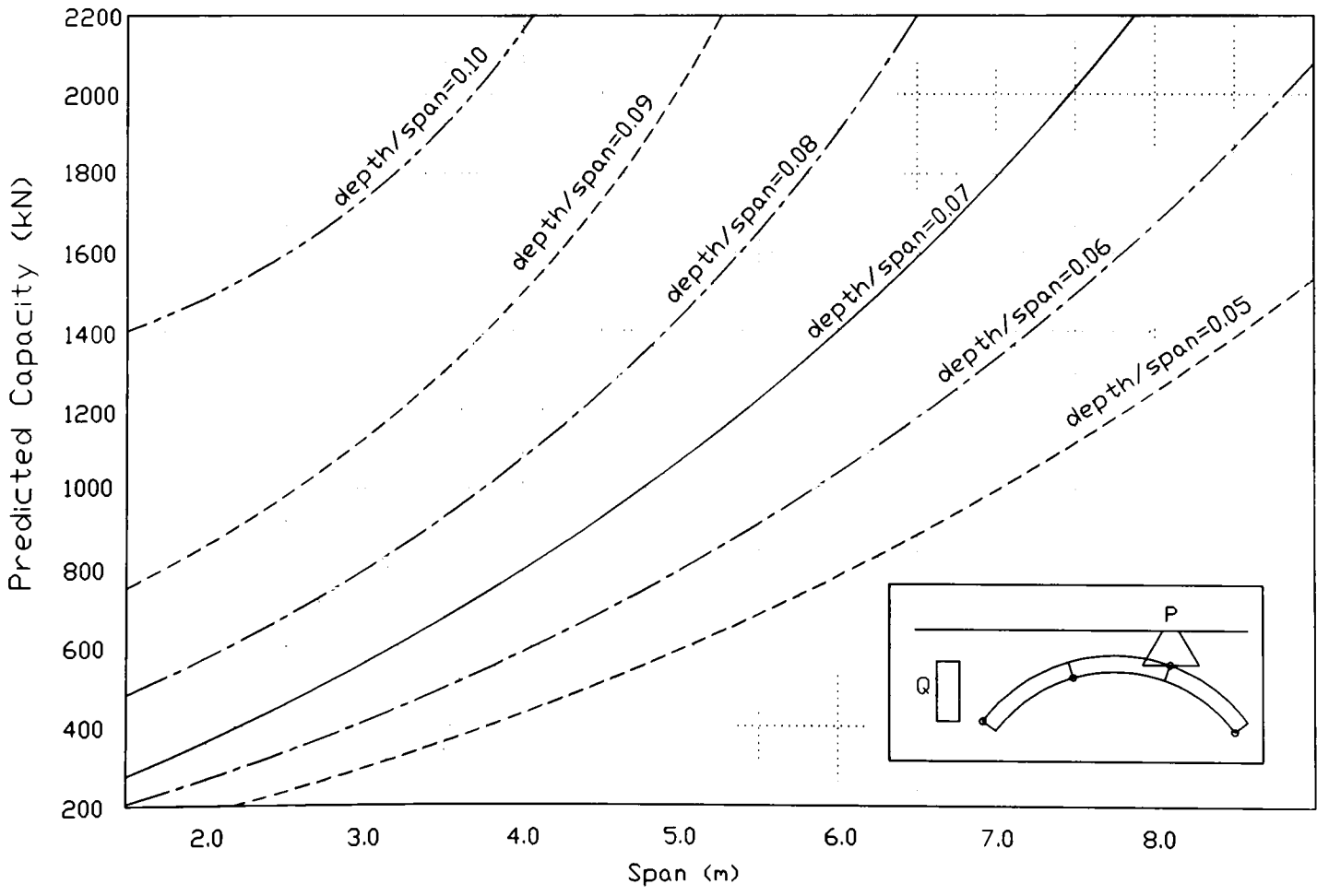

Figure 6.14 Predicted capacity of the square span voussoir arch

6.6 The three-dimensional indiscrete rigid block mechanism method

6.6.1 The simple hinge model of the skewed voussoir arch

6.6.1.1 Introduction

This three-dimensional modelling technique is based on the same assumptions as the two-dimensional technique presented in section 6.5 with the exception that it applies to the skewed voussoir arch.

An attempt to analyse the skewed arch using this approach is reliant upon visual observations of the collapse mechanism of each of the 3.0 m span skewed arch bridges documented in chapter 5. It can be concluded that each collapse mechanism resembled that which is shown in figure 6.15. It is assumed that the form of movement at each fracture will be simple hinging; the validity of this assumption will be determined by the ability of the technique to produce an admissible collapse mechanism.

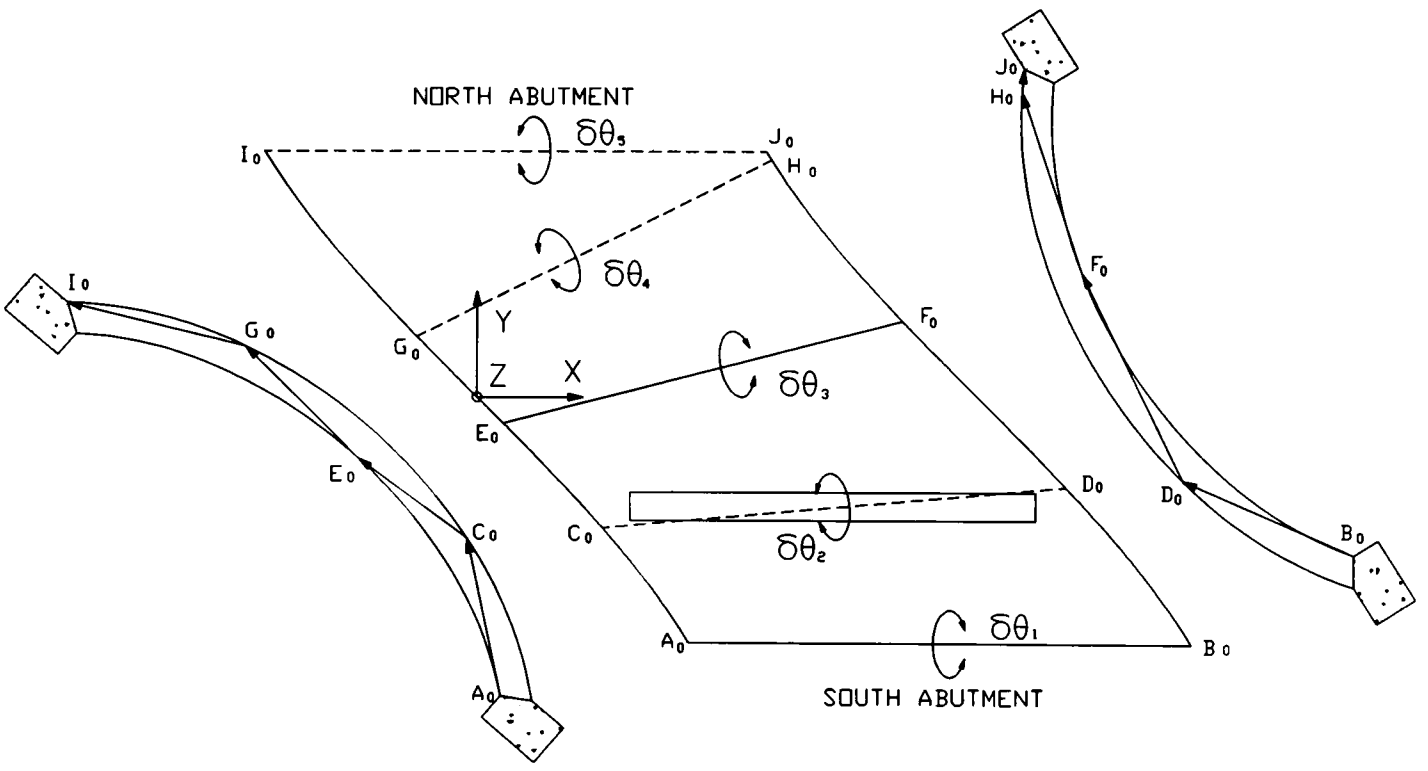

Figure 6.15 Generalised crack pattern associated with the global failure of a skewed arch

It is possible to generalise the crack pattern shown in figure 6.15 and to search for a mechanism, of this form, that would be associated with the minimum collapse load. Thus, in this technique, the skewed arch is idealised as a set of four incompressible contiguous blocks bounded by a total of five fractures. The position of each fracture is described by a set of three-dimensional vectors which can be varied so that the optimum position of each fracture can be determined. Each block is assumed to posses infinite compressive and tensile strength whereas only compressive forces can be transferred across each fracture plane.

If the extremes of each hinge are denoted by the letters A to J then the position of each, as yet unopened hinge, must be A_0 to J_0. These must be such that they lie on the extrados or the intrados of the arch, as shown in figure 6.15, at positions which will enable an admissible mechanism to form when the structure is subjected to a unit virtual displacement at the point of application of the load, which is assumed to coincide with the mid-point of hinge CD.

6.6.1.2 Development of the model

Consider a general hinge which extends from point K on the west edge of the arch to point L on the east edge of the arch. This hinge is inclined to the abutments and therefore forms a curve in three-dimensional space. However, this hinge is represented by the linear vector **KL** which provides an axis of rotation so that subsequent block movements can be described. The formation of a simple hinge at **KL** opening through an angle, $\delta\theta$, causes subsequent blocks to change position. The revised position of these blocks is described by rotating the vector which links hinge **KL** to each of their vertices.

The vector representation of the hinge lines act as axes of rotation about which each block must rotate in order to accommodate the imposition of the unit vertical displacement of the applied load. Therefore, the first step in the analysis of this reduced set of mechanisms is to develop the necessary mathematics which will enable the deformation of the structure to be described in terms of these rotations.

Let the vector **KL** be as defined in equation 6.29 in terms of its components in the global cartesian coordinate system.

$$\begin{aligned} \boldsymbol{KL} &= (X_L - X_K)\,\underline{i} + (Y_L - Y_K)\,\underline{j} + (Z_L - Z_K)\underline{k} \\ &= X_{KL}\underline{i} + Y_{KL}\underline{j} + Z_{KL}\underline{k} \end{aligned} \qquad \textbf{(6.29)}$$

Vector **KM** extends from one extreme of hinge **KL** to the point M situated at a vertex of a block to the north of the fracture line. A local coordinate system must be defined in order to calculate the new definition of **KM** after it undergoes a rotation of $\delta\theta$ due to the opening of hinge **KL**. This local coordinate system must be such that its x-axis lies along the hinge **KL**. Therefore, equation 6.30 defines the local x-axis in terms of its global components.

$$x = X_{KL}\underline{i} + Y_{KL}\underline{j} + Z_{KL}\underline{k} \qquad \textbf{(6.30)}$$

The orientation of the local y-axis and the local z-axis is unimportant provided that all three local axes form a mutually perpendicular right handed system. This is because rotations are

only permitted to take place about the local x-axis. The unimportance of the orientation of the other local axes means that the local y-axis can be selected so that it conveniently lies in the global XY-plane. This assumption simplifies the direction cosines so that one of them is zero.

$$\underline{y} = -Y_{KL}\underline{i} + X_{KL}\underline{j} \tag{6.31}$$

Therefore, the definition of the local y-axis, shown in equation 6.31, can be obtained from the dot product, $\mathbf{x}.\mathbf{y}=0$. It follows that the local z-axis is given by the cross product, $\mathbf{x} \wedge \mathbf{y}$ as defined in equation 6.32. Therefore, each local coordinate axis has been described in terms of the global coordinates of the hinge line.

$$\underline{z} = -X_{KL}.Z_{KL}\underline{i} - Y_{KL}.Z_{KL}\underline{j} + (X_{KL}^2+Y_{KL}^2)\underline{k} \tag{6.32}$$

The nine direction cosines relating the local coordinate system to the global coordinate system are as shown in equation 6.33.

$$\cos\alpha_{xX} = \frac{X_{KL}}{\sqrt{X_{KL}^2+Y_{KL}^2+Z_{KL}^2}} \quad , \quad \cos\alpha_{yX} = \frac{-Y_{KL}}{\sqrt{X_{KL}^2+Y_{KL}^2}} \quad , \quad \cos\alpha_{zX} = \frac{-X_{KL}.Z_{KL}}{\sqrt{(X_{KL}^2+Y_{KL}^2).(X_{KL}^2+Y_{KL}^2+Z_{KL}^2)}}$$

$$\cos\alpha_{xY} = \frac{Y_{KL}}{\sqrt{X_{KL}^2+Y_{KL}^2+Z_{KL}^2}} \quad , \quad \cos\alpha_{yY} = \frac{X_{KL}}{\sqrt{X_{KL}^2+Y_{KL}^2}} \quad , \quad \cos\alpha_{zY} = \frac{-Y_{KL}.Z_{KL}}{\sqrt{(X_{KL}^2+Y_{KL}^2).(X_{KL}^2+Y_{KL}^2+Z_{KL}^2)}}$$

$$\cos\alpha_{xZ} = \frac{Z_{KL}}{\sqrt{X_{KL}^2+Y_{KL}^2+Z_{KL}^2}} \quad , \quad \cos\alpha_{yZ} = 0 \quad , \quad \cos\alpha_{zZ} = \frac{X_{KL}^2+Y_{KL}^2}{\sqrt{(X_{KL}^2+Y_{KL}^2).(X_{KL}^2+Y_{KL}^2+Z_{KL}^2)}} \tag{6.33}$$

Each subsequent global vector, for example **KM**, must be transformed into **km** in the appropriate local coordinate system so that its components can be adjusted to take account of the rotation, $\delta\theta$, which takes place in the local yz-plane. Therefore in the local coordinate system:

$$\begin{aligned}\boldsymbol{km} = {} & (X_{KM}\cos\alpha_{xX}+Y_{KM}\cos\alpha_{xY}+Z_{KM}\cos\alpha_{xZ})\,\underline{i} \\ & +(X_{KM}\cos\alpha_{yX}+Y_{KM}\cos\alpha_{yY}+Z_{KM}\cos\alpha_{yZ})\,\underline{j} \\ & +(X_{KM}\cos\alpha_{zX}+Y_{KM}\cos\alpha_{zY}+Z_{KM}\cos\alpha_{zZ})\,\underline{k}\end{aligned} \tag{6.34}$$

which can be rewritten as equation 6.35.

$$\boldsymbol{km} = x_{KM}\underline{\boldsymbol{i}} + y_{KM}\underline{\boldsymbol{j}} + z_{KM}\underline{\boldsymbol{k}} \tag{6.35}$$

If this vector is transformed immediately back into its global components the following relationship can be established.

$$\begin{aligned}\boldsymbol{KM} = {} & (x_{KM}\cos\alpha_{xX} + y_{KM}\cos\alpha_{yX} + z_{KM}\cos\alpha_{zX})\ \underline{\boldsymbol{i}} + (x_{KM}\cos\alpha_{xY} + y_{KM}\cos\alpha_{yY} + z_{KM}\cos\alpha_{zY})\ \underline{\boldsymbol{j}} \\ & + (x_{KM}\cos\alpha_{xZ} + y_{KM}\cos\alpha_{yZ} + z_{KM}\cos\alpha_{zZ})\ \underline{\boldsymbol{k}}\end{aligned} \tag{6.36}$$

As previously shown in equation 6.23 in which use was made of small deflection theory, the new definition of the vector **km** after it has undergone a rotation of $\delta\theta$ about the hinge vector **KL** can now be redefined in equation 6.37.

$$\boldsymbol{km_1} = x_{KM}\,\underline{\boldsymbol{i}} + (y_{KM} + z_{KM}.\delta\theta)\underline{\boldsymbol{j}} + (z_{KM} - y_{KM}.\delta\theta)\underline{\boldsymbol{k}} \tag{6.37}$$

The vector shown in equation 6.37 must be transformed back into the global coordinate system. However, this does not result in the rotated vector, $\mathbf{KM_1}$, being expressed solely in terms of its rotation, its initial global components, and the global components of the hinge vector, **KL**. Local coordinate components must be removed by substituting into it the expressions for each as obtained from equation 6.34. Thus, equation 6.38 defines the vector $\mathbf{KM_1}$ in terms of the unknown rotation, $\delta\theta$, and the global coordinates of the hinges. This equation will be described as the simple hinge rotation equation.

$$\begin{aligned}\boldsymbol{KM_1} = {} & \left[\ X_{KM} + \frac{(Y_{KM}.Z_{KL} - Z_{KM}.Y_{KL})}{\sqrt{X_{KL}^2 + Y_{KL}^2 + Z_{KL}^2}}.\delta\theta\ \right]\underline{\boldsymbol{i}} + \left[\ Y_{KM} - \frac{(X_{KM}.Z_{KL} - Z_{KM}.X_{KL})}{\sqrt{X_{KL}^2 + Y_{KL}^2 + Z_{KL}^2}}.\delta\theta\ \right]\underline{\boldsymbol{j}} \\ & + \left[\ Z_{KM} + \frac{(X_{KM}.Y_{KL} - Y_{KM}.X_{KL})}{\sqrt{X_{KL}^2 + Y_{KL}^2 + Z_{KL}^2}}.\delta\theta\ \right]\underline{\boldsymbol{k}}\end{aligned} \tag{6.38}$$

The initial undeformed geometry of the arch is defined by the points A_0 to J_0. After hinge AB opens points C_0 to J_0 move to their new locations denoted C_1 to J_1. Similarly, after hinge CD opens points E_1 to J_1 move to their new locations denoted E_2 to J_2. This is continued until each hinge has opened at which juncture the deformed shape of the arch is defined by points denoted A_0, B_0, C_1, D_1, E_2, F_2, G_3, H_3, I_4, J_4, A_5, B_5. It therefore follows that the change in position of point J can be defined by the vector $\mathbf{J_0J_4}$ as shown in equation 6.39 and the change in position of point A can be defined by the vector $\mathbf{A_0A_5}$ as shown in equation 6.40.

$$\boldsymbol{J_0J_4} = \boldsymbol{B_0D_1} + \boldsymbol{D_1F_2} + \boldsymbol{F_2H_3} + \boldsymbol{H_3J_4} - \boldsymbol{B_0J_0} = 0 \tag{6.39}$$

$$A_0A_5 = A_0D_1 + D_1F_2 + F_2H_3 + H_3J_4 + J_4A_5 = 0 \quad \textbf{(6.40)}$$

Care must be taken when setting up the above vector equations since there are several paths through the structure which may pass through either end of each hinge. The sign convention is such that a clockwise hinge rotation is positive when viewed from a position with a positive local x-ordinate so that the rotation causes end M to moves towards the local y-axis. Therefore when using the local coordinate system that is based on the west end of a hinge, $+\delta\theta$ indicates an extrados hinge whereas $+\delta\theta$ would indicate an intrados hinge if the local coordinate system was based on the east end of the hinge.

Each abutment is assumed to be immovable. The assumption that only simple hinges occur at each fracture plane is valid if the mechanism can be found to be admissible. This is achieved if the combined effect of a positive rotation of each hinge can be accommodated by each abutment whilst remaining immovable. A mathematical description of this is given by equations 6.39 and 6.40 which are used to create four constraining equations 6.41 to 6.44 whose simultaneous solution determines the admissibility of the analysis. A similar set of constraints based on the movement of point I would be redundant because the assumption of simple hinges ensures that the vectors $\mathbf{I_0I_4}$ and $\mathbf{J_0J_4}$ are equal.

Equation 6.38 can be repeatedly substituted into itself as each successive hinge is opened in order to build up expressions for each vector defined in constraint 6.39. When these expressions are substituted into equation 6.38, the following three constraints are formed which state that point J must not translate in the X, Y or Z direction as a result of the formation of each hinge.

$$\frac{(Y_{DJ}.Z_{DC}-Z_{DJ}.Y_{DC})}{\sqrt{X_{DC}^2+Y_{DC}^2+Z_{DC}^2}}.\delta\theta_2-\frac{(Y_{FJ}.Z_{FE}-Z_{FJ}.Y_{FE})}{\sqrt{X_{FE}^2+Y_{FE}^2+Z_{FE}^2}}.\delta\theta_3+\frac{(Y_{HJ}.Z_{HG}-Z_{HJ}.Y_{HG})}{\sqrt{X_{HG}^2+Y_{HG}^2+Z_{HG}^2}}.\delta\theta_4 = 0 \quad \textbf{(6.41)}$$

$$\frac{(X_{DJ}.Z_{DC}-Z_{DJ}.X_{DC})}{\sqrt{X_{DC}^2+Y_{DC}^2+Z_{DC}^2}}.\delta\theta_2-\frac{(X_{FJ}.Z_{FE}-Z_{FJ}.X_{FE})}{\sqrt{X_{FE}^2+Y_{FE}^2+Z_{FE}^2}}.\delta\theta_3+\frac{(X_{HJ}.Z_{HG}-Z_{HJ}.X_{HG})}{\sqrt{X_{HG}^2+Y_{HG}^2+Z_{HG}^2}}.\delta\theta_4 = -Z_{BJ}.\delta\theta_1 \quad \textbf{(6.42)}$$

$$\frac{(X_{DJ}.Y_{DC}-Y_{DJ}.X_{DC})}{\sqrt{X_{DC}^2+Y_{DC}^2+Z_{DC}^2}}.\delta\theta_2-\frac{(X_{FJ}.Y_{FE}-Y_{FJ}.X_{FE})}{\sqrt{X_{FE}^2+Y_{FE}^2+Z_{FE}^2}}.\delta\theta_3+\frac{(X_{HJ}.Y_{HG}-Y_{HJ}.X_{HG})}{\sqrt{X_{HG}^2+Y_{HG}^2+Z_{HG}^2}}.\delta\theta_4 = -Y_{BJ}.\delta\theta_1 \quad \textbf{(6.43)}$$

The satisfaction of the constraining equations 6.41 to 6.43 adequately defines the collapse mechanism except for the magnitude of the rotation of the final hinge. Thus, the length of vector $\mathbf{A_0J_0}$ must be equal to that of vector $\mathbf{A_5J_4}$. Therefore only one component of the vector

$\mathbf{A_0A_5}$ need be defined since this will adequately define an immovable abutment AB. Hence, equation 6.38 can be substituted into itself as each consecutive hinge is opened so that the vectorial terms in equation 6.40 can be obtained and the constraining equation 6.44 produced.

$$\delta\theta_5 = \frac{(X_{DA}.Z_{DC}-Z_{DA}.X_{DC})}{Z_{JA}\sqrt{X_{DC}^2+Y_{DC}^2+Z_{DC}^2}}.\delta\theta_2 - \frac{(X_{FA}.Z_{FE}-Z_{FA}.X_{FE})}{Z_{JA}\sqrt{X_{FE}^2+Y_{FE}^2+Z_{FE}^2}}.\delta\theta_3 + \frac{(X_{HA}.Z_{HG}-Z_{HA}.X_{HG})}{Z_{JA}\sqrt{X_{HG}^2+Y_{HG}^2+Z_{HG}^2}}.\delta\theta_4 \qquad \textbf{(6.44)}$$

This equation is used only to define the magnitude of the rotation, $\delta\theta_5$, after the analysis of the mechanism has been performed.

The imposition of a unit vertical displacement of the applied load specifies the rotation, $\delta\theta_1$, at the south abutment as shown in equation 6.45.

$$(\frac{Y_C+Y_D}{2}-Y_A).\delta\theta_1 = 1 \qquad \textbf{(6.45)}$$

As can be seen in equation 6.45, the centroid of the applied load is assumed to coincide with the mid-point of hinge **CD**. Hence, by initially evaluating the rotation of the hinge at the south abutment, the three constraining equations 6.41 to 6.43 each contain three unknown rotations and three non-linear functions of the spatial coordinates.

6.6.1.3 Discussion

It should be noted that, within this model, the only form of relative block movement that is permitted to occur at each fracture plane is a simple hinge rotation. It is a long established fact, since the experimental work of Danyzy (1732), that an admissible mechanism can comprise four simple hinges provided that each fracture plane is parallel to the abutments. The experimental evidence, documented in chapter 5, indicates that five fracture planes occur in the skewed arch three of which are not parallel to the abutments. Furthermore, the respective failure loads of the skewed and square span arch bridges indicate that the fracture pattern shown in figure 6.15 is associated with a lower collapse load. The formation of a fracture that is inclined to the abutments means that a straight line drawn between its two ends does not remain in the plane of the arch. In this model, a simple hinge rotation occurs about an axis that is parallel to this line. Thus, an extrados hinge would create a single point of contact between the two adjacent blocks. Similarly, an intrados hinge would create two points of contact. In reality, the flexibility of the arch would result in full-length contact at a simple hinge. However, the constraints are valid whatever contact situation is created; the objective of the analysis is to

determine if an admissible mechanism can be formed with five simple hinges. The analysis will fail if any other form of movement is required, such as sliding or complex hinging. A complex hinge would cause the single point of contact at an extrados hinge to move and would result in the loss of one of the contact points at an intrados hinge.

The analysis of this model would require non-linear programming techniques. The determination of the optimum position of each hinge and the magnitude of each rotation required in an admissible mechanism that corresponds to the least possible collapse load could be carried out this way. However, this would require a similarly non-linear objective function to express the change in potential energy of the system in terms of each simple hinge rotation. However, the first task is to determine whether any admissible mechanism can be found. Thus, if the change in potential energy of the deformation is neglected, a search for a feasible set of hinge rotations can be carried out. This can be done by assuming reasonable hinge positions so that the three non-linear constraining equations 6.41 to 6.43 are transformed into three linear simultaneous equations.

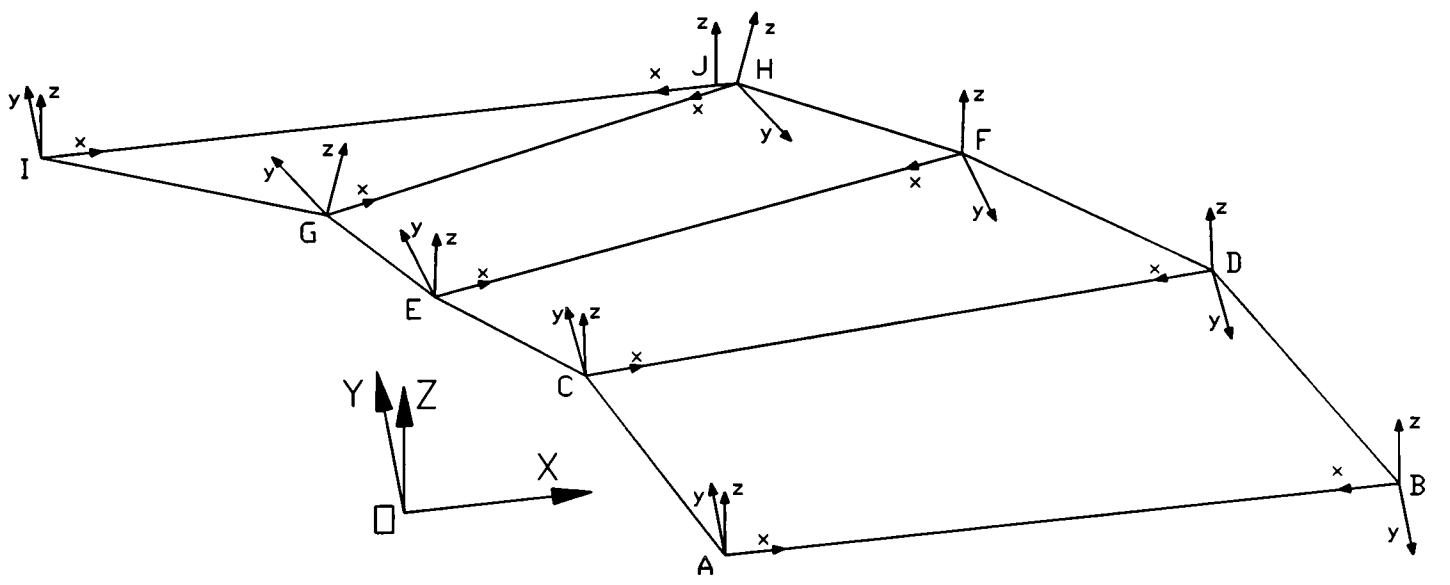

Figure 6.16 AutoCAD drawing of the idealised arch with simple hinges

Consider an arch bridge that is similar to skewed arch 3-2, i.e the 3.0 m span, 3.55 m wide, 45° skewed model arch, whose failure mechanism (as described in chapter 5), if ring separation is neglected, may be idealised as a set of simple hinges defined by the following values: $X_A=1.500, X_B=5.050, X_C=0.850, X_D=4.200, X_E=0.150, X_F=3.050, X_G=-0.350, X_H=2.000, X_I=-1.672, X_J=1.878$. The coordinates of each hinge can be determined, since $Y=-X$ or $Y=3.55-X$ and $Z=\sqrt{(2.09^2-Y^2)}$ or $Z=\sqrt{(1.875^2-Y^2)}$ depending on whether the particular point lies at the east or west edge of the arch and whether it lies on the extrados or the intrados. These points were used to create a three-dimensional AutoCAD drawing as shown in figure 6.16 which enabled the hinge opening equation to be validated against manual manipulation of the drawing.

The results of this exercise can be found in appendix C.1 which shows that the constraining equations are valid. Figure 6.16 can also be used to view the local coordinate system at either end of each hinge. As previously pointed out, the immovable abutment constraint 6.38 can be derived from any vectorial summation from one abutment to the other. The route taken through the structure determines the sign of the required hinge rotation.

Equation 6.45 is solved initially so that $\delta\theta_1 = 1.333$. Substituting this value and the above coordinate data into the constraining equations 6.41 to 6.43 and writing in matrix form:

$$\begin{bmatrix} -0.0969 & 0.0965 & -0.0358 \\ 0.6776 & -0.5640 & 0.1574 \\ 2.4556 & -1.3997 & 0.1593 \end{bmatrix} \cdot \begin{bmatrix} \delta\theta_2 \\ \delta\theta_3 \\ \delta\theta_4 \end{bmatrix} = \begin{bmatrix} 0 \\ -0.1720 \\ 4.2293 \end{bmatrix}$$

Which, after carrying out Gauss elimination becomes:

$$\begin{bmatrix} 2.4556 & -1.3997 & 0.1593 \\ 0 & -0.1778 & 0.1135 \\ 0 & 0 & -0.0031 \end{bmatrix} \cdot \begin{bmatrix} \delta\theta_2 \\ \delta\theta_3 \\ \delta\theta_4 \end{bmatrix} = \begin{bmatrix} 3.8549 \\ -1.2205 \\ -0.1315 \end{bmatrix}$$

Finally, equation 6.44 is used so that the required hinge rotations for this assumed mechanism are as follows: $\delta\theta_1 = 1.333$, $\delta\theta_2 = 19.888$, $\delta\theta_3 = 37.149$, $\delta\theta_4 = 46.398$ and $\delta\theta_5 = -51.684$.

The analysis is based on a mechanism which resembles that which was observed during each load test on the skewed arch bridges documented in chapter 5. Thus, whilst the position of the hinges must be adjusted so that the associated collapse load can be minimised, the occurrence of intrados or extrados hinges was based on the observed crack pattern.

There are several significant conclusions which can be made from this analysis which are as follows:

1. The assumed mechanism is infeasible. This is indicated by the negative rotation at hinge IJ. The negative value of $\delta\theta_5$ indicates that, although an extrados hinge was observed and therefore assumed to occur at this location, compatibility could only be maintained by an intrados hinge.

2. The theoretical mechanism can not be corrected by changing the north abutment hinge from an extrados hinge to an intrados hinge. This would conflict with visual observations. Furthermore, this rotation is found from a post-analysis calculation. In

other words, the error in the analysis is due to the assumption regarding the type of in-span hinges.

3. Simple hinges are insufficient to enable the formation of this mechanism. Although Gauss elimination of the rotation coefficient matrix did not produce a zero main diagonal term, the final main diagonal term did approach zero and is responsible for the order of magnitude difference between the rotation of the south abutment hinge and the rotation of every other hinge. This indicates an unrealistic selection of hinge types.

4. It can be concluded that a system of four simple hinges is sufficient to produce a failure mechanism provided that these hinges are parallel to the abutments. However, a system of five simple hinges is insufficient to produce a failure mechanism in a skewed arch if the hinges are inclined to each other.

5. In the skewed arch more complex hinge behaviour is required in order to produce a kinematically admissible deformed configuration of blocks.

6. The observed crack pattern at failure of bridge 3-2, as shown in figure 5.6, was attributed to the low shear strength of the mortar and the lack of compressive force within the arch due to the absence of backfill (Melbourne & Hodgson, 1994b). These were certainly valid statements. However, in light of the above conclusions, obtained from the failure of the simple hinge model to adequately analyse the mechanism, it is suggested that the observed sliding movements, the additional fracture and the appearance of cracking in the extrados and intrados were due to the necessary formation of a mechanism containing complex hinges.

It is therefore concluded that in order to successfully analyse the skewed arch a mathematical model which permits complex hinging at each fracture plane must be developed. Furthermore, the visual observations made of the 1.2 m span model arch tests, see section 5.2, would certainly verify the conclusion that the blocks of masonry must be allowed to undergo complex relative movements.

6.6.2 The complex hinge model of the skewed voussoir arch

6.6.2.1 Introduction

This, more general, theoretical model is an extension of the simple hinge model, presented in section 6.6, which incorporates complex hinges in which adjacent rigid blocks are also allowed to rotate about either extreme of the simple hinge as if connected by a ball and socket type joint. This model also applies to the skewed masonry arch without spandrel walls and does not incorporate the effects of the backfill. It is also assumed that the coefficient of separation is sufficiently high so that shear failures will not occur although the shearing associated with a torsional hinge is permitted but is not accompanied by dilatant movements.

6.6.2.2 Development of the model

The upper bound theorem of collapse requires that the assumed mechanism is admissible. This is partially satisfied by ensuring that adjacent blocks do not lose contact of each other and that they do not impinge on each other as they move to accommodate the displacement of the applied load. These requirements are fulfilled if each block is only permitted to rotate about an edge or a corner of an adjacent block. However, to achieve this, each axis of rotation must be selected so that bounds on the other rotations can be defined and used as constraints within which feasible values are to be sought. Linear programming techniques are based on the assumption that all variables must be non-negative. It is therefore both logical and convenient for each set of local axes to be selected so that the lower bound on each rotation is zero which corresponds to a closed hinge.

Figure 6.17 shows an isometric view of half of a cylinder which contains, within it, the skewed arch.

The local x-axis is selected so that it coincides with the vector which represents the fracture, **KL** as shown in equation 6.50.

$$\underline{x}_{KL}=X_{KL}\underline{i}+Y_{KL}\underline{j}+Z_{KL}\underline{k} \qquad \textbf{(6.50)}$$

The vector **KL** intersects the cylinder at two points at the east and west edge of the skewed arch. At point K or L the plane, P, is perpendicular to the vector, **KL**, and therefore contains the local y and z axes. The vector representing the local y-axis can be expressed as in equation 6.51 which when its dot product with the vector representing the local x-axis is equated to zero produces equation 6.52, since these two vectors represent mutually perpendicular axes.

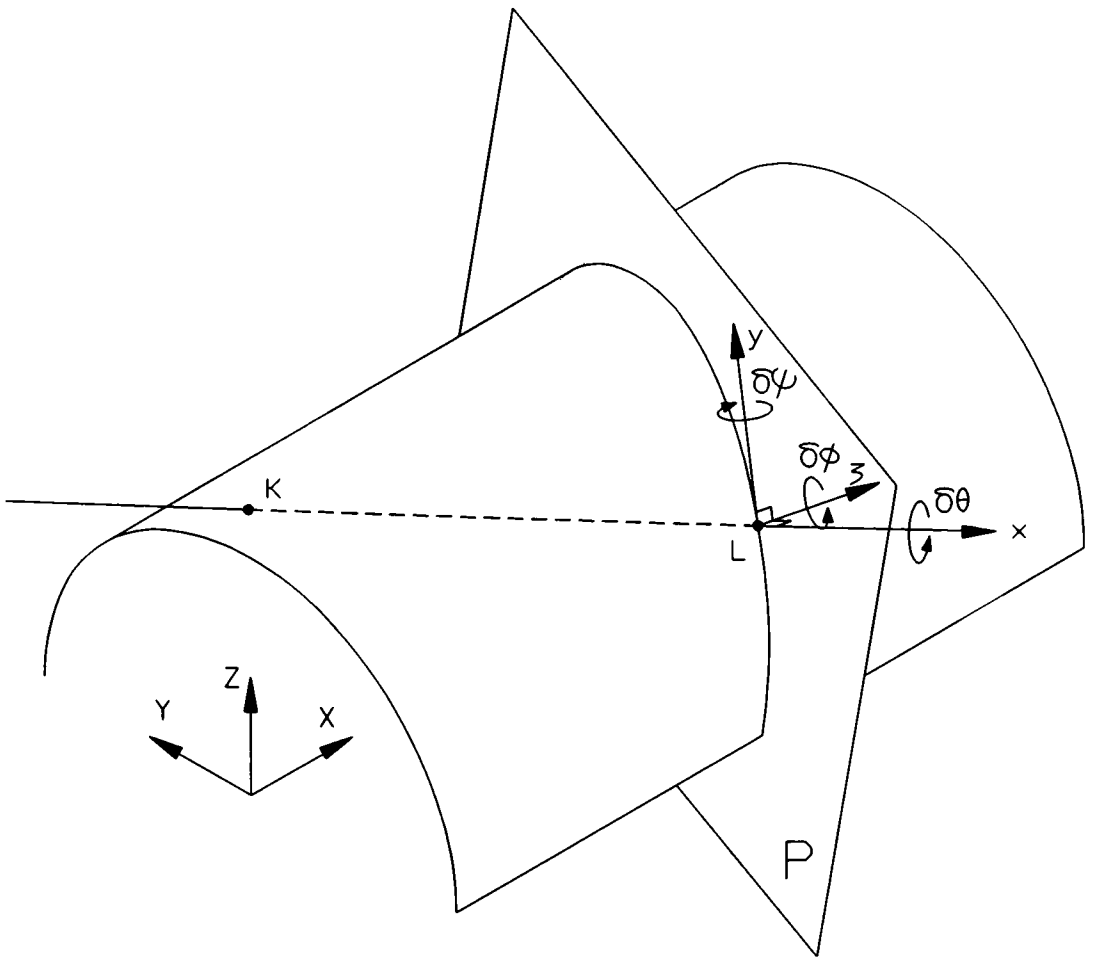

Figure 6.17 Local coordinate system in the skewed arch

$$y_{KL} = a\underline{i}+b\underline{j}+c\underline{k} \tag{6.51}$$

$$a.x_{KL}+b.y_{KL}+c.z_{KL} = 0 \tag{6.52}$$

Furthermore, the local y-axis also lies within the tangent plane to the cylinder at K. Hence, if equation 6.53 represents that of a cylinder of radius R_i, equation 6.54 represents the equation of the plane which is normal to the cylinder at K.

$$h = Y^2+Z^2-R_i^2 = 0 \tag{6.53}$$

$$\nabla h = 2Y_K\underline{j}+2Z_K\underline{k} \tag{6.54}$$

The vector $\nabla\underline{h}$ is normal to the local y-axis since it is normal to the tangent plane and y lies within the plane. Hence, the dot product, $\nabla\underline{h}.\underline{y}=0$, leads to equation 6.55 which can be solved simultaneously with equation 6.52.

$$b.Y_K+c.Z_K = 0 \tag{6.55}$$

Hence, the values of c and b in equation 6.51 can be expressed as functions of the variable a.

Since a affects only the magnitude of the vector $\mathbf{y_{KL}}$, it can be chosen arbitrarily so that each component has unit common denominator. Therefore equation 6.56 shows the vector representation of the local y-axis. The local z-axis can then be determined by taking the vector cross product of $\mathbf{x_{KL}}$ and $\mathbf{y_{KL}}$, i.e. $\mathbf{x_{KL}} \wedge \mathbf{y_{KL}}$, as shown in equation 6.57.

$$y_{KL} = (Z_{KL}.Y_K - Y_{KL}.Z_K)\underline{i} + (X_{KL}.Z_K)\underline{j} - (X_{KL}.Y_K)\underline{k} \tag{6.56}$$

$$z_{KL} = -X_{KL}(Y_{KL}Y_K + Z_{KL}Z_K)\underline{i} + [Y_K(X_{KL}^2 + Z_{KL}^2) - Y_{KL}Z_{KL}Z_K]\underline{j} + [Z_K(X_{KL}^2 + Y_{KL}^2) - Y_{KL}Z_{KL}Y_K]\underline{k} \tag{6.57}$$

Thus, the direction cosines relating the global axes with the local axes used in the general vector rigid block method are as shown in equation 6.58.

$$\cos\alpha_{xX} = \frac{X_{KL}}{\sqrt{X_{KL}^2 + Y_{KL}^2 + Z_{KL}^2}} \quad , \quad \cos\alpha_{xY} = \frac{Y_{KL}}{\sqrt{X_{KL}^2 + Y_{KL}^2 + Z_{KL}^2}} \quad , \quad \cos\alpha_{xZ} = \frac{Z_{KL}}{\sqrt{X_{KL}^2 + Y_{KL}^2 + Z_{KL}^2}} \quad ,$$

$$\cos\alpha_{yX} = \frac{Z_{KL}Y_K - Y_{KL}Z_K}{\sqrt{(Z_{KL}Y_K - Y_{KL}Z_K)^2 + X_{KL}^2(Y_K^2 + Z_K^2)}} \quad , \quad \cos\alpha_{yY} = \frac{X_{KL}Z_K}{\sqrt{(Z_{KL}Y_K - Y_{KL}Z_K)^2 + X_{KL}^2(Z_K^2 + Y_K^2)}} \quad ,$$

$$\cos\alpha_{yZ} = \frac{-X_{KL}Y_K}{\sqrt{(Z_{KL}Y_K - Y_{KL}Z_K)^2 + X_{KL}^2(Z_K^2 + Y_K^2)}} \quad ,$$

$$\cos\alpha_{zX} = \frac{-X_{KL}.(Y_{KL}Y_K + Z_{KL}Z_K)}{\sqrt{X_{KL}^2.(Y_{KL}Y_K + Z_{KL}Z_K)^2 + [Y_K.(X_{KL}^2 + Z_{KL}^2) - Y_{KL}Z_{KL}Z_K]^2 + [Z_K.(X_{KL}^2 + Y_{KL}^2) - Y_{KL}Z_{KL}Y_K]^2}} \quad ,$$

$$\cos\alpha_{zY} = \frac{Y_K.(X_{KL}^2 + Z_{KL}^2) - Y_{KL}.Z_{KL}.Z_K}{\sqrt{X_{KL}^2.(Y_{KL}Y_K + Z_{KL}Z_K)^2 + [Y_K.(X_{KL}^2 + Z_{KL}^2) - Y_{KL}Z_{KL}Z_K]^2 + [Z_K.(X_{KL}^2 + Y_{KL}^2) - Y_{KL}Z_{KL}Y_K]^2}} \quad ,$$

$$\cos\alpha_{zZ} = \frac{Z_K.(X_{KL}^2 + Y_{KL}^2) - Y_{KL}.Z_{KL}.Y_K}{\sqrt{X_{KL}^2.(Y_{KL}Y_K + Z_{KL}Z_K)^2 + [Y_K.(X_{KL}^2 + Z_{KL}^2) - Y_{KL}Z_{KL}Z_K]^2 + [Z_K.(X_{KL}^2 + Y_{KL}^2) - Y_{KL}Z_{KL}Y_K]^2}} \tag{6.58}$$

To the north of a particular hinge, **KL**, each global vector, for example **KM**, must be transformed into **km** in the local coordinate system. The effect of rotating this vector about the hinge can then be taken into account. The rotations, $\delta\theta$, $\delta\phi$, and $\delta\psi$ take place in the local yz-, xy-, and xz-plane respectively and are such that a clockwise rotation about each axis is positive when viewed from a positive position on that axis towards the plane defined by the other two axes. Therefore, in the local coordinate system, the rotated vector is as described in equation 6.59 which was formed on the basis of small deflection theory, i.e, by ignoring second order and higher terms in the expansion of the sine and cosine series.

$$\boldsymbol{km} = (x_{KM}+\delta\phi.y_{KM}\mp\delta\psi.z_{KM})\,\underline{i} + (y_{KM}+\delta\theta.z_{KM}-\delta\phi.x_{KM})\,\underline{j} + (z_{KM}-\delta\theta.y_{KM}\pm\delta\psi.x_{KM})\,\underline{k} \qquad \textbf{(6.59)}$$

Finally, by transforming the vector shown in equation 6.59 back into the global coordinate system and substituting into it the direction cosines defined in equation 6.58, the adjusted vector $\mathbf{KM_1}$ can be established in terms of its previous definition and functions of the unknown rotation, $\delta\theta$, $\delta\phi$, $\delta\psi$.

The global definition of this vector is shown in equation 6.60 and is called the complex hinge rotation equation.

$$\begin{aligned} K_iM_{i+1} =& [X_{K_iM_i}-\delta\theta(Y_{KM}f_1^{KL}-Z_{KM}f_2^{KL})+\delta\phi(Y_{KM}g_1^{KL}-Z_{KM}g_2^{KL})\mp\delta\psi(Y_{KM}h_1^{KL}+Z_{KM}h_2^{KL})]\,\underline{i} \\ &+[Y_{K_iM_i}+\delta\theta(X_{KM}f_1^{KL}-Z_{KM}f_3^{KL})-\delta\phi(X_{KM}g_1^{KL}+Z_{KM}g_3^{KL})\pm\delta\psi(X_{KM}h_1^{KL}-Z_{KM}h_3^{KL})]\,\underline{j} \\ &+[Z_{K_iM_i}-\delta\theta(X_{KM}f_2^{KL}-Y_{KM}f_3^{KL})+\delta\phi(X_{KM}g_2^{KL}+Y_{KM}g_3^{KL})\pm\delta\psi(X_{KM}h_2^{KL}+Y_{KM}h_3^{KL})]\,\underline{k} \end{aligned} \qquad \textbf{(6.60)}$$

where,

$$f_1^{KL} = [2Y_KZ_KY_{KL}Z_{KL}^2 - Y_K^2Z_{KL}(X_{KL}^2+Z_{KL}^2) - Z_K^2Z_{KL}(X_{KL}^2+Y_{KL}^2)] \;/\; (L_y^{KL}.L_z^{KL})$$

$$f_2^{KL} = [2Y_KZ_KZ_{KL}Y_{KL}^2 - Y_K^2Y_{KL}(X_{KL}^2+Z_{KL}^2) - Z_K^2Y_{KL}(X_{KL}^2+Y_{KL}^2)] \;/\; (L_y^{KL}.L_z^{KL})$$

$$f_3^{KL} = [2Y_KZ_KX_{KL}Y_{KL}Z_{KL} - Y_K^2X_{KL}(X_{KL}^2+Z_{KL}^2) - Z_K^2X_{KL}(X_{KL}^2+Y_{KL}^2)] \;/\; (L_y^{KL}.L_z^{KL})$$

$$g_1^{KL} = [Z_K(X_{KL}^2+Y_{KL}^2) - Y_KY_{KL}Z_{KL}] \;/\; (L_x^{KL}.L_y^{KL})$$

$$g_2^{KL} = [Y_K(X_{KL}^2+Z_{KL}^2) - Z_KY_{KL}Z_{KL}] \;/\; (L_x^{KL}.L_y^{KL})$$

$$g_3^{KL} = [X_{KL}(Y_KY_{KL}+Z_KZ_{KL})] \;/\; (L_x^{KL}.L_y^{KL})$$

$$h_1^{KL} = Y_KX_{KL}.(L_x^{KL}/L_z^{KL})$$

$$h_2^{KL} = Z_KX_{KL}.(L_x^{KL}/L_z^{KL})$$

$$h_3^{KL} = (Z_KY_{KL}-Y_KZ_{KL}).(L_x^{KL}/L_z^{KL})$$

$$L_x^{KL} = \sqrt{X_{KL}^2+Y_{KL}^2+Z_{KL}^2} \quad , \quad L_y^{KL} = \sqrt{(Z_{KL}Y_K-Y_{KL}Z_K)^2+X_{KL}^2(Y_K^2+Z_K^2)}$$

$$L_z^{KL} = \sqrt{X_{KL}^2.(Y_{KL}Y_K+Z_{KL}Z_K)^2+[Y_K.(X_{KL}^2+Z_{KL}^2)-Y_{KL}Z_{KL}Z_K]^2+[Z_K.(X_{KL}^2+Y_{KL}^2)-Y_{KL}Z_{KL}Y_K]^2}$$

The complete satisfaction of the upper bound theorem of collapse is achieved by ensuring that the formation of a mechanism does not require that the abutments move. The movement of the abutments can be incorporated into the analysis by prescribing a fixed amount in the same way as the movement of the applied load is prescribed. Multiple analyses of the structure would

then be required to determine the sensitivity of the analysis to a range of fixed abutment movements. It should be noted that it is not possible to make the abutment movement the subject of the analysis. The relative movement of the abutments must be prescribed in order to establish the constraints of the problem. Consideration, here, will be given to the case in which the abutments are immovable. This assumption is used when deriving constraints which enable feasible hinge rotations to be determined. These constraints are formed by beginning at hinge A_0B_0 and moving across the span of the arch from one hinge to the next, each vector representing the position of each block can be adjusted by repeatedly substituting equation 6.60 into itself. If it is assumed that only simple hinges occur at hinge AB and CD then ultimately, the deformed shape of the arch is described by vectors which link together the points A_0, B_0, C_1, D_1, E_3, F_3, G_5, H_5, I_7, J_7, A_8, B_8. This can be seen in figure 6.18 which shows a typical arrangement of hinges on the development of a skewed arch together with possible failure mechanisms shown on elevation.

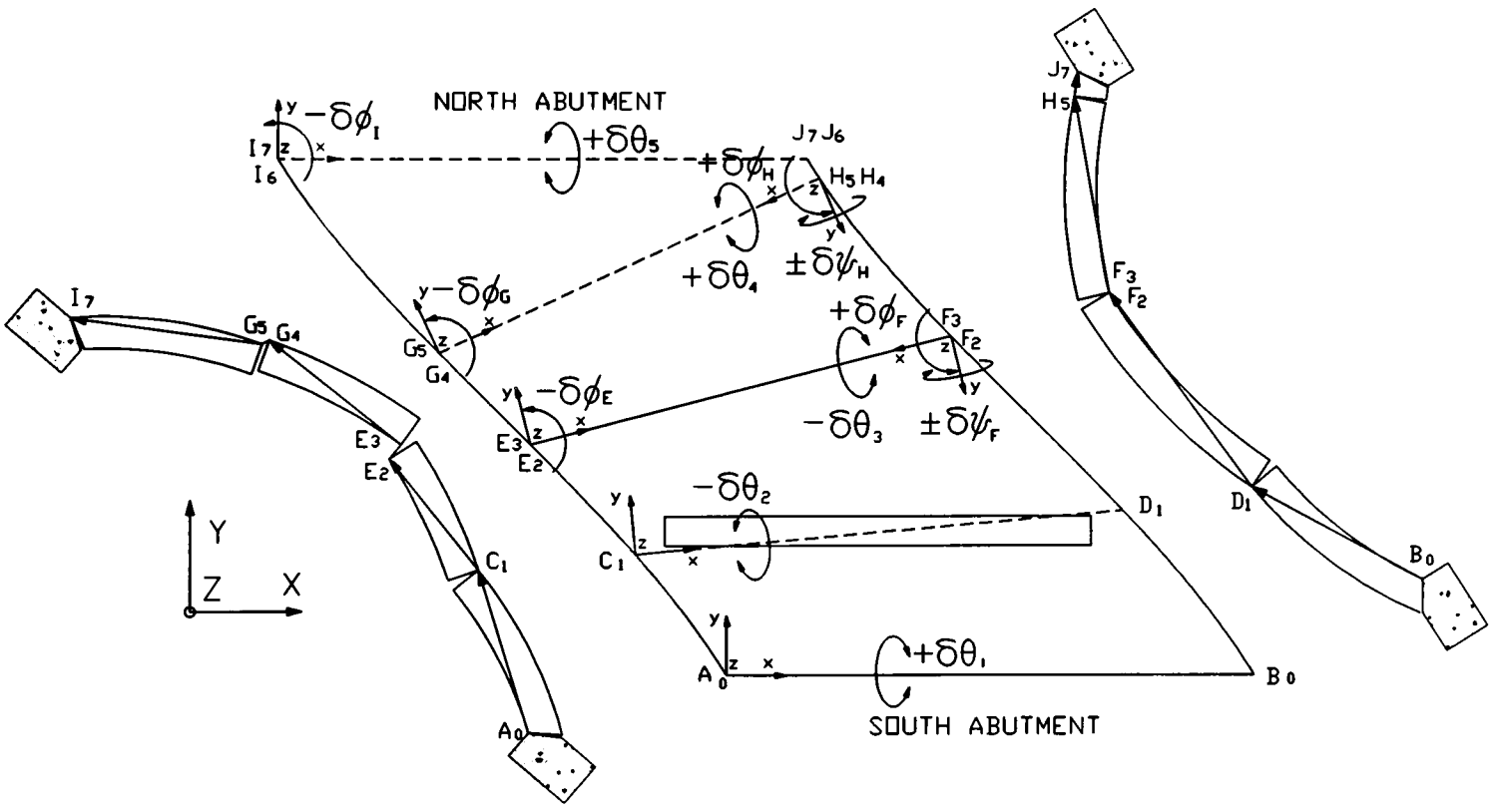

Figure 6.18 Typical position of complex hinges in the skewed arch

A feasible solution, in which the rotations at each complex hinge assume non-negative values and the abutments are not required to move in order to accommodate the deformation of the arch, indicates a kinematically admissible collapse state. The optimal solution is the one which minimises the change in potential energy during the deformation and this corresponds to the minimum failure load.

Mathematically, the constraint that the abutments must be immovable can be expressed in vector form by equation 6.61. The assumption that only a simple hinge occurs at AB means that it is not necessary to ensure that point B does not move. It is only necessary to ensure that points A, I and J do not move.

$$J_0J_7 = 0 \quad , \quad I_0I_7 = 0 \quad , \quad A_0A_8 = 0 \tag{6.61}$$

Dealing with each constraint shown in equation 6.61 in order, a closed loop of vectors which includes those which pass through the abutments can be formed which upon rearrangement produces the vector equation shown in equation 6.62; this provides the first three constraints.

$$J_0J_7 = A_0C_1 + C_1E_2 + E_2F_3 + F_3G_4 + G_4H_5 + H_5I_6 + I_6J_7 - A_0J_0 = 0 \tag{6.62}$$

Thus, each component of equation 6.62 provides a constraint which ensures that point J does not translate in the global X, Y or Z directions respectively. The satisfaction of these constraints means that the translation of point I can be similarly described by equation 6.63.

$$I_0I_7 = J_7I_7 - J_0I_0 = 0 \tag{6.63}$$

The above two equations provides the basis for determining the rotations which must take place at each hinge. Since the abutments are now fixed the satisfaction of the third constraint, viz. $A_0A_8=0$, provides the means for determining the simple hinge component of the rotation which takes place at hinge IJ.

$$A_0A_8 = J_7A_8 - J_0A_0 = 0 \tag{6.64}$$

It is necessary to calculate only one component of the vector $A_0A_8=0$ since the other two components are redundant. Two of the three components of the hinge rotation at IJ will be determined, along with the rotations at each other hinge, during the satisfaction of the constraints 6.62 and 6.63. The remaining unknown, viz. $\delta\theta_5$, must be selected so that constraint 6.64 is satisfied.

It should be reiterated that the imposition of a unit virtual vertical displacement at the centroid of the applied load, assumed to be the mid-point of hinge CD, provides a means of determining the rotation of the simple hinge AB, as shown in equation 6.65.

$$\left(\frac{Y_C+Y_D}{2} - Y_A\right).\delta\theta_1 = 1 \tag{6.65}$$

The displacement of the applied load creates the mechanism. The arch, being rigid, must accommodate this displacement by breaking into a number of discrete blocks which, in this idealisation, may only hinge about each other. The arch is free to form any mechanism of the

form shown in figure 6.17 since the position, the amount and the type of rotation at each hinge are variables of the problem.

The formation of the mechanism subject to compatibility is referred to as a kinematically admissible displacement configuration. The constraints of the problem, which ensure kinematic admissibility, can now be shown in equation 6.66 to 6.71 respectively.

$$\begin{aligned}&+\delta\theta_2(Y_{CJ}f_1^{CD}-Z_{CJ}f_2^{CD})\ -\delta\phi_E(Y_{EJ}g_1^{EF}-Z_{EJ}g_2^{EF})\ +\delta\theta_3(Y_{FJ}f_1^{FE}-Z_{FJ}f_2^{FE})\ +\delta\phi_F(Y_{FJ}g_1^{FE}-Z_{FJ}g_2^{FE})\\&\mp\delta\psi_F(Y_{FJ}h_1^{FE}+Z_{FJ}h_2^{FE})\ -\delta\phi_G(Y_{GJ}g_1^{GH}-Z_{GJ}g_2^{GH})-\delta\theta_4(Y_{HJ}f_1^{HG}-Z_{HJ}f_2^{HG})\\&+\delta\phi_H(Y_{HJ}g_1^{HG}-Z_{HJ}g_2^{HG})\mp\delta\psi_H(Y_{HJ}h_1^{HG}+Z_{HJ}h_2^{HG})\ -\delta\phi_I(Y_{IJ}g_1^{IJ}-Z_{IJ}g_2^{IJ})\ =\ \delta\theta_1(Y_{AJ}f_1^{AB}-Z_{AJ}f_2^{AB})\end{aligned}\qquad\textbf{(6.66)}$$

$$\begin{aligned}&+\delta\theta_2(X_{CJ}f_1^{CD}-Z_{CJ}f_3^{CD})\ -\delta\phi_E(X_{EJ}g_1^{EF}+Z_{EJ}g_3^{EF})+\delta\theta_3(X_{FJ}f_1^{FE}-Z_{FJ}f_3^{FE})\ +\delta\phi_F(X_{FJ}g_1^{FE}+Z_{FJ}g_3^{FE})\\&\mp\delta\psi_F(X_{FJ}h_1^{FE}-Z_{FJ}h_3^{FE})-\delta\phi_G(X_{GJ}g_1^{GH}+Z_{GJ}g_3^{GH})-\delta\theta_4(X_{HJ}f_1^{HG}-Z_{HJ}f_3^{HG})\\&+\delta\phi_H(X_{HJ}g_1^{HG}+Z_{HJ}g_3^{HG})\mp\delta\psi_H(X_{HJ}h_1^{HG}-Z_{HJ}h_3^{HG})-\delta\phi_I(X_{IJ}g_1^{IJ}+Z_{IJ}g_3^{IJ})\ =\ \delta\theta_1(X_{AJ}f_1^{AB}-Z_{AJ}f_3^{AB})\end{aligned}\qquad\textbf{(6.67)}$$

$$\begin{aligned}&+\delta\theta_2(X_{CJ}f_2^{CD}-Y_{CJ}f_3^{CD})-\delta\phi_E(X_{EJ}g_2^{EF}+Y_{EJ}g_3^{EF})+\delta\theta_3(X_{FJ}f_2^{FE}-Y_{FJ}f_3^{FE})+\delta\phi_F(X_{FJ}g_2^{FE}+Y_{FJ}g_3^{FE})\\&\pm\delta\psi_F(X_{FJ}h_2^{FE}+Y_{FJ}h_3^{FE})-\delta\phi_G(X_{GJ}g_2^{GH}+Y_{GJ}g_3^{GH})-\delta\theta_4(X_{HJ}f_2^{HG}-Y_{HJ}f_3^{HG})\\&+\delta\phi_H(X_{HJ}g_2^{HG}+Y_{HJ}g_3^{HG})\pm\delta\psi_H(X_{HJ}h_2^{HG}+Y_{HJ}h_3^{HG})-\delta\phi_I(X_{IJ}g_2^{IJ}+Y_{IJ}g_3^{IJ})\ =\ \delta\theta_1(X_{AJ}f_2^{AB}-Y_{AJ}f_3^{AB})\end{aligned}\qquad\textbf{(6.68)}$$

$$\begin{aligned}&+\delta\theta_2f_1^{CD}-\delta\phi_Eg_1^{EF}+\delta\theta_3f_1^{FE}+\delta\phi_Fg_1^{FE}\mp\delta\psi_Fh_1^{FE}-\delta\phi_Gg_1^{GH}-\delta\theta_4f_1^{HG}+\delta\phi_Hg_1^{HG}\\&\qquad\mp\delta\psi_Hh_1^{HG}-\delta\phi_Ig_1^{IJ}+\delta\phi_Jg_1^{JI}\mp\delta\psi_Jh_1^{JI}\ =\ 0\end{aligned}\qquad\textbf{(6.69)}$$

$$\begin{aligned}&+\delta\theta_2f_2^{CD}-\delta\phi_Eg_2^{EF}+\delta\theta_3f_2^{FE}+\delta\phi_Fg_2^{FE}\pm\delta\psi_Fh_2^{FE}-\delta\phi_Gg_2^{GH}-\delta\theta_4f_2^{HG}+\delta\phi_Hg_2^{HG}\\&\qquad\pm\delta\psi_Hh_2^{HG}-\delta\phi_Ig_2^{IJ}+\delta\phi_Jg_2^{JI}\pm\delta\psi_Jh_2^{JI}\ =\ 0\end{aligned}\qquad\textbf{(6.70)}$$

The object of the analysis is to determine the most onerous position of hinges and the set of associated rotations which will enable a mechanism to form at the lowest possible load. This is achieved by defining an objective function through which sets of compatible values of hinge rotations are related to the collapse load. A compatible set of rotations is one which simultaneously satisfies the constraining equations 6.65 to 6.71. The minimum collapse load is determined through the use of linear programming techniques. This is made possible because an assumption of the position of the hinges reduces the constraints and the objective function into a linear form.

Equation 6.71 may be used to obtain the final hinge rotation, $\delta\theta_5$, to completely describe the collapse mechanism because, as explained earlier, it alone is necessary to satisfy equation 6.64.

$$\begin{aligned}\delta\theta_5(X_{JA}f_1^{JI}-Z_{JA}f_3^{JI}) = {} & \delta\theta_2(X_{CA}f_1^{CD}-Z_{CA}f_3^{CD})-\delta\phi_E(X_{EA}g_1^{EF}+Z_{EA}g_3^{EF})+\delta\theta_3(X_{FA}f_1^{FE}-Z_{FA}f_3^{FE}) \\ & +\delta\phi_F(X_{FA}g_1^{FE}+Z_{FA}g_3^{FE})\mp\delta\psi_F(X_{FA}h_1^{FE}-Z_{FA}h_3^{FE})-\delta\phi_G(X_{GA}g_1^{GH}+Z_{GA}g_3^{GH}) \\ & -\delta\theta_4(X_{HA}f_1^{HG}-Z_{HA}f_3^{HG})+\delta\phi_H(X_{HA}g_1^{HG}-Z_{HA}g_3^{HG})\mp\delta\psi_H(X_{HA}h_1^{HG}-Z_{HA}h_3^{HG}) \\ & -\delta\phi_I(X_{IA}g_1^{IJ}+Z_{IA}g_3^{IJ})+\delta\phi_J(X_{JA}g_1^{JI}+Z_{JA}g_3^{JI})\mp\delta\psi_J(X_{JA}h_1^{JI}-Z_{JA}h_3^{JI})\end{aligned} \quad \textbf{(6.71)}$$

The change in potential energy of each block can be determined by treating each four sided block as a pair of triangular blocks that are rigidly connected together. Each triangular block can be described by two vectors **KM** ($= X_{KM}\mathbf{i}+Y_{KM}\mathbf{j}+Z_{KM}\mathbf{k}$) and **KN** ($= X_{KN}\mathbf{i}+Y_{KN}\mathbf{j}+Z_{KN}\mathbf{k}$). The weight of each triangular block is then proportional to its area which can be found using equation 6.72. The vectors were intended to be used to connect the vertices of each block so that admissible movements could be ensured. The above assumption that the vectors define the edges of the blocks is equivalent to replacing the segmental arch by a set of flat plates. This will lead to an underestimation of the collapse load because there is more weight associated with the actual curved members of the arch and, furthermore, the curvature of each actual member would shift its centroid. However, to avoid this added complexity, the above assumption will be adopted.

$$A_{KMN} = \tfrac{1}{2}|\boldsymbol{KM}\wedge\boldsymbol{KN}| = \tfrac{1}{2}|\boldsymbol{KM}|.|\boldsymbol{KN}|.\sin\beta \quad \textbf{(6.72)}$$

The angle between the two vectors, β, can be found by evaluating the dot product of the two vectors as shown in equation 6.73 and then substituting its value back into equation 6.72 to form equation 6.74.

$$\cos\beta = \frac{\boldsymbol{KN}\,.\,\boldsymbol{KM}}{|\boldsymbol{KN}|.|\boldsymbol{KM}|} \quad \textbf{(6.73)}$$

$$A_{KMN} = \tfrac{1}{2}\sqrt{|\boldsymbol{KM}|^2.|\boldsymbol{KN}|^2-(\boldsymbol{KM}.\boldsymbol{KN})^2} \quad \textbf{(6.74)}$$

Thus, the total weight of the triangular block of thickness, t, and unit weight, w, is given by equation 6.75.

$$W_{KMN} = \tfrac{1}{2}w.t.\sqrt{(X_{KM}Y_{KN}-X_{KN}Y_{KM})^2+(X_{KM}Z_{KN}-X_{KN}Z_{KM})^2+(Y_{KM}Z_{KN}-Y_{KN}Z_{KM})^2} \quad \textbf{(6.75)}$$

Initially, if the arch is assumed not to be backfilled so that the only forces which exist are the externally applied knife edge load and the self weight of the arch, the change in potential energy of the system of blocks and external load can be expressed as shown in equation 6.76.

$$P = \tfrac{1}{3}(C_0C_1\underline{k} + D_0D_1\underline{k}).w_{ACD} + \tfrac{1}{3}(D_0D_1\underline{k}).w_{ABD} + \tfrac{1}{3}(C_0C_1\underline{k} + D_0D_1\underline{k} + F_0F_2\underline{k}).w_{CDF}$$
$$+ \tfrac{1}{3}(C_0C_1\underline{k} + E_0E_2\underline{k} + F_0F_2\underline{k}).w_{CEF} + \tfrac{1}{3}(E_0E_3\underline{k} + F_0F_3\underline{k} + H_0H_4\underline{k}).w_{EFH} \quad \textbf{(6.76)}$$
$$+ \tfrac{1}{3}(E_0E_3\underline{k} + G_0G_4\underline{k} + H_0H_4\underline{k}).w_{EGH} + \tfrac{1}{3}(G_0G_5\underline{k} + H_0H_5\underline{k}).w_{GHJ} + \tfrac{1}{3}(G_0G_G\underline{k}).w_{GIJ}$$

The vertical component of each vector, as shown in equation 6.76, can be determined by carrying out repeated substitutions of equation 6.60 in to itself. As already described, equation 6.60 is used to develop a relationship for the movement of each point as it undergoes rotations about each successive hinge. For example, the change in position of point H can be determined as follows.

$$H_0H_4\underline{k} = A_0C_1\underline{k} + C_1F_2\underline{k} + F_2F_3\underline{k} + F_3H_4\underline{k} - A_0H_0\underline{k}$$

In which, successive applications of equation 6.60 enable each term to be determined as follows.

$$A_0C_1\underline{k} = Z_{AC} - \delta\theta_1 Y_{AC}$$
$$C_1F_2\underline{k} = Z_{CF} - \delta\theta_1 Y_{CF} + \delta\theta_2(X_{CF} f_2^{CD} - Y_{CF} f_2^{CD})$$
$$F_2F_3\underline{k} = -\delta\phi_E(X_{EF} g_2^{EF} + Y_{EF} g_3^{EF}) \mp \delta\psi_H(X_{EF} h_2^{EF} + Y_{EF} h_3^{EF})$$
$$F_3H_4\underline{k} = Z_{FH} - \delta\theta_1 Y_{FH} + \delta\theta_2(X_{FH} f_2^{CD} - Y_{FH} f_3^{CD}) - \delta\phi_E(X_{FH} g_2^{EF} + Y_{FH} g_3^{EF}) \mp \delta\psi_E(X_{FH} h_2^{EF} + Y_{FH} h_3^{EF})$$
$$- \delta\theta_3(X_{FH} f_2^{FE} - Y_{FH} f_3^{FE}) + \delta\phi_F(X_{FH} g_2^{FE} + Y_{FH} g_3^{FE}) \mp \delta\psi_F(X_{FH} h_2^{FE} + Y_{FH} Y_{FH} h_3^{FE})$$
$$A_0H_0\underline{k} = Z_{AH}$$

Therefore, upon simplification, equation 6.77 is produced which expresses the change in the vertical position of point H in terms of all possible rotations which may occur at the hinges between point A and point H.

$$H_0H_4\underline{k} = -\delta\theta_1 Y_{AH} + \delta\theta_2(X_{CH} f_2^{CD} - Y_{CH} f_3^{CD}) - \delta\phi_E(X_{EH} g_2^{EF} + Y_{EH} g_3^{EF}) \mp \delta\psi_E(X_{EH} h_2^{EF} + Y_{EH} h_3^{EF}) \quad \textbf{(6.77)}$$
$$- \delta\theta_3(X_{FH} f_2^{FE} - Y_{FH} f_3^{FE}) + \delta\phi_F(X_{FH} g_2^{FE} + Y_{FH} g_3^{FE}) \mp \delta\psi_F(X_{FH} h_2^{FE} + Y_{FH} Y_{FH} h_3^{FE})$$

Similar expressions can be derived for each term in equation 6.76 so that the change in potential energy of the system can be expressed in terms of both the rotations at each hinge and non-linear functions of the hinge coordinates as shown in equation 6.78.

$$P - \xi_1\delta\theta_1 = \xi_2\delta\theta_2 + \xi_3\delta\phi_E \mp \xi_4\delta\psi_E + \xi_5\delta\phi_F \mp \xi_6\delta\psi_F + \xi_7\delta\theta_3 + \xi_8\delta\phi_G \quad \textbf{(6.78)}$$
$$\mp \xi_9\delta\psi_G + \xi_{10}\delta\phi_H \mp \xi_{11}\delta\psi_H + \xi_{12}\delta\theta_4$$

Where the terms in ξ_1 to ξ_{12} inclusive are highly non-linear functions involving the weight of each block, as defined by equation 6.75, and geometrical expressions pertaining to the

orientation and location of the hinges, as shown in the appendix of equation 6.60, and are defined as follows.

$$\xi_1 = -[\ Y_{AC}(w_{ACD}+w_{CDF}+w_{CEF})/3\ +Y_{AD}(w_{ABD}+w_{ACD}+w_{CDF})/3\ +Y_{AE}(w_{CEF}+w_{EFH}+w_{EGH})/3 +Y_{AF}(w_{CDF}+w_{CEF}+w_{EFH})/3\ +Y_{AG}(w_{EGH}+w_{GHJ}+w_{GIJ})/3\ +Y_{AH}(w_{EFH}+w_{EGH}+w_{GHJ})/3 +Y_{AI}w_{GIJ}/3\ +Y_{AJ}(w_{GHJ}+w_{GIJ})/3\ ]$$

$$\xi_2 = [\ (X_{CE}f_2^{CD}-Y_{CE}f_3^{CD}).(w_{CEF}+w_{EFH}+w_{EGH})/3\ +(X_{CF}f_2^{CD}-Y_{CF}f_3^{CD}).(w_{CDF}+w_{CEF}+w_{EFH})/3] +(X_{CG}f_2^{CD}-Y_{CG}f_3^{CD}).(w_{EGH}+w_{GHJ}+w_{GIJ})/3\ +(X_{CH}f_2^{CD}-Y_{CH}f_3^{CD}).(w_{EFH}+w_{EGH}+w_{GHJ})/3 +(X_{CI}f_2^{CD}-Y_{CI}f_3^{CD}).w_{GIJ}/3\ +(X_{CJ}f_2^{CD}-Y_{CJ}f_3^{CD}).(w_{GHJ}+w_{GIJ})/3\ ]$$

$$\xi_3 = -[\ (X_{EF}g_2^{EF}+Y_{EF}g_3^{EF}).w_{EFH}/3\ +(X_{EG}g_2^{EF}+Y_{EG}g_3^{EF}).(w_{EGH}+w_{GHJ}+w_{GIJ})/3] +(X_{EH}g_2^{EF}+Y_{EH}g_3^{EF}).(w_{EFH}+w_{EGH}+w_{GHJ})/3\ +(X_{EI}g_2^{EF}+Y_{EI}g_3^{EF}).w_{GIJ}/3 +(X_{EJ}g_2^{EF}+Y_{EJ}g_3^{EF}).(w_{GHJ}+w_{GIJ})/3\ ]$$

$$\xi_4 = [\ (X_{EF}h_2^{EF}+Y_{EF}h_3^{EF}).w_{EFH}/3\ +(X_{EG}h_2^{EF}+Y_{EG}h_3^{EF}).(w_{EGH}+w_{GHJ}+w_{GIJ})/3] +(X_{EH}h_2^{EF}+Y_{EH}h_3^{EF}).(w_{EFH}+w_{EGH}+w_{GHJ})/3\ +(X_{EI}h_2^{EF}+Y_{EI}h_3^{EF}).w_{GIJ}/3 +(X_{EJ}h_2^{EF}+Y_{EJ}h_3^{EF}).(w_{GHJ}+w_{GIJ})/3\ ]$$

$$\xi_5 = [\ (X_{FE}g_2^{FE}+Y_{FE}g_3^{FE}).(w_{EFH}+w_{EGH})/3\ +(X_{FG}g_2^{FE}+Y_{FG}g_3^{FE}).(w_{EGH}+w_{GHJ}+w_{GIJ})/3] +(X_{FH}g_2^{FE}+Y_{FH}g_3^{FE}).(w_{EFH}+w_{EGH}+w_{GHJ})/3\ +(X_{FI}g_2^{FE}+Y_{FI}g_3^{FE}).w_{GIJ}/3 +(X_{FJ}g_2^{FE}+Y_{FJ}g_3^{FE}).(w_{GHJ}+w_{GIJ})/3\ ]$$

$$\xi_6 = [\ (X_{FE}h_2^{FE}+Y_{FE}h_3^{FE}).(w_{EFH}+w_{EGH})/3\ +(X_{FG}h_2^{FE}+Y_{FG}h_3^{FE}).(w_{EGH}+w_{GHJ}+w_{GIJ})/3] +(X_{FH}h_2^{FE}+Y_{FH}h_3^{FE}).(w_{EFH}+w_{EGH}+w_{GHJ})/3\ +(X_{FI}h_2^{FE}+Y_{FI}h_3^{FE}).w_{GIJ}/3 +(X_{FJ}h_2^{FE}+Y_{FJ}h_3^{FE}).(w_{GHJ}+w_{GIJ})/3\ ]$$

$$\xi_7 = -[\ (X_{EG}f_2^{FE}-Y_{EG}f_3^{FE}).(w_{EGH}+w_{GHJ}+w_{GIJ})/3\ +(X_{FH}f_2^{FE}-Y_{FH}f_3^{FE}).(w_{EFH}+w_{EGH}+w_{GHJ})/3] +(X_{EI}f_2^{FE}-Y_{EI}f_3^{FE}).w_{GIJ}/3\ +(X_{FJ}f_2^{FE}-Y_{FJ}f_3^{FE}).(w_{GHJ}+w_{GIJ})/3\ ]$$

$$\xi_8 = -[\ (X_{GH}g_2^{GH}+Y_{GH}g_3^{GH}).w_{GHJ}/3\ +(X_{GI}g_2^{GH}+Y_{GI}g_3^{GH}).w_{GIJ}/3\ +(X_{GJ}g_2^{GH}+Y_{GJ}g_3^{GH}).(w_{GHJ}+w_{GIJ})/3\ ]$$

$$\xi_9 = [\ (X_{GH}h_2^{GH}+Y_{GH}h_3^{GH}).w_{GHJ}/3\ +(X_{GI}h_2^{GH}+Y_{GI}h_3^{GH}).w_{GIJ}/3\ +(X_{GJ}h_2^{GH}+Y_{GJ}h_3^{GH}).(w_{GHJ}+w_{GIJ})/3\ ]$$

$$\xi_{10} = [\ (X_{HG}g_2^{HG}+Y_{HG}g_3^{HG}).(w_{GHJ}+w_{GIJ})/3\ +(X_{HJ}g_2^{HG}+Y_{HJ}g_3^{HG}).(w_{GHJ}+w_{GIJ})/3 +(X_{HI}g_2^{HG}+Y_{HI}g_3^{HG}).w_{GIJ}/3\ ]$$

$$\xi_{11} = [\ (X_{HG}h_2^{HG}+Y_{HG}h_3^{HG}).(w_{GHJ}+w_{GIJ})/3\ +(X_{HJ}h_2^{HG}+Y_{HJ}h_3^{HG}).(w_{GHJ}+w_{GIJ})/3 +(X_{HI}h_2^{HG}+Y_{HI}h_3^{HG}).w_{GIJ}/3\ ]$$

$$\xi_{12} = [\ (X_{GI}f_2^{HG}-Y_{GI}f_3^{HG}).w_{GIJ}/3\ +(X_{HJ}f_2^{HG}-Y_{HJ}f_3^{HG}).(w_{GHJ}+w_{GIJ})/3\ ]$$

6.6.2.3 Discussion

The rigid block model presented in section 6.6.1 could only accommodate the displacement of the load by forming a mechanism in which a simple hinge occurred at each fracture plane. This type of mechanism was found to be infeasible, the generality of the fracture was then increased. In this model two other forms of relative block movements are permitted, viz. twisting and radial rotations. However, the possibility of shear failures has not been incorporated nor has the shearing associated with torsional hinges.

It was noted in section 6.6.1.3 that, if each block is idealised as being incompressible and infinitely strong, the formation of a simple hinge at the extrados would create a single point of contact between the two adjacent blocks. In the simple hinge model the single point of contact was fixed. The tangent to the extrados at this point is parallel to the line drawn between the two ends of the fracture. Thus, the simple hinge rotation equation was correct. A similar idealisation of the arch in the complex hinge model means that the concurrent formation of a radial hinge would cause the point of contact to migrate towards either end of the fracture. Thereafter, the axis of rotation would remain fixed at this location. Furthermore, the movement of the point of contact would cause each axis of rotation to change. The orientation of the fracture plane determines the amount of radial rotation that is required before the axis is shifted to the end of the fracture plane. These effects were not incorporated because they would have introduced further complications into the analysis and would have required an iterative technique in which changes in the geometry of the arch are taken into account. Instead, a local coordinate system is defined at each end of the fracture plane; one of which is used, the other is disregarded depending on the direction of the radial rotation.

The assumption that radial or torsional hinging take place about fixed axes that pass through the end of the fracture means that the above iterative procedure is not required and the mathematics of the problem can therefore be simplified. The requirement that the blocks undergo complex relative movements was determined by the simple hinge model, see section 6.6. It is suggested that the difference in the required collapse load is small whether it is based on the change in potential energy due to relative block rotations about axes at the end of the fracture or about a set of variable axes that migrate towards that end. The ability of the three-dimensional modelling technique to provide a mathematical description of each relative block movement is, in itself, a significant contribution. However, the modelling technique can be extended to include other forms of relative block movements and to incorporate their contact in a more realistic way.

The assumption that shear failures cannot occur is relaxed in the presence of a torsional hinge. This form of relative block movement must be accompanied by a shearing movement of the two

adjacent surfaces. However, the dilatancy associated with this shearing has not been incorporated into the analysis because, in the development stage, it was necessary that the model was as simple as possible so that it could easily be validated.

These simplifications of the block interface are reasonable, they enable complex hinging requirements to be identified without inhibiting the development of the model. It is also argued that the modelling of rotational movements at the fracture plane in the more exact way described above is unnecessary. The assumption that each block is rigid requires that a variable set of local coordinate axes is required in order to produce an exact description of these movements. In reality the arch is not rigid nor is it infinitely strong so that full length contact is likely to occur even at an extrados hinge. Therefore, the assumption of the position of each rotation axis is valid.

When used in conjunction with the two-dimensional model of section 6.5, this model is a useful assessment tool and will serve to highlight the differences between a skewed arch and a square arch since each model is based on the same assumptions. It should be pointed out that this modelling technique cannot, at present, incorporate the backfill and, as will be shown, it also requies extending to include the dilatancy associated with torsional hinging and shear failures in general.

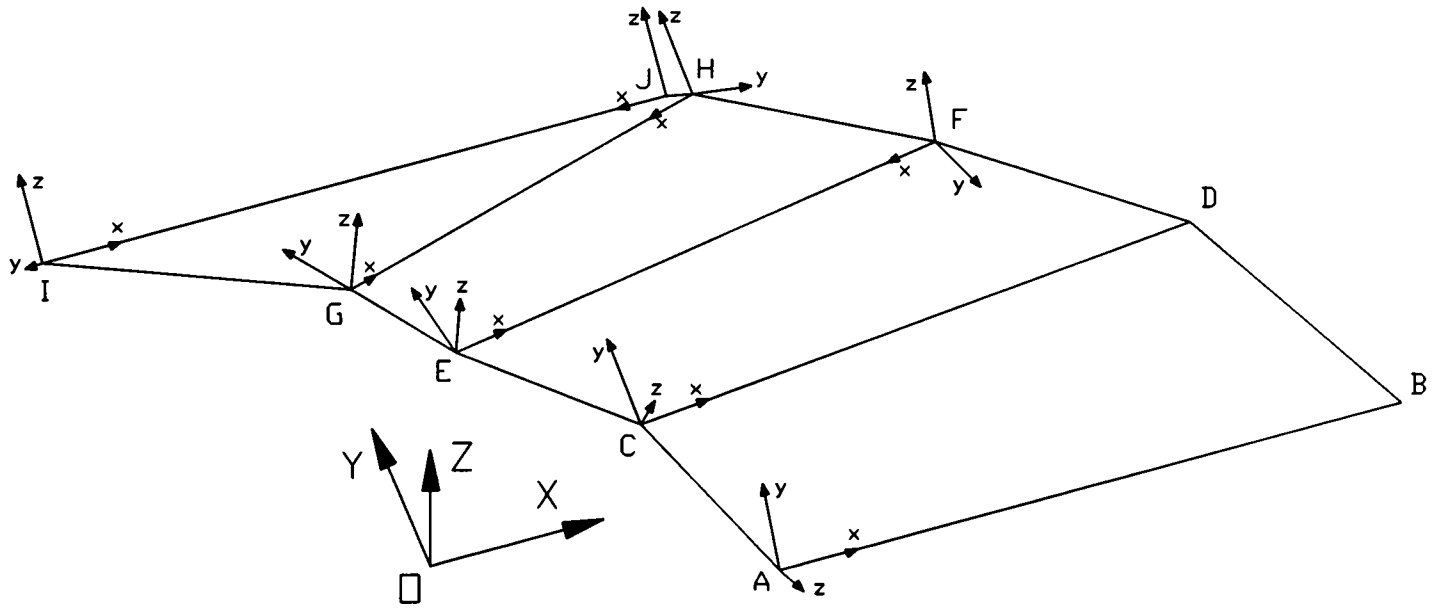

Figure 6.19 AutoCAD drawing of the idealised arch with complex hinges

Use of this vectorial modelling technique will now be demonstrated in the analysis of a 45° skewed voussoir arch whose proportions are similar to those of arch bridge 3-2. It will be assumed that the collapse mechanism of this bridge may be described by the following variables: $X_A=1.500, X_B=5.050, X_C=0.900, X_D=4.150, X_E=0.100, X_F=3.050, X_G=-0.350, X_H=2.000, X_I=-1.672, X_J=1.878$. The coordinates of the ends of each fracture can be determined since $Y=-X$ or $Y=3.55-X$ and $Z=\sqrt{(2.09^2-Y^2)}$ or $Z=\sqrt{(1.875^2-Y^2)}$ depending on whether the

particular point lies on the east or west edge of the arch and whether it lies on the extrados or the intrados.

The validity of the constraining equations was checked by creating a three-dimensional AutoCAD drawing of this skewed arch based on the above coordinates. This drawing is shown in figure 6.19 and the results of the validation are contained within appendix C.2. The validation entailed manually rotating each three-dimensional line in the AutoCAD drawing about each set of local axes in turn. A comparison of the new coordinates of the ends of each line with the new coordinates as predicted by equation 6.60 was then made. Equation 6.60 is based on small deflection theory so that an exact match would not be produced. However, it was found that a close correlation was produced when a 1° rotation was used. In this case the results were equal to three decimal places which is the accuracy of the small deflection theory. It was therefore established that the constraining equations are valid. Figure 6.19 can also be used to view the local coordinate system at either end of each fracture. The local coordinate systems at points E and F are each valid right handed systems. It can be seen that the effects of a clockwise rotation in the system at E would be reproduced by an anticlockwise rotation in the system at F. Therefore, the route taken through the structure, when establishing the constraints, determines the sign of the required hinge rotation.

A non-linear algorithm would be required in order to find the optimum value of the applied load. However, following the two-dimensional work shown in section 6.5 it can be concluded that reasonable estimates of the position of the hinges can be made which, in general, will not yield the minimum collapse load but will enable the constraints of the problem to be reduced to a linear form. The error between this upper bound value and the minimum upper bound value will be small if reasonable hinge positions are assumed. However, re-analyses can be carried out with the location of each fracture line adjusted in an attempt to minimise the calculated collapse load.

The imposition of a unit vertical displacement creates the necessity for a mechanism since the blocks are rigid and are incapable of accommodating this movement in any other way. Equation 6.45 can be solved so that $\delta\theta_1 = 1.33$. The above data representing the assumed position of each hinge can be substituted into constraint 6.66 to 6.70 which reduces them to a linear form. An artificial variable is added to each constraint so that the simplex linear programming tableau can be set up as shown in figure 6.20.

The first block of six rows in figure 6.20 shows the initial simplex linear programming tableau in which the first phase objective function has been introduced. The second block of six rows has been reduced to canonical form by carrying out several Gauss-Jordan transformations. Each subsequent block shows a further iteration of the first phase simplex method. It can be seen that

the value of the objective function is progressively improved with each iteration whilst the embedded identity matrix becomes dispersed throughout the tableau as structural variables replace the artificial variable in the basis.

$\delta\theta_2$	$\delta\phi_E$	$\delta\phi_F$	$\delta\theta_3$	$\delta\psi_F^a$	$\delta\psi_F^b$	$\delta\phi_G$	$\delta\phi_H$	$\delta\theta_4$	$\delta\psi_H^a$	$\delta\psi_H^b$	$\delta\phi_I$	$\delta\phi_J$	$\delta\psi_J^a$	$\delta\psi_J^b$	a_1	a_2	a_3	a_4	a_5	rhs
-0.149	-1.740	1.275	0.085	-0.216	0.216	-1.464	0.188	-0.036	-0.008	0.008					1.000					0.000
-0.664	-1.795	-1.148	0.567	-0.197	0.197	-2.253	-0.109	-0.157	-0.008	0.008	-2.130					1.000				0.172
2.470	0.139	-0.268	-1.382	0.875	-0.875	-0.352	-0.065	0.159	0.013	-0.013	-2.840						1.000			4.229
-0.035	-0.998	0.965	-0.022	0.261	-0.261	-0.959	0.721	0.242	0.650	-0.650	-0.600	0.600	0.800	-0.800				1.000		0.000
-0.092	0.047	0.260	0.199	-0.945	0.945	-0.244	0.678	-0.441	-0.588	0.588	-0.800	0.800	-0.600	0.600					1.000	0.000
0.000	0.000	0.000	0.000	0.000	0.000	0.000	0.000	0.000	0.000	0.000	0.000	0.000	0.000	0.000	1.000	1.000	1.000	1.000	1.000	0.000
-0.149	-1.740	1.275	0.085	-0.216	0.216	-1.464	0.188	-0.036	-0.008	0.008					1.000					0.000
-0.664	-1.795	-1.148	0.567	-0.197	0.197	-2.253	-0.109	-0.157	-0.008	0.008	-2.130					1.000				0.172
2.470	0.139	-0.268	-1.382	0.875	-0.875	-0.352	-0.065	0.159	0.013	-0.013	-2.840						1.000			4.229
-0.035	-0.998	0.965	-0.022	0.261	-0.261	-0.959	0.721	0.242	0.650	-0.650	-0.600	0.600	0.800	-0.800				1.000		0.000
-0.092	0.047	0.260	0.199	-0.945	0.945	-0.244	0.678	-0.441	-0.588	0.588	-0.800	0.800	-0.600	0.600					1.000	0.000
-1.529	4.347	-1.084	0.552	0.221	-0.221	5.272	-1.413	0.233	-0.059	0.059	6.370	-1.400	-0.200	0.200						-4.401
	-1.732	1.259	0.001	-0.163	0.163	-1.486	0.184	-0.026	-0.007	0.007	-0.172				1.000		0.060			0.256
	-1.757	-1.221	0.196	0.038	-0.038	-2.348	-0.127	-0.115	-0.004	0.004	-2.893					1.000	0.269			1.309
1.000	0.056	-0.109	-0.559	0.354	-0.354	-0.142	-0.026	0.064	0.005	-0.005	-1.150						0.405			1.713
	-0.996	0.961	-0.041	0.274	-0.274	-0.964	0.720	0.244	0.650	-0.650	-0.641	0.600	0.800	-0.800			0.014	1.000		0.061
	0.052	0.250	0.148	-0.912	0.912	-0.257	0.676	-0.435	-0.587	0.587	-0.906	0.800	-0.600	0.600			0.037		1.000	0.157
	4.433	-1.250	-0.304	0.763	-0.763	5.054	-1.453	0.332	-0.051	0.051	4.611	-1.400	-0.200	0.200			0.619			-1.782
	-1.476	1.013	0.012	-0.233	0.233	-1.239		-0.089	-0.173	0.173	-0.007	-0.154	-0.205	0.205	1.000		0.057	-0.256		0.240
	-1.933	-1.051	0.189	0.087	-0.087	-2.518		-0.072	0.110	-0.110	-3.006	0.106	0.141	-0.141		1.000	0.271	0.176		1.320
1.000	0.020	-0.073	-0.561	0.364	-0.364	-0.178		0.073	0.029	-0.029	-1.173	0.022	0.029	-0.029			0.405	0.037		1.715
	-1.385	1.336	-0.058	0.381	-0.381	-1.340	1.000	0.340	0.903	-0.903	-0.890	0.834	1.112	-1.112			0.020	1.390		0.084
	0.988	-0.652	0.187	-1.169	1.169	0.649		-0.665	-1.197	1.197	-0.304	0.237	-1.351	1.351			0.024	-0.939	1.000	0.100
	2.421	0.691	-0.387	1.316	-1.316	3.108		0.825	1.261	-1.261	3.318	-0.189	1.415	-1.415			0.648	2.019		-1.660
	-1.626	1.111	-0.016	-0.056	0.056	-1.337		0.012	0.008	-0.008	0.039	-0.190			1.000		0.053	-0.114	-0.152	0.225
	-1.830	-1.119	0.208	-0.035	0.035	-2.450		-0.141	-0.015	0.015	-3.038	0.130				1.000	0.274	0.078	0.104	1.330
1.000	0.041	-0.087	-0.557	0.339	-0.339	-0.164		0.059	0.003	-0.003	-1.180	0.027					0.406	0.016	0.022	1.717
	-0.572	0.799	0.096	-0.581	0.581	-0.806	1.000	-0.207	-0.082	0.082	-1.140	1.028					0.039	0.617	0.823	0.167
	0.731	-0.483	0.138	-0.865	0.865	0.480		-0.492	-0.886	0.886	-0.225	0.175	-1.000	1.000			0.018	-0.695	0.740	0.074
	3.456	0.008	-0.192	0.091	-0.091	3.787		0.129	0.007	-0.007	2.999	0.059					0.673	1.036	1.047	-1.555
	-1.540	1.054		-0.159	0.159	-1.280		-0.046	-0.097	0.097	0.012	-0.169	-0.118	0.118	1.000		0.055	-0.196	-0.064	0.234
	-2.929	-0.393		1.267	-1.267	-3.172		0.599	1.318	-1.318	-2.700	-0.133	1.504	-1.504		1.000	0.247	1.124	-1.009	1.218
1.000	2.986	-2.032		-3.147	3.147	1.770		-1.923	-3.567	3.567	-2.086	0.732	-4.028	4.028			0.477	-2.783	3.003	2.016
	-1.080	1.134		0.020	-0.020	-1.140	1.000	0.134	0.534	-0.534	-0.984	0.907	0.695	-0.695			0.027	1.100	0.309	0.115
	5.287	-3.491	1.000	-6.259	6.259	3.472		-3.559	-6.410	6.410	-1.627	1.266	-7.232	7.232			0.127	-5.026	5.353	0.537
	4.469	-0.661		-1.108	1.108	4.452		-0.553	-1.222	1.222	2.688	0.302	-1.386	1.386			0.697	0.072	2.073	-1.452
	-1.724	1.248		-0.155	0.155	-1.474	0.170	-0.023	-0.006	0.006	-0.156	-0.014			1.000		0.060	-0.009	-0.011	0.253
	-0.591	-2.850		1.224	-1.224	-0.705	-2.166	0.308	0.163	-0.163	-0.568	-2.097				1.000	0.188	-1.258	-1.677	0.969
1.000	-3.275	4.546		-3.032	3.032	-4.837	5.798	-1.143	-0.473	0.473	-7.793	5.990					0.635	3.594	4.792	2.684
	-1.554	1.633		0.029	-0.029	-1.640	1.439	0.194	0.768	-0.768	-1.417	1.305	1.000	-1.000			0.039	1.583	0.444	0.166
	-5.954	8.319	1.000	-6.053	6.053	-8.391	10.411	-2.159	-0.855	0.855	-11.873	10.706					0.411	6.424	8.565	1.737
	2.315	1.602		-1.069	1.069	2.179	1.995	-0.285	-0.157	0.157	0.724	2.111					0.752	2.267	2.689	-1.222
	-1.799	0.886				-1.564	-0.104	0.016	0.015	-0.015	-0.228	-0.280			1.000	0.127	0.084	-0.168	-0.224	0.376
	-0.483	-2.329		1.000	-1.000	-0.576	-1.770	0.252	0.133	-0.133	-0.464	-1.713				0.817	0.154	-1.028	-1.371	0.792
1.000	-4.740	-2.515				-6.583	0.433	-0.380	-0.069	0.069	-9.201	0.795				2.478	1.101	0.477	0.636	5.085
	-1.541	1.699				-1.624	1.490	0.186	0.764	-0.764	-1.403	1.354	1.000	-1.000		-0.023	0.035	1.612	0.483	0.143
	-8.878	-5.776	1.000			-11.876	-0.300	-0.635	-0.049	0.049	-14.684	0.336				4.946	1.342	0.202	0.269	6.528
	1.799	-0.886				1.564	0.104	-0.016	-0.015	0.015	0.228	0.280				0.873	0.916	1.168	1.224	-0.376
	-0.995					-0.717	-0.881	-0.081	-0.384	0.384	0.504	-0.986	-0.522	0.522	1.000	0.139	0.066	-1.009	-0.476	0.301
	-2.594			1.000	-1.000	-2.801	0.272	0.507	1.180	-1.180	-2.388	0.142	1.370	-1.370		0.785	0.202	1.182	-0.708	0.988
1.000	-7.019					-8.986	2.638	-0.104	1.062	-1.062	-11.278	2.799	1.480	-1.480		2.443	1.153	2.863	1.351	5.297
	-0.907	1.000				-0.956	0.877	0.110	0.450	-0.450	-0.826	0.797	0.588	-0.588		-0.014	0.021	0.949	0.284	0.084
	-14.114		1.000			-17.396	4.764	-0.001	2.549	-2.549	-19.454	4.939	3.399	-3.399		4.867	1.461	5.682	1.911	7.016
	0.995					0.717	0.881	0.081	0.384	-0.384	-0.504	0.986	0.522	-0.522		0.861	0.934	2.009	1.476	-0.301
	-1.908					-1.374	-1.690	-0.156	-0.736	0.736	0.967	-1.891	-1.000	1.000	1.917	0.266	0.126	-1.935	-0.913	0.578
	-5.209			1.000	-1.000	-4.684	-2.043	0.293	0.172	-0.172	-1.063	-2.450			2.627	1.150	0.374	-1.470	-1.960	1.780
1.000	-9.844					-11.020	0.137	-0.335	-0.027	0.027	-9.847	0.000			2.838	2.838	1.339	0.000	0.000	6.152
	-2.030	1.000				-1.764	-0.118	0.018	0.017	-0.017	-0.257	-0.316			1.128	0.143	0.095	-0.190	-0.253	0.424
	-20.601		1.000			-22.067	-0.980	-0.532	0.048	-0.048	-16.168	-1.490			6.517	5.773	1.888	-0.894	-1.192	8.979
															1.000	1.000	1.000	1.000	1.000	0.000

Figure 6.20 Each first phase simplex LP tableau for the complex hinge model

The final first phase LP tableau, shown in figure 6.20, produced a basic feasible solution, i.e. an objective function whose value is zero and whose structural variable coefficients are also zero. Furthermore, none of the artificial variables remained in the basis. Thus, several further conclusions can be made at this stage which include:

7. The three-dimensional collapse mechanism of a skewed arch can be successfully analysed if modelled as described in section 6.6.2 of this thesis.

8. The analysis was successful; an admissible collapse mechanism was found. This was identified by the presence of the basic feasible solution at the end of the first phase of the analysis.

9. As shown in the final LP tableau in figure 6.20, a feasible collapse mechanism of a skewed arch can be formed by four fractures provided that simple hinging is not the only form of relative block movement. In this model radial and torsional hinging was also required. The basic feasible solution of this example problem represents a mechanism described by a set of variables all of which have zero value except for $\delta\theta_1=1.33$, $\delta\theta_2=6.15$, $\delta\theta_3=8.98$, $\delta\phi_F=0.42$, $\delta\psi_F^a=1.78$, $\delta\theta_5=4.07$, and $\delta\psi_J^b=0.578$.

10. The requirement for the collapse mechanism to comprise complex hinges would result in full-depth tension and localised regions of high compression. These phenomena were observed in each 3.0 m span skewed arch and more prominently in the 1.2 m span arches, all of which are documented in chapter 5.

11. The collapse mechanism may comprise four simple hinges at either four or five fracture planes but must also include additional relative block movements to make it admissible. The type of additional, complex, rotations described by the basic feasible solution of this problem may occur at other fracture planes, i.e. any combination of non-zero values of $\delta\phi_F$, $\delta\psi_F^a$, $\delta\psi_F^b$, $\delta\phi_H$, $\delta\psi_H^a$, $\delta\psi_H^b$, $\delta\phi_J$, $\delta\psi_J^a$, or $\delta\psi_J^b$ may also produce an admissible mechanism.

12. The failure of the simple hinge model to obtain an admissible mechanism was not surprising. It could have been incorrectly concluded, from visual observations of the crack pattern within the intrados of skewed arch bridges 3-1, 3-3 and 3-4, that the fifth fracture plane was due to a simple hinge at the extrados of the arch. However, the observed crack in the extrados of skewed arch 3-2 confirms the predictions of these mathematical models, i.e. the necessity for radial or torsional hinging at the fifth fracture.

The second phase of the simplex method begins with the removal of the artificial variables since these have served their purpose in enabling a basic feasible solution to be obtained. The actual objective function, equation 6.78, can then be introduced into the LP tableau as shown in the first block of six rows in figure 6.21.

$\delta\theta_2$	$\delta\phi_E$	$\delta\phi_F$	$\delta\theta_3$	$\delta\psi_F^a$	$\delta\psi_F^b$	$\delta\phi_G$	$\delta\phi_H$	$\delta\theta_4$	$\delta\psi_H^a$	$\delta\psi_H^b$	$\delta\phi_I$	$\delta\phi_J$	$\delta\psi_J^a$	$\delta\psi_J^b$	rhs
	-1.908					-1.374	-1.690	-0.156	-0.736	0.736	0.967	-1.891	-1.000	1.000	0.578
	-5.209			1.000	-1.000	-4.684	-2.043	0.293	0.172	-0.172	-1.063	-2.450			1.780
1.000	-9.844					-11.020	0.137	-0.335	-0.027	0.027	-9.847	0.000			6.152
	-2.030	1.000				-1.764	-0.118	0.018	0.017	-0.017	-0.257	-0.316			0.424
	-20.601		1.000			-22.067	-0.980	-0.532	0.048	-0.048	-16.17	-1.490			8.979
61.15	1.735	-16.98	-25.64	60.58	-60.58	0.341	-19.99	8.434	19.028	-19.03					
	-1.908					-1.374	-1.690	-0.156	-0.736	0.736	0.967	-1.891	-1.000	1.000	0.578
	-5.209			1.000	-1.000	-4.684	-2.043	0.293	0.172	-0.172	-1.063	-2.450			1.780
1.000	-9.844					-11.020	0.137	-0.335	-0.027	0.027	-9.847	0.000			6.152
	-2.030	1.000				-1.764	-0.118	0.018	0.017	-0.017	-0.257	-0.316			0.424
	-20.601		1.000			-22.067	-0.980	-0.532	0.048	-0.048	-16.17	-1.490			8.979
	356.58					362.24	68.302	-2.178	11.77	-11.77	247.65	104.81			-246.6
	-2.594					-1.868	-2.297	-0.212	-1.000	1.000	1.314	-2.571	-1.359	1.359	0.785
	-5.656			1.000	-1.000	-5.006	-2.439	0.257			-0.837	-2.892	-0.234	0.234	1.915
1.000	-9.773					-10.97	0.199	-0.329			-9.883	0.070	0.037	-0.037	6.131
	-2.073	1.000				-1.796	-0.156	0.014			-0.235	-0.359	-0.023	0.023	0.438
	-20.73		1.000			-22.16	-1.090	-0.542			-16.11	-1.614	-0.065	0.065	9.017
	326.05					340.3	41.268	-4.675			263.11	74.546	-16.00	16.00	-237.3
36.930	-363.5					-407.0	5.058	-12.37	-1.000	1.000	-363.7	0.000			227.2
6.359	-67.81			1.000	-1.000	-74.8	-1.172	-1.837			-63.68	-2.450			40.899
27.172	-265.6					-298.1	5.411	-8.945			-268.5	1.891	1.000	-1.000	166.6
0.620	-8.129	1.000				-8.593	-0.033	-0.190			-6.359	-0.316			4.236
1.776	-38.09		1.000			-41.64	-0.736	-1.126			-33.66	-1.490			19.907
434.71	-3922.6					-4428	127.8	-147.8			-4033	104.8			2427.7

Figure 6.21 Each second phase simplex LP tableau for the complex hinge model

The transformation of the LP tableau into canonical form, as shown in the second iteration in figure 6.21, resulted in the value of the objective function becoming -246.6 kN. This value corresponds to the basic feasible solution but is not the value of the collapse load associated with this mechanism. The collapse load can be obtained by incorporating the additional work associated with the formation of the simple hinge at the south abutment, i.e. rotation $\delta\theta_1$, and correcting the sign of the value of the objective function since the negative sign is not important except that it indicates that a minimisation process was carried out. The collapse load associated with the mechanism described by the basic feasible solution is therefore 117.3 kN.

The third iteration of the second phase tableau produced an improvement in the value of the objective function in which the mechanism was essentially of the same form as the previous one except that a torsional hinge, $\delta\psi_H^b$, occurred at the fifth fracture plane rather than at point J on the north abutment. The collapse mechanism was thereby described by the following variables, $\delta\theta_1=1.33$, $\delta\theta_2=6.13$, $\delta\theta_3=9.02$, $\delta\phi_F=0.44$, $\delta\psi_F^a=1.92$, $\delta\theta_5=4.04$, and $\delta\psi_H^b=0.79$. However, further improvements were not possible. The next iteration distorted the tableau since the torsional hinge at J, $\delta\psi_J^a$, was required to reenter the basis in order to improve the objective function. After this iteration the value of the objective function became 2427.7 kN and the corresponding collapse load was -2556.9 kN. Further iterations were not possible since the

outcome of this one was that the problem is unbounded. Unboundedness is indicated by the presence of negative coefficients throughout the column of entries in the tableau of the variable which is next required to enter the basis, in this case, $\delta\phi_G$.

Some additional conclusions can be made following the termination of the second phase of the simplex method. These are as follows:

13. In its present form, the "augmented" model is unable to produce the minimum collapse load. This is because the problem is unbounded. This is not surprising, the physical interpretation of this unbounded situation is that the ability of two consecutive fracture planes to permit simple, radial and torsional hinging results in a ball-and-socket type joint at either edge of one of the rigid blocks. This enables the block to undergo torsional rotations ad infinitum.

14. In Livesley's (1992b) three dimensional work he remarked that the overall modelling process must generate a tractable computational problem. As it stands, this complex hinge "augmented" model violates this. However, the model is easily corrected, one possible way of doing this is by removing all but one of the possible torsional hinges.

Figure 6.22 shows each second phase LP tableau for the analysis of the "reduced" model of the arch shown in figure 6.19 in which only a single full ball-and-socket type joint, at point F, was permitted.

$\delta\theta_2$	$\delta\phi_E$	$\delta\phi_F$	$\delta\theta_3$	$\delta\psi_F^a$	$\delta\psi_F^b$	$\delta\phi_G$	$\delta\phi_H$	$\delta\theta_4$	$\delta\phi_I$	$\delta\phi_J$	rhs
	-1.974					-1.422	-2.271	-0.162	1.000	-1.957	0.598
	-7.308			1.000	-1.000	-6.195	-4.349	0.122		-4.529	2.415
1.000	-29.28					-25.02	-22.181	-1.925		-19.27	12.04
	-2.537	1.000				-2.130	-0.897	-0.024		-0.819	0.578
	-52.52		1.000			-45.054	-37.57	-3.142		-33.13	18.64
61.15	1.736	-16.98	-25.64	60.58	-60.58	0.341	-19.99	8.434			
	-1.974					-1.422	-2.271	-0.162	1.000	-1.957	0.598
	-7.308			1.000	-1.000	-6.195	-4.349	0.122		-4.529	2.415
1.000	-29.28					-25.02	-22.181	-1.925		-19.27	12.04
	-2.537	1.000				-2.130	-0.897	-0.024		-0.819	0.578
	-52.52		1.000			-45.054	-37.57	-3.142		-33.13	18.64
	845.5					714.3	621.4	37.81		589.4	-394.6

Figure 6.22 The second phase simplex LP tableau for the "reduced" model

The second phase of the analysis was successful. It determined that the optimum value of the objective function was -394.6 kN. This corresponds to a collapse load of 265.3 kN when the effects of the rotation $\delta\theta_1$ have been incorporated. The mechanism is described by the following variables: $\delta\theta_1=1.33$, $\delta\theta_2=12.04$, $\delta\theta_3=18.64$, $\delta\phi_F=0.58$, $\delta\psi_F{}^a=2.42$, $\delta\phi_I=0.60$, and $\delta\theta_5=8.08$.

It can be seen that this "reduced" model, in which torsional hinging was restricted to the fracture plane at EF, predicted the formation of a radial hinge at point I. This type of behaviour is not "realistic" since it does not conform to visual observations of the destructive load tests (documented in chapter 5). It can therefore be concluded that the reduced model is too restrictive; it does not permit the occurrence of a sufficient number of admissible deformed configurations. Thus, it is unable to select a realistic optimum set. The mechanism that was predicted for the arch shown in figure 6.19 was admissible and the collapse load was optimised. However, if the "reduced" model had been capable of predicting a realistic mechanism the associated collapse load would have been smaller.

In contrast, the "augmented" model, i.e the one in which torsional hinging was permitted at the fracture planes of EF, GH and IJ, predicted a "realistic" collapse mechanism. However, in this model the collapse load could not be optimised. The presence of several fracture planes that permit torsional rotations is not, in itself, responsible for the unboundedness of the mathematical model. This is because the fracture planes are not parallel to each other. It appears that at more than one torsional rotation is required to produce an admissible mechanism which may be satisfactory provided that some of the model's radial hinging ability is removed.

The surprising prediction of the "reduced" model that a radial hinge at point I must occur in order for the mechanism to be admissible is a result of this model being too constrained. This model possessed the appropriate rotational variables to enable a realistic mechanism to be predicted. However, it is likely that rotational movements must be accompanied by shear failures in order to maintain compatibility. Since the model cannot, at present, incorporate shear failures it could not predict a realistic mechanism and did not have a sufficiently large set of other admissible mechanisms to enable it to predict a reasonable alternative.

The validity of the above arguments can be established by examining the last "realistic" solution of the complex hinge model as shown in figure 6.21. For the assumed location of each fracture, as defined in figure 6.19, this model predicted a collapse load of 117.3 kN. Furthermore, the fact that this was not the optimum solution indicates that the actual minimum required collapse load would be lower than this value. In contrast, the "unrealistic" optimum solution of the "reduced" model was that the minimum collapse load was 265.3 kN. The difference can only be attributed to the inability of this model to produce a realistic admissible mechanism.

Further illustration of this can be found in the results of the parametric study shown in figures 6.23 and 6.24. The collapse load, as predicted by the "reduced" model, was investigated by adjusting the orientation of the fracture at CD and the location of the fracture at EF. In order that the results were comparable, the location of the mid-point of hinge CD (the point of application of the load) was fixed at the quarter span of the bridge.

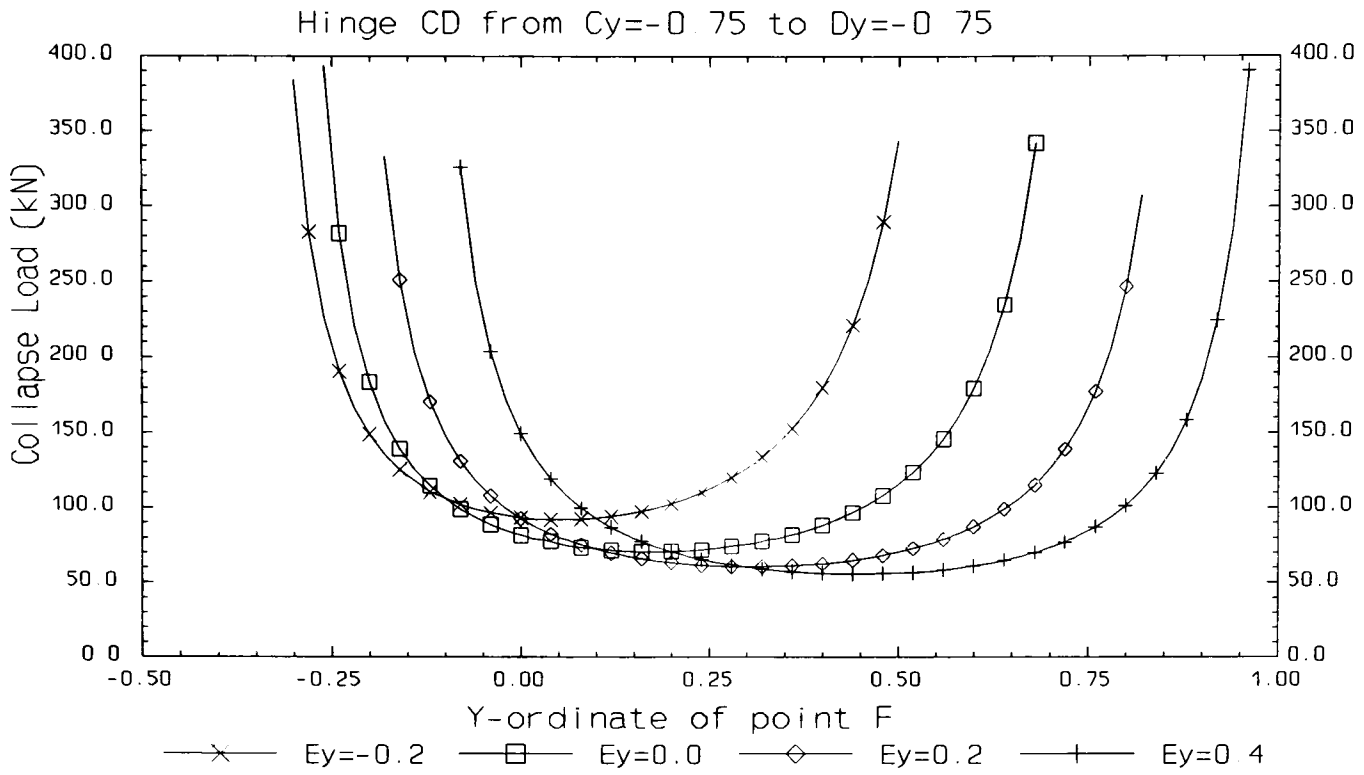

Figure 6.23 Predicted capacity of a 3.0 m span skewed arch

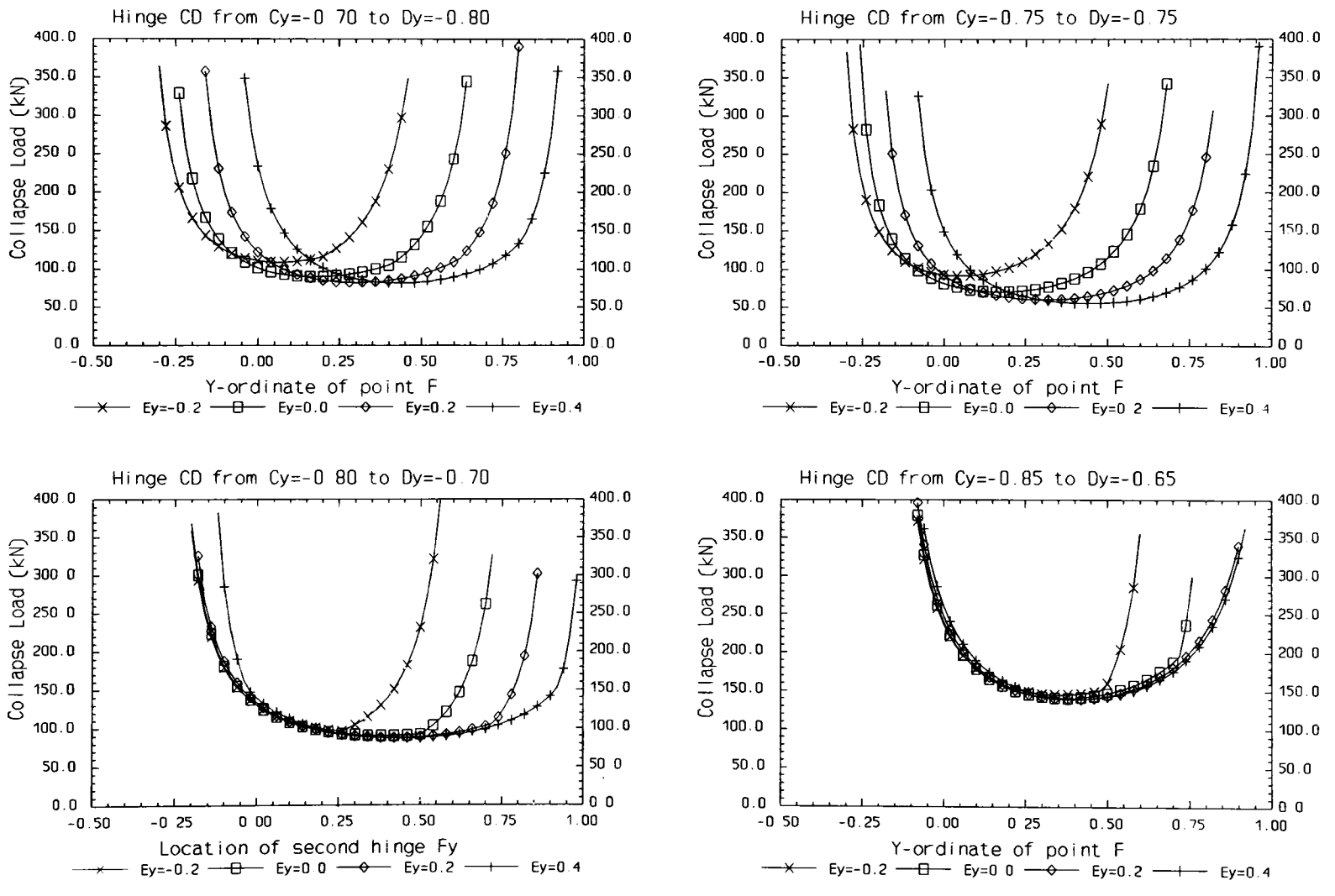

Figure 6.24 Predicted collapse load versus location of fracture planes

A general observation of the analyses was that each predicted collapse mechanism involved four simple hinges, $\delta\theta_1$, $\delta\theta_2$, $\delta\theta_3$ and $\delta\theta_5$, and three other forms of relative block movements. It was found that as the orientation of fracture EF was varied, the magnitude of the required torsional or radial hinges reduced so that, for instance, a radial hinge at F was eventually replaced by a

radial hinge at E and a clockwise torsional hinge eventually became an anticlockwise hinge. The location of the other radial hinges varied in order to accommodate this.

As can be seen in figure 6.23, the minimum collapse load was approximately 55.4 kN which was associated with a mechanism in which five fractures occurred. Three of these, viz. AB, CD, and IJ, were parallel to the abutments. The fracture at EF was inclined to the abutments by a small amount and the fifth fracture line was inclined to the abutments by a large amount. Figure 6.25 contains the final second phase LP tableau for the arch in which its fracture planes coincide with those described above and which correspond to the minimum point in figure 6.23. Each constraint in the LP tableau was active; the mechanism was therefore three-dimensional and comprised the following rotations: $\delta\theta_1=1.333$, $\delta\theta_2=5.022$, $\delta\theta_3=6.491$, $\delta\theta_5=2.803$, $\delta\phi_E=0.001$, $\delta\psi_F^a=0.095$, $\delta\phi_H=0.000$. The solution was unrealistic. If the rotation, $\delta\phi_E$, had occurred in the bridges tested as part of this research, compressive failures would have occurred in the vicinity of point E rather than in the vicinity of point F. However, this rotation was small as was the torsional hinge rotation at F, $\delta\psi_F^a$.

$\delta\theta_2$	$\delta\phi_E$	$\delta\phi_F$	$\delta\theta_3$	$\delta\psi_F^a$	$\delta\psi_F^b$	$\delta\phi_G$	$\delta\phi_H$	$\delta\theta_4$	$\delta\phi_I$	$\delta\phi_J$	rhs
		-16.640	1.000		0.000	-7.119		-0.702	-13.815	0.040	6.491
		-0.245		1.000	-1.000	-0.079		0.293	-0.185	-0.017	0.095
1.000		-8.712			0.000	-4.081		-0.512	-8.153	0.029	5.022
	1.000	-0.971			0.000	0.603		-0.057	-0.006	0.003	0.001
		0.042			0.000	-0.450	1.000	0.092	-0.993	0.993	0.000
		220.095			0.000	115.963		3.473	237.102	12.357	-184.89

Figure 6.25 The final second phase LP tableau for the set of fracture planes which produce the minimum possible collapse load

Despite a fifth fracture plane having been predicted, the value of the radial hinge at point H was zero. In other words, the model predicted the occurrence of four fracture planes each of which were parallel or only inclined by a small amount to the abutments. Furthermore, the magnitude of the required three-dimensional rotations was small; the mechanism was essentially two-dimensional. It is therefore, not surprising to find that the predicted simple hinge rotations and the associated collapse load for this set of fracture planes were almost identical to the predictions of the two-dimensional model discussed in section 6.5.3 when it was used to analyse a similarly proportioned square span arch. This close correlation provides further evidence of the validity of this three-dimensional model.

The fact that this "reduced" model could not predict a realistic three-dimensional collapse mechanism is, as already discussed, a product of its too restrictive modelling of the general fracture plane. Thus, it is not surprising that the minimum collapse load that it predicted was similar to that which was predicted by a two-dimensional analysis of an equivalent square span

structure. It has also been shown that a less restrictive model could predict a realistic three-dimensional mechanism that is associated with a smaller collapse load than a two-dimensional mechanism. Although this model was not restrictive enough, it did serve to provide bounds within which a more successful fracture plane model will lie. The search for this model is beyond the scope of this thesis. However, its existence is assured, the experimental evidence documented in chapter 5 indicates that a skewed arch is weaker than a square arch and this is attributable to the formation of a three-dimensional mechanism, idealised in figure 6.17. Furthermore, the three-dimensional mathematical model presented here will enable this search to be undertaken with relative ease.

In conclusion, the following investigatory work is seen as necessary in order to produce a "realistic" model so that the method becomes more useable.

15. In accordance with the normality rule, the shear failure that will coincide with a torsional hinge rotation must be incorporated into the model as a prerequisite part of its development.

16. The possibility of general shear failures may be included by enabling adjacent blocks to translate along the local x-axis and z-axis. These movements must be resisted by accompanying them with dilatant movements in the direction of the local y-axis. Some difficulty will be encountered here because the dilatant movement is proportional to the resultant shearing movement which cannot be put into an adequate linear form.

17. The complex hinge model provides the necessary mathematical description of relative block rotations. However, it has been found that it cannot provide an adequate description of the deformation of the entire structure if more than one fracture plane is modelled with it. A modified form of this model is required at the remaining fracture planes. It appears logical that a successful model would permit torsional movements at only two of its fracture planes. The most likely locations of these torsional movements would be any two fracture planes from EF, GH or IJ. However, the radial hinging ability of each of these fracture planes should be removed either individually or collectively in successive attempts to determine an appropriately "reduced" model. Thus, the investigation to determine which model can accurately reproduce observed bridge test behaviour would require several iterations before it reaches a successful conclusion.

18. Backfill can be incorporated as an additional weight so that it is included in the change in potential energy of the deformation of the structure and thus, affects the magnitude of the applied load. It can also be included, in the same way as it was in the two-

dimensional model, so that it subjects the arch to a horizontal passive pressure as well as providing a medium through which the applied load is dispersed.

19. The visual observations of the collapse mechanism of skewed arch 3-3 revealed that a system of hinge-like cracks occurred within its spandrel walls. It is not unreasonable to assume that these walls could not be included in the mathematical model at a later date. The single point of contact between the walls and the arch would enable the deformation of each to be compatible with the other. Furthermore, the effects of the end restraints to these walls could be investigated because if the walls cannot deform, neither can the arch. However, care would be needed to ensure that the model does not predict unrealistic collapse mechanisms. If the spandrel walls are so massive that they cannot deform, spandrel wall detachment may occur due to a shear failure between the arch and the spandrel walls. Alternatively, other forms of three-dimensional mechanisms would ensue so that the spandrel walls could be omitted from the mechanism. Thus, the inclusion of spandrel walls is possible but must form part of the future development of the model since a more sophisticated analysis will be required.

20. The assumption, in the present model, that a simple hinge must occur at the fracture at AB enabled the deformation of the arch to be adequately described by only five constraints. A further two rigid block movements were necessary to complete the mechanism, viz. the simple hinge component of movement at each abutment. The inclusion of a more general type of fracture plane at AB would result in further constraints to ensure that the south abutment was not required to move in order to create an admissible mechanism.

7.0 Finite element analysis of the brickwork arch

7.1 Introduction

The proposed finite element model of the brickwork arch, presented within this thesis, was developed using one of the most advanced commercially available finite element analysis (FEA) packages (ANSYS v.5.1 58, 1995). It was undertaken to provide an alternative analytical technique to the one proposed in chapter 6 but with the additional ability of incorporating separable brickwork rings. Furthermore, it was anticipated that this model could be more readily extended to incorporate other phenomena such as detachable spandrel walls and the effects of attempted repairs.

The multi-ring brickwork arch is a complex structure. Its exact analysis is beyond the scope of the mechanism method which can only analyse an idealised form of the arch at its ultimate limit state. Conversely, this means that it can therefore produce an assessment of the collapse load relatively quickly and is therefore inexpensive. However, it achieves this by making several assumptions regarding the behaviour of the structure either at its ultimate limit state or leading up to it. For instance, it is usually assumed that the arch is very stiff, or even rigid. This enables a mathematical description of its deformation during the formation of the collapse mechanism to be formulated based on its initial geometry. The collapse load that is predicted by the mechanism method is dependent upon this mathematical description because the more general it is, the more accurate the prediction becomes.

A phenomenon that was observed as part of the load carrying behaviour of each model arch bridge documented in chapter 5, whether square or skewed, was ring separation. This phenomenon has a pronounced effect upon the behaviour of an arch bridge; it increases its flexibility and, more significantly, it reduces its load carrying capacity. Thus, it is a fundamental aspect of the behaviour of multi-ring brickwork arch bridges. Therefore, an important part of this research must be to develop a theoretical model that can incorporate the effects of the progressive breakdown of composite action as ring separation propagates through the structure.

The requirement for a theoretical model that can predict the occurrence of ring separation and analyse its effects is a prerequisite part of the development of arch theory. Thus, in itself, this would be a significant contribution regardless of the fact that the model had been extended to incorporate other effects. It is likely that the vast majority of multi-ring brickwork arch bridges already contain partial ring separation as a consequence of their age and the effects of their dynamic loading.

The most general two-dimensional mechanism analysis model to date was proposed by Gilbert (1993) which attempted to incorporate ring separation as well as radial shear failures, simple hinging, and compressive failures. However, he could only justify the use of the "plastic shearing" model (see chapter 2) for the analysis of bridge 3-0c which supposedly had only damp sand between its brickwork rings. Consequently, he was unable to reproduce the measured failure load of this bridge without incorporating an unrealistic normality rule.

Using his "plastic cohesion" model in which the nature of the bond between adjacent rings was assumed to be rigid-perfectly plastic, see chapter 2, Gilbert (1993) was able to accurately reproduce the measured failure load of bridge 3-0d, whose brickwork rings were mortared together. To achieve this, he assumed that the applied load was uniformly dispersed through an angle of 45° and that the arch was subjected to a rectangular passive pressure block of magnitude 50H kN/m^2 where H is the total depth of backfill above the abutments.

Fundamentally, Gilbert's modelling of the rigid shear connection between adjacent brickwork rings was incorrect and led to the equally incorrect prediction that, given a sufficiently strong mortar, the multi-ring brickwork arch is at least as strong as the voussoir arch. In reality, the elasticity of the shear connection will result in the behaviour of the multi-ring arch being very much different to that of a voussoir arch. In a brickwork arch, the quality of the mortar may be highly variable with some regions possessing elastic-brittle properties and other regions possessing ductile post-failure behaviour. It is therefore reasonable to use an overall elastic-plastic behaviour as suggested by Stöckl and Hofmann (1988) so that the most appropriate analytical technique is the finite element method.

In this thesis, the failure of the mortar bond between adjacent brickwork rings is described as ring separation, i.e. non-composite behaviour, although this is represented by a plastic failure rather than a brittle failure. Thus, the formation of circumferential cracks is not a prerequisite part of this phenomenon; it merely indicates excessive plastic deformation. Composite behaviour refers to the interaction of each brickwork ring prior to the formation of ring separation. However, due to the elasticity of the mortar bond this is somewhat less than the homogeneous behaviour of a voussoir arch bridge.

Gilbert (1993) found that the assumed behaviour of the backfill, in terms of the method of load dispersal and the mobilisation of passive pressure, has a significant effect on the predicted collapse load. Gilbert's uniform load dispersal was not in accordance with the work presented in section 4.4.1 of this thesis and likewise the magnitude of the passive pressures appears to be lower than those adopted herein. However, this indicates that there may be several combinations of these values that will produce realistic analyses. Therefore it is recognised that further research into soil-structure interaction is required before any analysis can be proclaimed

as correct in all respects. Notwithstanding this, it is suggested that the treatment of ring separation presented within this thesis represents a significant contribution to present arch theory.

The continual deterioration of the mortar within an arch bridge would ultimately result in it being unsafe to assume that it will contribute to the strength of the arch (Heyman, 1992). Thus, the inability of the mechanism method to incorporate the bond strength of the mortar would result in its prediction of the collapse load being erred on the side of safety. However this may not address the present desire, based on the current economic situation, to avoid unnecessary weight restrictions or replacement schemes by producing a realistic assessment of a bridge based on its current condition. In order to achieve this, a more sophisticated analytical technique is required which can incorporate the bond strength of the mortar, if only in terms of that which enables adjacent brickwork rings to act compositely.

The finite element method is a general numerical procedure for the analysis of continua; an example of which is the distribution of stress within an arch bridge. The distinct advantage of this technique, as compared with all others, is that it can be used to analyse any structure regardless of its geometric or material complexity. It is this ability that led to its use within this research.

The finite element method is the most appropriate method for the analysis of ring separation since, as already discussed, the mechanism method cannot, at present, incorporate the elastic-plastic properties of the mortar bond. Thus, the development of this FE model would form the foundation upon which future research would depend. The effects of skew must be considered in conjunction with ring separation. The three-dimensional mechanism method developed in chapter 6 has the potential to analyse a skewed arch and thereby describe its behaviour in a more direct, albeit simplified, way but nevertheless cannot, at present, incorporate ring separation. The inclusion of spandrel walls and other three-dimensional effects (such as eccentric loading, areas of damage, and areas in which repairs have been attempted) cannot be carried out in the absence of ring separation if its presence may overshadow the effects produced by them. The development of this finite element model may also be of use in the analysis of proposed strengthening measures such as concrete saddles and linings. In effect, these would behave in a similar manner as a brickwork ring and be subjected to similar shear forces tending to separate them from the remaining arch.

7.2 Structural Non-linearities

The use of the finite element method was initially directed towards the determination of the distribution of stress within a continuum. Thus, several assumptions were implied regarding the behaviour of the structure. Firstly, its rigidity and the magnitude of the applied loads were assumed to be such that the effects of the deformation of the structure could be neglected. Furthermore, the adhesion between the component parts of the structure was assumed to be sufficiently strong so that it could not fragment as a result of the loads. Secondly, the relationship between the applied loads and the deformation of the structure was assumed to be perfectly linear regardless of the magnitude of the loads, i.e. it possessed no elastic limit.

Geometric non-linearities refer to the change in stiffness of a structure, or the change in the point of application of the loads, due to its deformation. These non-linearities are ever present within all structure. However, the magnitude of their effects may be small enough for the analyst to neglect them. Consider the cantilever beam, shown in figure 7.1a, that is subjected to a point load at its free end. The beam is assumed to comprise perfectly linear elastic material. As the load is monotonically increased, the increasingly large deflection of the beam causes the lever arm of the load to diminish. Furthermore, the load is initially resisted by only the bending strength of the beam. However, as its deflection increases the resistance of the beam to the load is supplemented by its axial strength. Hence, the parabolic load-deflection response of a perfect cantilever, as shown in figure 7.1b.

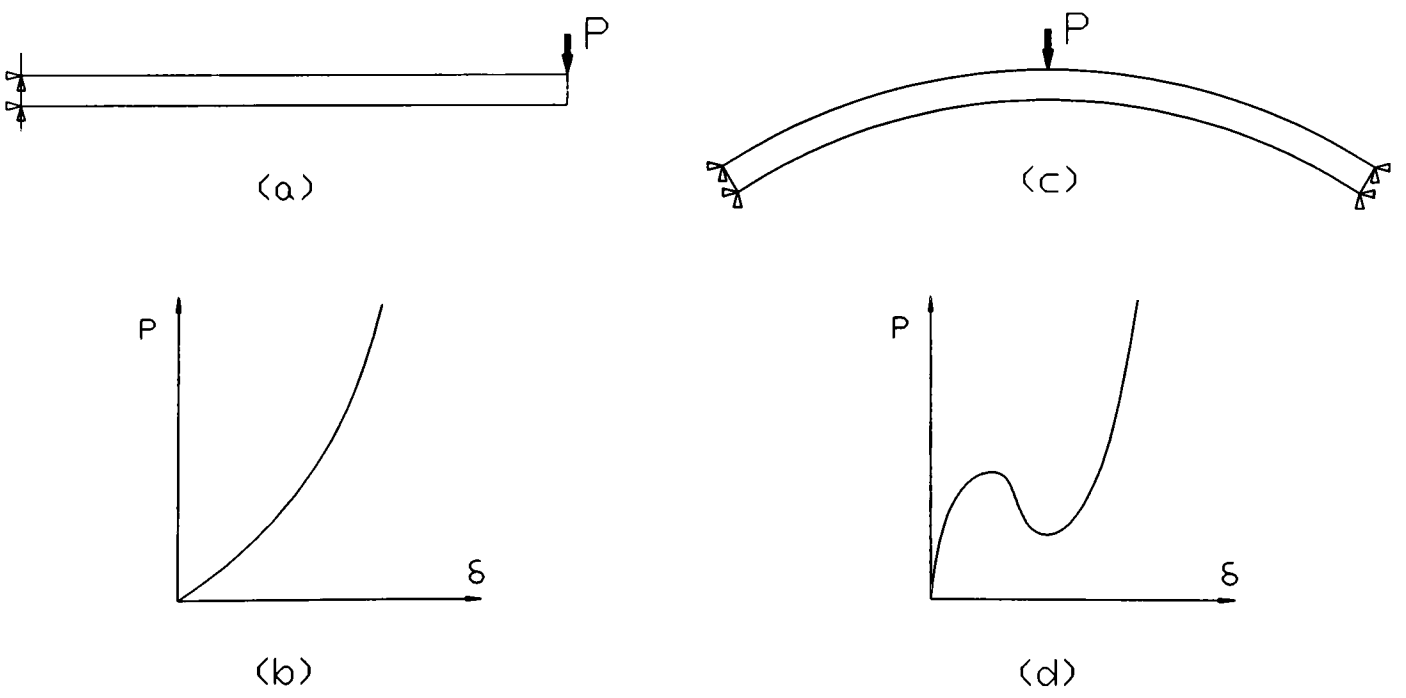

Figure 7.1 Geometric non-linearities

A shallow arch, as shown in figure 7.1c, that comprises perfectly linear elastic material and is subjected to a monotonically increasing concentrated load applied at its crown will exhibit a cubical load-deflection relationship as shown in figure 7.1d. As the magnitude of the load is increased, the arch deforms and the compression within it builds up. There will come a point

at which its deflection and compression will be such that the arch will buckle thus causing a dramatic decrease in the load. However, beyond this point, the arch will behave as a beam so that further load increments will be resisted by its bending strength and an increasingly significant tensile strength.

With reference to the masonry arch, its low tensile strength would mean that the post-buckling stage does not exist; the bridge merely collapses. The TRRL destructive test of Torksey bridge (Page & Grainger, 1987) was reported to produce a three-hinge snap through failure. The amount of compression of the arch, either as an elastic shortening or as a compressive failure, or the amount of spreading of the abutments that would be required to facilitate this makes this conclusion incredible. It is suggested that a more realistic description of the collapse mechanism was that it comprised three hinges and a shear failure. However, the observation of a possible buckling failure indicates that geometric non-linearities may be significant and may warrant inclusion in an analysis. In contrast, the deflection, at failure, of each model arch bridge documented in chapter 5, was small. Thus these effects were justifiably neglected in the finite element analysis of the brickwork arch, carried out in this thesis.

Another form of geometric non-linearity is associated with the fragmentation of the structure. With reference to the multi-ring brickwork arch, a set of monotonically increasing applied loads may cause the spandrel walls to become detached, or may create radial cracks (consistent with the formation of hinges), or may propagate ring separation. In each case the geometry of the structure is altered so that its stiffness may be reduced accordingly. It may be possible to define the material properties of a finite element model in such a way that some of these effects can be incorporated without having to add further complications to the model. It certainly seems reasonable to do this in the case of the formation of simple hinges (Choo et al.,1990; Crisfield, 1985; Loo & Yang, 1992). However, it will be shown that this approach weakens the finite element method as an accurate analysis technique if ring separation or spandrel wall detachment are treated in this way. These phenomena change the fundamental nature of the structure from a continuum to a surface-to-surface contact problem whereas the formation of hinges can be merely a separation problem.

Material non-linearities refer to the relationship between stress and strain exhibited by the constituent materials of the structure. Figure 3.1 shows the highly non-linear relationship between uniaxial compressive stress and compressive strain within sample brickwork prisms. It can be seen that the initial portion of each response can be adequately approximated as linear. Thus, provided that the stress does not exceed the limit of proportionality, a linear analysis can be performed. The stress at which the elastic limit is exceeded is known as the yield stress. Beyond this point, a brittle failure may ensue or the material may become plastic. In a three-dimensional system the yielding of the material is governed by the interaction of the principal

stresses within it. Many theories have been proposed to predict the point at which yielding will occur. Ford (1963) and Mendelson (1968) have published comprehensive reviews of these theories and detailed information regarding plasticity. Essentially, each theory dictates how the principal stresses should be combined to create a single equivalent stress which can be related to the uniaxial stress-strain relationship to determine if yielding will occur.

The yield surface can be drawn in principal stress space. An elastic-perfectly plastic material will posses a yield surface whose size will remain constant. In other words, no matter how much the material yields under load, if it is unloaded then loaded again, it will begin to yield at the same constant stress level. Less perfect materials may become strain hardened. Upon removal of the load such materials will take on a permanent set and reapplication of load will produce yielding at an increased yield stress, equal to the previous maximum stress. Thus the yield surface expands as a result of previous yielding. The expansion of the yield surface is governed by the hardening law.

The flow rule predicts the direction in which yielding occurs. An associative flow rule is derived from the yield criterion such as the "normality rule" which defines that plastic strains develop in a direction normal to the yield surface.

The finite element idealisation of a structure leads to a large set of simultaneous linear equations of the form shown in equation 7.1 in which $\{P\}$ is a vector of nodal loads (most of which are prescribed), $\{\delta\}$ is a vector of nodal displacements (some of which are prescribed) and [K] is the structure stiffness matrix.

$$\{P\} = [K].\{\delta\} \qquad \textbf{(7.1)}$$

To analyse a non-linear problem, of whatever nature, ANSYS carries out a series of successive linear approximations with corrections as depicted in figure 7.2. The load is applied in increments as a series of sub-steps and each is solved in turn. A balance must be found between the number of sub-steps and the number of iterations since fewer sub-step will result in an increased number of iterations.

At the end of the previous sub-step the state of stress within the structure is such that its nodal forces and nodal displacements can be represented by point (δ_i, P_i) in figure 7.2. The tangent to the non-linear load-deflection curve at this point represents the stiffness of the structure, K_t.

During the present sub-step the load is increased to P_{i+1}. The structure, i.e equation 7.1, is solved to determine the nodal displacements δ'_{i+1}. With reference to the actual non-linear load-

deflection relationship of the structure, the set of nodal loads, P'_{i+1}, which correspond to this set of displacements will generally not be those that correspond to the applied load. Thus, the process must be repeated from the new point (δ'_{i+1}, P'_{i+1}) until the error in the predicted nodal loads is acceptably small. The convergence tolerance of the analysis determines the acceptability of this error.

Several methods have been proposed in order to carry out subsequent iterations. The Newton-Raphson iteration procedure was adopted within the present work. One of the Newton-Raphson procedures updates the stiffness matrix at every iteration so that the stiffness of the structure is always based on the tangent to the load-deflection curve, as marked (b) in figure 7.2. The initial stiffness Newton-Raphson procedure, as marked (a) in figure 7.2, does not update the stiffness matrix and results in the stiffness of the structure during each subsequent iteration being based on the tangent to the load-deflection curve at the beginning of the present sub-step.

More equilibrium iterations are required in the initial stiffness method whereas additional work is required in repeatedly formulating the revised stiffness matrix if the former method is used.

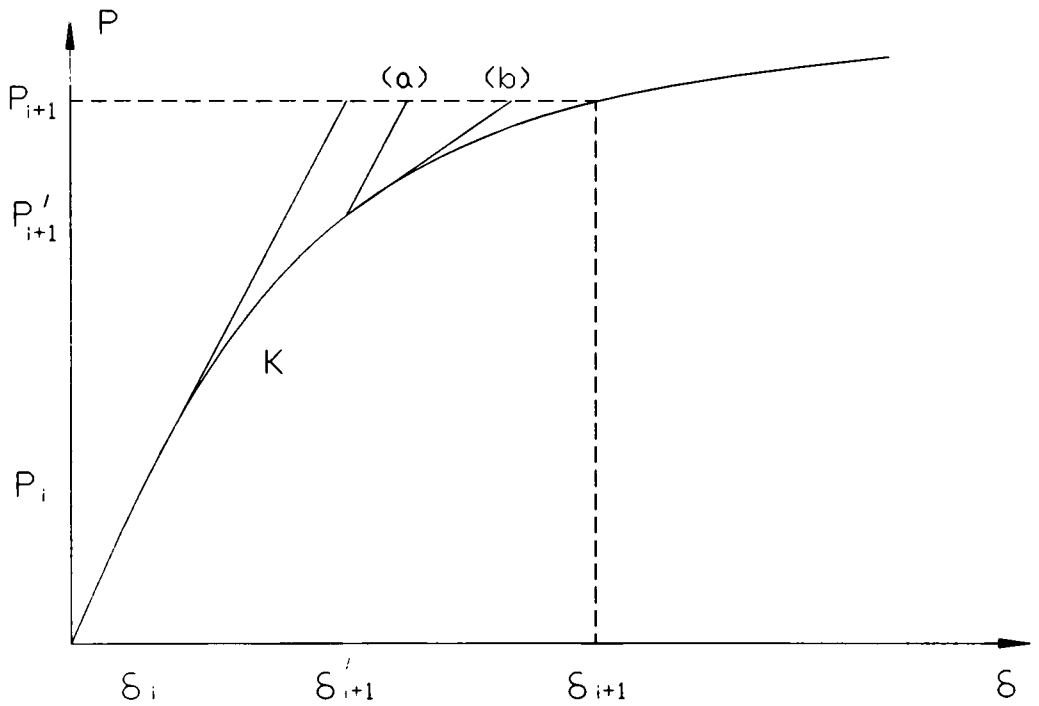

Figure 7.2 Iterative solution of a non-linear problem

7.3 The ANSYS "concrete" material model

The "concrete" material model (William & Warnke, 1975) that is contained within the ANSYS suite assumes that the material is initially isotropic and exhibits a linear relationship between its deformation and its internal stress.

The intersection of the three-dimensional failure surface used in this material model with the plane in which one of the principal stresses is zero is shown in principal stress space in figure 7.3. In the compression-compression-compression region a stress state that causes the failure criterion to be satisfied will result in crushing. In this situation it is assumed that there is a complete deterioration of the structural integrity of the material in the region of the compressive failure, i.e spalling occurs. The region of compressive failure takes no further part in the calculation of the stiffness of the element in further load increments.

In any other region in principal stress space, tensile failures occur when the stress state causes the failure criterion to be satisfied. The concrete material is capable of cracking in three mutually perpendicular directions corresponding to the principal stresses. Cracks are modelled through an adjustment of material properties so that they are effectively treated as a "smeared band" of cracks rather than as discrete cracks. The adjustment of material properties effectively creates a plane of weakness that is perpendicular to the direction of the smeared crack. This is achieved by reducing the stiffness of the appropriate section of the element to zero in that direction. Thus, the level of stress that can be sustained by the cracked material is maintained at its yield value and is not reduced to zero. Therefore, the initial state of isotropy can become one of orthotropy if tensile failures occur in each principal stress direction.

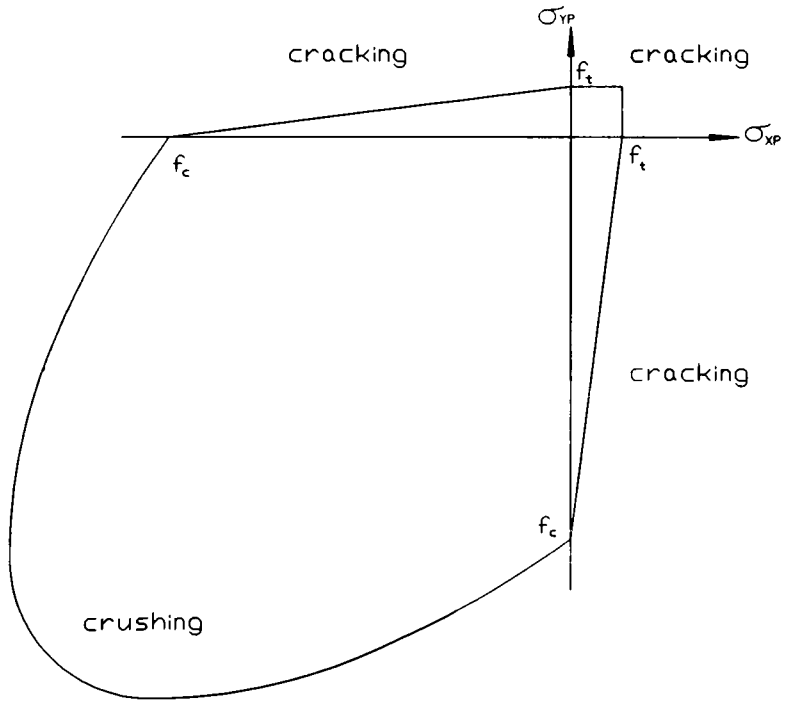

Figure 7.3 Failure Criterion for the 3-d solid element when $\sigma_{ZP}=0$

The failure criterion of the "concrete" material resembles that which was used by Loo & Yang

(1991a). However, in their two-dimensional analysis, the von Mises failure criterion in the compression-compression zone was used whereas in this model the failure surface is defined by a more complex relationship. Loo and Yang defined a strain softening parameter with which the post failure behaviour of the material could be modelled. Essentially this parameter defined the rate at which the stresses were reduced after failure occurred. In contrast, the material failure in the ANSYS "concrete" model results in a sudden loss of all compressive stress or a curtailment of further increases in tensile stress. The failure criterion used by Choo et al. (1992, 1995) appears to be a very simplistic one-dimensional relationship in which the stress must not exceed a given maximum value.

The "concrete" failure surface can be defined by a set of eight parameters (William & Warnke, 1975). The first two parameters are shear transfer coefficients across an open, β_o, and closed, β_c, crack respectively. These are used to reduce the shear strength of the structure for those loads that, subsequent to a tensile failure, will induce sliding along the crack face. The third and fourth parameters are the uniaxial tensile strength, f_t, and the uniaxial compressive strength, f_c, respectively. These two parameters are the ones that are most readily obtainable in practice. Brickwork cores can be extracted from an existing structure or brickwork specimens can be constructed concurrently with the model arch bridge, as in the case of this research. It is noteworthy that William and Warnke (1975) suggested simple linear relationships that could be used to determine the other strength parameters from these uniaxial strengths. These relationships were reported as being valid only when there exists a relatively low hydrostatic stress component. If other situations are anticipated it was recommended that the ultimate biaxial compressive strength, f_{cb}, be obtained, in conjunction with the ultimate compressive strengths, f_1 and f_2, for states of biaxial compression superimposed on a known hydrostatic stress state, σ^a_h, respectively.

In the case of a square span arch bridge, the hydrostatic stress state is relatively low so that the failure surface can be adequately defined by the two uniaxial strength parameters. This is a particularly important conclusion because it would be unreasonable to expect the assessment engineer to carry out complex biaxial material tests to determine the exact shape of the failure surface. Hence, even if the state of hydrostatic stress is not relatively small it would be desirable to use the simplified failure criterion based on just two easily obtainable strength parameters.

7.4 The square span multi-ring arch without spandrel walls

The finite element (FE) model developed as part of this research used a combination of element types from the ANSYS library in order to incorporate ring separation. An array of three-dimensional (SOLID65) elements was used to model each brickwork ring. Composite action was achieved by connecting together each set of brickwork elements with (CONTAC12 and COMBIN40) gap elements as depicted in figure 7.4.

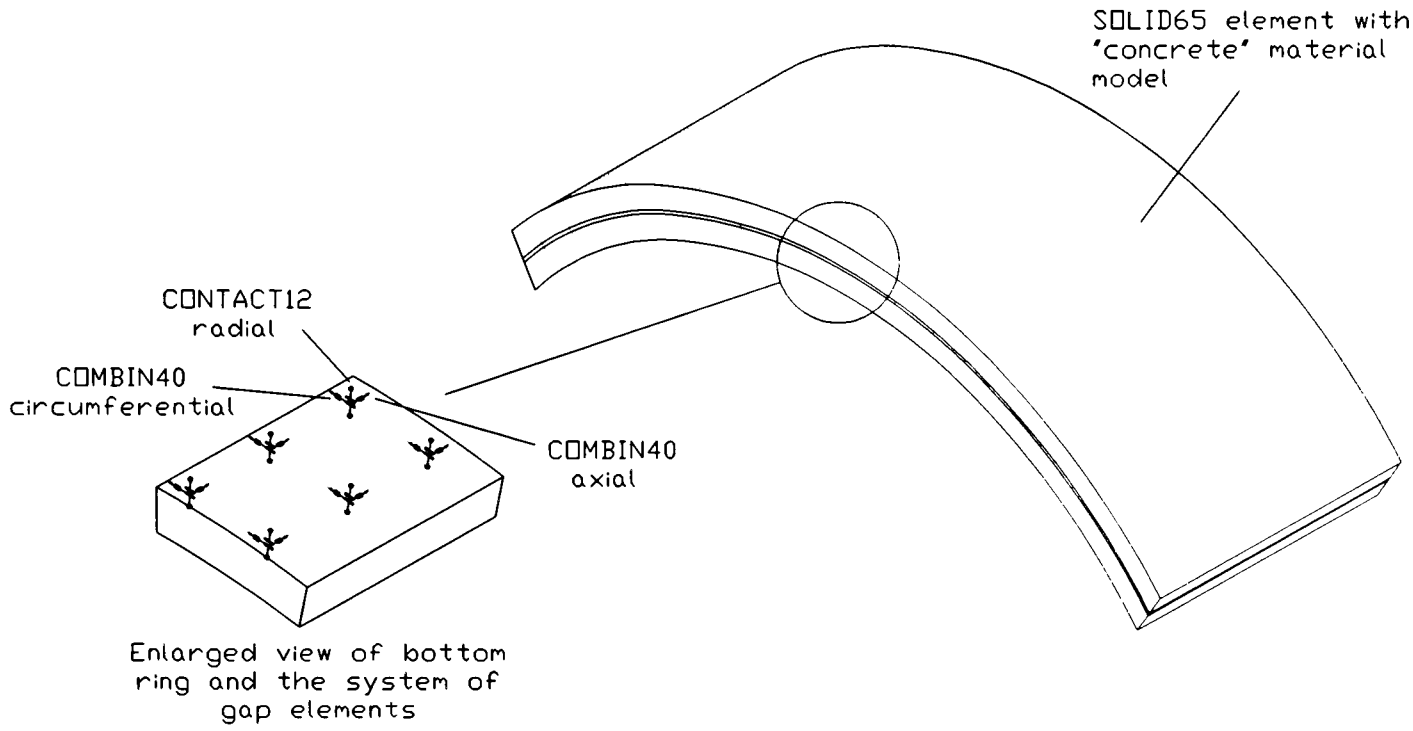

Figure 7.4 Finite element idealisation of the brickwork arch

The SOLID65 element is a three-dimensional eight node element that can incorporate reinforcing bars (rebars). This element, without its rebar capability, can be used to model the behaviour of unreinforced concrete or masonry when it is used in conjunction with the "concrete" material model (William & Warnke, 1990) as described in section 7.3.

The SOLID65 element was used to model the arch because of its ability to incorporate the "concrete" material model whereas inadequate, one-dimensional yield criteria, would have been required if other elements had been used. In actual fact, the behaviour of each square span model arch bridge with detached spandrel walls, as documented in chapter 5, was essentially two-dimensional when subjected to the full-width load used in the destructive tests. Thus, a two-dimensional analysis of this type of loading would have been adequate. For this reason, the finite element analysis of these square span arch bridges was based on a metre width strip and contained only one element across its width. However, it was anticipated that the analysis of the square arch, which is essentially a special case, would enable the modelling technique to be perfected so that a fully three-dimensional model could be created for the analysis of skew of other three-dimensional effects in which the magnitude of each principal stress may be such that a three-dimensional yield criterion is required.

It is not advocated that a two-dimensional analysis should be carried out if spandrel walls are attached to the arch. The destructive load tests carried out by Gilbert (1993) show that the behaviour of his model arch bridges remained essentially two-dimensional although their stiffness was increased by the spandrel walls. This may not have been the case if the spandrel walls had been more massive or had been more effectively restrained, as they may be in practice. Therefore, a three-dimensional analysis would be required in order to determine the effects of the spandrel walls; this study is beyond the scope of this thesis.

The two-dimensional finite element analysis carried out by Loo and Yang (1991a) used what was essentially the two-dimensional equivalent of the three-dimensional element and the "concrete" material model that was used in the FE analysis carried out as part of this research. However, their model was applicable only to the voussoir arch because it could not incorporate the relative shearing of adjacent rings. Their analyses of the bridges at Bargower and Bridgemill, both of which were voussoir arches, revealed that the respective collapse loads of these bridges could be reproduced by several combinations of the tensile strength and strain softening parameters. However, they did not report on the correlation between the experimental and theoretical load-deflection responses so that the success of their analysis cannot be determined.

Stöckl and Hofmann (1988) carried out shear tests on brickwork prisms that were constructed with mortars as weak as those used in the construction of each model arch bridge documented in chapter 5 and those used in the construction of most in-service bridges. As reproduced in figure 7.5, their tests revealed that, when loaded in shear, brickwork built with weak mortar exhibits a behaviour that can be represented by an elastic-perfectly plastic relationship.

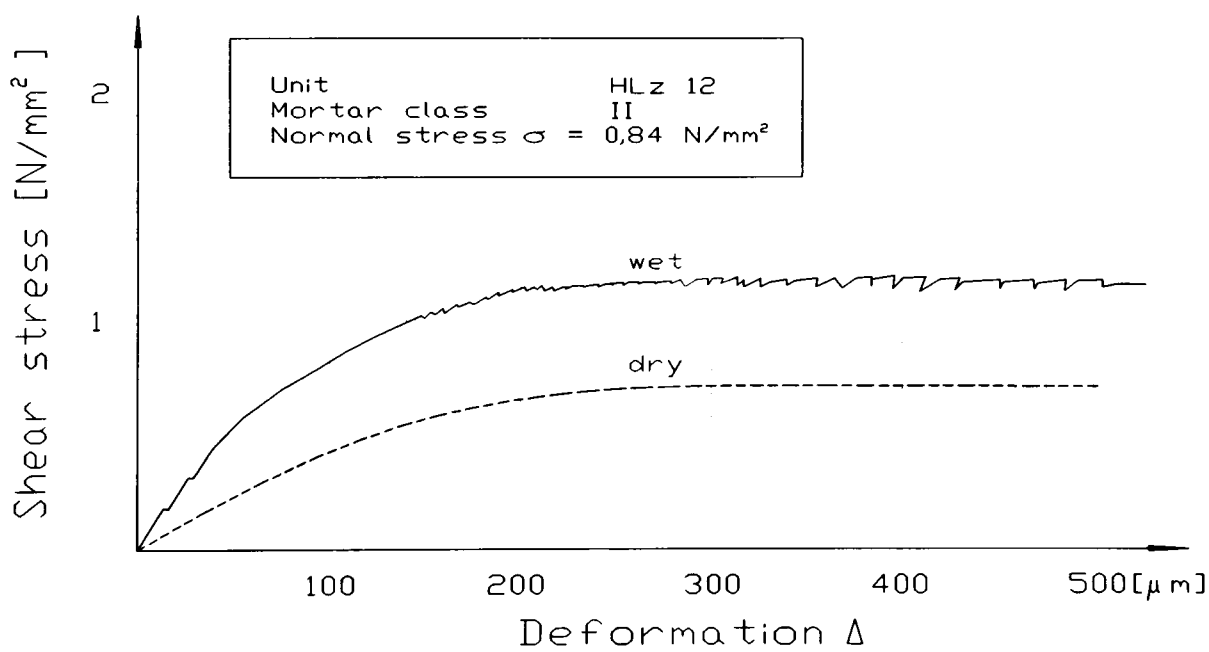

Figure 7.5 Shear stress v. shear deformation response of brickwork (from Stöckl and Hofmann)

It can be inferred from figure 7.5 that, due to the post-failure plasticity of the mortar bond, the effects of ring separation may be produced irrespective of the formation of circumferential cracks between the mortar and the brickwork. These cracks will only occur when the plastic deformation becomes large or when localised regions of higher strength mortar fail in a brittle way. This work was incorporated into the finite element modelling of ring separation presented in this thesis. The two parameters which define the mortar bond are therefore, its stiffness and its yield stress.

A fundamental requirement of a finite element model is that it has the ability to mimic the behaviour of the actual structure that it represents when each is subjected to an applied load. This is more important than ensuring that the model and the structure have similar appearances.

Figure 7.6 shows the non-linear load-deflection response of each of the model 3.0 m span square arch bridges that were constructed with detached spandrel walls (Gilbert, 1993) and subjected to a monotonically increasing line load as documented in chapter 5. The results of finite element analyses of these bridges are shown in which the arch was idealised as a "continuum", using the SOLID65 element only, and as two continua connected together with gap elements in the "ring separation" model.

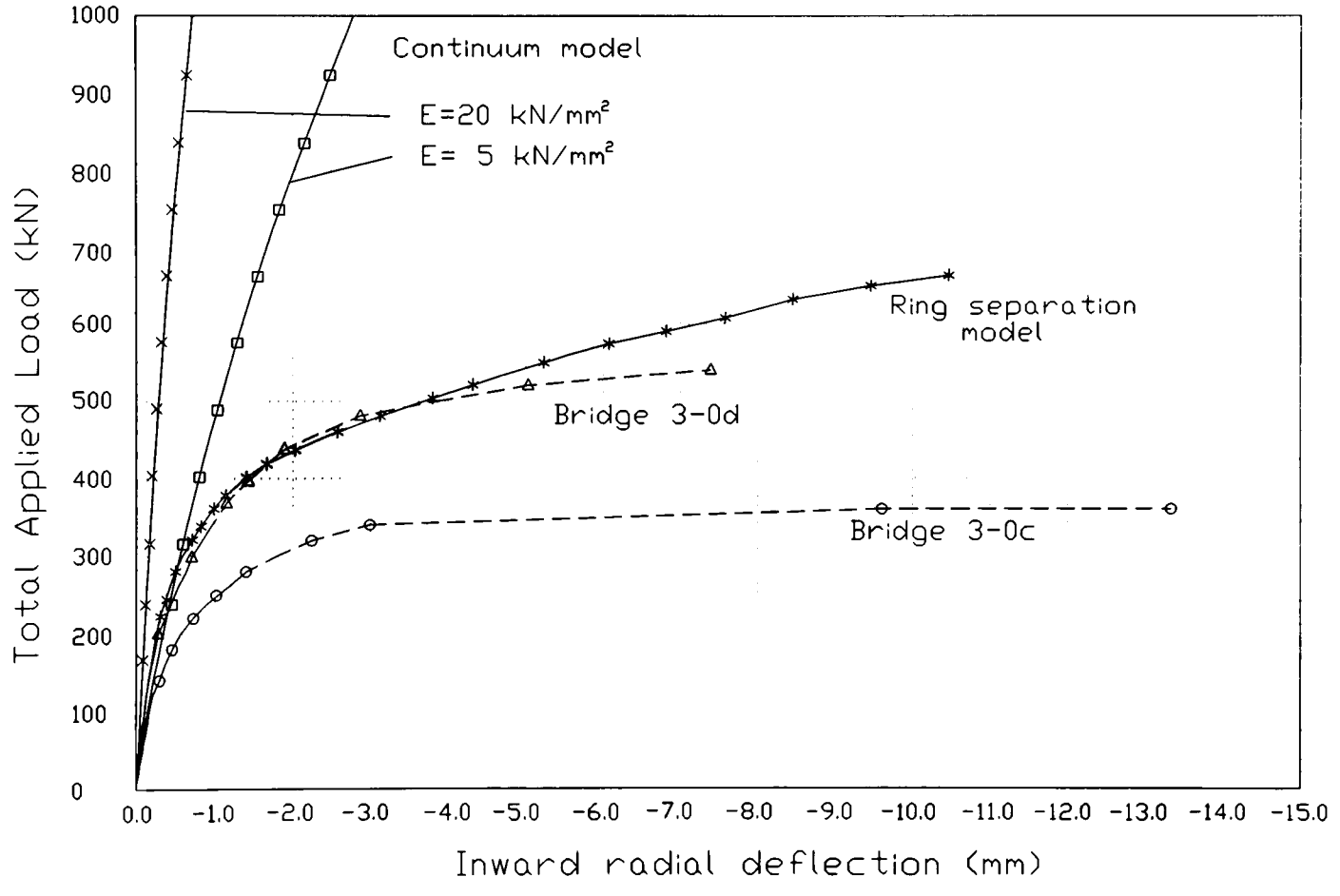

Figure 7.6 Comparison of FE results with/without ring separation

The "continuum" model is flawed in the sense that it does not mimic the behaviour of the actual structure that it represents. In contrast, the "ring separation" model is able to reproduce similar load-deflection behaviour as measured experimentally. It can be seen that a reduction in the

elastic modulus of the "continuum" model caused its load-deflection response to become more realistic. The results could also have been made more realistic by reducing the compressive strength of the material so that failure would occur at an appropriate load. This would have been sheer folly; this methodology may create the appearance that the analysis is correct but it would not be based on actual measurable material properties and would therefore be of little use to the Assessment Engineer who would be unable to determine what material properties should be used in the analysis.

The modelling of tensile failures in other models (Choo et al. 1990; Loo & Yang, 1991a) would result in their predictions of the load-deflection response being more non-linear. The difference would be due to the fact that in these models, tensile failures are brittle or cause strain softening respectively whereas the tensile failure of the ANSYS "concrete" material is plastic.

The highly non-linear load-deflection response of bridge 3-0c and bridge 3-0d, as shown in figure 7.6, is not entirely due to the formation of tensile cracks consistent with the development of a hinged failure mechanism. The bond between the ring of mortar and each ring of brickwork is relatively very flexible. This means that, even if the bond is not overcome, the behaviour of a multi-ring arch will be dissimilar to that of a voussoir arch. It can therefore by deduced that the strain profile on each fascia is unlikely to be linear. Furthermore, the load-deflection response of a multi-ring arch bridge will be more non-linear than that of a voussoir arch bridge.

The "ring separation" model, shown in figure 7.6, was based on the actual measured material properties of bridge 3-0d as documented in chapter 3. However, the bond strength of the mortar was given an unrealistically high value so that yielding of the mortar bond could not occur. This was done to highlight the fact that the load-deflection response becomes non-linear as a result of the flexibility of the mortar bond. The occurrence or ring separation makes the pronounced change in gradient of the load-deflection response occur at an earlier load level and makes the gradient less steep after its initiation. The results of the finite element analysis of the "ring separation" model revealed that this bridge could sustain an applied load of approximately 540 kN provided that, at this load, the shear bond strength was not less than 0.25 N/mm^2.

In order to successfully model the behaviour of a multi-ring brickwork arch bridge it is necessary to allow adjacent brickwork rings to shear relative to each other when the mortar bond strength has been exceeded. The relative movement of each ring must be controlled so that they are not able to move through each other but are free to separate if they should desire. It is also necessary to allow relative shear movements, both before and after the bond has yielded, to occur in the direction that corresponds to the principal stress at the interface. At every point within a square span arch, when subjected to a full-width patch load, this will be

in the circumferential direction parallel to the edge of the structure. However, in a skewed arch or when the square arch is subjected to eccentric patch loads, the direction of shear movements may vary throughout the structure.

ANSYS does not posses a three-dimensional gap element which can perform the above functions. Thus, it was necessary to use several elements in combination to create the same effect. This combination of gap elements was intended to reproduce the actual behaviour of a multi-ring brickwork arch bridge. The achievement of this must be judged on the ability of the model to reproduce the measured load-deflection response and the ultimate load whilst being based on actual measured material properties.

The CONTAC12 element is a two-dimensional element which is capable of supporting only compression in the direction normal to the contact surface and shear in the tangential direction. Figure 7.7 shows the force-deflection relationship for this element in which it can be seen that the contact surfaces are free to separate in the normal direction. The stiffness, KN, of the element inhibits the movement of the two contact surfaces through each other but does not prevent it. A slight overlap will occur and this is used to calculate the normal force between the contact surfaces. Coulomb friction is used to relate this normal force to the maximum sustainable shear force. The adjacent brickwork rings will shear relative to each other before the gap elements have reached their elastic limit. However, the shear movement will occur much more freely if the shear force exceeds this maximum sustainable value.

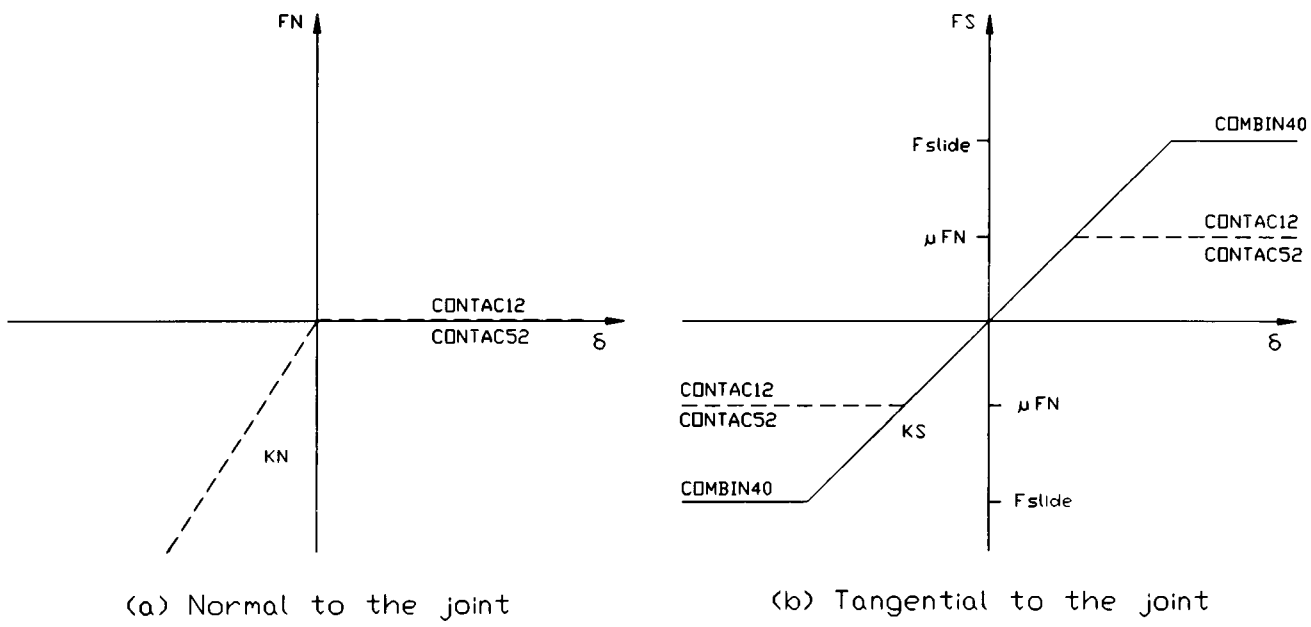

Figure 7.7 Force-deflection relationships of the gap elements

The two-dimensional FE model proposed by Choo et al. (1992) for the analysis of ring separation used a gap element that was more simple than the CONTAC12 element. Gap elements were only introduced into their model "when the tensile stress across an element boundary exceeded its tensile strength". This appears to suggest that they had assumed that ring separation was due to a radial tensile failure rather than a circumferential shear failure. They

used a one-dimensional element which could only resist compression normal to the two contact surfaces. The one-dimensional nature of this element meant that it had no stiffness in the circumferential direction so that unrestrained movements could occur in this direction. To resist these movements, two equal but opposite forces, of an arbitrary value, were applied at either end of each gap element. Consequently, their predicted load-deflection response of the 5.0 m span arch bridge with ring separation, which was load tested at the Bolton Institute of Higher Education (Melbourne & Gilbert, 1992) was very much different to its actual measured response. Furthermore, they managed to accurately reproduce the experimentally obtained failure load despite (or perhaps, *because of*) their analysis being based on unrealistically low material properties.

The initial finite element analyses of the brickwork arch presented within this research revealed that the normal force across the joint between adjacent brickwork rings was so low that shear movements were effectively unrestrained by the CONTAC12 element. In other words, if only CONTAC12 elements were used, the analysis would fail at an unrealistically low load. CONTAC12 elements were retained for their ability to prevent adjacent rings overlapping. However, a COMBIN40 element was used to increase the circumferential shear bond strength, as shown in figure 7.7, and, in order to complete the triad of elements, a further COMBIN40 element was used in the direction parallel to the abutments as shown in figure 7.4.

The COMBIN40 element is a one-dimensional element which has several capabilities, most of which were not used in this application. The aspect of this element which was retained was its spring-slider capability. In other words, the load-deflection relationship of this element, as shown in figure 7.7, resembled the shear stress-shear deformation of the mortar bond as determined experimentally by Stöckl and Hofmann (1988). Unlike the CONTAC12 element, the one-dimensional nature of the COMBIN40 element results in its behaviour being unaffected by a load effect that occurs in a direction that is perpendicular to it. More explicitly, when defined in the circumferential direction, the COMBIN40 element will continue to resist ring separation until its strength is exceeded regardless of the fact that the rings may separate in the radial direction. However, it was found that a radial separation occurred within the arch only in the vicinity of each hinge when the material throughout the full depth of one of the brickwork rings had yielded in tension so that the radial gap in this case is unimportant.

7.4.1 The analysis of bridge 3-0c and bridge 3-0d

Where possible, the material properties used in the finite element analysis of these structures were based on actual measured values, as outlined in chapter 3. They required no adjustment because the model was able to behave in a realistic way. Material tests carried out on brickwork samples and on mortar cubes provided the data with which the stiffness and strength of the corresponding finite elements were determined. The exception to this was the derivation of the properties of the shear bond between the brickwork rings of bridge 3-0c (which was supposedly attributable to only damp sand). These properties were obtained empirically by carrying out several analyses of this structure.

	Bridge 3-0d	**Bridge 3-0c**
Brickwork properties		
Young's modulus	15.0 kN/mm^2	15.0 kN/mm^2
Compressive strength	25.0 N/mm^2	25.0 N/mm^2
Tensile strength	0.1 N/mm^2	0.1 N/mm^2
Poisson's ratio	0.15	0.15
Shear transfer coeff.	0.9	0.9
Mortar properties		
Normal stiffness	10.0×10^6 kN/m	10.0×10^6 kN/m
Tangential stiffness	5.0×10^6 kN/m	0.1×10^6 kN/m
Tangential strength	0.25 N/mm^2	0.08 N/mm^2

Table 7.1 Finite element material properties for the square span arch bridges

The finite element analyses carried out by Choo et al. (1991) incorporated the backfill by modelling it with a set of one-dimensional spring elements that were attached to the extrados of the arch. Thus, the backfill transferred loads to the arch that were related to its deformation. The finite element model presented in this thesis does not include backfill elements. This is because they would add a further complication to an already complicated model and therefore make its development difficult. Furthermore, the behaviour of the backfill is not well understood and is certainly unpredictable at present so it would be unwise to attempt to model its effects in any way other than applying a set of predetermined vertical and horizontal loads. However, the approach adopted by Choo et al. (1991) is at least a step in the right direction.

Each finite element analysis was carried out with the live load being applied at a location which would correspond to the actual loading position used during the respective destructive load test. In accordance with section 4.4.1 the applied load was assumed to disperse through the backfill, to the extrados of the arch, at 30° to the vertical. Moreover, the shape of the influence lines

shown in figure 4.24 would indicate that the distribution of pressure on the extrados was of a sinusoidal form. Therefore, in the present finite element model a sinusoidal distribution of pressure was assumed at the surface of the backfill (Smith, 1991). The load that was applied to the arch at each extrados node contained within the load dispersal lines, see figure 7.8, was proportional to the area of the pressure distribution curve that was bounded by lines draw from the edges of the loaded length of the node to the point of intersection of the dispersal lines.

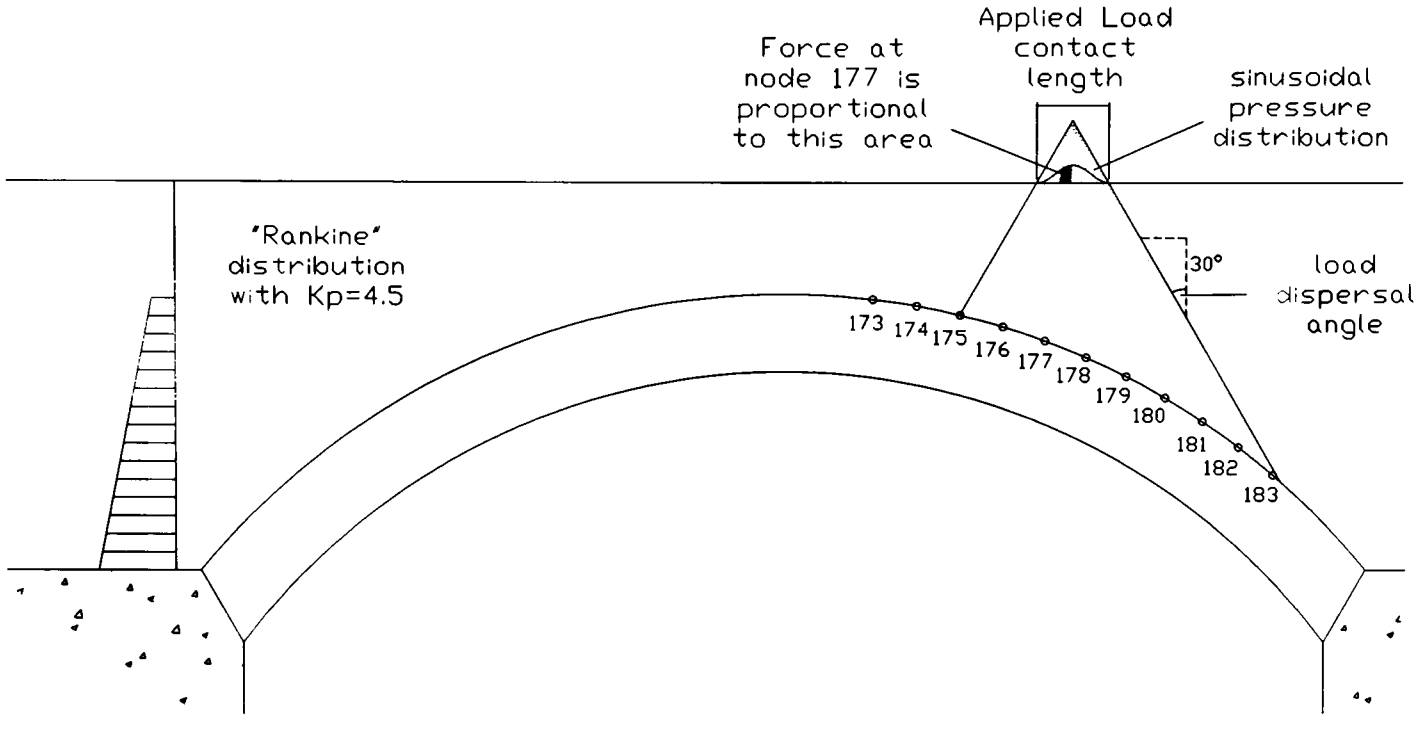

Figure 7.8 Assumed soil-structure interaction

Backfill pressure cells were not installed within bridges 3-0c and 3-0d so no data were available with which the horizontal loads due to the passive resistance of the backfill could be calculated. In the absence of these data, horizontal forces were applied to each finite element model in accordance with a Rankine (1862) pressure distribution in which the value of $K_p=4.5$ was adopted. This value was selected because it would limit the horizontal forces to approximately 33% of those that could occur if the actual coefficient of passive earth pressure was used. The value of the angle of internal friction of the spandrel fill was found to be approximately 60° which would correspond to a passive earth pressure coefficient of 13.9. However, figure 5.29 shows that the spandrel fill is able to mobilise only a fraction of this maximum amount before the arch reaches failure. Thus, an upper limit of 33% was deemed to be reasonable. However, to verify the reasonableness of the adopted value of $K_p=4.5$, a parametric study was carried out to ascertain the effects of varying the magnitude of the passive pressure.

Figure 7.9 shows the results of the finite element analyses of bridges 3-0c and 3-0d when idealised as described in section 7.4 and based on the material properties listed in table 7.1.

It can be seen, in figure 7.9, that the finite element analysis of ring separation, presented within

this thesis, was successful. The failure load of each model arch bridge was reproduced fairly accurately, there was a close correlation between the experimental and FEA predicted load-deflection relationships throughout their entire load histories, and the FE models were based on actual measured material properties.

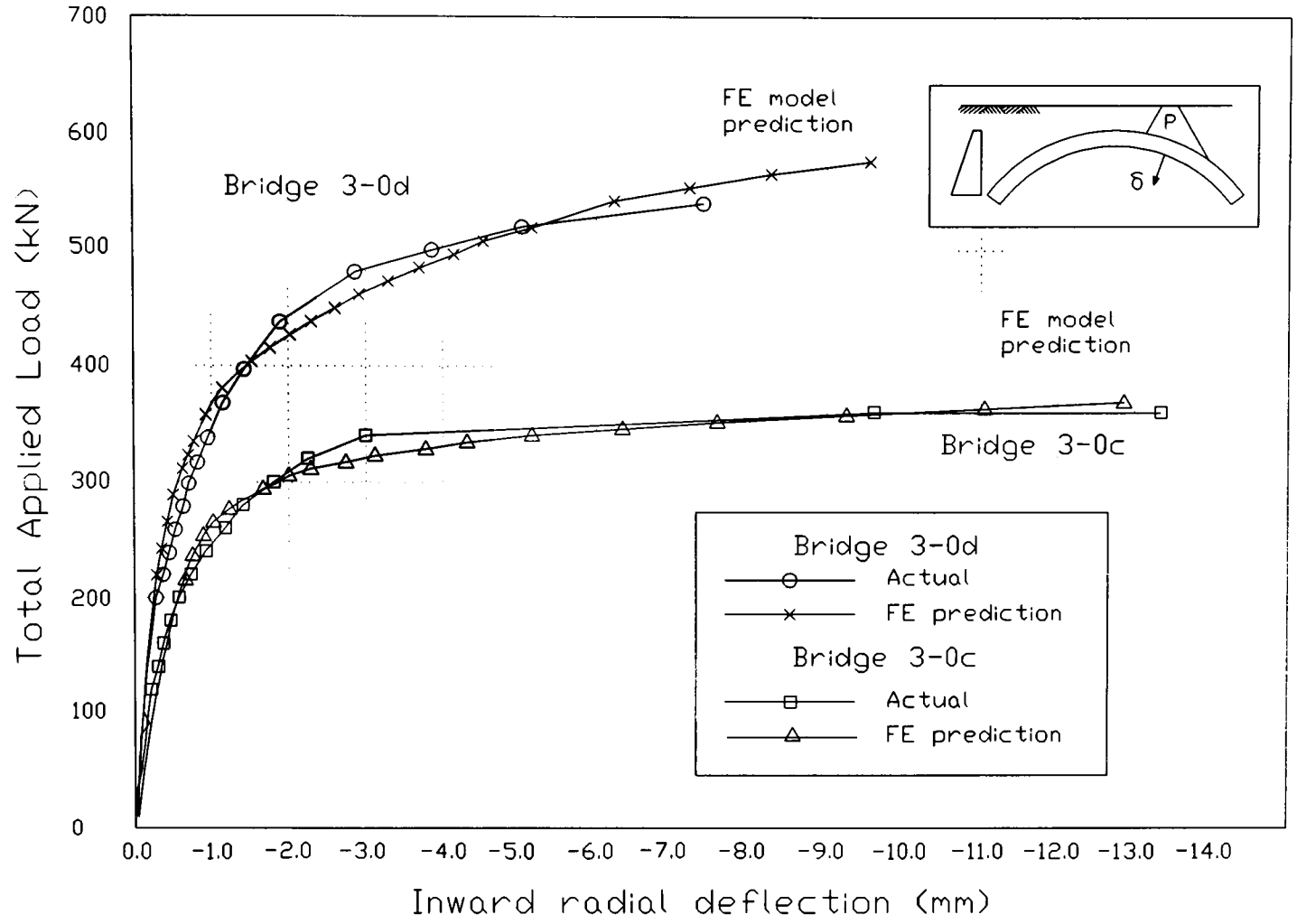

Figure 7.9 Finite element analysis of bridge 3-0c and bridge 3-0d

It was found that the finite element model of bridge 3-0d, in which the shear bond strength was 0.25 N/mm^2, resisted the initiation of ring separation until the applied load was increased beyond 280 kN. The actual value of the load at which radial cracking was visually detected within this bridge was 240 kN (Melbourne & Qazzaz, 1989). Circumferential cracks were not recorded but this does not indicate the absence of ring separation; it may only indicate that the ductility of the mortar bond was such that it failed in a plastic manner as opposed to a brittle manner. Within the finite element model, the initial failure of the mortar bond was confined to the vicinity of the first in-span hinge. Furthermore, as Gilbert (1993) suggests, the formation of a simple hinge requires a relative shear movement of adjacent rings in order for compatibility to be maintained. Thus, the close correlation between the initiation of ring separation in the finite element model and the formation of the first in-span hinge within the actual bridge is further confirmation of the accuracy of the analysis.

The analysis carried out using the present finite element model is certainly more accurate than that of Choo et al. (1991a) whose FE analysis of bridge 3-0c predicted a failure load of 188 kN. They also predicted that 81% of the strength of a "well bonded" arch would be attainable if the

brickwork shear bond strength was only 0.05 N/mm^2. However, the material tests documented in chapter 3 produced a shear bond strength of 0.25 N/mm^2 and the use of this value in the proposed FE model produced a failure load of 576 kN for bridge 3-0d which is within 7% of its actual failure load. Ring separation was predicted in the FE analysis and must also have occurred within the actual structure during its load test. If this bridge was assumed to be "well bonded", a similar bridge in which the shear bond strength of its brickwork is assumed to be 0.05 N/mm^2 should fail at 460 kN in accordance with the assertion of Choo et al. (1991a). However, figure 7.22 shows that, for a shear bond strength of 0.05 N/mm^2, the failure load would be approximately 230 kN, i.e. 40% of the strength of a "well bonded" arch. Conversely, a shear bond strength of 0.15 N/mm^2 would produce a failure load of 460 kN.

The objective of the analysis of bridges 3-0c and 3-0d was to demonstrate the validity of the modelling technique, not to obtain an incredibly close correlation between the experimental and numerical results. However, given sufficient time and effort, slight adjustments to the material properties could have been carried out within the tolerances specified in table 3.5 in order to obtain a much closer correlation between the numerical and experimental results. However, an exact match could only be produced if every gap element was given its own unique stiffness and strength to reflect the variability of the masonry. However, the results show that this is unnecessary, the analyses are sufficiently accurate if each gap element has identical properties.

An interesting, and reassuring, observation is that the two finite element models were similar to each other. The exception to this was in the stiffness and strength of their respective gap elements, see table 7.1. This difference was intended to reflect the fact that the materials used to connect each brickwork ring were very dissimilar to each other.

It was anticipated that in the FE model of bridge 3-0c Coulomb friction would be sufficient to create the required amount of load sharing so that the experimental load-deflection relationship could be reproduced. However, this was found not to be the case; COMBIN40 elements were required in order to increase the shear bond strength to 0.08 N/mm^2. The coefficient of friction between the adjacent brickwork rings, a property of the CONTAC12 elements, could be increased ad infinitum, the low value of the normal force between the brickwork rings curtailed its effect, see figure 7.7. Furthermore, the relatively low normal stress between the brickwork rings and the relatively low stress parallel to the abutments indicates that it was acceptable to define the yield surface as determined by William and Warnke (1975) in terms of only the uniaxial compressive and tensile strengths of the masonry thereby accepting their suggested default values.

This does not explain the apparent anomaly that a shear resistance was required in the FE model of bridge 3-0c (with total ring separation) in excess of that which would be provided by

Coulomb friction. However, the following conjecture is offered as an explanation of this. Bridge 3-0c was constructed with a layer of damp sand between each of its brickwork rings. The bottom ring would have been constructed first and then the 10 mm thick layer of sand would have been placed over each haunch. The top ring, of each haunch would have been constructed next. Finally, the layer of sand and subsequent in-fill section of brickwork of the top ring would have been placed at the crown of the arch. It is not unreasonable to assume that the layer of sand was not of a uniform thickness. Furthermore, it is likely that mortar and individual bricks would penetrate the sand layer as each brick was laid. Thus, these ingressions of mortar or bricks would act as shear studs so that an enhancement of the shear strength was produced. The 0.08 N/mm^2 bond strength was therefore a strength which was equivalent to the combined effects of these construction defects; its use created a successful finite element analysis.

Material properties similar to those used in the analysis of bridge 3-0c may represent lower bound values pertaining to the behaviour of in-service multi-ring brickwork arch bridges. In contrast, the material properties used in the analysis of bridge 3-0d may represent reasonable upper bound values. Bridge 3-0d was constructed with a weak, flexible mortar similar to those used in most in-service arch bridges. However, this bridge was not subjected to similar weathering and a dynamic loading history of 100 to 200 years. Therefore, the assessment of an in-service bridge could be carried out with appropriate parameters within the above range.

Figure 7.10 shows the effects that increasing the number of finite elements has upon the results of the analyses. As previously stated, the finite element method is a numerical procedure in which the most complex structure can be discretised into a number of small elements so that it can be solved with relative ease. In order to achieve this, the deformation of each element is assumed to be of a certain form, i.e. linear or quadratic etc. so that the structure can be represented by a set of linear equations relating the nodal displacements to the nodal forces. This limited form of the assumed deformation creates the approximate nature of the method. The infinite number of particles within the actual structure would not generally deform in a similar way as the FE model. Therefore the FE model will be stiffer than the actual structure. Hence, if additional or higher order elements are used, the results of the finite element analysis will converge towards the exact solution. It can be seen in figure 7.9 that when the number of SOLID65 elements is increased to 60×6 (i.e 60 elements in the circumferential direction and two rings of 3 elements in the radial direction), the results of the analysis show that the stiffness of the model is reduced as expected. When the number of SOLID65 elements is increased to 90×8 the results of the analysis are virtually unchanged. It can therefore be concluded that if the model contains 60×6 SOLID65 elements the analysis is, to all intents and purposes, exact. Furthermore, the results of the analysis of the model containing 30×4 SOLID65 elements are sufficiently accurate and has the added benefit that the analysis requires much less time to

perform. It can also be seen that the predicted failure load becomes more accurate as the number of finite elements is increased.

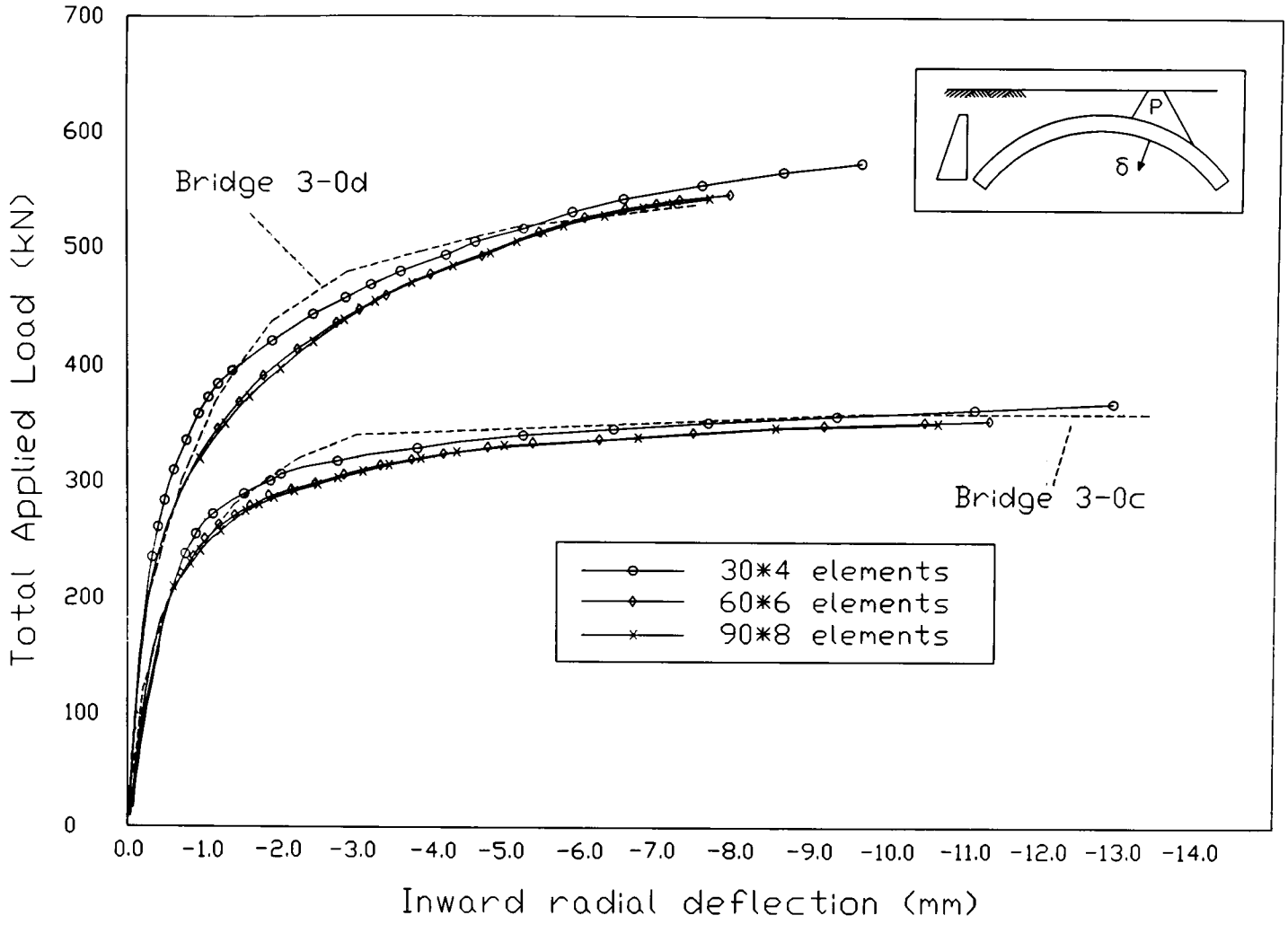

Figure 7.10 The results of the FE analysis versus number of elements

The following figures, viz. 7.11 to 7.22, show the results of the finite element analysis of bridges 3-0c and 3-0d at corresponding stages throughout their load histories.

The distribution of circumferential stress within the arch barrel of each bridge, when the magnitude of the applied load was approximately 75 kN (see figures 7.11 and 7.12 respectively), highlights the fundamental difference between the behaviour of a multi-ring brickwork arch containing ring separation and one whose brickwork rings are "well bonded" together. The plots also reveal that the behaviour of a multi-ring brickwork arch is very much different to that of a voussoir arch.

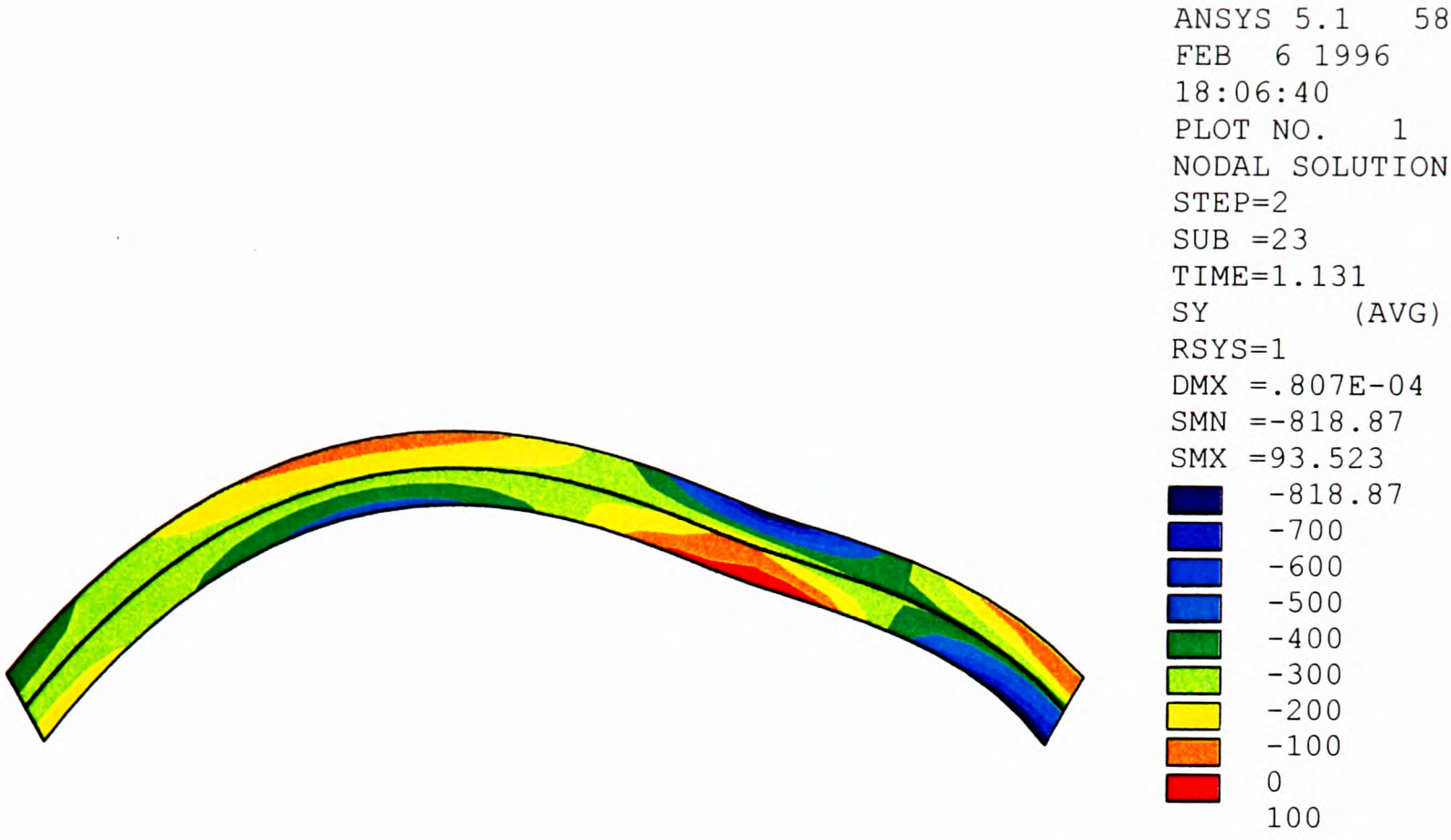

Figure 7.11 Circumferential stress in arch 3-0d at 75.5 kN

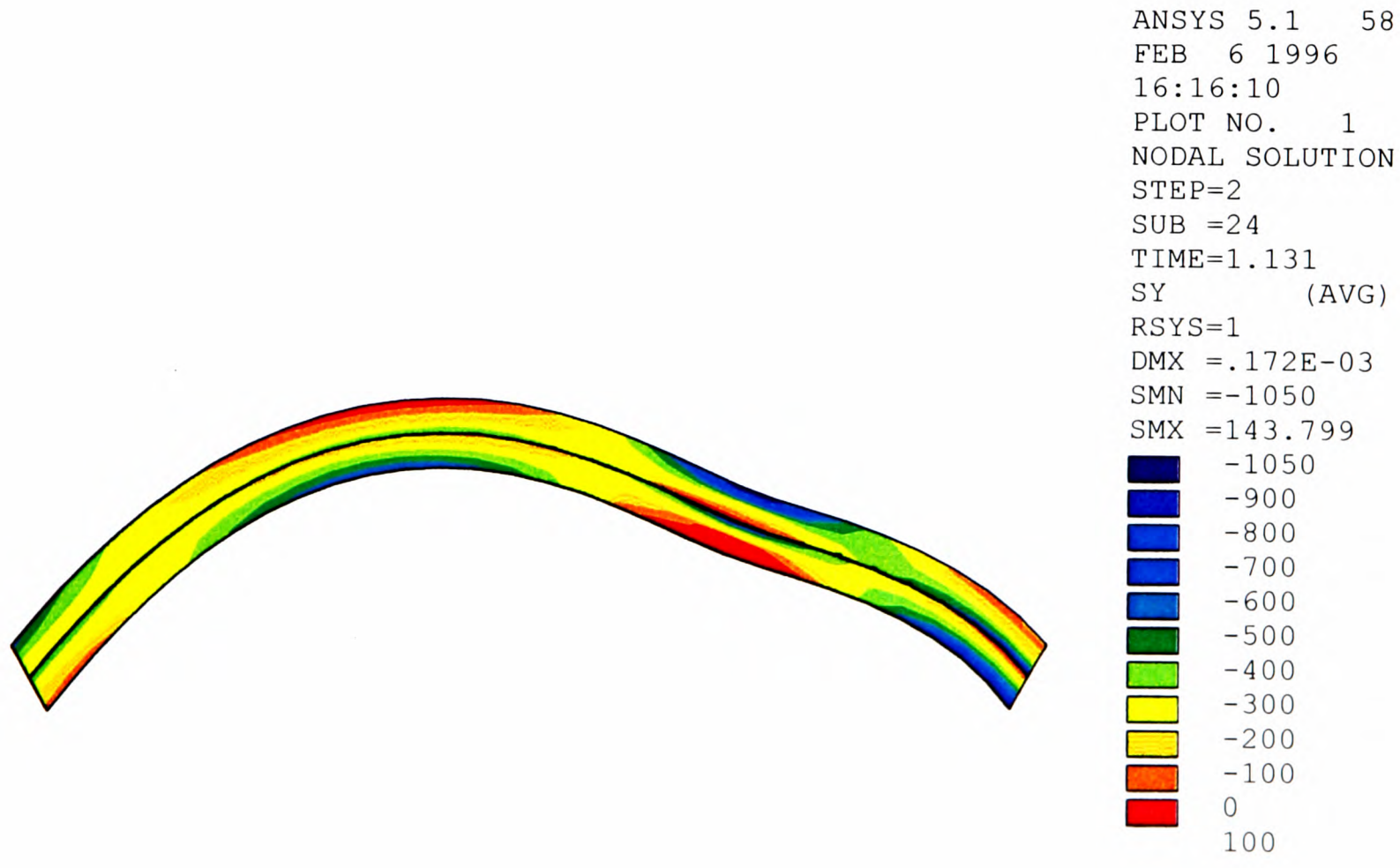

Figure 7.12 Circumferential stress in arch 3-0c at 75.5 kN

In the finite element model of bridge 3-0d, see figure 7.11, the distribution of circumferential stress appears to be proportional to depth, i.e. as if there is no discontinuity across the mortar joint. However, this was not the case. In the right hand side haunch a stress discontinuity can be observed. Here, the deformation of the arch is such that the upper ring is pulled away from the abutment. The thrust within the arch must therefore move from the top ring, in the vicinity of the loaded area, to the bottom ring, in the vicinity of the right hand side abutment, and must therefore cross the mortar joint. The thrust is not sufficiently large to initiate ring separation, the shear bond strength of the mortar resists this but its relative flexibility enables the brickwork rings to move relative to each other.

From this, it can be concluded that the stress is not proportional to depth at any section of a multi-ring arch, unless the mortar between each of its brickwork rings is capable of rigidly connecting them together. Thus, the behaviour of this type of bridge is fundamentally different to that of a voussoir arch bridge; its stiffness and probably its strength will be reduced.

In contrast, the distribution of circumferential stress within the finite element model of bridge 3-0c, see figure 7.12, when the magnitude of the applied load was 75 kN indicates that each of its brickwork rings acted non-compositely. There was a pronounced discontinuous stress distribution in which relatively large tensile and compressive stresses occurred within each ring rather than at the extremities of the barrel as in the model of bridge 3-0d. Consistent with this non-composite behaviour, the magnitude of the deflection and the maximum tensile and compressive stresses were larger in bridge 3-0c than in bridge 3-0d. However, the small but non-zero shear strength between the "damp sand" layer and each brickwork ring meant that the degree of load sharing between the brickwork rings was such that they did not behave in an independent manner as they would if only friction had existed between them.

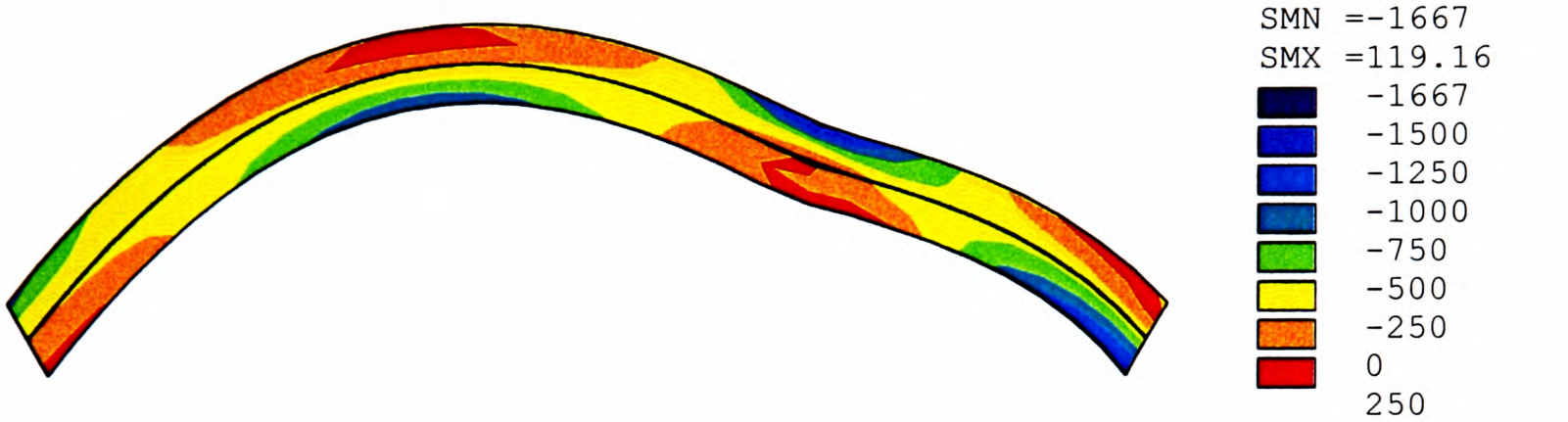

Figure 7.13 Circumferential stress in arch 3-0d at 150.3 kN

Figure 7.14 Circumferential stress in arch 3-0c at 150.3 kN

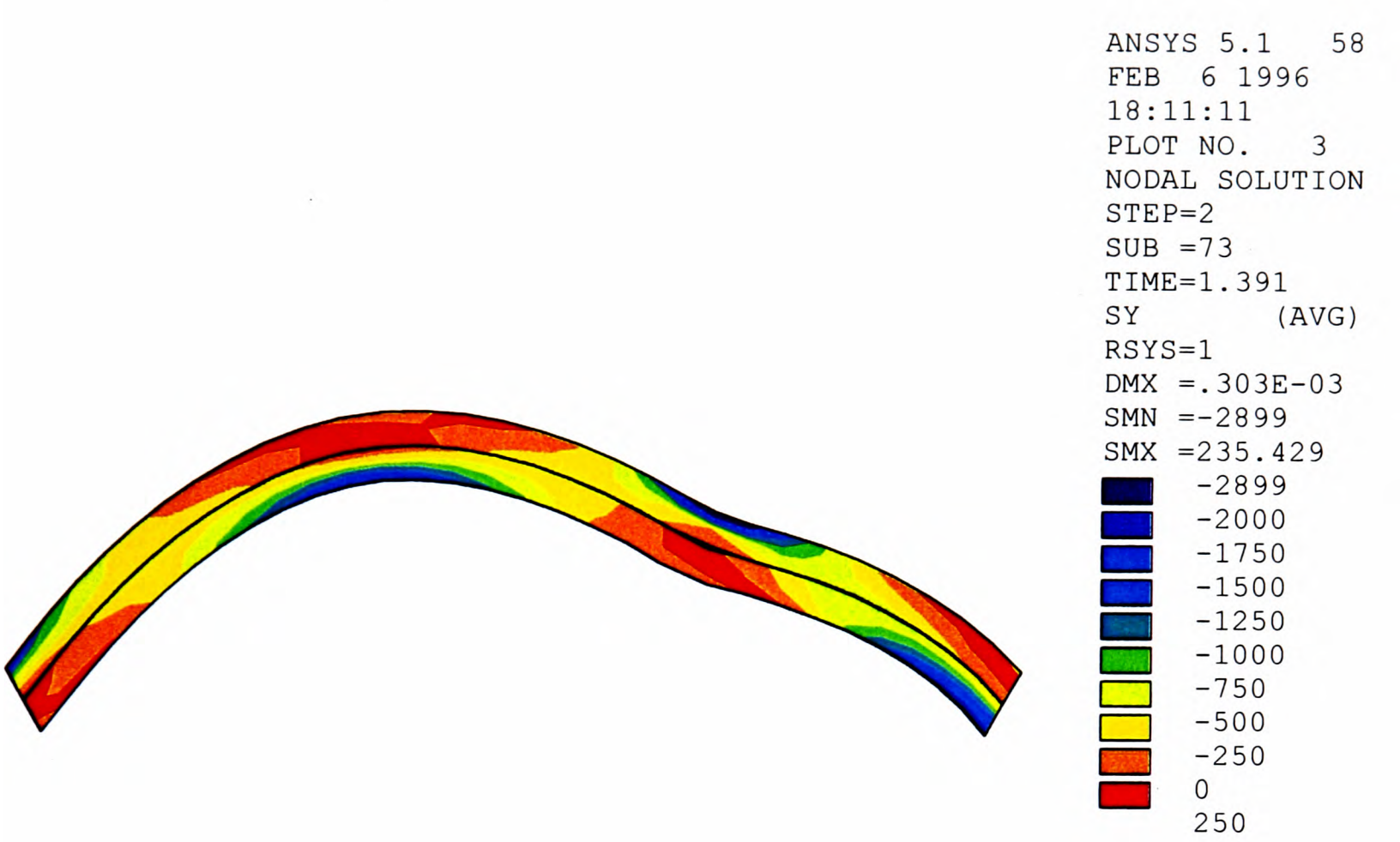

Figure 7.15 Circumferential stress in arch 3-0d at 225.2 kN

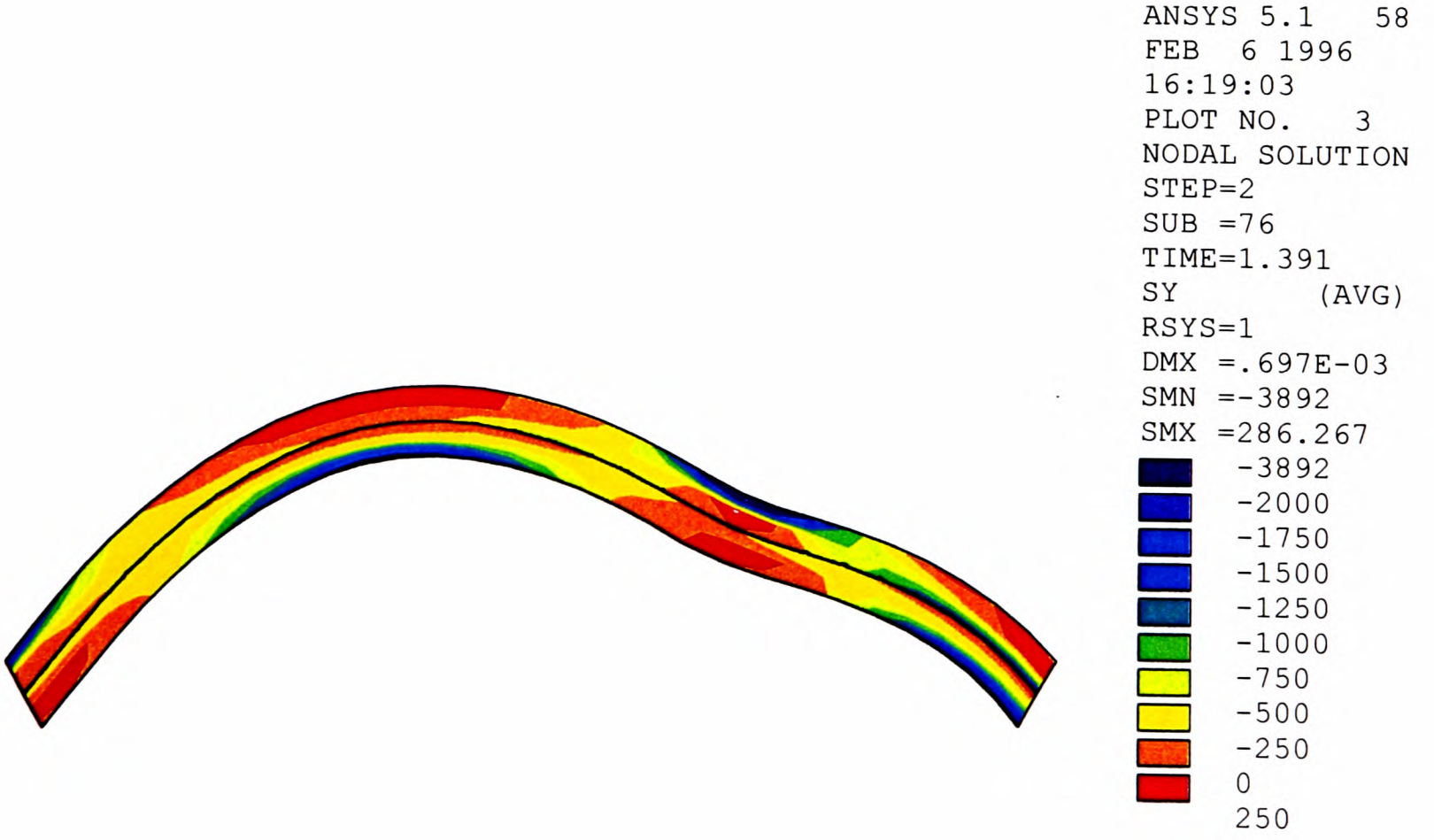

Figure 7.16 Circumferential stress in arch 3-0c at 225.2 kN

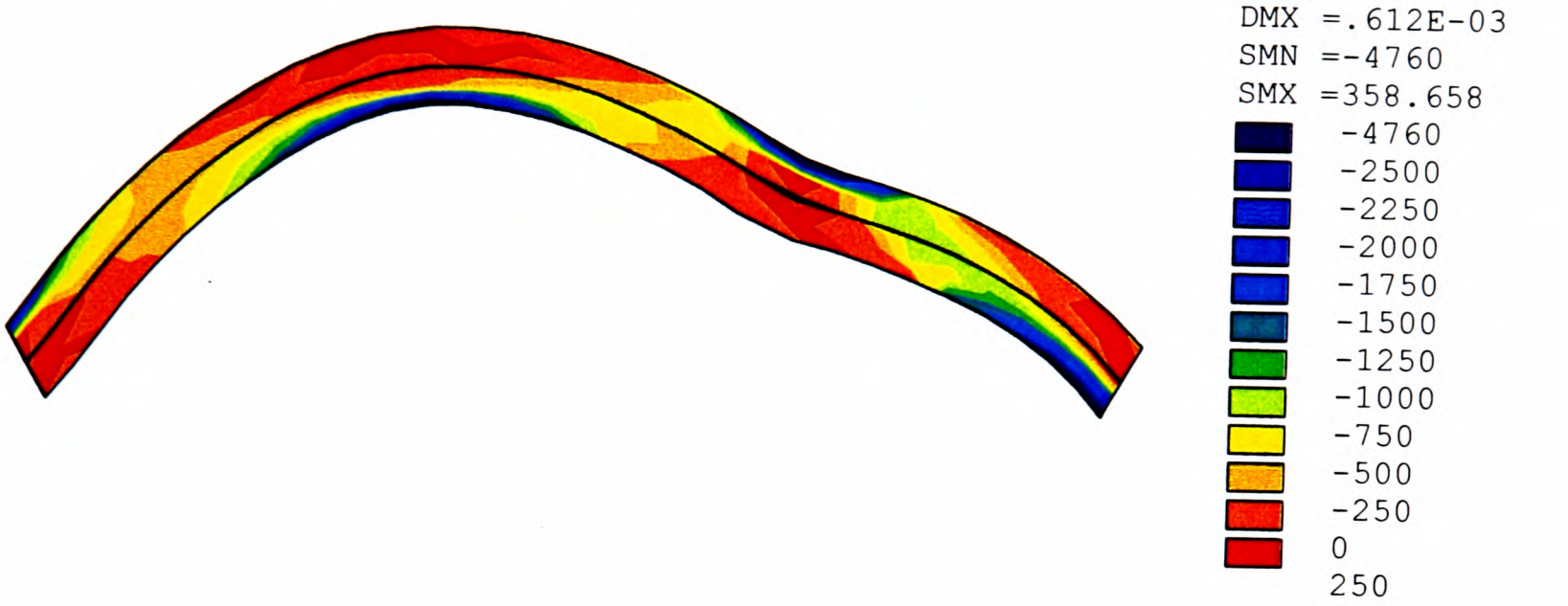

Figure 7.17 Circumferential stress in arch 3-0d at 300.1 kN

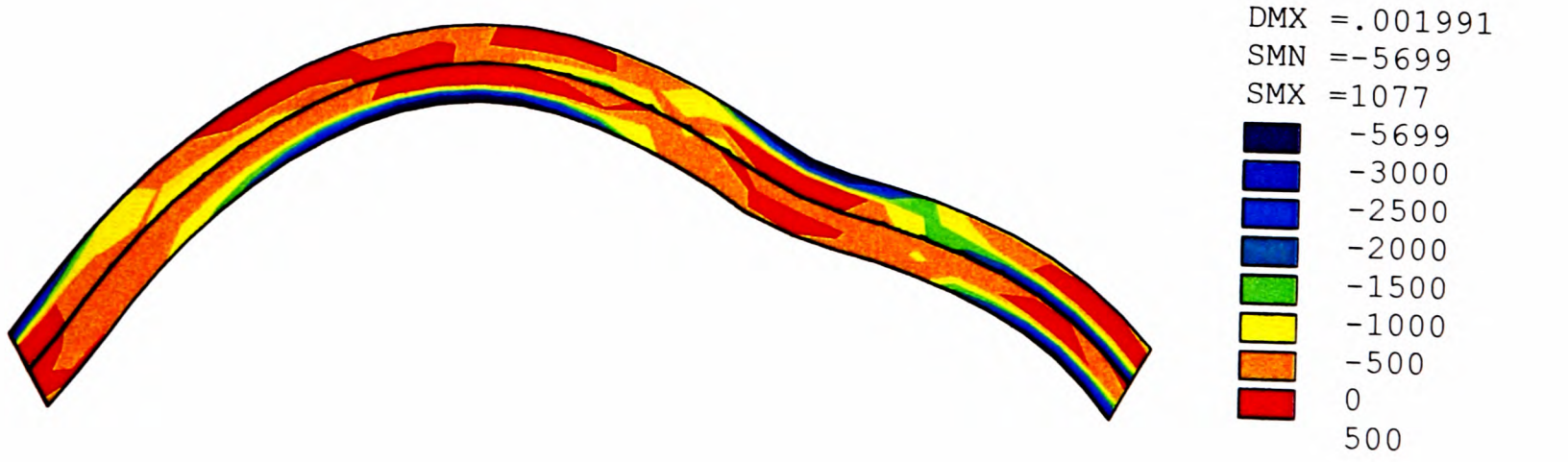

Figure 7.18 Circumferential stress in arch 3-0c at 300.1 kN

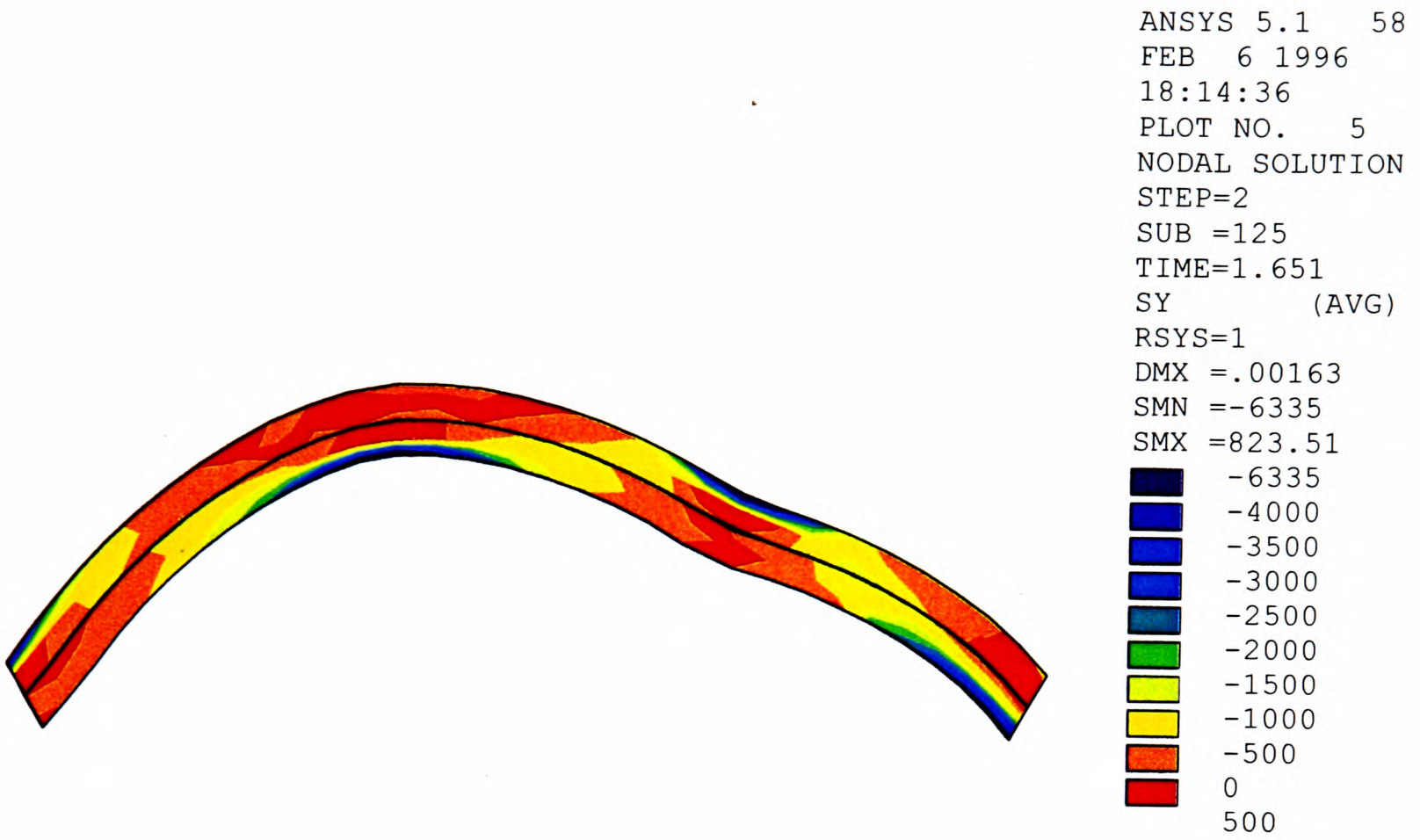

Figure 7.19 Circumferential stress in arch 3-0d at 375.0 kN

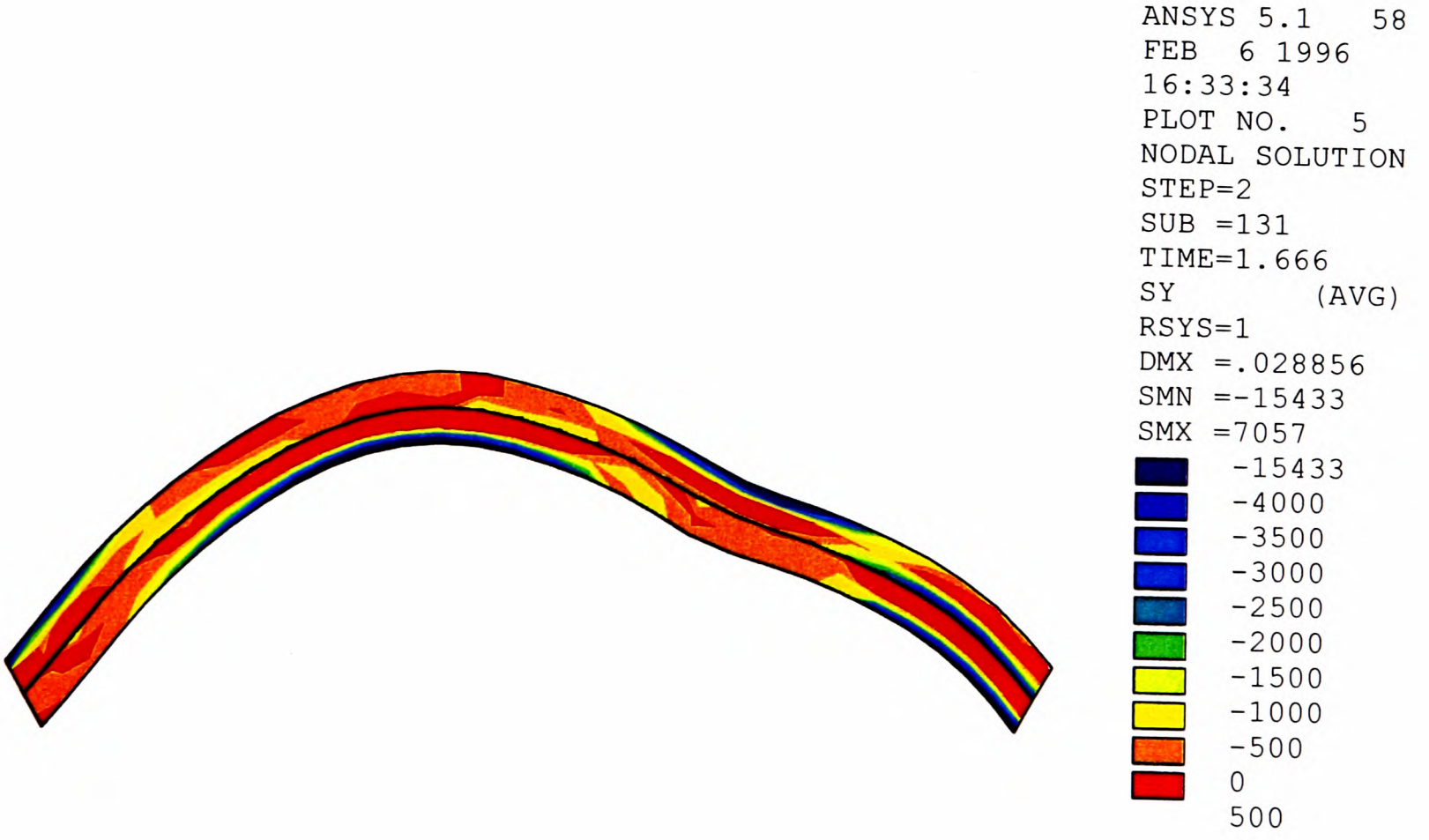

Figure 7.20 Circumferential stress in arch 3-0c at 383.6 kN

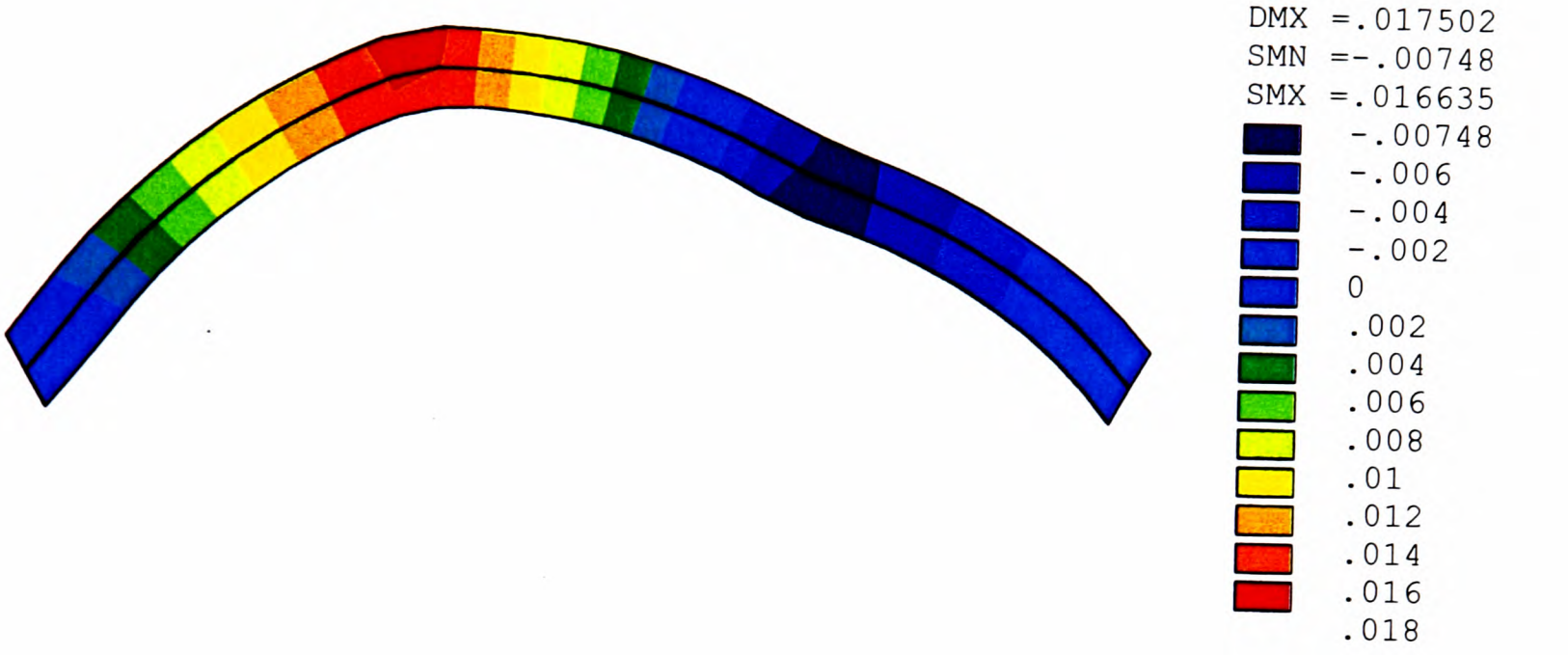

Figure 7.21 Radial deflection of arch 3-0d at 539.1 kN

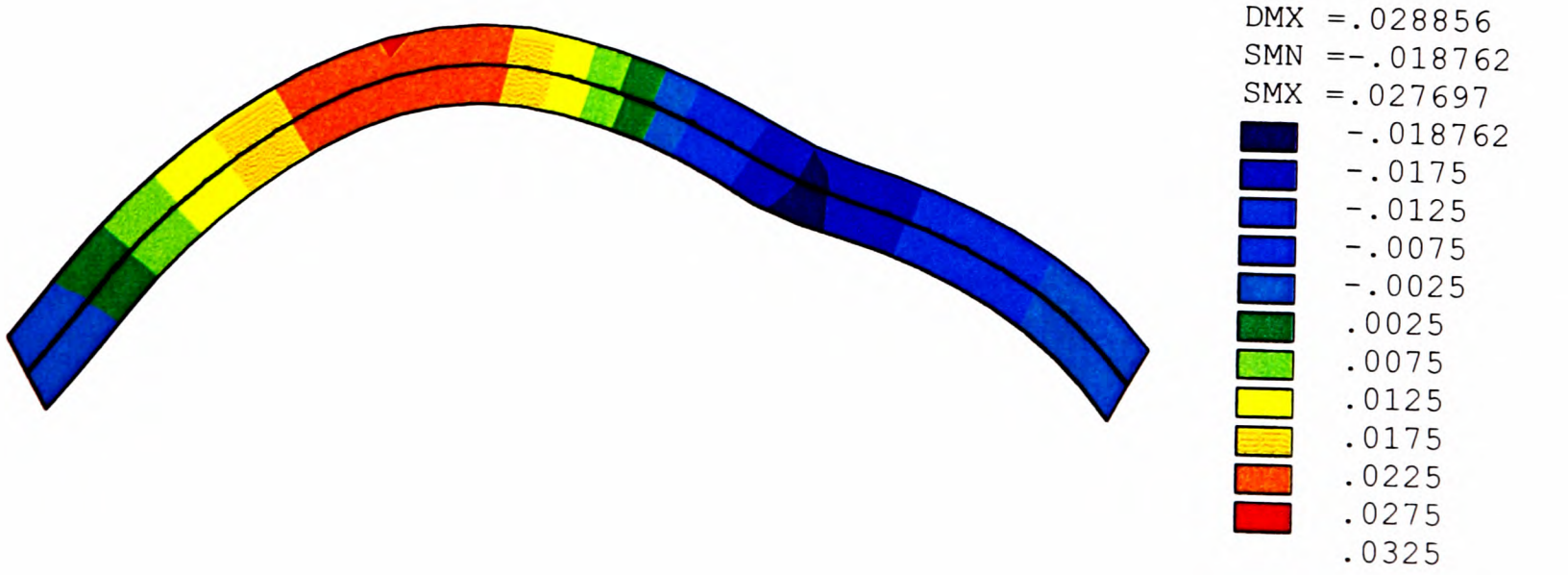

Figure 7.22 Radial deflection of arch 3-0c at 383.6 kN

Figures 7.13, 7.15 and 7.17 show the circumferential stress within bridge 3-0d when the magnitude of the applied load was 150 kN, 225 kN and 300 kN respectively. It can be seen that, at each section, the discontinuity in the stress across the mortar joint becomes more pronounced as the load is increased. This is particularly apparent in the vicinity of the applied load where ring separation was initiated at 280 kN.

Figures 7.14, 7.16 and 7.18 show the circumferential stress within bridge 3-0c when the magnitude of the applied load was 150 kN, 225 kN and 300 kN respectively. It can be seen that as the load was increased tensile failures occurred within each brickwork ring in the vicinity of each hinge. In other words, the finite element analysis predicted a hinged mechanism in which the hinges were diffused. This is in agreement with the predictions of Gilbert (1993). In this FE model the low shear bond strength was sufficient to produce a limited amount of load sharing. The application of the load caused the top ring to deflect. The bottom ring was therefore pushed downwards due to the normal stress between the adjacent brickwork rings. In order to maintain compatibility the left hand side haunch of the bottom ring must deflect upwards and therefore pushed the top ring upwards with it. These regions are the only regions within the arch in which the normal stress across the joint is sufficiently large to enable a reasonable amount of Coulomb friction to be developed so that load sharing is created. In other regions, the normal stresses are small so that each brickwork ring will act independently unless a sufficiently large shear bond strength exists to enable them to act otherwise. Thus, in the absence of the COMBIN40 elements, each brickwork ring within the FE model will act independently and failure will occur at an unrealistically low load.

Figures 7.21 and 7.22 show the radial deflection of each arch at failure. The ring separation within arch bridge 3-0c resulted in its rings acting non-compositely which created the non-uniform deflections.

7.5 Discussion

Figures 7.23 and 7.24 show the results of varying the tensile strength of the brickwork in the FE model of bridges 3-0d and 3-0c respectively. It can be seen that as the tensile strength increases, there is a diminution in the correlation between the results of the finite element analysis and those that were obtained experimentally.

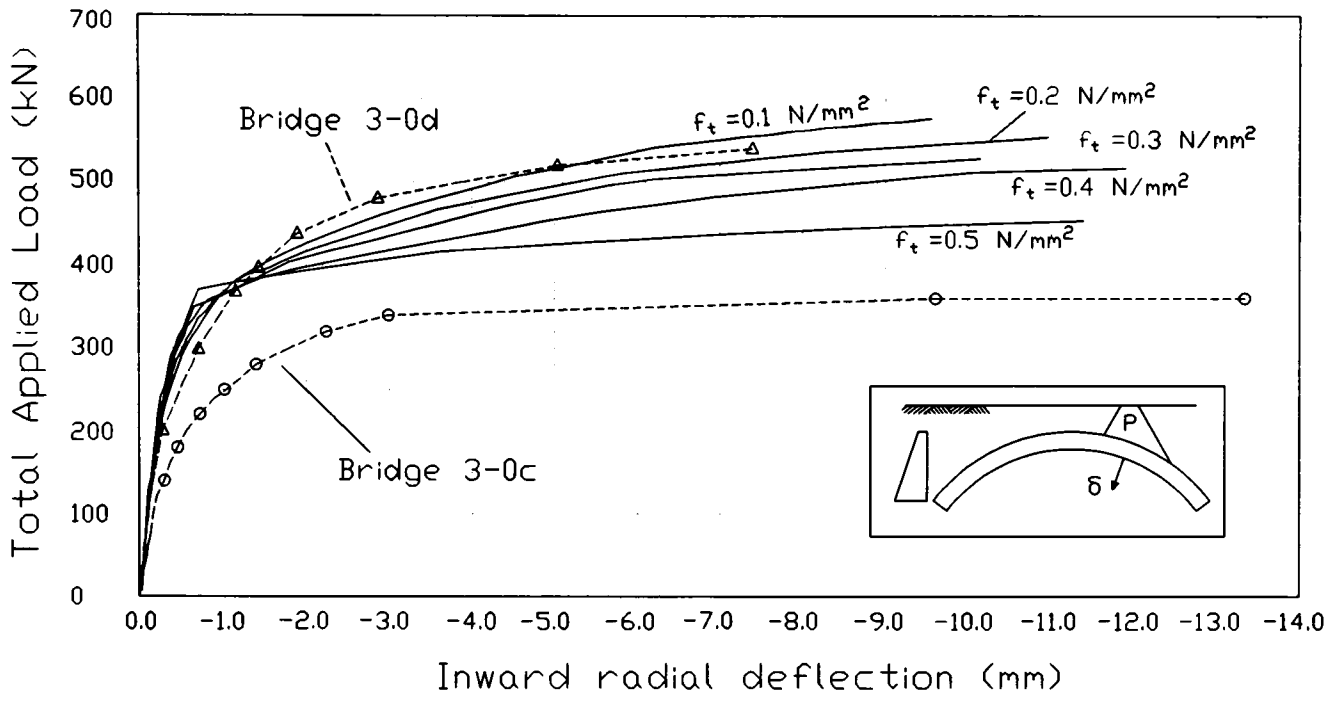

Figure 7.23 The influence of brickwork tensile strength on the FE analysis of Bridge 3-0d

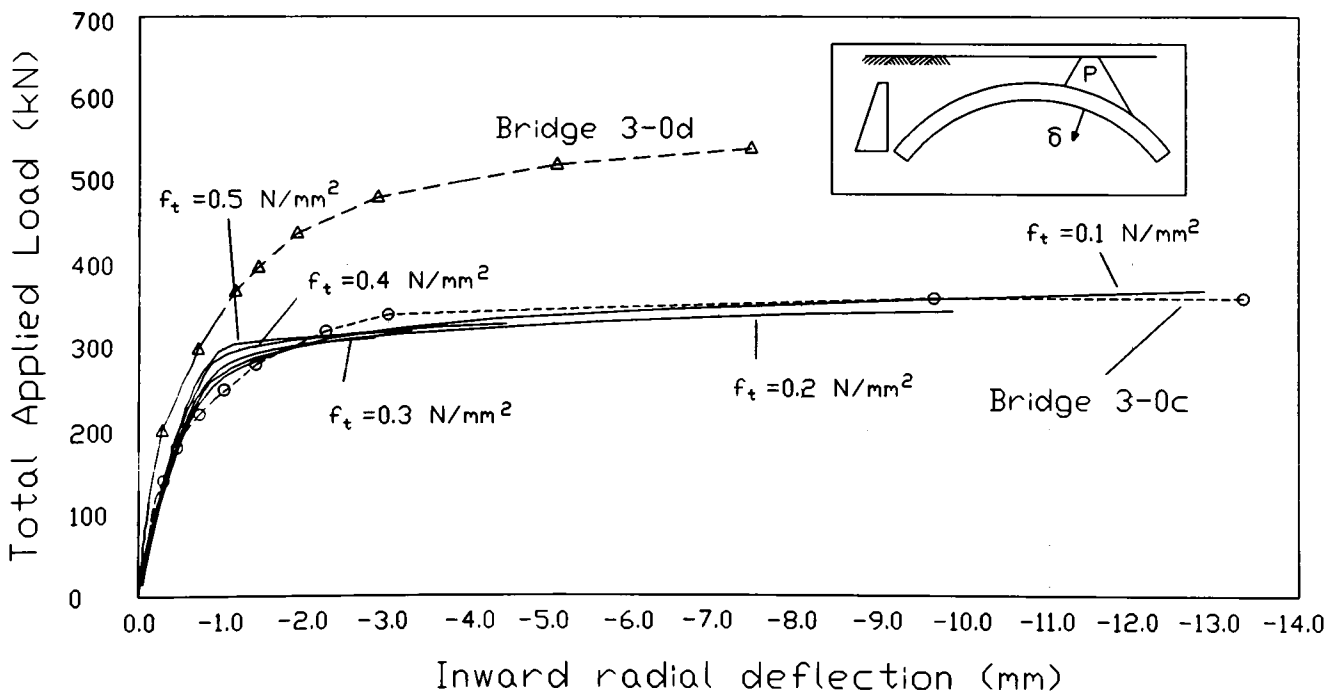

Figure 7.24 The influence of brickwork tensile strength on the FE analysis of Bridge 3-0c

The stiffness of the structure is generally increased by stronger brickwork because the formation of tensile cracks is delayed. In practice, the delayed formation of tensile cracks will often result in catastrophic failures. This was also found to occur in these finite element analyses in which

convergence problems arose when the tensile strength was increased. In other words, the analysis was unable to trace the highly non-linear response of the model, which became more non-linear as the tensile strength was increased. The analyses could only be achieved if the convergence tolerance, see section 7.2, was relaxed and the load was applied in smaller increments.

Figures 7.25 and 7.26 show the results of varying the shear bond strength between adjacent brickwork rings in the FE model of bridges 3-0c and 3-0d respectively.

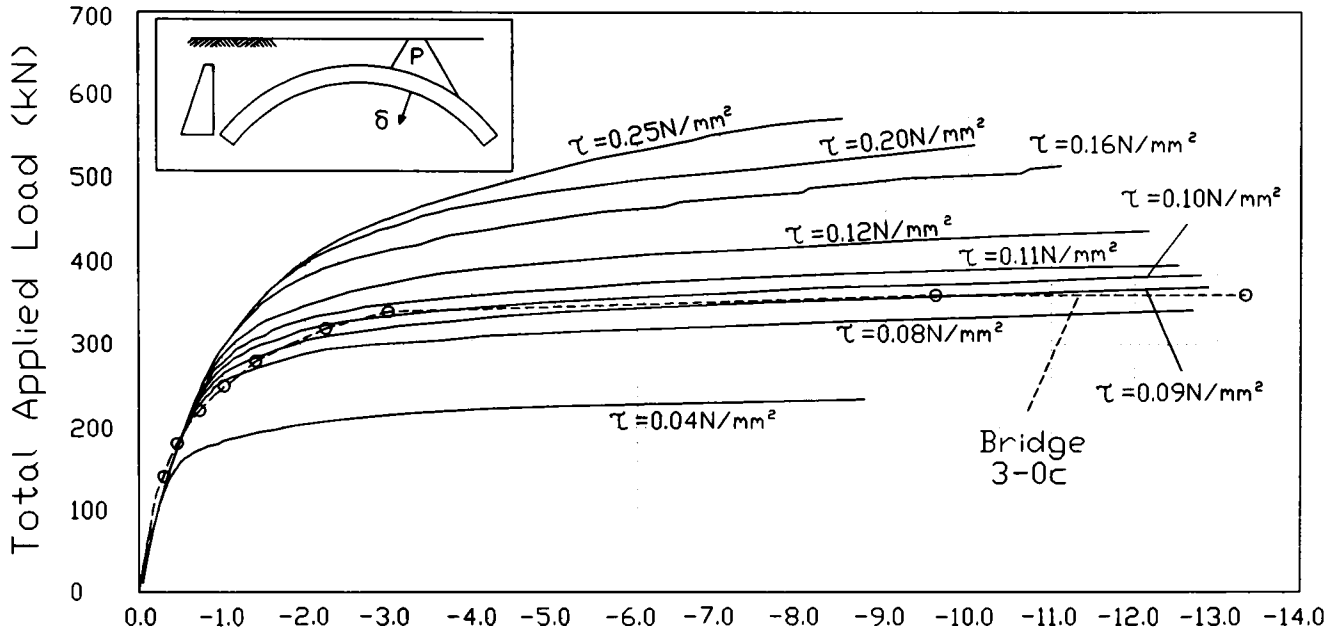

Figure 7.25 The influence of the shear bond strength, τ, on the behaviour of the finite element model of bridge 3-0c

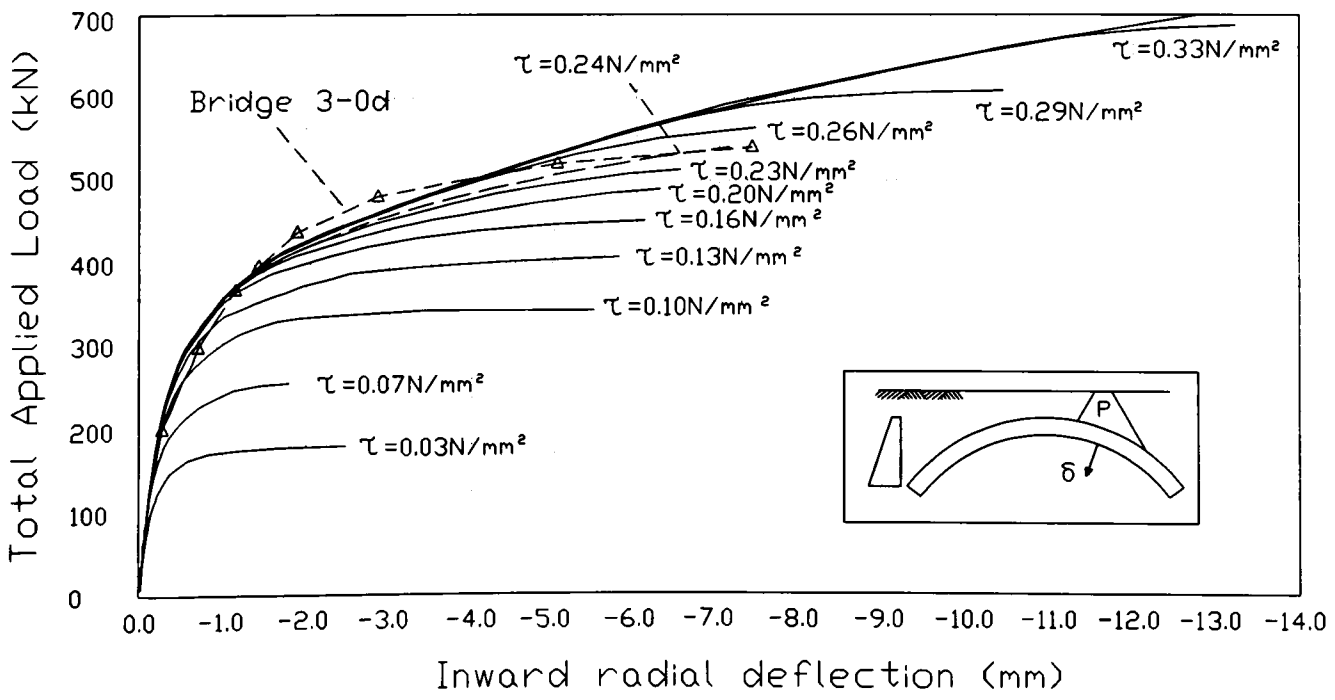

Figure 7.26 The influence of the shear bond strength, τ, on the behaviour of the finite element model of bridge 3-0d

Initially, it can also be seen that a reduction in the strength of the bond between adjacent brickwork rings can dramatically reduce the predicted capacity of an arch bridge, this is shown in figure 7.27. This is reasonable because if ring separation occurs, the brickwork rings must begin to act non-compositely so that they are less able to resist the applied load.

The relatively high initial stiffness of the mortar bond in the model of bridge 3-0d makes it difficult for the analysis to converge when the strength of the mortar has been overcome. Thus, the post-ring separation part of each load-deflection response shown in figure 7.26 is relatively short. In contrast, the post-ring separation part of each load-deflection response of the bridge 3-0c models, shown in figure 7.25, is relatively long. This is analogous to the corollary of the work of Stöckl and Hofmann in that brickwork built with higher strength mortars will exhibit increasingly more brittle failures.

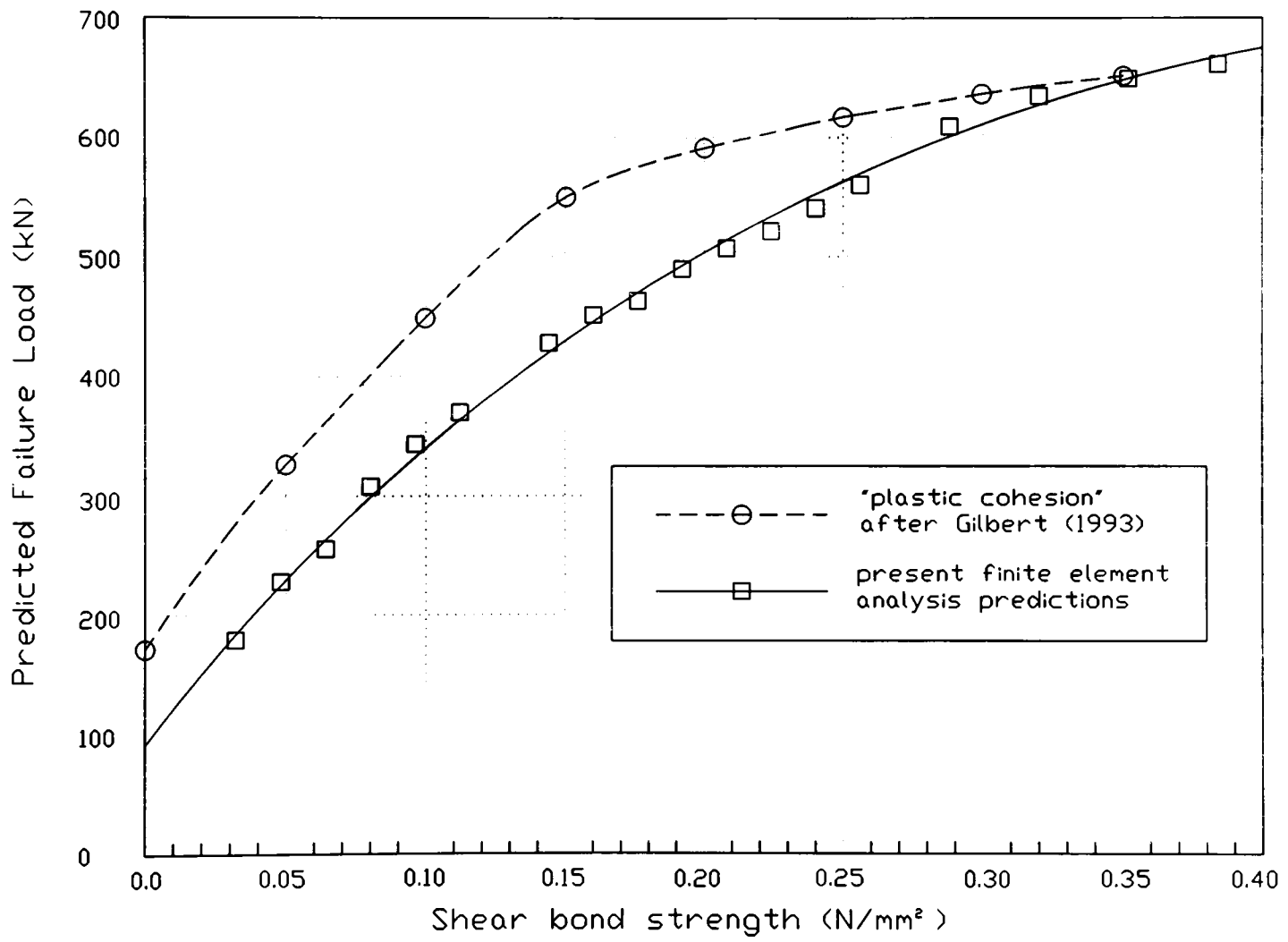

Figure 7.27 Predicted capacity of bridge 3-0d versus shear bond strength

It can also be seen that the bond strength does not appear to influence the stiffness of the structure until ring separation begins to propagate through it. The behaviour of the "ring separation" model (in which its unrealistically high shear bond strength was 1.6 N/mm^2), shown in figure 7.6, defines the underlying load-deflection response of the finite element model of bridge 3-0d. A reduction in the shear strength of the mortar bond will only affect the point at which the load-deflection response of the model departs from that of the almost perfect "ring

separation" model. However, beyond this point the stiffness of the structure is greatly reduced since the brickwork rings begin to act non-compositely.

The relationship between the predicted capacity and the shear bond strength, shown in figure 7.27, was produced by carrying out multiple analyses on the FE model of bridge 3-0d. A parabolic curve was fitted through the results of these analyses from which the actual value of its shear bond strength can be seen to be 0.23 N/mm^2. It can be seen that a 10% error in selecting this value will produce only a 5% error in the predicted capacity. In contrast, the "plastic cohesion" model (Gilbert, 1993) predicts that the shear bond strength of bridge 3-0d must have been 0.15 N/mm^2. It is suggested that the inability of Gilbert's model to incorporate the elasticity of the bond would account for some of this discrepancy whilst the differences in the representation of the backfill may account for the remainder.

The unpredictable and probably highly variable nature of the bond strength within most in-service arch bridges would result in it being very difficult to assess their load carrying capacity. However, it is suggested that the properties used in the analysis of bridge 3-0d may not be too dissimilar to those of a particular in-service arch bridge provided that it is similarly well maintained.

A close correlation was found between the measured shear bond strength, i.e. 0.25 N/mm^2, and the value obtained from the present finite element analyses, i.e. 0.23 N/mm^2. Furthermore, the present finite element model possessed similar load-deflection characteristics as the actual bridge. Therefore, the accuracy of the proposed model is confirmed. Furthermore, if the properties that are assumed are not exact the analysis will not be excessively inaccurate.

Figures 7.28 and 7.29 show the results of varying the stiffness of the bond between adjacent brickwork rings in the FE model of bridges 3-0c and 3-0d respectively.

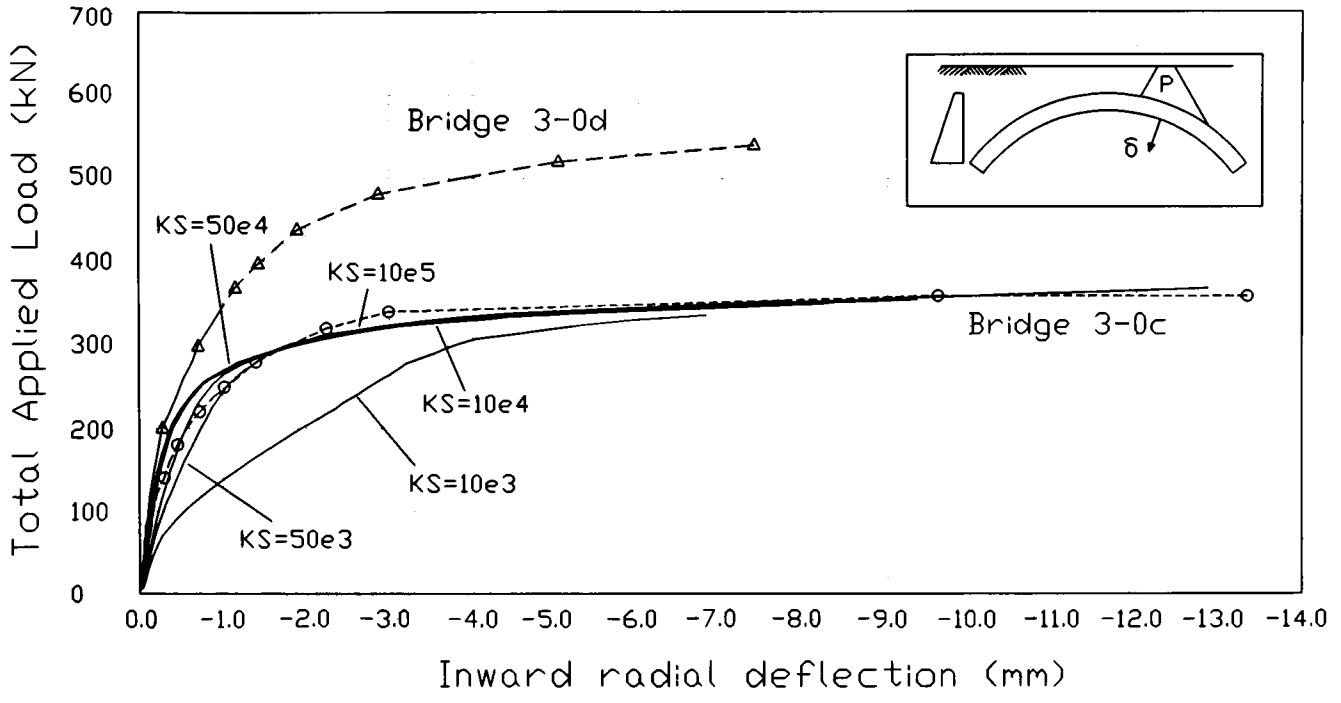

Figure 7.28 The influence of the stiffness of the mortar bond, KS, on the behaviour of the finite element model of bridge 3-0c

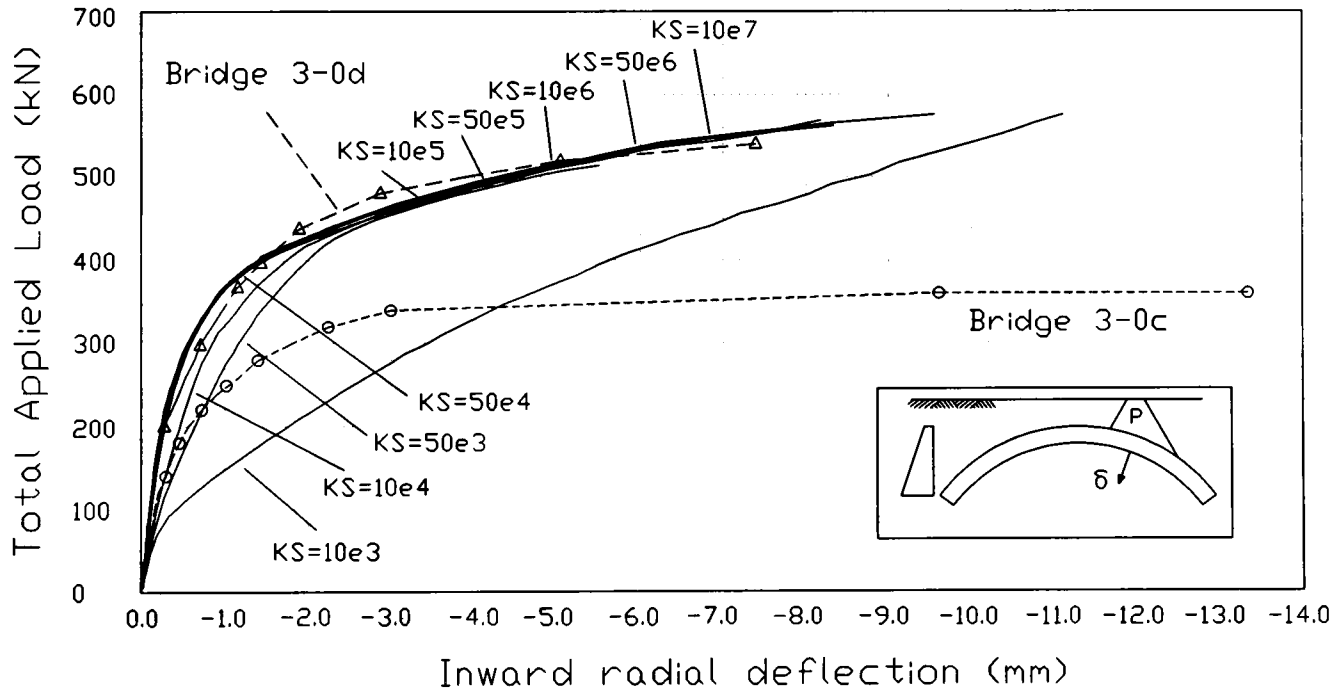

Figure 7.29 The influence of the stiffness of the mortar bond, KS, on the behaviour of the finite element model of bridge 3-0d

It can be seen that small changes in the stiffness of the mortar bond have a pronounced effect on the behaviour of the model when its initial value is relatively low. However, when the stiffness of the mortar bond is already relatively high, an increase in its value will have a negligible effect on the overall stiffness of the arch. This is reassuring because it indicates that any value of stiffness within an order of magnitude of the value that was used in the model of bridge 3-0d will probably be applicable to most in-service arch bridges. Moderate changes in

its value will not produce significant changes in the behaviour of the finite element model.

It can be seen that the load-deflection response of the "ring separation" model shown in figure 7.6 was highly non-linear despite the exceptionally high value of the shear bond strength between its brickwork rings. It can be seen in figure 7.29 that a decrease in the stiffness of the mortar bond will affect a decrease in the initial stiffness of the structure but, each load-deflection response converges towards that of the "ring separation" model. Only the point at which the two load-deflection responses become similar is affected by the stiffness of the mortar bond.

The stiffness of the mortar bond can create the effects of ring separation without its strength being exceeded because a low stiffness permits the occurrence of excessive shear movements of one ring relative to another.

Additionally, there is a threshold value of the bond stiffness above which any value will produce a load-deflection relationship that is similar to that of the "ring separation" model shown in figure 7.6.

The finite element model of bridge 3-0d behaved in a way that was similar to that of the actual bridge. This is because the assumed behaviour of the backfill within this finite element model was similar to its actual behaviour. However, figure 7.30 shows the results of varying the magnitude of the total horizontal passive pressure in the FE model of bridge 3-0d.

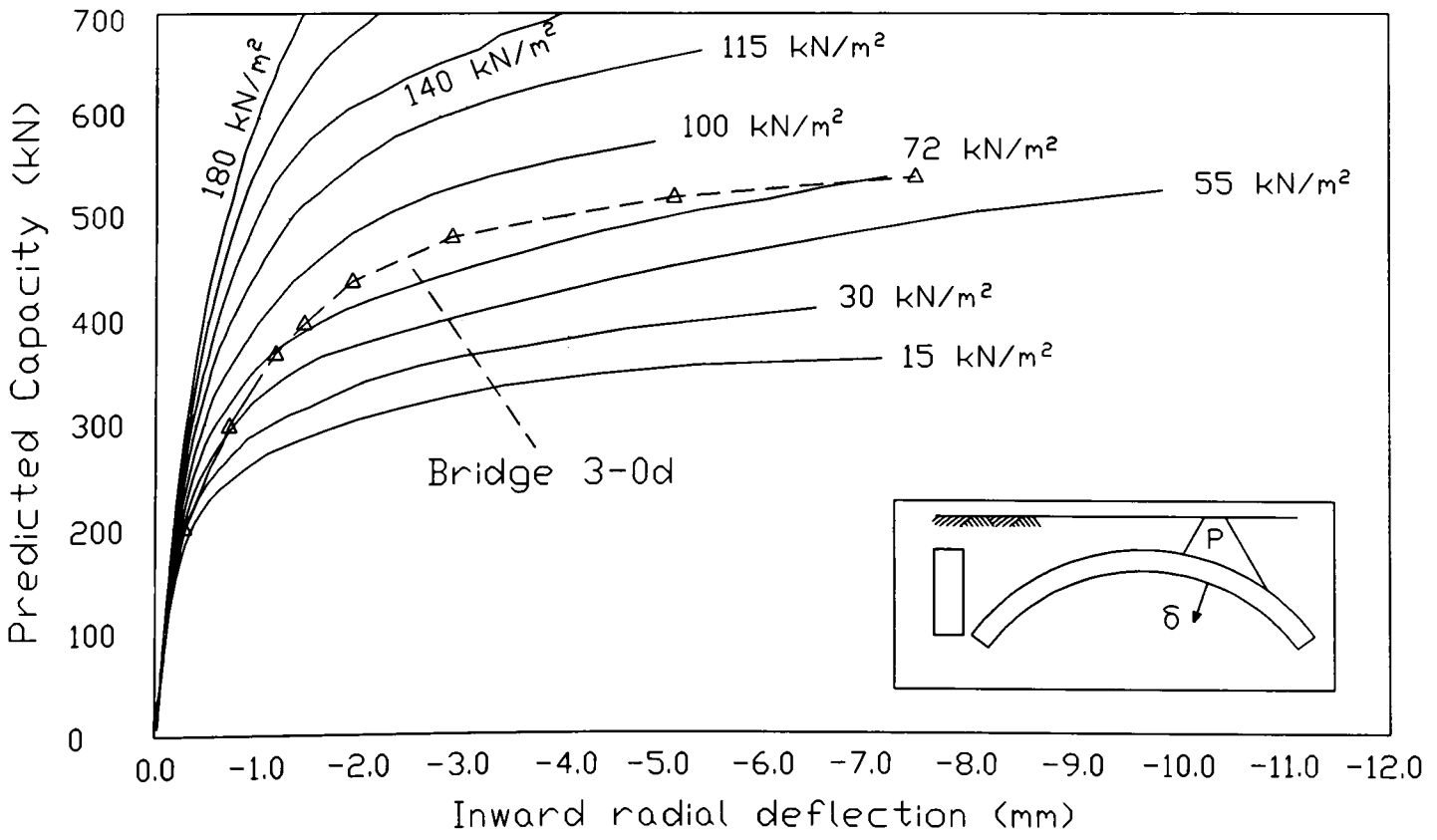

Figure 7.30 The influence of passive pressure on the behaviour of the finite element model of bridge 3-0d

In order that comparisons could be made, the "Rankine" passive pressure distribution was replaced by a rectangular pressure block as proposed by Gilbert (1993). The magnitude of the passive pressure was varied and the finite element model was repeatedly reanalysed. However, it is pointed out that this passive pressure distribution is as equally incorrect as the hydrostatic pressure distribution proposed by Rankine (1862). In reality, the ambient pressure on the passive side of the arch is a combination of a "Rankine" at-rest distribution and that produced by compaction, upon which the increase produced by the deformation of the arch is superimposed. However, the parametric studies will serve to illustrate the significant contribution of the backfill towards the stiffness and strength of a masonry arch bridge.

Figure 7.31 shows the predicted capacity of arch bridge 3-0d as a function of the magnitude of the rectangular passive pressure block. The relationships were developed either from the results of the finite element analyses presented in figure 7.30 or from the analyses of the mechanism model proposed by Gilbert (1993). The inherent assumption in each relationship is that the deformation of the arch and the confinement of the backfill will enable these passive pressures to be mobilised. However, figure 7.31 successfully reveals that the backfill can stabilise the arch so that it can significantly increase the ability of the structure to sustain an applied load.

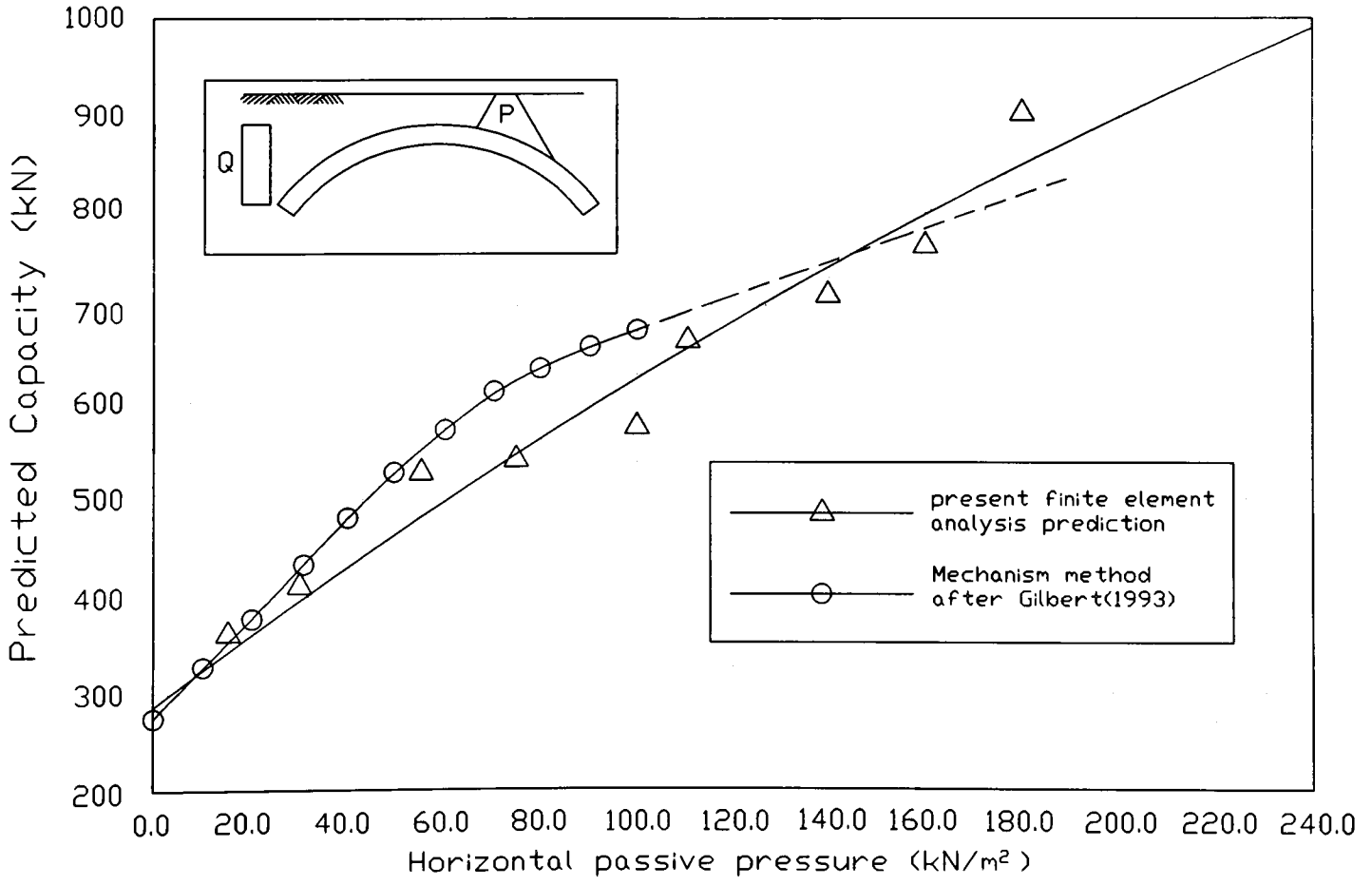

Figure 7.31 Magnitude of passive pressure versus predicted failure load of arch 3-0d

It can be seen that the predictions of each model are similar to each other. However, Gilbert's predictions are generally higher than those of the present finite element analyses. Not withstanding the differences in the modelling of ring separation, it is suggested that the

differences in the predicted load capacity may be attributable to the way in which the load was dispersed through the backfill. Gilbert dispersed the load through the backfill at 45° and applied the load uniformly whereas the load dispersal used in the present finite element analyses was, as shown in section 7.4.1, based on experimental observations described in section 4.4.1. Thus, in the latter case the load is more concentrated towards the middle of the distribution so that more onerous effects will be produced thus leading to lower predicted arch capacities than the method adopted by Gilbert.

Figure 7.32 shows the effects of varying the angle of load dispersal on the behaviour of bridge 3-0d. In each case, the load was dispersed through the backfill as depicted in figure 7.8.

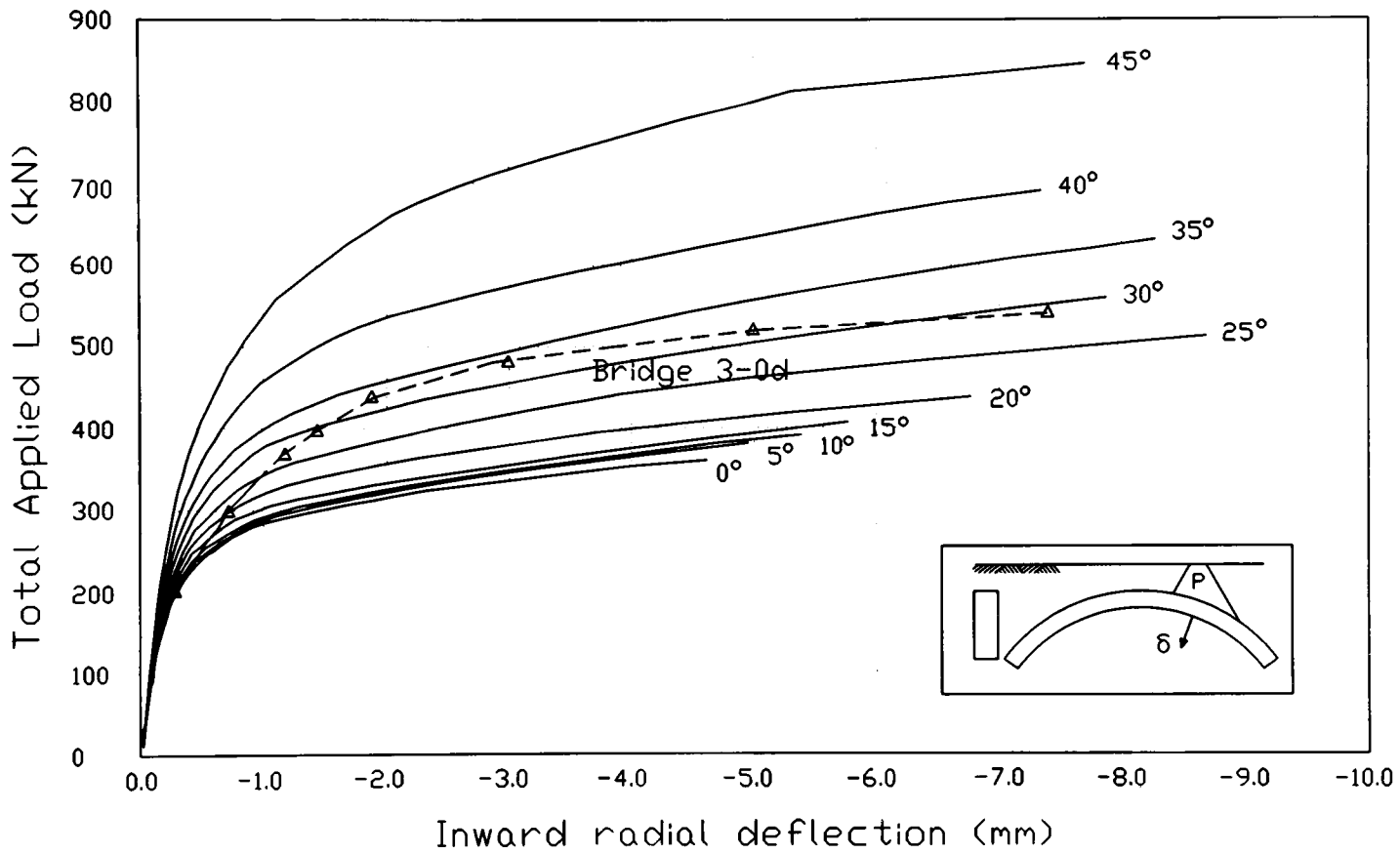

Figure 7.32 The influence of the angle of load dispersal on the behaviour of the finite element model of bridge 3-0d

Figure 7.33 shows the predicted capacity of this bridge as a function of the angle of load dispersal. The relationship was developed from the results of the analyses presented in figure 7.32. It can be seen that there is a significant increase in the capacity of the arch as the angle of load dispersal is increased. A more concentrated load, produced by steeper load dispersal lines, initiated ring separation at an earlier load. Thus, the capacity of the arch was reduced by a concentrated load. Furthermore, it can be seen that the load dispersal angle that is most appropriate for arch bridge 3-0d is of the order of 30° which confirms the experimental value obtained in section 4.4.1.

It is perhaps a little disappointing that the equivalent parametric study carried out by Gilbert (1993) was done in the absence of horizontal passive pressures so that comparisons are not possible. However, each load dispersal method produced an increase in the predicted capacity of the arch as the angle of load dispersal is increased, the method adopted by Gilbert appears to create only a slight increase although this relationship may become more non-linear if passive pressures are included.

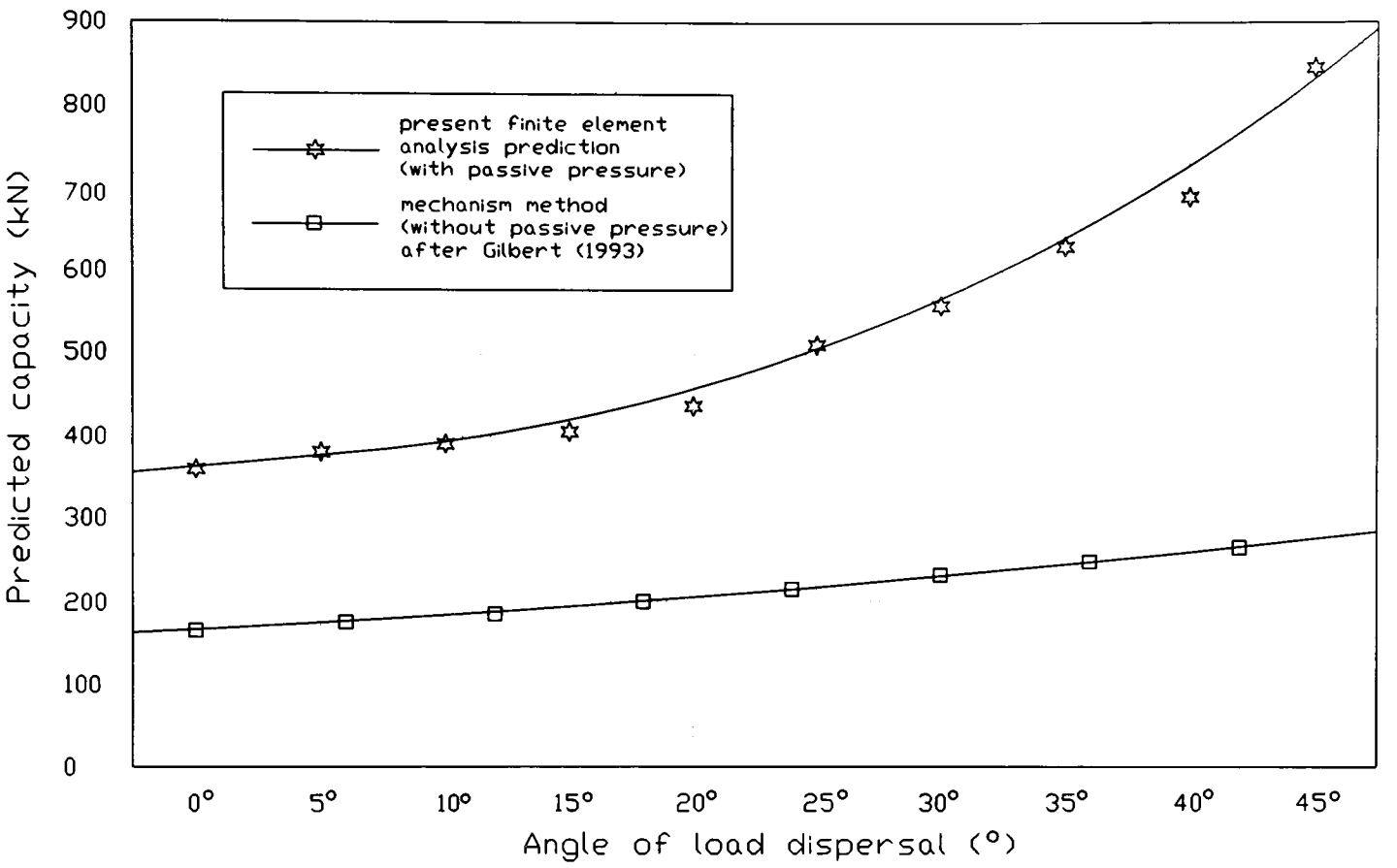

Figure 7.33 Angle of load dispersal versus predicted failure load

Thus, the backfill has been identified as a major contributory element. However, in retrospect, it is therefore possible for inaccuracies accrued in dispersing the applied load to be compensated by inaccuracies in applying passive pressures. It is also possible for each of these to compensate for deficiencies in the model of the arch. The finite element model presented herein is based on actual measured material properties and therefore possesses realistic load-deflection characteristics that are similar to those of the actual bridge. Thus, the proposed modelling of the arch is correct. However, in order to avoid criticisms of self compensating errors in the representation of the backfill, the sinusoidal load dispersal method, adopted herein, was experimentally verified. Therefore, a realistic passive pressure distribution could be assumed rather than selecting it arbitrarily so that it created realistic results.

7.6 The three-dimensional analysis of multi-ring brickwork arch bridges

7.6.1 The square span arch

In order to analyse a three-dimensional structure using a finite element model of the form presented in section 7.4 it is necessary to use a three-dimensional array of SOLID65 elements. The model which was only a single element wide was essentially two-dimensional, although it required two sets of gap elements at each radial section. It would therefore not produce a sufficiently accurate analysis of an arch bridge when it is subjected to eccentric patch loads, or when spandrel walls are included, or when the structure is skewed. Furthermore, ANSYS does not contain an appropriate single gap element that can be used to model the breakdown of composite action and allow relative sliding movements to occur in an arbitrary direction. However, in the two-dimensional model, this deficiency was overcome whereas in the three-dimensional model this deficiency may be surmountable but would require more complex treatment.

In a finite element model, adjacent brickwork rings can be prevented from overlapping each other by a variety of means. However, it is not quite so easy to model their relative sliding movement. ANSYS contains several generic one-, two- and three-dimensional gap elements which can prevent overlapping as well as perform other functions. The two-dimensional CONTAC12 element appears to be useful since it can resist compression in the direction normal to the joint (within its two-dimensional plane of application). It can also create a limited amount of composite action since it can resist shear movements provided that the normal force within it is sufficiently large. However, its two-dimensional nature precludes its use in a three-dimensional model because, unless it was fortuitously defined in a plane that is parallel to the principal stress, it would only resist a component of this stress, the other component would create unrestrained movement in the perpendicular direction. The corresponding three-dimensional element, viz. CONTAC52, will orient itself in the direction of principal stress but, like the CONTAC12 element, it cannot create a sufficient amount of composite action through friction because, within the arch, there is not a sufficiently large normal force between the brickwork rings. Neither of these elements can model the shear bond strength between the mortar and the brickwork rings. Therefore they are of no use except for preventing adjacent elements moving through each other.

The only gap element, within ANSYS, that can directly model the shear bond strength between the brickwork rings appears to be the one-dimensional COMBIN40 element. Its one-dimensional nature means that it will be susceptible to the above problem regarding its orientation relative to the orientation of the principal stress. However, it may be possible to define several of these elements so that, in combination, ring separation may be modelled

successfully without it causing the model to become unstable.

In order to illustrate the difficulties associated with using one-dimensional COMBIN40 elements in a three-dimensional model, first consider the square span arch that is subjected to a full width patch load and whose spandrel walls are detached from it. It has already been shown that the two-dimensional nature of this problem can be adequately represented by a two-dimensional model, as presented in section 7.4. In this model, a COMBIN40 element was defined in the circumferential and transverse direction at each interface node. However, the transverse gap elements were not required because they were found to carry no force; this was not by chance. The geometry of the structure and the nature of the applied load were such that the principal stress was parallel to the circumferential COMBIN40 elements. Furthermore, the relative stiffness and strength of each circumferential COMBIN40 element along a particular row was such that the direction of the principal stress was not altered by them. In other words, along each row, the force within one COMBIN40 element was the same as in the other and each would fail during the same load increment. Thus, their orientation relative to the orientation of the principal stress remained correct throughout the analysis.

Significant problems arise if the finite element model is extended to comprise several SOLID65 elements across its width because the number of sets of COMBIN40 elements must also increase. In this case, the determination of their relative stiffness and strength is no longer straight forward. Suitable values must be obtained so that, at each load increment, the extension of each COMBIN40 element along a particular row must be the same and, furthermore, the load increment at which each fails must also be the same. Otherwise, the behaviour of the structure will be forced to become three-dimensional and the analysis will be incorrect. This will probably be as a result of the incorrect definition of the COMBIN40 elements preventing the occurrence of ring separation. The selection of the stiffness and strength parameters requires an iterative approach which has been found to take a considerable length of time to produce values which, ultimately, yield similar results as the two-dimensional model, when the loading is essentially two-dimensional as stated earlier. The difficulties associated with obtaining suitable stiffness and strength parameters stem from the fact that the relative values of each parameter along a particular row will vary from one row to the next.

Figure 7.34 contains the results of a three-dimensional finite element analysis of bridge 3-0d in which five SOLID65 elements were used across its 2.88 m width. It appears that the behaviour of the model was two-dimensional, as anticipated. However, the analysis did not terminate at the correct failure load; it continued until the maximum load of 595 kN was applied. A closer inspection of the deformed shape of this bridge under the maximum applied load, as shown in figure 7.34, indicates that its behaviour was not exactly two-dimensional.

It took a considerable length of time to adjust the stiffness and strength of each set of COMBIN40 elements so that the analysis could converge towards the actual measured behaviour of the bridge. The slight three-dimensional behaviour of the model was due to the stiffness and strength of each one-dimensional COMBIN40 element being (marginally) incorrect. Thus, ring separation was not as extensive as it should have been. However, the exercise was useful in verifying that a three-dimensional analysis of this structure when subjected to the full-width loading is neither practical (when it involves cumbersome one-dimensional elements) nor necessary. A two-dimensional analysis was more accurate, less expensive, and quicker to perform.

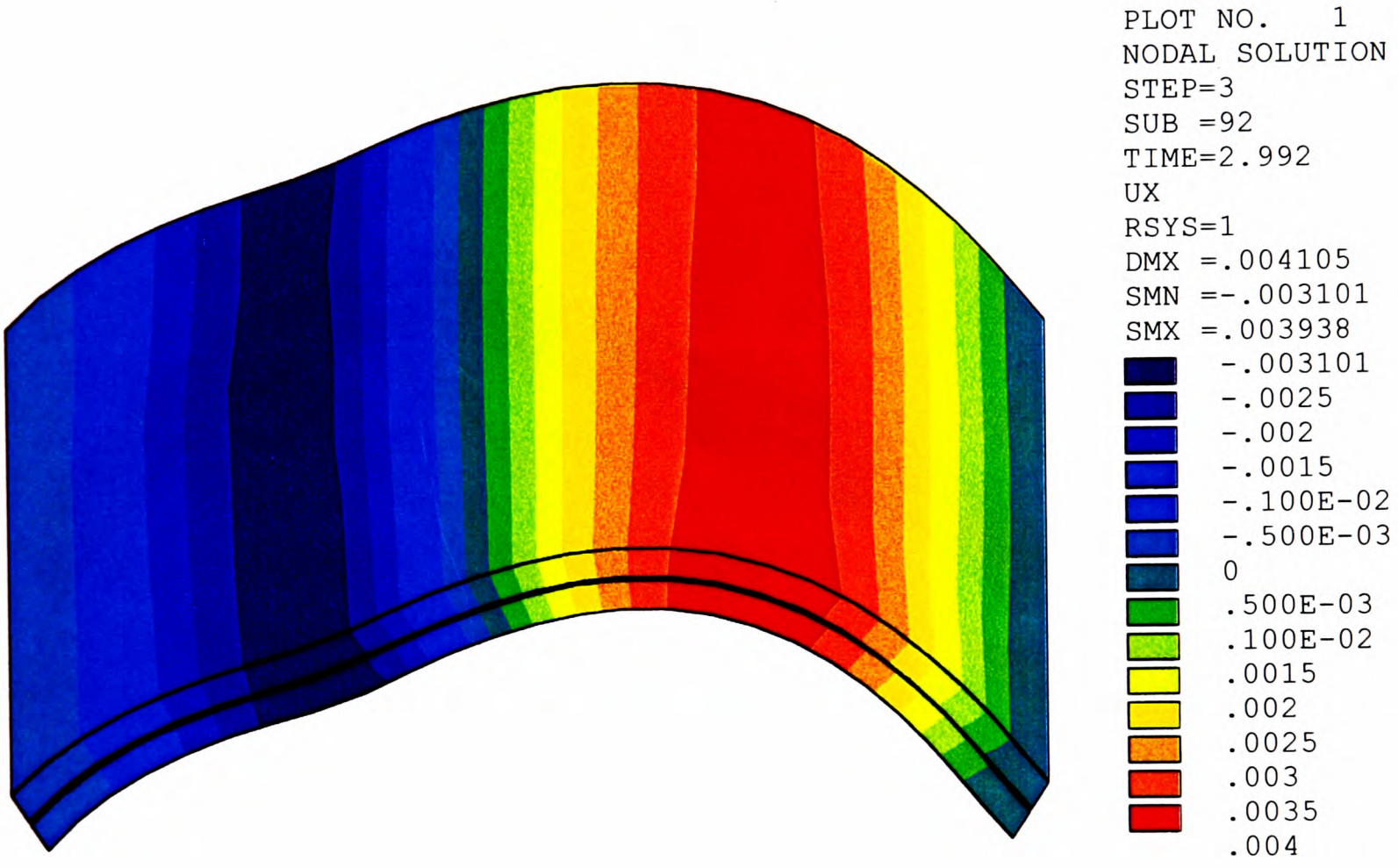

Figure 7.34 Deflected shape at failure of the three-dimensional model of bridge 3-0d

It is perhaps useful, at this stage, to present the results of a three-dimensional analysis of the above model in which COMBIN40 elements were omitted. In other words, the two brickwork rings acted independently of each other except for the small amount of load sharing that could be generated by Coulomb friction. The behaviour of this model was more two-dimensional than the model in which COMBIN40 elements were used. However, the analysis could not proceed beyond time $=1.15$, i.e the model could only sustain 15% of the 600 kN live load.

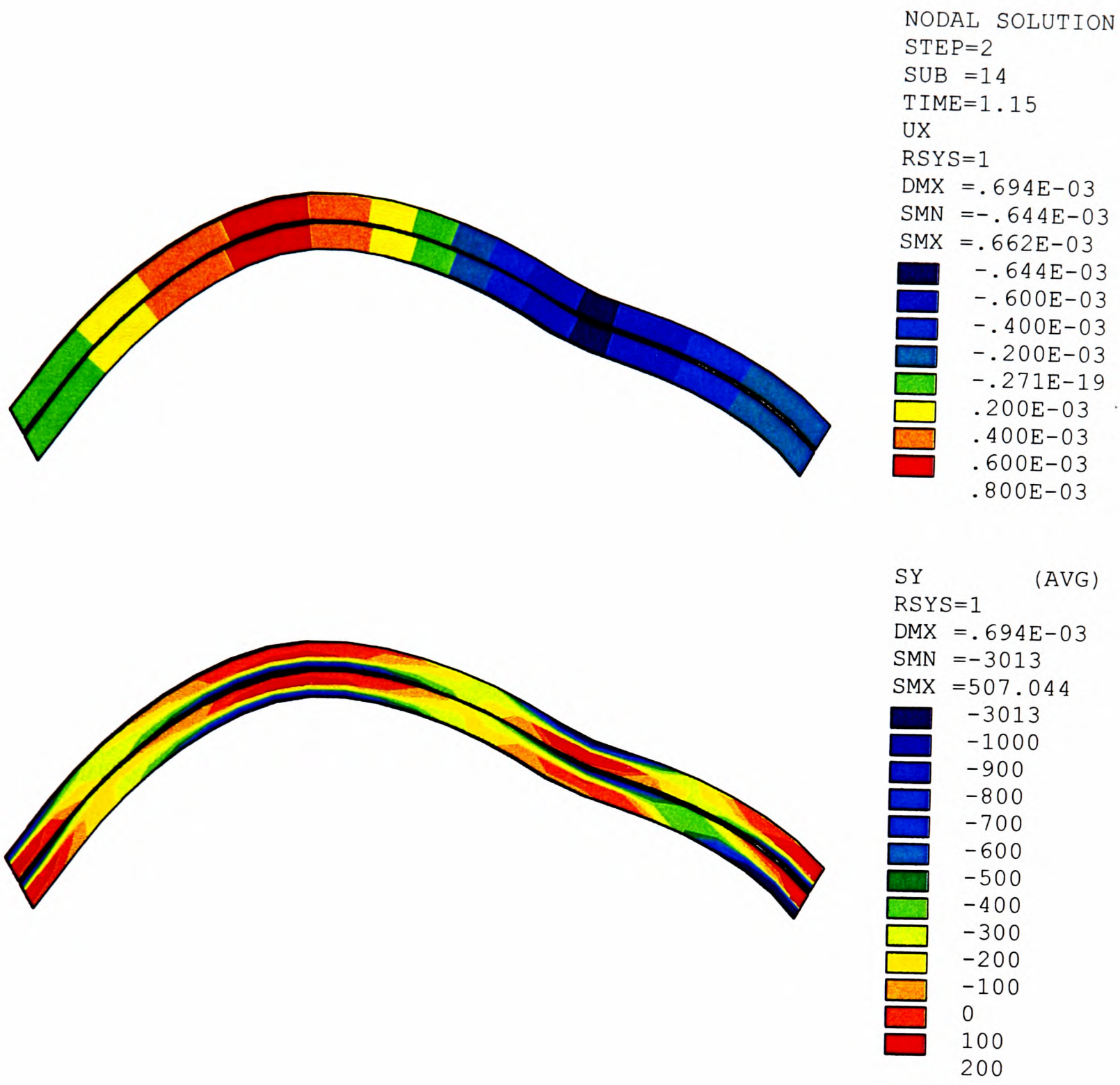

Figure 7.35 The behaviour of a multi-ring square arch (without shear bond strength) at 90 kN

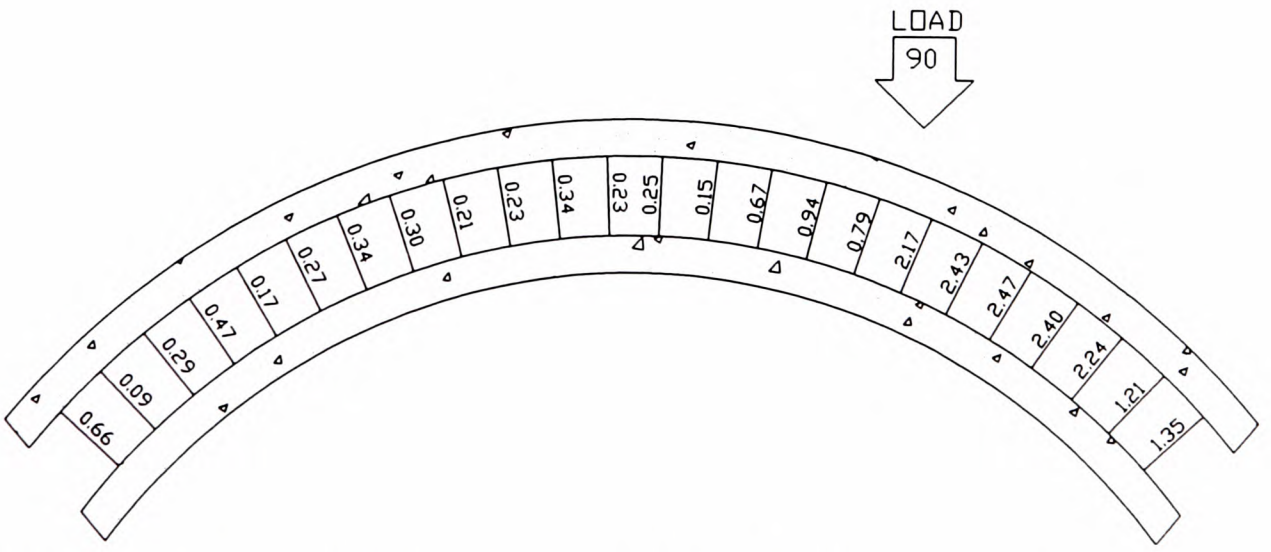

Figure 7.36 Normal force (kN) between the brickwork rings of the above FE model

Figure 7.35 contains the radial deflection of the arch and the circumferential stress within it during the last converged sub-step of the analysis, i.e. when the magnitude of the applied load was 90 kN. Figure 7.36 shows the average normal force between its brickwork rings.

Due to the independent behaviour of the brickwork rings, the distribution of circumferential stress was very much different to that of the FE model of bridge 3-0c, shown in figure 7.12, whose brickwork rings acted non-compositely but were able to generate a small amount of load sharing because of the assumed shear bond strength of the damp sand layer. It can be seen in figure 7.35 that tensile failures had occurred in each ring in the vicinity of each hinge and were accompanied by areas of relatively large compressive stresses in each ring. Compressive failures occurred during the next sub-step which caused the arch to collapse, i.e the analysis could not converge.

The values of the normal force between the brickwork rings were obtained by interrogating the results of the analysis to obtain the force within each CONTAC12 element. It can be seen that even the largest normal force, i.e 2.47 kN (which is equivalent to 35 kN/m^2), was not sufficiently large to enable friction to prevent the rings sliding relative to each other. Thus, it is essential that an element such as a COMBIN40 element is used so that the shear bond strength between the brickwork rings can be incorporated into the analysis.

Not withstanding the problems encountered when a three-dimensional model is used to analyse a two-dimensional behaviour, further problems are encountered when COMBIN40 elements are used in a three-dimensional model that is used to analyse a structure that, either due to its geometry or to its loading, will produce a three-dimensional behaviour. These modelling problems are large but may not be insurmountable. The ability of the two-dimensional model, presented herein, to incorporate ring separation was a significant achievement. The nature of this surface to surface contact problem is by no means simple which is probably why, to date, most FE researchers, with the exception of Choo et al. (1992), have avoided the problem. However, the model presented in section 7.4 can be extended into three-dimensions in order to investigate the effects of ring separation in a skewed arch or indeed, in combination with any other three-dimensional effect. The problems associated with its extension are due to the fact that either a combination of gap elements are required or additional procedures are necessary because, even the most sophisticated (arguably) commercial finite element analysis package viz. ANSYS, does not posses a single three-dimensional gap element that will perform the desired functions.

7.6.2 The multi-ring brickwork skewed arch

Figure 7.37 shows the proposed finite element model of skewed arch bridge 3-4. This model comprised two three-dimensional arrays of SOLID65 elements that were held together by a two-dimensional array of gap elements. It can be seen that the model comprised no fewer than five SOLID65 elements across its width and therefore required six sets of gap elements at each transverse section.

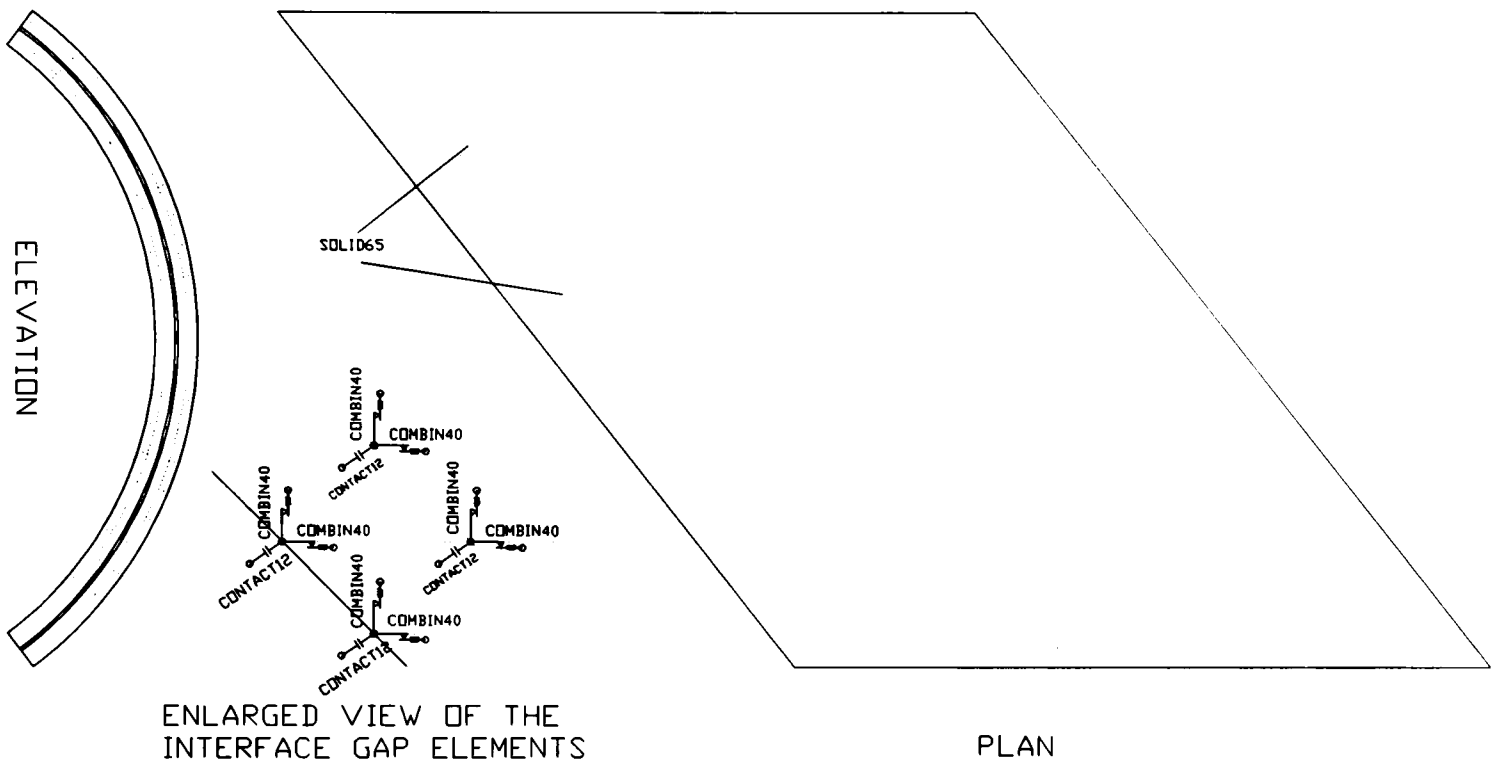

Figure 7.37 Finite element model of multi-ring brickwork skewed arch bridge 3-4

An attempt was made to model composite behaviour and its breakdown, as in the two-dimensional model presented in sections 7.4 and 7.6.1, by using a triad of essentially one-dimensional gap elements at each node within the interface. A CONTAC12 element was used to prevent the brickwork rings overlapping each other whilst allowing them to freely separate in the radial direction if they should desire. COMBIN40 elements were used in the circumferential and transverse direction, as before, to model the shear bond strength between the rings. In essence, the above finite element model was similar to the model of the square arch presented in section 7.6.1 except that it was skewed.

In the skewed arch model, the same problems arise as in the three-dimensional model of a square arch when it is used to investigate the three-dimensional effects produced by, for instance, eccentric patch loads or spandrel walls. At each nodal point on the interface between the adjacent brickwork rings, the principal stress will generally not be parallel to either the circumferential COMBIN40 element or the transverse COMBIN40 element. There may be several ways in which this situation may be dealt with, these will be discussed in chapter 8. In the present model, the stiffness of each pair of mutually perpendicular COMBIN40 elements are

adjusted so that their resultant stiffness will be parallel to the direction of the principal stress. Likewise, their strengths are adjusted so that they will both fail concurrently during the same load increment. If this was not carried out correctly, the extension of the circumferential COMBIN40 element relative to the extension of its transverse partner will be such that the movement of one ring relative to the other would be forced to occur in an incorrect direction. This would, in turn, cause the direction of principal stress at the site of a nearby triad of gap elements to change. Furthermore, the eventual yielding of a particular COMBIN40 element may have such a large effect on the direction of the principal stress that its partner may never fail. In this way, composite action may not be allowed to breakdown.

An iterative procedure was devised which was intended to produce the stiffness and strength of each COMBIN40 element throughout the interface. However it was found to possess an extremely slow convergence ability, i.e after 56 reanalyses each taking approximately 5.5 hours it still had not converged on an appropriate set of values). This is because there are 144 sets of gap elements each of which, if not working correctly, will adversely effect the performance of the nearby sets. The iterative technique involved interrogating the results of the previous analysis to determine the load increment at which each COMBIN40 element failed. The forces within each pair of elements at the load increment just before the first one of them failed were used to redefine the stiffness and strength parameters in order to carry out the present analysis.

The situation is further complicated by the occurrence of tensile failures within the SOLID65 elements. These elements become orthotropic when this occurs and this will change the direction of principal stress. In other words, the above iterative procedure may never produce suitable stiffness and strength parameters because values which are appropriate up to a particular load increment may not be valid beyond that load due to the tensile failure of the SOLID65 elements. Consequently, the modelling technique described herein was unsuccessful. A single unique set of stiffness and strength parameters for the COMBIN40 elements could not be ascertained. Thus, as defined, the COMBIN40 elements are unable to realistically model the breakdown of composite action, i.e ring separation was prevented. Therefore, it can be concluded that the cumbersome use of a triad of one-dimensional gap elements at each interface node is certainly impractical but may also represent an inadequate way of modelling the occurrence of ring separation in a three-dimensional model.

The material properties used in the analysis of skewed arch 3-4 were identical to those of square arch 3-0d, as listed in table 7.1, so that the results of the analyses could be comparable. In terms of the properties of the masonry and those of the backfill, the above assumption was valid. However, it was known that bridge 3-4 contained partial ring separation so that the properties of the mortar bond should have been reduced accordingly. It was anticipated that, as soon as a feasible set of properties for the COMBIN40 elements could be ascertained their

strength and stiffness could be adjusted on a pro rata basis.

As previously explained, a set of feasible stiffness and strength parameters for the COMBIN40 elements could not be obtained. Thus, at a live load of 350 kN, ring separation existed only at isolated regions throughout the interface. Consequently, the maximum radial deflection of the arch at this load was less than 1.0 mm, as shown in figure 7.38. The finite element analysis of this bridge revealed that it could sustain a load far in excess of 350 kN. It can be seen in figure 5.13 that the actual failure load of bridge 3-4 was 337 kN at which its maximum inward deflection was approximately 6.0 mm. This was due to the prevalence of ring separation; a phenomenon whose occurrence was prevented in the present finite element model. Therefore, it is not suggested that the skewed arch is stronger than the equivalent square arch. On the contrary, it is suggested that the present finite element model cannot adequately incorporate the actual non-linear behaviour of the arch as it approaches the ultimate limit state. Further discussion regarding the deficiencies in the present model can be found in chapter 8.

It is, however, reassuring to find that the underlying behaviour of the present finite element model is legitimate. The predicted deformed shape of the intrados of the arch, shown in figure 7.38, is remarkably similar to the measured deformed shape of the actual arch, shown in figure 5.13. The apparent twisting of the finite element model can also be seen in elevation in figure 7.39 which shows the distribution of circumferential stress. Therefore, there is no reason to conclude that the proposed modelling technique will not be as accurate for the analysis of the skewed arch as it was for the square arch. However, to achieve a similar level of accuracy the modelling of the three-dimensional surface to surface contact of adjacent brickwork rings requires further investigatory work; it may be beyond the capability of commercially available finite element packages such as ANSYS.

The underlying legitimacy of the deformed shape of the finite element model adds credence to the conclusion that, although it cannot trace the behaviour of the arch up to its ultimate limit state, it can analyse the multi-ring skewed arch when subjected to loads in the serviceability range.

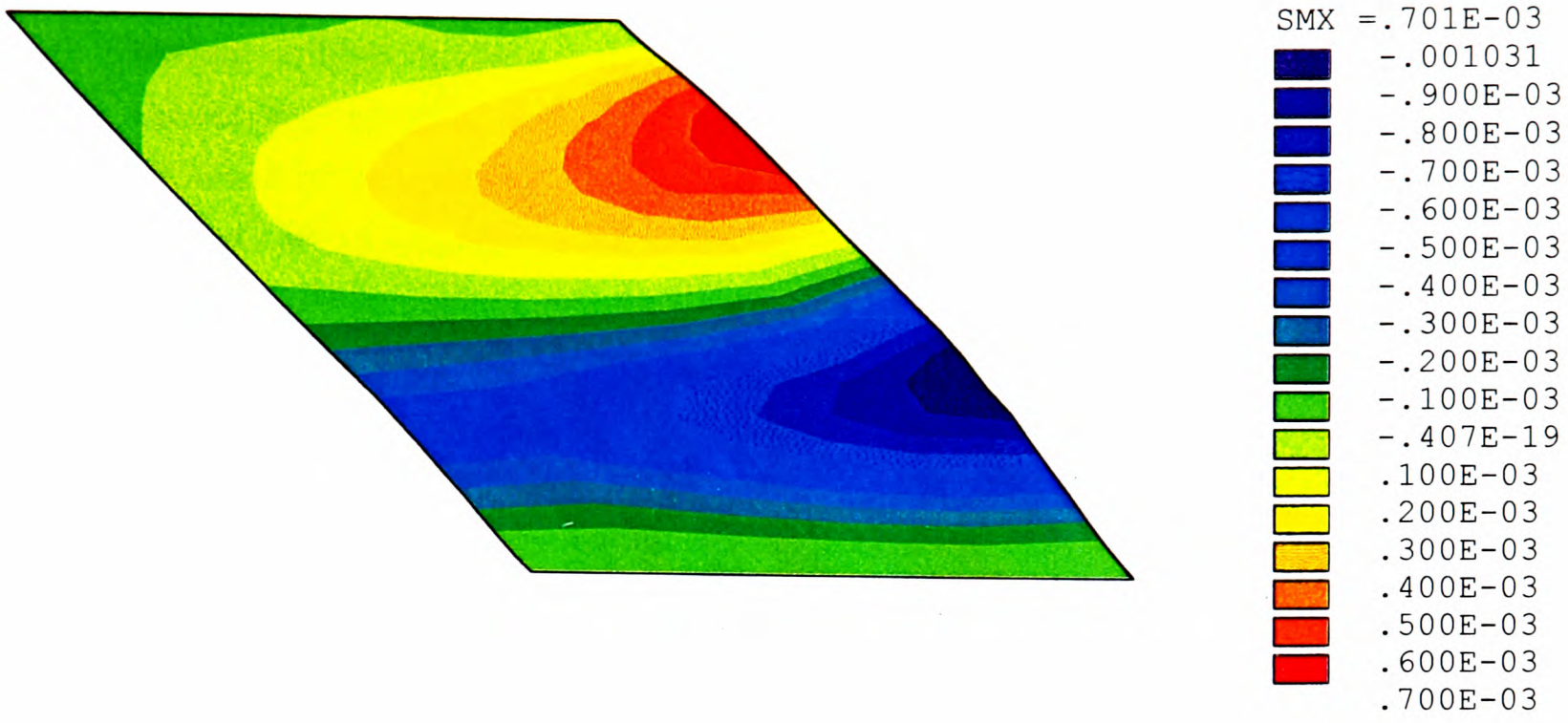

Figure 7.38 Radial deflection of the intrados of the FE model of arch 3-4 at 350 kN live load

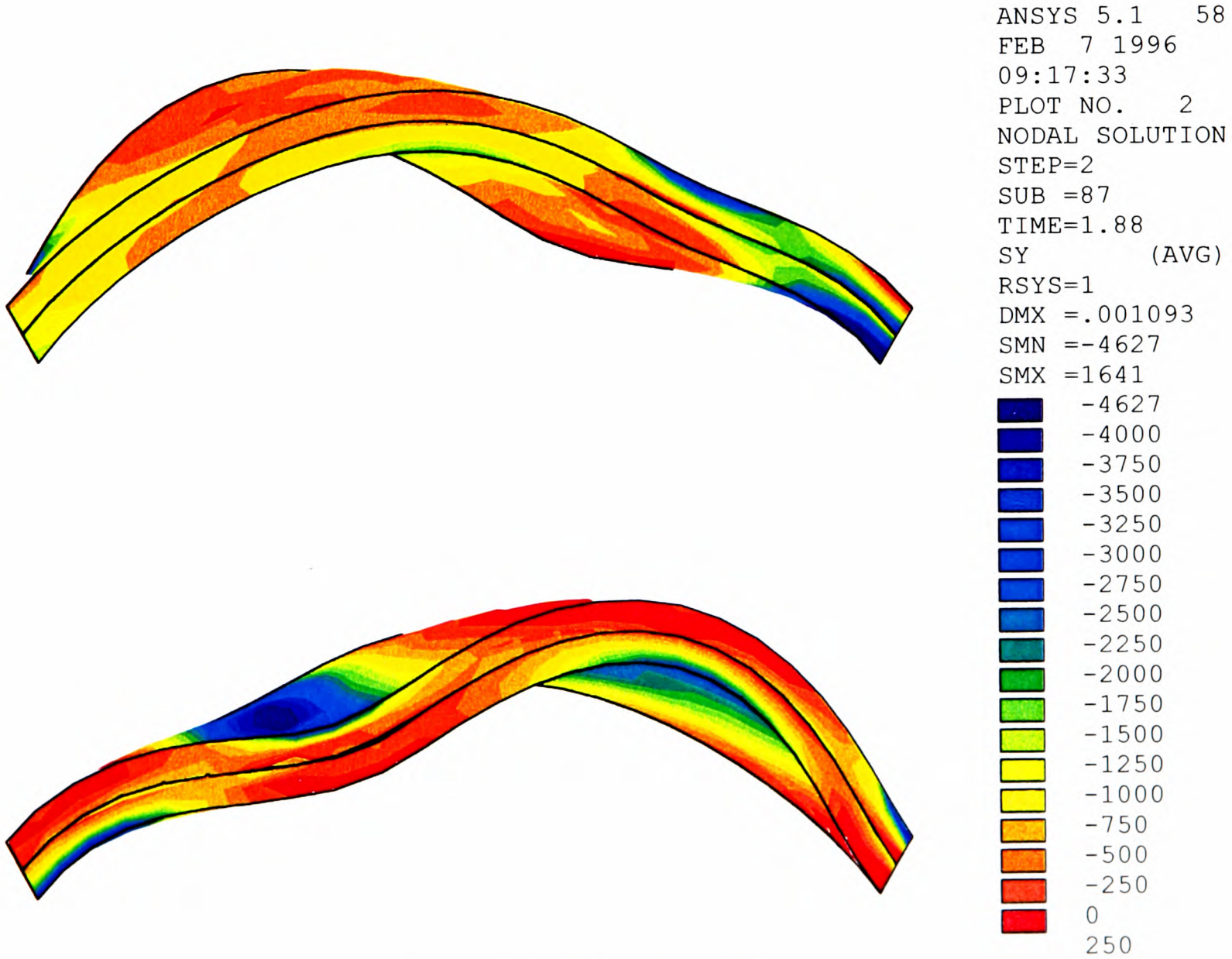

Figure 7.39 Circumferential stress in the FE model of arch 3-4 at 350 kN live load

The remarkable resemblance between the predicted deformed shape of skewed arch 3-4, using the proposed finite element model, and its actual deformed shape is in conflict with the finite element analyses of Choo et al. (1993) as reproduced in figure 7.40. Their analysis of the skewed arch predicted that it behaves in a two-dimensional manner that is similar to the behaviour of the square arch, i.e that the arch does not undergo an apparent twist and the four fractures are each parallel to the abutments.

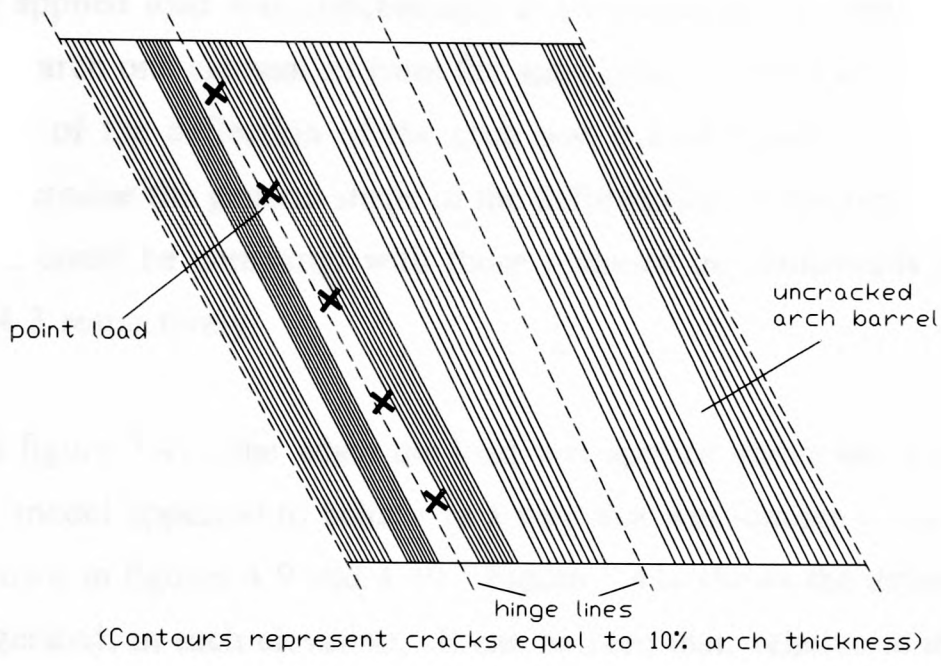

Figure 7.40 Crack distribution and hinge lines in arch ring after Choo et al. (1993)

In their later work (Choo et al., 1995), they used this apparently flawed model to compare the capacity of a skewed arch with that of an equivalent square arch and consequently incorrectly concluded that, "the load carrying capacity increases as the skew angle of the arch increases". It is not clear on what basis a square arch was said to be equivalent to a skewed arch. However, they reported that in each case the strength was increased by skew. They found that the case that produced the least increase in strength was the one in which the angle of skew was increased whilst keeping the square span, the rise, and the width of the bridge constant. This appears to be similar to the way, within this thesis, that a skewed arch is related to the equivalent square arch although here, it has been shown experimentally that an increase in skew produces a reduction in strength.

However, if the constant width to which they refer is the width perpendicular to the spandrel walls then the apparent increase in strength could be due to the additional width of the structure as measured parallel to the abutments. In other words, if they had kept constant the clear distance between the spandrel walls, an increase in skew would have required that the length of the abutments must be increased and, given that their model is unable to predict any three-dimensional effects, the predicted strength will be proportional to the length of the abutments. Nevertheless, it is incorrect to talk in terms of an increase in strength being associated with an increase in skew. One of the outcomes of this research is the conclusion that skew weakens the arch.

The present finite element model was used to analyse skewed arch 3-4 when subjected to eccentric point loads P_1 and P_4 at its south quarter-span section as described in chapter 4. Figure 7.41 and figure 7.42 contain the results of each respective analysis in which (a) the deformed shape of the arch in elevation, (b) the radial deflection of the intrados, and (c) the circumferential stress on the intrados are shown consecutively. Each analysis was performed without horizontal backfill pressures and without load dispersal through the spandrel fill. Furthermore, the applied load was concentrated at two adjacent circumferential nodes at the quarter span of the arch one element in from the appropriate edge of the structure. Thus, the absolute magnitude of the deflection of the arch was not of interest. The objective of the analyses was to determine the general shape of the deformation of the arch and the distribution of stress so that it could be compared with those obtained experimentally as documented in sections 4.2 and 4.3 respectively.

It can be seen, in figure 7.41, that when the load was applied above the acute angled haunch the finite element model appeared to behave in a way that was similar to the behaviour of the actual arch, as shown in figures 4.9 and 4.19. Figure 7.41a shows the deformed shape of the arch, albeit exaggerated, in each elevation. It can be seen that, relative to the east fascia, the load effects visible on the west fascia were seemingly negligible. There is a close correlation between this prediction and the measured surface strains on each fascia as shown in figure 4.19. Figure 7.41b shows the predicted radial deflection of the arch whereas figure 4.9 shows its actual measured deflection. Here, also, there is a high degree of similarity between the two sets of data in that, in each case the region of downward deflection extended across almost the entire width of the structure towards its obtuse angled corner and a comparatively small region of upward deflection occurred at its north east edge. Additionally, the distribution of circumferential stress on the intrados, figure 7.41c, indicates stress concentrations at locations around the arch similar to the sites at which high compressive and tensile strains were recorded experimentally, as depicted in figure 4.19.

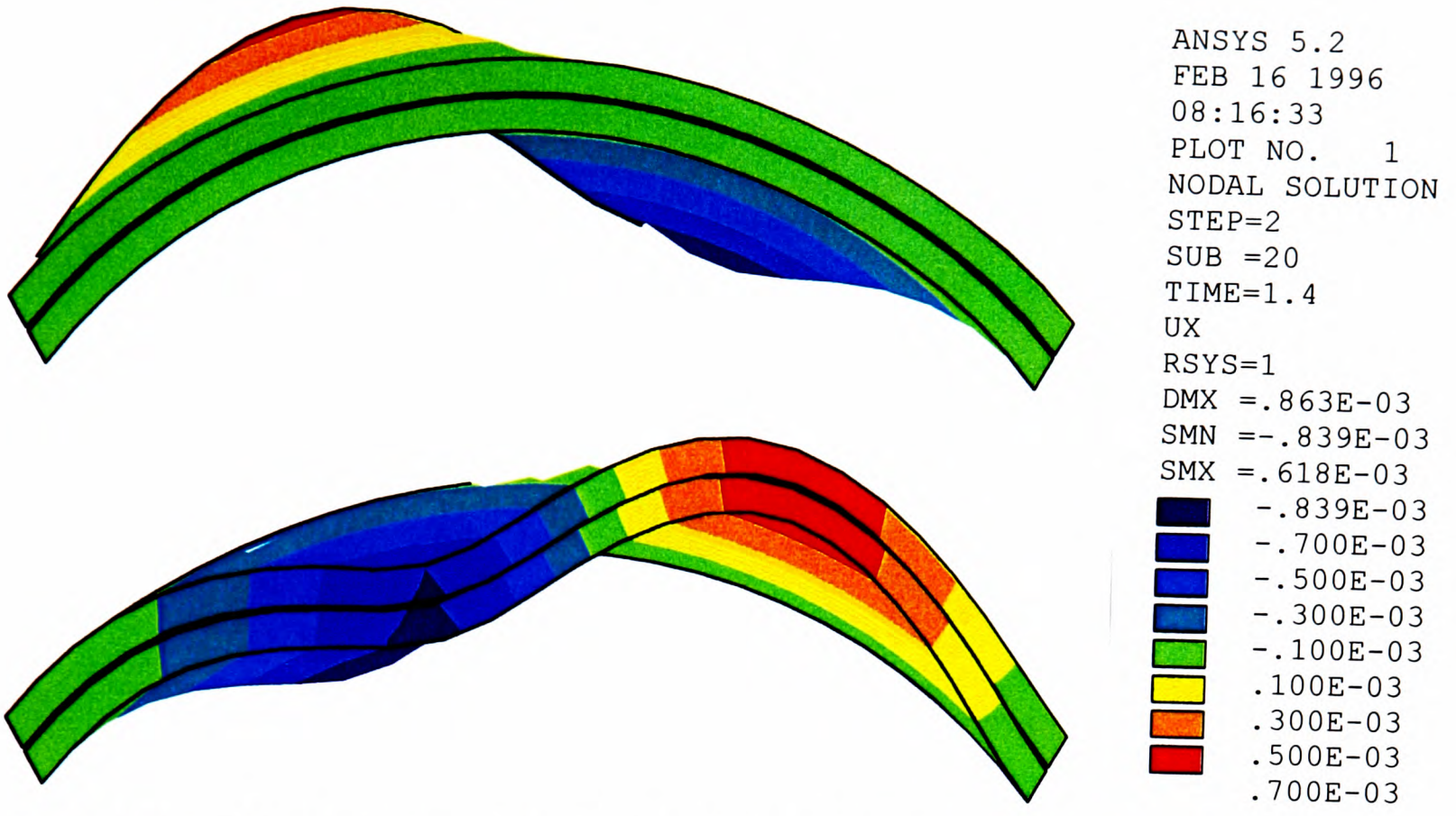

Figure 7.41a Deformed shape of the FE model when loaded at P_1

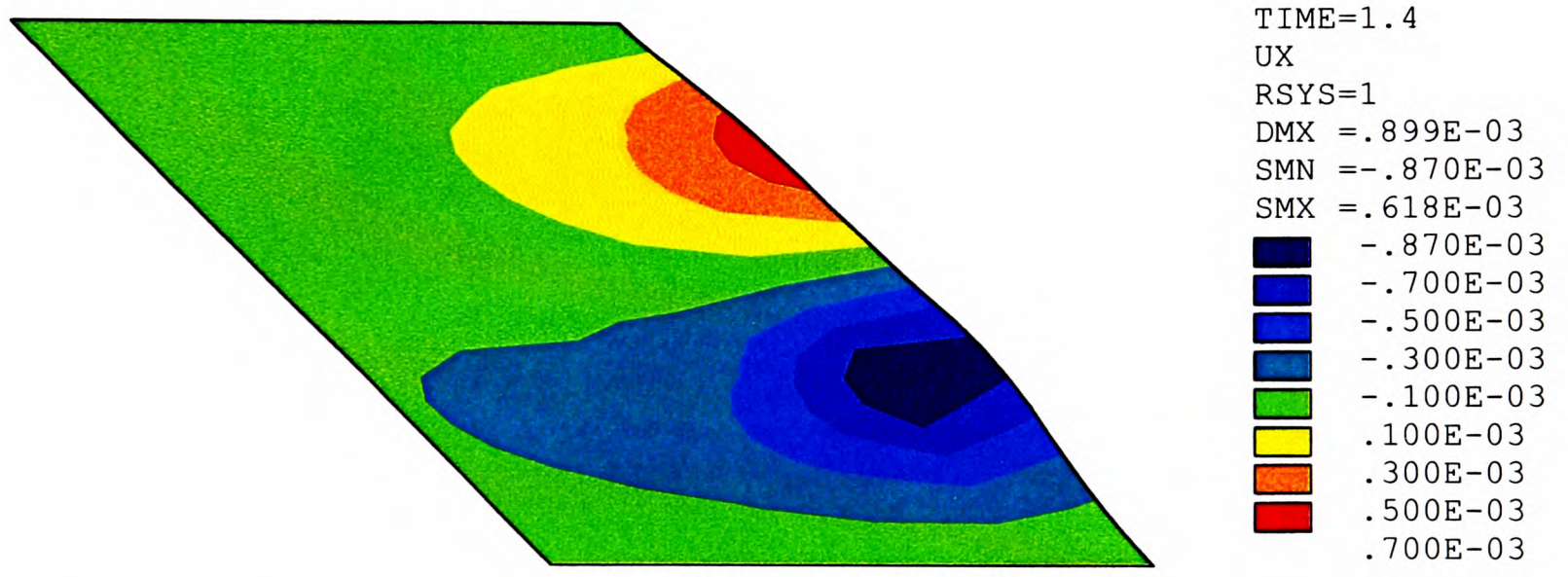

Figure 7.41b Radial deflection of the intrados of the FE model when loaded at P_1

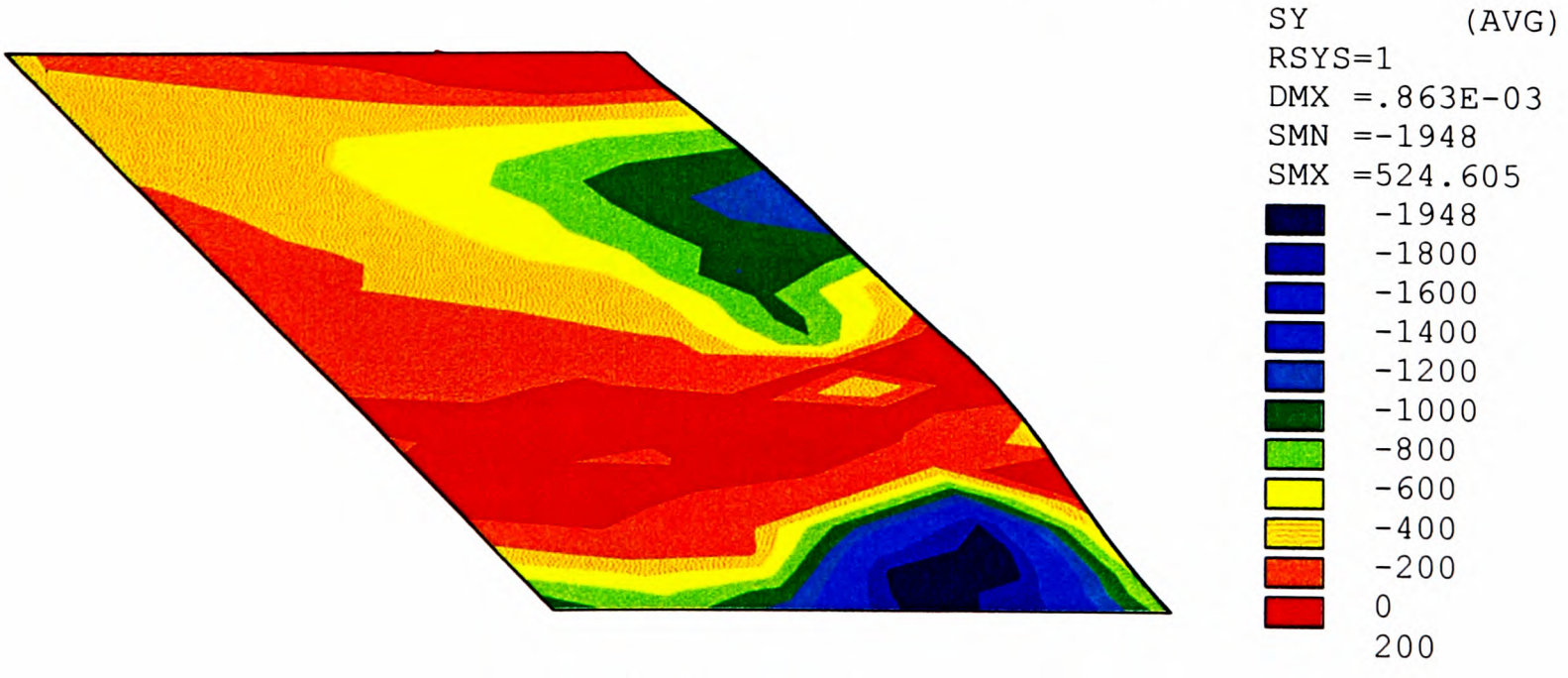

Figure 7.41c Circumferential stress on the intrados of the FE model when loaded at P_1

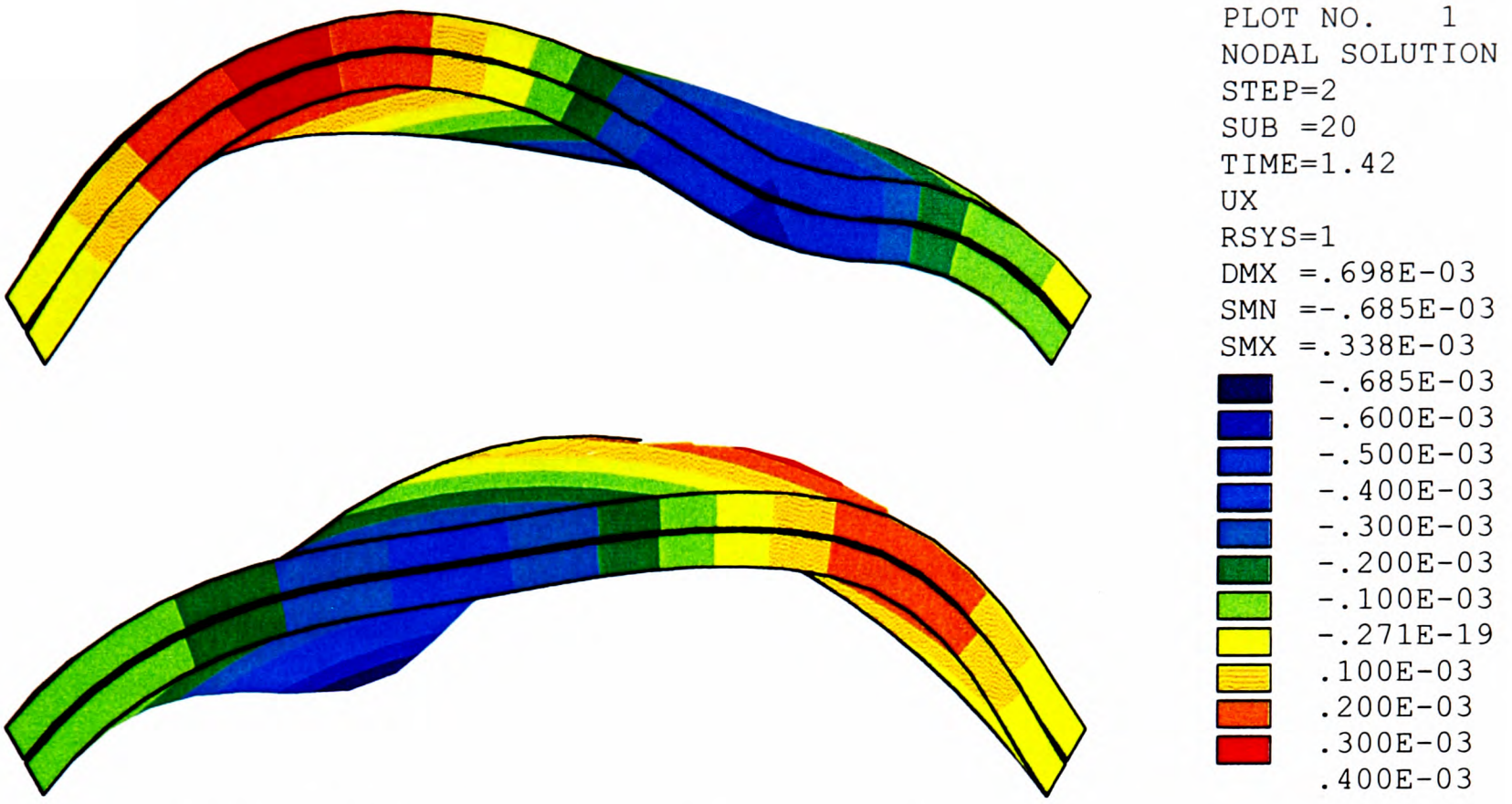

Figure 7.42a Deformed shape of the FE model when loaded at P_4

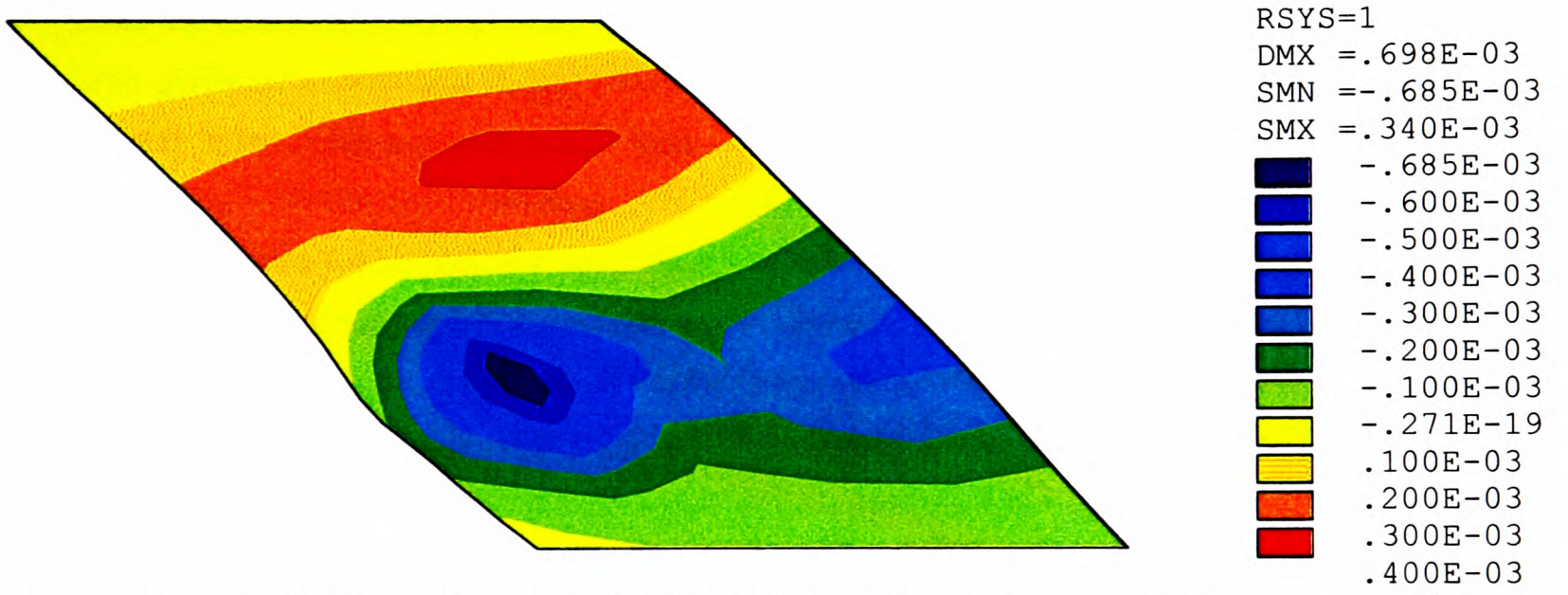

Figure 7.42b Radial deflection of the intrados of the FE model when loaded at P_4

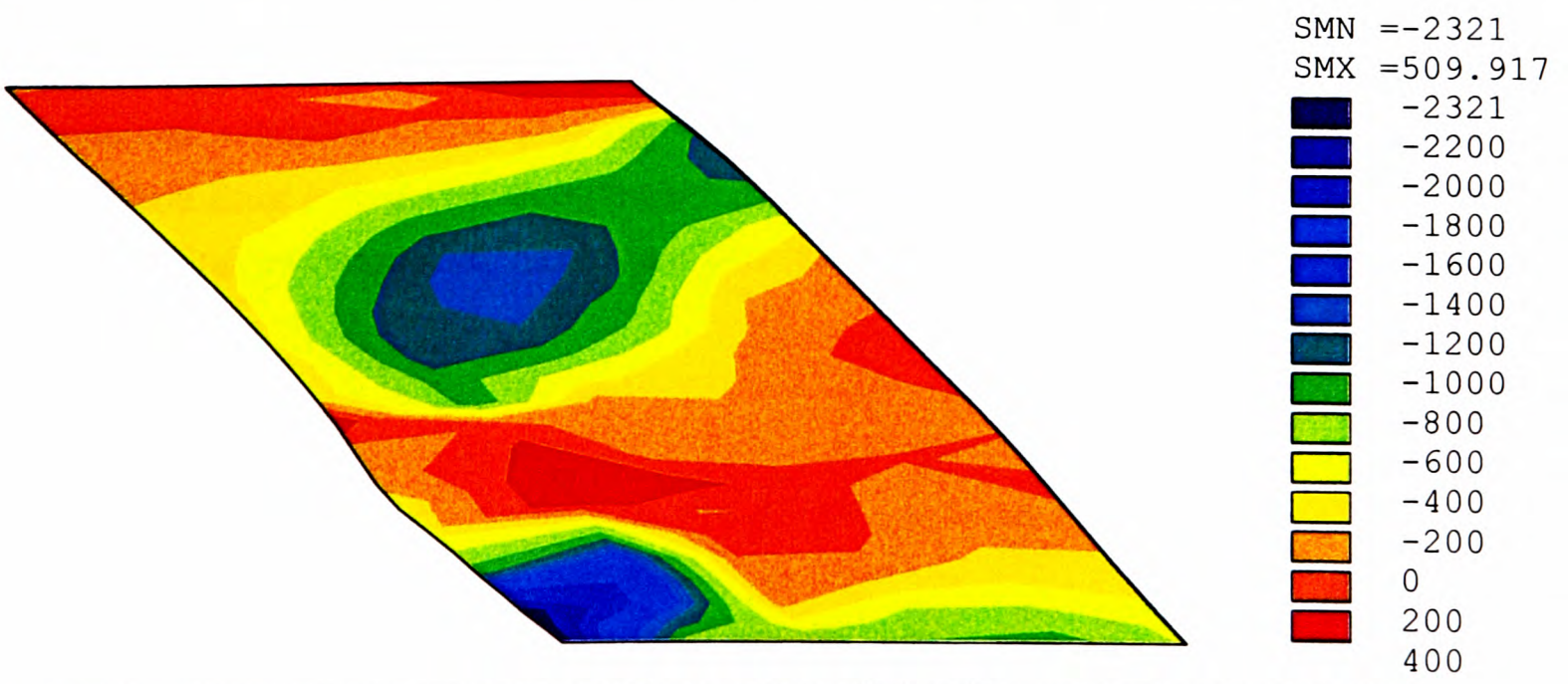

Figure 7.42c Circumferential stress on the intrados of the FE model when loaded at P_4

It can be seen, in figure 7.42, that when the load was applied above the obtuse angled haunch, once again, the finite element model appeared to behave in a way that was similar to the actual behaviour of the arch, as shown in figures 4.10 and 4.20. Figure 7.42a shows the deformed shape of the arch, albeit exaggerated, in each elevation in which detectable load effects are visible on each fascia. Figure 4.20 contains the surface strain measurement on each fascia of the arch which confirm this prediction. Furthermore, these surface strains are smaller in magnitude than those that occurred when the load was applied above the acute angled haunch. Likewise, the finite element analysis yielded a similar diminution in the predicted magnitude of the deflection of the arch. The geometry of the structure is responsible for this effect. Firstly, the stiffness of the obtuse angled haunch relative to that of the acute angled haunch decreases the downward deflection of the arch in the vicinity of the applied load. Secondly, the circumferential load effects that emanate from the obtuse angled haunch may disperse into the structure more rapidly than those that emanate from the acute angled haunch.

With the exception of the small downward deflection of its south east haunch, the radial deflection of the intrados of the finite element model, shown in figure 7.42b, was very much alike the measured radial deflection of the actual arch, shown in figure 4.10. In each case, the arch deflected downwards in the vicinity of the load and upwards in the vicinity of the north quarter span along a perpendicular path between the load position and the north abutment. Consistent with this deformed shape, the predicted distribution of circumferential stress on the intrados, figure 7.42c, indicates four regions of relatively high stress along this square span load path. Surface strain measurements shown in figure 4.20 are generally in agreement with this prediction in which the magnitude of the maximum surface strain along each row diminishes and the extent of the relatively highly strained region increases in proportion to the distance along the span of the arch.

Therefore, it has been shown that the present finite element model can produce a sufficiently accurate analysis of a skewed multi-ring brickwork arch bridge provided that the applied loads are within the serviceability range. The analysis of these eccentric point loads provides important validation of the proposed modelling technique. Moreover, they also provide important clues as to the necessary modifications that are required in order for the accuracy of the model to be extended to the ultimate limit state. These will be discussed in chapter 8.

8.0 Discussion

8.1 The three-dimensional behaviour of the masonry arch

The discussion of the behaviour of the masonry arch bridge that is presented within this thesis is confined to the single span structure whose abutments are effectively immovable and whose shape is segmental with a span/rise ratio of 4.0. Furthermore, two structures are herein defined as being equivalent, so that their respective load carrying behaviour is comparable, if their geometries are identical to each other in every detail except one. For example, the effects of a change in the width of the arch barrel can only be considered if every other detail remains constant. Otherwise, like is not being compared with like. Similarly, the effects of a change in its angle of skew can only be considered if the square span of the arch and its width measured parallel to the abutments remains constant. In this latter case, the structure has a mass of arch and a mass of spandrel fill that is the same as that of its equivalent structure.

The masonry arch is a three-dimensional structure although its geometry and applied loading may sometimes conspire to produce a behaviour that is essentially two-dimensional i.e. in which the three-dimensional effects are small and may therefore be neglected. However, as its geometry is changed, certain aspects of its load carrying behaviour become more, or less, significant so that ultimately its mode of failure will also change.

The imposition of an applied load on the arch will cause it to deform but it will not collapse if it can find a safe statically admissible deformed state. Conversely, it will collapse if it can find an admissible collapse state i.e if its deformation is such that it is transformed into a mechanism. The configuration of each potential mechanism is associated with a particular collapse load. The optimum mechanism, i.e. the one that is associated with the least collapse load, is the one that will actually occur. This is because, as the applied load is monotonically increased, the first encountered deformed configuration of the structure that satisfies the upper bound theorem of collapse is the one that is the optimum mechanism. The downward deflection of the arch in the vicinity of the applied load is accommodated by an upward deflection at a remote location in the longitudinal direction. However, this longitudinal arching is accompanied by the three-dimensional phenomenon of transverse arching. This effect is produced as a result of torsion, in section, or twisting, on plan, or shearing in a direction parallel or perpendicular to the bedding joints. As previously mentioned, the significance of the transverse arching phenomenon is dependent upon the geometry of the arch and the nature of its applied loading. This phenomenon was first observed by Davey (1953) and again by Chettoe and Henderson (1957) and was observed within this research during the non-destructive load tests documented in chapter 4 and the destructive load tests documented in chapter 5.

In the special case of the square arch of normal proportions, when subjected to a full-width patch load, the magnitude of the three-dimensional aspects of its behaviour is small, see figures 5.10a and 5.10d. These transverse aspects of its behaviour become more significant if spandrel walls are attached to the arch, see figures 5.10b and 5.10c. However, the relative proportions of the walls and the arch barrel in the structures tested as part of this research were such that the attached spandrel walls did not affect a significant change in the ultimate behaviour of the arch. Consequently, each full-scale model square arch bridge behaved in an essentially two-dimensional manner. Furthermore, when subjected to an eccentric point load, the three-dimensional aspects of its behaviour continue to remain small. The deflected shape of full-scale model square arch 3-0d, see figure 4.11, shows that when it was subjected to an eccentric 100 kN point load it underwent transverse arching although this was not sufficiently large to produce upward movements at remote locations in the transverse direction. However, the equivalent 3.55 m wide square arch with spandrel walls, viz. 3-0a, did produce an upward movement in this direction, see figure 4.11. These structures were not loaded to failure in this way so it is not possible to determine the ultimate significance of the observed three-dimensional behaviour. However, small-scale model square arch 1-2 had proportions that were similar to its full-scale counterparts and its ultimate behaviour, see figure 5.39, was essentially two-dimensional in which there were only slight differences in its measured load-deflection response across its width to suggest any other form of behaviour. These experimental observations generally confirmed the theoretical predictions of Livesley (1992b).

Livesley proposed a mathematical model for the analysis of three-dimensional failure mechanisms within the special case of the square arch when idealised as comprising four similarly shaped rigid blocks. It was discovered that as the eccentricity of the applied load was increased, so was the significance of the three-dimensional aspects of its behaviour. Thus, the optimal failure mechanism ceased being two-dimensional. More importantly, the maximum sustainable load was found to diminish in proportion to the increased complexity of the relative block movements at each fracture. In other words, depending on the proportions of the arch, a three-dimensional mechanism may enable failure to occur at a lower load than if the mechanism was two-dimensional. Thus, it can be concluded that failure is governed by the combination of transverse and longitudinal load effects relative to each respective resistance.

The behaviour of small-scale model square arch 1-3, which was unrealistically wide, was also generally in agreement with the findings of Livesley (1992b). The three-dimensional aspects of its behaviour were much more pronounced than those of arch 1-2. However, instead of each fracture being associated with complex relative block movements, such as torsional hinging, its transverse arching, see figure 5.41, produced a three-dimensional system of cracks, as shown in figure 5.40. The magnitude of the relative block movements that occurred at the diagonal cracks was small compared with those at the four fractures that were each parallel to the

abutments. Its mode of failure was therefore essentially two-dimensional although it is suggested that if the eccentricity of the applied load is increased this would become three-dimensional. However, it seems more appropriate to conclude that a local three-dimensional failure mechanism rather than, as Livesley suggests, a global three-dimensional failure mechanism would become optimal as the eccentricity of the applied load is increased.

A change in the geometry of the arch in some other way, such as an increase in its angle of skew, may also change its mode of behaviour because the three-dimensional aspects of its behaviour may become more significant.

When subjected to a full-width uniformly distributed patch load, i.e one that is parallel to the abutments, the arch will undergo transverse arching. This effect has already been shown to be relatively small, see figure 5.10, when the angle of skew is small. However, as the angle of skew is increased so is the significance of this effect. When the angle of skew is 22.5° the apparent twist of the arch is already quite pronounced, for example just before failure, the difference in outward deflection of skewed arch 3-1 along its second in-span fracture, shown in figure 5.11, was approximately 1.2 mm which corresponds to a torsional rotation of 0.36×10^{-3} radians. Moreover, when the angle of skew is 45° the apparent twist is relatively large. The difference in outward deflection of skewed arch 3-4 along its second in-span fracture, shown in figure 5.13, was approximately 3.0 mm which corresponds to a torsional rotation of 1.13×10^{-3} radians.

The combination of its longitudinal behaviour and its transverse behaviour causes the arch to fail at a lower load than when the magnitude of its transverse behaviour is comparatively small. More succinctly, the capacity of an arch reduces as its angle of skew increases because of the increased significance of the transverse load effects. The combination of these effects causes fractures to occur in directions which are inclined to the planes of the abutments and may also increase the number of fractures. However, the orientation of these fractures is also influenced by the bedding joints. Thus, the failure mechanism of each full-scale model skewed arch comprised five fractures which were generally inclined to the abutments, as shown in figures 5.5 to 5.8 inclusive.

In accordance with BS 5628, the flexural strength of masonry in the direction of the bedding joints is three times less than its flexural strength in the perpendicular direction. However, this ratio applies to uniform bending. Within the arch, transverse bending is produced by localised effects. For example, the deformed shape of 45° skewed arch 3-4, see figure 5.13, shows comparatively small regions of large inward and outward deflections along its eastern edge. Thus, the flexural strength of the masonry in the direction parallel to the bedding joints will only be governed by its global ability to undergo transverse bending if its mortar-brick shear

bond strength is sufficiently large to enable each course to act compositely. Hence, depending on the shear strength of the mortar, localised twisting of the arch may create longitudinal fractures due to a failure in bending or may create diagonal fractures due to a failure in shear i.e. relative translational movements or torsional hinging. Conversely, the formation of a three-dimensional failure mechanism indicates the presence of significant transverse behaviour. It also indicates that the observed mechanism is optimal, otherwise it would not have formed, and therefore it is associated with a lower collapse load than a two-dimensional mechanism or, indeed, any other form of potential mechanism. This is in agreement with what can be concluded from Livesley's work on the special case of the square arch.

When the three-dimensional mathematical modelling technique developed in chapter 6 was used to create the "simple hinge" model for the analysis of the collapse mechanism of a skewed arch it could not obtain a feasible set of simple hinge rotations for a three-dimensional set of fractures. Further to the above discussion, this should not have been surprising because a three-dimensional set of fractures is associated with three-dimensional behaviour. Consequently, the "complex hinge" models, in which torsional and radial hinging were also permitted, were able to obtain feasible sets of relative block movements. The "augmented" model could not determine the optimum mechanism because, as is suggested in section 6.6.2.3, the inclusion of more than one fracture that permits radial and torsional hinging allows the blocks in between to undergo unrestrained rotations. In contrast, the "reduced" model was able to determine the optimum mechanism although because it was too restrictive in the number of possible relative block movements it found that the optimum mechanism was two-dimensional. However, it was reassuring to find that, in this case, the magnitude of the collapse load was similar to the magnitude of the minimum collapse load that was predicted by the two-dimensional analysis of the equivalent square arch using the technique proposed in section 6.5. In other words, the collapse load associated with a two-dimensional mechanism is independent of the angle of skew of the arch provided that the arches being compared are equivalent to each other. This conclusion is important if only to establish that an increase in the angle of skew of an arch is associated with a decrease in its strength. Otherwise, if the collapse load associated with a two-dimensional mechanism (in which each fracture is parallel to the abutments and permits only simple hinging) was a function of the angle of skew it would not be possible to conclude that skew weakens the arch.

In the three-dimensional arch, collapse will occur if a sufficient number of fractures form so that it is transformed into a mechanism. The minimum number of fractures required to create a hinged mechanism is four. However, this situation will occur only if the geometry of the arch and its applied loading are such that each fracture is parallel to the abutments. Additional, complex, relative block movements and perhaps additional fractures are required if the fractures are inclined to the abutments. Conversely, the radial and torsional hinging that must occur if

some of the fractures are inclined to the abutments can be considered as being required in order to produce an overall effect in the direction perpendicular to the abutments that is equivalent to four simple hinges.

The aforementioned three-dimensional mathematical modelling technique indicates that, if a simple hinge is the only form of relative block movement at the south abutment fracture and other fractures are inclined to the abutments, there must be a total number of seven relative block movements in order that an admissible three-dimensional mechanism can be created within the skewed masonry arch. Consequently, the complexity of the relative block movements that occur at each fracture is inversely proportional to the number of fractures. However, the magnitude of the simple hinge rotation at the south abutment is predetermined so that the point of application of the load undergoes the required unit vertical displacement. The magnitude of each other relative block movement is selected so that the displacement of the applied load is accommodated. The final step in the analysis is to determine the magnitude of the simple hinge component of movement at the north abutment since it is dependent upon the other values. Thus, the analysis of the collapse mechanism can be reduced to a problem in which the optimum combination of five relative block movements must be selected from a finite number of possibilities and therefore linear programming techniques are most appropriate.

The failure of each small-scale model skewed arch, documented in section 5.2, was due to the formation of a three-dimensional mechanism and therefore required complex relative block movements at each fracture. The configuration of each collapse mechanism should not be considered as definitive but merely indicative of the type of fracturing that may occur. However, the observed complex relative block movements validate the predictions of the theoretical models developed in chapter 6.

Small-scale arch 1-6 and 1-7 each failed due to the formation of a mechanism in which there were only four fractures, see figures 5.44 and 5.45 respectively. The fracture that passed through the point of application of the load, marked 2, was associated with several types of relative block movements including radial and torsional rotations which produced full-depth tension at the western extremity of the fracture and relative upward and downward sliding movements at opposite ends of the fracture. Furthermore, the stress concentration that occurred at the single point of contact between blocks marked A and B caused a section of brick to spall away. Similar movements at the fracture at the north abutment were also observed. Here, upward and downward relative sliding movements at the opposite extremes of the fracture occurred that were consistent with torsional hinging. However, it can be seen, in figures 5.44 and 5.45, that seven relative block movements occurred which is exactly the number predicted by the three-dimensional mechanism method proposed in section 6.6.2.3.

Small-scale model arch 1-4 and 1-5 each failed due to the formation of a three-dimensional mechanism in which there were five or six fractures, as shown in figures 5.42 and 5.43 respectively. It is more difficult to identify the total number of relative block movements because the fractures are generally indiscrete. However, it is possible to identify seven relative block movements which is also in accordance with the three-dimensional mechanism method proposed in section 6.6.2.3. It can also be seen that three of the fractures were parallel to the abutments and permitted only simple hinging. Compatibility requires that the combined effect of each relative block movement at the remaining fractures must be equivalent to a fourth simple hinge. However, the fact that a two-dimensional mechanism did not occur indicates that each mechanism is associated with a lower collapse load than this upper bound value. An interesting observation of the collapse mechanism of each of these small-scale model arches is that they resemble the collapse mechanism of each full-scale model skewed arch and therefore provide insight into the behaviour of these structures. For example, if the eccentric patch load that was applied on the south obtuse angled haunch of small-scale model skewed arch 1-5 was replaced by a full-width patch load at the north quarter-span section, similar to the way in which each full-scale model arch was loaded, the pattern of fractures shown in figure 5.43 may describe the failure mechanism in each load case. Thus, complex relative block movements equivalent to those that occurred at the fractures marked 2 and 3/4 must occur at the corresponding fractures in each full-scale model skewed arch in order to maintain compatibility.

It has been established that within the skewed arch, if a simple hinge occurs at the south abutment, there must be a further six relative block movements at the remaining fractures if the three-dimensional behaviour of the arch is sufficiently large to cause them to occur inclined to the abutments. Thus, the presence of radial and torsional hinging at the second and third in-span fractures, in accordance with both the three-dimensional mechanism model proposed in section 6.6.2.3 and the above discussion, in the full-scale model skewed arches would explain the observed full-depth tension, see figure 5.25, and regions of spalling brickwork, see figure 5.8, that occurred within these structures.

The three-dimensional collapse mechanism that may occur in a skewed arch, as a result of an increase in its angle of skew increasing the significance of its transverse behaviour, produces a corresponding reduction in its load carrying capacity. This anticipated reduction in strength as a function of the angle of skew is shown diagrammatically in figure 8.1.

It can be seen that there may be a particular angle of skew below which a two-dimensional mechanism is optimal since the collapse load associated with it is less than that associated with a three-dimensional mechanism. Above this value, a three-dimensional mechanism will be optimal. However, figure 8.1 also illustrates the importance of formulating a mathematical model that is sufficiently general to enable each potential mechanism to be investigated. In this

way, the one that is predicted can, with confidence, be said to be associated with the least possible collapse load. If, on the other hand, the model is too restrictive and therefore cannot behave in a realistic way its predicted collapse load is likely to be an upper bound value.

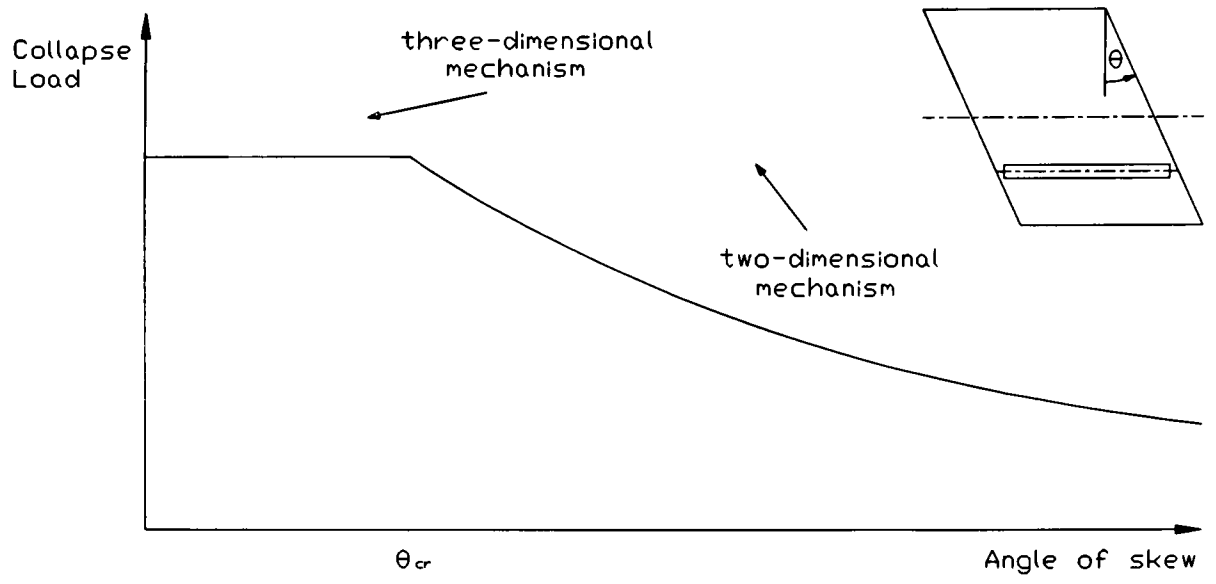

Figure 8.1 Anticipated relationship between angle of skew and arch capacity

It is suggested that the omission of diagonal fractures within the model that was proposed by Livesley (1992b) and the apparent inability of the three-dimensional finite element model that was proposed by Choo et al. (1993) to predict three-dimensional behaviour indicate that each of these models will produce upper bound values of the maximum sustainable load. It is also pointed out that the "reduced" mechanism analysis model developed in section 6.6.2.3 and the proposed finite element model developed in section 7.6.2 are included within this group. The minimum collapse load that the "reduced" model predicted was associated with a two-dimensional mechanism. However, the alternative "augmented" model proved to be unbounded. Thus, it can be concluded that an appropriate "realistic" model will lie within these two bounds.

The proposed finite element model of the skewed arch, depicted in figure 7.37, is at present unable to reproduce the load-deflection response of the actual arch beyond its serviceability range and therefore it cannot reproduce the measured failure load. To illustrate some of the deficiencies in the above model, an analysis of a similar model was carried out except that it comprised only a single 102 mm thick brickwork ring and therefore contained only SOLID65 elements; gap elements were not used. The material properties of this model were also identical to those of the model of square arch 3-0d as listed in table 7.1 with the exception that its compressive strength was ascribed a value of 7.5 N/mm^2. The absence of the highly non-linear gap elements meant that the analysis did not encounter convergence difficulties; the load could therefore by applied in relatively few increments. Thus, after 27 sub-steps the maximum applied load of 400 kN was reached which caused a maximum deformation of the model of approximately 4.5 mm as shown in figure 8.2.

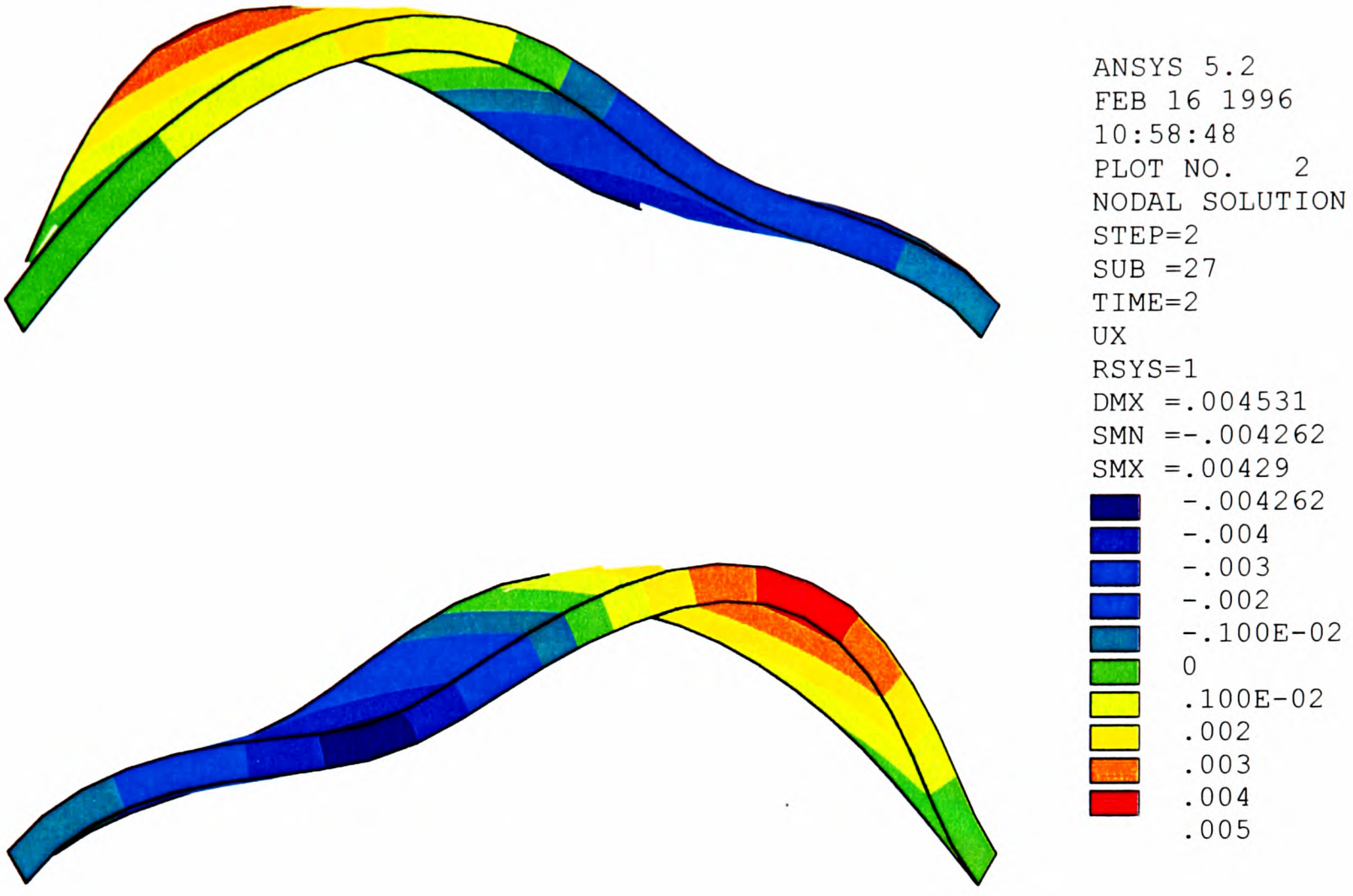

Figure 8.2a Deflected shape of the FE model of a single ring skewed arch when subjected to 400 kN live load

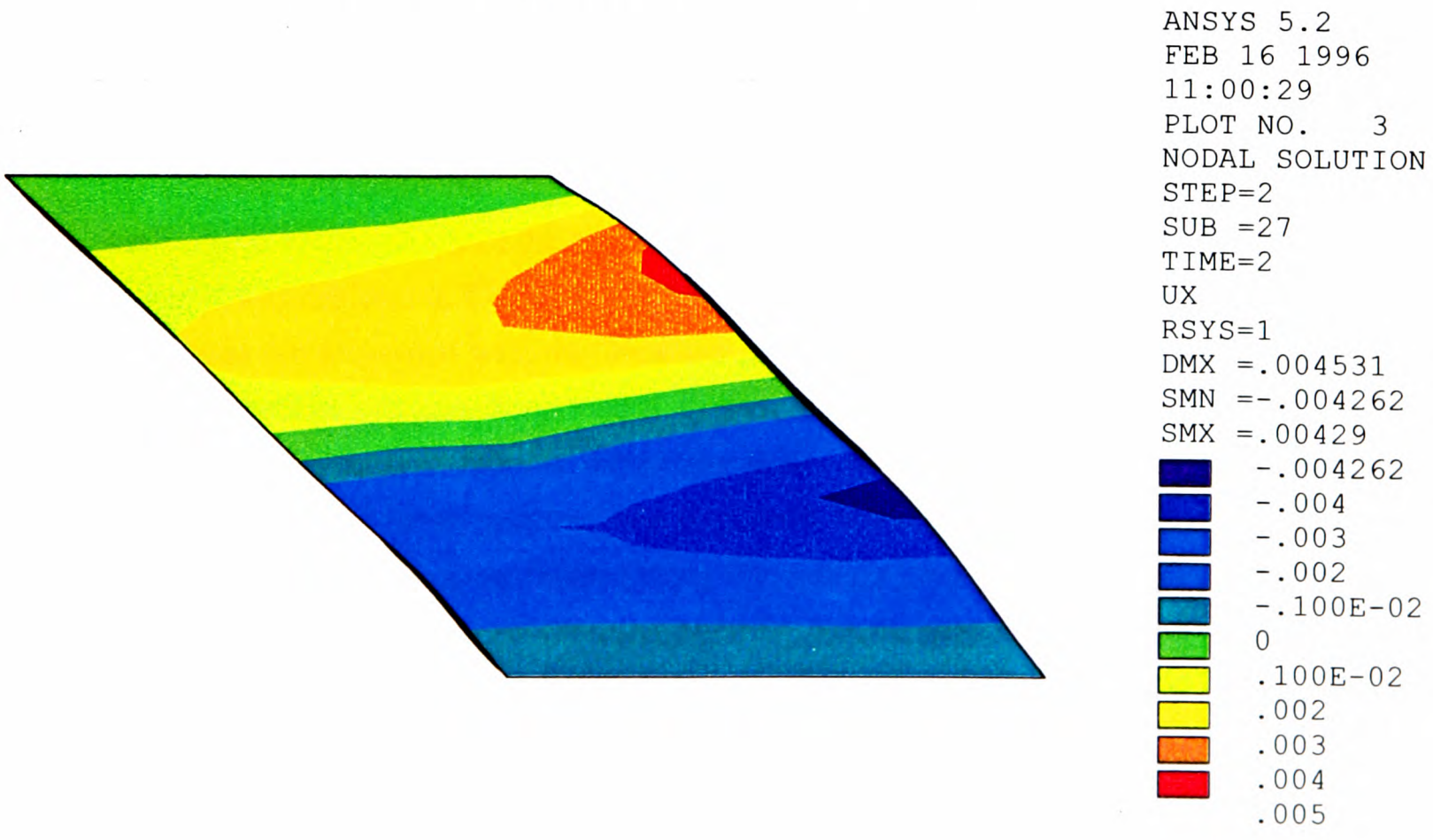

Figure 8.2b Radial deflection of the FE model of a single ring skewed arch when subjected to 400 kN live load

It can be seen that the model of the skewed arch shown in figure 8.2 can sustain an applied load of 400 kN despite it being only 102 mm thick. This is clearly incorrect; it would therefore be most inappropriate to conclude from these results that the strength of an arch increases in proportion to the increase in its angle of skew. A more reasonable conclusion is that the masonry is inappropriately modelled. Thus, this analysis can be used to establish how the finite element model proposed in section 7.6.2 should be amended.

It has already been discussed in section 7.4 that, in tension, the post-failure behaviour of the ANSYS "concrete" model does not realistically represent the behaviour of masonry. If the actual elastic-brittle properties of masonry were used in a finite element analysis it may create convergence problems, this is why Loo and Yang (1991a) adopted a post-failure strain softening approach. This would certainly increase the non-linearity of the load-deflection response of the model but it cannot be concluded that this will be significant if compared with a model that uses elastic-plastic properties especially if the tensile strength is small. Thus, although incorrect the use of the ANSYS "concrete" material model is adequate in this respect.

The analysis of the two-ring square arch shown in figure 7.35, in which only CONTAC12 elements were used (and which ensured that the rings could not overlap each other), could not sustain more than 90 kN of live load because beyond this load, compressive failures occurred due to the absence of composite action. In contrast, the analysis of the single-ring skewed arch shown in figure 8.2 revealed that (even with an unrealistically low compressive strength and a relatively large applied load) compressive failures were not predicted. Thus, the analysis could not terminate at a realistic load. It can be seen in figure 7.3 that the shape of the yield surface means that a combination of relatively large compressive principal stresses is less likely to cause failure than if only one of them is large. The deformed shape of the model, see figure 8.2b, was realistic. Its maximum outward deflection can be seen to be confined to a comparatively small region in the vicinity of the north east edge of the structure similar to the actual behaviour of arch 3-4 as depicted in figures 5.13. Thus, the pronounced transverse and longitudinal load effects that are associated with this localised peak outward deflection indicate the presence of at least two large compressive principal stresses at this location. This would account for the absence of compressive failures within the finite element model. However, the ANSYS "concrete" material model assumes that transverse bending, due to the above localised peak deflection, cannot cause shear failures along the bedding joints of the masonry. Thus, there is justification for a more appropriate material model than the one that is contained within ANSYS (William and Warnke, 1975).

As its title suggests, the ANSYS three-dimensional "concrete" material model only applies to concrete-like continua in which the material properties are isotropic and, consequently, the compressive strength is independent of the orientation of the principal stress. However, it can

be used to model the behaviour of masonry provided that one of the principal stresses is perpendicular to the bedding joints and the others are relatively small. This stress state was found to exist within the square arch when subjected to a full-width patch load, as shown in the work presented in section 7.4.1 and in the results shown in figures 7.35 and 7.36. Thus, when subjected to this type of loading, it would make little difference as to whether the yield surface, outlined in section 7.3, is described by accepting the suggested default values (William and Warnke, 1975) or if each of its parameters are experimentally obtained. However, if as Livesley (1992b) had done, the present model of the square arch was used to investigate the three-dimensional effects produced by an increasingly eccentric applied load the analysis would be incorrect. This is a situation which could not be rectified by correctly obtaining the strength parameters used to define the yield surface of the ANSYS "concrete" material model; it would require a restructuring of this material model in order to incorporate the planes of weakness created by the bedding joints within masonry.

It was pointed out by Dhanasekar et al. (1985) and Bernardini et al. (1982), that the compressive strength and elastic modulus of masonry are approximately twice as great in a direction perpendicular to the bedding joints as they are in a direction parallel to the bedding joints. Furthermore, they found that the resistance to compression, when the principal stress is inclined to the bedding joints, was also dependent upon the shear bond strength of the mortar. Therefore, failure was ultimately governed by a combination of the shear failure of the mortar bond and the compressive failure of the brickwork depending on the orientation of the uniaxial compression relative to the bedding joints. Thus, the "masonry" material models that they proposed for two-dimensional situations correctly attempted to account for the presence of mortar joints acting as planes of weakness. In contrast, the ANSYS "concrete" material model cannot predict shear failure although it can, through the use of its shear transfer coefficients, reduce the resistance of the material to shear forces after tensile failures have occurred. Hence, in the skewed masonry arch, where the principal stress is likely to be inclined to the bedding joints, the use of the ANSYS "concrete" material model is inappropriate. This is not so much because it assumes that the material is isotropic, and therefore cannot accurately predict compressive failures, but because it cannot incorporate the planes of weakness created by the bedding joints since it cannot predict shear failures associated with either translational fractures or torsional hinging. Notwithstanding this, the use of the ANSYS "concrete" material model proved to be successful in the analysis of the multi-ring square arch documented in section 7.4.

It can therefore be concluded that in a three-dimensional model of a masonry structure the material properties must be anisotropic and must take into consideration the presence of bedding joints in a similar way to the proposed material models of Dhanasekar et al. (1985) and Bernardini et al. (1982). However, ANSYS does not, at present, contain a "masonry" material model.

Thus, one option is to recognise the limitations of the ANSYS "concrete" material model by abandoning it so that orthotropic material properties can be assigned to the finite elements. This is not ideal because it does not explicitly recognise the presence of the bedding joints. However, the behaviour of the model may be improved by using realistic material properties (i.e. the elastic modulus and shear modulus) in each mutually perpendicular direction and by orienting each element so that these properties apply in the appropriate directions, i.e. parallel or perpendicular to the bedding joints. The strength of the material in each direction must also be specified. These one-dimensional yield criteria are unsatisfactory. Failure of an isotropic material is governed by the combination of principal stresses being greater than a given yield stress. This can only be modelled by a three-dimensional yield surface such as the one contained within the ANSYS "concrete" material model. Furthermore, it is inferred (Samarasinghe et al., 1981) that the failure of a three-dimensional material such as masonry which possesses distinctly directional properties requires a five-dimensional yield surface involving each principal stress and their orientation relative to the plane of the bedding joints. The development of a satisfactory "masonry" material model is beyond the scope of this research although it is recognised that, in fact, a three-dimensional yield surface of the form proposed by Dhanasekar et al. (1985) may prove to be successful. This is because the out-of-plane principal stress is relatively small and may therefore be neglected. Furthermore, if gap elements are used to connect the adjacent brickwork rings this potential plane of weakness has already been accounted for and need not figure in the yield surface. However, it is apparent from the above discussion that this option has several potential drawbacks.

The alternative modelling technique would be to retain the ANSYS "concrete" material model and thereby accept the limitations produced by its assumption of isotropy. Potential shear failures could be modelled by incorporating gap elements into the model at sections where fractures are anticipated. Superficially, it may appear spurious to claim that the present model can be corrected by using gap elements in this way especially when the difficulties associated with these elements, as discussed in section 7.6.2, are considered. However, a more critical examination of the results of the analysis of the single-ring skewed arch, shown in figure 8.2 reveals that the geometry of the arch caused significant transverse and longitudinal bending to occur but ANSYS could not recognise the significance of the transverse bending component of its behaviour since its representation of masonry was incorrect. In other words, ANSYS did not realise than this model was a masonry structure. Thus, irrespective of whether it would or would not fail in compression it could not fail in shear. Hence, it is suggested that gap elements are used to model potential shear failures and thereby correct the deficiency in the "concrete" material model. It would be impractical to model several potential fracture planes, i.e. as if they are diffused, because gap elements are highly non-linear and require that the applied load is increased in relatively small increments to ensure convergence. Therefore, they adversely effect run-times. Hence, multiple analyses would be required in order to obtain the optimum

position of each fracture in much the same way as in the three-dimensional mechanism method proposed in chapter 6. It should also be pointed out that the problems associated with gap elements being used to create composite action between adjacent brickwork rings, as discussed in section 7.6.2, will not be present in the modelling of fractures. In this case, the normal stress at the fractures should be sufficient to ensure that friction can prevent the adjacent blocks of masonry sliding relative to each other until the appropriate load is reached. At this point, the three-dimensional CONTAC52 gap element would allow sliding to occur in the desired direction so that torsional hinging or relative translational movements may occur. However, as discussed in section 7.2, the CONTAC52 gap element cannot resist tension, nor can its two-dimensional equivalent, viz. the CONTAC12 element. In order to incorporate the mortar bond strength the CONTAC52 gap element could be prestressed by an appropriate amount. Alternatively, a COMBIN40 element with elastic-brittle properties could be superimposed on the CONTAC52 element so that separation can only occur when the COMBIN40 element has failed.

The results of the finite element analyses of the model of skewed arch 3-4 when subjected to an eccentric point load on its south obtuse angled haunch, see figure 7.42, may confirm the requirement for fractures to be modelled by gap elements if not in-span then certainly at the abutments. Figure 7.42b shows that a downward deflection was predicted in the south acute angled haunch where experimental evidence, documented in chapters 4 and 5, would suggest that an upward deflection should occur. This may be attributable to the incorrect assumption of isotropic material properties but it is suggested that it may also be attributable to the fixity of the model at its abutments. It can be seen in figure 7.42c that the large compressive stress at the south west corner of the arch decreased rapidly in the easterly direction but then increased again towards the acute angled corner of the arch. It is suggested that by restraining the nodes of the model it is unable to deform in a realistic way and this causes the aforementioned downward deflection of the south acute angled haunch. If gap elements are used to separate the model from its supports the model could undergo slight rotations, on plan or in section, at its abutments and its deformed shape will be corrected.

The stiffness of the arch is dependent upon a number of parameters such as the presence of attached spandrel walls and the extent of ring separation. It also increases in proportion to an increase in its angle of skew.

When the angle of skew is small, i.e a square arch, the out-of-plane stiffness of the arch barrel increases due to the spandrel walls and decreases due to the presence of ring separation, this can be seen in figure 5.10. Moreover, the ratio of maximum outward deflection to maximum inward deflection was found to be related to the attachment of spandrel walls. When spandrel walls are attached to the arch barrel the arch deflects inwards, in the vicinity of the applied load,

more than it does outwards, at the second in-span hinge. This ratio is inverted when spandrel walls are detached from the arch barrel. However, as the angle of skew is increased the above ratio decreases irrespective of whether or not the spandrel walls are attached or detached. This can be seen in figures 5.11 and 5.13 and figure 5.12. It has been shown, see figure 8.2, that the occurrence of transverse bending is not a function of the material properties but is related to the geometry of the structure. The behaviour of the structure, in response to this effect in combination with the longitudinal load effects is, however, a function of its anisotropic material properties. It is suggested that the reason why the arch becomes stiffer as its angle of skew is increased is because the axes of rotation for longitudinal and transverse bending are inclined to the planes of the bedding joints. This is also the reason why the arch becomes weaker as its angle of skew is increased, i.e. because the combination of the longitudinal and transverse effects produce a more onerous condition and that the orientation of the bedding planes is such that each effect is resisted by a combination of shear and flexural strength, the latter term being comparatively low.

The increase in stiffness that is created by an increase in the angle of skew is discussed here to illustrate the difficulties involved in carrying out field tests on structures in which only their deflection is recorded. Chettoe and Henderson (1957) incorrectly remarked that they, "could see no reason to conclude that skew weakens the arch". They did not carry out any destructive load tests but observed that the stiffness of the arch was not decreased by skew although other effects such as attached spandrel walls and ring separation can also influence its stiffness. It is clear that there is no relationship between stiffness and strength. Therefore, it would have been more expedient to have issued the rather inconsequential remark that they, "could see no reason to conclude that skew decreases the stiffness of the arch". Furthermore, if several loads of different magnitudes are applied to a particular in-service bridge a non-linear load-deflection response may provide the Assessment Engineer with a subjective indication of its behaviour if loads of a greater magnitude are applied on it. However, a linear load-deflection response should not be used to conclude that the structure is safe when subjected to loads that are only marginally in excess of those used during the tests unless the gradient of the response can be compared with those produced by a history of similar load tests. In fact, if a non-destructive load test is to have any use at all, other than as a proof load test, its results must be predictable by a theoretical model that can proceed to produce an estimate of the capacity of the bridge.

8.2 Ring separation

It was shown by Gilbert (1993) that the problems associated with the construction of multi-ring brickwork arch bridges were appreciated as long ago as the beginning of the Nineteenth century. Despite this apparent knowledge, many bridges of this form were constructed in the U.K. throughout the remainder of this century. Construction details were sometimes amended so that, for instance, an arch requiring four rings was built with headers so that the number of rings was halved. However, this only reduces the problem; it does not solve it. Moreover, Engineers such as Fowler (Mackay, 1990) demonstrated this lack of understanding of the behaviour of this form of structure by continuing to construct them. In 1890 Fowler had faith enough in the availability of "very superior quality" brick and high quality mortar (which "possessed a degree of cohesive strength and a regularity of quality" that were hitherto unknown) to undertake the widening of the Maidenhead bridge using stretch bonded brickwork. The very fact that the presence of several circumferential bands of mortar affects a fundamental change in the behaviour of the arch, when compared with that of a voussoir arch, was largely overlooked. Furthermore, weathering, accidental damage and heavy trafficking over many decades may only serve to increase the difference between the two forms of arch by causing the brickwork rings to act non-compositely.

The "safe theorem" expounded by Heyman (1982), see section 2.4.3, relies on the assumption that shear failures cannot occur. Heyman was referring to the relative movement of two adjacent blocks of masonry along a radial fracture. However, in the multi-ring arch, shear failures can also occur in the circumferential direction. In this case, the safe theorem is invalidated if the trajectory of the line of thrust is calculated without taking into account the relative circumferential movement of the rings. Furthermore, any analytical method that idealises the arch as if it is a voussoir arch, and therefore assumes that plane sections remain plane, is not applicable to multi-ring brickwork arch bridges because, even if composite behaviour is maintained, the elasticity of the mortar bond ensures that plane sections do not remain plane. This was observed in the full-scale model bridge tests carried out by Gilbert (1993) and those that were carried out as part of this research, see figures 5.22 to 5.25. However, if the non-linearity of the strain profiles is overlooked it remains inherently unsafe to assume that the multiple rings of masonry in the barrel can behave in a way that is similar to that of a voussoir arch. In other words, the assumption is flawed that large shear forces can be transferred from one ring to another. This was recently recognised by Hendry (1990) who suggested that the assessment of a multi-ring arch bridge must include a check on possible circumferential shear failures.

The difference between the behaviour of a voussoir arch and that of a multi-ring arch can be seen in their respective load-deflection responses shown in figure 7.6. The "continuum" model

represents a voussoir arch whereas the "ring separation" model represents a multi-ring arch whose mortar is sufficiently strong to prevent ring separation. The flexibility of the mortar bond between each brickwork ring enables them to translate relative to each other in the circumferential direction without the bond failing. Thus, the overall flexibility of the multi-ring arch is greater than that of the equivalent voussoir arch. The shear failure of the mortar bond, i.e. ring separation, may occur in a plastic manner (Stöckl & Hofmann, 1988) without the formation of the cracks that are associated with brittle materials although excessive plastic strains will eventually cause cracking. The corollary of this is that a more flexible mortar will not prevent the brickwork rings acting non-compositely regardless of how strong it is. In other words, the total shear strain, i.e. elastic plus plastic, at a section at which a shear failure has already occurred may be equal to the elastic shear strain at a section at which the mortar is more flexible but sufficiently strong to prevent the shear failure. However, with each section straining by similar amounts the effect at each is equivalent to ring separation. Thus, non-composite behaviour is a function of both stiffness and strength of the mortar bond, as shown in figures 7.25 and 7.28 respectively. It can therefore be concluded that the flexibility of the mortar diminishes the amount of load sharing between adjacent rings, see figures 5.22 to 5.25, which will eventually lead to a reduction in the strength of the multi-ring arch, when compared with that of the equivalent voussoir arch, see figure 7.6.

The breakdown of composite action is hastened by a weaker mortar so that ultimately ring separation will lead to a significant reduction in the capacity of the arch. This was observed experimentally (Gilbert, 1993) and predicted by the proposed finite element analyses documented in chapter 7, see figure 7.27. In fact, the realism of the proposed finite element models enabled them to reproduce the load-deflection responses of Gilbert's square arch bridges, see figure 7.9, with a maximum error of only 5%. The reduction in strength due to ring separation was also predicted by Gilbert (1993) in his two-dimensional discrete rigid block mechanism method. However, Gilbert's model was based on the mechanism method, therefore he was forced to use a rigid-plastic model to represent the bond between adjacent brickwork rings as opposed to its actual elastic-plastic behaviour. Consequently, he incorrectly predicted that, given a suitably strong mortar a multi-ring arch would be stronger than the equivalent voussoir arch.

It is clear, from figure 7.27, that the accuracy of the predicted behaviour of an arch bridge, including its capacity, is dependent upon the magnitude of the shear bond strength that is used in the analysis. However, this parameter may be largely unquantifiable in a particular in-service bridge because, as Hendry (1990) points out, sufficiently large samples may be unobtainable. Non-destructive tests and radar surveys are available with which the extent of existing ring separation can be ascertained. Despite this, the Assessment Engineer is left with little guidance regarding the selection of an appropriate shear bond strength although BS 5628 states that a

horizontal shear strength of 0.15 N/mm^2 is applicable in a vertical wall if the vertical load is neglected. However, it is suggested that the properties listed in table 7.1 may be considered as upper and lower bounds within which an appropriate value will lie.

It can be seen in figure 7.35 that when the shear bond strength is assumed to be zero, the analysis will predict an unrealistically low arch capacity. Furthermore, the lower bound value of 0.08 N/mm^2 is perhaps also conservative since it was selected to represent the shear bond strength of damp sand. However, it was also suggested that this non-zero value was selected to make allowance for the possibility of mortar or brick intrusions into the damp sand layer that would act as shear studs. This is equally possible within an in-service bridge since it is very unlikely that the surfaces of each ring are continuous curves. Any discontinuity, albeit small, will enhance the resistance to relative sliding movements. Thus, it is suggested that the upper-bound value of 0.25 N/mm^2 is a value that may reasonably be applied to most in-service arch bridges. The justification for this is that it was experimentally obtained from brickwork samples pertaining to square arch bridges 3-0c and 3-0d and consequently enabled an accurate analysis of these structures to be performed, see figure 7.9. Furthermore, these structures contained mortar that is representative of those that occur in actual arch bridges (Temple & Kennedy, 1989). It seems reasonable to suggest that a finite element model of an in-service bridge may be developed by adopting this value of shear bond strength factored to take account of the ratio of areas of existing ring separation to areas of intact bond. This ratio can be obtained by carrying out a radar survey or another form of non-destructive test. The alternative approach, i.e. to use a shear bond strength that varies throughout each interface, would be impractical.

The shear bond strength of 0.25 N/mm^2 that enabled the present finite element model to reproduce the measured load-deflection response of bridge 3-0d must be contrasted with the value of 0.15 N/mm^2 that was used by Gilbert (1993). It is suggested that Gilbert's rigid-plastic model of the shear bond between adjacent rings as opposed to the present elastic-plastic model (Stöckl & Hofmann, 1988) will account for some of this difference. The remaining component of the difference will be attributable to the respective modelling of the spandrel fill. Notwithstanding these modelling differences, each of these methods produced a predicted relationship between arch capacity and shear bond strength that was not too dissimilar to each other, see figure 7.27. However, Choo et al. (1991a) concluded, from their finite element analysis of ring separation, that a shear bond strength of 0.05 N/mm^2 is sufficient for the arch to attain over 80% of the strength of an equivalent "well bonded" arch; a fact that is not borne out in the results shown in figure 7.27.

The finite element analysis of ring separation that was documented in chapter 7 was applicable only to the square arch that is subjected to a full-width patch load and whose spandrel walls are detached. This is because ANSYS does not contain an appropriate gap element that can allow

relative sliding movements to occur in any arbitrary direction after a given bond strength has been overcome. Ring separation could only be modelled because in this essentially two-dimensional problem the orientation of the COMBIN40 gap elements, i.e. those elements that control when the rings are allowed to slide relative to each other, remain fortuitously aligned with the invariant direction of movement throughout the analysis.

The inability of the triad of essentially one-dimensional gap elements to model ring separation in a three-dimensional finite element model was discussed in section 7.6.2. It was concluded that it would take an inordinate number of iterations to obtain the stiffness and strength parameters of each pair of COMBIN40 elements. In other words, unless these values could be obtained, ring separation may be prevented from occurring because of the flaw within the finite element model. However, the results of the analysis of the single ring skewed arch, depicted in figure 8.2, show that another reason for the excessive number of iterations was that the gap elements were not required. The inability of the SOLID65 element to represent the behaviour of masonry meant that ANSYS considered each ring to be adequate if acting alone. However, given the assumption that the modelling of masonry can be improved, further investigation into obtaining a successful way of modelling the interaction of each brickwork ring is required.

It is suggested that in order to model ring separation in a three-dimensional model of a multi-ring brickwork arch another three-dimensional gap element is required, which is currently unavailable within ANSYS. This hybrid element could be formed from a COMBIN40 element and a CONTAC52 element. In other words, it must prevent adjacent brickwork rings overlapping each other but must possess elastic-brittle properties in the opposite direction so that separation is resisted until its bond strength is overcome. The element must also possess elastic-plastic properties in shear, and must align itself with the direction of the resultant sliding force. However, if the tensile bond strength has been overcome its shear resistance should be reduced to that which can be created through friction. Conversely, the shear failure of the mortar bond should not effect the tensile bond strength.

In lieu of the above extension of the ANSYS element library it is suggested that the following options could be investigated in order to determine an alternative method of modelling the interaction of adjacent rings. One option is to use a CONTAC12 element to resist penetration and a single COMBIN40 element to incorporate the shear bond strength between them. During each load increment an iterative process would be required in order to orientate each element in the direction of relative movement. However, it seems reasonable to conclude that this method will converge even slower than the method that required a triad of gap elements. Another option is to use only small, i.e 10 mm long, elastic-plastic beam elements to connect the adjacent rings. These will bend in the desired direction within the elastic range and undergo relatively large deformations when their elastic limit has been exceeded, i.e allow ring

separation. However, it is unfortunate that ANSYS does not contain such an element. Another option is to use solid elements to model each mortar ring that are similar to those within each brickwork ring with the exception that their material properties are adjusted to ensure that ring separation takes place at an appropriate load.

A further option is to use CONTAC52 elements between each brickwork ring because these will orientate themselves in the direction of the relative movement although they cannot model the shear bond strength. With reference to figure 7.7b, if the shear strength of this element can be increased from μFN to F_{slide} it would appear that the element can be made to provide the desired functions. In retrospect, this idea proved to be flawed. The coefficient of friction of the element can be set to 1.0 and it can be prestressed by F_{slide}. This would, if FN is small, produce the required resistance to sliding movements. However, it was found that in the square arch even a prestress of 0.1 kN changed the mode of behaviour of the arch to that of a voussoir arch, i.e the arch shown in figure 7.35 could sustain the maximum applied load of 400 kN and produced a load-deflection response that exhibited only small non-linearities. It is suggested that the initial compression of these elements attracts load effects towards them. Thus, the normal force within them increased in proportion to the magnitude of the applied load. Consequently, ring separation did not occur. Although it proved to be an unsuccessful method of modelling ring separation, when it was used within the model of the skewed arch it provided insight into the deficiencies of the modelling of the behaviour of masonry. In this case it was found that a prestress was not required. In other words, each individual ring was capable of sustaining the load without calling on composite action with the other ring via the gap elements. This was illustrated in the subsequent analysis of a single ring skewed arch, the results of which are shown in figure 8.2. Thus the "masonry" material model was unrealistic since the applied load should only have been sustainable if composite action had been created by, in this case, prestressing the gap elements.

The finite element model that was developed in section 7.4 has applications beyond the modelling of ring separation in a multi-ring brickwork arch bridge. For example the change in behaviour of an arch caused by the addition of a concrete saddle or a concrete lining can be investigated with this modelling technique. At present, there is little documented evidence that these proposed strengthening measures are successful in this respect. Furthermore, it is not known what effect they will have upon the behaviour of the existing structure. This is particularly important in the case of concrete saddles where any reduction in the compression within the arch may create further problems. Although the bond between the concrete and the top ring may be sound, the effects that this has upon the bond between subsequent brickwork rings requires further study.

A strengthening measure that was studied by Gilbert (1993) was to stitch each brickwork ring together so that, with the aid of these steel bars, the performance of the arch becomes comparable with that of an equivalent voussoir arch. The three-dimensional equivalent of the proposed finite element model would enable the effects of this proposed strengthening measure to be investigated. In particular, the required spacing of the steel bars could be obtained as a function of strength. This would enable the Assessment Engineer to cost his proposed strengthening measures.

Outside the field of arch assessment but within the global field of bridge assessment and repair, a proposed strengthening measure is to glue carbon fibre reinforced plastic sheets onto the soffit of concrete bridges. This material is light and very strong and has been shown to produce a significance increase in the strength of concrete beams when tested in bending. However, a hitherto unobserved failure mode (Peshkam et al., 1985) has been encountered. The concrete cover to the existing reinforcing bars along with the composite sheets "peel" off the structure as a result of a longitudinal shear failure. The existing reinforcing bars create a potential plane of weakness, especially if they are too closely spaced, which requires incorporation into the theoretical model. It is suggested that the use of gap elements similar to the way in which they were used in the finite element model of the arch presented in section 7.4 will be directly applicable to this particular problem as, indeed it will to any other two-dimensional surface-to-surface contact problem.

8.3 The influence of the spandrel walls

The change in the behaviour of the arch due to its interaction with the spandrel walls is very much dependent upon the relative dimensions of these elements of the structure, their condition, and their respective supports. The attached spandrel walls of the relevant full-scale model structures listed in table 3.1 were of fairly limited extent (they were only 375 mm high at the crown of the arch), with free ends, and without the added restraint that external soil may introduce. These walls were also well maintained as were the arch barrels (with the exception of arch 3-0b which contained the defect of ring separation). The collapse mechanism of skewed arch 3-3, shown in figure 5.7, and square arch 3-0a and 3-0b (Gilbert, 1993) indicate how the walls of the above form interact with the arch barrel. Each wall was broken into several blocks of masonry by the formation of discrete hinge-like cracks within them. Consequently, the arch barrel is stiffened and the three-dimensional aspects of its behaviour are increased, see figure 5.10, but the configuration of the collapse mechanism, compared with that of the equivalent structure with detached spandrel walls, is only marginally changed.

Given that the collapse mechanism of the structure with detached spandrel walls is optimal then, the change in configuration due to the attachment of spandrel walls represents an increase in the required collapse load. Furthermore, the inclusion of the spandrel walls within the mechanism must also add to the required collapse load. Therefore an increase in the capacity of the arch would be expected. Royles and Hendry (1991) observed this increase during their tests on small-scale voussoir arches. The experimental evidence documented in section 5.1.4.1 indicates that the presence of attached spandrel walls (at least within a structure of a form whose proportions are similar to these full-scale model bridges) affects a significant increase in the stiffness of the arch. They also appear to increase the extent of ring separation but do not appear to significantly alter the maximum sustainable load. In fact, on a pro rata basis, the indications are that attached spandrel walls weaken the structure. However, no firm conclusions can be made in this respect without developing a theoretical model with which the effects that are produced by attached spandrel walls can be investigated. It is suggested that the stiffening effect produced by spandrel walls increases the shear stress within the arch which, in turn, will increases the likelihood of ring separation if the arch is a multi-ring construction. However, the increased stiffness of the arch may also diminish its ability to mobilise passive pressures. The quality of the materials and the construction of each model arch was controlled in order to minimise the variability of the material properties of each structure, see table 3.5. Thus, it is unlikely that the increased extent of ring separation within each arch that had attached spandrel walls is due a mortar whose shear bond strength was relatively low.

With the exception of the two-dimensional discrete rigid block mechanism method that was proposed by Gilbert (1993), analysts have generally ignored spandrel walls. In fact, Gilbert,

by analysing a section of arch and a section through the spandrel walls could only include them on a pro rata basis. Consequently, he predicted that his 3.0 m span arch bridges with attached spandrel walls should have been approximately 50% stronger that the equivalent structures with detached spandrel walls. Notwithstanding the inaccuracies inherent within his modelling of the shear bond between adjacent brickwork rings, it is clear that a three-dimensional analytical tool is required in order to investigate the interaction of the arch barrel and the spandrel walls. However, the computational difficulties involved have, to date, deterred analysts from carrying out this study although the assumed unreliability of their strengthening effect may have been used as a further reason to neglect them. Conversely, this could have been used as a positive argument for carrying out this investigation.

The discretisation of the attached spandrel walls of the full-scale model arch bridges suggests a simple way in which they can be included in a three-dimensional analysis of the form presented in section 6.7. They can be represented by simple mechanisms that must be compatible with the arch barrel. Figure 5.15 reveals that the spandrel walls of skewed arch 3-3 were broken into several blocks of masonry which underwent complex relative movements. An insufficient number of deflection gauges were used to monitor the movement of the spandrel walls of the equivalent square arch bridges. However, it can be inferred from the changes in passive backfill pressure, when comparing figure 5.32 with figure 5.35, that the outward movement of the walls inhibited the build-up of passive pressure at the edge of the structure irrespective of the angle of skew of the arch. In other words, a complex hinged mechanism may also occur within the spandrel walls.

To include the spandrel and wing walls in an analysis by assuming that they will interact with the barrel in the way that is depicted in figure 5.15 is to limit the applicability of the model to structures whose proportions are similar to those of the full-scale model arch bridges documented in chapter 5. If the bond between each individual element within the perimeter walls is without tensile strength the walls will provide less restraint to the barrel. If the walls are relatively large, well maintained, or are restrained at their ends, for example if the bridge is across a cutting and is founded on bedrock, they may affect a change in the behaviour of the arch so that it fails in a way that does not require that the walls are displaced by the mechanism within the arch barrel. This is particularly apparent in the case where spandrel walls interlock with the arch barrel. In this case, spandrel wall detachment may occur as a result of the shear failure of the arch along a path that is parallel to the walls. The load required to produce this failure may be in excess of that which is required to cause the remaining portion of the arch to fail. Consequently, collapse will occur simultaneously with the detachment of the walls. However, there are innumerable in-service bridges, which are subjected to dynamic loads, in which longitudinal cracks such as these exist. The following conjecture that shear failures, such as these, may be progressive as a result of fatigue is offered as explanation. If the edge of the

arch is restrained by the spandrel walls whilst the interior is deformed by the applied loads. The interior of the arch may not fully recover after the load is removed, although the shortfall may be imperceptible, so that the cumulative effect of these relatively small dynamic loads is the formation of cracks that will eventually detach the spandrel walls. Furthermore, vertical cracks within the piers in the vicinity of the obtuse angled corners of a skewed arch may also occur as a result of this accumulation of stress.

In the case of the analysis of an arch bridge when subjected to a static load it is apparent that if spandrel walls are to be included the model must be capable of forming several different mechanisms so that the optimum one can be ascertained. In a finite element model, the spandrel walls could be included in the way that is advocated by Choo et al. (1993), i.e non-linear spring elements. It is suggested that a more realistic method would be to use three-dimensional solid elements within which potential fractures could be modelled with gap elements that could hold the structure together if fractures are deemed not to be required. In this way, support conditions can be more realistically incorporated into the analysis rather than arbitrarily adjusting a set of spring stiffnesses. Furthermore, the influence of the soil outside the structure could also be incorporated. However, the elements within each spandrel wall must be connected to the arch barrel by gap elements in a way that reflects the actual construction details of the modelled structure. In essence, if the material model cannot accurately represent masonry, gap elements must be used to allow the model to fracture in a realistic way. Without, these although the model may resemble the modelled structure in appearance, it cannot allow it to behave in a realistic way.

8.4 The behaviour of the backfill

It is clear from the results of the finite element analyses presented in section 7.5 that the behaviour of the arch is greatly influenced by its interaction with the spandrel fill, see figures 7.30 and 7.31. Conversely, the predicted behaviour that any analytical technique will produce is dependent upon the assumed contribution of the backfill. This is pointed out in the DoT advice note BA 16/93 in which it is suggested that many mechanism models "may not be appropriate for arch bridges where soil resistance is important". It is clear that there is concern regarding the ability of a theoretical model that is based on the mechanism method to correctly incorporate the backfill. It is suggested that this concern should be directed towards all theoretical models because, even though the alternative finite element method (for example) is capable of including the backfill in a more realistic way, it does not necessarily follow that the assumptions upon which the particular model is based are correct. However, it is recognised that the spandrel fill is an important component of a masonry arch bridge and therefore a comprehensive investigation into their interaction is a prerequisite part of the development of arch theory.

It can be seen in figure 7.30 that the behaviour of the finite element model of square arch 3-0d is dependent upon the magnitude of the horizontal passive pressure that is assumed to act on it. However, when subjected to its maximum applied load of 540 kN, the maximum inward deflection of the arch, in the vicinity of its first in-span hinge, was found to be approximately 7.5 mm. Thus, if the assumed passive pressure enables the model to deflect more than 7.5 mm or does not stabilise it so that it fails prematurely, the assumption was too low. Likewise, if the model does not deflect enough or it sustains too much load it can be concluded that the assumed magnitude of the passive pressure was too high. In this way, provided that the behaviour of the model and the method of load dispersal are realistic, the assumptions pertaining to the behaviour of the backfill can be validated. Clearly, direct back substitution of experimentally obtained data or carrying out multiple analyses until the input parameters enable the observed behaviour to be reproduced are techniques that can only be employed when a given bridge has been extensively instrumented and load tested to failure. Therefore, the procedure of applying predetermined loads or, for that matter, predetermined spring stiffnesses (Choo et al., 1991) are not applicable to "real" bridges. As previously discussed, a more representative model of the backfill is required.

In the case of the full-scale model arch bridges, the rate at which horizontal passive backfill pressures increased as the arch rotated into the soil mass, see figure 5.31, was dependent upon several factors.

Figure 8.3 shows the relationship between the horizontal strain within a dense sand, as a vertical retaining wall translates in the horizontal direction, and the ratio of the horizontal to vertical stress within it (Chen, 1975).

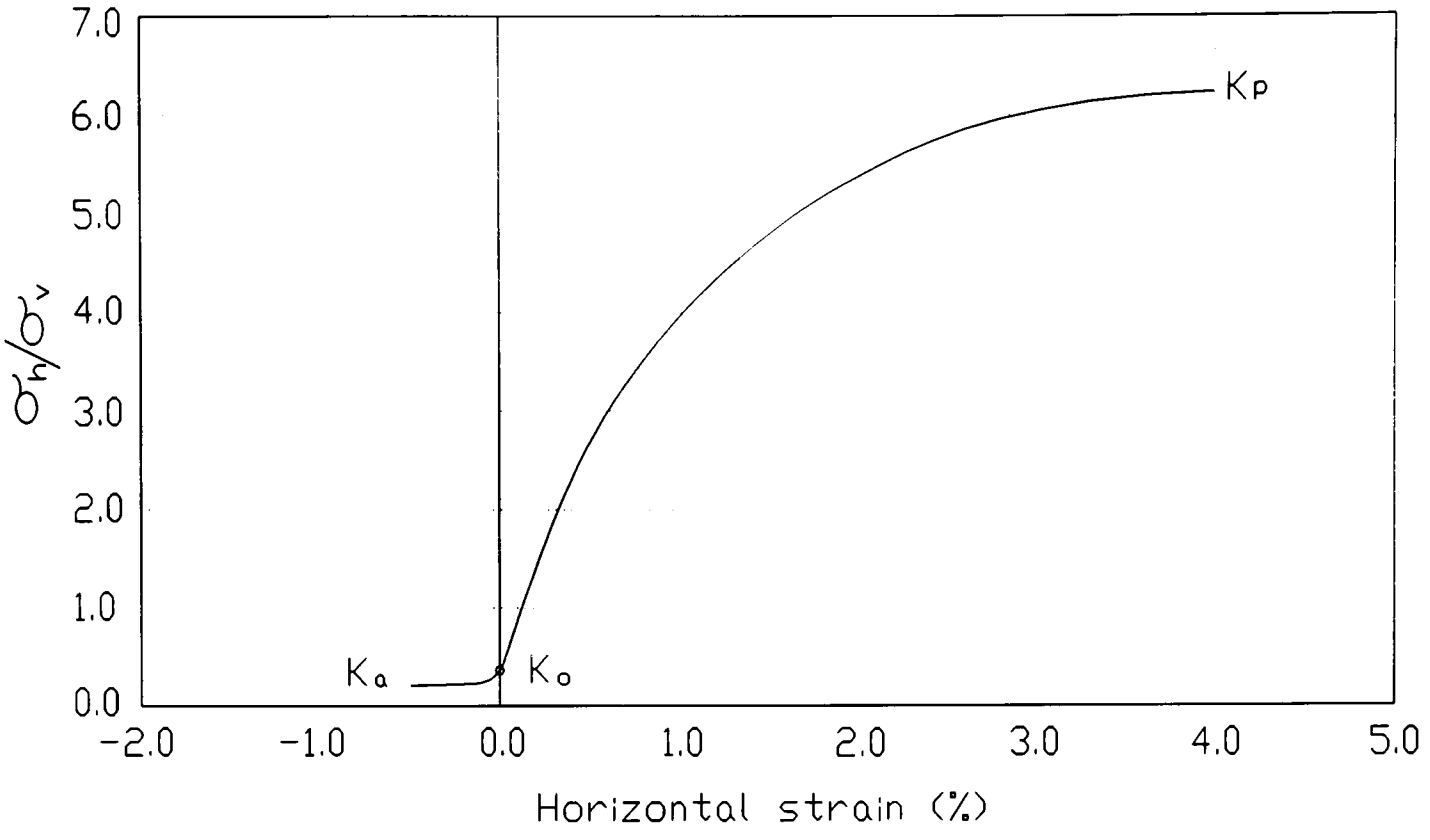

Figure 8.3 Movement related pressures in a dense sand

It can be seen that very little horizontal strain, i.e. approximately -0.5%, is required to reach the active state. However, much larger strains, i.e. approximately 4.0% are required to mobilise the maximum passive resistance. It was also noted by Chen (1975) that in loose sands the maximum passive resistance may be mobilised only after strains as large as 15.0% occur. Thus, the degree of compaction of the material effects how rapidly the passive pressures are mobilised. It also effects how much pressure is present in the so called un-loaded state.

The spandrel walls also effect the rate of increase of movement related passive pressures. They stiffen the arch, see figure 5.9, so that it is less able to deform and therefore cannot mobilise passive pressures of a similar magnitude as those that can be mobilised by the equivalent arch with detached spandrel walls, compare figure 5.31d with figure 5.31e. Furthermore, in each full-scale model, when spandrel walls were attached to the arch an upper limit was imposed on the mobilisation of pressures, see figures 5.31a, 5.31b and 5.31d. In contrast, when spandrel walls were detached from the arch passive pressures continued to increase well beyond the point at which the arch became unstable and was transformed into a mechanism, see figures 5.31c and 5.31e. The deformation of these arches was not sufficient to mobilise the maximum passive

resistance of the backfill. Therefore it can be concluded that, depending on the proportions of the arch, failure may occur due to relatively small movements whose destabilising effects must therefore outweigh the strengthening effects of a potential increase in passive pressure.

Depending on their form, attached spandrel walls may be displaced by the arch as it deforms, see figure 5.7, and broken into several blocks of masonry. These blocks are therefore more readily displaced outwards by the movement of the arch and the pressure within the spandrel fill than they would be if the walls were detached and therefore remain intact. This situation is increased if the walls are constructed with poor quality mortar or if the angle of skew of the bridge is increased because, in this case, it is not only the lateral pressure within the fill but the component of the longitudinal pressure that forces the walls outwards. Consequently, the movement of the walls reduces the confinement of the spandrel fill and therefore prevents passive pressures increasing beyond a particular value. When spandrel walls are detached, they should be capable of both confining the fill and allowing the arch to deform more freely so that it can generate higher passive pressures. It was found that as the angle of skew increases the perimeter walls become less able to resist the outward pressure so that in the case of skewed arch 3-4 they were displaced outwards even though they were detached from the arch. Thus, the passive pressures within this structure were not as large as they could have been if the movement of the perimeter walls had been prevented by, for instance, the presence of soil outside the structure. In fact, any medium outside the structure that assists in the confinement of the spandrel fill is beneficial, whether its continual presence can be relied upon is another issue.

The increased stiffness of the arch due to its angle of skew results in its outward deflection being less than that of the equivalent arch with a smaller angle of skew. Consequently, the passive pressures that it mobilises are also smaller. Furthermore, the change in geometry due to the increase in the angle of skew causes the maximum outward deflection of the arch to migrate towards a comparatively small region at the edge of the structure in its obtuse angled haunch, see figures 5.13 and 8.2. Likewise, the mobilisation of stabilising passive pressures is confined to a small region in the vicinity of the obtuse angled haunch. Figure 5.33 reveals that the maximum increase in passive pressure in bridge 3-3 was smaller and much less widespread than the equivalent pressures in bridge 3-0a, as shown in figure 5.32.

The spandrel fill also enhances the load carrying capacity of an arch bridge by dispersing the applied loads, see figures 7.32 and 7.33. The DoT design note, BD 21/93, recommends that the load should be applied uniformly over a section of the extrados contained within load dispersal lines drawn at 2 vertical : 1 horizontal (26.6°) from the edges of the load at the surface of the spandrel fill as shown in figure 8.4.

This appears to have been selected arbitrarily because of its simplicity. As such, it does not indicate to the Assessment Engineer the importance of the spandrel fill. Nevertheless Gilbert (1993) adopted this method in his analyses although he used a 45° load dispersal for the 3.0 m span arches and, despite the same backfill material being used, a 30° load dispersal for the 5.0 m span arches. In contrast, the method of load dispersal used within this thesis was based on the sinusoidal distribution suggested by Smith (1991) as shown in figure 7.8. This method was adopted because it would produce a distribution similar to that which was observed in the results of the moving point load tests shown in figure 4.24.

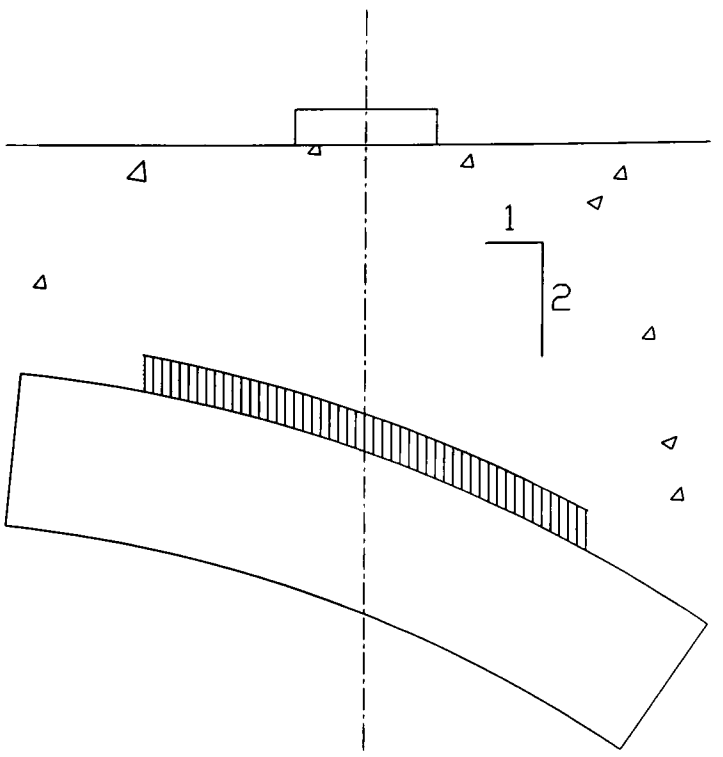

Figure 8.4 Load dispersal from BD 21/93

It can be seen in figures 7.32 and 7.33 that a significant increase in the predicted capacity of an arch bridge can be achieved by increasing the load dispersal angle. Moreover, there should be a more significant increase in the predicted capacity if the uniform distribution advocated in the DoT design note, BD 21/93, is used because with the sinusoidal distribution the load is more concentrated directly beneath the position of the load irrespective of the angle of dispersal.

It can also be seen, in figures 7.30 and 7.31, that the assumed magnitude of the passive pressure is significant in determining what capacity will be predicted. Therefore, it can be concluded that if the analyst selects a method of load dispersal that is incorrect, an equally incorrect assumption pertaining to the passive pressure distribution can make the results of the analysis appear to concur with experimental observations. In this case, the model must be used only with caution as a predictive tool, i.e. where experimental observations are not available, because multiple modelling errors cannot be assumed to remain self compensating. In the present finite element model, the method of load dispersal was verified experimentally and the behaviour of the model was realistic because of the gap elements. Therefore, despite the backfill pressure not having been measured in the modelled structures, the assumptions pertaining to its distribution must have been reasonable because the other two components of the model, that could potentially compensate for any errors, were reasonable.

9.0 Conclusions

1. The load carrying behaviour of the masonry arch is a function of its geometry, the applied load and its anisotropic material properties. The geometry and applied load may conspire to produce a behaviour within which there are pronounced three-dimensional effects. Its anisotropic material properties will increase the significance of these effects.

2. The masonry arch is essentially a one-way spanning structure. Its failure is determined by the combination of its transverse load effects and its longitudinal load effects relative to their respective resistances. An increase in the eccentricity of the applied load or a change in geometry such as an increase in the angle of skew increases the three-dimensional aspects of its load carrying behaviour and, consequently, will cause failure to occur at a lower load.

3. The three-dimensional aspects of the behaviour of the square arch, of normal proportions, were found to be sufficiently small to enable its behaviour to be reproduced by a two-dimensional analysis. The results of the destructive load tests on the small-scale model arches indicate that, when subjected to an eccentric point load applied at the edge of the structure at its quarter-span section, the arch will behave in an essentially two-dimensional way even when its span/width ratio is decreased to 0.5.

4. Two-dimensional discrete rigid block analytical techniques have been developed, based on the upper-bound and lower-bound theorem of collapse respectively. The duality between the two methods has been demonstrated.

5. A two-dimensional indiscrete rigid block analytical technique has been devised, based on plastic theory, which can be used to investigate the ultimate behaviour of the square voussoir arch. The analysis of a theoretical model formed using this technique proved to be as accurate as either of the above discrete rigid block mechanism methods. Furthermore, it proved to be quicker to perform, requires much less computer effort, and produces more information regarding the effect that varying the fracture locations has upon the predicted collapse load.

6. When subjected to a full-width patch load, situated in the vicinity of the quarter-span section and placed parallel to the abutments, each full-scale model square arch bridge failed due to the formation of a simple hinged mechanism. An increase in the angle of skew of the arch caused the failure mechanism to become three-dimensional in which there were five fractures of which those that occurred in-span were inclined to the abutments.

7. The large-scale model skewed brickwork arch bridges failed at lower loads than their respective equivalent square arch counterparts.

8. A three-dimensional indiscrete rigid block analytical technique has been devised which can be used to investigate the ultimate behaviour of the skewed masonry arch. Using this modelling technique to analyse the observed collapse mechanisms it was found that, to be admissible, the blocks of masonry bounded by each fracture must undergo relative movements that are more complex than the simple hinges hitherto associated with the two-dimensional collapse mechanism of a square arch bridge.

9. The minimum number of fractures required to create a hinged mechanism is four. However, this situation will occur only if the geometry of the arch and its applied loading are such that each fracture is parallel to the abutments. Within the skewed arch, the collapse mechanism contains fractures that are inclined to the abutments. In accordance with the above three-dimensional mechanism method, if a simple hinge is assumed to occur at the south springing, the collapse mechanism must contain seven relative block movements.

10. The compatibility requirement for each block of masonry, bounded by the fractures that form within the arch at failure, to undergo complex relative movements when accommodating the displacement of the applied load was verified during the destructive load tests on the small-scale model skewed arches. Full-depth tension, consistent with the formation of a radial hinge, upward and downward relative sliding movements at opposite ends of a given fracture, consistent with the formation of a torsional hinge, were observed in conjunction with the formation of simple hinges.

11. When subjected to an eccentric point load situated on its acute angled haunch, the behaviour of the small-scale model arch was clearly three-dimensional in which complex relative block movements occurred at some of the fractures. In contrast, when loaded on the obtuse angled haunch the geometry and applied load conspired to produce an overall behaviour in which the three-dimensional effects were comparatively small. However, in this case, the requirement for complex relative block movements remains valid.

12. Small-scale model arch bridges can be constructed and tested in a similar way as full-scale models. Within the small-scale model arches, the bond strength of the mortar may have increased the strength of the arch and may have resulted in the formation of fractures at locations where they would not occur if the mortar was less strong. The behaviour of the structures can be made comparable by reducing the bond strength of

the mortar by applying a debonding agent onto the bricks or by re-tempering the mortar by adding water to it and then remixing it.

13. The behaviour of a multi-ring arch is fundamentally different from that of a voussoir arch. The relatively high flexibility of the bond between each ring of masonry means that plane sections do not remain plane. Therefore, the multi-ring arch cannot be analysed in the same way as a voussoir arch. Consequently, in order to assess the load carrying capacity of the arch by using the safe theorem of collapse, which states that "collapse will not occur if the thrust line lies entirely within the bounds of the arch", the relative movement of the adjacent rings (before and after possible shear failures) must be taken into account.

14. A three-dimensional finite element model has been developed for the analysis of the multi-ring square arch bridge without spandrel walls. This model behaves in a realistic way because it uses gap elements to create composite action between each brickwork ring. Within their elastic range the flexibility of these elements allows the rings to displace relative to each other in the circumferential direction. Ultimately, when their strength is overcome ring separation is able to propagate through the structure. The model is based on actual measured material properties and reproduces the measured load-deflection responses of the relevant full-scale model bridges throughout their load histories.

15. The stiffness of the arch is decreased if it is constructed from several rings of masonry as opposed to a single ring. It is decreased further if the rings separate due to the shear failure of the bond between each ring. It is also decreased by the detachment of its spandrel walls. However, its stiffness is increased if the angle of skew of the arch is increased because the orientation of the axes of bending become inclined to the bedding joints.

16. There is no simple relationship between stiffness and strength.

17. The load carrying capacity of each square arch bridge that suffered ring separation during its load test was greater than that of the equivalent structure containing total ring separation prior to the load test. The initiation of ring separation is very unpredictable relying, as it does, on the shear bond strength of the mortar; a property that in practice will vary throughout the particular structure and will be difficult to ascertain.

18. The results of the load tests on the full-scale model arch bridges have indicated that attached spandrel walls, of these proportions, have a significant effect upon the behaviour of the bridge in terms of increasing its stiffness but not its strength. In fact, the results indicate that the strength may be decreased by attached spandrel walls of the form used in the test programme. The increased stiffness of the arch results in it being unable to mobilise passive pressures as freely as if the walls were detached. Furthermore, the prevalence of ring separation within the structures whose spandrel walls were attached to the arch indicates that the shear stress within the arch may be increased if spandrel walls are attached to it. Consequently, ring separation may become more likely. In arch bridges whose geometry is different from these test structures the ability of the spandrel walls to strengthen it will depend on the construction details of the arch, the fixity of the walls into the arch, their end supports, their extent and their relative condition.

19. The modelling technique that was used in the proposed finite element model to create composite action between adjacent brickwork rings has applications beyond the study of the behaviour of multi-ring arch bridges. Any continuum that may fragment into a number of smaller parts due to a shear failure and which therefore remain in contact with each other can be modelled using this technique. For example, the interaction of the arch with a concrete saddle or a concrete lining can be modelled in this way, as can detachable spandrel walls. The "peel off" problem associated with the failure of concrete beams when strengthened using external reinforcement is another application.

20. The results of the analyses of the proposed theoretical models, whether mechanism or finite element, and the results of the load tests on the full-scale model arch bridges indicate that the mobilisation of passive pressure significantly strengthens the arch. The distribution of passive pressure is related to the deformation of the arch rather than being proportional to depth. It is also dependent upon the degree of compaction of the spandrel fill. It was observed that the deformation of the arch at failure was insufficient to mobilise the maximum passive resistance. However, in other structures this situation will be dependent upon the proportions of the arch.

21. As the angle of skew increases, the arch becomes stiffer and its twisting behaviour increases. Thus, the extent and the magnitude of the movement related passive pressure that it mobilises diminish as the angle of skew increases. This provides a further reason why the load carrying capacity of the arch reduces as its angle of skew increases.

22. The backfill also has a significant influence on the load carrying capacity of the arch in terms of the stability it provides due to its weight and its ability to disperse the applied load. The results of the analyses of the above finite element model and the mechanism model indicate that the greater its ability to spread the applied load, the greater is the load carrying capacity of the structure.

23. The distribution of vertical load on the extrados of the arch due to its dispersal through the spandrel fill was found to be of a sinusoidal form confined within dispersal limits of 30° to the vertical. Experimental observations indicate that the angle of load dispersal may reduce as the applied load in monotonically increased.

24. A three-dimensional finite element model of the skewed multi-ring brickwork arch has been developed. The analysis of this model was able to reproduce the observed behaviour of the full-scale model skewed arch bridges when subjected to applied loads that do not exceed the elastic limit of the structure.

25. In order to increase its usefulness the three-dimensional finite element model requires the development of a more sophisticated material model, that is applicable to masonry i.e. incorporates the planes of weakness created by the bedding joints, and a three-dimensional gap element, to create composite action between adjacent rings. These improvements will enable it to produce a realistic analysis of the entire load history, including its ultimate behaviour, of the multi-ring arch bridge when subjected to eccentric loads, when spandrel walls are in contact with it, or when skewed. The required three-dimensional gap element must prevent adjacent brickwork rings overlapping each other but must possess elastic-brittle properties in the opposite direction so that separation is resisted until its bond strength is overcome. The element must also possess elastic-plastic properties in shear, and must align itself with the direction of the resultant sliding force. However, if the tensile bond strength has been overcome its shear resistance should be reduced to that which can be created through friction.

10.0 Suggestions for future work

1. The finite element analyses of the full-scale model multi-ring square arch bridges revealed the importance of obtaining reasonable material properties particularly those that pertain to the mortar bond between each brickwork ring. This is possible when laboratory controlled tests are carried out. Measured values of the shear bond strength were used in the theoretical model and enabled it to behave in a way that was similar to the particular arch bridge that it represented. However, the properties of the bond within in-service bridges will be difficult to ascertain. It would be useful to perform an extensive field study on the state of the brick/mortar bond within as many of the U.K. stock of bridges as possible. Rather than simply load testing to collapse a redundant structure it could be dismantled so that large undisturbed samples of brickwork can be obtained and tested. Further development of non-destructive test methods would also be useful in obtaining the extent of existing ring separation. The measured shear bond strengths could then be linked to the results of the non-destructive tests and to visual observations of the state of the bridge so that the Assessment Engineer is provided with effective guidance on the selection of the material properties to be used in an analysis.

2. The inclusion of detachable spandrel walls in a theoretical model is required in order to increase its usefulness. The interaction of the arch barrel and the spandrel walls in the full-scale model bridges tested as part of this research was not significant enough to affect a change in their ultimate behaviour. The method of attachment, the condition of the walls and the arch, their relative proportions, the presence of fill outside the structure, and the support conditions of the walls may significantly alter the behaviour of the structure from that which was observed and recorded within this thesis. It would be useful to carry out such an investigation by first developing the proposed theoretical models contained herein, and later, if deemed necessary, carry out a series of large-scale model bridge tests to verify the conclusions of these theoretical models. In any case, the inclusion of spandrel walls must be carried out if the non-destructive load tests on in-service bridges are to be used as anything other than proof load tests. The credibility of a finite element model can be enhanced by comparing its predictions with the experimental observations from such tests. It is suggested that the usefulness of a finite element model must be based on its ability to make accurate predictions of the behaviour of a structure throughout its load history. If it cannot do this the close correlation between the predicted and observed failure loads is coincidental. It remains preferable to compare their entire load histories including the failure loads but this is expensive and defeats the objective of the exercise (unless the structure is redundant).

3. The investigations documented within this thesis have concentrated on arch bridges constructed from very strong Engineering bricks. The span/rise ratio of each structure was 4.0 and the square span was 3.0 m. The abutments were rigid and the backfill was a high quality well-graded cohesionless material. The expense associated with carrying out large-scale model bridge tests in order to investigate the effects produced by varying each of the above parameters would result it is being more viable to extend current theoretical models. The requirement for these tests would remain but the risk associated with carrying out a poorly planned experimental test programme would be minimised if it lagged behind the development of suitable theoretical models.

4. It would be useful to carry out the development of the proposed three-dimensional finite element model so that the analysis of multi-ring skewed arch bridges can be carried out up to their ultimate limit state. This would require the development of a material model that can realistically represent the behaviour of masonry. As such, it must possess anisotropic material properties to reflect the presence of bedding joints within the brickwork. Possible shear failures must be allowed to occur at these planes of weakness rather than assuming that each course of brickwork acts compositely so that the material is able to accommodate bending in this direction. Three-dimensional gap elements can be used to model these potential planes of weakness although it would be preferable to carry out further research to develop an appropriate "masonry" material model. Several workers have already carried out some investigatory work towards this objective; it remains to implement this material model into a finite element model be it commercial or private package.

5. It would be useful to carry out further investigatory work into the use of the proposed three-dimensional indiscrete rigid block modelling technique. The search for a suitable "realistic" model remains outstanding and further work could be undertaken to obtain this model. The analysis of the "reduced" model revealed that the optimal mechanism was two-dimensional. This was because it was too restrictive in terms of the number of permissible relative movements. Using the "augmented" model three-dimensional mechanisms were predicted which were associated with lower collapse loads than the equivalent mechanism in the "reduced" model. This model could not be optimised. However, a "realistic" model will lie within the bounds represented by these two models.

6. Following the successful determination of the above "realistic" model, the effects of the spandrel fill can be incorporated into the analysis. However, this is not a prerequisite part of its development since a comparison with its two-dimensional counterpart will enable a strength reduction factor due to skew to be obtained. Nevertheless, the simple

mechanisms that were observed within the attached spandrel walls can be incorporated into the analysis since they must be compatible with the mechanism within the arch barrel.

7. The effects of dynamic loading have not been adequately considered to date. Despite this, in-service bridges are subjected to cyclical loading which may produce fatigue effects and progressive damage. It would be useful to carry out prolonged dynamic load tests on large-scale model arch bridges to establish their behaviour when subjected to dynamic effects. In particular the establishment of the most onerous load effect is outstanding. This may be the concurrent imposition of dynamic loads consistent with two-way moving traffic. However, it is suggested that this investigation should follow the completion of the programme of research directed towards the understanding of the behaviour of the arch when subjected to static loads. If this understanding is not present, dynamic effects are beyond comprehension.

8. It would be useful to carry out further investigations into the mobilisation of passive pressure. The results of the analyses of the theoretical models contained herein indicate that a reasonable assumption of the magnitude and distribution of the passive pressure will lead to an accurate predicted load carrying behaviour. However, there is nothing to prevent the analyst making unreasonable assumptions which will lead to incorrect assessments of the behaviour of the structure. For that matter, there is nothing to prevent the analyst disguising a flawed model by using unrealistic backfill parameters. The inclusion of the spandrel fill needs to be related to the deformation of the arch but must also take account of its initial at-rest state of stress. It would be useful to carry out a series of large-scale tests to determine this effect.

11.0 References

Alexander & Thomson (1900) *Scientific Design of Masonry Arches*, Dublin Private Printing, University Press

Andreaus U. (1988) *A 3-D Finite element model for the analysis of masonry structures*, Proceedings of the 8th Int. Brick & Block masonry conference, Dublin

ANSYS v.5.1 58 (1995) *The "Theory", "Procedures", and "Elements" manuals*, Swanson Analysis Systems inc., Houston, U.S.A.

Argyris and Kelsey (1954) *Energy theorems and structural analysis*, Butterworths, London (collection of papers published in "Aircraft Engineering" in 1954 and 1955)

Austrian Society of Engineers (1895) *Bericht des Gewölbe-Ausschusses*, Und Architekten Vereins Zeitschrift, Vienna, p 131

Baker I.O. (1900) *A Treatise on masonry Construction*, 9th Edition, John Wiley & Sons, New York

Barlow W.H (1846) *The existence (practically) of the line of equal horizontal thrust in arches, and the mode of determining it*, paper no. 728, Proc. of I.C.E., 1846

Bélidor B.F. (1729) *La science des Ingénieurs dans la conduite des travaux de fortification et d'Architecture civile*, Jombert, Paris, 6 volumes

Bell W. (1872) *On the stresses of rigid arches, continuous beams and curved structures*, Min. Proc. I.C.E., Vol. 33, pp 58-165

Bernardini A., Modena C. Vescovi U. (1982) *An anisotropic biaxial failure criterion for hollow clay brick masonry*, International Journal of masonry construction, Volume 2, No. 4, pp 165-171

Boistard L.C. (1800) *Experiences sur la stabilite des voûtes*, in Lesage's (1810) , "à l'usage de MM. les ingénieurs", Paris, Vol. 2, p 171

Boothby T.E. (1992a) *Stability of systems of rigid bodies by bounding theorems*, 9th Engineering Mechanics Conference, A.S.C.E.

Boothby T.E. (1992b) *Stability of Masonry piers and arches*, J. Eng. Mech., A.S.C.E., Vol. 118, No. 2, pp 367-383

Boothby T.E. (1992c) *Collapse modes of Masonry Arch Bridges*, Int. Historic Bridges Conf., Ohio Historical Society, Columbus, U.S.A.

Boothby T.E. (1993) *A general lower- and upper-bound theorem of static stability*, Engrg. Structures, Vol. 15, Part 3, pp 189-196

Boothby T.E. (1994) *Stability of Masonry Piers and Arches including Sliding*, J. of Engrg. Mechanics, A.S.C.E., Vol. 20, No. 2

Brierley (1979) *The mediaeval Exe Bridge*, Proceedings of the I.C.E., Part 1, Vol. 66, pp 127-139

Castigliano C.A.P. (1879) *Théorie de l'equilibre des systèmes élastiques et ses applications*, Augusto Federico Negro. Translated by Andrews in "Elastic Stresses in Structures", Scott Greenwood and Son, London (1919)

Chandler H.W & Chandler C.M (1995) *The analysis of skew arches using shell theory*, in "Arch bridges", Thomas Telford, U.K.

Chapman W. (1819) *Oblique arches*, in "Encyclopaedia or universal dictionary of arts, sciences and literature", Longman, Hurst, London

Charlton T. (1973) *Energy Principles*, in "Theory of Structures", Oxford University Press

Charnes A. & Greenberg H.J. (1951) *Plastic Collapse and linear programming*, Summer meeting, American Mathematics Society, bulletin no. 57

Charnes A., Lemke E. & Zienciewicz (1959) *Virtual Work, Linear Programming and Plastic Limit Analysis*, Proc. Royal Society, Series A: Mathematics and Physical Sciences, Vol. 251, p 110

Chen W.F. (1975) *Soil plasticity*, Elsevier Scientific Publishing, Oxford

Chettoe & Henderson (1957) *Masonry Arch Bridges: A Study*, Proc. I.C.E., Vol. 7, p 723

Choo B., Coutie M. & Gong N. (1990) *Analysis of Masonry Arch Bridges by a Finite Element Method*, Proc. of Forth Rail Bridge Centenary Conf., Edinburgh

Choo B., Coutie M. & Gong N. (1991a) *Finite Element Analysis of Masonry Arch Bridges using tapered elements*, Proc. I.C.E., Part 2, Vol. 91, pp 755-770

Choo B., Coutie M. & Gong N. (1991b) *The effects of cracks on the behaviour of masonry arches*, Proceedings of the 9th International Brick/Block Masonry Conference, Berlin, pp 948-955

Choo B., Coutie M. & Gong N. (1992) *Finite Element Analysis of brick arch bridges with multiple ring separation*, Proceedings of the 6th Canadian Masonry Symposium, pp 789-799

Choo B., Coutie M. & Gong N.G. (1993) *Finite Element Analysis of Masonry Arch Bridges using shell elements*, 13th Australian Conf. on Mechanics of Structures and Materials, Wollongong, Australia, Vol. 1, pp 201-208

Choo B., Coutie M. & Gong N. (1995) *Effects of skew on the strength of masonry arch bridges*, in "Arch bridges", Thomas Telford, London, pp205-214

Clayton C.R.I. & Milititsky J. (1987) *Earth Pressure and Earth Retaining Structures*, Surrey University Press, Ch. 6, pp 59-68

Clayton C.R.I. & Symons I.F. (1992)
The pressure of compacted fill on retaining walls, Géotechnique 42, No. 1, pp 127-130

Collins I.F. (1969)
The Upper bound theorem for rigid/plastic solids generalised to include Coulomb friction, J. Mech. Phys. Solids, Vol. 17, pp 323-338

Cook D., Melkus D. & Plesha (1989)
Concepts and applications of finite element analysis, 3rd edition, John Wiley & sons, New York

Cooke N. (1987)
Instability of Masonry Arches, Proc. I.C.E., Part 2, Vol. 83, pp 497-515

Cooke N. (1988)
Instability of Masonry Arches, Discussion, Proceedings of the I.C.E., Part 2, Vol. 85, pp 373-387

Cooke N. (1990)
Strength of Masonry Arch Bridges, Proc. 5th North American Masonry Conf., Univ. of Illinois, pp 981-993

Coulomb (1773)
Mémoires de mathématique et de physique, présentés à l'Académie Royale des Science, pars divers savans, et lûs dans ses assembées, Vol. 7, Paris (1776), pp 343-382

Couplet (1729)
De la poussée des voûtes, in "Histoire de l'Académie Royale des Sciences", p 79

Couplet (1730)
De la poussée des voûtes, in "Histoire de l'Académie Royale des Sciences", p 117

Crisfield M. (1984)
A finite element computer program for the analysis of masonry arches, T.R.R.L. Report 1115, Crowthorne, U.K.

Crisfield M. (1985a)
Finite element and mechanism methods for the analysis of masonry and brickwork arches, T.R.R.L. Report RR 19, Crowthorne, U.K.

Crisfield M. (1985b)
Computer Methods for the analysis of masonry arches, Proc. 2nd Conf. on Civil and Structural Engineering Computing, Vol. 2, Civil-Comp. Press, Edinburgh, pp 213-220

Crisfield M.A. & Packham A.J. (1987)
A mechanism program for computing the strength of masonry arch bridges, T.R.R.L. research report 124, Crowthorne, U.K.

Crisfield M. (1987)
Plasticity Computations using Mohr-Coulomb yield criterion, Engineering Computers, Vol. 4, pp 300-308

Crisfield M.A. & Wills J. (1987)
Nonlinear analysis of concrete and masonry structures, in "Finite element methods for nonlinear problems", ed Bergan P.G. et al., Springer-Verlag, Berlin, pp 639-652

Crisfield M. (1988)
Numerical Methods For Non-linear Analysis of Bridges, Computers & Structures, Vol. 30, No. 3, pp 637-644

Dantzig et al. (1951) *Activity analysis of production and allocation*, Ed. Koopmans, Wiley, New York

Danyzy (1732) *Histoire de la Societé Royale des Sciences établie à Montpellier*, Vol. 2, Lyon (1778), p40

Davies S.R. (1985) *The assessment of load carrying capacity of masonry arch bridges*, Proceedings of the 2nd Conf. on Civil and Structural Engineering Computing, Vol. 2, Civil-Comp. Press, Edinburgh, pp 203-206

Davey (1953) *Tests on Road Bridges*, Building Research Station, National Building Studies Research Paper 16, H.M.S.O., London

Delbecq J.M. (1982) *Analyse de la stabilité des voûtes en maçonnerie par le calcul à la rupture*, J. de Mécanique théorique et appliquée, Vol. 1, Part 1, pp 91-121

Del Piero G. (1989) *Constitutive equations and compatibility of external loads for linearly elastic masonry-like materials*, Meccanica, Vol. 24, No. 3, pp 150-162

Dhanesehar et al. (1985) *The failure of brick masonry under biaxial stress*, paper 8871, Proc. ICE, Part 2, Vol. 79, pp 295-313

Drucker D.C. (1953) *Coulomb friction, plasticity and limit load*, Journal of Applied Mechanics, A.S.M.E., Vol. 21, pp 71-74

DoT (1984a) *The assessment of highway bridges and structures*, Departmental Standard BD 21/84

DoT (1984a) *The assessment of highway bridges and structures*, Advice Note BA 16/84

Encyclopedia Britannica (1876) *Encyclopaedia Britannica, 9th Ed.*, Edinburgh, Pub. Adam & Charles Black, Vol.2, pp 327-332

Encyclopedia Britannica (1984a) *Encyclopaedia Britannica, 15th Ed.*, Edinburgh, Vol.3, p 452

Encyclopedia Britannica (1984b) *Encyclopaedia Britannica, 15th Ed.*, Edinburgh, Vol. 3, p 175

Fomba G.T (1990) *The assessment of masonry arch bridges using a thinning elastic analysis*, MPhil Thesis, University of Wales, Cardiff

Ford H. (1963) *Advanced Mechanics of materials*, Longmans

Foulds L.R. (1981) *Optimisation techniques: an introduction*, Springer-Verlag, New York

Franciosi C. (1986) *Limit behaviour of masonry arches in the presence of finite displacements*, International J. Mech. Science, Vol. 28, No. 7, pp 463-471

Franciosi V. & Franciosi C. (1988) *The Cells Method in masonry arch analysis*, Proceedings of the 8th International Brick and Block Masonry Conference, Dublin, pp 1290-1301

Frézier (1737) *La théorie et la pratique de la coupe des pierres et des bois pour la construction des voûtes et autres parties des batimens civils et militaires, ou traité de stéréotomie à l'usage de l'architecture*, 3 Volumes, Doulsseker le fils, Strasbourg

Fuller (1875) *Curve of Equilibrium for a rigid arch under vertical forces*, Proc. I.C.E., Vol. 40

Gallagher R.H. (1973) *Finite Element Analysis of Geometrically Nonlinear Problems*, in "Theory and practice in finite element structural analysis", Tokyo University Press, 1973

Gass S.I. (1969) *Linear Programming, Methods and applications*, 3rd edition, McGraw Hill

Gautier H. (1717) *Traité des Ponts*, Paris

Gauthey (1809) *Traité de la construction des Ponts*, Ed. Navier, 2 Volumes, Didot, Paris (1809, 1813)

Gavarini C. (1966) *Plastic Analysis of Structures and Duality in Linear Programming*, Meccanica, No. 3/4

Gay C. (1924) *Ponts en Maçonnerie*, Paris, Librairie J.-B. Baillière et Fils, 19 Rue Hautefeuille

Gilbert M. (1993) *The behaviour of masonry arch bridges containing defects*, Ph.D. Thesis, Bolton Institute of Higher Education

Gregory D. (1697) *Catenaria*, Philosophical Transactions, No. 231, p 637

Harvey W. & Smith F. (1985) *The assessment and design of masonry arch structures using a microcomputer*, Proc. 2nd Int. Conf. Civil and Structural Engineering Computers, London, pp 207-212

Harvey W. (1986) *Testing times for arches*, New Scientist, 15 May, pp 54-59

Harvey W. & Smith F. (1987) *Semicircular Arches*, Proceedings I.C.E., Part 2, Vol. 83, pp 845-849

Harvey W. & Smith F. (1988) *Semicircular Arches Discussion*, Proc. I.C.E., Part 2, Vol. 85, pp 739-742

Harvey W., Maxwell J. & Smith F. (1988) *Arch Bridges are Economic*, Proc. 8th Int. Brick/Block Masonry Conference, Dublin, Elsevier, pp 1302-1310

Harvey W. (1988) *Application of mechanism analysis to masonry arches*, The Structural Engineer, Vol. 66, No. 5, pp 77-82

Harvey W., Vardy A., Craig R., & Smith F. (1989) *Load tests on a full-scale model 4.0 m span masonry arch bridge*, Department of Transport, T.R.R.L. contractor report 155, Crowthorne, U.K

Harvey W. (1991) *Stability, Strength, Elasticity and Thrust lines in masonry structures*, The Structural Engineer, Vol. 69, No. 9, pp 181-184

Harvey W. & Smith F. (1991) *The behaviour and assessment of multi-span arches*, The Structural Engineer, Vol. 69, No. 24, p 17

Harvey W. (1994) *Demolition of arch bridges*, The Structural Engineer, Vol. 72, No. 5, pp 87-88

Hayes J. (1938) *Strengthening & Reconstruction of weak Bridges under the Road & Rail Traffic Act, 1933*, Students' Paper No. 953, Proc. I.C.E., Vol. 10, pp 15-40

Hendry A., Davies S. & Royles R. (1985) *Test on Stone Masonry Arch at Bridgemill-Girvan*, Department of Transport, TRRL contractor report 7, Crowthorne, U.K

Hendry A. et al. (1986) *Test on masonry arch bridge at Bargower*, Department of Transport, TRRL contractor report 26, Crowthorne, U.K

Hendry A. (1990) *Masonry properties for assessing arch bridges*, Department of Transport, TRRL contractor report 244, Crowthorne, U.K

Hendry & Royles (1991) *Model tests on masonry arches*, Proc. I.C.E., Part 2, Vol. 91, pp 299-321

Heyman J. (1966) *The Stone Skeleton*, International Journal of Solids and Structures, Vol. 2, pp 249-279

Heyman J. (1967) *On shell structures for masonry domes*, Int. J. Solids and Structures, Vol. 3, pp 227-241

Heyman J. (1968) *On the Rubber Vaults of the middle ages, and other matters*, in "Gazette Des Beaux-arts", Vol. 71, pp 177-188

Heyman J. (1969) *The safety of Masonry Arches*, International J. Mech. Science, Vol. 11, pp 363-385

Heyman J. (1971) *Plastic Design of Frames*, Vol. 2, Ch. 4, Cambridge University Press, pp 60-83

Heyman J. (1972) *Coulomb's Memoir on Statics*, cambridge University Press

Heyman J. & Threlfall B. (1972) *Two Masonry Bridges: Telford's Bridge at Over*, Proc. I.C.E., Part 1, no. 52, pp 319-330

Heyman J. & Padfield C. (1972) *Two Masonry Bridges: Clare College Bridge*, Proceedings I.C.E., Part 1, Vol. 52, pp 305-318

Heyman J., Threlfall B. & Padfield C. (1973) *Two Masonry Bridges: Clare College Bridge Telford's Bridge at Over*, Discussion, Proc. I.C.E., Vol. 52, pp 495-505

Heyman J. (1976) *Couplet's Engineering Memoirs, 1726-1733*, in "History of Technology" Edited by Hall R. & Smith N., Mansell, London. pp 21-44

Heyman J., Hobbs N. & Jermy B. (1980) *The rehabilitation of Teston Bridge*, Proceedings of I.C.E., Volume 68, p 489

Heyman J. (1980) *The Estimation of the Strength of Masonry Arches*, Proc. I.C.E., Part 2, Vol. 69, pp 921-937

Heyman J. (1982) *The Masonry Arch*, Ellis Horwood Ltd., Chichester

Heyman J. (1988) *Poleni's Problem*, Proc. I.C.E., Part 1, Vol. 84, pp 737-759

Heyman J. (1992) *The maintenance of masonry*, in "The design life of structures", Ed. Somerville & Blackie, p 121

Hooke R. (1676) *Description of Helioscopes and some other Instruments*, London

Howe (1897) *A Treatise on Arches*, John Wiley & Sons, New York

Hughes T.G. & Vilnay O. (1988) *The Analysis of Masonry Arches*, Proc. 8th International Brick/ Block Masonry Conference, Dublin

Hughes T.G., Blackler & Bridle R.J. (1990) *A new approach to masonry arch assessment*, Structures 2000: 2nd Kerensky conference, Glasgow

Hughes T.G. & Bridle R.J. (1990) *An Energy method for arch bridge analysis*, Proceedings of I.C.E., Part 2, Vol. 89, pp 375-385

Hughes T.G. & Bridle R.J. (1991) *An Energy method for arch bridge analysis*, Discussion, Proceedings of I.C.E., Part 2, Vol. 91, pp 617-630

Hutton C. (1812) *Tracts on Mathematical and Philosophical Subjects*, Wilkie and Robinson, London, 3 Volumes

Jenkin H.C.F. (1876) *Bridges*, in "Encyclopaedia Britannica, 9th edn", Edinburgh

Jennings A. (1985) *Use and Misuse of Fuller's construction for the analysis of masonry arches*, The Structural Engineer, Vol. 63A, pp 352-355

Jennings A. (1986) *Stability Fundamentals in relation to masonry arches*, The Structural Engineer, Vol. 64B, No. 1, pp 10-12

Jennings A. (1988) *Assessment of the Collapse Load for Masonry Arches*, Proc. of the 8th International Brick/Block Masonry Conference, Dublin, pp 1330-1339

Knapp R.G. (1992) *China's Bridges: Craft and Symbolism*, Proc. Int. Historic Bridges Conference, Columbus, Ohio, pp 91-132

Kooharian A. (1952) *Limit Analysis of Voussoir (Segmental) and Concrete Arches*, Proc. American Concrete Institute, Vol. 24, No. 4

Labelye C. (1751) *A Description of Westminster Bridge*, London

Lamé & Clapeyron (1823) *Mémoire sur la stabilité des voûtes*, Annales des Mines, Vol. 8, p 789

La Hire P. De (1695) *Traité de Mécanique*, Annison, Paris

La Hire P. De (1712) *Sur La Construction des Voûtes dans les édifices*, in "Mémoires de l'Académie Royale des Sciences", Paris (1731), p 69

Ling-Xi Q. (1987) *New Insight into an Ancient Stone Arch Bridge: the Zhao-Zhou Bridge of 1400 years old*, Int. Journal of Mechanic Science, Vol. 29, No. 12, pp 831-843

Livesley R.K. (1973a) *A compact Fortran sequence for limit analysis*, International J. of Numerical Methods in Engineering, Vol. 5, pp 446-449

Livesley R.K. (1973b) *Linear Programming in Structural Analysis and Design*, in "Optimum Structural Design", Ed. Gallagher & Zienkiewicz, John Wiley, Ch. 6, pp 79-108

Livesley R.K. (1974) *Matrix Methods of Structural Analysis*, 2nd Edition, Ch. 7, Pergamon

Livesley R.K. (1978) *Limit Analysis of Structures formed from Rigid Blocks*, Int. J. Numerical Methods in Engineering, Vol. 12, pp 1853-1871

Livesley R.K. (1992a) *The Collapse Analysis of Masonry Arch Bridges*, Proc. Conf. Applied Solid Mechanics, Elsevier, pp 261-274

Livesley R.K. (1992b) *A Computational Model For the Limit Analysis of 3-dimensional Masonry Structures*, Meccanica, Vol. 27,pp 161-172

Loo Y.-C. ,Yang Y. & Best R. (1988) *Behaviour of Stanwell Park Viaduct, A multi-span brick masonry arch system on tall piers*, Proceedings of the 8th Int. Brick & Block masonry conference, Dublin

Loo Y.-C. & Yang Y. (1991a) *Cracking and Failure Analysis of Masonry Arch Bridges*, Journal of Structural Engineering, A.S.C.E., Vol. 117, No. 6, pp 1641-1659

Loo Y.-C. & Yang Y. (1991b) *Tensile Strength, Strain Softening, and the Failure analysis of Masonry Arch Bridges*, in "Computational Mechanics" Ed. Cheung, Lee & Leung, Balkema, Rotterdam

Mackay T. (1900) *The life of Sir John Fowler*, John Murray, London

McKenning R. (1987) *Bridge Assessments for heavy loads: computer aids*, Municipal Engineer, Vol.4, pp 101-110

McNeely D.K., Archer G.C. & Smith K.N. (1989) *Structural Analysis of old stone arch bridges*, Canadian J. Civil Engineers, Vol. 16, pp 789-797

Melbourne C. & Walker P. (1988) *Load tests to collapse of model brickwork masonry arches*, Proc. 8th Int. Brick/Block masonry conference, Dublin

Melbourne C. (1988) *A New Construction Technique*, Structural Engineering Review, Vol. 1, pp 81-85

Melbourne C. & Qazzaz (1989) *Load test to collapse of a 3.0 m span brickwork masonry arch bridge with detached spandrel walls and mortar bonded rings*, B.I.H.E. report ref: CE/1/89

Melbourne C. & Walker P. (1990a) *The load test to collapse of a 6.0 m span brickwork arch bridge* Department of Transport, T.R.R.L. contractor report 189, Crowthorne, U.K

Melbourne C. & Walker P. (1990b) *Load test to collapse of a 3.0 m span brickwork masonry arch bridge with attached spandrel walls and unbonded rings*, B.I.H.E. report ref: CE/1/90

Melbourne C. (1990) *The Behaviour of Brick Arch Bridges*, Proc. British Masonry Society, No. 4, pp 54-57

Melbourne C. (1991) *The assessment of masonry arch bridges*, 9th Int. Brick/ block masonry Conference, Berlin

Melbourne C. & Gilbert M. (1991) *Load test to collapse of a 3.0 m span brickwork masonry arch bridge with attached spandrel walls and mortar bonded rings*, B.I.H.E. report ref: CE/1/91 to British Rail Research

Melbourne C. & Gilbert M. (1992) *Load test to collapse of a 3.0 m span brickwork masonry arch bridge with detached spandrel walls and unbonded rings*, B.I.H.E. report ref: CE/1/92 to British Rail Research

Melbourne C. & Hodgson J. (1993a) *Load test to collapse of a 3.0 m span 22.5° skewed brickwork masonry arch bridge with detached spandrel walls*, B.I.H.E. report ref: CE/2/93 to L.G.Mouchel & Partners

Melbourne C. & Hodgson J. (1993b) *Load test to collapse of a 3.0 m span 45° skewed brickwork masonry arch barrel only*, B.I.H.E. report ref: CE/3/93 to L.G.Mouchel & Partners

Melbourne C. & Hodgson J. (1994a) *Load test to collapse of a 3.0 m span 45° skewed brickwork masonry arch bridge with attached spandrel walls*, B.I.H.E. report ref: CE/1/94 to L.G.Mouchel & Partners

Melbourne C. & Hodgson J. (1994b) *The behaviour of skew brickwork arches*, in "bridge assessment, management and design", Elsevier, pp 187-192

Melbourne C. & Hodgson J. (1995a)
Load test to collapse of a 3.0 m span 45° skewed brickwork masonry arch bridge with detached spandrel walls, B.I.H.E. report ref: CE/1/95 to L.G.Mouchel & Partners

Melbourne C. & Hodgson J. (1995b)
The behaviour of skew brickwork arches, in "Arch bridges", Thomas Telford, London, pp 309-320

Melbourne C. & Tao H.Y. (1995)
The behaviour of open spandrel masonry arch bridges, in "Arch bridges", Pub. Thomas Telford, London, pp 239-244

Mendelson A. (1968)
Plasticity: Theory and Application, Macmillan

Military Engineering Experimental Establishment (1952)
Classification of masonry arch bridges, Military Engineering Experimental Station, Christchurch, U.K

Min. of Transport (1973)
The Assessment of highway bridges for construction and use vehicles, Ministry of Transport, London, Technical Memorandum BE 3/73

Morley A. (1912)
Theory of Structures, Ed. Longmans, Green & Co., 39 Paternoster Row, London

Morgan T. (1764)
On The bridge at Pontypridd, in "The Gentleman's Magazine", Vol. XXXIV, p 534

Moseley (1835)
Equilibrium of the arch and theory of equilibrium of bodies in contact, Transactions of the Cambridge Philosophical Society, No. 5/6

Moseley (1843)
The mechanical principles of engineering and architecture, London

Navier (1826)
Résumé des leçons données à l'École des ponts et Chaussées, sur l'application de la mécanique a l'établissement des constructions et des machines, Firmin Dodet, Paris

Page J. (1987)
Loads tests to collapse in two arch bridges at Preston, Shropshire and Prestwood, Staffordshire, Department of Transport T.R.R.L. research report 110, Crowthorne, U.K.

Page J. & Grainger J. (1987)
Load test to collapse on a brick arch bridge at Torksey, Working Paper WP/B/134/87, Transport and Road Research Laboratory, Crowthorne, U.K.

Page J. (1988)
Load tests to collapse on two arch bridges at Torksey and Shinafoot, Department of Transport, T.R.R.L. research report 159, Crowthorne, U.K.

Page J. (1989a)
Load tests to collapse on two arch bridges at Strathmashie and Barlae, T.R.R.L. research report 201, Crowthorne, U.K.

Page J. (1989b) *A Guide to Masonry Arch Bridges*, T.R.R.L. technical paper BD/TP/1/89, Transport and Road Research Laboratory, Crowthorne, U.K.

Page J. (1990) *Assessment of Masonry arch bridges*, Proceedings of the Institution of Highways and Transportation national Workshop, Leamington Spa

Page J. (1993) *Masonry arch bridges*, Transport research laboratory HMSO publication

Perronet J.-R. (1783) *Description des projets*, Paris, 2 volumes

Peshkam V. et al. (1995) *The role of finite element analysis in composite plate bonding*, in "Composites in infrastructure design and rehabilitation", NAFEMS research working group, London

Pippard A.J.S., Tranter E. & Chitty L. (1936) *Mechanics of the Voussoir Arch*, Proceedings I.C.E., Vol. 4, pp 281-306

Pippard A.J.S. & Ashby R. (1939) *An Experimental Study of the Voussoir Arch*, Proc. I.C.E., Vol. 10, pp 383-404

Pippard A.J.S. & Chitty L. (1941) *Repeated Load Tests on a Voussoir Arch*, Proc. I.C.E., Vol 17, pp 79-86

Pippard A.J.S. (1948) *The Approximate Estimation of the Safe Loads on Masonry Bridges*, Civ. Engineer in War, I.C.E., pp 365-372

Pippard A.J.S. (1951) *A Study of the Voussoir Arch*, Nat. Building Studies Research Paper 11, HMSO

Pippard A.J.S. & Baker J.F. (1957) *The Analysis of Engineering Structures*, 3rd Edition, Arnold E. & Co., London, pp 385-403

Poleni (1748) *Memorie istoriche della gran cupola del Tempio Vaticano*, Padova

Powell B. & Hodgkinson H.R. (1976) *The determination of the stress/strain relationship of brickwork*, Proc. 4th Int. brick masonry Conference, Brugge

Prager W. (1953) *Limit Analysis and Design*, Journal of American Concrete Society, Vol. 25, No.4, p 297

Prentis J.M. (1977) *Use of upper and lower bounds in evaluating friction effects in mechanics*, S.Y.R.O.M. Conf., Bucharest

Rankine (1862) *Civil Engineering and Applied Mechanics*, Charles Griffin & Co., London

Rankine (1898) *A Manual for Civil Engineering*, Charles Griffin & Co., London, article 295, pp 429-432

Robinson (1985) — *Early FEM Pioneers*, Robinson & Associates, Dorset, England

Robison J. (1822) — *The Arch*, in "supplement to Encyclopaedia Britannica 3rd edn.", Edinburgh, pp 14-31

Rondelet (1812) — *Traité théoretique et pratique de l'art de batin*, 3 vols., Goeury, Paris

Ruddock E.C. (1974) — *Hollow spandrels in arch bridges: a historical study*, Structural Engineer, part 2, pp 281-293

Ruddock T. (1979) — *Arch Bridges and their Builders: 1735-1835*, Cambridge University Press

Samarasinghe W., Page A. Hendry A.W. (1981) — *Behaviour of brick masonry shear walls*, The Structural Engineer, Vol. 59B, no. 3, pp 42-48

Sawko & Towler (1982a) — *Limit State Behaviour of brickwork arches*, Proc. 6th Int. Conf. on Brick Masonry, Rome, pp 412-442

Sawko & Towler (1982b) — *Structural Behaviour of brickwork Arches*, 7th Int. Conf. on load bearing brickwork, British Ceramic Soc., London, Vol. 30, pp 160-168

Sawko & Rouf (1984) — *On the stiffness properties of masonry*, Proc. I.C.E., Part 2, Vol. 77, pp 1-12

Sawko & Rouf (1985) — *A proposed numerical model for structural masonry*, Masonry International, Vol. 5, pp 22-27

Schofield (1979) — *Benjamin Outram (1764-1805), Canal Engineer Extraordinary*, Proc. I.C.E., Part 1, Vol. 66, pp 539-555

Séjourné P. (1913) — Grandes voûtes, 6 vols., Bourges

Selberg A. (1953) — *On the Bearing Capacity of Voussoir Arches*, I.A.B.S.E. publication, Vol. 13, pp 322-326

Smeaton J. (1754) — *Designs by the late John Smeaton, FRS*, The Royal society of London, Vol IV

Smith F., Harvey W. & Vardy A.E. (1990) — *Three-hinge analysis of masonry arches*, The Structural Engineer, Vol. 68, No. 11, pp 203-213

Smith F. (1991) — *Load path analysis of masonry arches*, PhD Thesis, University of Dundee

Smith N.A.F. (1993) — *The Roman Bridge-Builder: Some aspects of his work*, The Structural Engineer, Vol. 74, No. 9, pp 160-165

Snell G. (1846) — *On the Stability of arches, with practical methods for determining, according to the pressure to which they will be subjected, the best form of section, or variable depth of voussoir, for any given intrados or extrados*, Proceedings of the I.C.E., Vol. 5, p 439

Stöckl & Hofmann (1988) *Tests on the shear bond behaviour in the bed joints of masonry*, 8th international Brick/Block masonry conference, Dublin

Taylor N. & Mallinder P. (1987) *On the limit state properties of masonry*, Proc. I.C.E., Part 2, Vol. 83, pp 33-41

Taylor N. (1991) *Moment-thrust limit state properties of masonry*, Masonry International, Vol. 5, No. 2, pp 55-58

Taylor N. & Mallinder P. (1993) *The brittle hinge in masonry arch mechanisms*, The Structural Engineer, Vol. 71, No. 20, pp 359-366

Tellet J. (1983) *A Review of the literature on brickwork arches*, Proc. 8th Int. Symposium on load bearing brickwork, Technical Session 2: Structures, Building Materials section of the British Ceramic Society, London

Temple & Kennedy (1989) *The engineering properties of old bricks*, BRR technical memorandum, Derby

Toi & Yoshida (1991) *Numerical Simulation of Non-linear Behaviour of two-dimensional Block Structures*, Computers & Structures, Vol. 41, pp 593-603

Towler (1981) *The structural behaviour of brickwork arches*, PhD thesis, University of Liverpool, U.K.

Van Beek G.W. (1987) *Arches and Vaults in the Ancient Near East*, Scientific American, Vol. 256, pp 78-86

Villarceau Y. (1845) *Mémoires présentés par divers Savants*, Vol. 12, p 503

Vilnay O. (1984) *Buckling of Masonry Arches*, Proceedings of I.C.E., Part 2, Vol. 77, pp 34-41

Vilnay & Cheung (1986) *Stability of Masonry Arches*, J. Structural Engineering, Vol. 112, No. 10, pp 2185-2199

Vilnay O. (1988) *The Critical Load Effect on the Failure of Masonry Arches*, Proc. of the 8th International Brick/Block Masonry Conference, Dublin, pp 1330-1339

Walklate & Mann (1983) *A Method for Determining the Permissible Loading of brick and masonry Arches*, Proc. I.C.E., Part 2, Vol. 75, pp 585-597

Walklate & Mann (1984) *A Method for Determining the Permissible Loading of brick and masonry Arches*, Discussion, Proc. I.C.E., Part 2, Vol. 77, pp 401-404

Ware (1809) *A treatise of the properties of arches, and their abutment piers*, London

William K.J. & Warnke E.D. (1975) — *Constitutive model for the triaxial behaviour of concrete*, Proc. International Assoc. for bridges and structural engineering, Vol. 19, ISMES, Bergamo, Italy, p174

Williams E.O. (1927) — *The Philosophy of Masonry Arches*, Proc. I.C.E., Selected Engineering Papers, Paper No. 56

Winkler (1879) — *Beitrag zur Theorie der Elastischen Bogenträger*, Vienna Carl Gerold's Sohn

Wood R.D. & Zienkiewicz (1977) — *Geometry of non-linear finite element analysis of beams, frames, arches and axisymmetrical shells*, Computers and Structures, Vol. 7, pp 725-735

Yamada, Takatsuka & Iwata K. (1973) — *Nonlinear analysis by the finite element method and some expository examples*, in "theory and practice in finite element structural analysis, Tokyo University Press

Yi-Sheng M. (1978) — *Bridges in China: Old and New*, Foreign Language Press, Peking

Zienkiewicz (1977) — *The Finite Element Method in Engineering Science*, 3rd edition, McGraw-Hill, London

Appendix A Terminology

The following is a glossary of some terms used within this thesis when referring to component parts of an arch bridge. Some of which can be seen in figure 1.1 and readers are referred to Page (1993) for a comprehensive list.

Archivolt	A projecting moulding which follows the curve of an arch on top of the extrados,
Centring	The temporary structure used to support an arch during its erection,
Counter arch	Sometimes used to mean an inverted or reversed arch in a spandrel, and sometimes used to mean a secondary arch above the primary or springing across the intermediate pier between adjacent arches,
Crown	The highest point of an arch,
Haunch	Part of an arch midway between its springing and its crown,
Segmental Arch	An arch whose shape is only part of a semi circle, having a ratio (span/rise) greater than 2.0,
Spandrel	The space between the extrados of an arch, or two adjacent arches, and the road surface,
Springing	The surface of contact between the first voussoir and the skewback,
Voussoir	a tapered or wedge shaped arch stone as seen on the facade of a bridge.

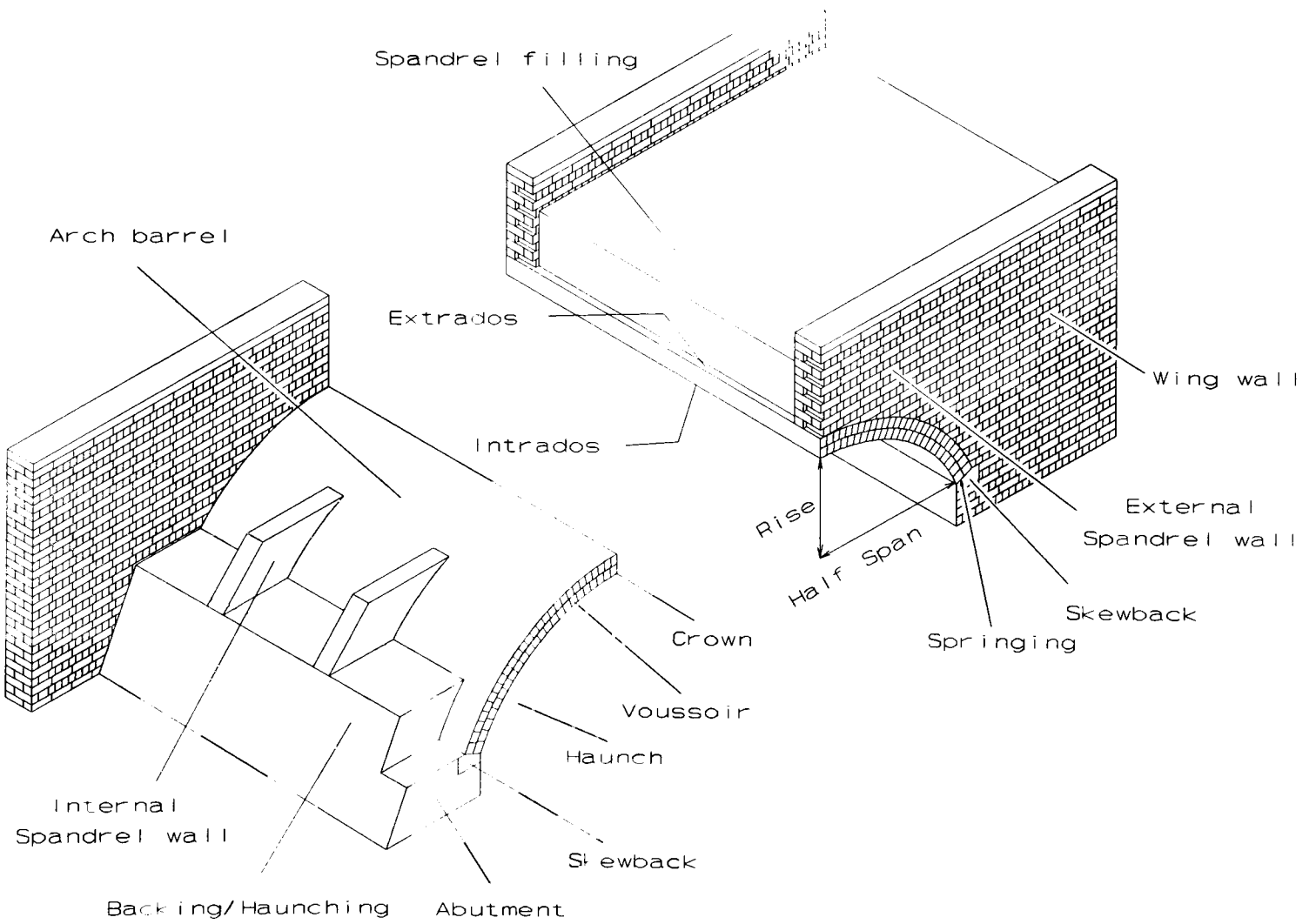

Figure A.1 Arch Nomenclature

Appendix B Duality of the lower bound and upper bound techniques

In linear programming (L.P.) terminology the minimum upper bound technique, described in chapter 6.4.2, may be described as the primal problem. In this case the maximum lower bound technique, described in chapter 6.4.3, would be called the dual problem in accordance with Charnes & Greenberg (1951). However, the dual problem can also be formed directly from the constraints of the primal problem. Figure B.1 shows the initial LP tableau for the primal problem presented in chapter 6.4.2. Figure B.2 shows the initial LP tableau for the dual problem and was set up by converting the primal tableau as follows (Foulds, 1981):

1. Replace each primal equality constraint by a less than or equal to constraint and a greater than or equal to constraint,
2. Since the primal is a minimisation problem transform all constraints to the form of greater than or equal to by multiplying them by -1 where necessary,
3. Define a unique non-negative dual variable for each primal constraint,
4. The dual problem is defined as a maximisation problem since the primal was a minimisation problem,
5. The right hand side constraint constants of the dual problem are defined as being the coefficients of the objective function of the primal problem,
6. Reverse the sign of each constraint to a less than or equal to form for the required maximisation problem,
7. Transpose the matrix of primal constraint coefficients to form the dual constraint coefficient matrix.

Figure B.3 shows the final L.P tableau of the dual problem which was achieved after 38 Gauss-Jordan iterations.

$\delta\theta_1^A$	$\delta\theta_1^B$	δr_1^u	δr_1^d	$\delta\theta_2^A$	$\delta\theta_2^B$	δr_2^u	δr_2^d	$\delta\theta_3^A$	$\delta\theta_3^B$	δr_3^u	δr_3^d	$\delta\theta_4^A$	$\delta\theta_4^B$	δr_4^u	δr_4^d	$\delta\theta_5^A$	$\delta\theta_5^B$	δr_5^u
6.84	-6.49	1.00	-0.20	6.07	-5.80	1.09	-0.48	5.11	-4.94	1.11	-0.72	4.04	-3.98	1.05	-0.92	2.94	-2.99	0.92
0.55	-0.29	-0.50	1.10	1.34	-0.99	-0.22	1.01	1.90	-1.49	0.07	0.84	2.19	-1.75	0.36	0.62	2.19	-1.75	0.62
1.00	-1.00			1.00	-1.00			1.00	-1.00			1.00	-1.00			1.00	-1.00	
-1.32	0.97	-1.00	0.20	-0.55	0.28	-1.09	0.48											
-7.07	6.80	0.50	-1.10	-7.86	7.51	0.22	-1.01	-8.02	7.44	-1.19	-0.12	-7.24	6.74	-1.42	0.29	-6.13	5.75	-1.55

δr_5^d	$\delta\theta_6^A$	$\delta\theta_6^B$	δr_6^u	δr_6^d	$\delta\theta_7^A$	$\delta\theta_7^B$	δr_7^u	δr_7^d	$\delta\theta_8^A$	$\delta\theta_8^B$	δr_8^u	δr_8^d	Q_1	Q_2	Q_3	Q_4	rhs
-1.05	1.87	-2.04	0.72	-1.11	0.91	-1.18	0.48	-1.09	0.14	-0.49	0.20	-1.00	1.00				0.00
0.36	1.90	-1.49	0.84	0.07	1.34	-0.99	1.01	-0.22	0.55	-0.29	1.10	-0.50		1.00			0.00
	1.00	-1.00			1.00	-1.00			1.00	-1.00					1.00		0.00
																1.00	1.00
0.69	-4.77	4.54	-1.57	1.04	-3.26	3.18	-1.49	1.31	-1.69	1.78	-1.30	1.50	0.00	0.00	0.00	0.00	-1.00

Figure B.1 Initial LP tableau for the primal upper bound problem

Figure B.2 Initial LP tableau for the dual of the upper bound problem

x1	x2	x3	x4	x5	x6	x7	x8	S1	S2	S3	S4	S5	S6	S7	S8	S9	S10	S11	S12	S13	S14	S15	S16	S17	S18	S19	S20	S21
6.85	-6.85	0.56	-0.56	1.00	-1.00	-1.33	1.33	1.00																				
6.49	-6.49	0.29	-0.29	1.00	-1.00	-0.98	0.98		-1.00																			
1.00	-1.00	-0.50	0.50			-1.00	1.00			1.00																		
0.20	-0.20	-1.10	1.10			-0.20	0.20				-1.00																	
6.07	-6.07	1.35	-1.35	1.00	-1.00	-0.55	0.55					1.00																
5.80	-5.80	1.00	-1.00	1.00	-1.00	-0.28	0.28						-1.00															
1.10	-1.10	-0.22	0.22			-1.10	1.10							1.00														
0.48	-0.48	-1.01	1.01			-0.48	0.48								-1.00													
5.12	-5.12	1.90	-1.90	1.00	-1.00											1.00												
4.94	-4.94	1.50	-1.50	1.00	-1.00												-1.00											
1.12	-1.12	0.07	-0.07															1.00										
0.73	-0.73	-0.85	0.85																-1.00									
4.05	-4.05	2.19	-2.19	1.00	-1.00															1.00								
3.99	-3.99	1.76	-1.76	1.00	-1.00																-1.00							
1.06	-1.06	0.36	-0.36																			1.00						
0.93	-0.93	-0.63	0.63																				-1.00					
2.94	-2.94	2.19	-2.19	1.00	-1.00																			1.00				
3.00	-3.00	1.76	-1.76	1.00	-1.00																				-1.00			
0.93	-0.93	0.63	-0.63																							1.00		
1.06	-1.06	-0.36	0.36																								-1.00	
1.87	-1.87	1.90	-1.90	1.00	-1.00																							1.00
2.04	-2.04	1.50	-1.50	1.00	-1.00																							
0.73	-0.73	0.85	-0.85																									
1.12	-1.12	-0.07	0.07																									
0.92	-0.92	1.35	-1.35	1.00	-1.00																							
1.19	-1.19	1.00	-1.00	1.00	-1.00																							
0.48	-0.48	1.01	-1.01																									
1.10	-1.10	0.22	-0.22																									
0.14	-0.14	0.56	-0.56	1.00	-1.00																							
0.49	-0.49	0.29	-0.29	1.00	-1.00																							
0.20	-0.20	1.10	-1.10																									
1.00	-1.00	0.50	-0.50																									
34.55	34.55	-5.79	5.79	-8.00	8.00	1.94	-1.94	0.00	1.00	0.00	1.00	0.00	1.00	0.00	1.00	0.00	1.00	0.00	1.00	0.00	1.00	0.00	1.00	0.00	1.00	0.00	1.00	0.00

S22	S23	S24	S25	S26	S27	S28	S29	S30	S31	S32	A1	A2	A3	A4	A5	A6	A7	A8	A9	A10	A11	A12	A13	A14	A15	A16	rhs
											1.00																60.30
												1.00															53.97
													1.00														17.99
														1.00													3.60
															1.00												47.08
																1.00											42.91
																	1.00										16.90
																		1.00									7.42
																			1.00								33.39
																				1.00							31.20
																					1.00						14.34
																						1.00					9.36
																							1.00				20.93
																								1.00			20.34
																									1.00		10.87
																										1.00	9.51
-1.00																											10.98
	1.00																										11.43
		-1.00																									7.13
			1.00																								8.15
				-1.00																							4.21
					1.00																						5.09
						-1.00																					3.74
							1.00																				5.73
								-1.00																			0.72
									1.00																		1.42
										-1.00																	1.24
1.00	0.00	1.00	0.00	1.00	0.00	1.00	0.00	1.00	0.00	1.00	0.00	0.00	0.00	0.00	0.00	0.00	0.00	0.00	0.00	0.00	0.00	0.00	0.00	0.00	0.00	1.00	2.82
																											0.00
																											0.00
																											0.00
																											-212.94

	X1	X2	X3	X4	X5	X6	X7	X8	S1	S2	S3	S4	S5	S6	S7	S8	S9	S10	S11	S12	S13	S14	S15	S16	S17	S18	S19	S20	S21	S22
									1.00	1.36							1.18													2.07
										-0.29				1.00			1.23													1.21
										1.03	1.00						2.24													2.96
										0.57			1.00				0.56													0.88
	1.00									1.13					1.00		-0.19	1.00												0.72
																	1.29													0.84
																	2.75													4.02
																	0.63													-0.37
																	0.23													2.06
																	1.08													2.45
																	-0.43													-0.54
																	0.97													2.06
																	3.14													4.77
																	0.44													2.06
																	-0.14													0.18
																	1.00 -0.39													0.37
																	0.80													1.52
																	0.45													1.75
																	0.15													0.88
																	0.19													-1.00
																	0.39													0.84
																	0.90													2.45
																	0.44													1.52
																	0.36													1.36
																														-0.54
																	0.44													1.21
																	0.69													2.06
																	-0.27				1.00									1.36
																	0.44													0.64
																	0.07													-0.37
																	0.29													0.18
																	0.90													2.34
	0.00	0.00	0.00	0.00	0.00	0.00	0.00	0.00	0.00	0.00	0.00	0.00	0.00	0.00	0.00	0.00	3.14	0.00	0.00	0.00	0.00	0.00	0.00	0.00	0.00	0.00	0.00	0.00	0.00	4.77

	A1	A2	A3	A4	A5	A6	A7	A8	A9	A10	A11	A12	A13	A14	A15	A16	rhs	
											-2.07						15.77	S1
											-1.21						7.64	S6
											-2.96						22.37	S3
											-0.88	-1.00					8.51	S24
					-1.00						-0.72						6.37	S5
							-1.00				-0.84						7.49	S10
											-4.02						27.58	S7
											0.37						2.63	S14
						-1.00					-2.06						7.99	S17
											-2.45						14.30	S12
								-1.00			0.54						2.74	S11
											-2.06						12.47	S16
											-4.77						24.94	X7
											-2.06						8.39	S21
					-1.00						-0.18						5.15	S15
										-1.00	-0.37						4.27	S8
										-1.00	-1.52						10.62	S20
											-1.75						13.47	S4
									-1.00		-0.88						7.66	S19
											1.00						0.06	S18
											-0.84				-1.00		8.81	S30
											-2.45						17.43	S31
											-1.52						10.53	S23
											-1.36						5.93	S25
											0.54				-1.00		2.61	S32
											-1.21						8.33	X5
											-2.06						13.78	S27
											-1.36						5.13	S13
											-0.64						11.58	X1
											0.37		-1.00				2.74	S26
											-0.18			-1.00			5.92	S28
											-2.34						17.95	X4
	0.00	0.00	0.00	0.00	0.00	0.00	0.00	0.00	0.00	0.00	-4.77	0.00	0.00	0.00	0.00	0.00	24.94	

	S23	S24	S25	S26	S27	S28	S29	S30	S31	S32	A1	A2	A3
							1.25				-1.36		
							0.69				0.29		-1.00
							1.75				-1.03		
		1.00					0.32						
							0.48				-0.57		
							0.55						
							2.39				-1.13		
							0.84						
							1.37						
							-0.11						
							1.09						
							2.66				-1.03		
							0.62						
							0.32						
							0.27				0.49		
							0.73						-1
							1.10						
							0.73				0.20	-1.00	
							-0.19						
							1.45	1.00					
							1.55		1.00				
							1.09						
			1.00										
	1.00												
							-0.53			1.00			
							1.78						
					1.00		1.37						
							0.62						
							0.19						
			1.00				0.56						
				1.00			-0.11						
							1.45						
	0.00	0.00	0.00	0.00	0.00	0.00	2.66	0.00	0.00	0.00	-1.03	0.00	0.00

Figure B.3 Final LP tableau for the dual of the upper bound problem

Appendix C.1 Validation of the simple hinge rotation equation

The initial position of each hinge is defined by the variables listed on page 164 and illustrated in figure 6.16. These variables are repeated here for convenience:

$X_A = 1.50$, $Y_A = -1.50$, $Z_A = 1.125$
$X_B = 5.05$, $Y_B = -1.50$, $Z_B = 1.125$
$X_C = 0.85$, $Y_C = -0.85$, $Z_C = 1.909$
$X_D = 4.20$, $Y_D = -0.65$, $Z_D = 1.986$
$X_E = 0.15$, $Y_E = -0.15$, $Z_E = 1.869$
$X_F = 3.05$, $Y_F = 0.50$, $Z_F = 1.807$
$X_G = -0.35$, $Y_G = 0.35$, $Z_G = 2.060$
$X_H = 2.00$, $Y_H = 1.55$, $Z_H = 1.402$
$X_I = -1.672$, $Y_I = 1.672$, $Z_I = 1.254$
$X_J = 1.878$, $Y_J = 1.672$, $Z_J = 1.254$

After a positive rotation, $\delta\theta_1 = 1°$, for an intrados hinge at AB

Manipulation of AutoCAD drawing	Prediction using equation 6.37
$X_C = 0.85$, $Y_C = -0.8364$, $Z_C = 1.8979$	$X_C = 0.85$, $Y_C = -0.8363$, $Z_C = 1.8980$
$X_D = 4.20$, $Y_D = -0.6351$, $Z_D = 1.9714$	$X_D = 4.20$, $Y_D = -0.6350$, $Z_D = 1.9715$
$X_E = 0.15$, $Y_E = -0.1372$, $Z_E = 1.8453$	$X_E = 0.15$, $Y_E = -0.1370$, $Z_E = 1.8454$
$X_F = 3.05$, $Y_F = 0.5116$, $Z_F = 1.7721$	$X_F = 3.05$, $Y_F = 0.5119$, $Z_F = 1.7722$

After a negative rotation, $\delta\theta_2 = -1°$, for an extrados hinge at CD

Manipulation of AutoCAD drawing	Prediction using equation 6.37
$X_E = 0.1497$, $Y_E = -0.1497$, $Z_E = 1.8819$	$X_E = 0.1497$, $Y_E = -0.1496$, $Z_E = 1.8819$
$X_F = 3.0494$, $Y_F = 0.5025$, $Z_F = 1.8283$	$X_F = 3.0494$, $Y_F = 0.5027$, $Z_F = 1.8283$
$X_G = -0.3503$, $Y_G = 0.3467$, $Z_G = 2.0826$	$X_G = -0.3503$, $Y_G = 0.3469$, $Z_G = 2.0826$
$X_H = 1.9985$, $Y_H = 1.5589$, $Z_H = 1.4427$	$X_H = 1.9985$, $Y_H = 1.5593$, $Z_H = 1.4426$

After a positive rotation, $\delta\theta_3 = 1°$, for an intrados hinge at EF

Manipulation of AutoCAD drawing	Prediction using equation 6.37
$X_G = -0.3509$, $Y_G = 0.3530$, $Z_G = 2.0500$	$X_G = -0.3509$, $Y_G = 0.3531$, $Z_G = 2.0501$
$X_H = 2.0012$, $Y_H = 1.5425$, $Z_H = 1.3802$	$X_H = 2.0012$, $Y_H = 1.5427$, $Z_H = 1.3801$
$X_I = -1.6702$, $Y_I = 1.6605$, $Z_I = 1.2161$	$X_I = -1.6703$, $Y_I = 1.6609$, $Z_I = 1.2160$
$X_J = 1.8797$, $Y_J = 1.6619$, $Z_J = 1.2297$	$X_J = 1.8797$, $Y_J = 1.6622$, $Z_J = 1.2296$

Appendix C.2 Validation of the complex hinge rotation equation

The initial position of each hinge is defined by the variables listed on page 178 and illustrated in figure 6.19. These variables are repeated here for convenience:

$X_A = 1.50$, $Y_A = -1.50$, $Z_A = 1.125$
$X_B = 5.05$, $Y_B = -1.50$, $Z_B = 1.125$
$X_C = 0.90$, $Y_C = -0.90$, $Z_C = 1.886$
$X_D = 4.15$, $Y_D = -0.60$, $Z_D = 2.002$
$X_E = 0.10$, $Y_E = -0.10$, $Z_E = 1.872$
$X_F = 3.05$, $Y_F = 0.50$, $Z_F = 1.807$
$X_G = -0.35$, $Y_G = 0.35$, $Z_G = 2.060$
$X_H = 2.00$, $Y_H = 1.55$, $Z_H = 1.402$
$X_I = -1.672$, $Y_I = 1.672$, $Z_I = 1.254$
$X_J = 1.878$, $Y_J = 1.672$, $Z_J = 1.254$

After a positive rotation, $\delta\theta_1 = 1°$, for an intrados hinge at AB

Manipulation of AutoCAD drawing	Prediction using equation 6.60
$X_C = 0.900$, $Y_C = -0.8867$, $Z_C = 1.8758$	$X_C = 0.900$, $Y_C = -0.8868$, $Z_C = 1.8757$
$X_D = 4.150$, $Y_D = -0.5847$, $Z_D = 1.9863$	$X_D = 4.150$, $Y_D = -0.5848$, $Z_D = 1.9862$
$X_E = 0.100$, $Y_E = -0.0870$, $Z_E = 1.8479$	$X_E = 0.100$, $Y_E = -0.0872$, $Z_E = 1.8478$
$X_J = 1.878$, $Y_J = 1.6743$, $Z_J = 1.1986$	$X_J = 1.878$, $Y_J = 1.6738$, $Z_J = 1.1986$

After a negative rotation, $\delta\theta_2 = -1°$, for an extrados hinge at CD

Manipulation of AutoCAD drawing	Prediction using equation 6.60
$X_E = 0.0995$, $Y_E = -0.1003$, $Z_E = 1.8875$	$X_E = 0.0995$, $Y_E = -0.1004$, $Z_E = 1.8875$
$X_F = 3.0490$, $Y_F = 0.5027$, $Z_F = 1.8280$	$X_F = 3.0490$, $Y_F = 0.5025$, $Z_F = 1.8280$
$X_J = 1.8754$, $Y_J = 1.6836$, $Z_J = 1.2971$	$X_J = 1.8754$, $Y_J = 1.6832$, $Z_J = 1.2972$

After a negative rotation, $\delta\phi_E = -1°$, for a radial hinge at EF

Manipulation of AutoCAD drawing	Prediction using equation 6.60
$X_F = 3.0396$, $Y_F = 0.5514$, $Z_F = 1.8099$	$X_F = 3.0391$, $Y_F = 0.5513$, $Z_F = 1.8099$
$X_G = -0.3580$, $Y_G = 0.3421$, $Z_G = 2.0604$	$X_G = -0.3579$, $Y_G = 0.3420$, $Z_G = 2.0604$
$X_H = 1.9716$, $Y_H = 1.5834$, $Z_H = 1.4045$	$X_H = 1.9713$, $Y_H = 1.5831$, $Z_H = 1.4045$
$X_J = 1.8476$, $Y_J = 1.7033$, $Z_J = 1.2564$	$X_J = 1.8474$, $Y_J = 1.7031$, $Z_J = 1.2564$

After a positive rotation, $\delta\phi_F$=1°, for a radial hinge at FE

Manipulation of AutoCAD drawing	Prediction using equation 6.60
X_E= 0.0896, Y_E=-0.0504, Z_E=1.8586	X_E= 0.0900, Y_E=-0.0503, Z_E=1.8586
X_G=-0.3537, Y_G=0.4071, Z_G=2.0450	X_G=-0.3532, Y_G=0.4072, Z_G=2.0450
X_H= 2.0195, Y_H=1.5679, Z_H=1.3978	X_H= 2.0197, Y_H=1.5677, Z_H=1.3979
X_J= 1.9003, Y_J=1.6920, Z_J=1.2493	X_J= 1.9004, Y_J=1.6919, Z_J=1.2494

After a negative rotation, $\delta\theta_3$=-1°, for an intrados hinge at FE

Manipulation of AutoCAD drawing	Prediction using equation 6.60
X_G=-0.3508, Y_G=0.3531, Z_G=2.0512	X_G=-0.3508, Y_G=0.3530, Z_G=2.0512
X_H= 2.0010, Y_H=1.5427, Z_H=1.3804	X_H= 2.0011, Y_H=1.5425, Z_H=1.3805
X_J= 1.8795, Y_J=1.6621, Z_J=1.2299	X_J= 1.8795, Y_J=1.6619, Z_J=1.2300

After a positive rotation, $\delta\psi_F^{a}$=1°, for a torsional hinge at FE

Manipulation of AutoCAD drawing	Prediction using equation 6.60
X_E= 0.0983, Y_E=-0.0863, Z_E=1.9231	X_E= 0.0988, Y_E=-0.0862, Z_E=1.9230
X_G=-0.3465, Y_G= 0.3664, Z_G=2.1171	X_G=-0.3460, Y_G= 0.3665, Z_G=2.1170
X_H= 1.9981, Y_H= 1.5534, Z_H=1.4157	X_H= 1.9982, Y_H= 1.5534, Z_H=1.4157
X_J= 1.8742, Y_J= 1.6754, Z_J=1.2693	X_J= 1.8744, Y_J= 1.6755, Z_J=1.2693

After a negative rotation, $\delta\psi_F^{b}$=1°, for a torsional hinge at FE

Manipulation of AutoCAD drawing	Prediction using equation 6.60
X_E= 0.1017, Y_E=-0.1137, Z_E=1.8216	X_E= 0.1021, Y_E=-0.1136, Z_E=1.8216
X_G=-0.3535, Y_G= 0.3336, Z_G=2.0039	X_G=-0.3530, Y_G= 0.3337, Z_G=2.0039
X_H= 2.0019, Y_H= 1.5466, Z_H=1.3883	X_H= 2.0020, Y_H= 1.5466, Z_H=1.3883
X_J= 1.8818, Y_J= 1.6686, Z_J=1.2387	X_J= 1.8819, Y_J= 1.6686, Z_J=1.2388